AEDC TR-94-10

Temperature Effects on Accoustic Interactions between Altitude Test Facilities and Jet Engine Plumes

K. K. Ahuja and K. C. Massey
Georgia Tech Research Institute
Georgia Institute of Technology
Atlanta, GA
and
C. K. W. Tam
Consultant
Florida State University
Tallahassee, FL
and
R. R. Jones, III
Sverdrup Technology, Inc./AEDC Group

October 1994

Final Report for Period February 1992 through May 1994

**ARNOLD ENGINEERING DEVELOPMENT CENTER
ARNOLD AIR FORCE BASE, TENNESSEE
AIR FORCE MATERIEL COMMAND
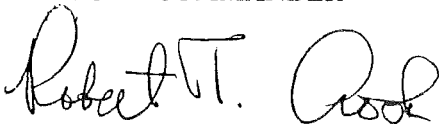UNITED STATES AIR FORCE**

NOTICES

APPROVAL STATEMENT

This report has been reviewed and approved.

DANIEL MAGEE, Capt, CF
Propulsion Technology
Applied Technology Division
Test Operations Directorate

Approved for publication:

FOR THE COMMANDER

ROBERT T. CROOK
Assistant Chief, Applied Technology Division
Test Operations Directorate

REPORT DOCUMENTATION PAGE

Public reporting burden for this collection of information is estimated to average 1 hour per response, including the time for reviewing instructions, searching existing data sources, gathering and maintaining the data needed, and completing and reviewing the collection of information Send comments regarding this burden estimate or any other aspect of this collection of information, including suggestions for reducing this burden, to Washington Headquarters Services, Directorate for Information Operations and Reports, 1215 Jefferson Davis Highway, Suite 1204, Arlington, VA 22202-4302, and to the Office of Management and Budget, Paperwork Reduction Project (0704-0188), Washington, DC 20503.

1. AGENCY USE ONLY (Leave blank)	2. REPORT DATE September 1994	3. REPORT TYPE AND DATES COVERED Final Report for February 1992 - May 1994

4. TITLE AND SUBTITLE Temperature Effects on Acoustic Interactions Between Altitude Test Facilities and Jet Engine Plumes	5. FUNDING NUMBERS Contract No. NAS1-19061

6. AUTHOR(S)
Ahuja, K. K. and Massey, K. C., Georgia Tech Research Institute; Tam, C. K. W., Consultant, Florida State University; and Jones, R. R. III, Sverdrup Technology, Inc., AEDC Group

7. PERFORMING ORGANIZATION NAME(S) AND ADDRESS(ES) Georgia Tech Research Institute Georgia Institute of Technology Atlanta, GA 30032-0800	8. PERFORMING ORGANIZATION REPORT NUMBER AEDC-TR-94-10

9. SPONSORING/MONITORING AGENCY NAMES(S) AND ADDRESS(ES) National Aeronautics and Space Administration Langley Research Center Hampton, VA 23665-5225	10. SPONSORING/MONITORING AGENCY REPORT NUMBER

11. SUPPLEMENTARY NOTES

Available in Defense Technical Information Center (DTIC).

12a. DISTRIBUTION/AVAILABILITY STATEMENT Approved for public release; distribution is unlimited.	12b. DISTRIBUTION CODE

13. ABSTRACT (Maximum 200 words)

The overall objective of the present investigation was to determine the mechanisms responsible for engine/test cell resonance observed at the AEDC facility. The specific objective was to determine the effect of heating the jet on its coupling with the diffuser used in a typical engine/test cell facility. This objective was to be accomplished through systematic measurements of cold and heated free and ducted jets using a subscale facility. An additional objective was to analytically examine the behavior of jet instability waves as a function of temperature, and to identify any potential of strong coupling between the jet instabilities and diffuser duct resonance modes directly attributable to heating of the jet. Model cold and heated jet experiments are performed with an axisymmetric convergent nozzle in a test setup that simulates a supersonic jet exhausting into a cylindrical diffuser. The measured data consist of a free and ducted plume for a range of jet exit Mach numbers and four reservoir temperatures: ambient, 400°F, 750°F, and 1,000°F. Analytical results on the growth of instability waves and the duct resonance have been introduced. It is shown that the screech frequency increases with increasing operating temperature ratio. The measured in-duct microphone signatures contain a number of discrete tones, and almost all of them can be associated with duct resonances. The amplitudes increase with increasing Mach number and operating temperature ratios. At certain operating conditions, the acoustic fluctuations associated with these ejector duct modes excite the most amplified wave of the jet. Once excited, the instability wave grows rapidly to its maximum amplitude as it propogates downstream, causing the jet to oscillate violently, which in turn pumps energy into the duct modes. The feedback cycle thus formed is believed to be the mechanism responsible for the AEDC test cell resonance.

14. SUBJECT TERMS screech, altitude test facilities, instability waves, flow/acoustic interactions, jet noise, ejectors, receptivity, duct resonance, ducted jets, high temperature jets	15. NUMBER OF PAGES 310
	16. PRICE CODE

17. SECURITY CLASSIFICATION OF REPORT UNCLASSIFIED	18. SECURITY CLASSIFICATION OF THIS PAGE UNCLASSIFIED	19. SECURITY CLASSIFICATION OF ABSTRACT UNCLASSIFIED	20. LIMITATION OF ABSTRACT SAME AS REPORT

PREFACE

CONTENTS

ILLUSTRATIONS

APPENDICES

1.0 INTRODUCTION

1.1 BACKGROUND

Altitude test cells are routinely used to test aero-engines during their development phases. Often, these cells are also used to test propulsion system enhancements after entering service. In a typical installation, the engine is contained in a large test cell where the engine inlet is supplied with conditioned air through a direct connection to the test cell air supply system. The engine inlet is aerodynamically isolated from the test cell. The test cell is maintained at the desired altitude pressure through the combined action of the facility exhaust compressors and the pumping action of the engine exhaust as it enters the test cell exhaust gas management system (EGMS) which, in its most common form, is a cylindrical diffuser. In such an installation, the high-energy engine exhaust stream may contain acoustic and/or fluid dynamic characteristics that can couple with the resonant modes of the test cell and/or the EGMS to produce strong, undesirable pressure fluctuations.

In isolated full-scale engine tests conducted at Arnold Engineering Development Center (AEDC) in Tennessee, it has become apparent that, for certain operating conditions and test geometries, when engines exhaust supersonically into the EGMS, high-intensity discrete tones (whistles) are heard (Ref. 1.1). Sound pressure levels as high as 170 dB have been measured within the facility exhaust system. These whistles appear to be unrelated to the screech commonly observed in free jets and whose frequency can now be calculated with a high degree of accuracy (Ref. 1.2).

When these high-intensity tones are heard, it appears that the phenomenon responsible for these tones also is directly or indirectly responsible for producing large vibrations in the test cells and other related test facility ducting (Ref. 1.1).

The above-described phenomenon has been observed for both axisymmetric, underexpanded nozzles and for two-dimensional, convergent-divergent (2-D, C-D) nozzles. For the 2-D, C-D nozzle, it appears that for certain flow operating conditions, the whole jet body physically deflects in the manner of a fluidic jet. This is also accompanied by a high-amplitude (in excess of 165 dB) discrete tone.

The physical mechanisms responsible for the discrete tones described above and their interactions with the flow need to be understood so that a corrective action can be taken in a timely manner. Or if it is known in advance as to what range of flow conditions for given geometric test configuration produces an unacceptable interaction, then that range of flow conditions can be avoided until an appropriate control methodology has been implemented.

In an effort to develop an understanding of the physical mechanisms involved in the flow/ acoustic interactions experienced in the full-scale altitude test facilities at AEDC, an extensive set of measurements was carried out in 1991 by the authors using a 1/48th-scale model facility at the Georgia Tech Research Institute (GTRI) (Ref. 1.3). Model cold-jet experiments with an axisymmetric convergent nozzle were performed in a test setup that simulated a supersonic jet

7

exhausting into a cylindrical diffuser. The measured data consisted of detailed flow visualization and acoustic spectra for a free and a ducted plume. To complement the experimental study, a theoretical model was also developed. It was shown that duct resonance is most likely responsible for the low-frequency, high-intensity whistles experienced in the AEDC full-scale facilities, and the higher frequencies are related to the screech phenomenon.

While we were able to replicate the frequencies, scaled appropriately for the model scale test configuration, we were unable to reproduce the high amplitudes (as high as 170 dB) experienced in the full-scale facilities. To establish if this could have been a result of the small scale of the model, a nominally 25 times larger (the diffuser was 66 in. in diameter by 108 in. long) test setup was built and tested in NASA Lewis Research Center wind tunnel altitude test cell PSL-3. These measurements were also made only for cold-flow simulations and are described in Ref. 1.4. In these measurements also, we were able to replicate a duct resonance frequency which linearly scaled with the geometry of the full-scale facility and the 1/48th-scale GTRI facility alluded to above. Unfortunately, similar to the cold-flow measurements of the GTRI sub-scale facility, these measurements also failed to reproduce the high amplitudes experienced in the full-scale facilities.

It was established from these measurements that the scale of the test facility was not responsible for the reduced whistle amplitudes. Since the high-amplitude whistles in the full-scale facilities were obtained for higher jet temperatures, it was speculated that the amplitude of the duct resonance for our test geometry may increase for certain operating conditions if the plume is operated at higher temperatures. This is because growth rates of the instability waves in a jet are expected to be different at different temperatures (Ref. 1.5). Their most preferred frequencies are expected to change with temperature and if the most preferred frequency of the jet instability at a given operating condition matches a duct resonance frequency for our model scale facility, high amplitudes are likely to result.

It is to understand this effect of temperature on the flow/acoustic interactions between the altitude test facility and a jet engine plume that the study described in the present report was initiated.

1.2 PROGRAM OBJECTIVE

The overall objective of the present investigation was to determine the mechanisms responsible for engine/test cell resonance observed at the AEDC facility. The specific objective was to determine the effect of heating the jet on its coupling with the diffuser used in a typical engine/test cell facility.

This objective was to be accomplished through systematic measurements of cold and heated free and ducted jets using a sub-scale facility.

An additional objective was to analytically examine the behavior of jet instability waves as a function of temperature and to identify any potential of strong coupling between the jet instabilities and diffuser duct resonance modes directly attributable to heating of the jet.

1.3 REPORT OUTLINE

The model-jet diffuser test facility setup and test procedures are described in Section 2. This is followed, in Section 3, by a description of the effect of temperature on the screech phenomenon of a free jet. The results are compared with the theoretical model of Tam (Ref. 1.6). Results for the ducted jet are then presented in Section 4.

Also, a number of spin-off results became available at the end of the present study. For the sake of completeness, these results are included in this report in appendices at the end of the report. Analytical calculations performed by Dr. Tam in support of the experimental study appear in Section 6. This section also includes a summary of the study together with a concise discussion. Finally, the overall conclusions and recommendations are also provided in Section 6. Equations used for mass flow calculations are included in Appendix D, and the nomenclature in Appendix H.

It should be noted that, throughout this report, the words "diffuser" and "ejector" are used interchangeably. For all experimental observations reported, the exhaust diffuser was operated in an unstarted condition, (i.e., subsonic flow existed in portion of diffuser allowing communication from entrance to exit). The term "ducted" indicates the complete subscale facility consisting of the jet, the diffuser, and the cell sections surrounding the jet nozzle and downstream of the jet nozzle.

2.0 EXPERIMENTAL SETUP AND TEST PROCEDURES

2.1 COMPLETE MODEL CONFIGURATION AND AIR SUPPLY PLENUM

Based upon the specifications provided by personnel at AEDC, the model jet/diffuser/test cell configurations shown in Figs. 2.1 - 2.3 were designed and fabricated. The air for the jet is provided by a compressor capable of providing up to 17 lbm/sec of dry air continuously. The jet exhausts from a 0.484-in.-diam round convergent nozzle.

All of the experiments reported here were conducted in GTRI's Hot Jet Facility which is described in detail in Refs. 2.1 and 2.2. As shown in Fig. 2.4, the primary flow enters through a 10-in.-diam plenum to a 4-in.-diam supply duct followed by a 4-in. to 2-in. converging section. The test nozzle used in this program has an exit diameter of 0.484 in. and is attached to this converging section. This provides an overall plenum-to-nozzle area contraction ratio of 427. A 1-in.-diam convergent circular nozzle was available to us at the beginning of the program while the smaller nozzle (D_j = 0.484 in.) was being fabricated. For selected tests with the free jet, this 1-in.-diam nozzle was used to examine the variation of screech frequency with temperature, and results along with those for the smaller diameter nozzle are compared in this report.

The air flow in this facility is heated by a propane burner. The plenum temperatures can be heated to an excess of 1,700°R at pressure ratios exceeding 4.5.

DIFFUSER

NOZZLE

Scale Factor	= 48
Nozzle D_j	= 0.484 in.
Test Cell Dia.	= 6.50 in.
Ejector D_{ej}	= 2.62 in.
Ejector Length	= 1 D_{ej} and 3 D_{ej}
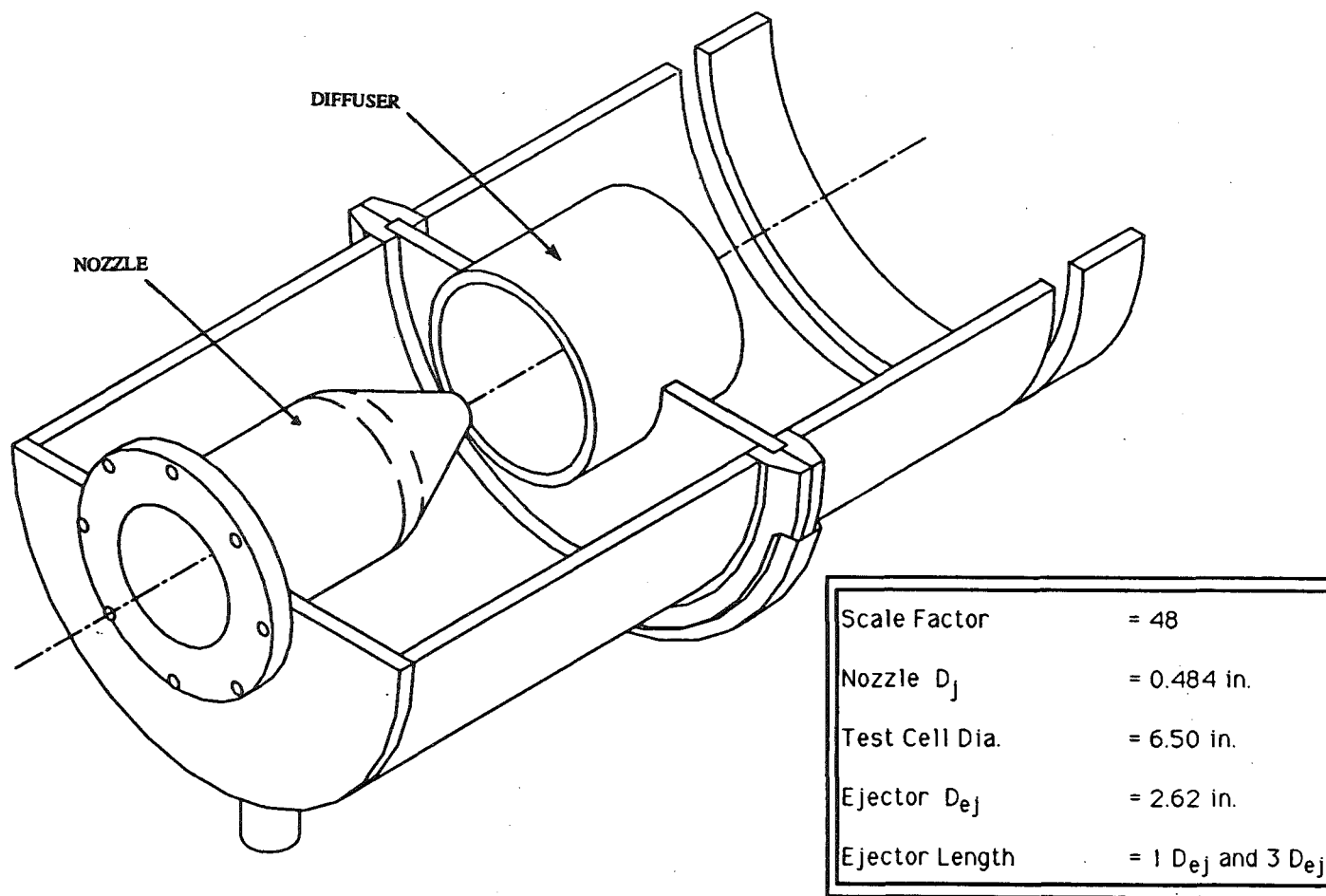
Figure 2.1. Sub-scale axisymmetric ducted jet configuration.
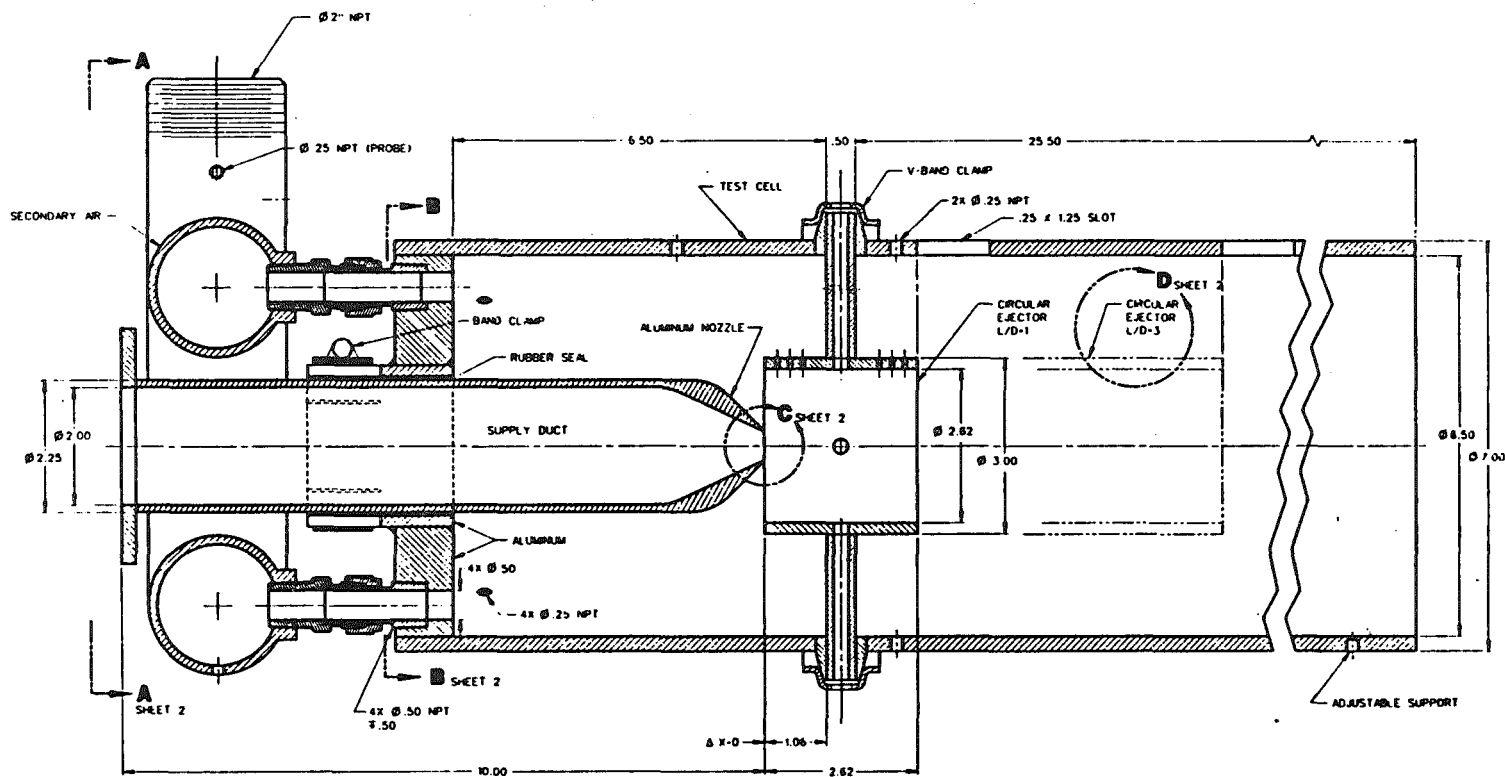
Figure 2.2. Critical dimensions for the ducted jet configuration.
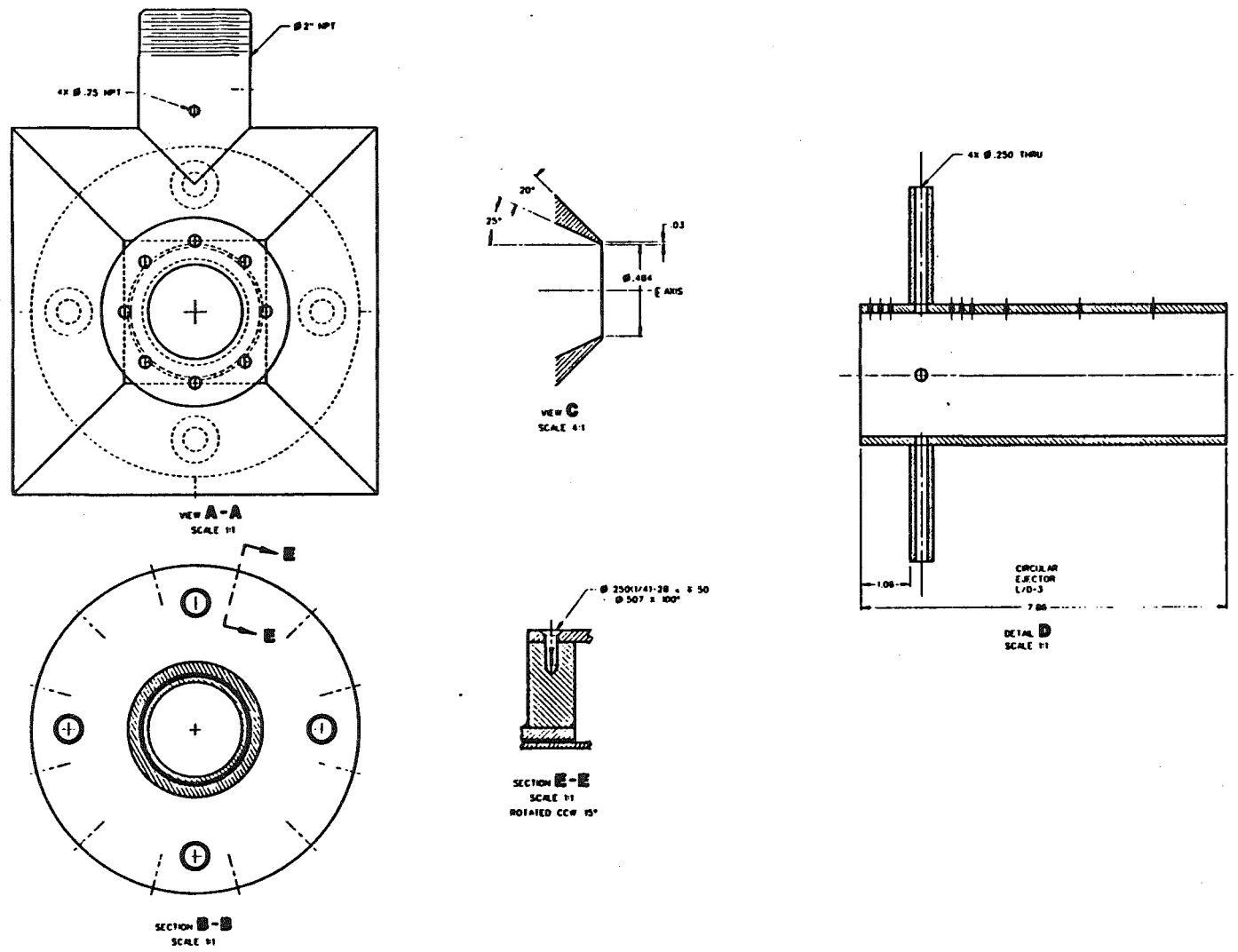
Figure 2.3. Details of the ducted jet configuration.
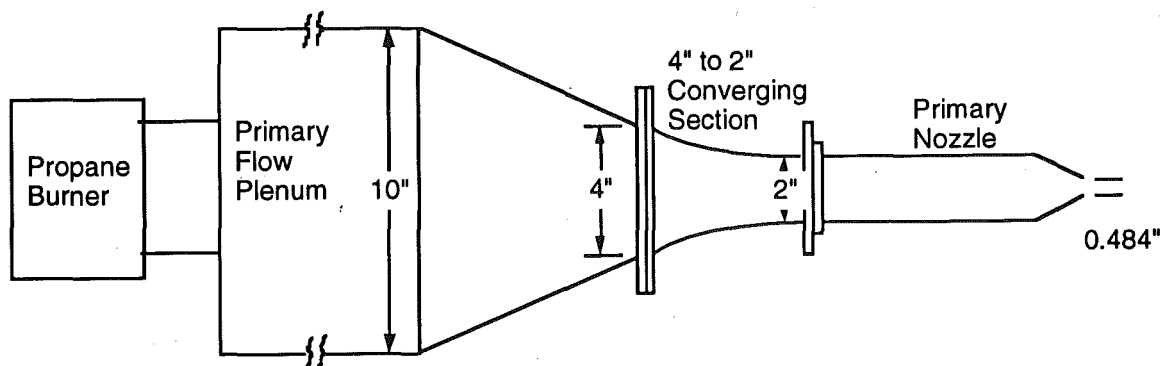
Figure 2.4. Hot Jet Facility cross-sectional view.

2.2 FREE-JET CONFIGURATION

The free-jet nozzle is constructed of a high-temperature steel alloy. The nozzle consists of a 10-in.-long duct with an inner diameter of 2 in. that ends in a 1-in.-long converging section to a final exit of 0.484 in. The nozzle was initially designed so that the end of the nozzle could be screwed on and off. This was done to facilitate the addition of a boundary-layer trip upstream of the nozzle lip and, if needed, to provide an additional section of duct to lengthen the nozzle. Figure 2.5 shows the free jet as mounted in the hot jet facility for free-jet data acquisition. Figure 2.6 is a side view of the end of the nozzle and the boundary-layer trip. Figure 2.7 shows an end view of the converging section of the nozzle with the boundary-layer trip in place.
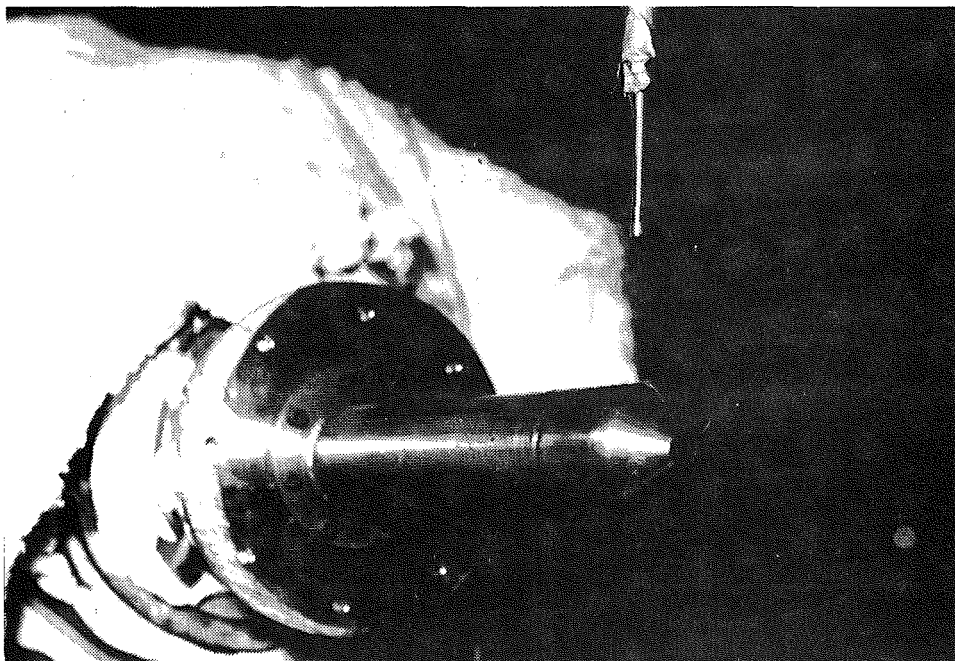
Figure 2.5. Experimental setup for the free jet.
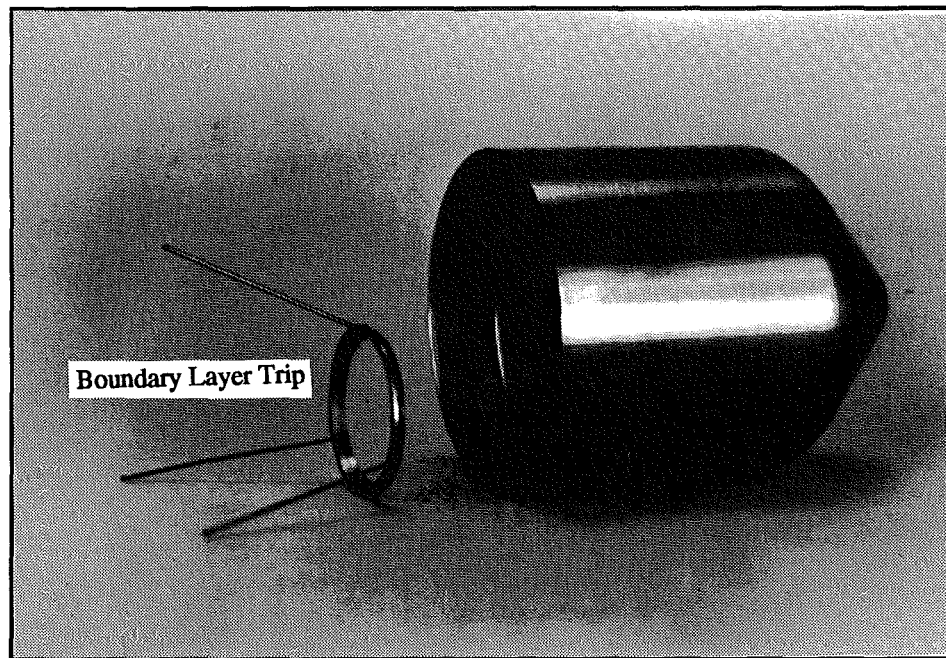
Figure 2.6. Side view of nozzle and boundary-layer trip.
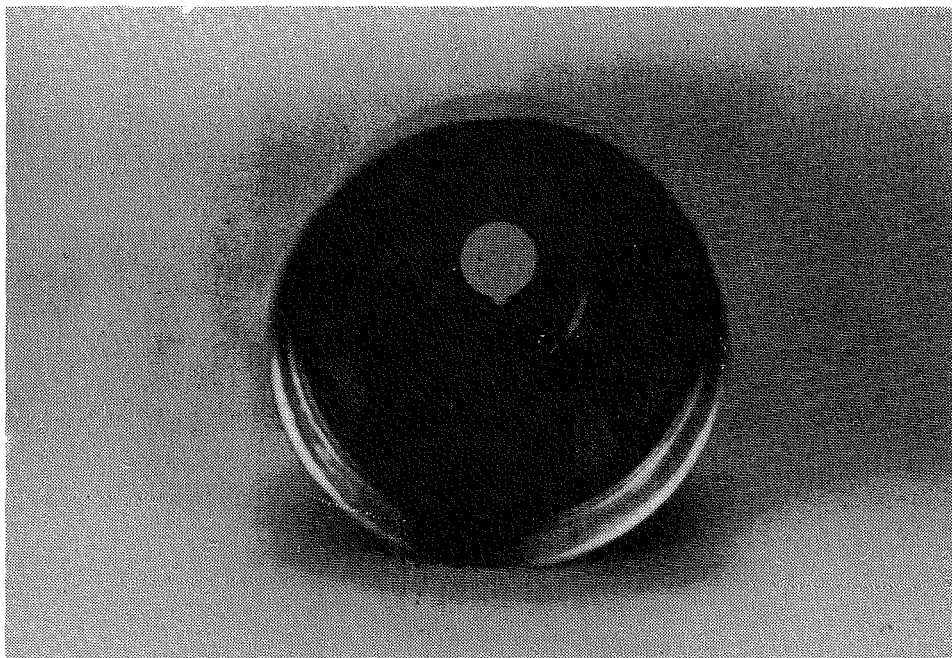
Figure 2.7. End view of nozzle with boundary-layer trip in place.

2.3 DUCTED JET CONFIGURATION

The ducted jet configuration is based on a scaled-down version of the AEDC test facility with a slightly simplified geometry. It consists of the jet described above exhausting into a test cell with a diffuser located slightly downstream. The test cell is constructed from steel and is 6.5 in. in diameter. To simulate the test conditions typical of those used at AEDC during the full-scale tests, a manifold is attached to the test cell through which secondary air can be entrained for cooling purposes. This secondary air enters the test cell through four inlets. The secondary air is entrained through the manifold opening. The diffuser is constructed of a high-temperature steel alloy and has a diameter of 2.62 in. The diffuser is constructed with a length-to-diameter ratio (L/D) of 3. Downstream of the diffuser wall, the test cell wall continues with a constant diameter of 6.5 in. for another 25.5 in. A cutaway view of the ducted configuration appears in Fig. 2.1 while the critical dimensions appear in Figs. 2.2 and 2.3 .

The ducted jet components are shown before assembly in Fig. 2.8, and the ducted jet configuration is shown mounted in Fig. 2.9. The L/D = 3 diffuser is shown in Fig. 2.10 .

Note that the component shown seated second from left in Fig. 2.8 is the ejector (or diffuser) equipped with high-temperature transducers mounted in water jackets. These transducers and water jackets are described in detail later in Appendix F. These high-temperature transducers were not used in the present study due to a change in the scope of the program. Figure 2.8 is included merely for the sake of completeness. A second ejector shown in Fig. 2.10 without room for water jackets and transducers was used for all tests reported here. This diffuser is mounted inside the long test cell shown in Fig. 2.9.
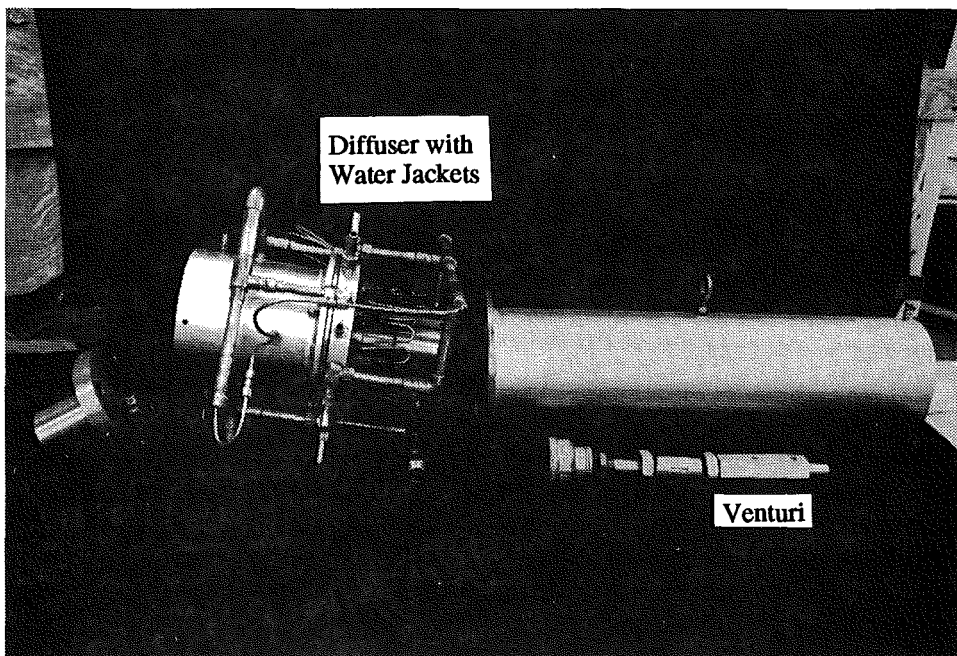
Figure 2.8. Individual components of the ducted jet assembly.

15
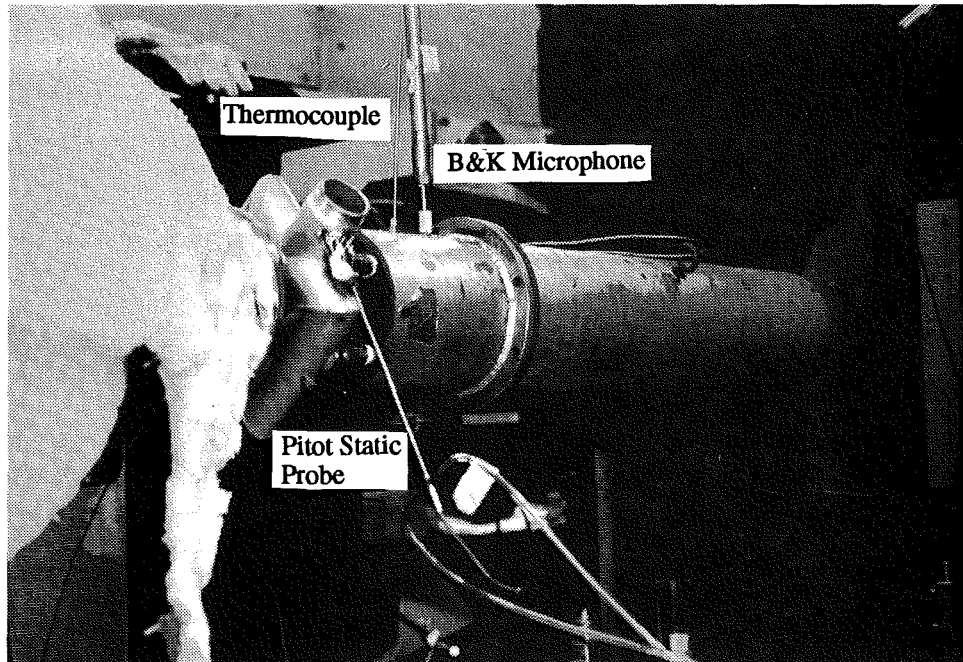
Figure 2.9. Ducted jet configuration as tested in hot-jet facility.
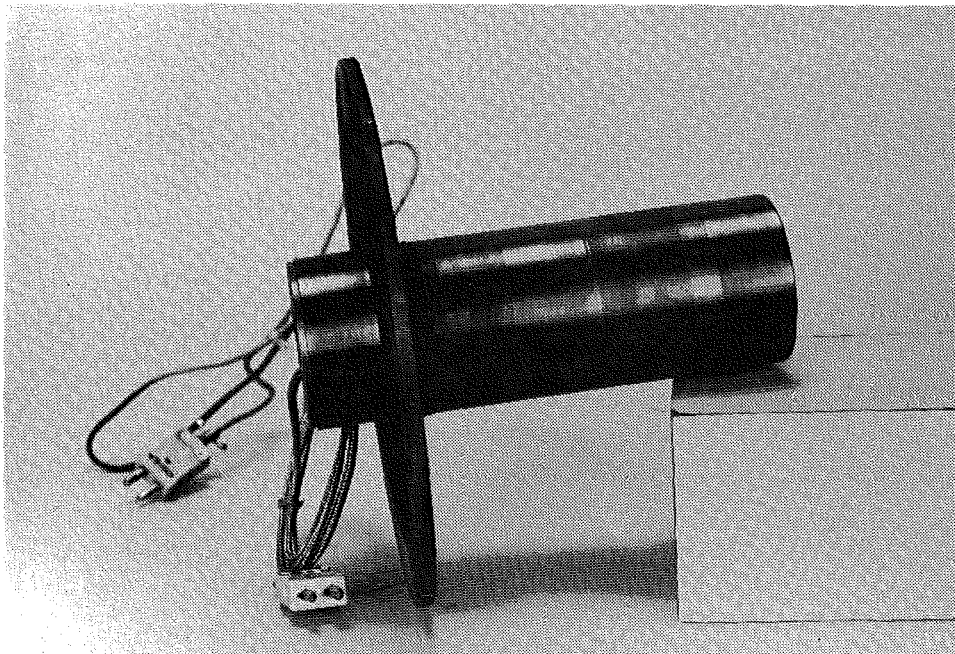
Figure 2.10. Side view of L/D = 3 diffuser.

2.4 INSTRUMENTATION

All acoustic data were acquired using a type 4136 Bruel and Kjaer 1/4-in.-diam microphone located at 7.3 exit diameters (7.3 De) above and slightly behind the nozzle (θ = 110.92 deg). The data from this microphone were analyzed from 0 to 100 kHz using a Hewlett Packard (HP) narrow band real-time analyzer with a bandwidth resolution (Δf) of 128 Hz.

For the ducted conditions, the microphone was mounted flush with the wall of the test cell. For the heated conditions, this meant that the microphone could potentially be exposed to high temperatures. A wooden sheath for the microphone was constructed to protect the microphone from heat from the surroundings. This sheath is shown in Fig. 2.11 as it mounted over the B&K microphone. A test was conducted to ensure that the sensitivity of the microphone was not jeopardized. This is described separately in Section 4.2.2.

Additional tests were conducted to measure the temperatures in the test cell and at locations downstream of the diffuser. These temperature measurements were made using Chromel-Alumel® thermocouples. For the test cell temperature, the thermocouple was located roughly in between the test cell wall and nozzle wall (1-1/4 in. beneath the test cell wall). The location of this thermocouple relative to the nozzle is shown in Fig. 2.12. Although it is appreciated that temperature measurement made only at one location may not be a true indicator of the test cell temperature, it does provide a qualitative insight into the effects of the changing secondary mass flow rate since this temperature was a strong function of the secondary mass flow rate. This temperature location was also close to the nozzle exit and hence was used to determine the operating temperature ratio of the jet for a given reservoir temperature.

The thermocouple in the diffuser was located 1/2 in. from the diffuser exit and 1/2 in. from the diffuser wall, as is shown in Fig. 2.13. The temperatures measured here are very likely representative of the average temperatures in the diffuser as the flow is expected to be well-mixed at this stage.

The test cell static pressure was measured for all tests as this pressure was necessary to calculate the jet pressure ratio that determined the operating conditions. This static pressure was measured near the upstream wall of the test cell. The location of this static pressure port, as well as the microphone and thermocouple locations on the test cell, are shown in Fig. 2.14.

Pressure measurements were also made to allow the calculation of the secondary mass flow rate. The secondary air was entrained either through a venturi that was attached to the manifold or through the manifold opening itself. For those tests for which the venturi was used, the pressure was measured at the inlet and at the throat of the venturi as depicted in Fig. 2.15. For the tests where the secondary air manifold was left open, a pitot static probe was inserted into the manifold and the pressure difference was measured and used to calculate the velocity in the manifold. It was found that the pressure difference was constant across the cross section of the manifold intake. Figure 2.16 shows the setup for a test where the open manifold was used. The manometer used to measure the pressure difference across the pitot probe can be seen in the foreground, and the pitot probe can be seen protruding from the manifold.

In the final test conducted where a portion of the inlet of the diffuser was closed off by using an orifice baffle, an additional thermocouple was installed in the upstream portion of the diffuser. This addition of the orifice baffle to the diffuser and the thermocouple are shown in Fig. 2.17.

Wooden Sheath
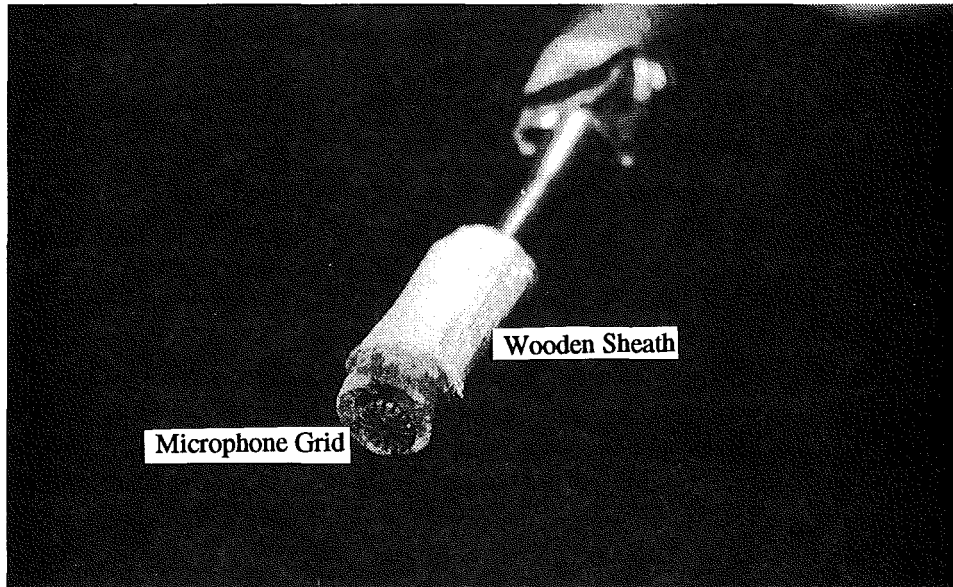
Microphone Grid

Figure 2.11. B&K microphone with protective wooden sheath.
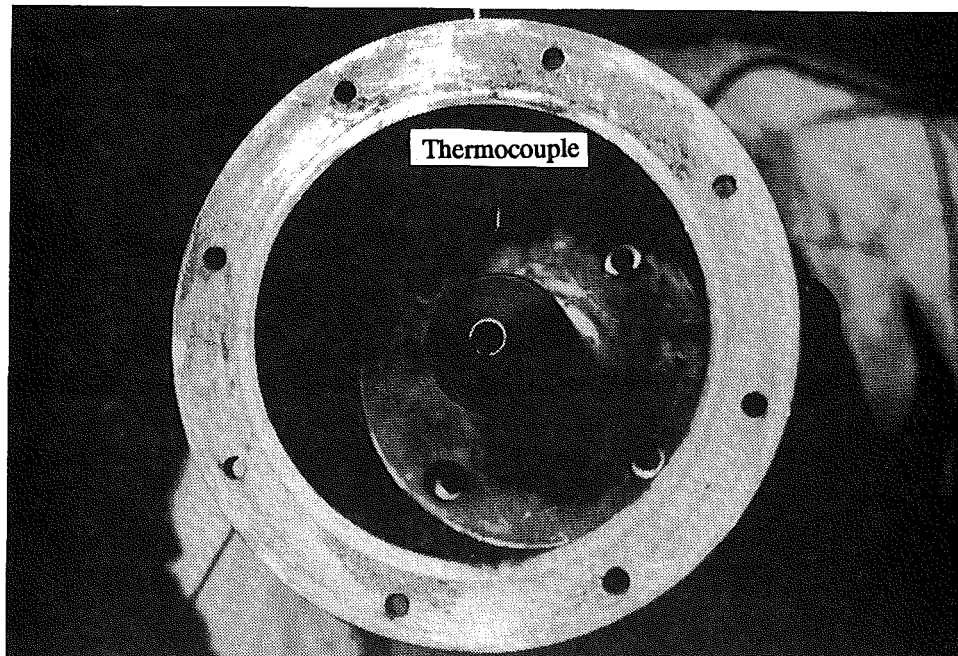
Thermocouple

Figure 2.12. Thermocouple used to measure test cell temperature.
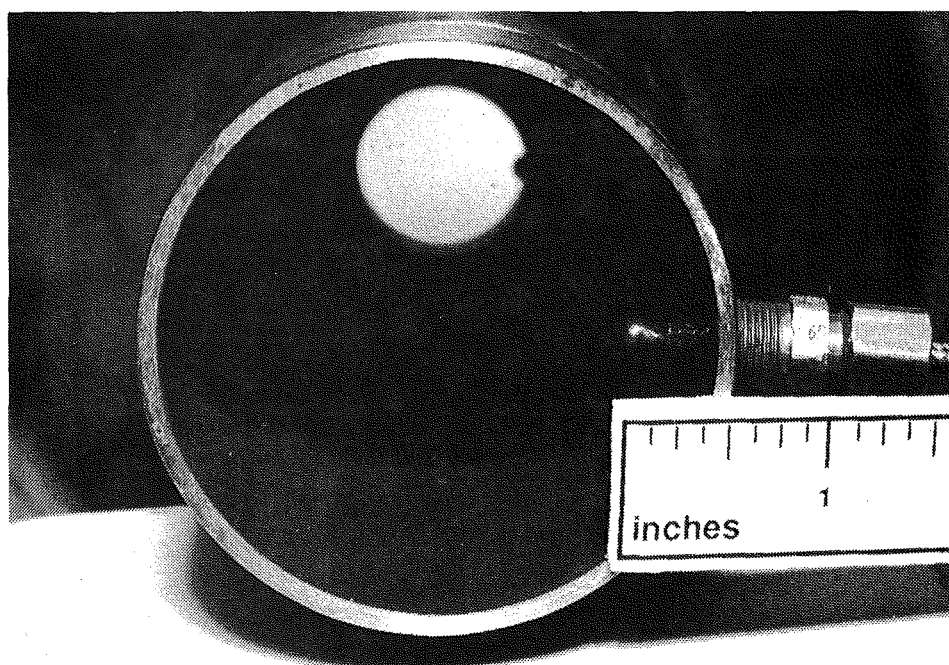
Figure 2.13. Thermocouple used to measure diffuser temperature.
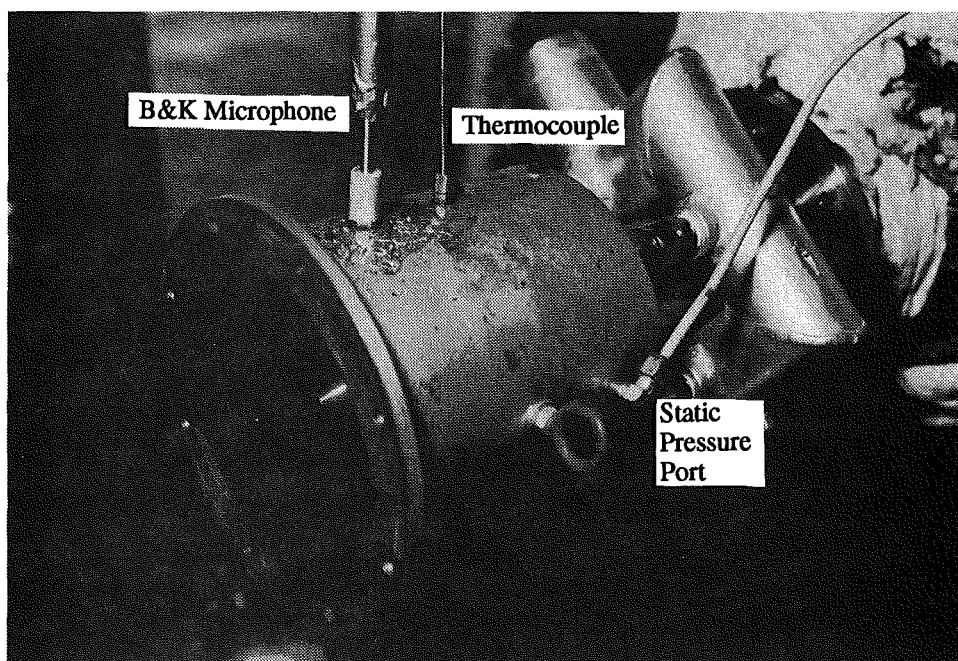
Figure 2.14. Relative locations of the static pressure port, microphone and thermocouple on the test cell.
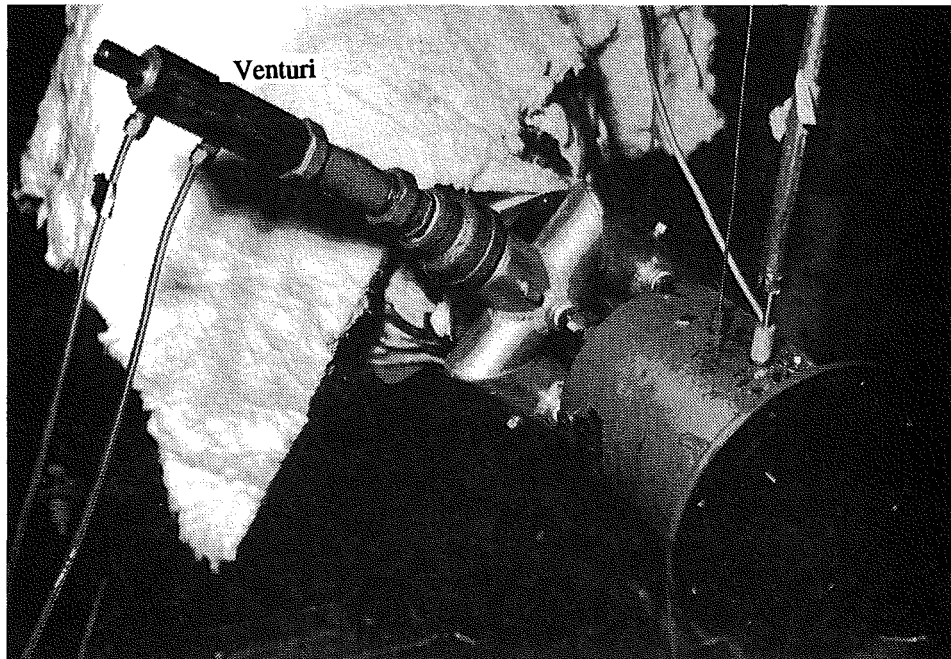
Figure 2.15. Ducted jet configuration using the venturi.
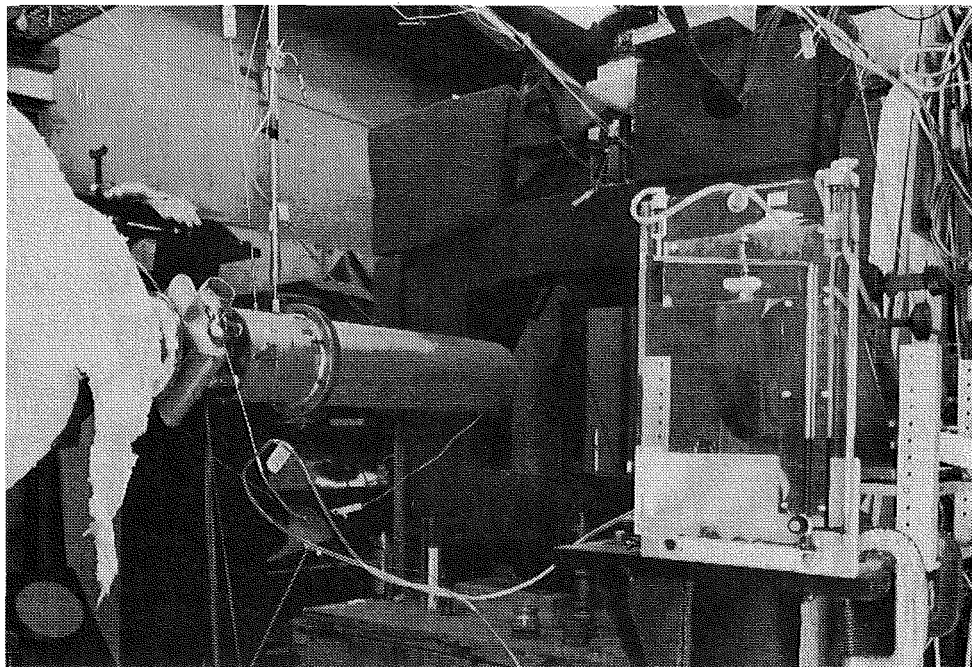
Figure 2.16. Ducted jet configuration using the open manifold.
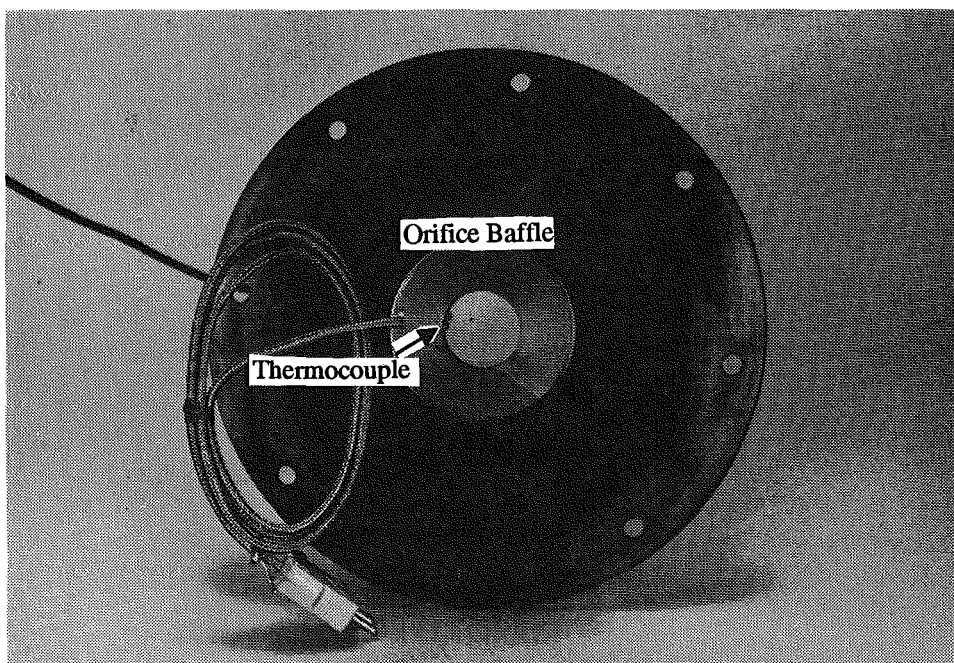
Figure 2.17. Orifice baffle added to the diffuser and additional upstream thermocouple.

2.5 TEST CONDITIONS

All tests with the smaller diameter nozzle (i.e., D_j = 0.484 in.) were first conducted with the free jet and then with the ducted configuration. For the ducted configuration, the nozzle exit was located at a distance of 0.3 nozzle exit diameters from the ejector inlet for all tests. In both cases the microphone location with respect to the nozzle center did not change. For the 1-in. nozzle, for which only the free-jet data were obtained, the microphone was located in the plane of the nozzle exit at a distance of 4 ft from the nozzle center.

The free jet was operated at plenum pressure ratios corresponding to fully developed Mach numbers (nominal values) of 0.8, 1.0, 1.1, 1.2, 1.3, 1.4, 1.5, and 1.6. Thus, for the ducted jet, these Mach numbers were slightly higher since the jet was expanding into a region of lower pressure. For each Mach number, the acoustic data were acquired for plenum chamber temperatures of ambient, 400, 750, and 1,000°F. Depending upon the secondary mass flow rate for the ducted jet, this provided different temperature ratios at the nozzle exit for a constant plenum temperature, T_r. The temperature ratios as a function of jet Mach number, M_j, are shown in Figs. 2.18 and 2.19 for reservoir temperatures of 750°F and 1,000°F, respectively. Figure 2.19 also shows selected data for the manifold 1/2-open. (Half of the manifold opening was covered by a steel plate in this case.)
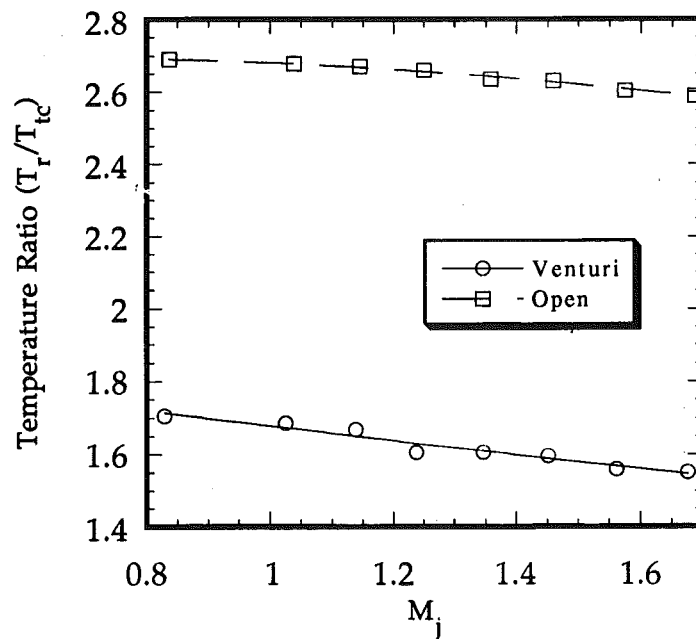
Figure 2.18. Operating temperature ratio for venturi on and open manifold configurations for reservoir temperature of 750°F.
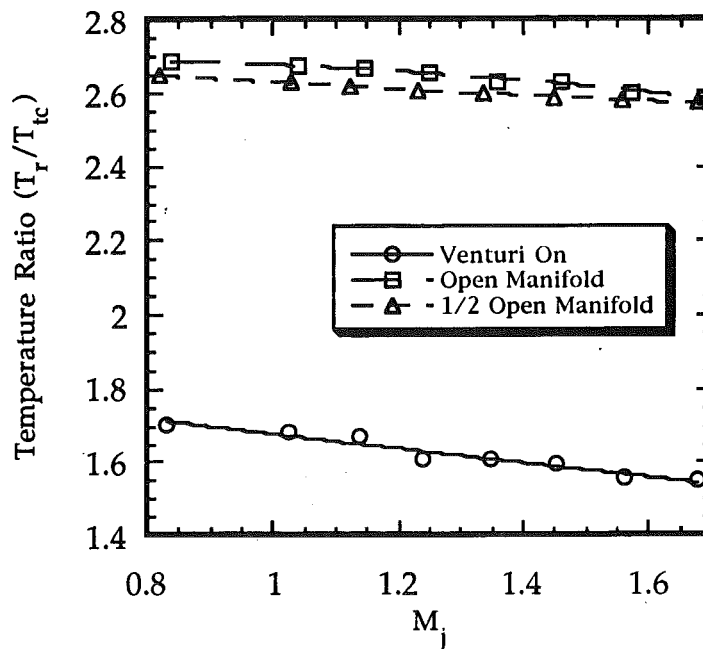
Figure 2.19. Operating temperature ratio for venturi on and open and 1/2-open manifold configurations for reservoir temperature of 1,000°F.

3.0 FREE-JET RESULTS

The results for the free jet only are presented in this section. Particular attention is paid to the variation of screech frequency and amplitude with jet temperature. It is shown that the effect of the boundary-layer trip on the free-jet acoustic spectra was negligible. The screech frequencies measured for a range of test conditions are compared with those predicted by Tam's theory (Ref. 3.1), and excellent agreement is found with measurements. The effect of temperature is to decrease the amplitude of the screech and also to reduce the normalized frequency at a fixed fully expanded jet Mach number.

It should be pointed out here that the sound pressure level (SPL) spectra presented in this report were obtained in a semi-anechoic chamber. Caution should, therefore, be exercised in attempting to compare these spectra with similar spectra obtained in large anechoic chambers. The free-jet data are presented here to examine the trends and to examine the variation of frequency peaks as a function of temperature. Suffice it to say, however, that subsequent data obtained in a large anechoic chamber produced similar results and conclusions (Ref. 3.2).

Also, for the sake of completeness, the free-jet noise spectra are presented separately in Appendices A and B for the 1-in. and the 0.48-in.-diam nozzles, respectively.

3.1 EFFECT OF BOUNDARY-LAYER TRIP

Since the test nozzle had a small diameter and since with heating the kinematic viscosity of air increases with temperature, there was concern that the resulting low values of Reynolds numbers may produce laminar boundary layers at the exit of the nozzles. To ensure that the boundary layer at the exit of our nozzle was turbulent, and thus a more realistic representation of the flow in the full-scale system, we introduced a boundary-layer wire trip located just upstream of the nozzle exit as shown earlier in Fig. 2.7. A similar trip was installed in earlier heated jet studies by the first author (Ref. 3.3) using the same facility as used here, and it successfully rendered the boundary layer turbulent. (Note that this boundary-layer trip was used only with the 0.48-in.-diam nozzle in the present study.)

The boundary-layer trip was found to have a negligible effect upon the jet acoustics as shown in Fig. 3.1 for a jet Mach number, M_j, of 0.8 and in Fig. 3.2 for $M_j = 1.45$. Similar results were obtained at other Mach numbers. Due to mechanical difficulties in removing and replacing the boundary-layer trip, it was eventually left in the nozzle and the majority of the tests were conducted with the trip in place.

3.2 EFFECT OF TEMPERATURE RATIO

3.2.1 Subsonic Case

Although acoustic data were acquired for only one subsonic Mach number, the effect of the temperature ratio on the spectra follows the anticipated trend. Increasing the temperature ratio serves to increase the broadband noise across the entire frequency range. This is as expected, since the noise in the subsonic case is primarily mixing noise. For a constant jet exit Mach
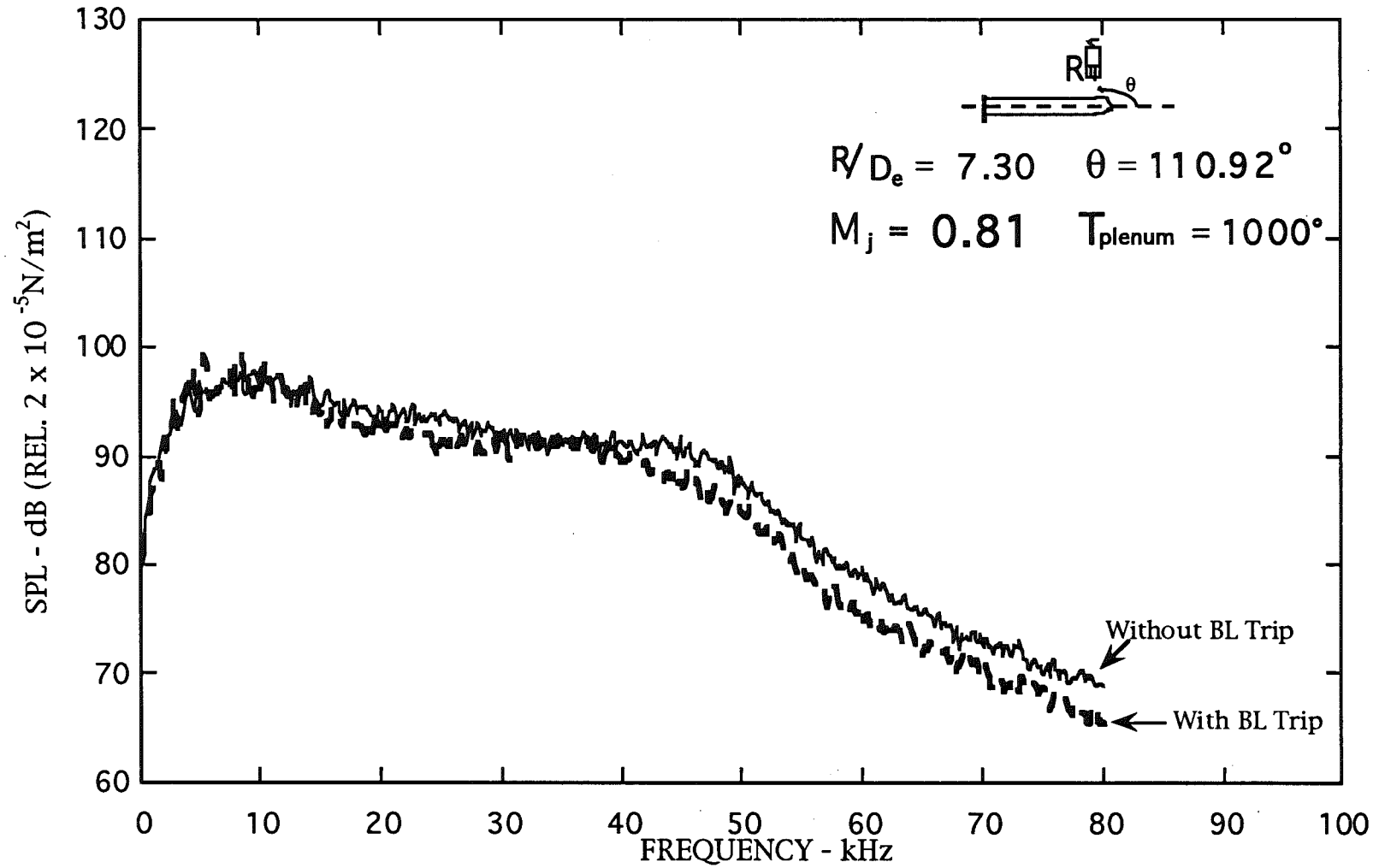
Figure 3.1 Narrow band (Δf = 128 Hz) noise spectra of the free jet, M_j = 0.81.
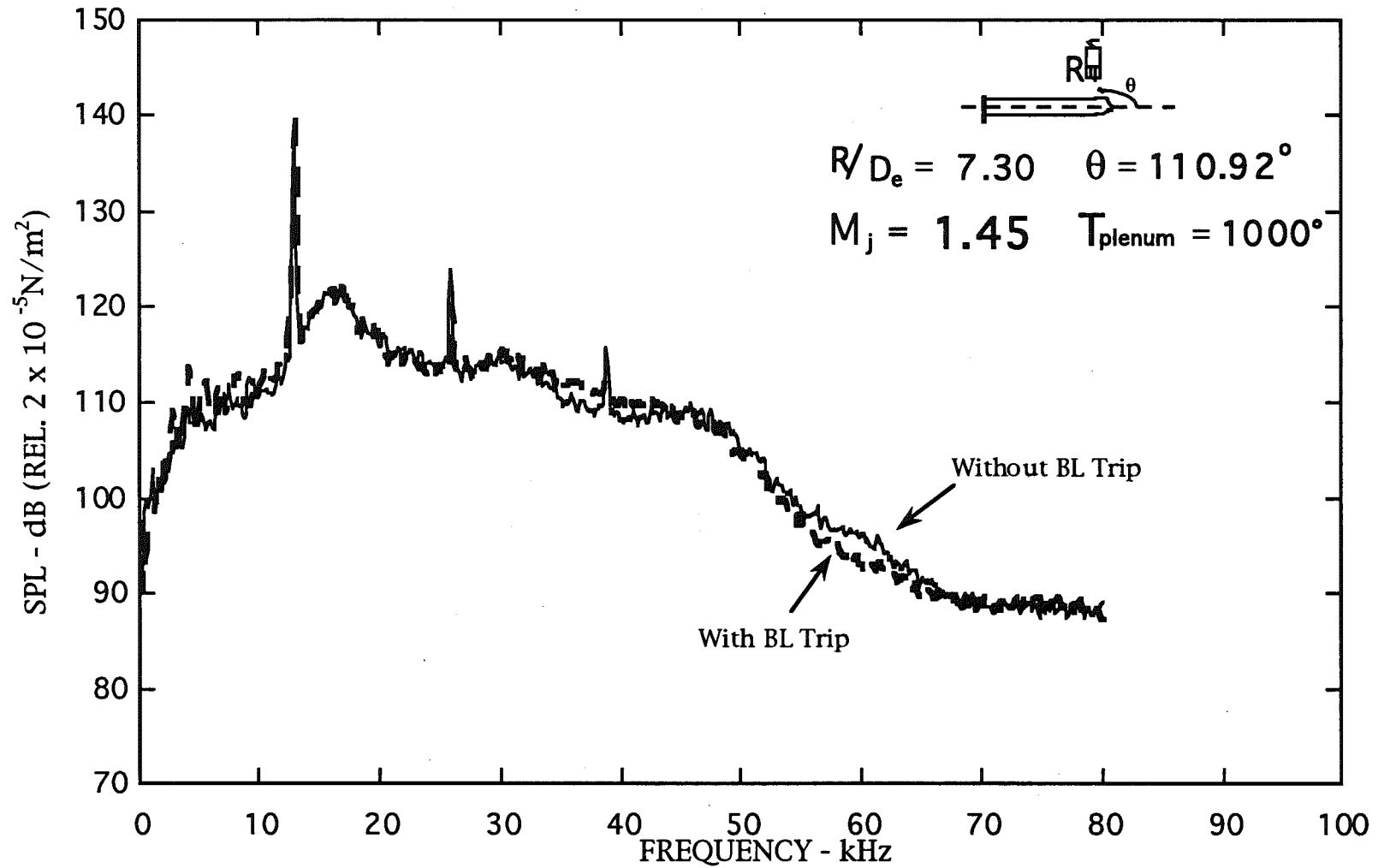
Figure 3.2. Narrow band ($\Delta f = 128$ Hz) noise spectra of the free jet, $M_j = 1.45$.

The figure shows SPL - dB (REL. 2×10^{-5} N/m^2) on the vertical axis versus FREQUENCY - kHz on the horizontal axis.

$R/D_e = 7.30 \qquad \theta = 110.92°$

$M_j = 1.45 \qquad T_{plenum} = 1000°$

Without BL Trip

With BL Trip

Figure 3.3. Narrow band (Δf = 128 Hz) noise spectra of the free jet, M_j = 0.81.

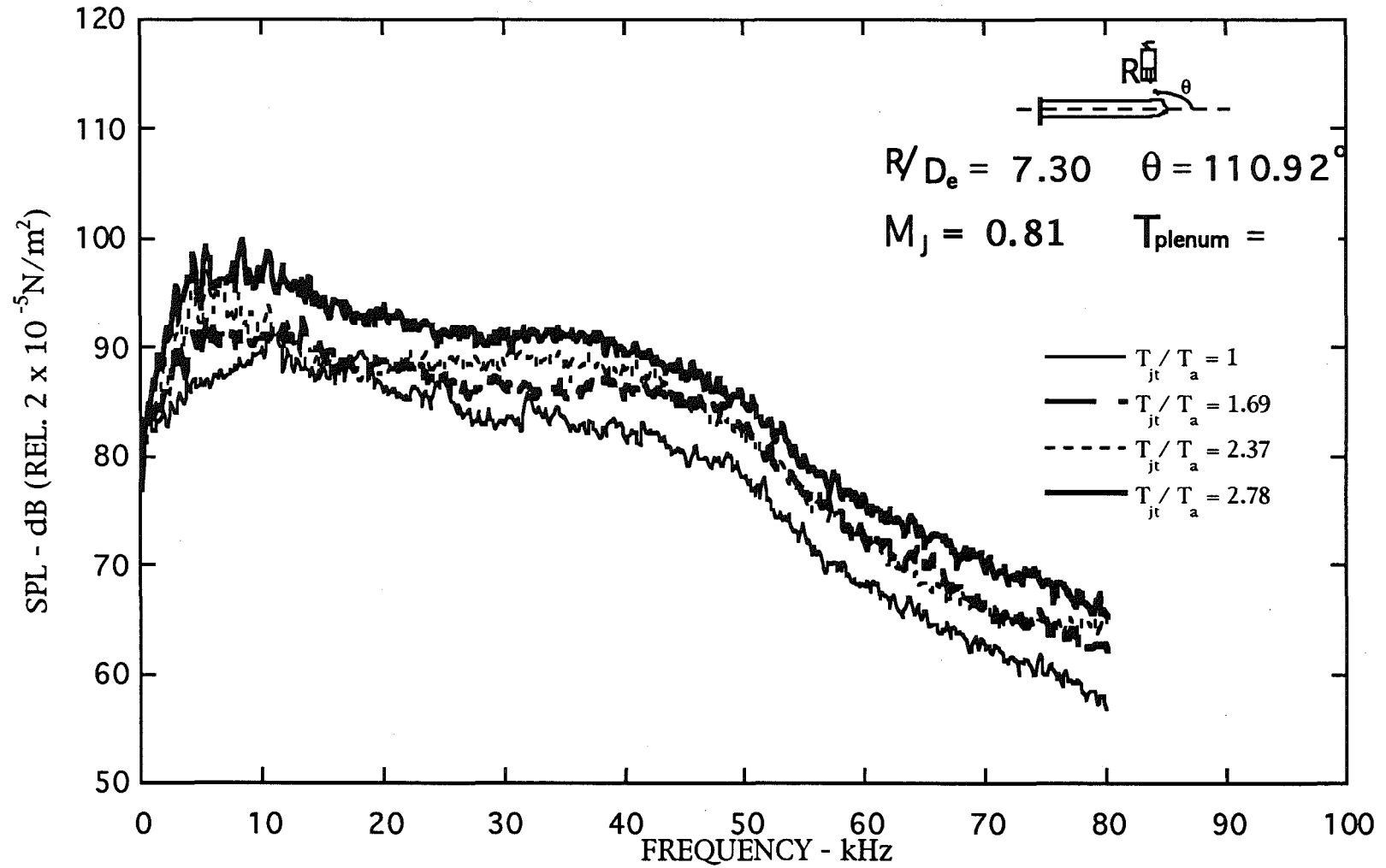number, the jet velocity increases with increasing temperature ratio. Since the mixing noise is a function of the jet velocity, one would expect an increase in mixing noise with increasing velocity. This trend is clearly seen in Fig. 3.3. Increasing the temperature ratio from 1 to 2.87 (plenum temperature = 54°F to 1,000°F) results in an increase of approximately 10 dB below 10 kHz and roughly 5-7 dB at higher frequencies.

3.2.2 Supersonic Case

The effect of temperature is best seen by comparing the spectra of the 1-in.-diam nozzle at M_j = 1.2 at three temperature ratios, 0.99, 2.24, and 2.76 as shown in Figs. 3.4a -c, respectively. Two effects are quite obvious. First, for each Mach number, the frequencies change with increasing temperature. Second, the amplitude has a tendency of decreasing with increasing temperature. Because of a multiplicity of screech tones at this Mach number, it is difficult to establish if the screech frequency increases or decreases with jet temperature. After a careful examination of all spectra, for other Mach numbers and jet exit diameters, it became clear that the screech frequencies actually increased with increasing jet diameter. This is discussed below in relation to the spectra for the 0.48-in.-diam nozzle.

Typical spectra for the 0.48-in.-diam nozzle are shown in Figs. 3.5 - 3.7 for three fully expanded jet Mach numbers, namely 1.12, 1.34, and 1.56, respectively. In each figure, data for four temperature ratios, 1, 1.69, 2.37, and 2.78, are presented. These temperature ratios correspond to plenum temperatures of ambient, 400, 750, and 1,000°F, respectively. Here it is found that for a Mach number of 1.12, the screech frequencies increase from 19.1 to 22.2 to 23.9 to 24.8 kHz on increasing the temperature ratio from 1 to 1.69 to 2.37 to 2.78, respectively. Similarly, for a Mach number of 1.56, these frequencies are 9.3, 10.8, and 11.2 kHz for temperature ratios of 1, 2.37, and 2.78, respectively.

Also note that the amplitude of screech decreases with increasing temperature only at the lower jet Mach numbers up to 1.2; at the higher Mach numbers, it is difficult to draw firm conclusions. At Mj = 1.56, temperature has no effect on the amplitude of the fundamental screech tone.

3.3 COMPARISON WITH THEORY

It is well known that the screech tones in shock-containing supersonic jets are generated by a feedback loop. The loop consists of three main components. They are the downstream propagating instability wave, the shock cell structure in the jet plume, and the feedback acoustic waves immediately outside the jet. Figure 3.8 shows a schematic of the screech tone feedback loop. An instability wave of the jet is generated by acoustic disturbances near the nozzle exit where the mixing layer is thin and is most receptive to excitation. The instability wave grows as it propagates downstream by extracting energy from the mean flow of the jet. At a distance of about four to five shock cells downstream, the instability wave, having acquired large enough amplitude, interacts strongly with the shock cell structure inside the jet plume. The unsteady interaction results in the emission of intense acoustic waves, part of which propagate upstream outside the jet. Upon reaching the jet nozzle exit, the acoustic disturbances excite the shear layer of the jet, thus generating a new instability wave. In this way the feedback loop is completed.
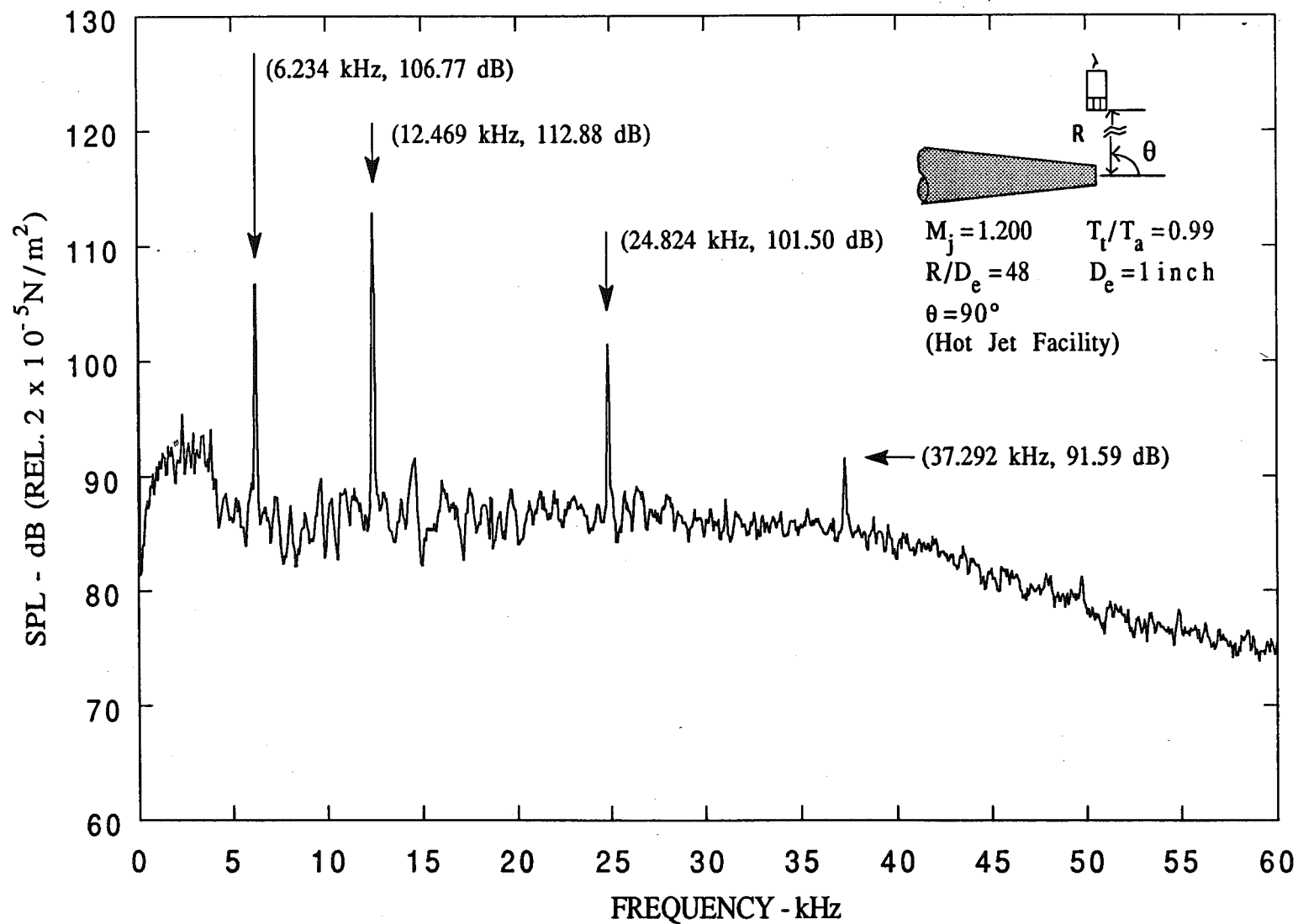
a. $\Delta f = 62.5$ Hz, $M_j = 1.200$, $T_t/T_a = 0.99$

Figure 3.4. Narrow band spectra.
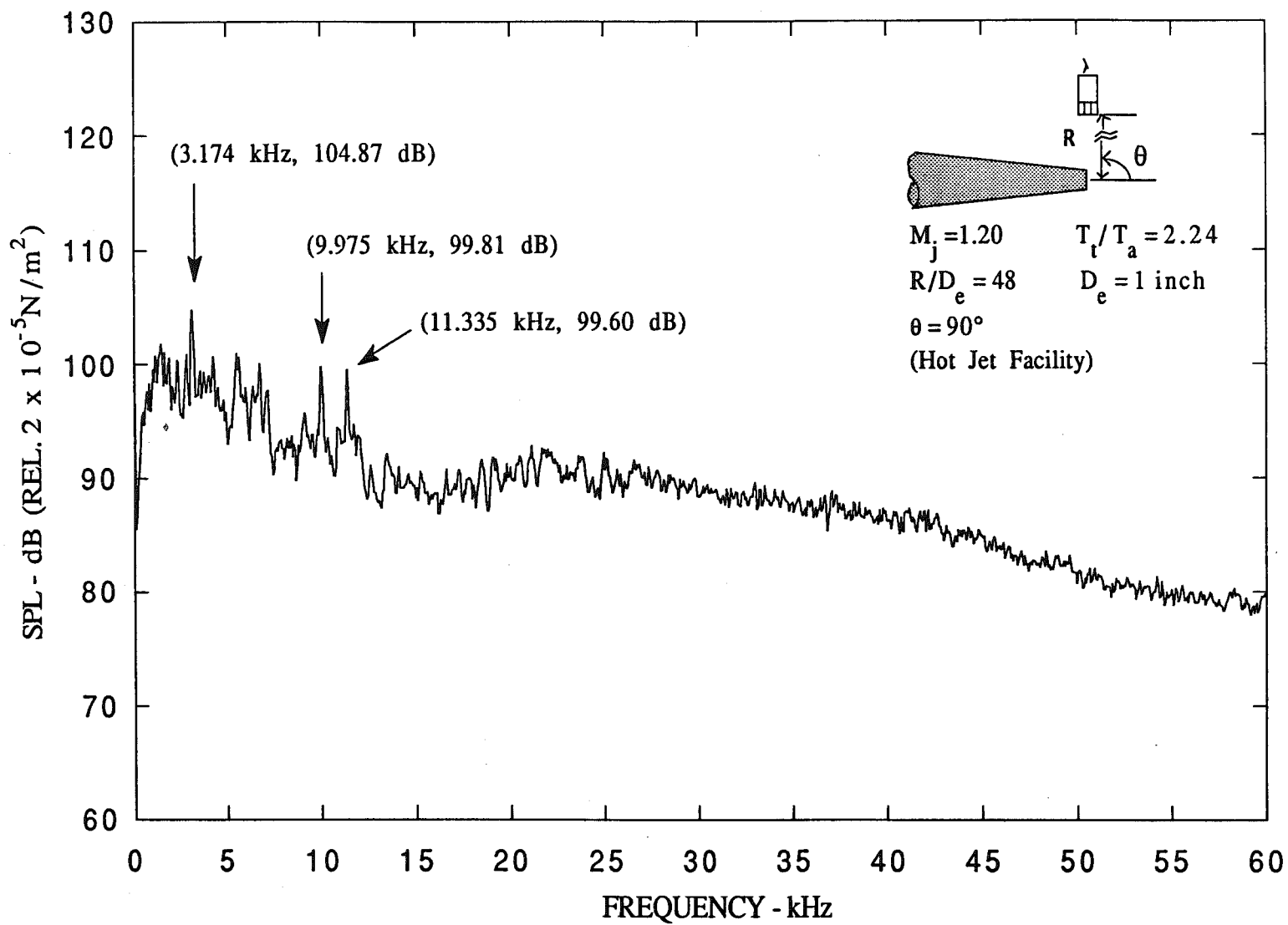
b. $\Delta f = 62.5$ Hz, $M_j = 1.200$, $T_t/T_a = 2.24$
Figure 3.4. Continued.
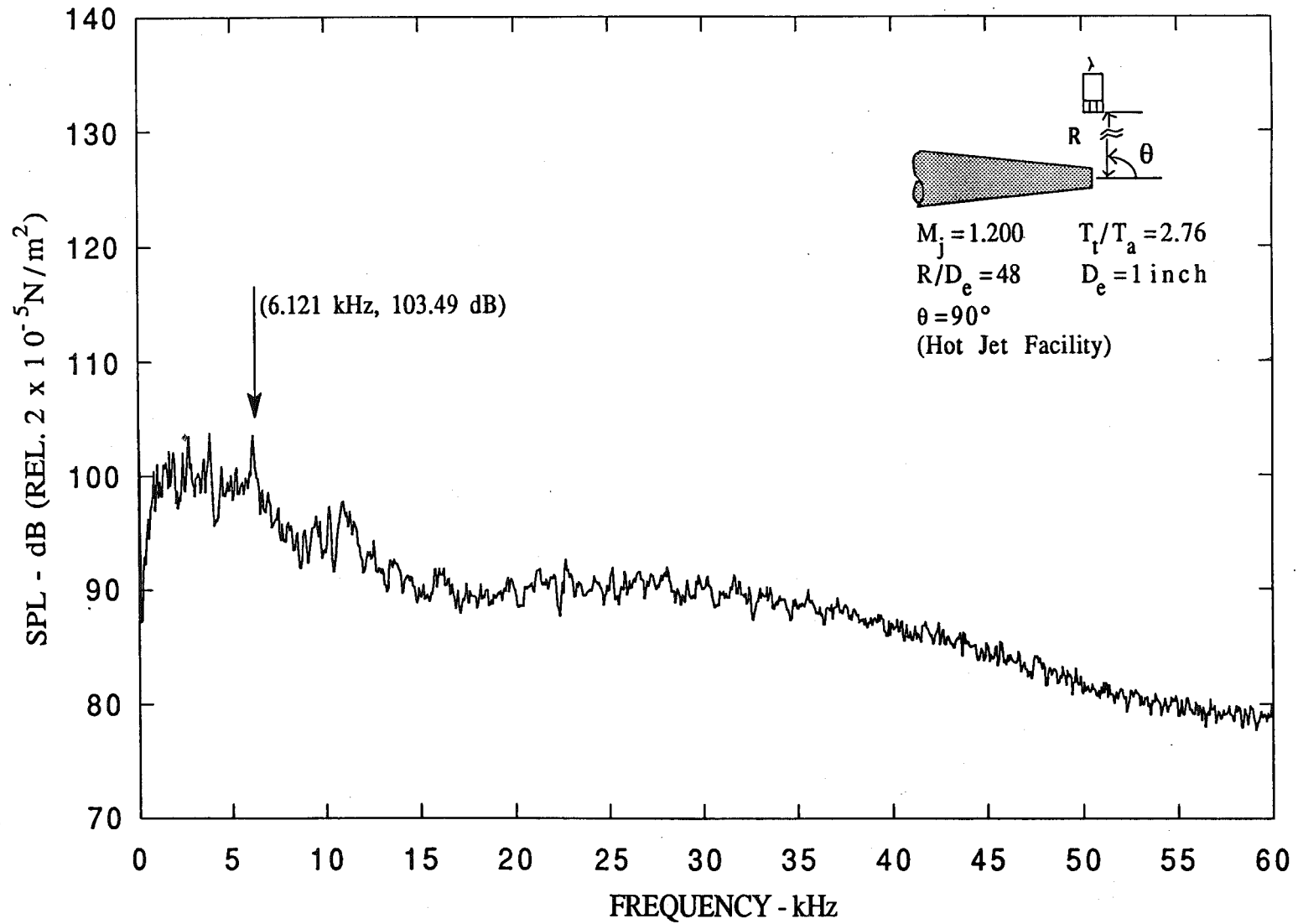
c. $\Delta f = 62.5$ Hz, $M_j = 1.200$, $T_t/T_a = 2.76$

Figure 3.4. Concluded.

The figure is a noise spectra plot. The y-axis is labeled "SPL - dB (REL. 2 x 10^{-5} N/m^2)" ranging from 70 to 140. The x-axis is labeled "FREQUENCY - kHz" ranging from 0 to 100.

Parameters shown on the figure:

$R/D_e = 7.30$ $\theta = 110.92^{\circ}$

$M_j = 1.12$ $T_{plenum} =$

Legend:
- $T_{jt}/T_a = 1$
- $T_{jt}/T_a = 1.69$
- $T_{jt}/T_a = 2.37$
- $T_{jt}/T_a = 2.81$

Figure 3.5. Narrow band ($\Delta f = 128$ Hz) noise spectra of round nozzle, $M_j = 1.12$.
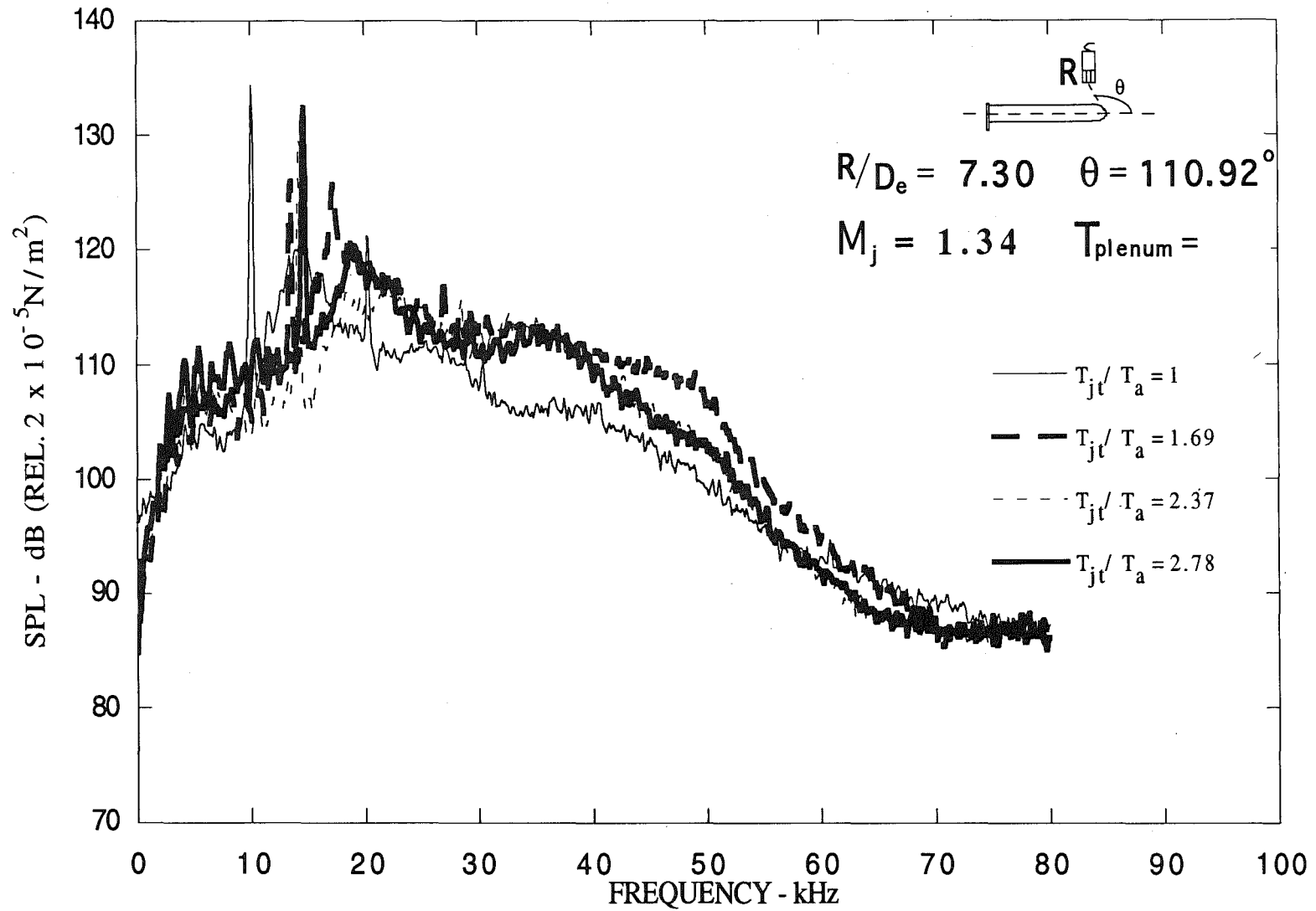
Figure 3.6. Narrow band (Δf = 128 Hz) noise spectra of round nozzle, M_j = 1.34.
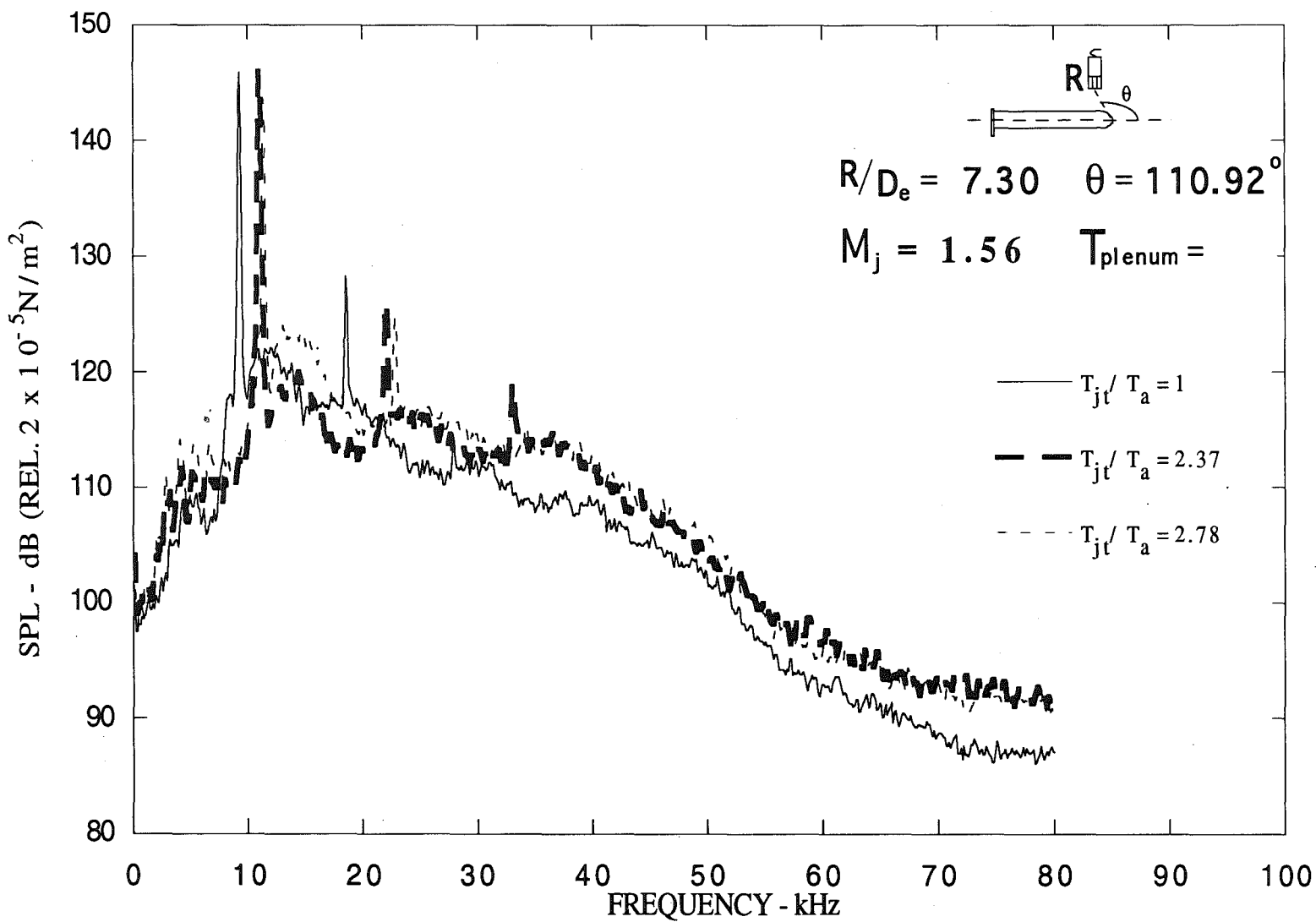
Figure 3.7. Narrow band (Δf = 128 Hz) noise spectra of round nozzle, M_j = 1.56.
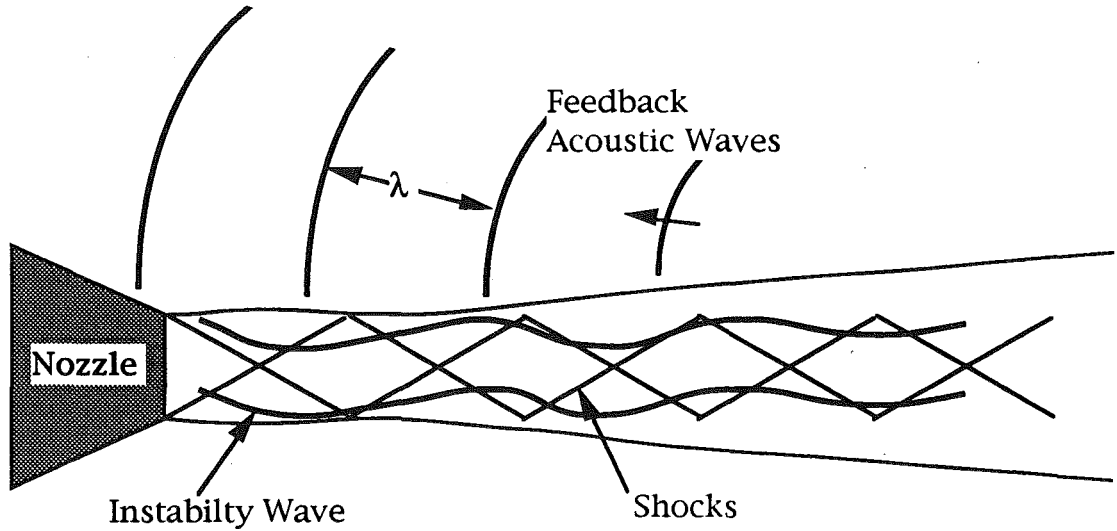
Figure 3.8. Jet screech feedback loop.

Each of the three components of the feedback loop alluded to above plays a different but essential role in the maintenance of the feedback loop. Tam, Seiner, and Yu (Ref. 3.4) examined the feedback loop and suggested that feedback acoustic waves were the "weakest link" of the loop. As in the case of the broadband shock-associated jet noise, the principal direction of the feedback acoustic waves is related to its frequency. In order that enough acoustic waves reach the nozzle lip to maintain the feedback loop, the principal direction must be in the 180-deg upstream direction. By imposing this upstream radiation condition, Tam, Seiner, and Yu derived the following screech tone frequency formula

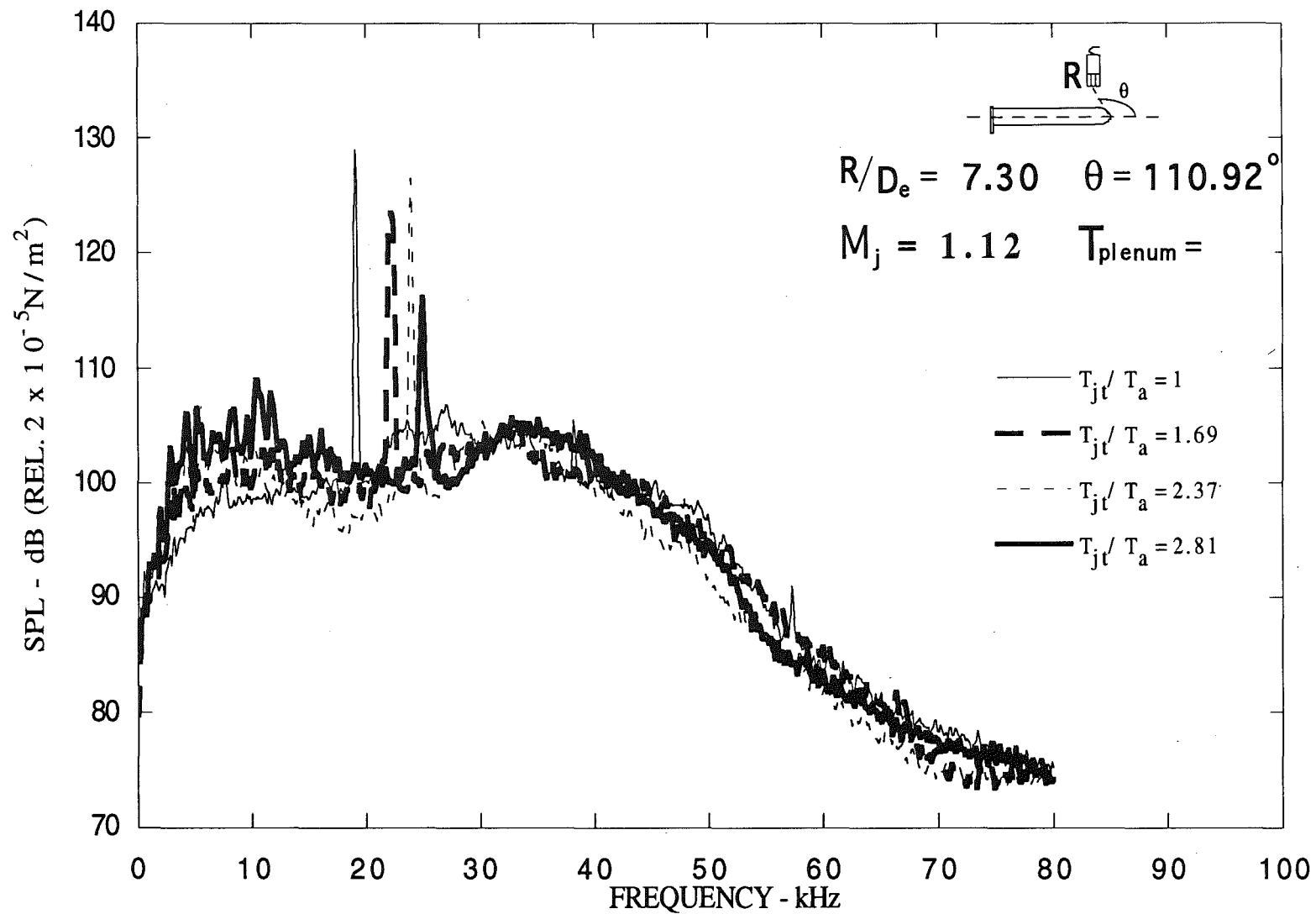$$\frac{fD_j}{U_j} = 0.67 \frac{1}{\sqrt{M_j^2 - 1}} \left[1 + 0.7 M_j \cdot \left(1 + \frac{\Upsilon - 1}{2} M_j^2 \right)^{\frac{1}{2}} \sqrt{\frac{T_r}{T_a}} \right]^{-1} \tag{1}$$

where f is the frequency, D_j is the effective jet diameter, U_j is the jet velocity, M_j is the fully expanded jet Mach number, T_R is the reservoir temperature, and Ta is the temperature of the medium into which the jet expands.

Here D_j, the fully expanded jet diameter, is related to the nozzle exit diameter, D, and the nozzle design Mach number, Md, by the following relation (Ref. 3.5).

$$\frac{D_j}{U} = \left[\frac{1 + \frac{\Upsilon - 1}{2} M_j^2}{1 + \frac{\Upsilon - 1}{2} M_d^2} \right]^{\frac{\Upsilon + 1}{4(\Upsilon - 1)}} \sqrt{\frac{M_d}{M_j}} \tag{2}$$

Equation (1) is valid for both hot and cold jets. A quick inspection of this equation indicates that the normalized screech frequency (i.e., fD_j/U_j) decreases with increasing jet Mach number and temperature ratio. Note, however, that the absolute screech frequency actually increases with increasing temperature for a fixed Mach number. This is because although the jet velocity increases as $T_j^{1/2}$, the decrease in Strouhal number is faster than $T_j^{-1/2}$.

The measured screech frequencies for the free jet are compared here with the predicted frequency for jet total temperatures of 60, 400, 750, and 1,000°F using Tam's formulation (Ref. 3.1). Only limited data were available for the 400°F temperature, while for all other temperatures, the frequencies were measured both for the 0.484-in. nozzle and for a 1-in. nozzle. Data obtained from previous tests for the unheated conditions (Ref. 3.6) using the 0.484-in. nozzle are also included.

The screech Strouhal numbers, fD_j/U_j, corresponding to the measured data for four temperature ratios are compared with the predicted values in Fig. 3.9. Data for each temperature are compared separately in Figs. 3.10 - 3.13.

As is seen in Fig. 3.9, the experimental data follow the predicted trend quite well. The screech Strouhal number for a given Mach number decreases as the jet total temperature ratio increases. For all conditions, the measured screech frequencies match the predicted frequencies closely at all Mach numbers except in the range $M_j = 1.2 - 1.35$. In this range of Mach numbers, the predicted values of screech Strouhal numbers are higher than those measured. This is particularly clear for the results for the unheated condition shown in Fig. 3.10 for which a large number of data points were available in the range $M_j = 1.2 - 1.4$. Recall (Ref. 3.6) that it is between $M_j = 1.2$ and 1.35 that the instabilities switch from axisymmetric to helical or flapping mode. The discrepancy observed between the measurements and prediction by Tam's theory may be due to the jet switching modes in this region for which the assumptions of a constant convection Mach number in Tam's theory for the feedback frequency may not be valid.

Comparison of Tam's theory with other researchers' data was also performed, as was the relationship between the screech tones and the growth rate of instabilities as a function of jet temperature. These were discussed in a recent AIAA paper by the authors (Ref. 3.7).

3.4 CONCLUDING REMARKS

Although the main objective of the present program was to study the ducted jets, it was important to ensure that our understanding of the free jet was correct. As shown here, the free jet appears to be well-behaved. Our data are credible and it is safe to conclude that the effect of temperature is to reduce the peak Strouhal number of the screech frequency and the absolute frequency actually increases with temperature. Clearly, this implies that if for unheated conditions, the duct resonance tones did not match with the screech tones, it is possible for them to match the screech frequencies at heated conditions which can result in very high amplitude discrete tones.
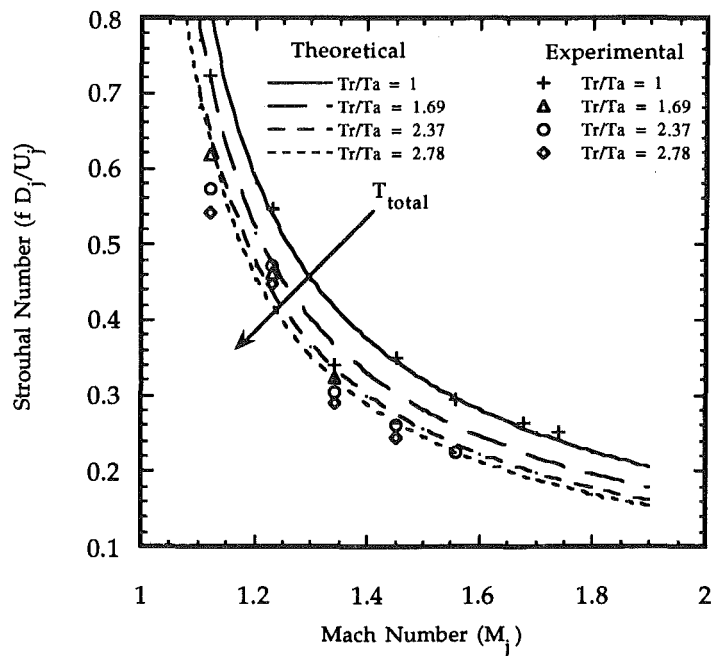
Figure 3.9. Strouhal number as a function of Mach number and temperature ratio. (Lines: Prediction; Symbols: Measurements.)
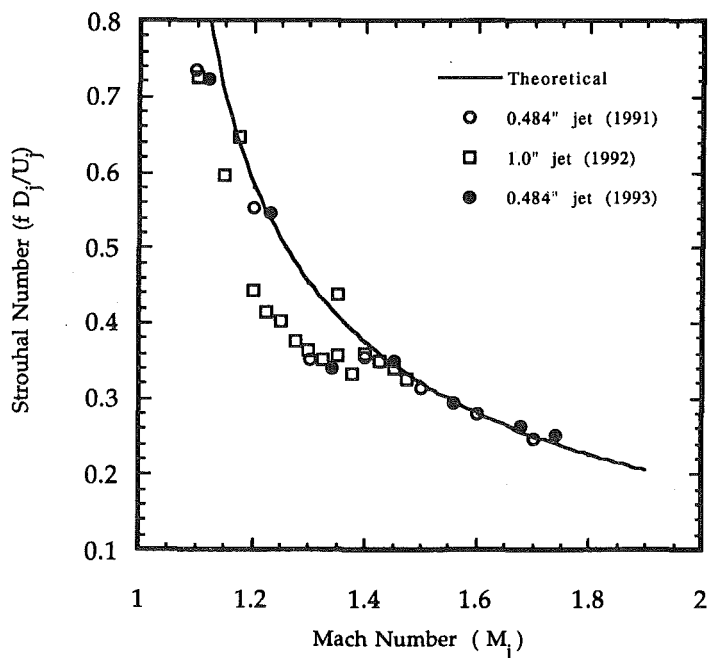

Figure 3.10. Strouhal number as a function of Mach number for temperature ratio of 1.
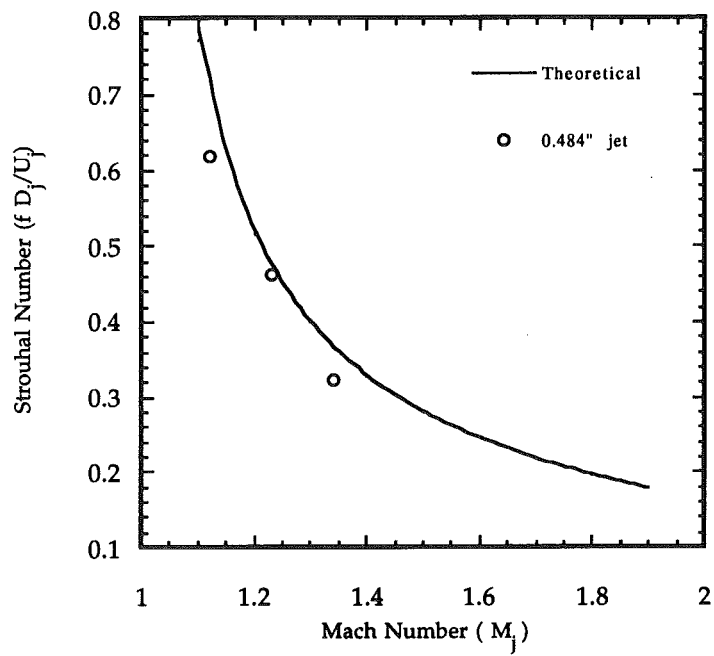
Figure 3.11. Strouhal number as a function of Mach number for temperature ratio of 1.69.
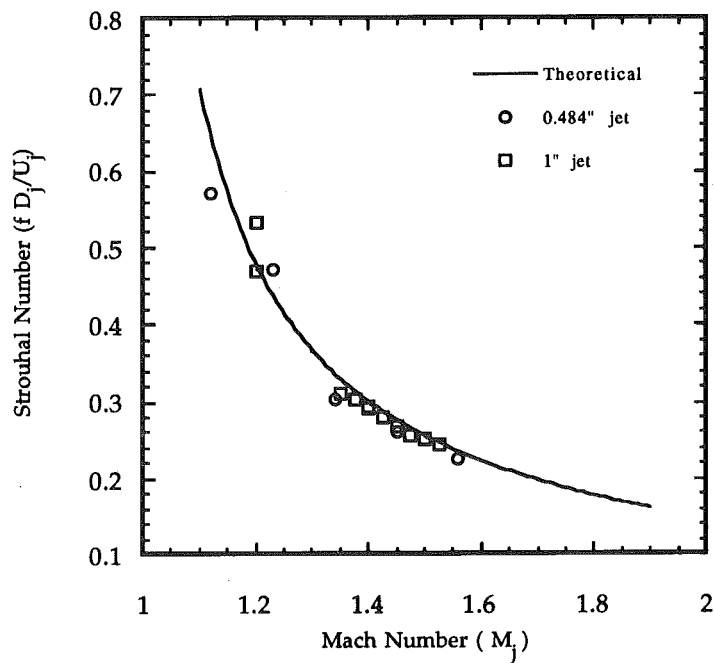

Figure 3.12. Strouhal number as a function of Mach number for temperature ratio of 2.37.
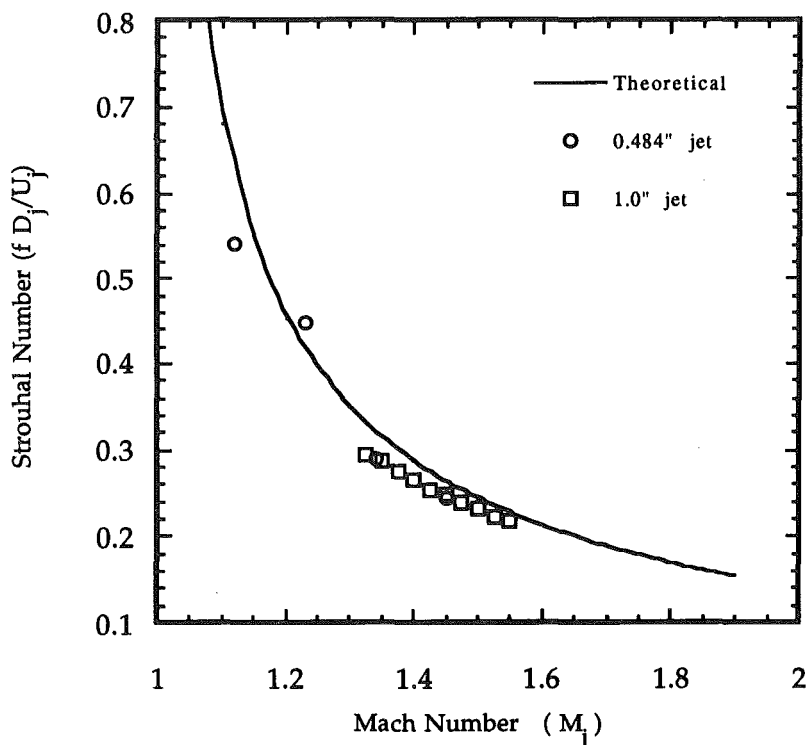
Figure 3.13. Strouhal number as a function of Mach number for temperature ratio of 2.78.

4.0 DUCTED JET RESULTS

4.1 SUMMARY OF PREVIOUS RESULTS

In the Phase 1 study (Ref. 4.1), an experimental and theoretical study was carried out to understand the aeroacoustics of the jet/diffuser flows. Model cold-jet experiments with an axisymmetric convergent nozzle were performed in a test setup that simulated a supersonic jet exhausting into a cylindrical diffuser. The measured data consisted of detailed flow visualization data and acoustic spectra for a free and a ducted plume. Theoretical calculations were also performed. It was shown that duct resonance is most likely responsible for the low-frequency, high-intensity whistles experienced in the AEDC full-scale facilities, and the higher frequencies are related to the screech phenomenon.

While we were able to replicate the frequencies, scaled appropriately for the model scale test configuration, we were unable to reproduce the high amplitudes (as high as 170 dB) experienced in the full-scale facilities. To establish if this could have been a result of the small scale of the model, a 25 times larger scale test setup was built and tested in NASA Lewis Research Center altitude test cell PSL-3. These measurements were also made only for cold flow simulations and are described in Ref. 4.2. In these measurements also, we were able to replicate a

duct resonance frequency which linearly scaled with the geometry of the full-scale facility and the 1/48th-scale GTRI facility alluded to above. Unfortunately, similar to the cold-flow measurements of the GTRI subscale facility, these measurements also failed to reproduce the high amplitudes experienced in the full-scale facilities.

It was established from these measurements that the scale of the test facility was not responsible for the reduced levels. Since the high-amplitude whistles in the full-scale facilities were obtained for higher jet temperatures, it was speculated that the amplitude of the duct resonance for our test geometry may increase for certain operating conditions if the plume is operated at higher temperatures. This is because growth rates of the instability waves in a jet are expected to be different at different temperatures (Ref. 4.3). Their most preferred frequencies are expected to change with temperature and if this most preferred frequency of the jet instability at a given operating condition matches a duct resonance frequency for our model scale facility, high amplitudes are likely to result.

It is to understand this effect of temperature on the flow/acoustic interactions between the altitude test facility and a jet engine plume that the study described in the present report was initiated.

4.2 PREPARATORY TESTS

Before acquiring the detailed acoustic data for the ducted configuration, a number of preparatory tests had to be performed to obtain confidence in our data. These are described briefly below.

4.2.1 Effect of Venting Air

Because of the small size of the test nozzle (D = 0.48 in.), the mass flow rate was inadequate for the burner to operate stably for the duration of the test. To keep the burner lit during a given test, therefore, we increased the mass flow rate through the burner and before exhausting through the test nozzle we let an appropriate amount of air vent out to the atmosphere. This air was vented away from the experimental setup through a 4-in.- diam pipe which is shown in Fig. 4.1. Unfortunately, due to the high temperature and pressure in the burner, this vented air was at a fairly high velocity and was extremely loud. To ensure that the noise created by venting this air did not affect our data, several acoustic measurements were made at the in-duct microphone location, once with and then without the vent in operation. As is seen in Figs.4.2 and 4.3, the noise created by venting this air had insignificant effect on the acoustic data over the majority of the spectral range.
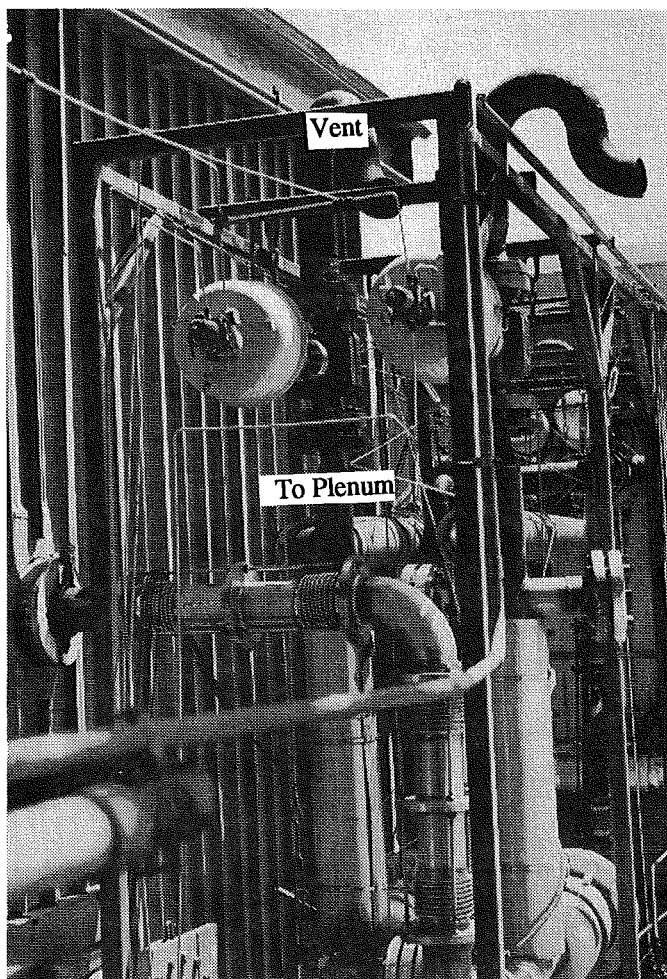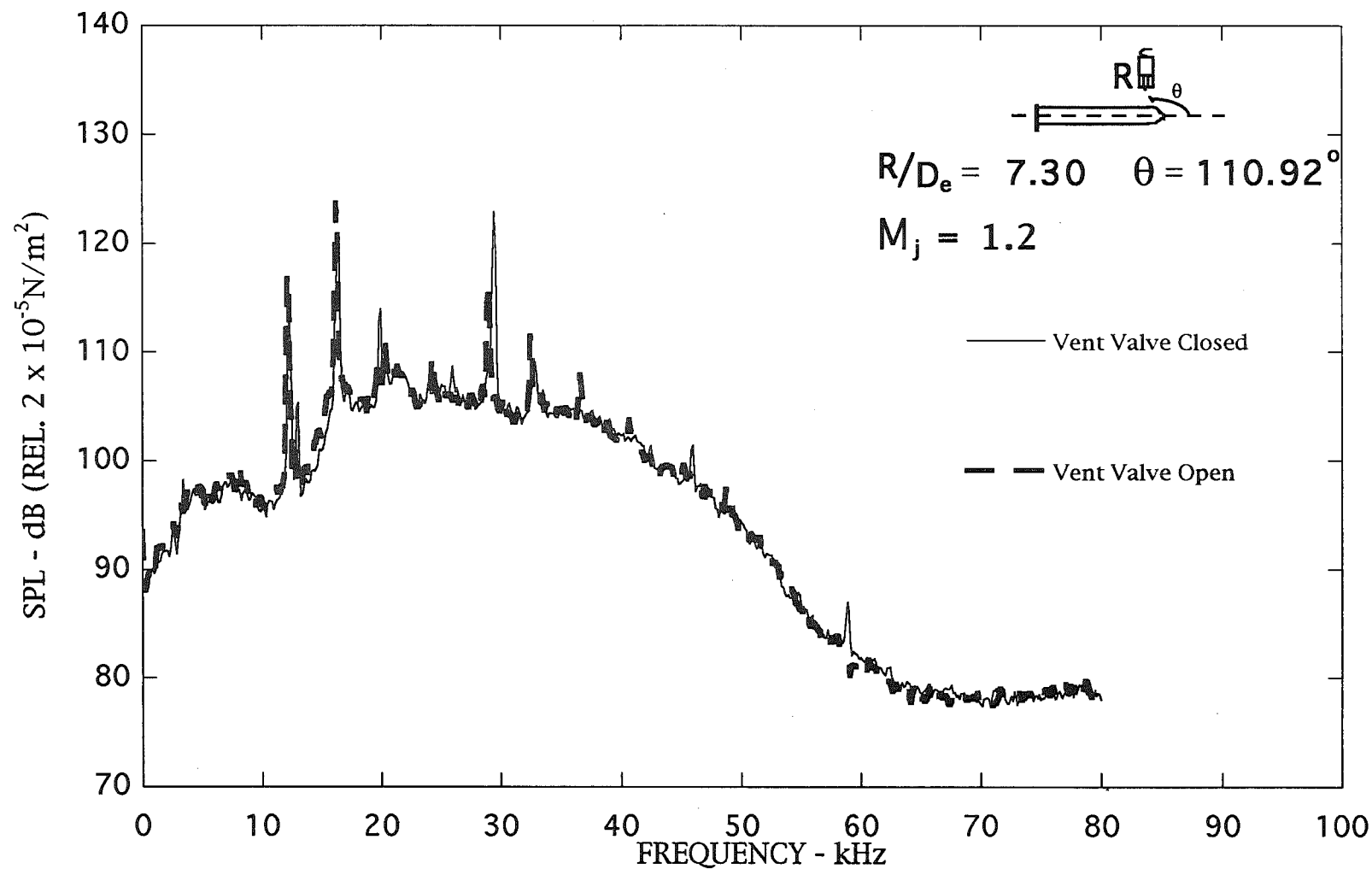
Figure 4.1. Vent outside of Hot Jet Facility.

Figure 4.2. Narrow band (Δf = 128 Hz) noise spectra of round nozzle (cold flow), M_j = 1.2.
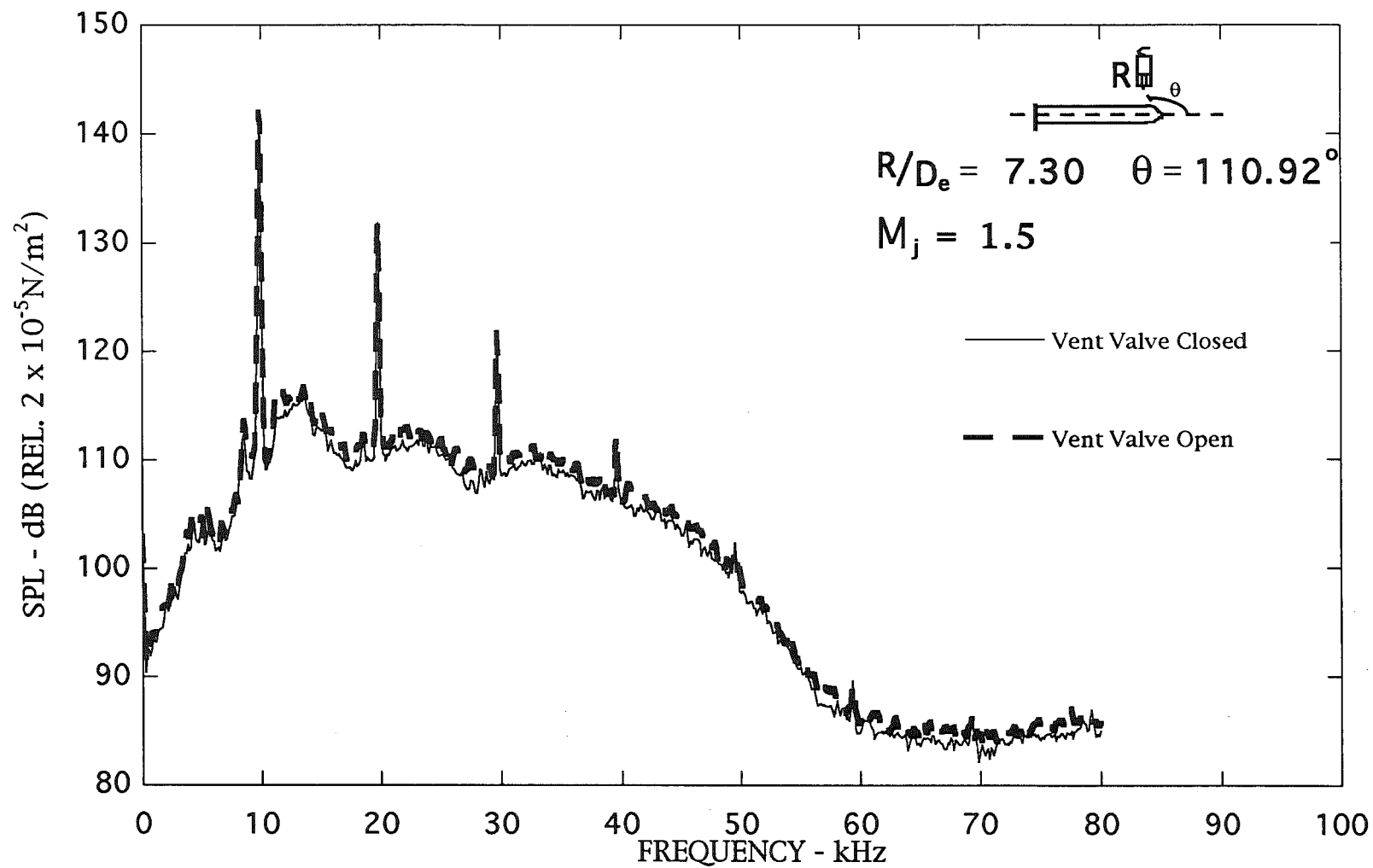
Figure 4.3. Narrow band (Δf = 128 Hz) noise spectra of round nozzle (cold flow), M_j = 1.5.

4.2.2 Microphone Temperature Tests

For the ducted conditions, the microphone was mounted flush with the wall of the test cell. For the heated conditions, this meant that the microphone was exposed to potentially high temperatures. According to the B&K specifications on 4136 microphones, their sensitivity starts to change at temperatures greater than 100°C (or 212°F). Since the wall temperature had been measured to be as high as 200°F (See Fig. 4.5), several tests were done to ensure that the microphone was working properly, even though attempts were made before the test began to shield the microphone from heat transfer from the wall. Temperature measurements were made at three locations: (1) on the test cell wall (2) at a typical interior location of the test cell, and (3) at a representative location just upstream of the diffuser exit. These three locations are shown schematically in Figs.4.4a-c, respectively.

It was found that the temperature in the test cell decreased dramatically as the secondary mass flow rate increased (See Fig. 4.6) and vice versa (See Fig. 4.7). With the secondary manifold fully open (i.e., with the venturi removed), the highest test cell temperature was about 100°F at all jet Mach numbers (See Fig. 4.6). The highest ejector temperature in this case was about 525°F for a reservoir temperature of 1,000°F. These values were significantly higher when the venturi was added, as shown in Fig. 4.7 by arrows.

The most crucial temperature for the microphone occurred when the jet was the hottest and the mass flow rate was the lowest. For the tests presented here, this condition occurred when the jet was at 1,000°F and the venturi described earlier was used to control the secondary mass flow rate. Since the secondary air was entrained by the pumping effect of the ejector, the addition of the venturi decreased the effective area of the air entrainment through the secondary air manifold and hence contributed to an increase in the test cell temperature.

Recall from Section 4.1 that a wooden sheath was used to protect the microphone from heat. We believe that our microphone's performance remained unchanged because of this wooden sheath and because it was flush mounted and as shown in Fig. 4.5, the wall temperature barely exceeds 200°F for most tests. The jet was operated at 1,000°F with the venturi removed, and then with the venturi in place. In addition, several acoustic spectra were acquired as a function of time during which the temperature in the test cell increased gradually. The temperature rose rapidly during the first 30 sec and then gradually achieved a steady value of 400°F as shown in Fig. 4.8. The test cell wall temperature still never exceeded 200°F. The microphone's performance remained unchanged as the same spectra could be measured in many of repeat runs for both the unheated and heated operating conditions over a span of some 18 months by the physically same microphone.

4.3 EFFECT OF TEMPERATURE RATIO ON IN-DUCT ACOUSTIC SPECTRA

As mentioned earlier, data at the in-duct microphone were acquired for four reservoir temperature conditions: unheated, 400°, 750°, and 1,000°F. These measurements were first made with a venturi in place, and then with it removed. The presence of the venturi, which had a small-diameter (0.080-in.) throat, restricted the pumping of the secondary mass flow through the secondary manifold and as such the temperature in the test cell which was used to define the jet operating temperature stayed rather high. It was only when the venturi was removed and the 2-
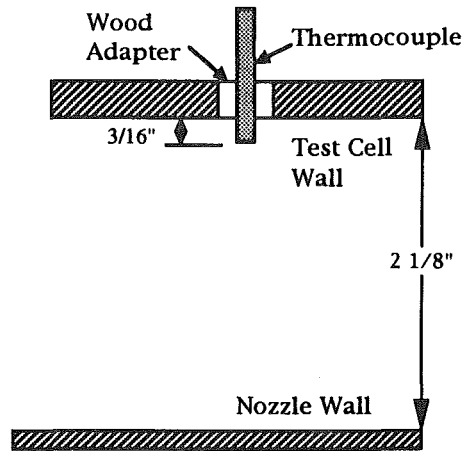
Figure 4.4a. Position of thermocouple relative to test cell wall to measure temperature at microphone location.
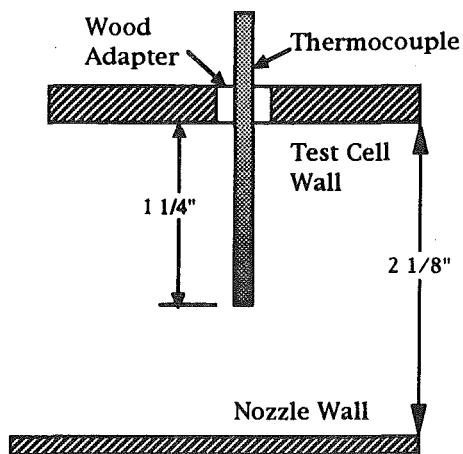

Figure 4.4b. Position of thermocouple relative to test cell wall to measure temperature in the test cell.
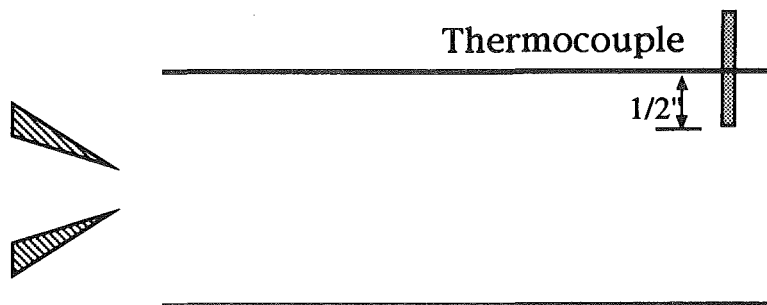

Figure 4.4c. Position of thermocouple relative to test cell wall to measure temperature in diffuser.

in.-diam secondary manifold was allowed to entrain as much air as its operating conditions demanded that the ambient temperature inside the test cell in the vicinity of the jet exit became low enough to be very close to that of the lab air. This provided reasonably high jet total temperature to the test cell temperature ratios.

It will be shown below that changing the ratio of the jet total temperature to the test cell temperature had a significant effect on the noise produced in the ducted configuration. In previous tests conducted at GTRI (Ref. 4.1), it was found that the noise generated was independent of the secondary mass flow for an unheated jet in the far field. It is assumed that the in-duct data are also independent of the secondary flow and any changes observed in the in-duct acoustic signatures are therefore assumed to be due to the changes in the flow temperature.
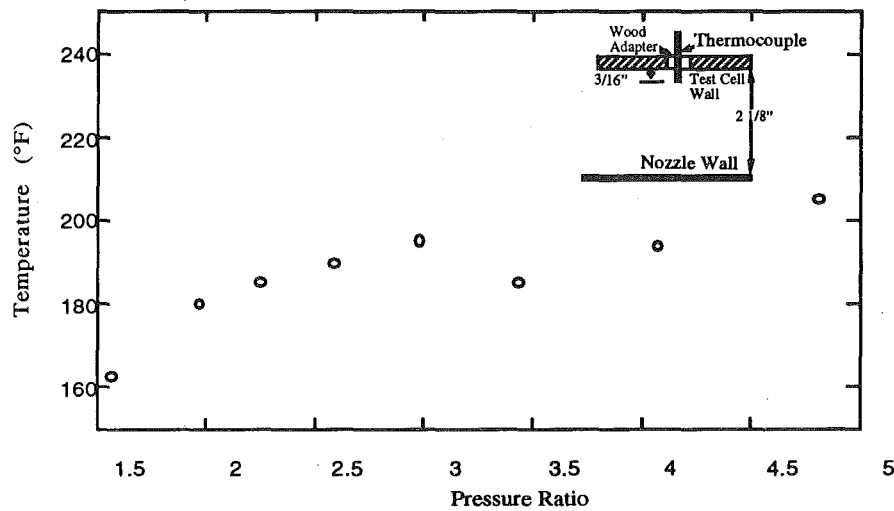

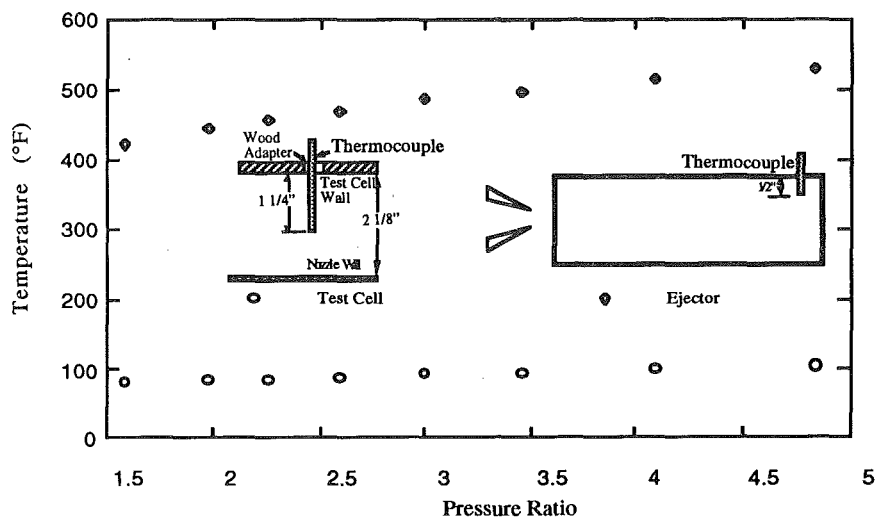**Figure 4.5. Temperature below microphone location with venturi-mounted configuration.**

Figure 4.6. Temperature in test cell and ejector for T_{plenum} = 1,000°F with venturi removed.
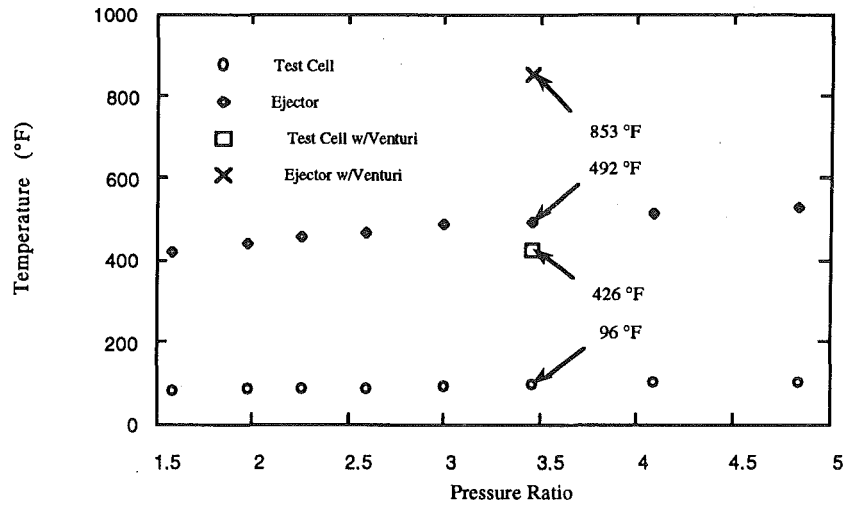
45

Figure 4.7. Temperature in test cell and ejector for plenum temperature of 1,000°F.

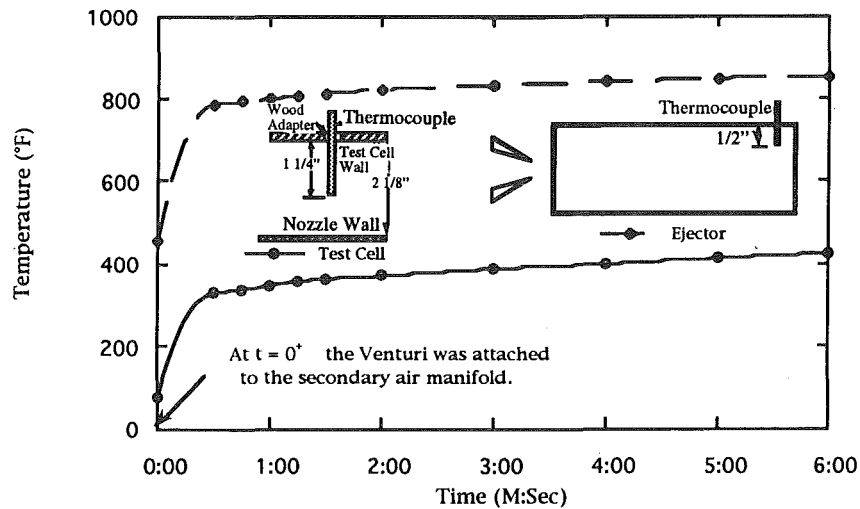**Figure 4.8. Temperature in test cell and ejector for T_{plenum} = 1,000°F and pressure ratio of 3.41 as a function of time after venturi mounted.**

Individual spectra measured at the in-duct microphone locations with the venturi in place are included in Appendix D for various Mach numbers and temperatures. Similar data are then presented in Figs. 4.9 - 4.17 with the venturi removed. In each figure, frequencies of obvious tones have also been labeled. The spectra for three temperatures, namely, 53°, 750°, and 1,000°F are compared for Mach numbers shown below.

46

Figures	Mach Number	T_{plenum} (°F)	$T_{plenum}/T_{ambient}$ (Nominal)	$T_{plenum}/T_{test\ cell}$ (Nominal)
4.9a-d	0.81	53, 400, 750, 1,000	1, 1.69, 2.35, 2.86	1, N/A, 1.83, 1.71
4.10a-d	1.02	53, 400, 750, 1,000	1, 1.69, 2.35, 2.86	1, 1.27, 1.64, 1.69
4.11a- d	1.12	53, 400, 750, 1,000	1, 1.69, 2.35, 2.86	1, 1.24, 1.61, 1.67
4.12a-d	1.23	53, 400, 750, 1,000	1, 1.69, 2.35, 2.86	1, N/A, 1.55, 1.61
4.13a-d	1.34	53, 400, 750, 1,000	1, 1.69, 2.35, 2.86	1, N/A, 1.52, 1.61
4.14a-c	1.45	53, 750, 1,000	1, 2.35, 2.86	1, 1.48, 1.60
4.15 a, b	1.56	53, 1,000	1, 2.86	1, 1.56
4.16 a, b	1.68	53, 1,000	1, 2.86	1, 1.55
4.17	1.74	53	1	1

Note that although our primary interest was to examine the spectra for the supersonic Mach numbers, we have also included data for a subsonic Mach number, namely, $M_j = 0.8$, so that we can distinguish a duct resonance tone from screech. The spectra for $M_j = 0.8$ indeed show a number of tones in the low-frequency region up to about 15 kHz, which, as discussed below can indeed be identified to match the duct-resonance tones. For the supersonic case, both the duct resonance tones and those clearly identifiable with the screech tones discussed earlier in Section 3 were measured.

It was pointed out in our earlier studies that the duct resonance frequency is a mild function of the flow Mach number. It does, however, change proportional to the square root of the flow static temperature as the duct resonance frequency is directly proportional to speed of sound. To demonstrate that a number of tones observed in our measured spectra are indeed due to the duct resonance, we have plotted various measured tone frequencies as a function of the ejector temperature in Fig. 4.18. In the same figure, we show the calculated resonance frequencies associated with various modes in the ejector. (The equations used to calculate these frequencies are described in Section 4.3.2.) It is clear that the measured tones match very well with those predicted. These tones were measured for all flow conditions for which data were acquired.

We had two sets of data available to us: one set with the venturi connected to the secondary manifold and another without. A close examination of the two sets of data showed that for a fixed operating Mach number, increasing the absolute temperature of the jet air alone has little effect on the amplitudes of the acoustic tones mentioned above. However, if the ratio of the jet total (or the plenum total) temperature and the temperature of the test cell into which the jet exhausts, increased tone levels are observed. In other words, it is the actual operating temperature ratio that is important.

This is best seen in Figs. 4.19 and 4.20 where the in-duct acoustic data acquired with the secondary manifold area restricted by the venturi and then with an open manifold are compared for $M_j = 0.81$ and 1.34, respectively. In each figure, the dotted line curve is for the configuration with the venturi and the full line without. The spectral amplitudes with the venturi in place for which the test cell temperature remained high because of the restricted mass flow rate from the secondary manifold are lower than those for the manifold open. In the latter case, secondary flow cooled the test cell and thus for a given plenum temperature the operating jet temperature

increased with the plenum temperature, the tones as well as the broadband noise of the in-duct spectra increased with increasing temperature. At times new high-level tones surfaced in the measured spectra on heating the jet.

The best example of increased tonal content in the in-duct spectra as a result of increasing the operating temperature ratio is seen in Fig. 4.21. This figure contains data for spectra acquired over a period of 6 min. At the start, the secondary manifold was kept open and the spectrum shown in this line was obtained. With this configuration the secondary mass flow rate was approximately 90 percent that of the primary mass flow rate, and the temperature ratio ($T_{plenum}/T_{test cell}$) was 2.35. The secondary mass flow rate was reduced to only 1.5 percent by adding the venturi. This provided a temperature ratio of 1.48. Spectra acquired 30 sec, 2 min, and 6 min after adding the venturi to the secondary manifold are also shown in Fig. 4.21. Clearly, the tonal content is not as high as for the higher temperature ratio. Even the broadband noise content is lower.

In summary, higher temperature ratio appears to increase the discrete tone levels in the frequency range 3 to 20 kHz, the largest increase taking place at 3.6 kHz. It is shown later that even though the amplitudes measured at the in-duct microphone located upstream of the nozzle exit were not as high as 170 dB, those measured inside the diffuser were close to 165 dB.

One glaring conclusion that can be drawn from these results is that the tones at new frequencies with relatively high amplitudes can surface as the ratio of the jet temperature and that of the surrounding is changed. It thus highlights the importance of the key objective of the present program i.e., the importance of the operating jet temperature ratio in understanding jet/facility acoustic interactions.

The data acquired with the manifold open, where a more realistic temperature ratio has been simulated, have been used in the presentation below.
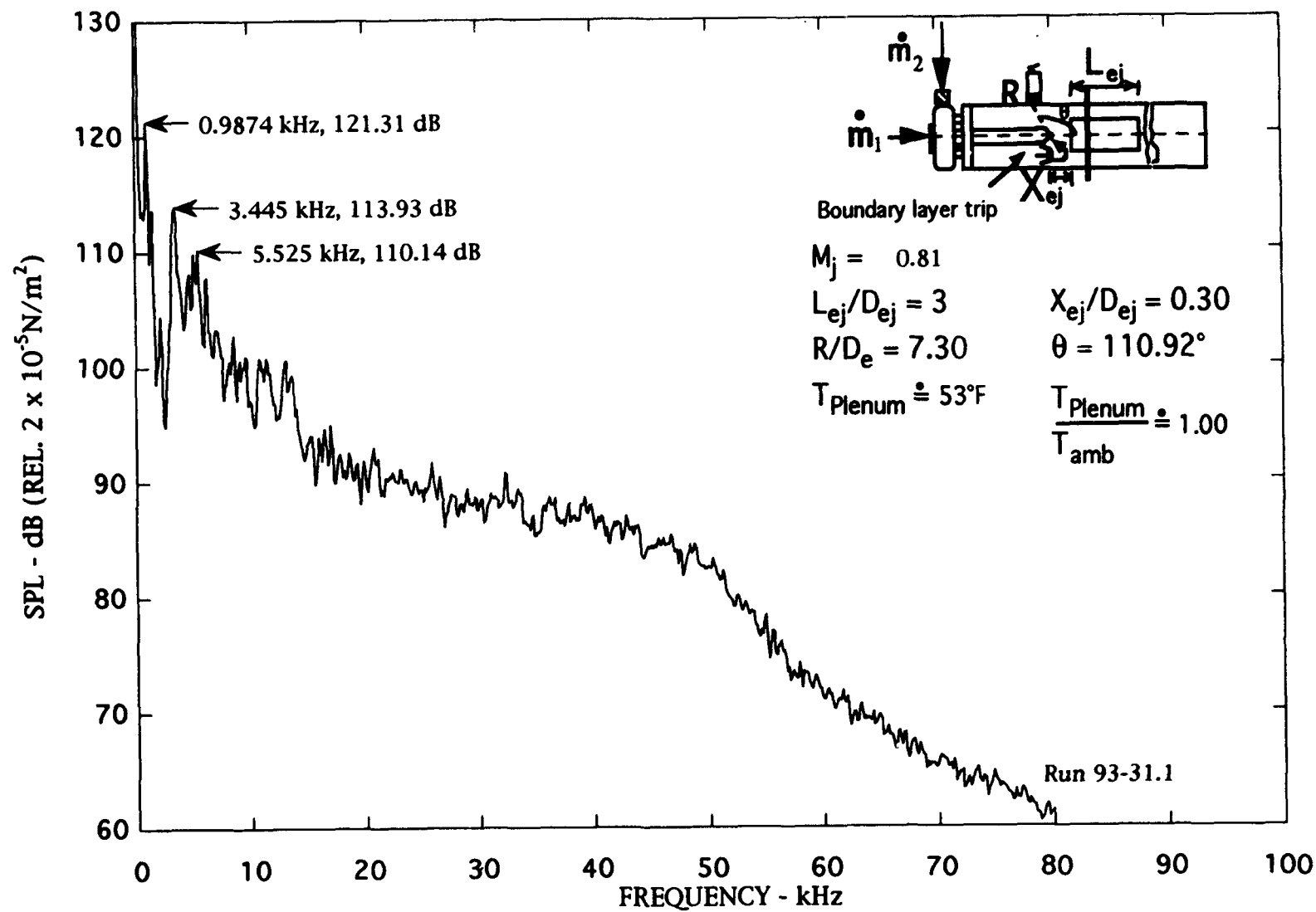
Figure 4.9a. Narrow band ($\Delta f = 128$ Hz) noise spectra of tripped and ducted jet with open manifold, $M_j = 0.81$.
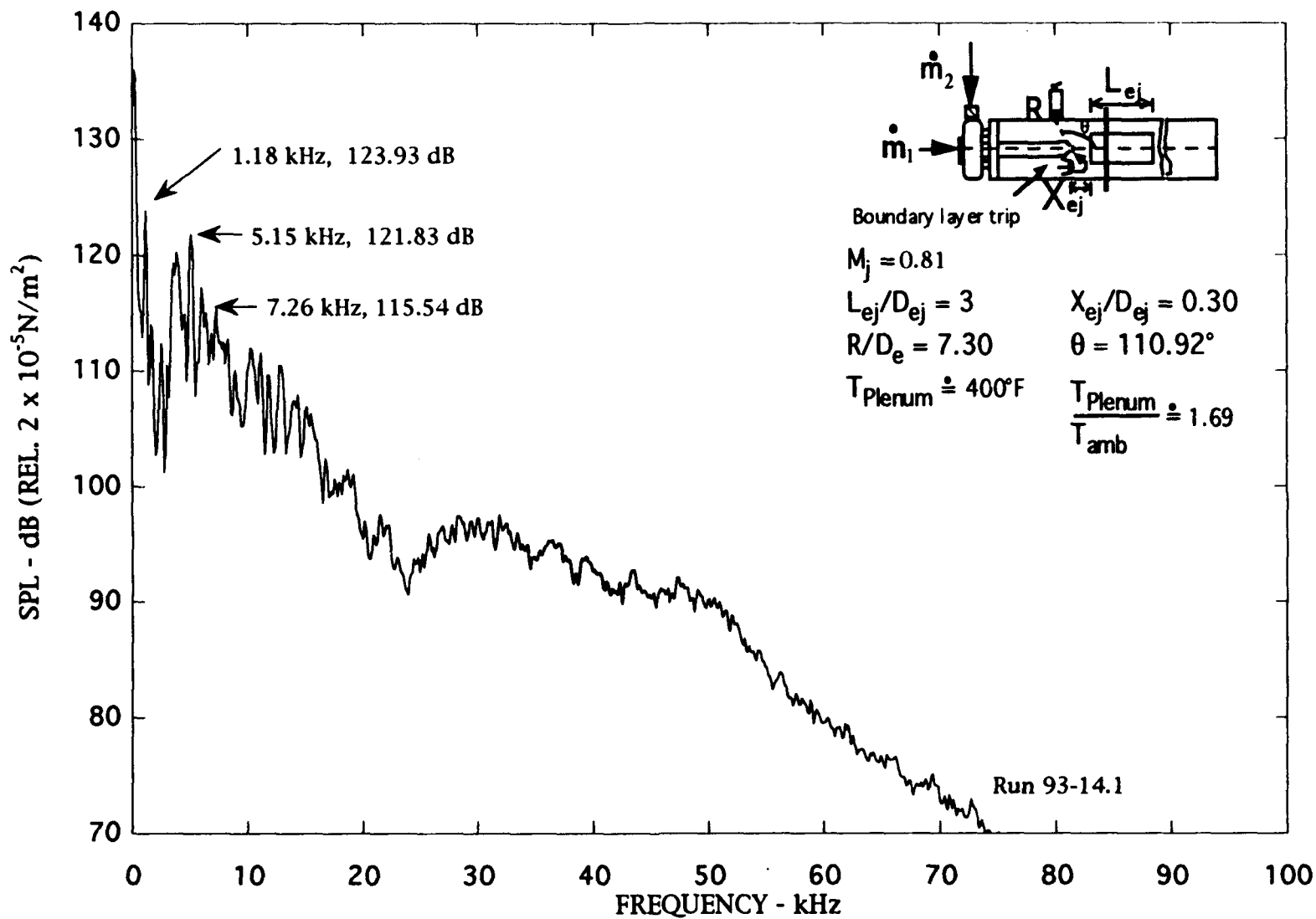
Figure 4.9b. Narrow band ($\Delta f = 128$ Hz) noise spectra of tripped and ducted jet with open manifold, $M_j = 0.81$.

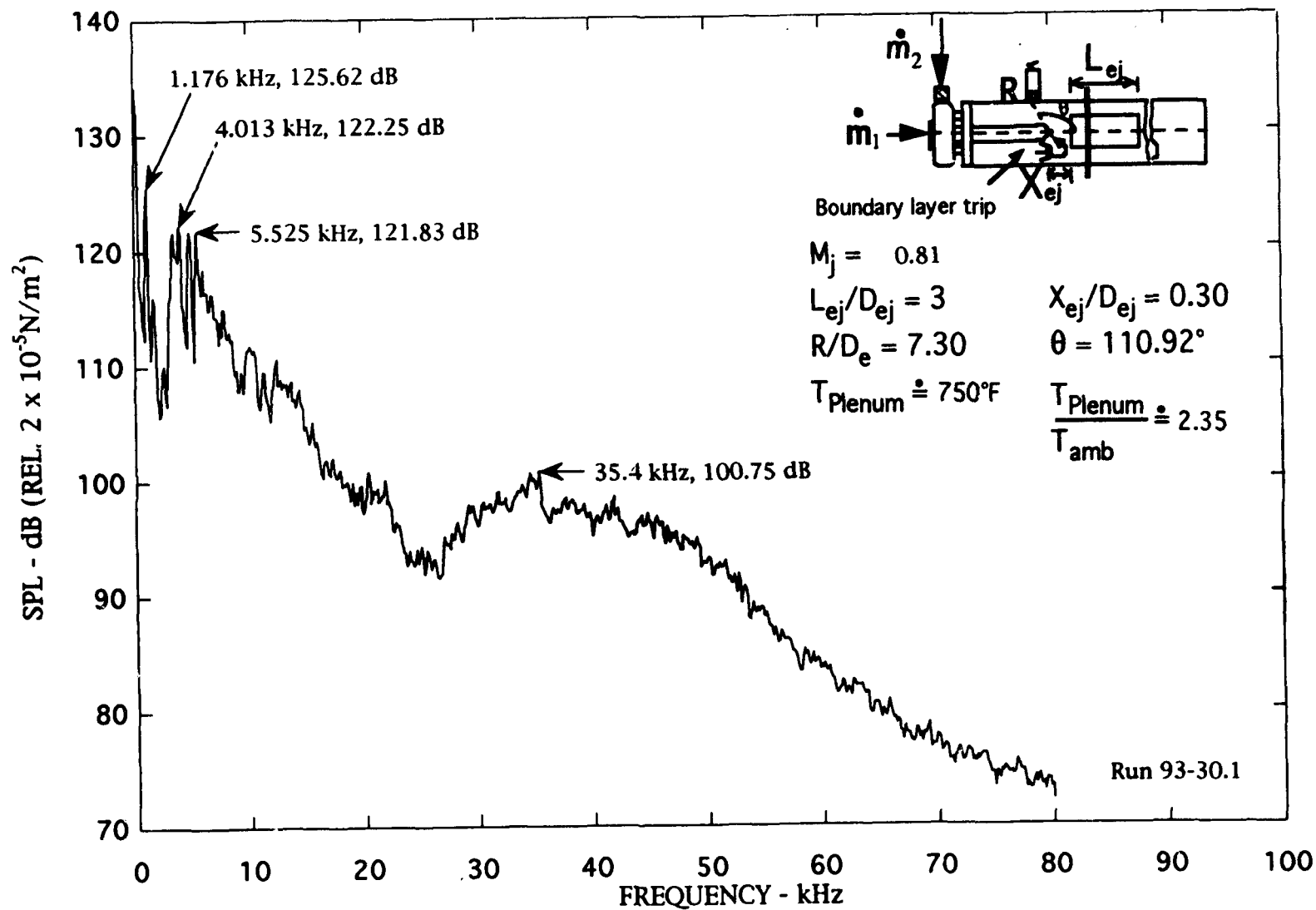Figure 4.9c. Narrow band ($\Delta f = 128$ Hz) noise spectra of tripped and ducted jet with open manifold, $M_j = 0.81$.
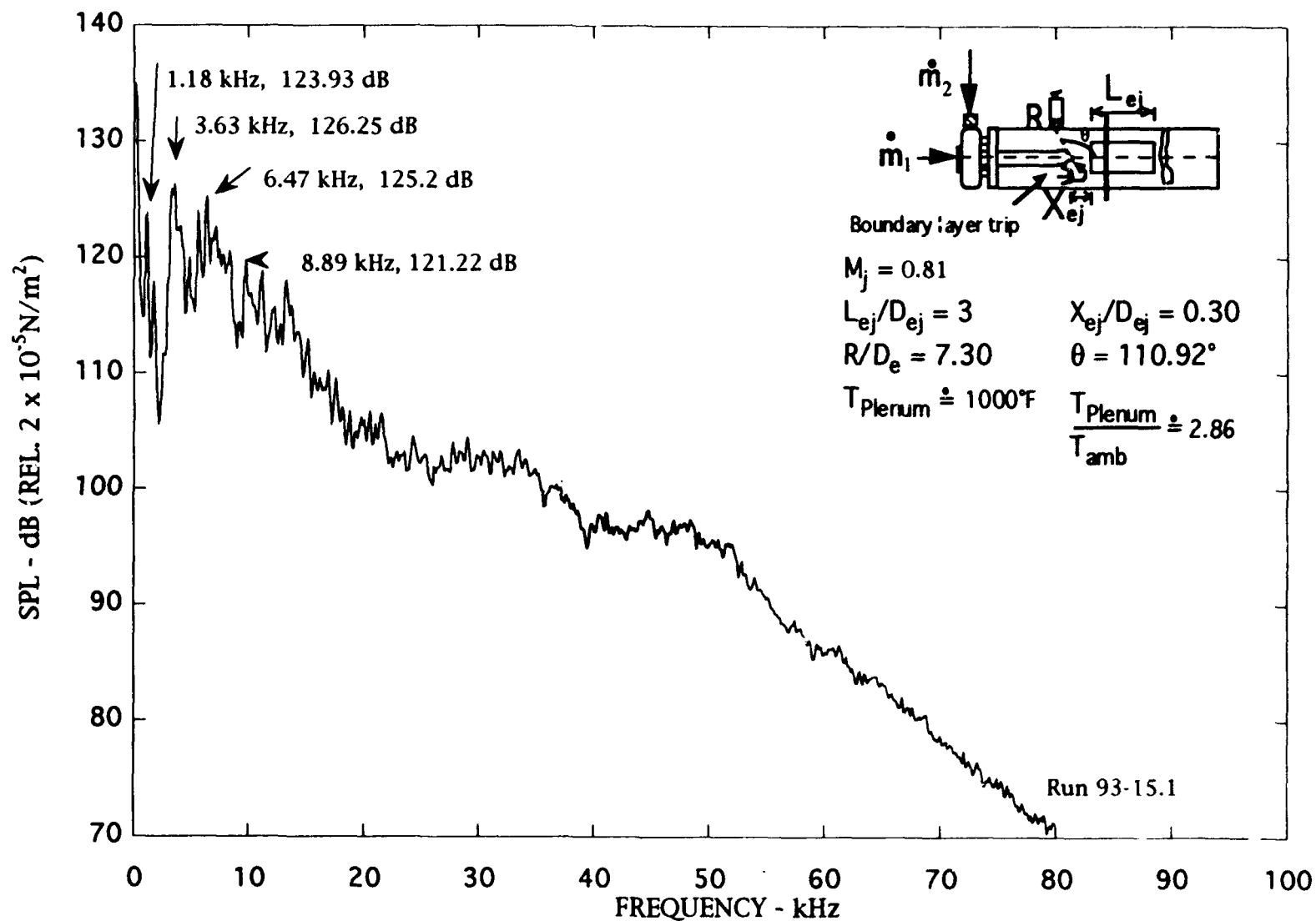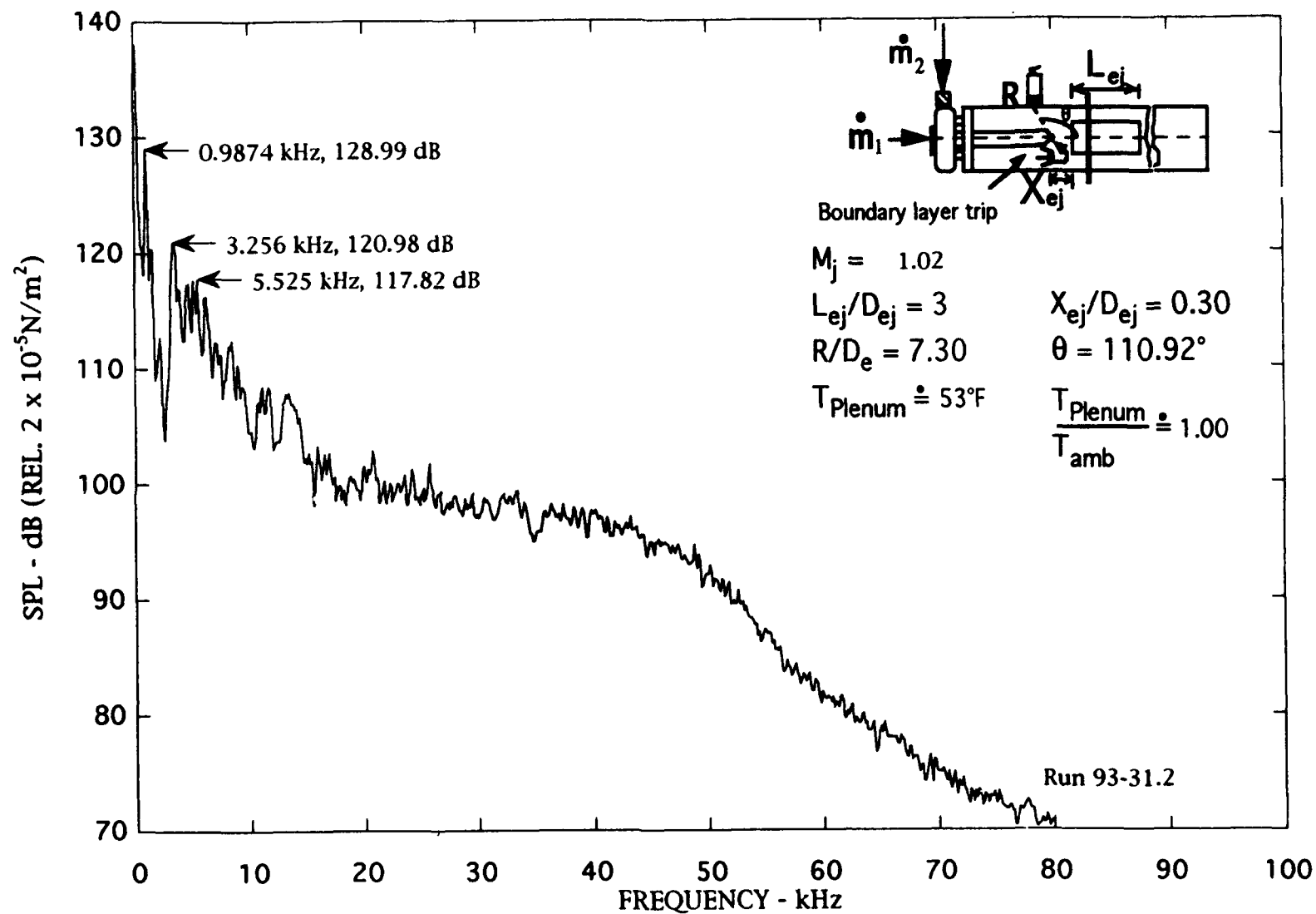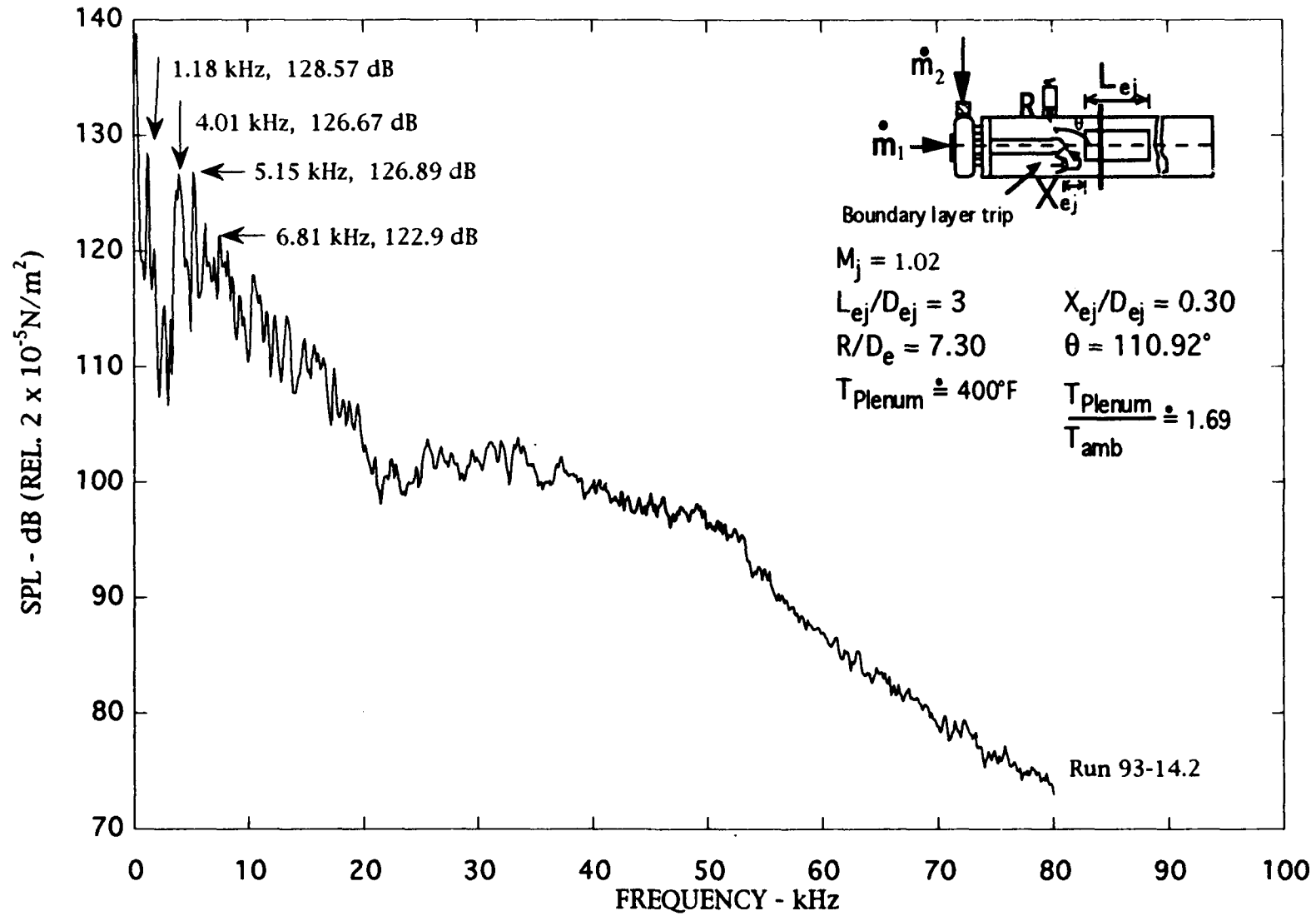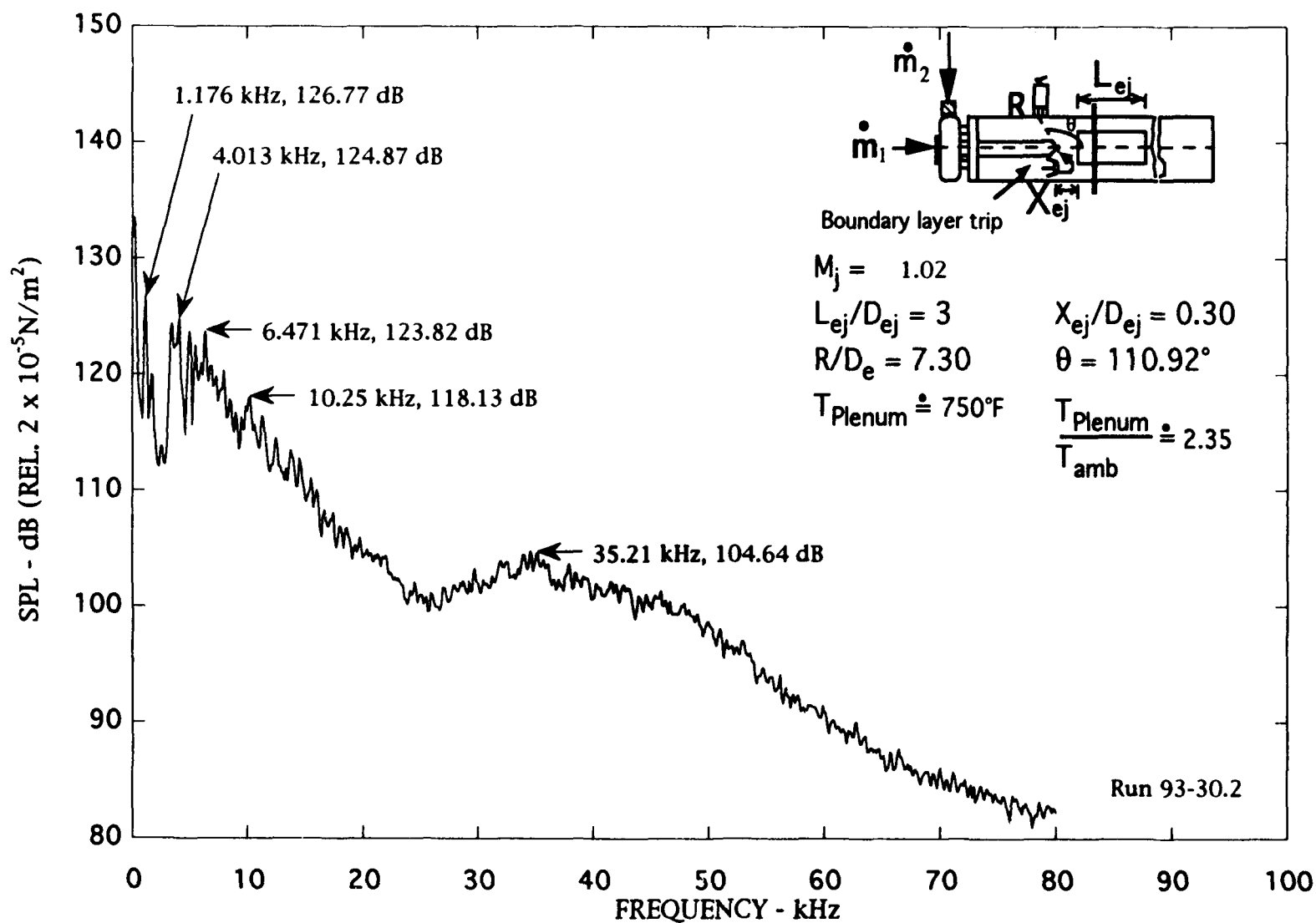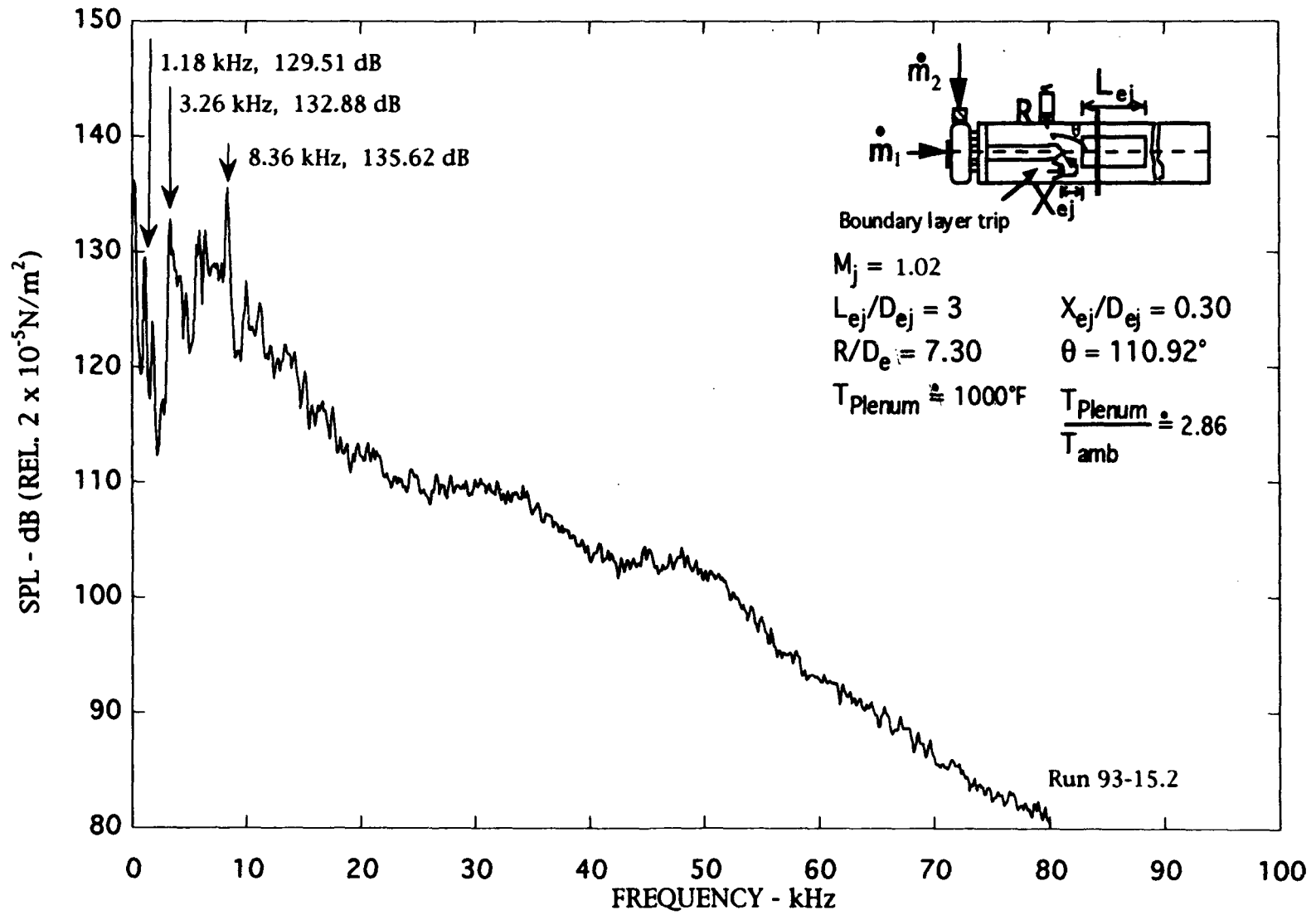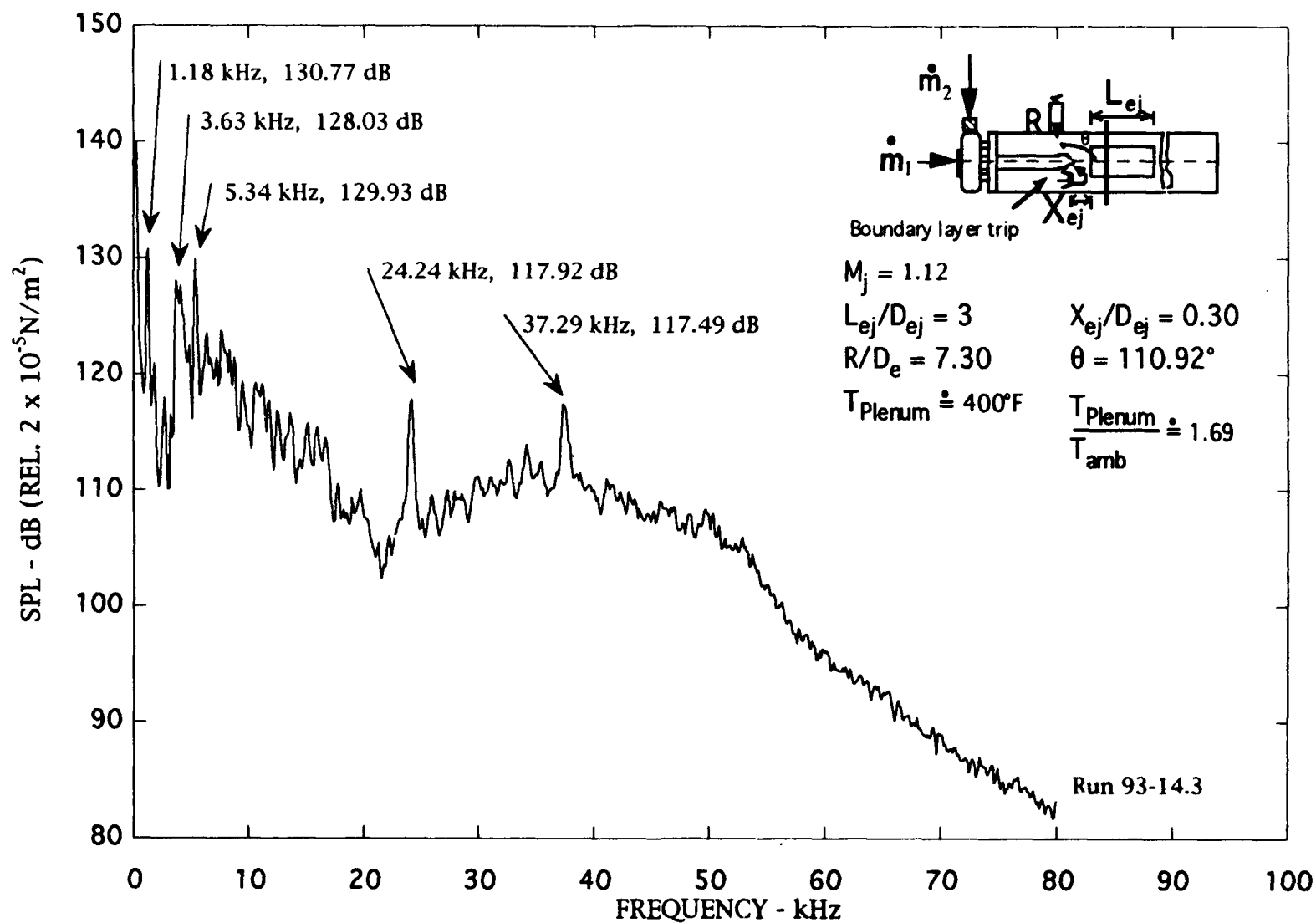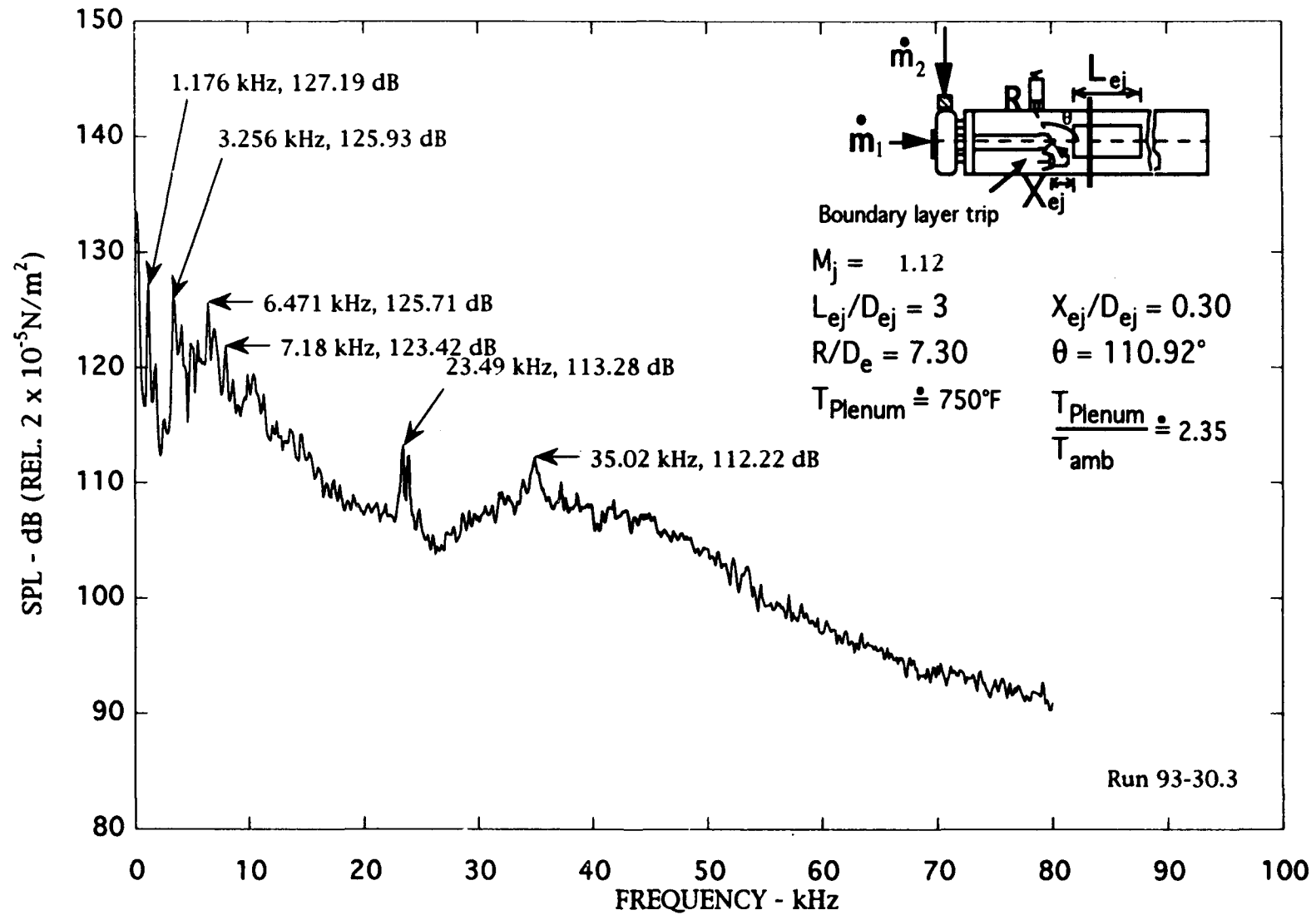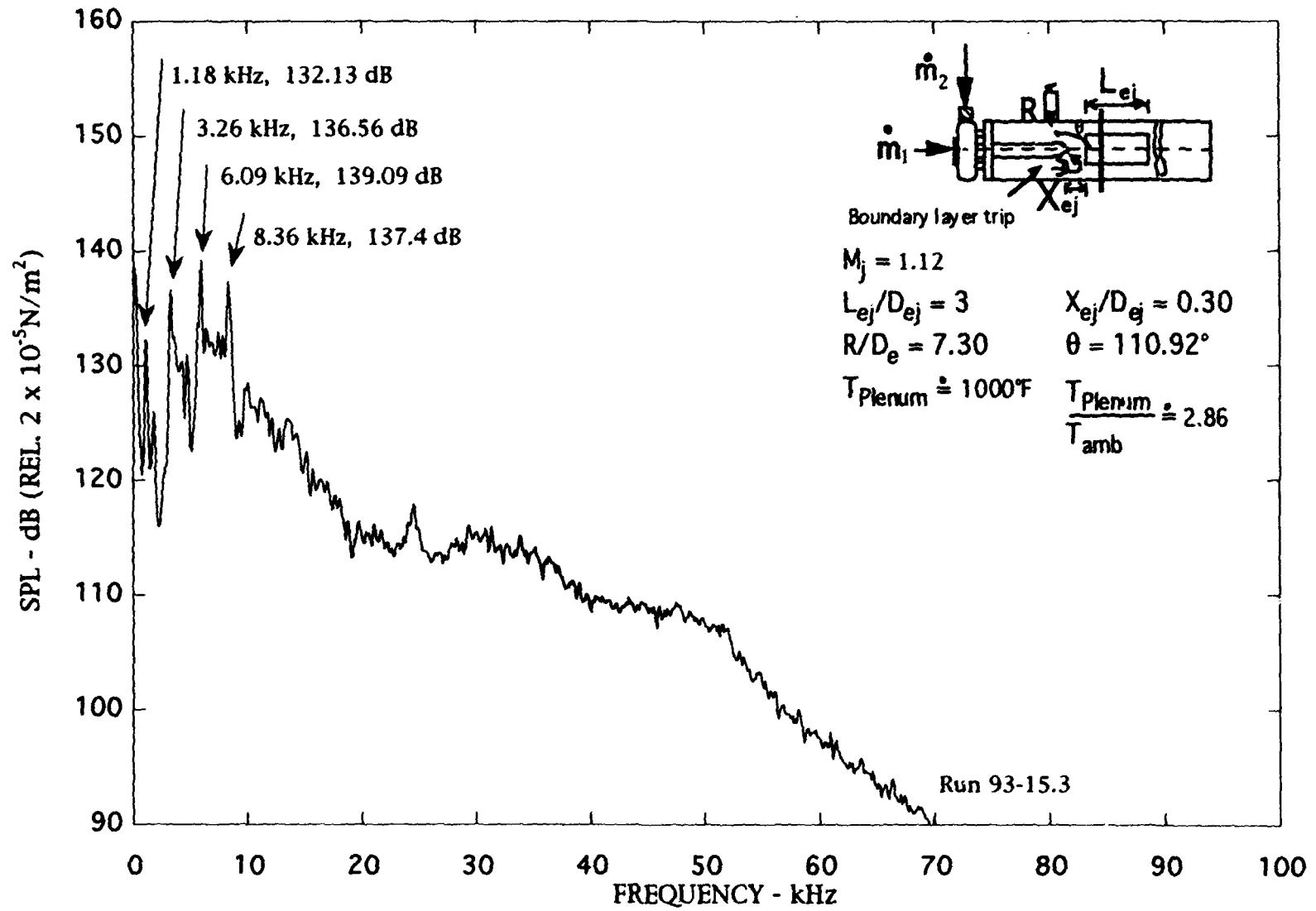
Figure 4.9d. Narrow band ($\Delta f = 128$ Hz) noise spectra of tripped and ducted jet with open manifold, $M_j = 0.81$.
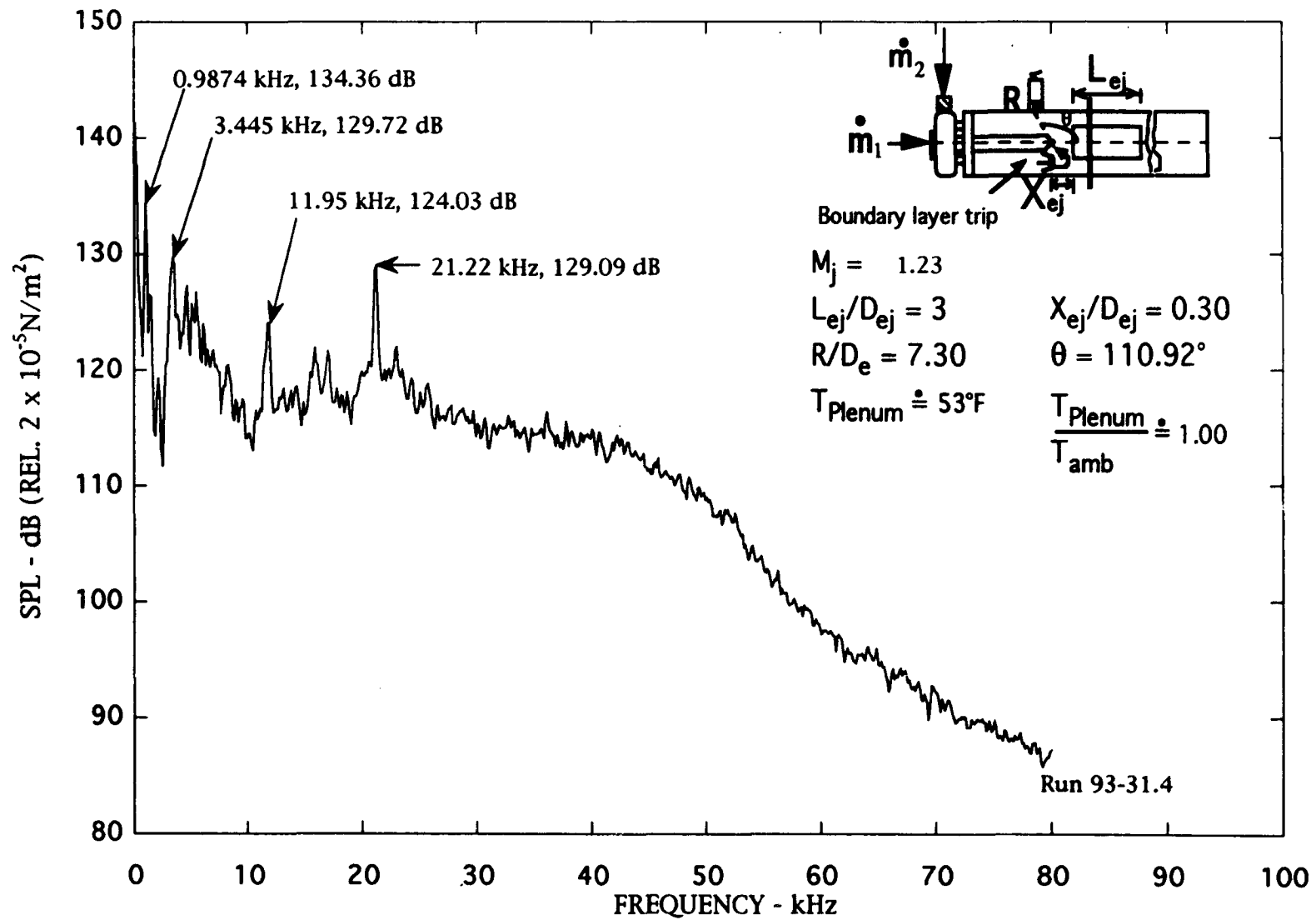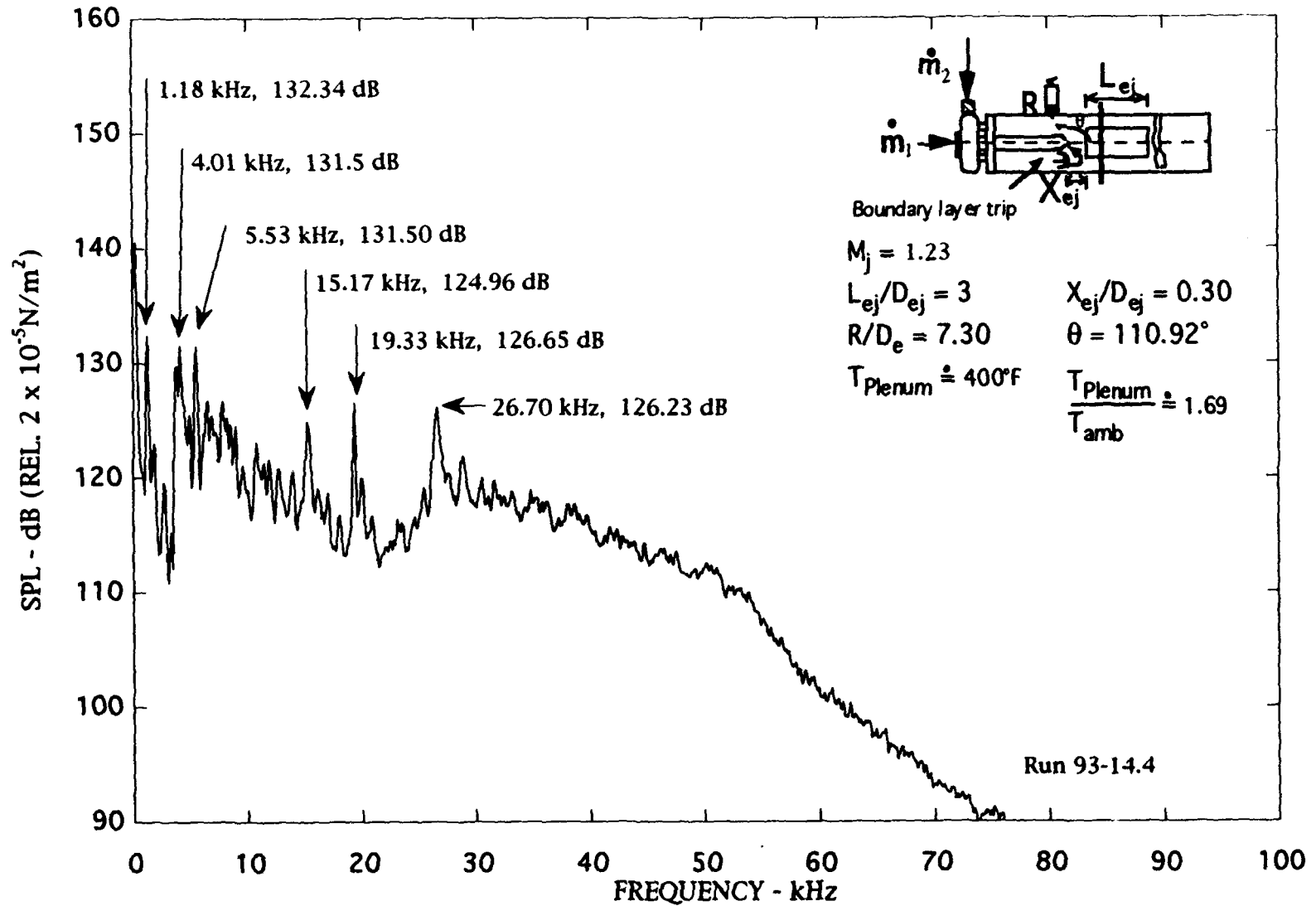
Figure 4.10a. Narrow band (Δf = 128 Hz) noise spectra of tripped and ducted jet with open manifold, M_j = 1.02.

Figure 4.10b. Narrow band (Δf = 128 Hz) noise spectra of tripped and ducted jet with open manifold, M_j = 1.02.

Figure 4.10c. Narrow band ($\Delta f = 128$ Hz) noise spectra of tripped and ducted jet with open manifold, $M_j = 1.02$.

Figure 4.10d. Narrow band ($\Delta f = 128$ Hz) noise spectra of tripped and ducted jet with open manifold, $M_j = 1.02$.
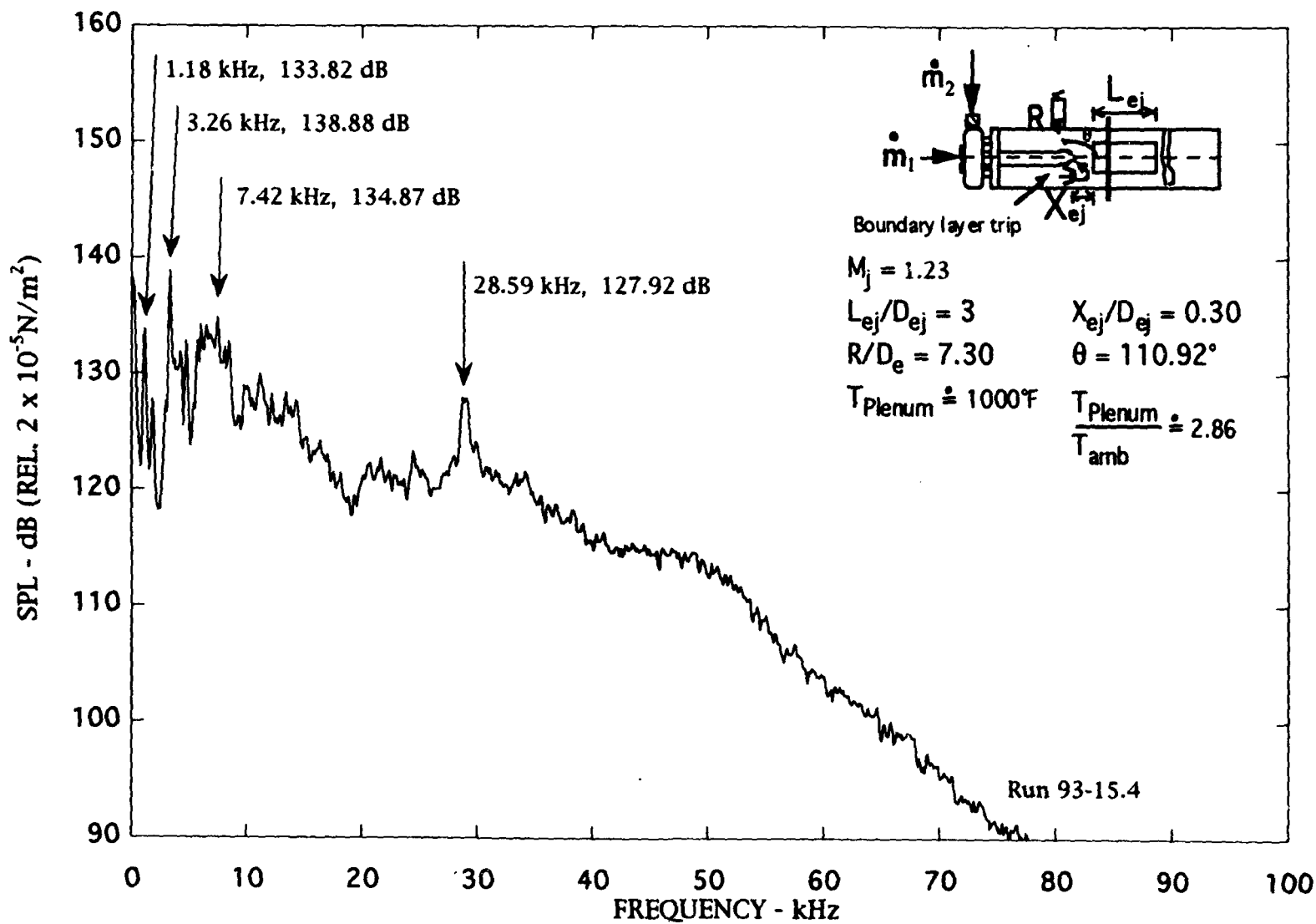
Figure 4.11a. Narrow band ($\Delta f = 128$ Hz) noise spectra of tripped and ducted jet with open manifold, $M_j = 1.12$.
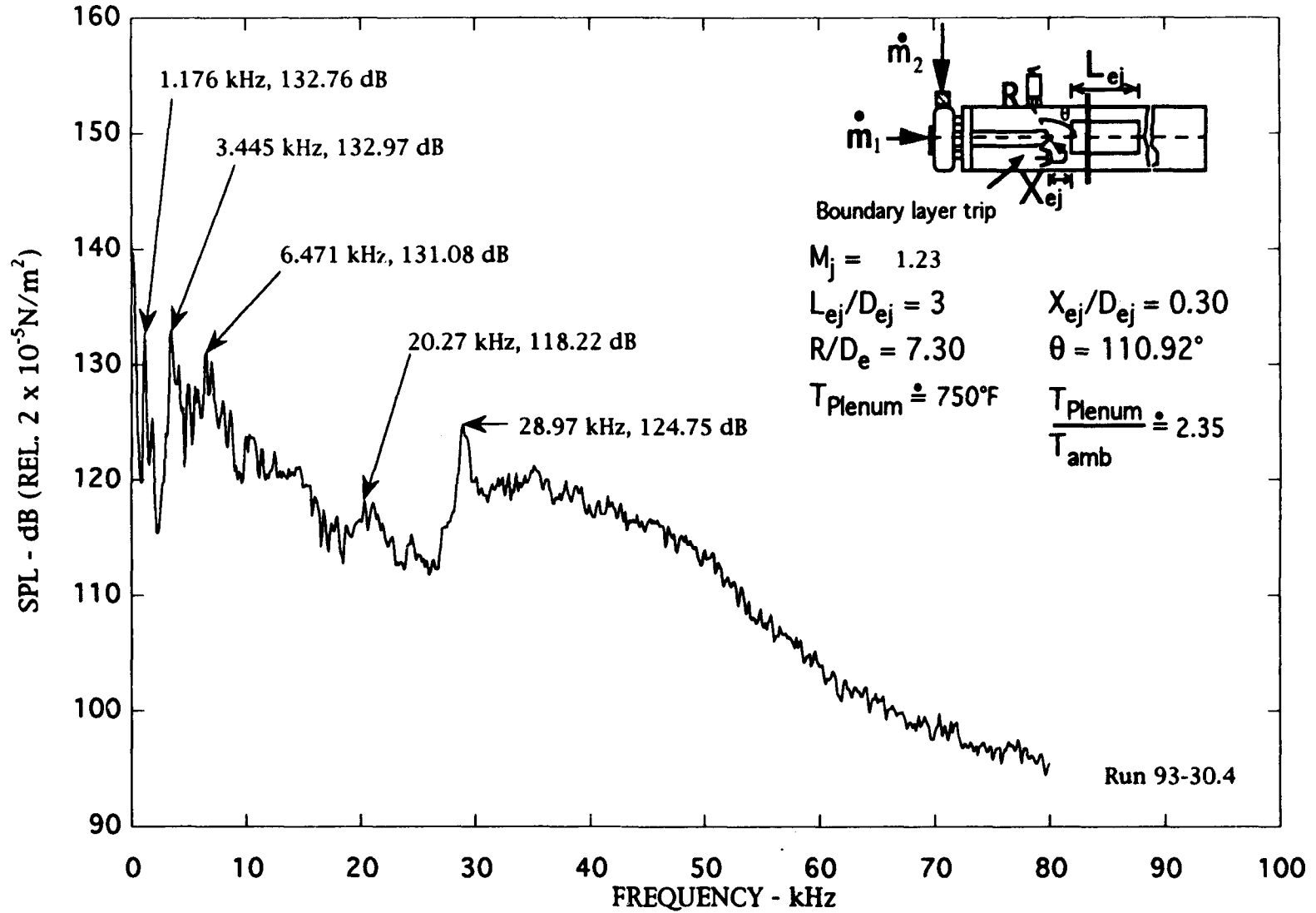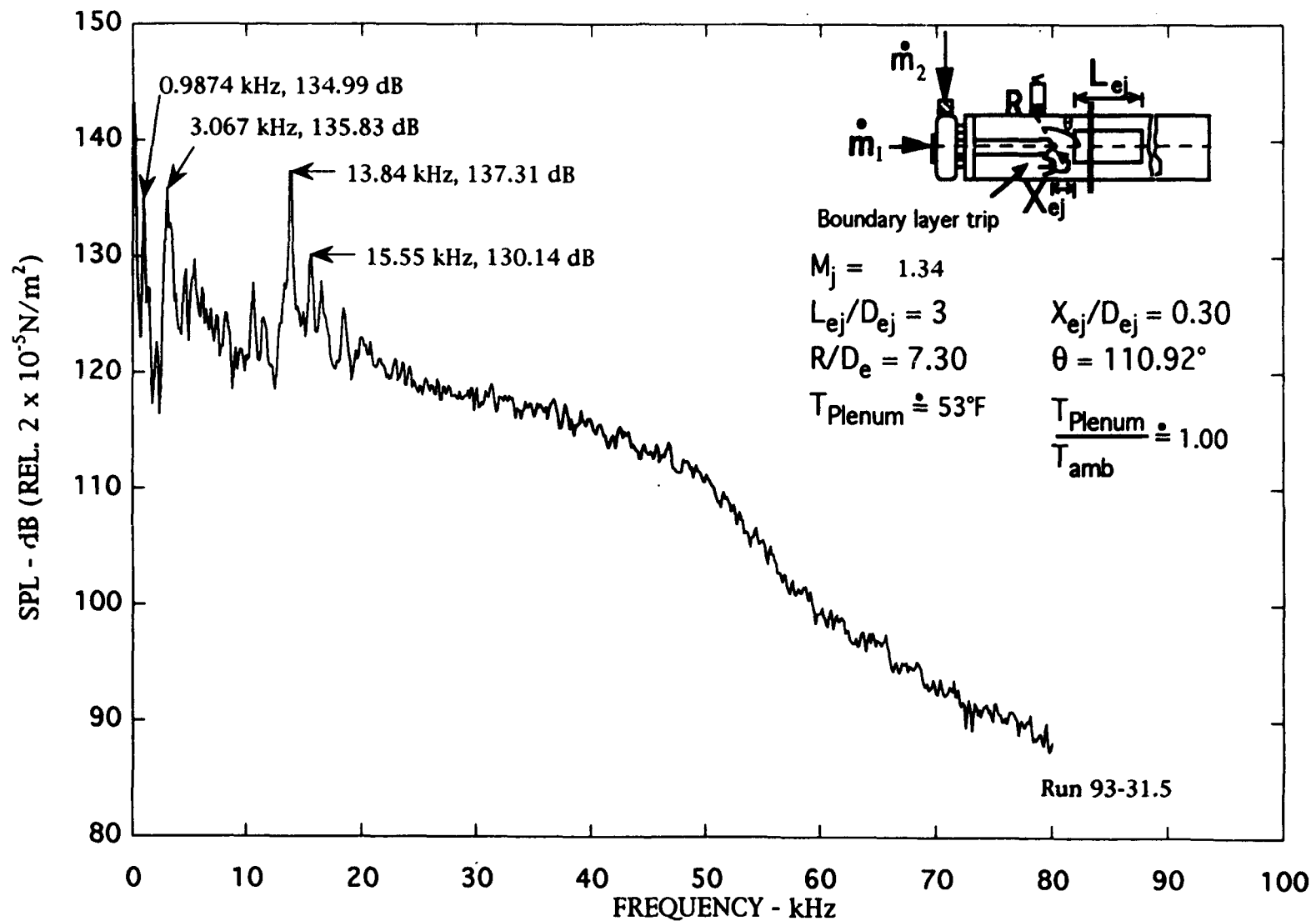
Figure 4.11b. Narrow band (Δf = 128 Hz) noise spectra of tripped and ducted jet with open manifold, M$_j$ ≈ 1.12.

Figure 4.11c. Narrow band ($\Delta f = 128$ Hz) noise spectra of tripped and ducted jet with open manifold, $M_j = 1.12$.

Figure 4.11d. Narrow band ($\Delta f = 128$ Hz) noise spectra of tripped and ducted jet with open manifold, $M_j = 1.12$.

Figure 4.12a. Narrow band ($\Delta f = 128$ Hz) noise spectra of tripped and ducted jet with open manifold, $M_j = 1.23$.
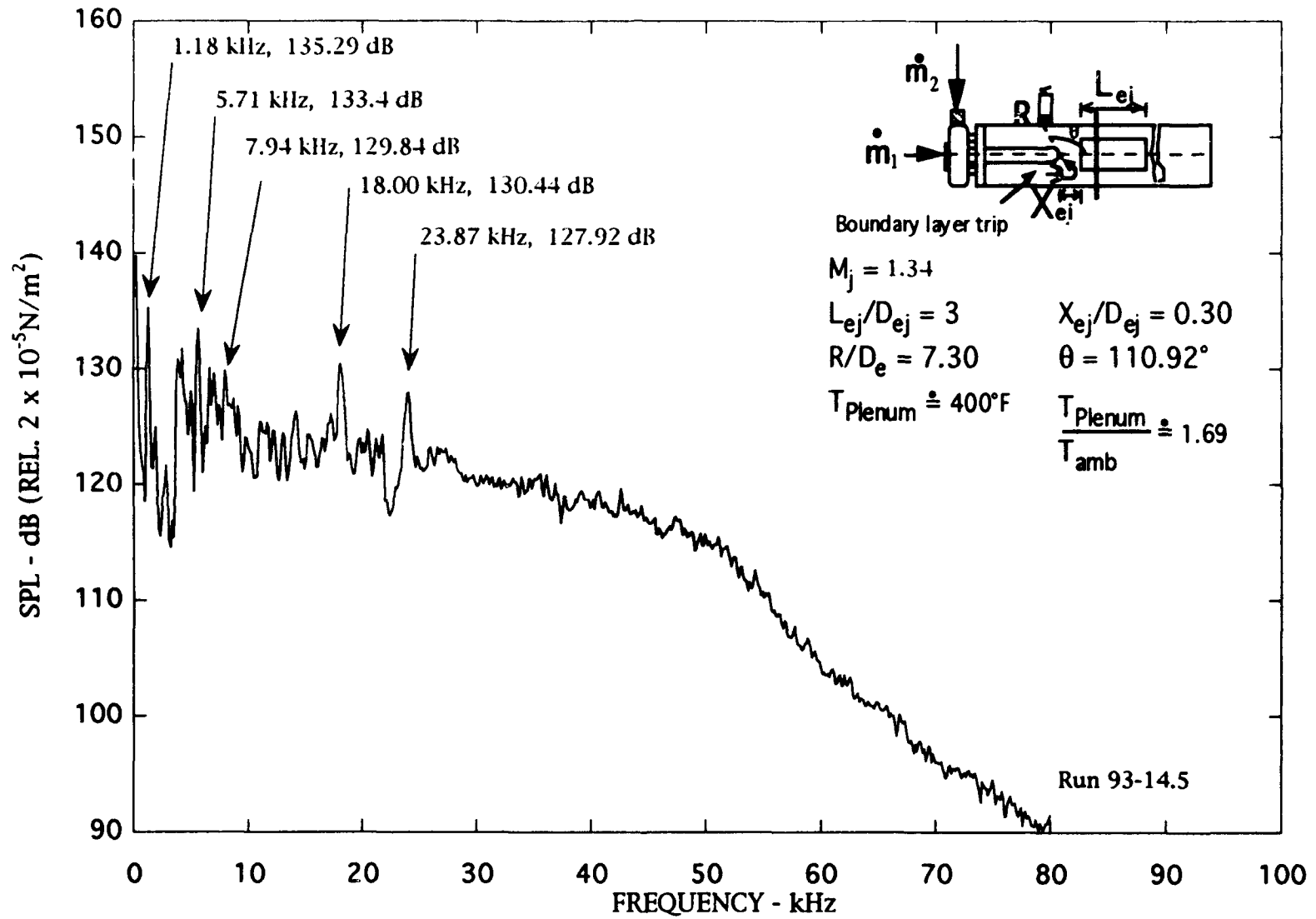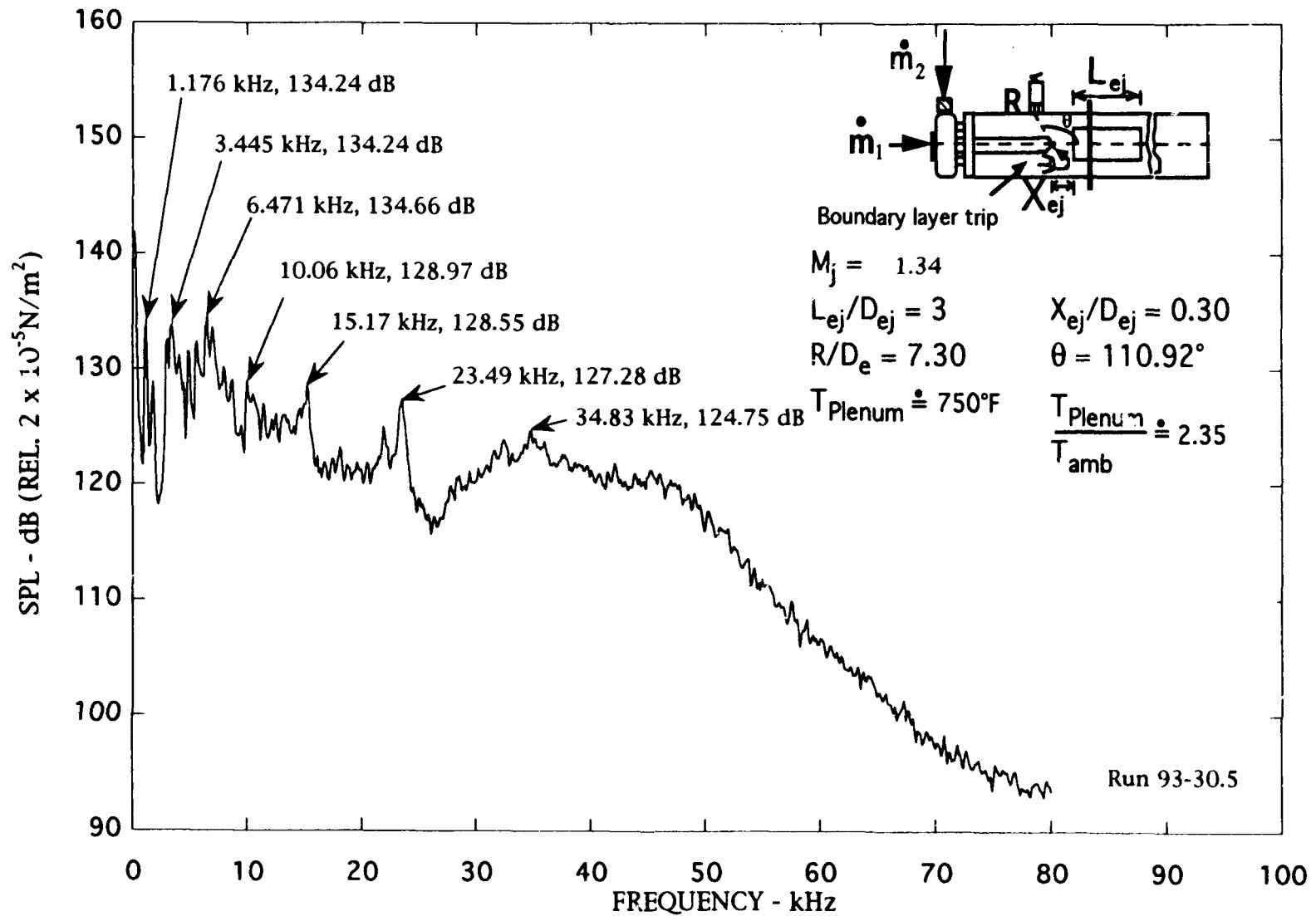
Figure 4.12b. Narrow band ($\Delta f = 128$ Hz) noise spectra of tripped and ducted jet with open manifold, $M_j = 1.23$.

Figure 4.12c. Narrow band ($\Delta f = 128$ Hz) noise spectra of tripped and ducted jet with open manifold, $M_j = 1.23$.
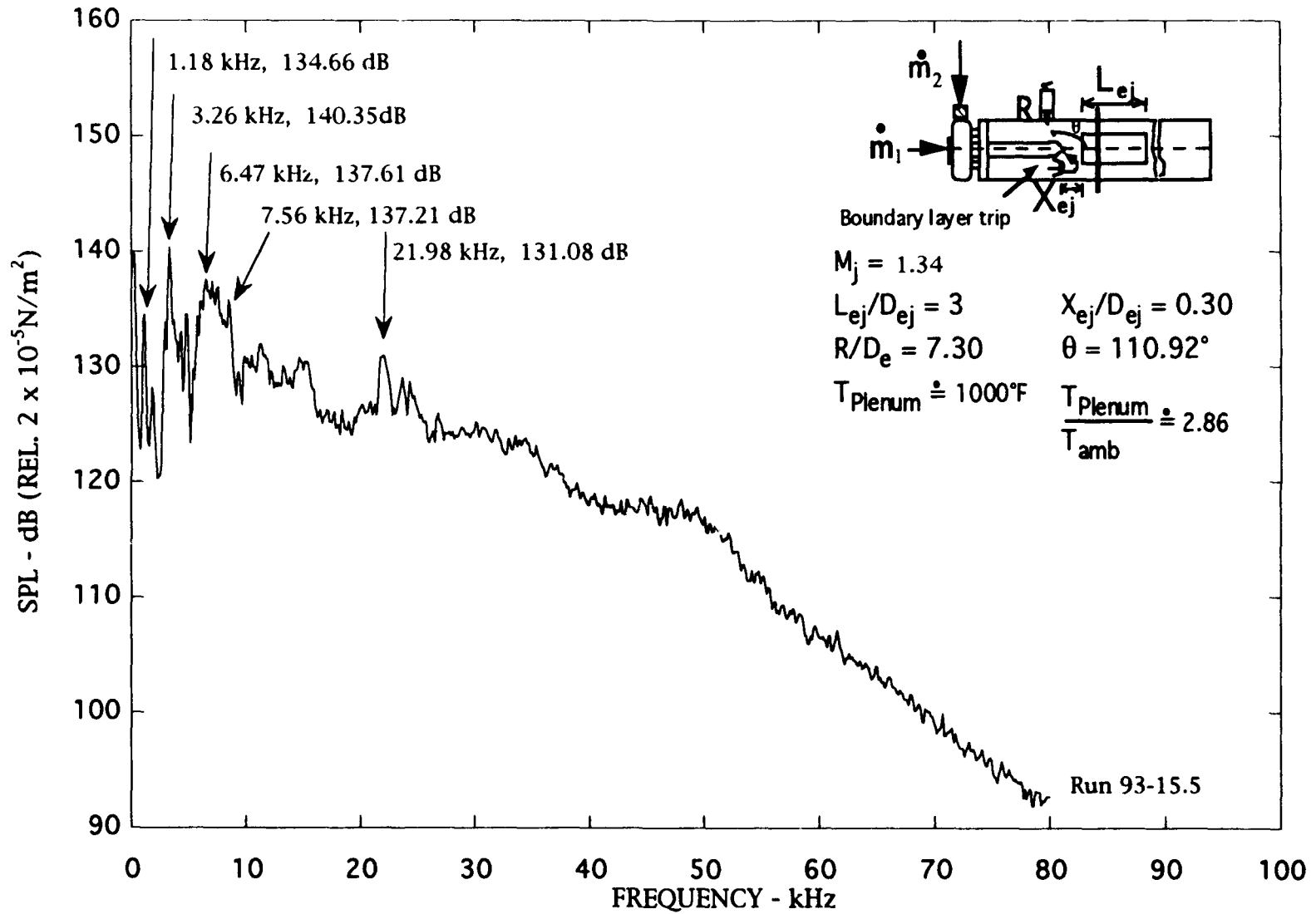
Figure 4.12d. Narrow band ($\Delta f = 128$ Hz) noise spectra of tripped and ducted jet with open manifold, $M_j = 1.23$.
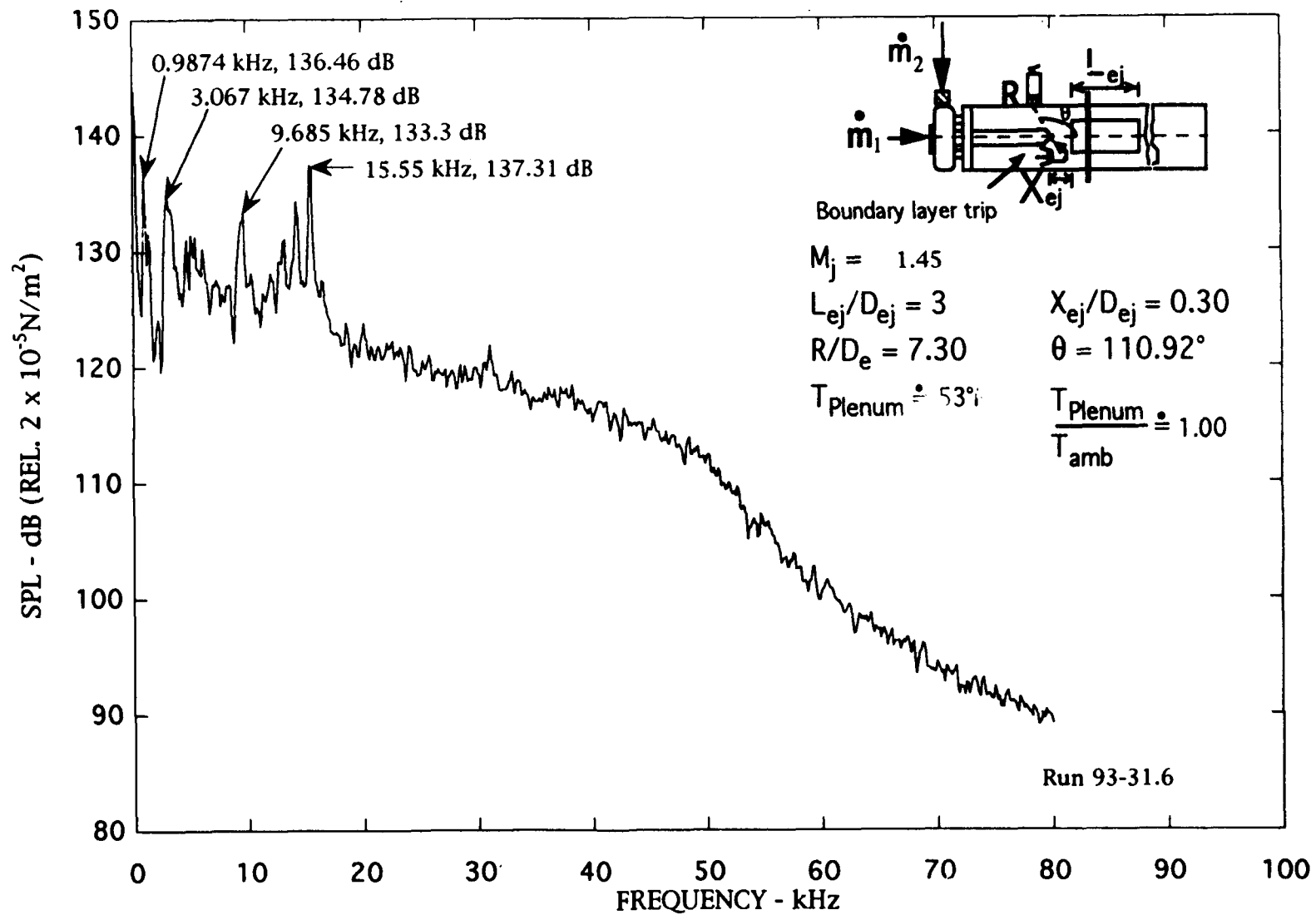
Figure 4.13a. Narrow band ($\Delta f = 128$ Hz) noise spectra of tripped and ducted jet with open manifold, $M_j = 1.34$.

Figure 4.13b. Narrow band (Δf = 128 Hz) noise spectra of tripped and ducted jet with open manifold, M_j = 1.34.

Figure 4.13c. Narrow band ($\Delta f = 128$ Hz) noise spectra of tripped and ducted jet with open manifold, $M_j = 1.34$.

Text visible within the figure:

1.176 kHz, 134.24 dB
3.445 kHz, 134.24 dB
6.471 kHz, 134.66 dB
10.06 kHz, 128.97 dB
15.17 kHz, 128.55 dB
23.49 kHz, 127.28 dB
34.83 kHz, 124.75 dB

Boundary layer trip

$M_j = 1.34$
$L_{ej}/D_{ej} = 3$
$R/D_e = 7.30$
$T_{Plenum} \doteq 750°F$

$X_{ej}/D_{ej} = 0.30$
$\theta = 110.92°$
$\dfrac{T_{Plenum}}{T_{amb}} \doteq 2.35$

Run 93-30.5

SPL - dB (REL. 2×10^{-5} N/m^2)

FREQUENCY - kHz

Figure 4.13d. Narrow band ($\Delta f = 128$ Hz) noise spectra of tripped and ducted jet with open manifold, $M_j = 1.34$.
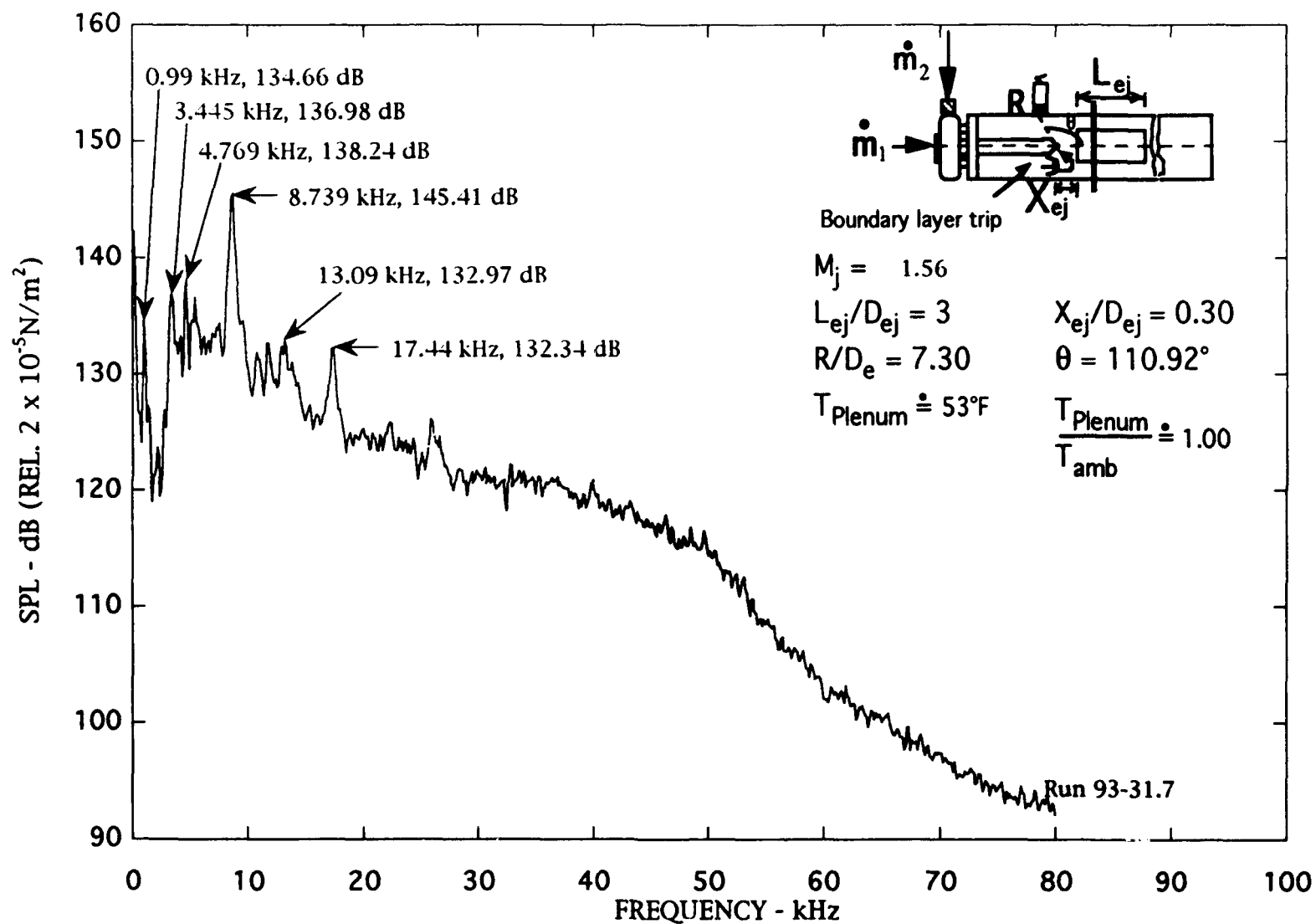
Figure 4.14a. Narrow band ($\Delta f = 128$ Hz) noise spectra of tripped and ducted jet with open manifold, $M_j = 1.45$.
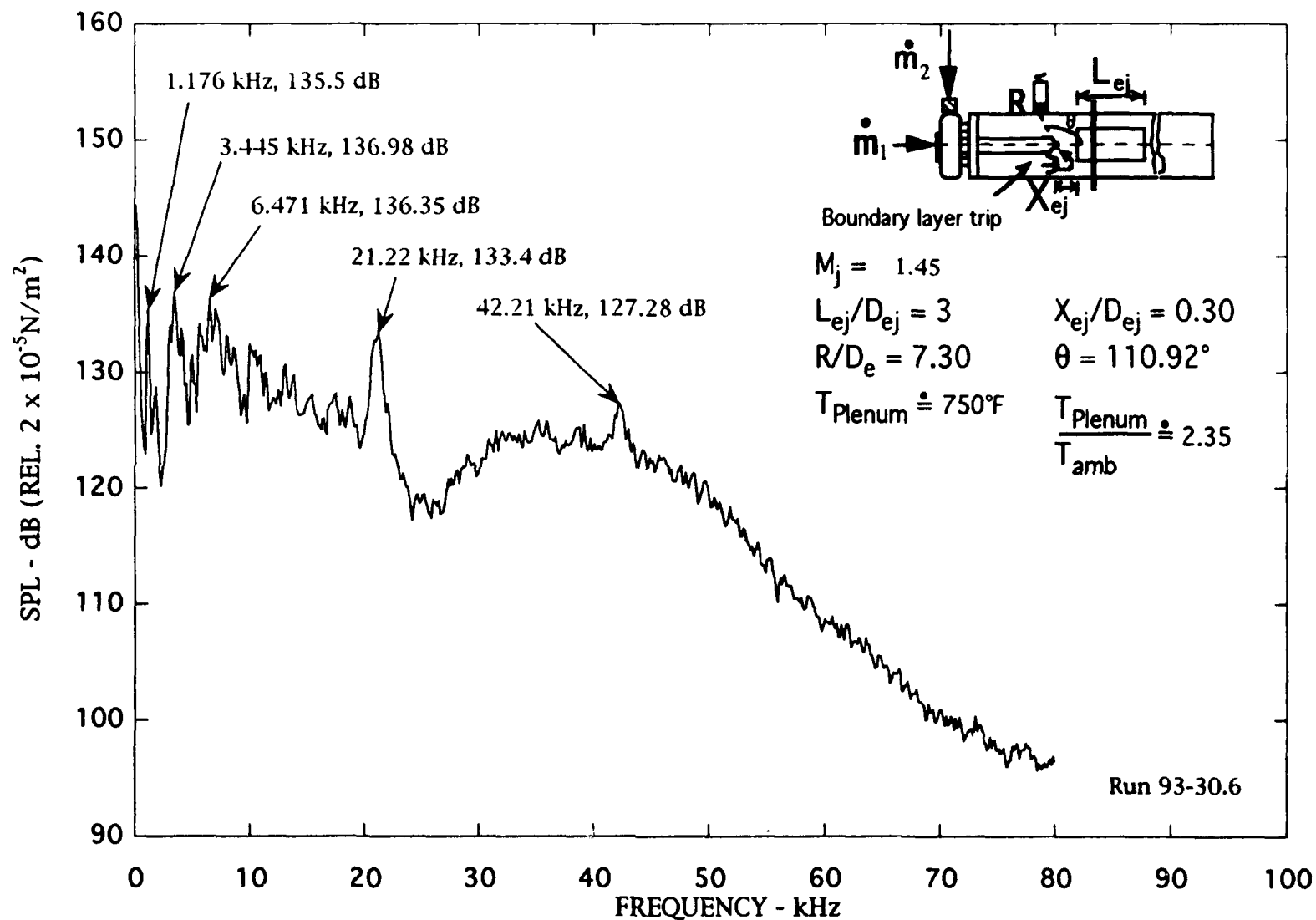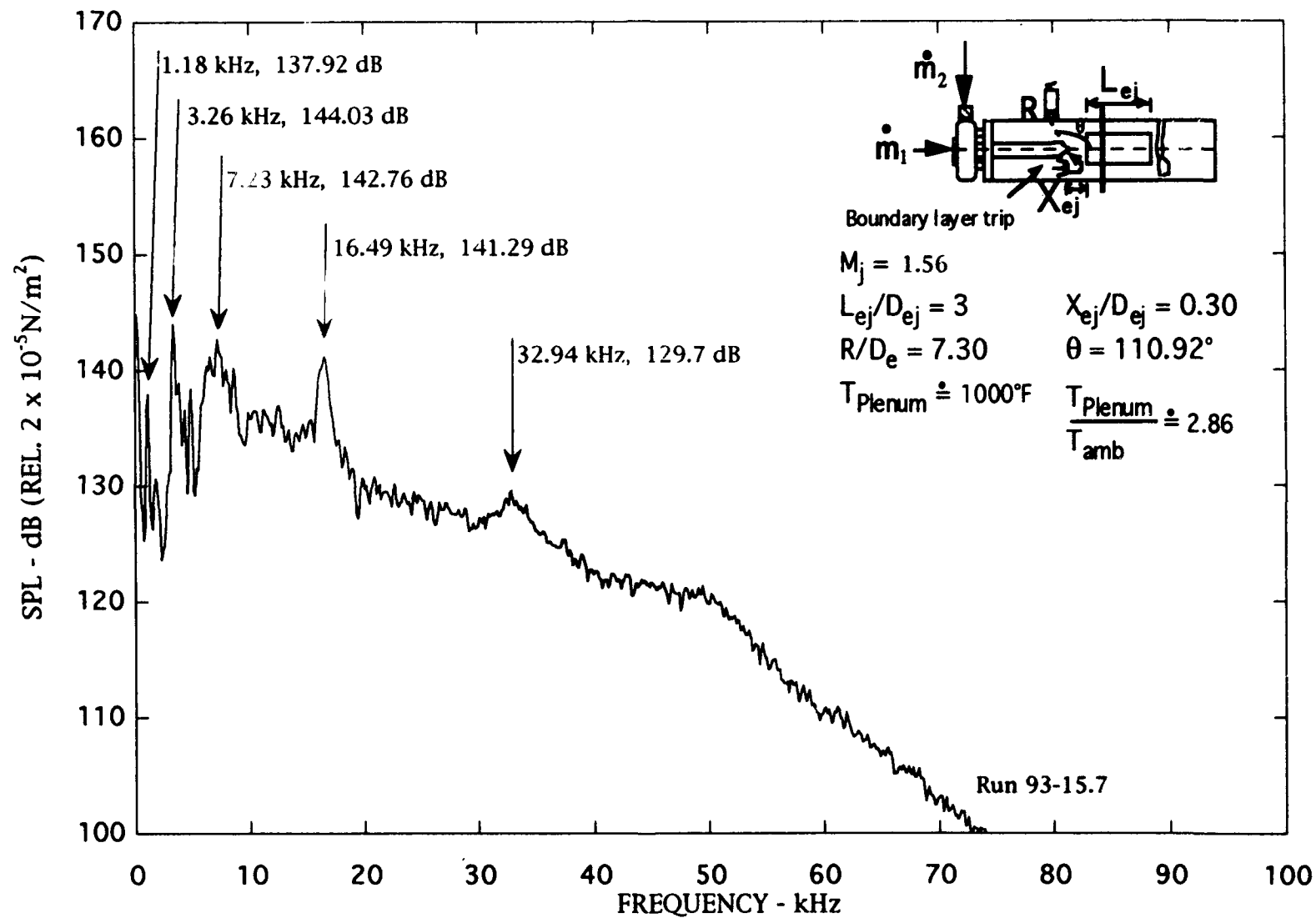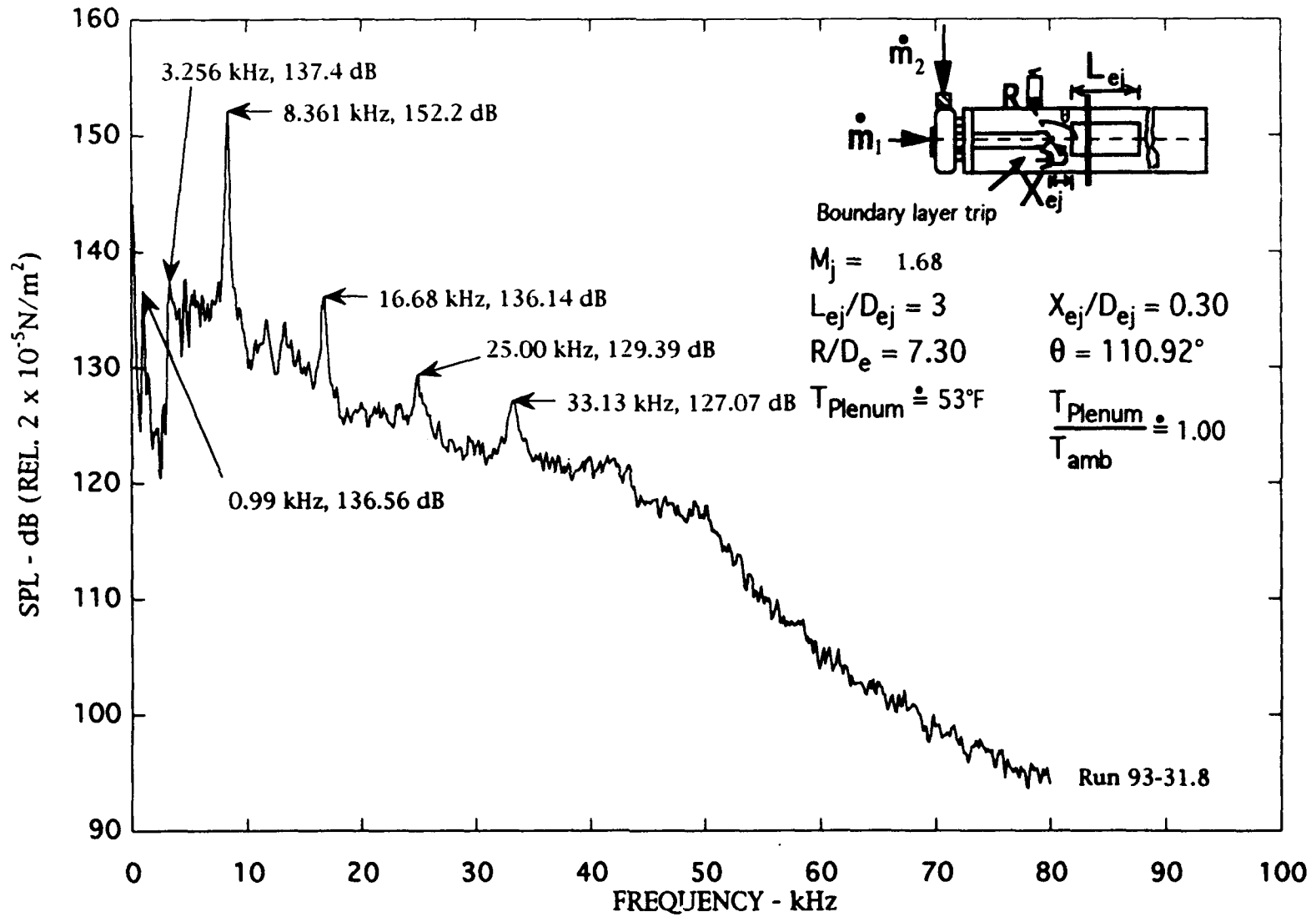
Figure 4.14b. Narrow band (Δf = 128 Hz) noise spectra of tripped and ducted jet with open manifold, M_j = 1.45.
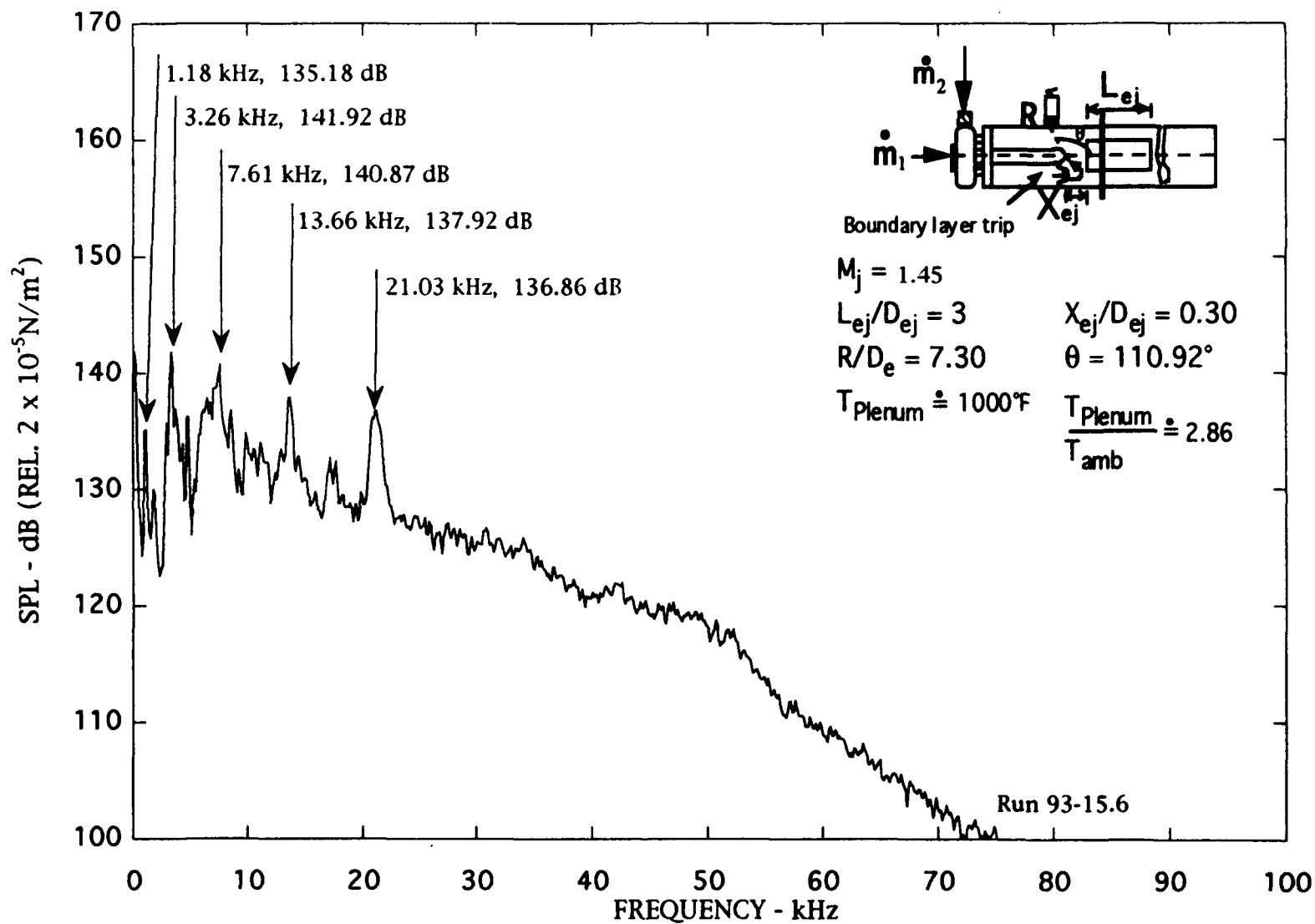
Figure 4.14c. Narrow band ($\Delta f = 128$ Hz) noise spectra of tripped and ducted jet with open manifold, $M_j = 1.45$.

Figure 4.15a. Narrow band (Δf = 128 Hz) noise spectra of tripped and ducted jet with open manifold, M_j = 1.56.

Figure 4.15b. Narrow band ($\Delta f = 128$ Hz) noise spectra of tripped and ducted jet with open manifold, $M_j = 1.56$.

Figure 4.16a. Narrow band ($\Delta f = 128$ Hz) noise spectra of tripped and ducted jet with open manifold, $M_j = 1.68$.
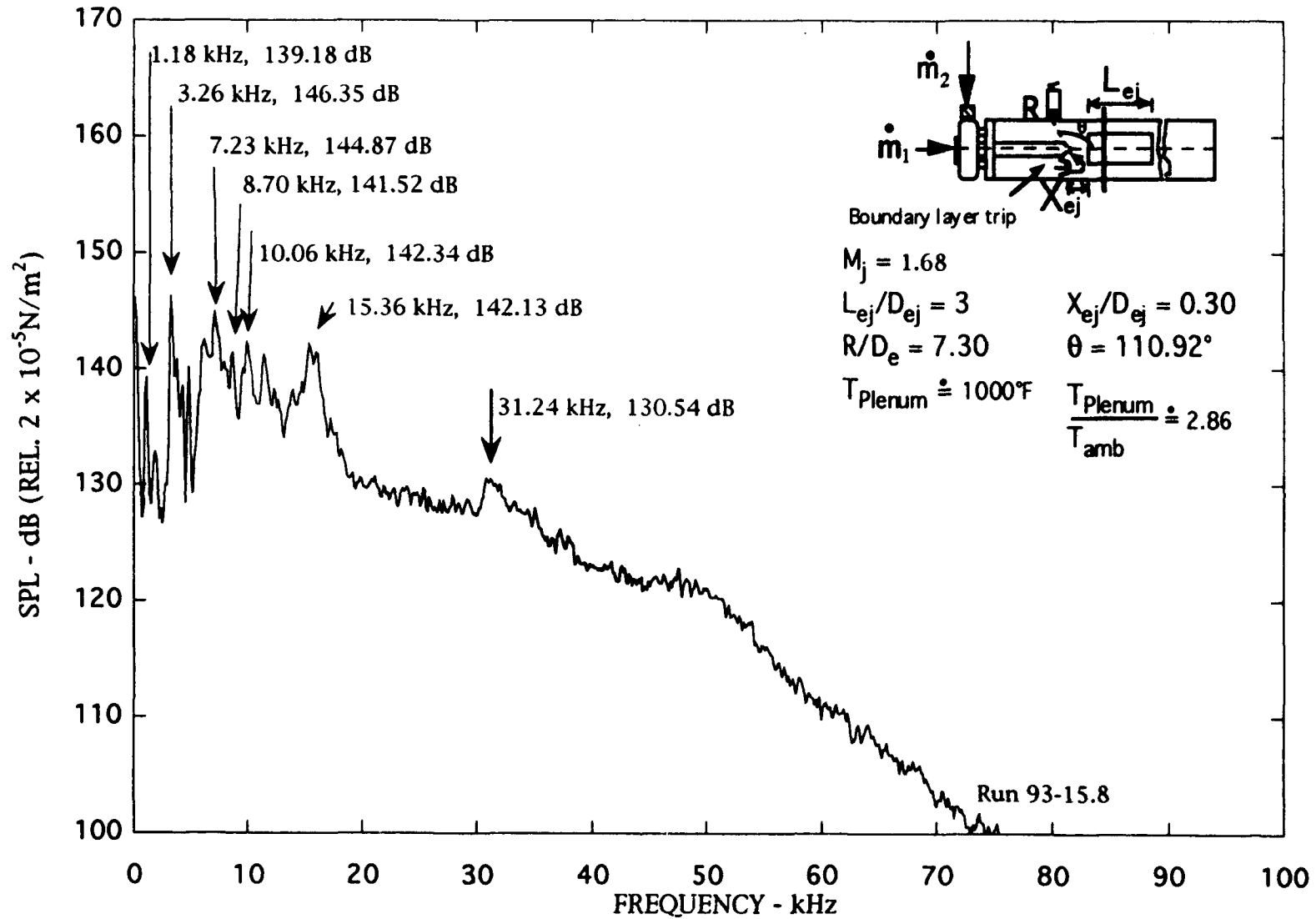
Figure 4.16b. Narrow band ($\Delta f = 128$ Hz) noise spectra of tripped and ducted jet with open manifold, $M_j = 1.68$.

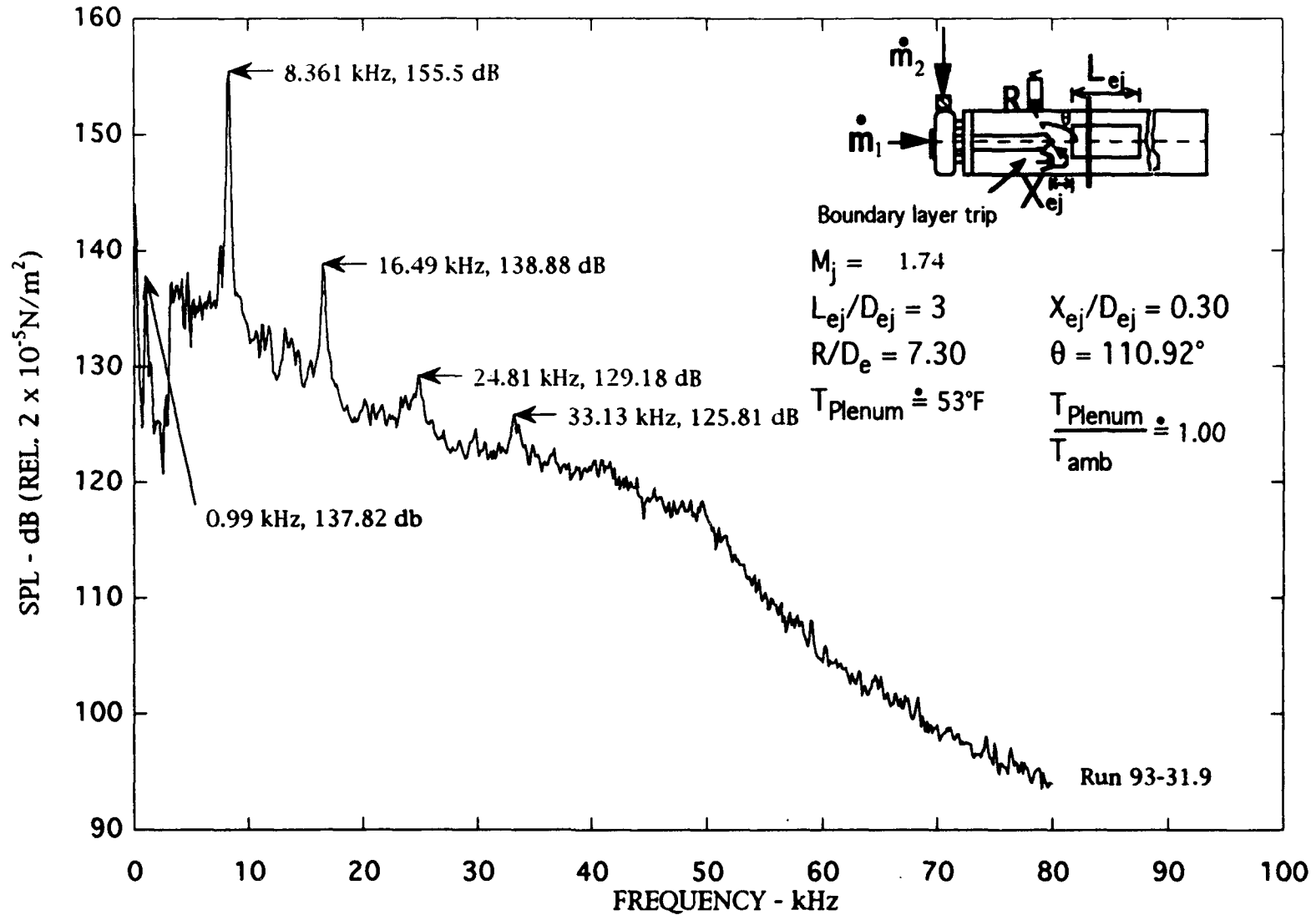Figure 4.17. Narrow band (Δf = 128 Hz) noise spectra of tripped and ducted jet with open manifold, M_j = 1.74.
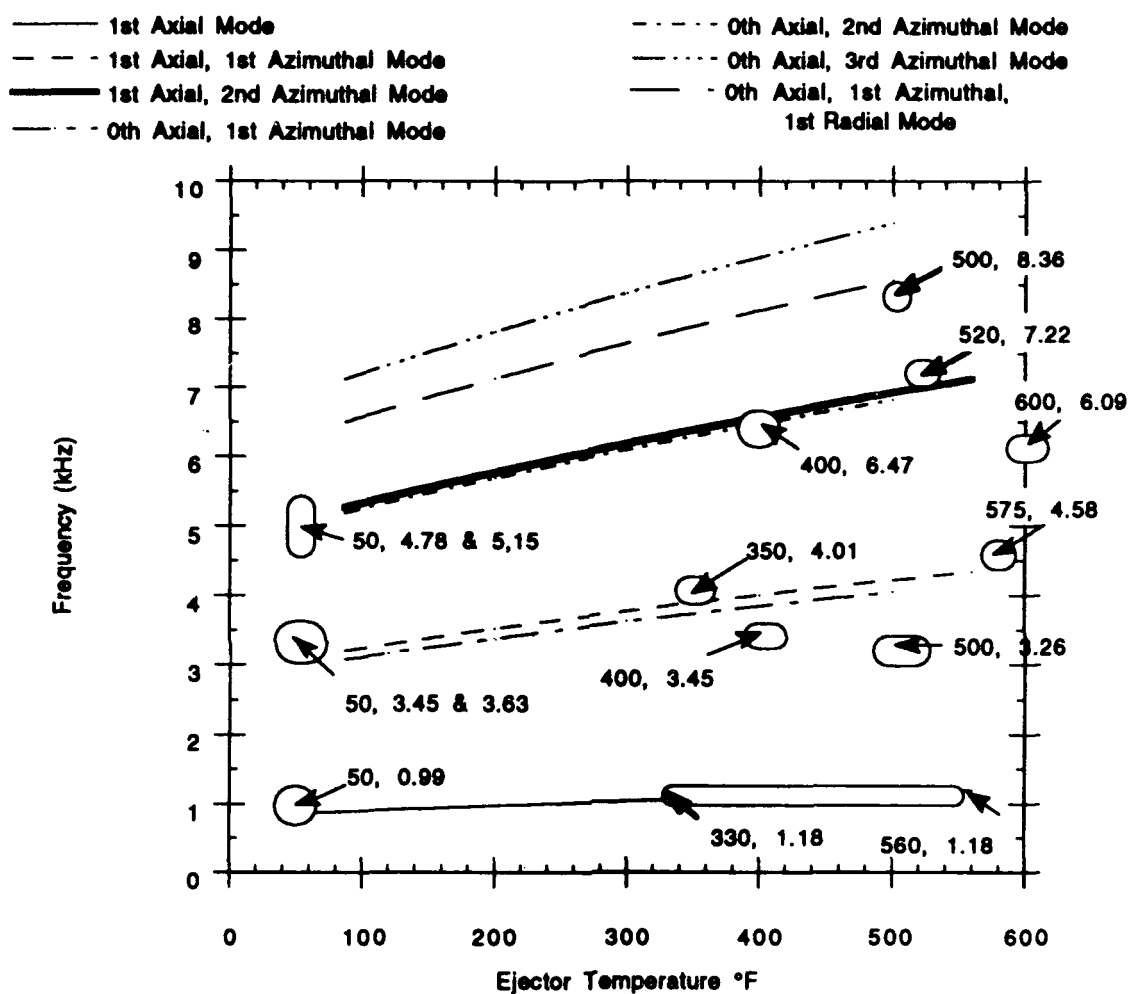
Figure 4.18. Predicted diffuser resonant frequency ranges and measured results. (The numbers adjacent to arrows indicate the ejector temperature, first number, and tone frequency in kHz, second number)
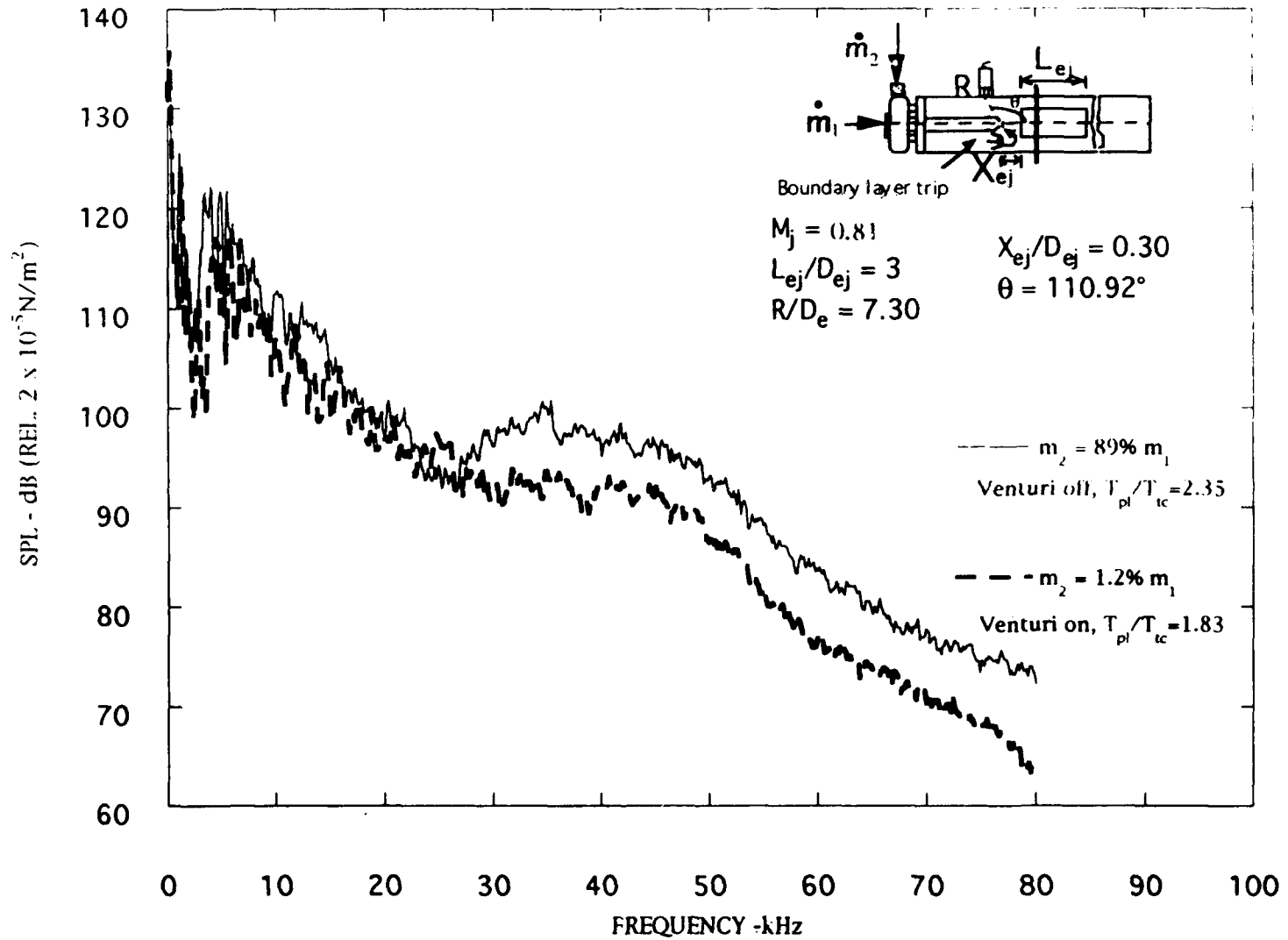
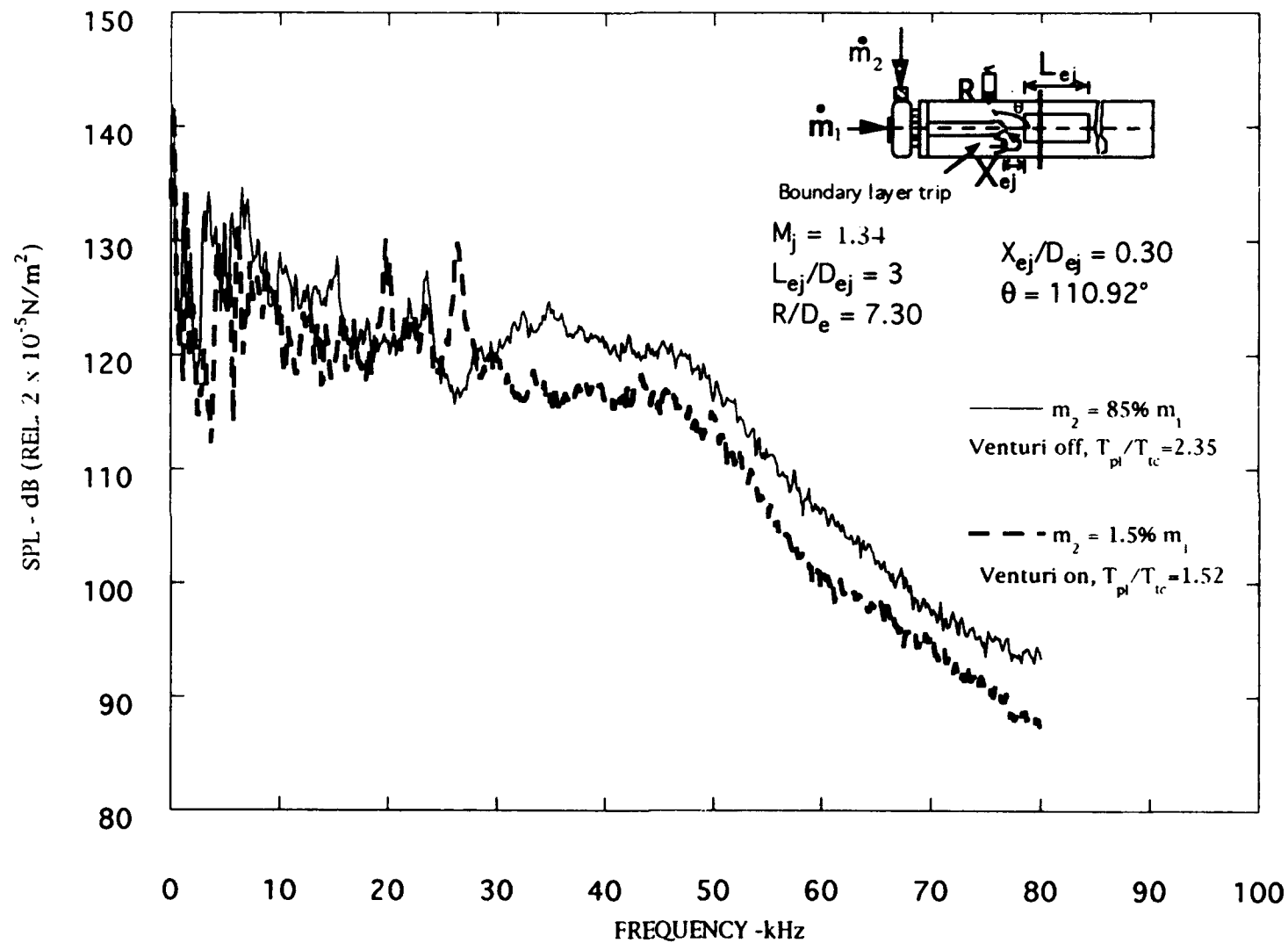Figure 4.19. Narrow band ($\Delta f = 128$ Hz) noise spectra of ducted jet, $M_j = 0.81$, $T_{plenum} = 750°F$.

Figure 4.20. Narrow band ($\Delta f = 128$ Hz) noise spectra of ducted jet, $M_j = 1.34$, $T_{plenum} = 750°F$.
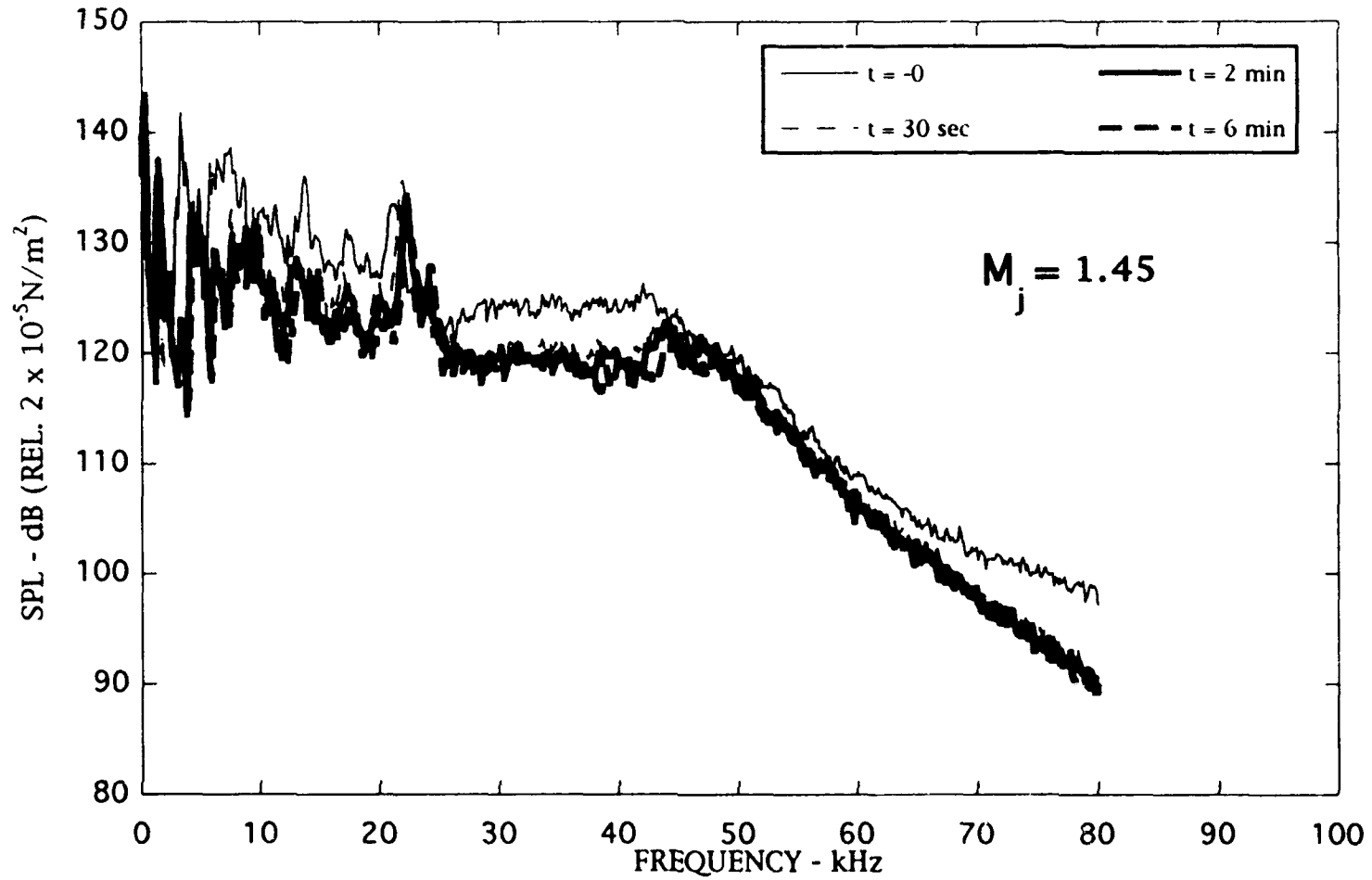
Figure 4.21. Comparison of venturi manifold open vs. time after manifold is closed.

4.3.1 Presence of Screech in the Ducted Configuration

Because of the predominance of tones in the in-duct spectra, it is difficult to separate the duct resonance tones and those associated with screech. An experienced researcher who has exar .ned a number of noise spectra for the free jet containing screech may be able to identify the scre. .h frequencies in the spectra obtained with the same jet enclosed in a duct, which we were able to do. Yet, to obtain confidence in our measure of success, we have plotted the frequencies of the tones that we believe are screech related in the fashion shown in Figs. 4.22, 4.23, and 4.24. Here, we have plotted the normalized frequencies (i.e., fD_j/U_j) of these tones against the jet Mach number and have superimposed the theoretical curves for the free jet obtained by using Tam's theory discussed earlier in relation to the screech of the free jets. Data for three temperature ratios 1, 2.37, and 2.78, are shown in these figures. We have included data with (square symbols) and without the venturi (circular symbols). Thus, data for two separate test cell temperatures appear in each figure. The ratios of the plenum temperatures and the test cell temperatures are also given in these figures.

It can be seen that we have been able to identify the screech frequencies in the duct correctly. As in the case of the free jet, it is seen that these frequencies for the ducted configuration also change with increasing temperature ratio. (Recall that the Strouhal number decreases and the frequency increases with increasing temperature.) A comparison of the spectra for the free jet shown earlier and the ducted jet shown here will indicate that the amplitudes of the sound pressures at these frequencies are much higher for the ducted case than for the free jet.
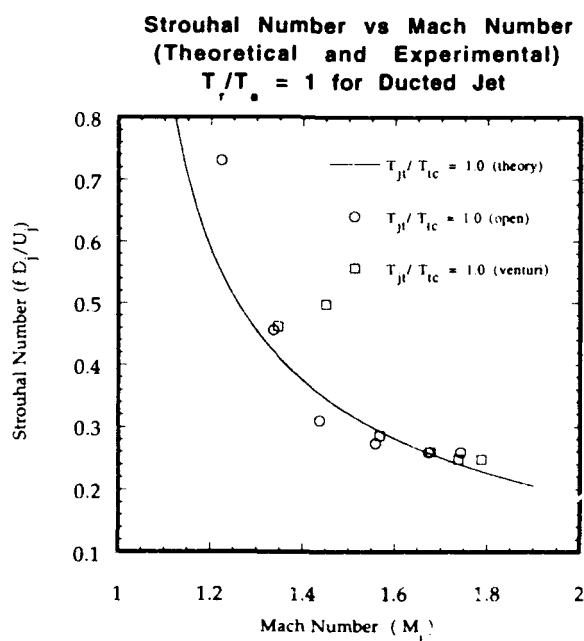

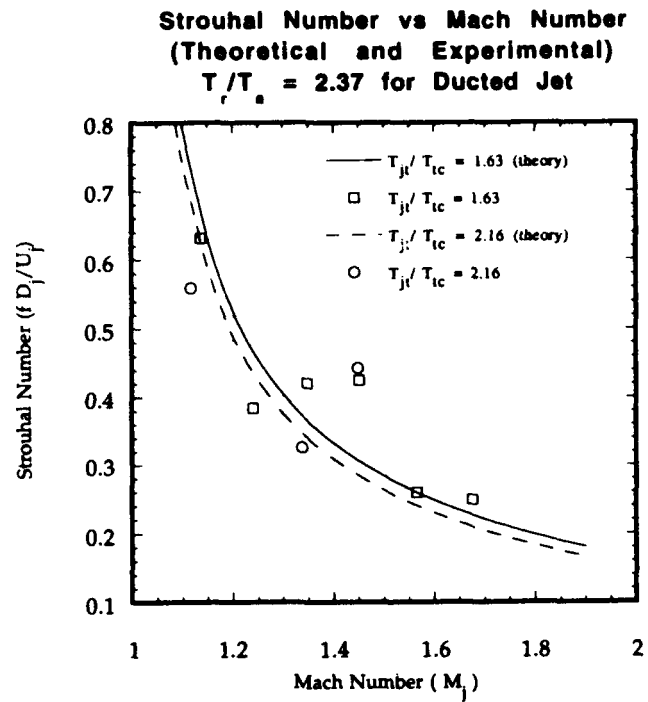Figure 4.22. Strouhal number as a function of Mach number for the unheated ducted jet.

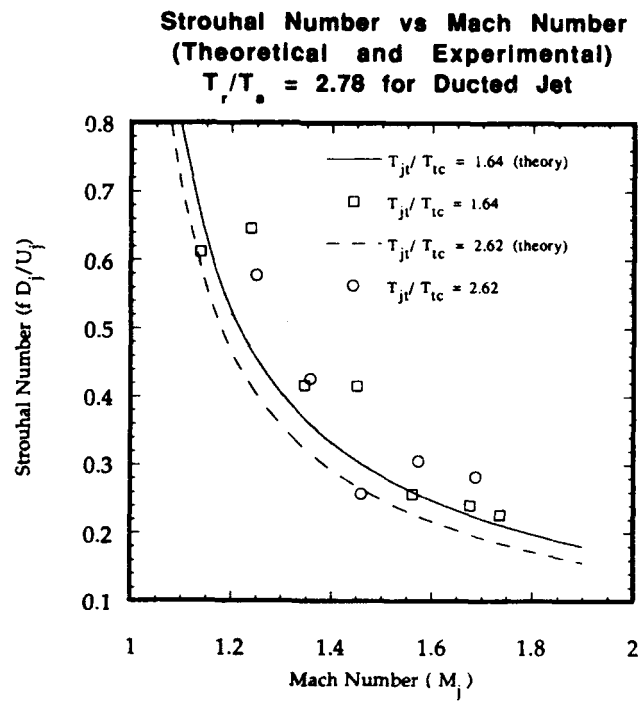**Figure 4.23. Strouhal number as a function of Mach number for the ducted jet at 750°F.**

Figure 4.24. Strouhal number as a function of Mach number for the ducted jet at 1,000°F.

4.3.2 Duct Resonance

As mentioned earlier, our previous experiments (Ref. 4.1) indicated that the high-level discrete tones measured in the model jet diffuser may be associated with duct resonance modes. It will not be possible to examine the variation of all tones with flow parameters. Some of the tones that we have definitely identified to be associated with the duct resonance modes will first be considered. From the acoustic data taken for underexpanded jet Mach numbers ranging from 0.8 to 1.79, with jet total temperatures (nominal) of 50, 400, 750, and 1,000°F, with various secondary mass flow rates, several trends in the acoustic spectra were noted. The most notable among these trends was a discrete tone that appeared in all test conditions near 1 kHz and a less well-defined hump that appeared in the range of 3.2 to 3.6 kHz. Another tone around 8.3 kHz appeared at higher Mach numbers for the unheated condition which switched to a higher frequency at higher temperatures. Since these trends appear to be present regardless of the Mach number or jet total temperature and their levels appear to change with Mach numbers and operating temperature ratios at selected operating conditions only, these tones are, in all likelihood, not due to the jet alone, but result from duct resonance. If suitable flow conditions are present, they may excite instability waves of the same frequency and then through a feedback mechanism (see Section 6 for more details) may produce a very large amplitude tone in the duct by locking on to the duct resonance frequencies.

To establish if the discrete tones referred to above were indeed the duct resonance tones and if so, what duct modes they corresponded to, the resonant frequencies of the diffuser were calculated for its various axial, radial, and azimuthal modes as a function of the temperature in the diffuser using the following equation (Ref. 4.1).

$$f_{lmn} \sqrt{\sigma_{nm}^2 + l^2 \left(\frac{\Pi D}{2L}\right)^2} \frac{a_0}{\Pi D}$$

$$l, n = 0, 1, 2, \dots$$
$$m = 1, 2, 3, \dots$$

(4.1)

where l, n, m are the longitudinal, azimuthal, and radial mode numbers, respectively. a_0 is the speed of sound inside the duct. σ_{nm} is the mth root of J_n' (prime denotes derivatives; i.e. J_n' (σ_{nm}) = 0.) J_n is the Bessel function of order n.

Note that in this terminology (referred to here as terminology 1) n = 0, m = 1 or (0,1) refers to a plane wave and n = 1, m = 1 or (1,1) refers to the circumferential mode, etc. Here m represents the mth zero of the derivatives σ_n'. This convention introduces confusion for those used to dealing with mode numbers in rectangular ducts where n and m represent the number of ...odes in the transverse pressure distribution. To avoid this confusion and to introduce a similar connotation for circular ducts, many authors use n to denote the number of cylindrical nodes in the pressure distribution. With this notation, a plane wave mode would have the (0,0) label in the circular and rectangular ducts. Likewise, n and m would have the same connotation, that is, the number of nodes in the respective direction (m: along the azimuthal and n: along the radial direction, in the transverse pressure distribution.) We refer to this terminology as terminology 2.

Values of frequencies calculated using the above equation for our ejector (L/D = 3) are presented in Table 4.1 for the zeroth axial mode ($l = 0$) and in Table 4.2 for the first axial mode ($l = 1$). Calculated frequencies are provided both for a duct with both ends open and for a duct with one end open and one end closed, since it was not known how the presence of the supersonic jet modified the boundary conditions at one end of the diffuser. Typical curves for various modes for the "both ends open" case were shown earlier in Fig. 4.18. Measured tone frequencies from most of the measured in-duct noise spectra are also superimposed in this figure. The comparison between the measured discrete tones and those calculated is excellent, indicating that the tones are indeed related to the duct resonance.

If one examines the case of the 1-kHz tones, one finds an extremely good match between the measured tones and the predicted ones. For the first axial or (1,0,0) mode of the diffuser, the predicted frequency varies from 0.86 kHz at 50°F to 1.2 kHz at 600°F (Fig. 4.25). Further, noting that all of the 0.99-kHz data corresponded to cold flow while all of the heated data corresponded to the slightly higher frequency of 1.18 kHz, one can see that the temperature trend was followed as well. (The analysis bandwidth was 128 Hz.) One would assume that since this mode is the lowest order mode that can be supported in an open duct like the one in the current test, that this mode would always be excited and this seems to be true of the experimental data as this 1-kHz tone is almost always present.

It should be added here that in our previous studies (Ref. 4.1), when we used a diffuser length different from that used in the present study, the 1-kHz tone was absent in the measured in-duct spectra. Also in the previous study, we found that in a test where we tried to excite various resonances in the diffuser by exciting the duct configuration with white noise injected from an acoustic driver with no flow passing through the duct system, a 1-kHz tone was found only when the length of the diffuser was same as that used in the present study (e.g., L/D = 3).

The other two prominent tones that were noticed in these spectra and those measured in the previous study by the authors were at nominal frequencies of 3.6 and 8.3 kHz. These are associated with the first and the second radial or transverse modes of the diffuser.

In summary, the dominant tones observed at the in-duct microphone location are either those associated with the jet screech or those associated with the duct resonances, and we have been able to identify them by comparing them with the predicted frequencies. This we have done by calculating the screech frequencies using the screech equation developed by Tam and provided above and by calculating the duct resonance frequency by using the standard organ pipe resonance frequency equation involving terms with Bessel's function and also provided above

4.3.3 Mach Number Dependence of Discrete Tone Amplitudes

A careful examination of all of the prominent tone levels will indicate that these levels increase monotonically with increasing Mach number. This is shown in Fig. 4.26 for a nominal frequency of 1 kHz. The level of this tone is approximately 123 dB at a jet Mach number of 0.8 and steadily increases to 139 dB at a jet Mach number of 1.7. It is interesting to note that the levels appear to be fairly independent of the jet total temperature and remain in a narrow band of

Table 4.1 Duct resonance frequencies for the zeroth axial mode. (The numbers 0, 1, 2, ... typed in bold represent the azimuthal mode number n in the horizontal row and radial mode number m in the vertical column. Terminology 2 discussed earlier applies.)

gamma	1.40		Duct dia (ft)	0.21833333	
g	32.174		Duct length (ft)	0.655	
gas constant	53.33		Axial Mode	0	
Temp (°F)	75		Freq Div (Hz)	1000	
Temp (R)	535				
speed of sound	1133.67	ft/s			
	m = 0	**m = 1**	**m = 2**	**m = 3**	**m = 4**
			σmn		
n = 0	0	3.8317	7.0156	10.1735	13.3237
n = 1	1.8412	5.3314	8.5363	11.706	14.8636
n = 2	3.0542	6.7061	9.9695	13.1704	16.3475
n = 3	4.2012	8.0152	11.3459	14.5859	17.7888
n = 4	5.3176	9.2824	12.6819	15.9641	19.196
n = 5	6.4156	10.5199	13.9872	17.3128	20.5755
open open cylinder		(both ends open)			
	m = 0	**m = 1**	**m = 2**	**m = 3**	**m = 4**
		(frequency values in kHz)			
n = 0	0.000	6.333	11.595	16.815	22.021
n = 1	3.043	8.812	14.109	19.348	24.566
n = 2	5.048	11.084	16.478	21.768	27.019
n = 3	6.944	13.247	18.752	24.107	29.401
n = 4	8.789	15.342	20.961	26.385	31.727
n = 5	10.604	17.387	23.118	28.614	34.007
closed open cylinder		(one end open, one end closed)			
	m = 0	**m = 1**	**m = 2**	**m = 3**	**m = 4**
		(frequency values in kHz)			
n = 0	0.433	6.348	11.603	16.820	22.026
n = 1	3.074	8.822	14.115	19.352	24.570
n = 2	5.066	11.092	16.483	21.772	27.022
n = 3	6.957	13.255	18.757	24.111	29.404
n = 4	8.800	15.348	20.965	26.389	31.730
n = 5	10.612	17.393	23.122	28.618	34.010

Table 4.2 Duct resonance frequencies for the first axial mode. (The numbers 0, 1, 2, ... typed in bold represent the azimuthal mode number n in the horizontal row and radial mode number m in the vertical column. Terminology 2 discussed earlier applies.)

gamma	1.40		Duct dia (ft)	0.21833333	
g	32.174		Duct length (ft)	0.655	
gas constant	53.33		Axial Mode	1	
Temp (°F)	75		Freq Div (Hz)	1000	
Temp (R)	535				
speed of sound	1133.67	ft/s			
	m = 0	**m = 1**	**m = 2**	**m = 3**	**m = 4**
			σ_{mn}		
n = 0	0	3.8317	7.0156	10.1735	13.3237
n = 1	1.8412	5.3314	8.5363	11.706	14.8636
n = 2	3.0542	6.7061	9.9695	13.1704	16.3475
n = 3	4.2012	8.0152	11.3459	14.5859	17.7888
n = 4	5.3176	**9.2824**	12.6819	15.9641	19.196
n = 5	6.4156	**10.5199**	13.9872	17.3128	20.5755
open open cylinder	(both ends open)				
	m = 0	**m = 1**	**m = 2**	**m = 3**	**m = 4**
		(frequency	values	in	kHz)
n = 0	0.865	6.392	11.628	16.837	22.038
n = 1	3.164	8.854	14.135	19.367	24.582
n = 2	5.122	11.118	16.500	21.785	27.033
n = 3	6.997	13.276	18.772	24.123	29.414
n = 4	8.831	15.366	20.978	26.400	31.739
n = 5	10.639	17.409	23.134	28.628	34.018
closed open cylinder	(one end open, one end closed)				
	m = 0	**m = 1**	**m = 2**	**m = 3**	**m = 4**
		(frequency	values	in	kHz)
n = 0	0.865	6.392	11.628	16.837	22.038
n = 1	3.164	8.854	14.135	19.367	24.582
n = 2	5.122	11.118	16.500	21.785	27.033
n = 3	6.997	13.276	18.772	24.123	29.414
n = 4	8.831	15.366	20.978	26.400	31.739
n = 5	10.639	17.409	23.134	28.628	34.018

2-3 dB regardless of the jet total temperature. Similar results were obtained for two other prominent frequencies i.e., 3.6 kHz, and 8.3 kHz (nominal values), the data for which are shown in Figs. 4.27 and 4.28, respectively. Developing a theoretical model to predict this behavior is beyond the scope of this work, but intuitively one would expect that as the excitation levels increase as a result of increased broadband noise of the jet, more energy will be injected into the resonance of the acoustic modes.
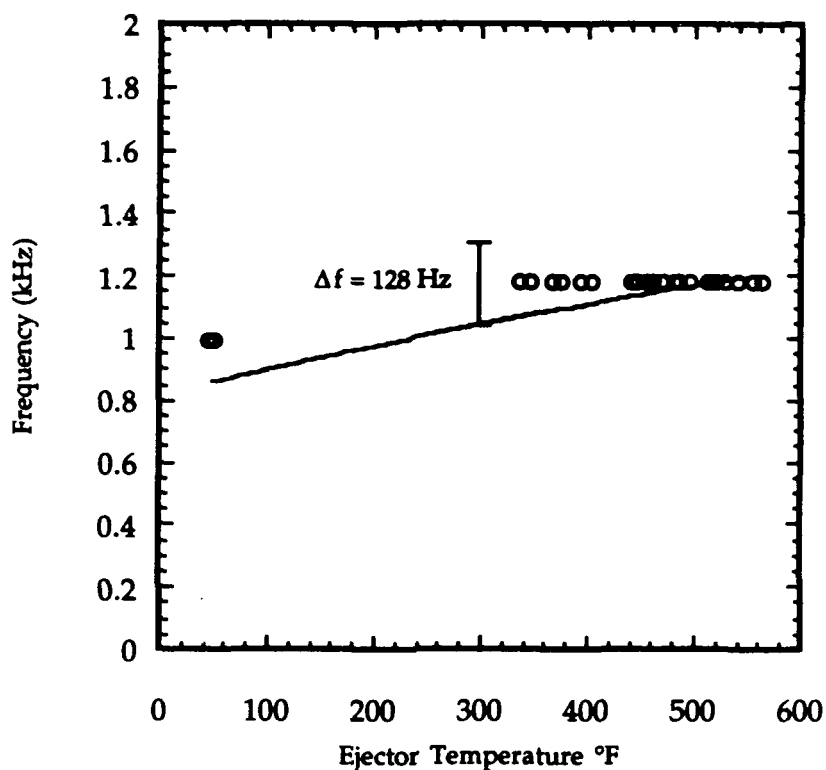
Figure 4.25. Predicted diffuser resonant frequency ranges and measured results for first axial mode as a function of ejector temperature.
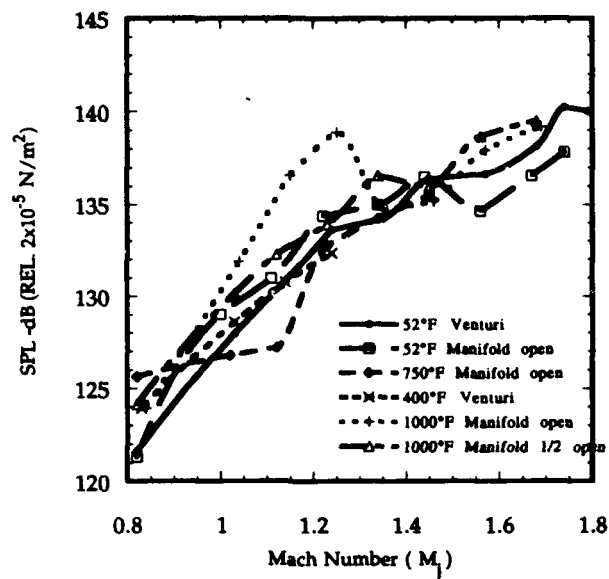
Figure 4.26. Sound Pressure Level of the first axial mode resonance as a function of Mach number.
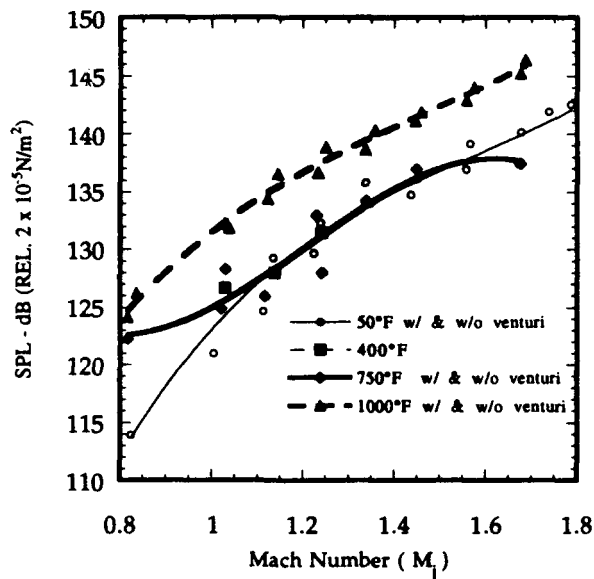
Figure 4.27. Sound Pressure Level for the 3.4-kHz tones as a function of Mach number.
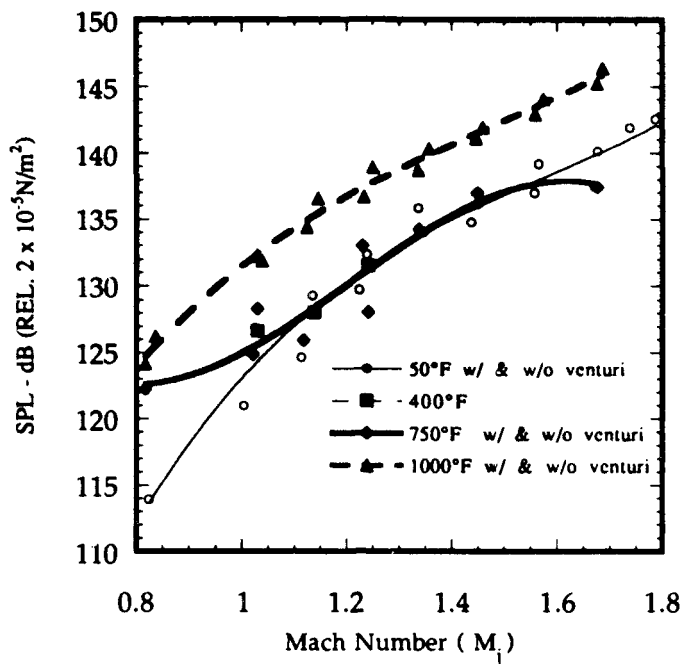
Figure 4.28. Sound Pressure Level for the 8.3-kHz tones as a function of Mach number.

4.3.4 Temperature Dependence of Discrete Tone Amplitudes

All of the spectra shown here for L/D of 3 (ejector length was three times its diameter) displayed a tone at a nominal frequency of 1 kHz for the unheated condition. As pointed out above, this tone is associated with the first axial mode frequency of the diffuser. How the amplitude measured at the in-duct microphone at this frequency changes with increasing temperature is shown in Fig. 4.29. Clearly, there is little change by increasing the temperature in the amplitude of this frequency.

Similar plots obtained for the nominal frequency of 3.4 kHz are shown in Fig. 4.30. In this case, the result of heating the flow is to increase the noise levels by up to 5 to 7 dB at all Mach numbers.

4.3.5 In Search of Conditions That Produce High-Amplitude Tones

All of the data presented so far show that, indeed, discrete tones are present in the in-duct microphone signature and that many of these tones increase with increasing jet Mach number and temperature ratio. But with the exception of the unheated condition of $M_j = 1.68$ and 1.74 where SPLs of 152.2 dB and 155.5 dB were measured at a frequency of 8.361 Hz (See Figs. 4.15 and 4.17), the highest amplitudes in other measured spectra were not as high as we had expected.

89

Based upon the tone amplitudes measured in the AEDC facility (Ref. 6.2), we were expecting to measure tone levels as high as 170 dB.

It is because of this lack of high tonal amplitude that AEDC personnel suggested that a better simulation of the AEDC diffuser is needed. Recall that the AEDC diffuser is conical (diverging in the direction of the flow) and we used a cylindrical diffuser for the case of obtaining theoretical and experimental data for identical configurations. The baffle orifice plate or diffuser insert described earlier (See Fig. 2.17) was installed to examine if there were major changes in the measured in-duct spectra. Two inserts with thicknesses of 0.77 in. and 0.105 in. and inner hole diameter of 1.20 in. as shown in Fig. 4.31 were installed at the inlet of the diffuser. The data for the thin insert are shown in Figs. 4.32 - 4.34 for M_j = 0.81, 1.34, and 1.56, respectively. Up to 6 to 7 dB increase is obtained in the highest tone amplitudes, although the broadband noise amplitude measured by the test cell microphone is considerably lower now. This is attributable to the fact that the mixing noise and other noise sources located downstream of the diffuser insert are being shielded, thus reducing the noise reaching the microphone located upstream of jet exit in the test cell. By the same token, one could argue that it implies that the much higher level tones are also being generated in the diffuser, much of which is being shielded by the diffuser insert as the tone sound travels from the diffuser to the test cell microphone. (See the sketch on the top right corner of any plot containing in-duct spectra for the location of the microphone.)

It is found as with the tones without the diffuser insert, the tones with the diffuser insert also increase in amplitude with temperature. This is shown for the thin insert in Figs. 4.35 - 4.37 for three Mach numbers.

Finally, Figs. 4.38 - 4.40 compare the in-duct spectra for the thin and thick diffuser inserts. Except for minor switching of some discrete tone frequencies, no major changes are obtained in the tone amplitudes.

In summary, the exercise carried out with diffuser inserts indicated that the noise levels of the tones may be higher for a configuration that closely simulates the inlet and the exit areas of the AEDC diffuser. Yet our result did not reproduce the high amplitudes that we were expecting, as alluded to above. Another test was therefore carried out to resolve this issue further as discussed below.

4.3.6 Tone Amplitude Measurements in the Ejector

All of the in-duct measurements reported up to this point were acquired at a microphone located upstream of the nozzle exit above the jet supply duct and inside the test cell. Although when we started the program, we had intended to carry out extensive measurements of sound field inside the ejector, changes in the scope of the experiments during the course of the investigation prevented us from carrying out these measurements. In retrospect, it was a mistake not to continue with ejector in-duct transducer measurements, as we have been forced to draw conclusions about the tone amplitudes based upon the measurements by a microphone located outside the diffuser duct. Since the diffuser has a diameter of 2.62 in., much of the sound at

frequencies higher than that corresponding to first longitudinal mode will decay significantly before reaching our microphone located in the test cell. For a 2.62-in.-diam duct, the cut-off frequency for the plane wave mode is 3.02 kHz at 50°F. Thus, even if higher level tones are generated in the diffuser, they may not appear that high at our test cell microphone location.

To confirm this, we mounted a flush-walled microphone on the diffuser. To do this, we had to remove the large test cell section located downstream of the plate that holds the diffuser in place. As these experiments were conducted very near the end of the program, only limited tests were conducted and for unheated test conditions only. Tone levels as high as 166 dB were obtained as shown in Figs. 4.41 and 4.42. These figures also show the test configuration and the relative location of the microphone on the top right corner.

Although these data are for the high Mach numbers, there is no reason why the tone levels could not be as high at low Mach numbers if the combined Mach number and jet temperatures were just right to produce coupling between the jet instabilities and the duct modes. Considerably more discussion on this topic appears later in Section 6.
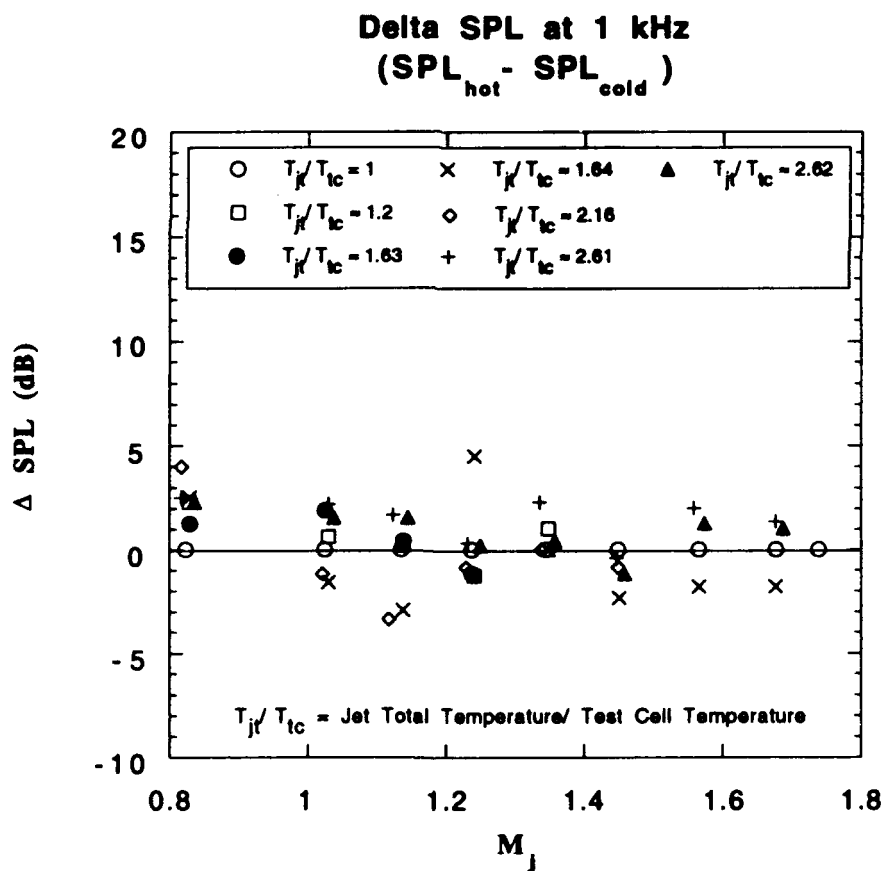
Figure 4.29. Effect of temperature ratio on the 1-kHz tone. (ΔSPL = SPL$_{hot}$ - SPL$_{cold}$)
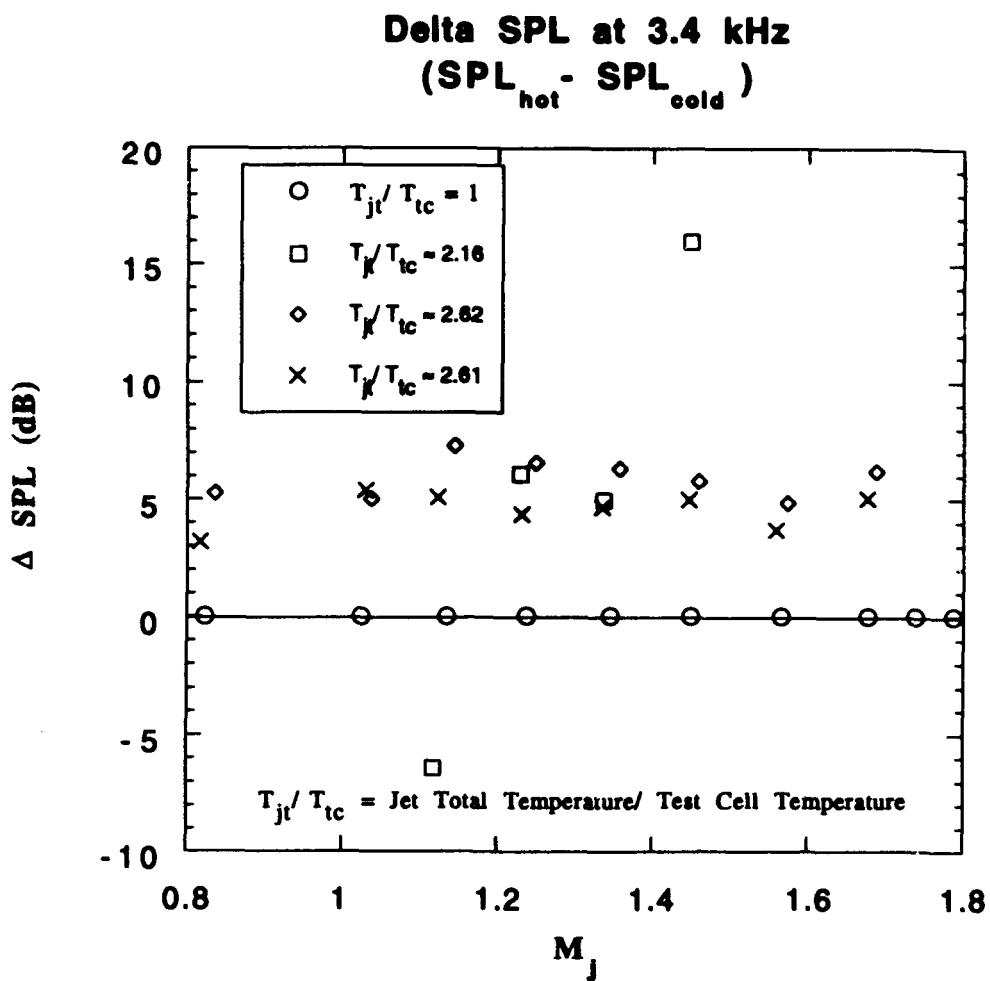
Figure 4.30. Effect of temperature ratio on 3.4-kHz tone. (ΔSPL = SPL$_{hot}$ - SPL$_{cold}$)

Thick Insert   **Thin Insert**
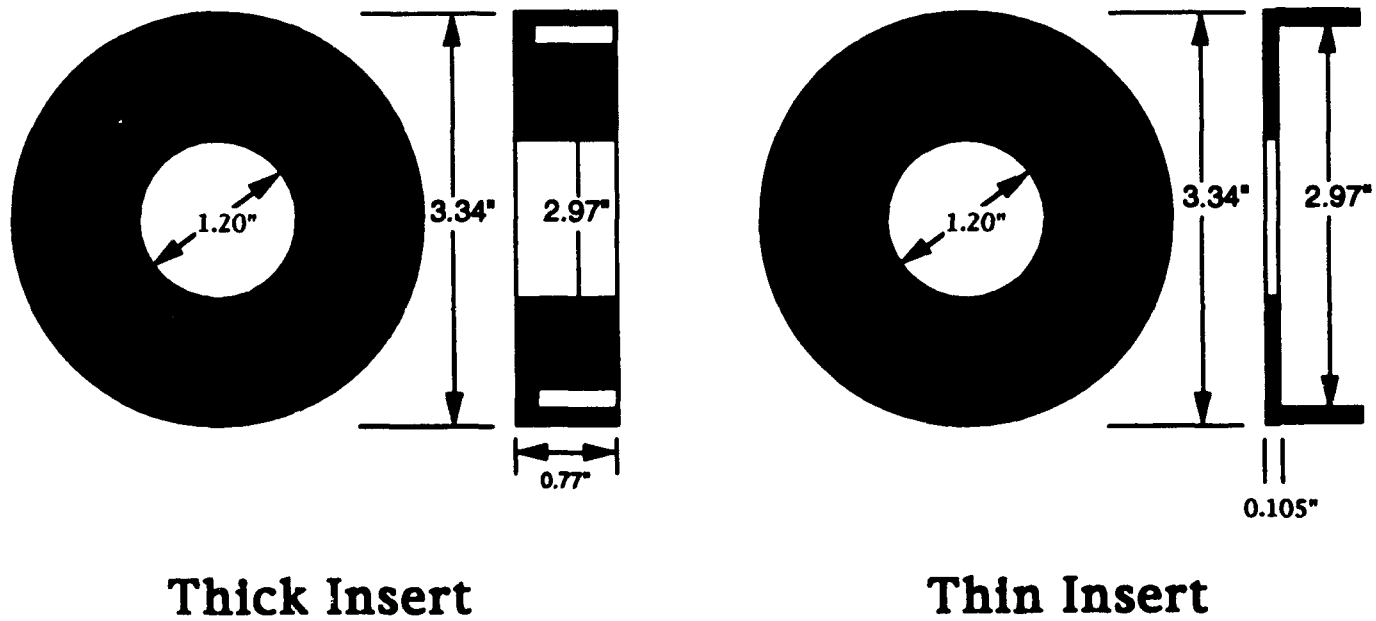
Figure 4.31. Schematic of thick and thin orifice baffle inserts.
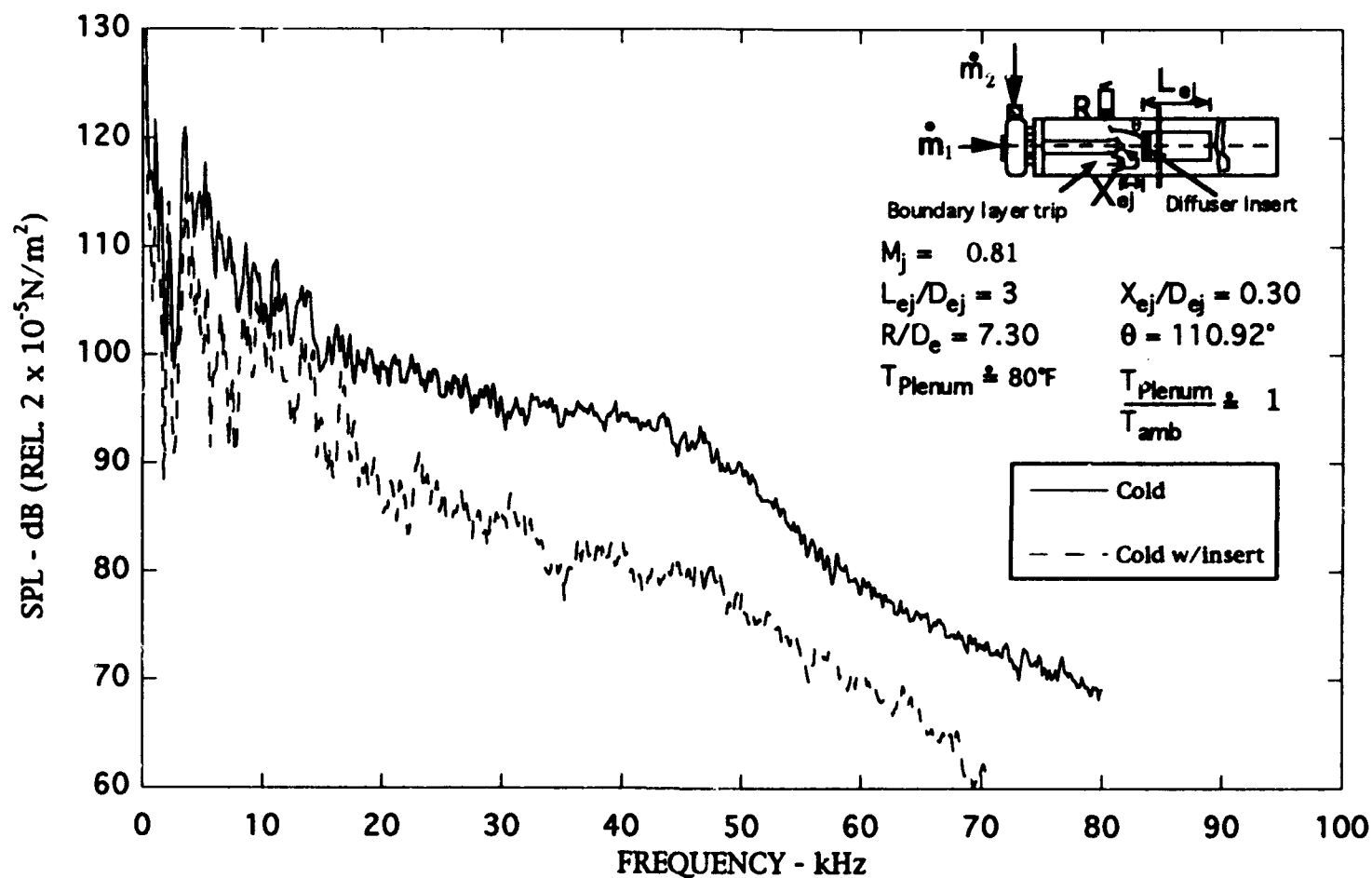
Figure 4.32. Narrow band (Δf = 128 Hz) noise spectra of the ducted jet w/ &w/o diffuser insert, M_j = 0.81.
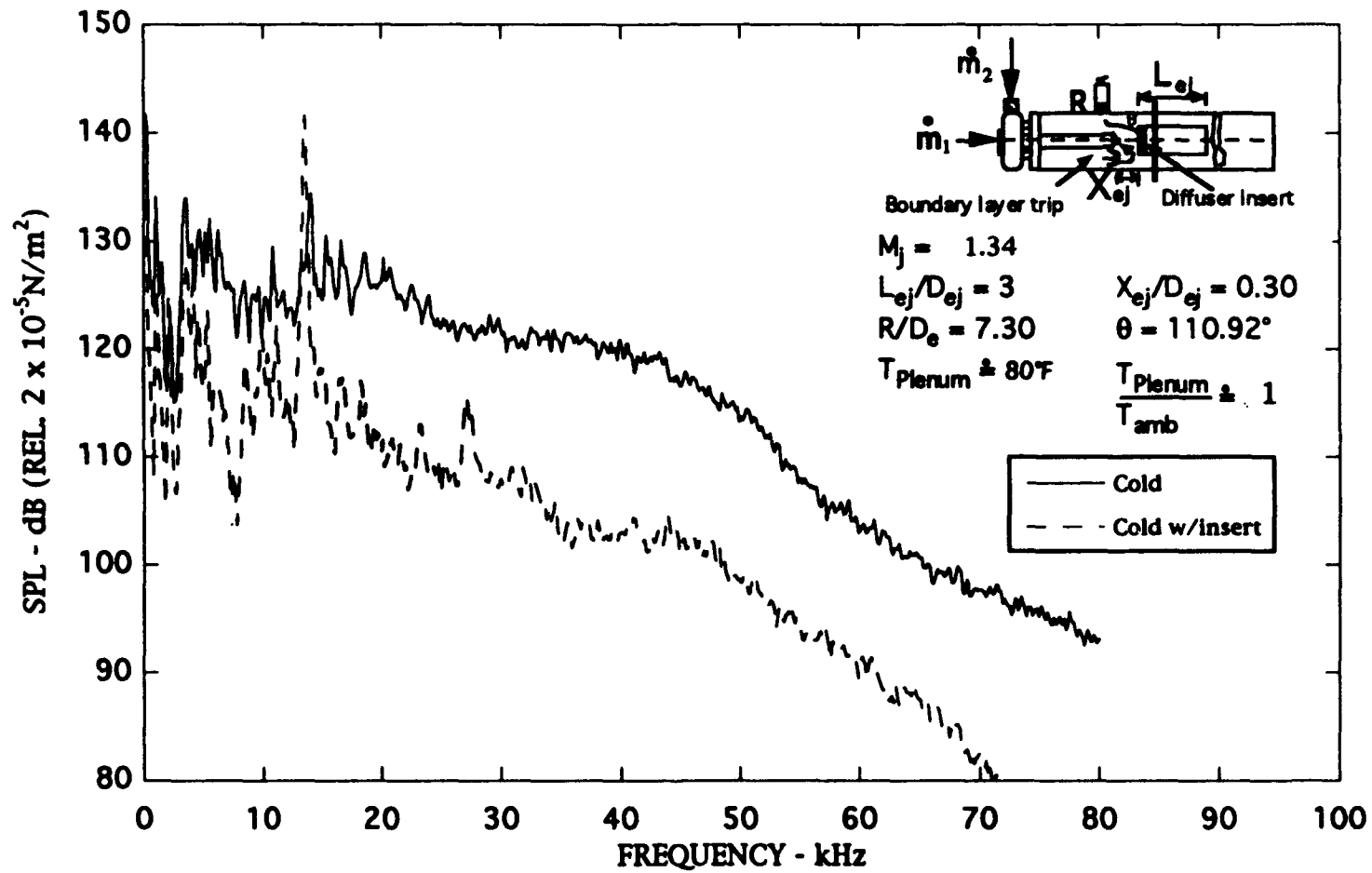
Figure 4.33. Narrow band (Δf = 128 Hz) noise spectra of the ducted jet w/ &w/o diffuser insert, M_j = 1.34.
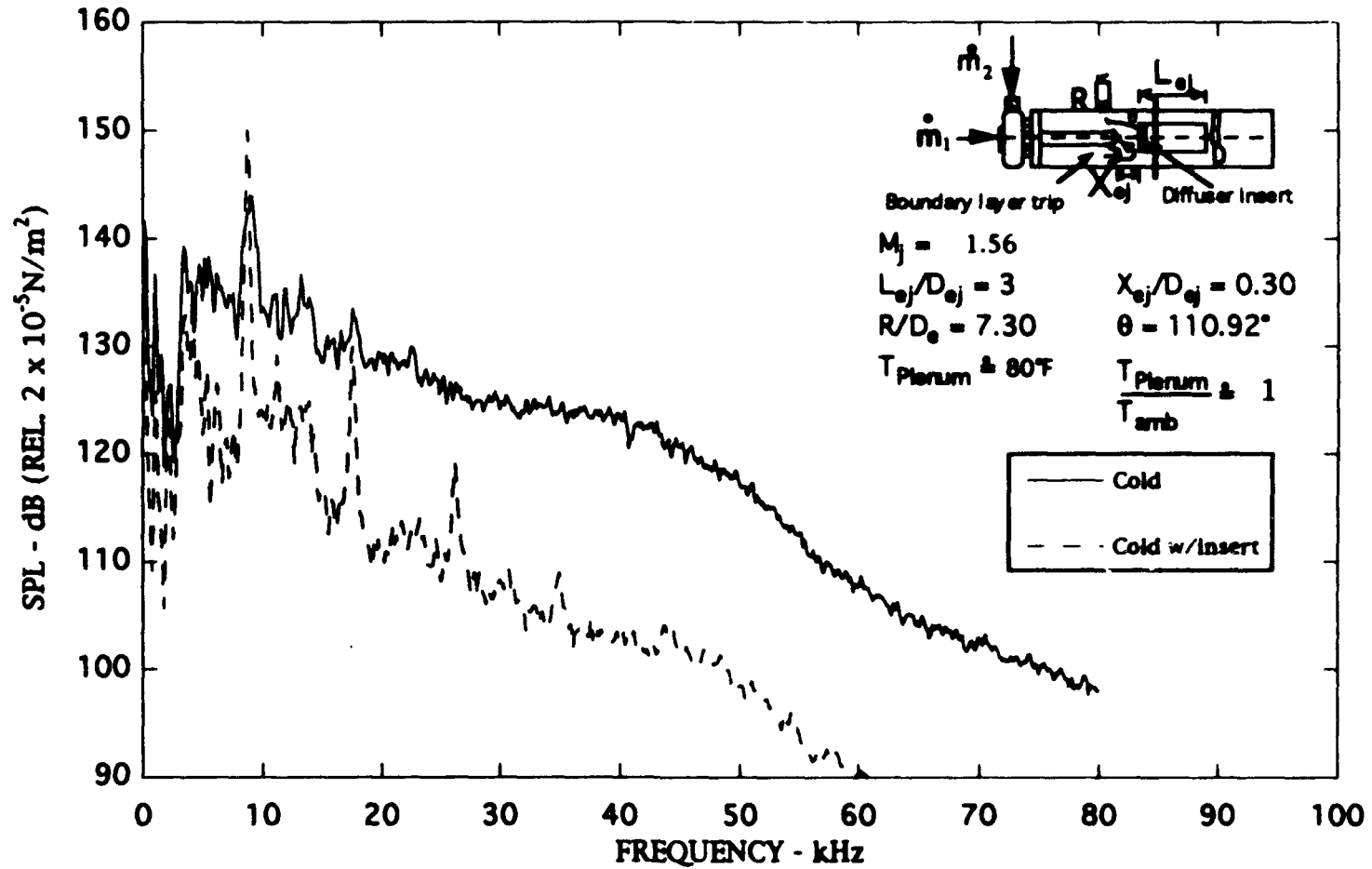
Figure 4.34. Narrow band (Δf = 128 Hz) noise spectra of the ducted jet w/ &w/o diffuser insert, M_j = 1.56.
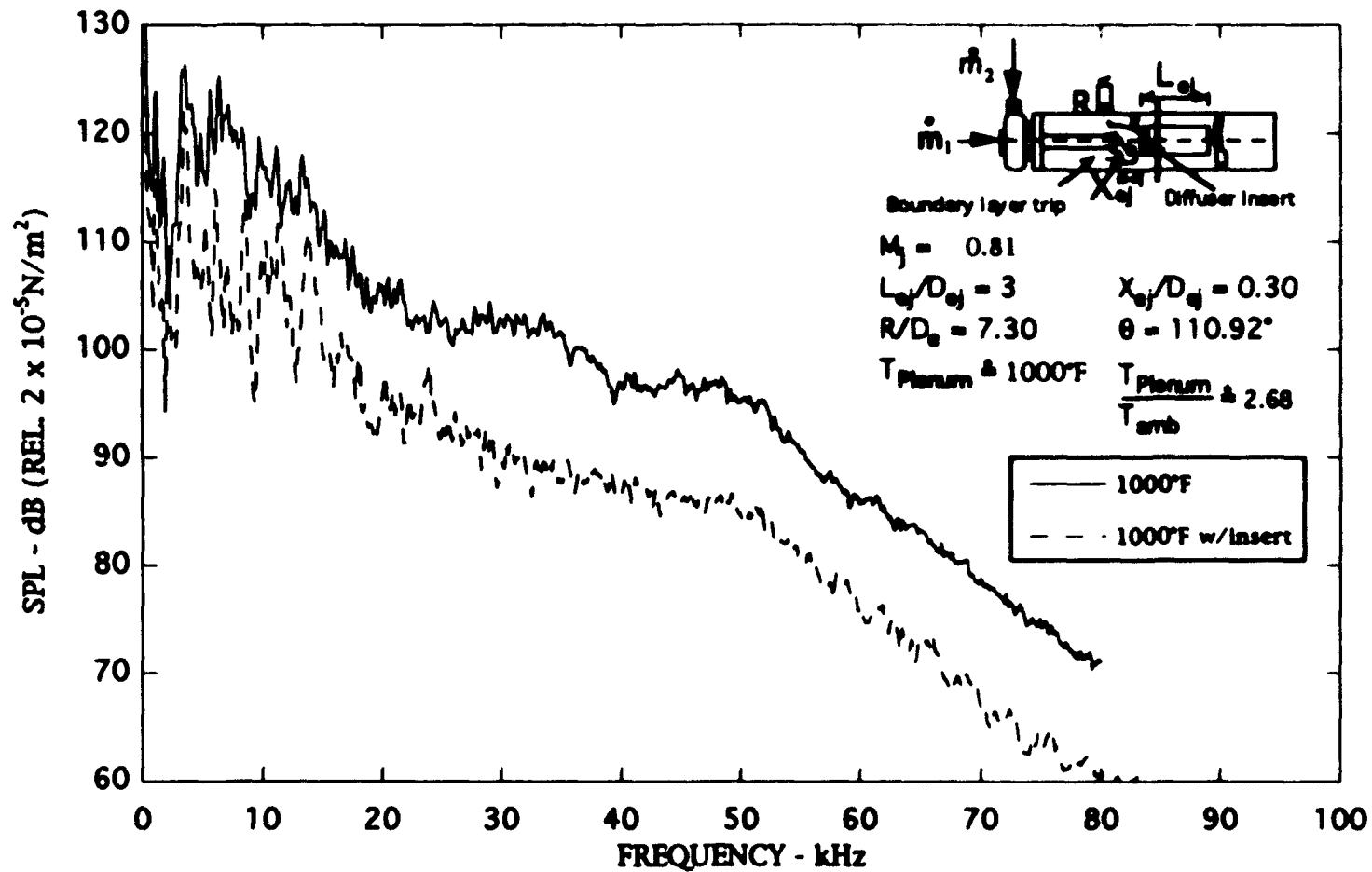
Figure 4.35. Narrow band ($\Delta f = 128$ Hz) noise spectra of the ducted jet w/ &w/o diffuser insert, $M_j = 0.81$.
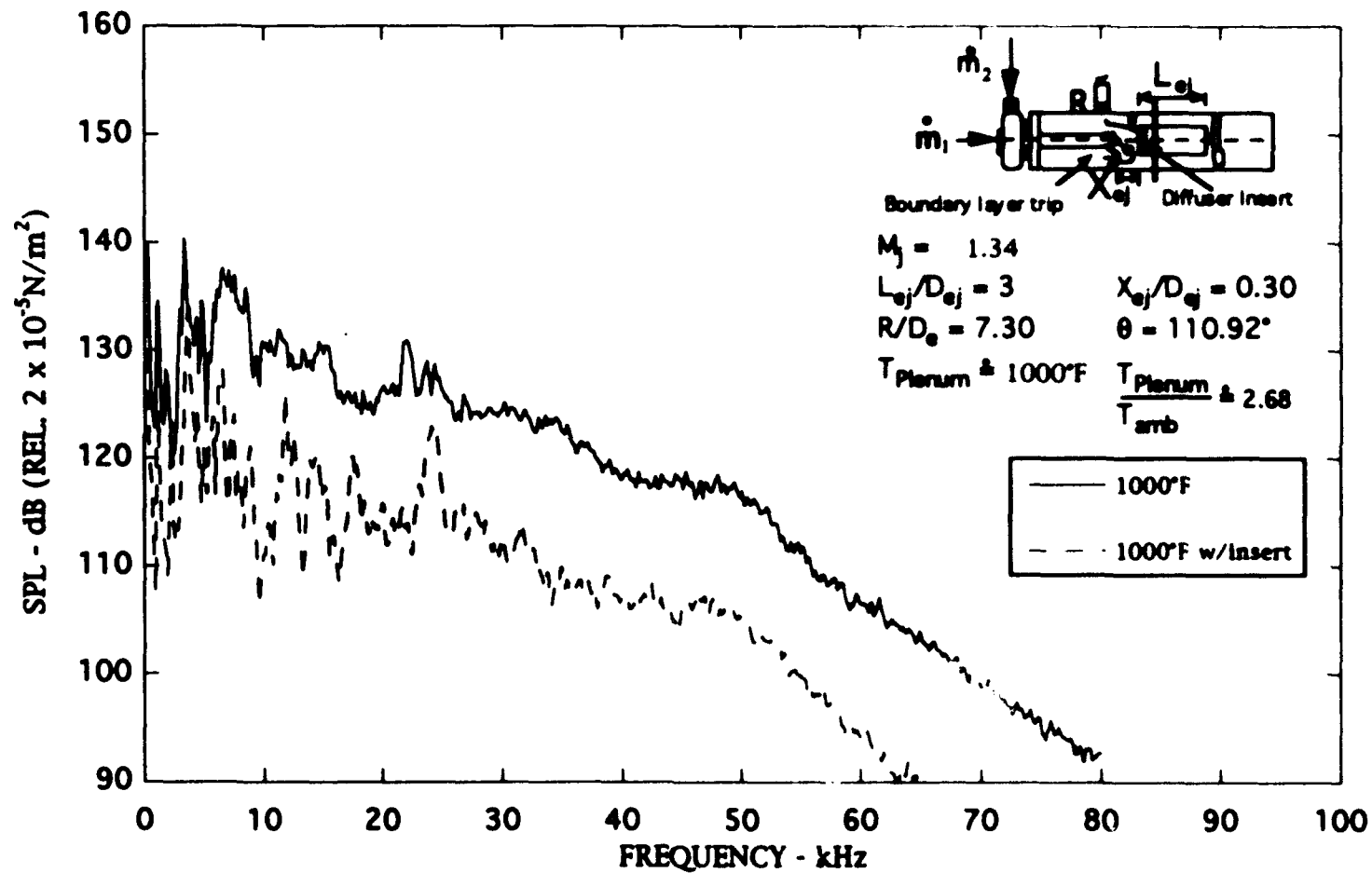
Figure 4.36. Narrow band (Δf = 128 Hz) noise spectra of the ducted jet w/ &w/o diffuser insert, M_j = 1.34.
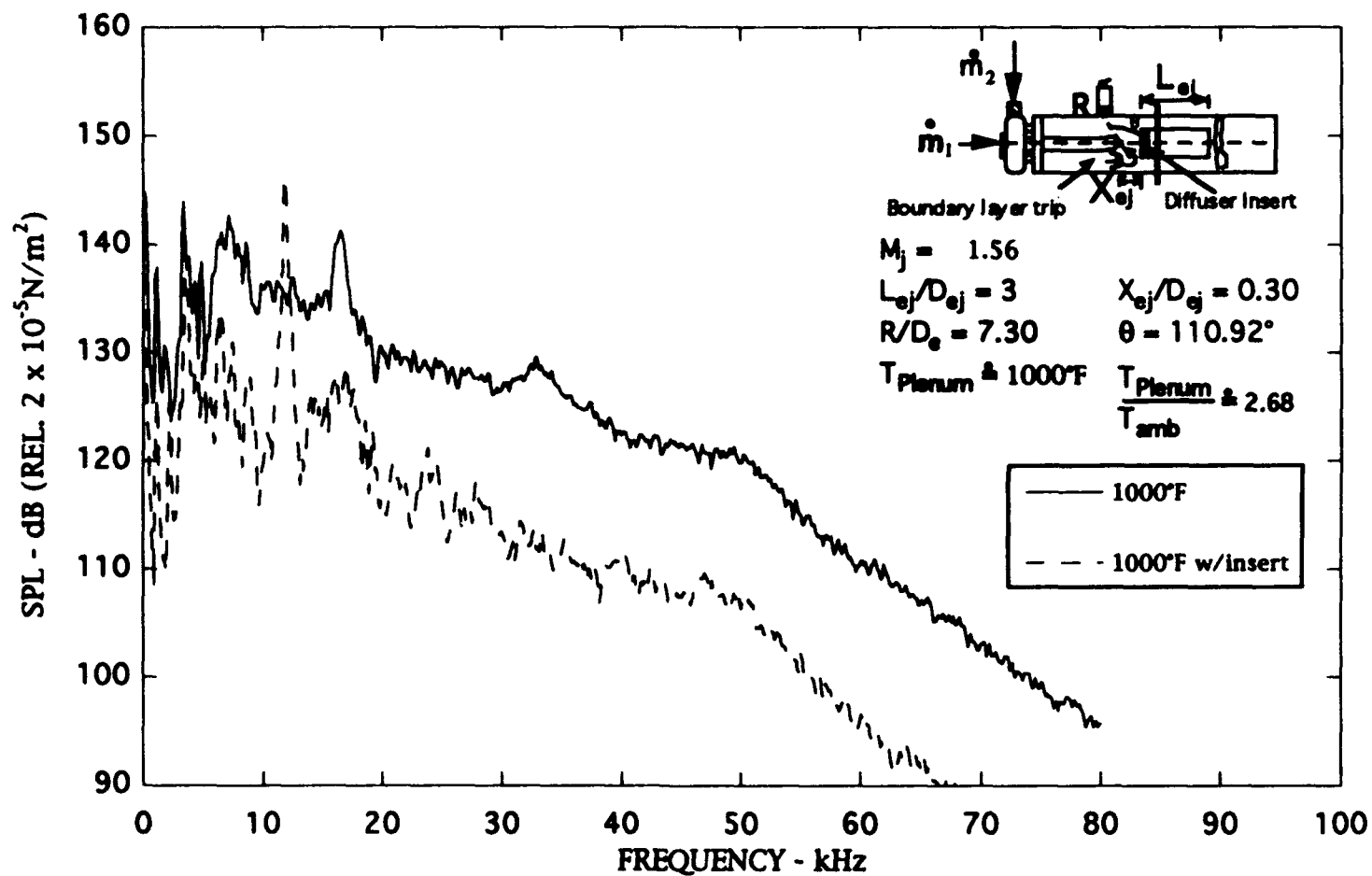
Figure 4.37. Narrow band (Δf = 128 Hz) noise spectra of the ducted jet w/ &w/o diffuser insert, M_j = 1.56.
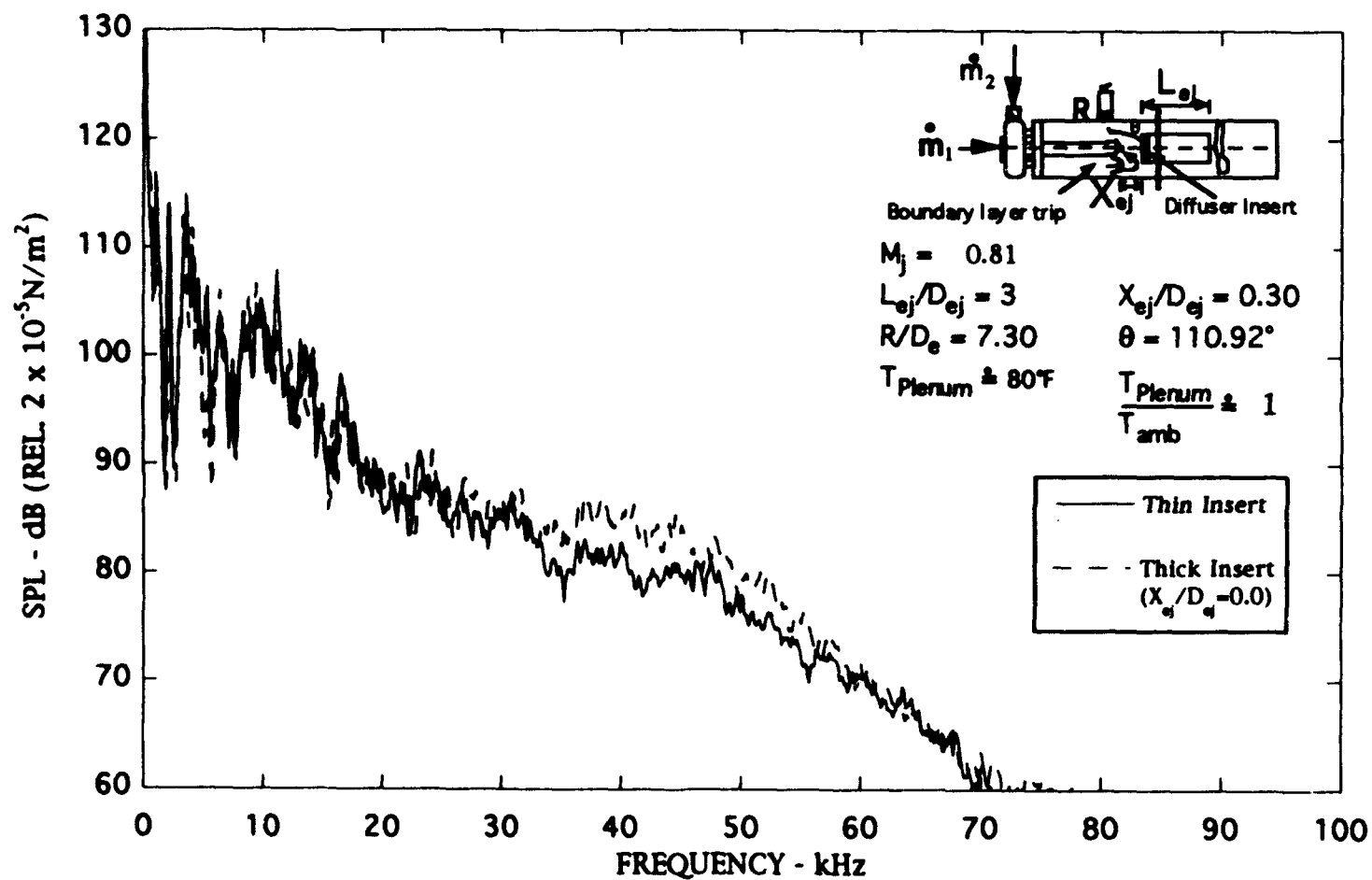
Figure 4.38. Narrow band (Δf = 128 Hz) noise spectra of the ducted jet with diffuser insert, M_j = 0.81.
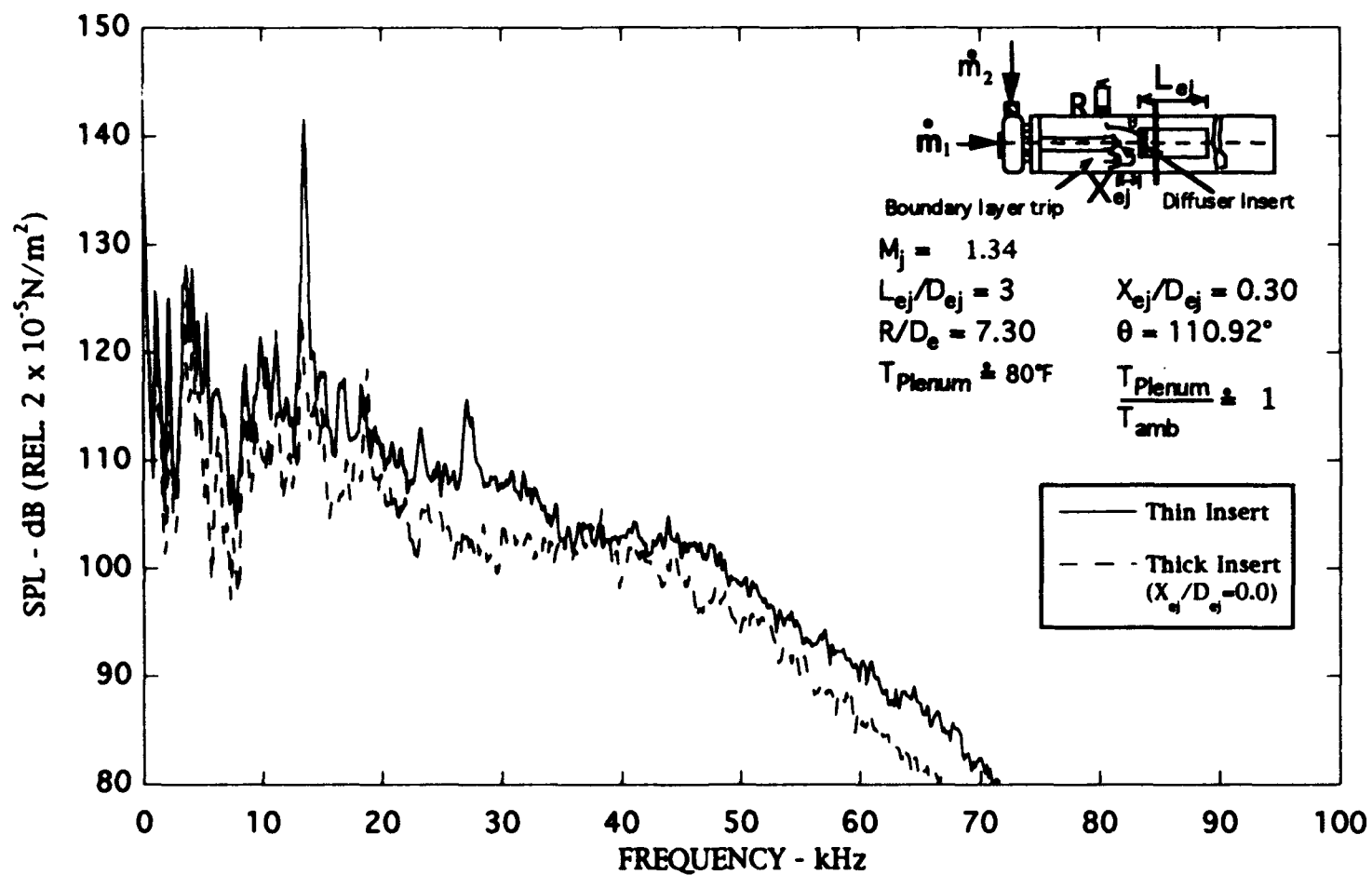
Figure 4.39. Narrow band ($\Delta f = 128$ Hz) noise spectra of the ducted jet with diffuser insert, $M_j = 1.34$.
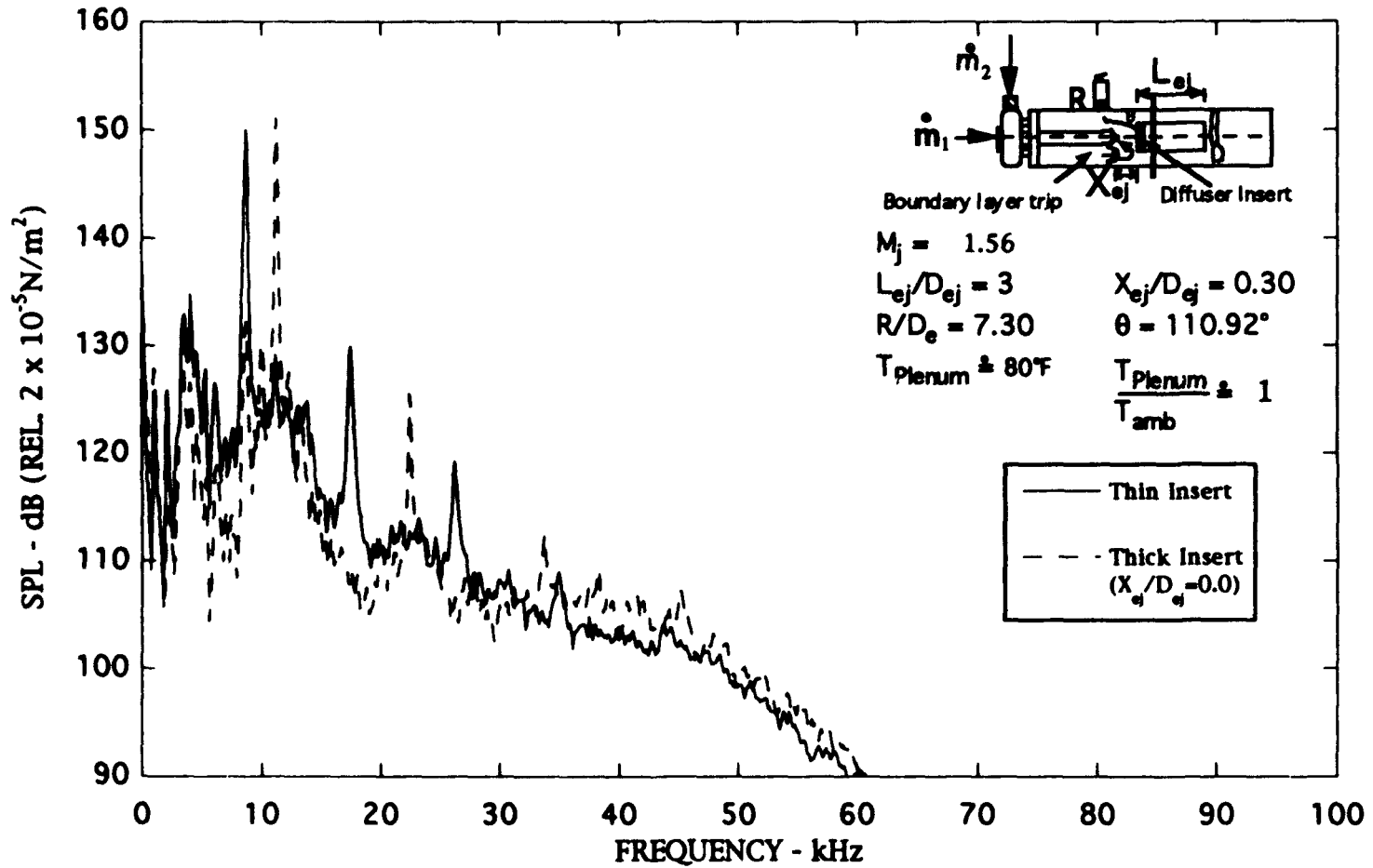
Figure 4.40. Narrow band ($\Delta f = 128$ Hz) noise spectra of the ducted jet with diffuser insert, $M_j = 1.56$.
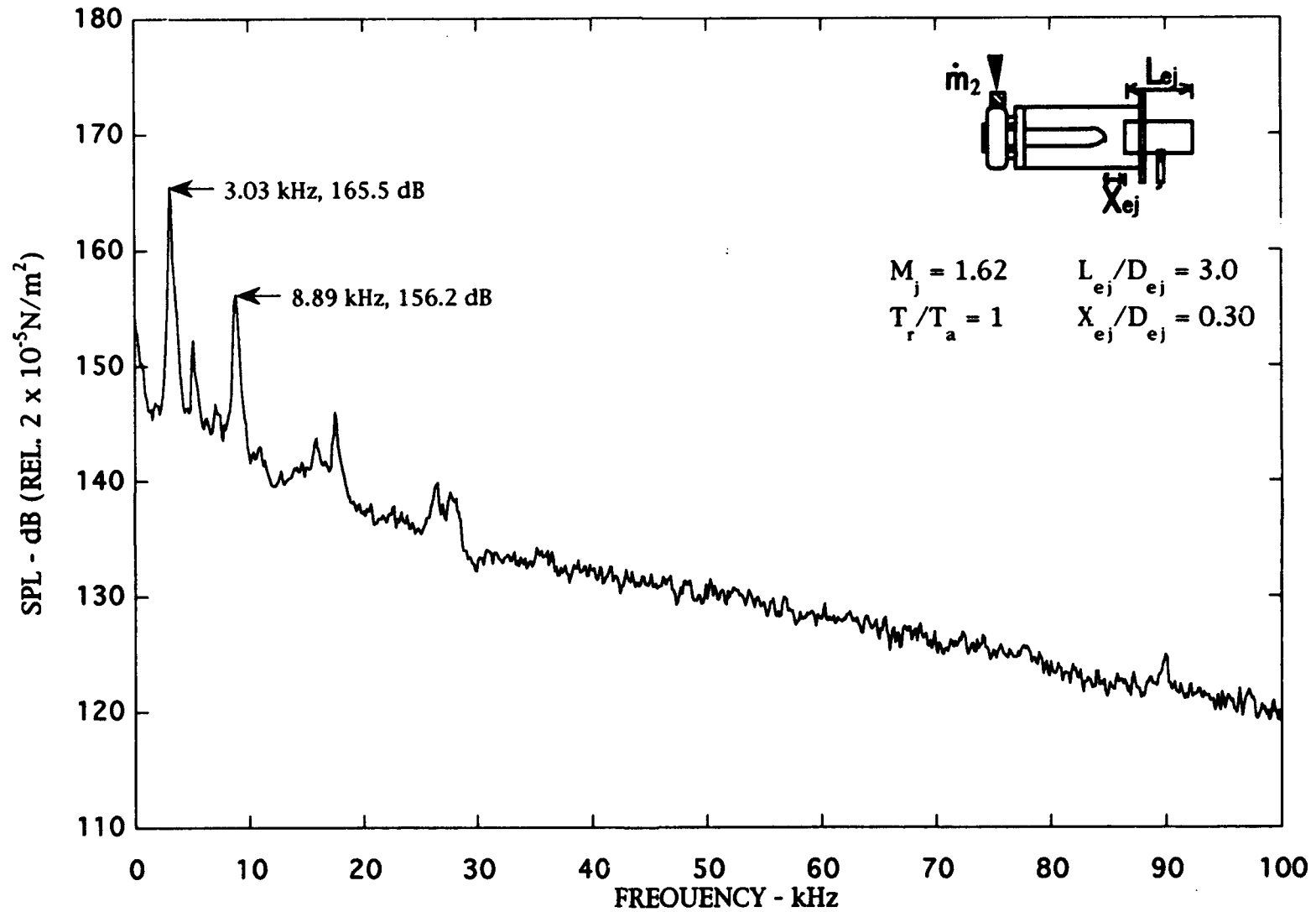
Figure 4.41. Narrow band ($\Delta f = 128$ Hz) noise spectra of tripped and ducted jet with open mainfold, $M_j = 1.62$.
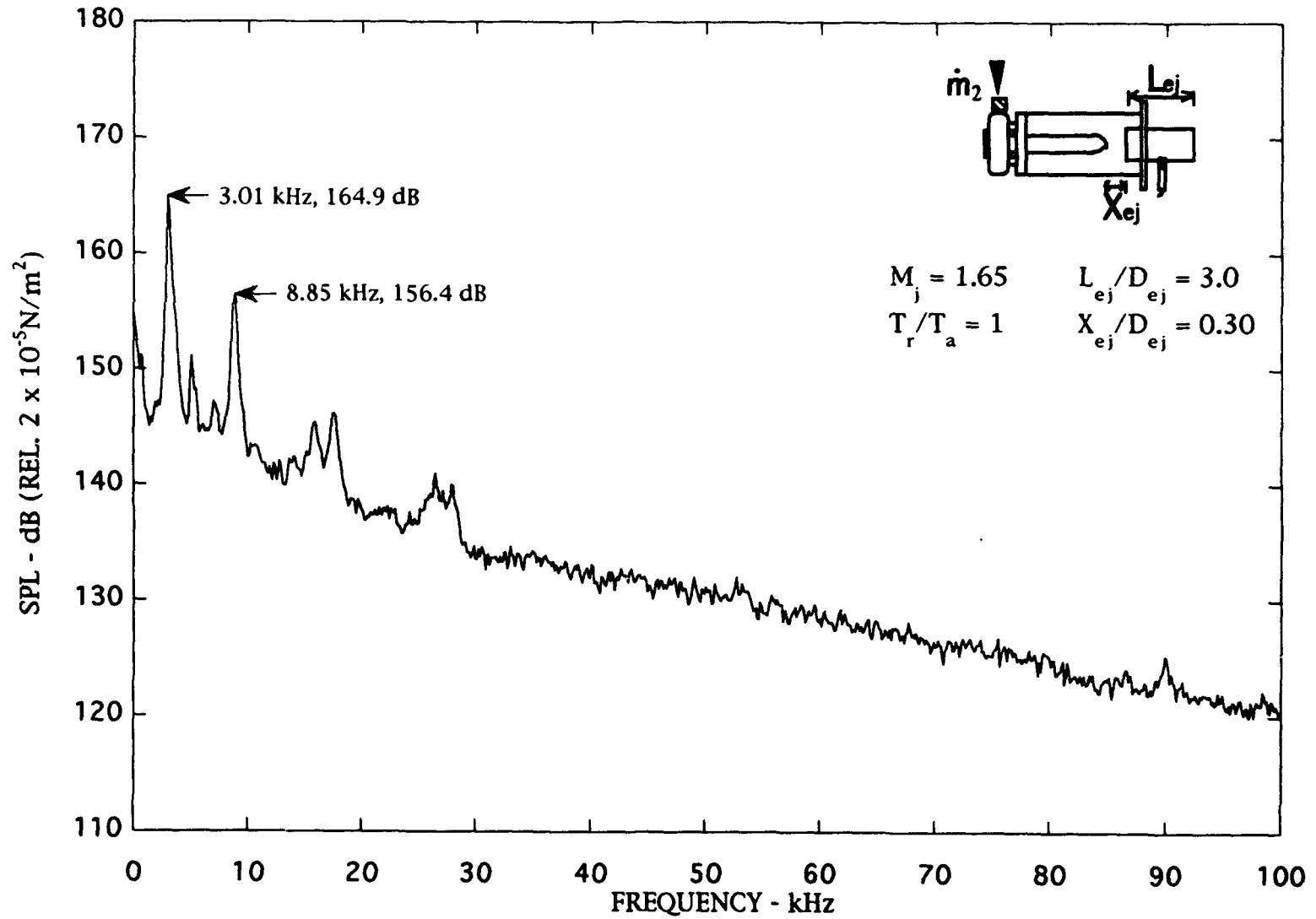
Figure 4.42. Narrow band ($\Delta f = 128$ Hz) noise spectra of tripped and ducted jet with open manifold, $M_j = 1.65$.

5.0 SELECTED SPIN-OFF RESULTS

To support the experimental work reported earlier, several additional tests were conducted. For example, because of a change in the scope of the present work during the course of this investigation, the high-temperature transducers equipped with water jackets were mounted on the diffuser wall but could not be used because of the budgetary and time constraints. Some valuable information on the method of their calibration was, however, obtained and is reported in Appendix E. Similarly, Appendix F includes the description of the diffuser fitted with water jackets, and Appendix G contains results of additional tests on the effect of L/D.

6.0 SUMMARY AND DISCUSSION

6.1 INTRODUCTION

The main goal of this project was to determine the mechanism responsible for engine test cell resonance observed at the AEDC facility (Ref. 6.1). Resonance occurred for both axisymmetric and rectangular jets. In this report consideration is confined only to axisymmetric jets.

Figure 6.1 shows the cross-section of a baseline test cell configuration. The jet from the engine issues into the test cell through an opening of a cylindrical/conical duct. A strong resonance at 140 Hz is reported under the following operating condition.

Jet Mach Number $(M_j) \cong 1.3$

Total temperature of the jet $(T_r) \cong 1,800^{\circ}R$

Temperature of gas around jet $\cong 250^{\circ}F$

Diameter of jet $= 2$ ft

Prior to the beginning of the present project, a 1/12-scaled model experiment and theoretical analysis were carried out at the University of Tennessee Space Institute (UTSI) (Ref. 6.2). The experiments were performed with jet total temperature equal to room temperature (cold jet). However, it was reported that no strong resonance tone at 140 Hz (full scale) was observed.

In order not to duplicate the UTSI effort, it was decided that a more traditional type test cell was to be used in the present investigation. That is, instead of the cylindrical/conical duct piece, a cylindrical ejector duct is used. Earlier, Abdel-Fattah and Favaloro (Ref. 6.3) had carried out a series of experiments using a similar flow configuration (See Fig. 6.2). The purpose of their experiments was to study thrust and mixing enhancement. Thus, the duct-to-nozzle diameter ratio, as well as the length-to-diameter ratio of the ejector duct are different from the present project. Although the geometry of the test facility is proportionally not the same as that of the present study, their measured results are of interest to the current investigation. The Abdel-Fattah and Favaloro experiments clearly demonstrated that by putting a jet inside an ejector, a large number of the normal duct acoustic modes of the ejector were simultaneously excited. Figure 6.3 shows the measured tone frequencies as a function of the pressure ratio of the jet at five duct-to-nozzle area ratios. The discrete tone frequencies match closely with the calculated normal mode frequencies of the ejector. Abdel-Fattah and Favaloro observed that the thrust of an ejector

reached maximum at a special pressure ratio. At the maximum thrust condition, they found optically that the jet went into violent resonant oscillations, as shown in Fig. 6.4. At other pressure ratios, the jet flow was very stable, even though tones of the duct modes were emitted.

6.2 REVIEW OF THE THEORETICAL WORK CONDUCTED UNDER THIS PROJECT

At the inception of this research program, it was believed that the violent ejector resonance at maximum thrust condition observed by Abdel-Fattah and Favaloro was a form of super-resonance. Here super-resonance is referred to the special jet operating condition under which the ejector duct mode and the most amplified instability wave of the jet form a feedback loop. What happens is that when super-resonance occurs the acoustic fluctuations associated with the ejector duct mode excite the most amplified instability wave of the jet. Once excited, the instability wave grows rapidly to its maximum amplitude as it propagates downstream, causing the jet to oscillate violently. The violent oscillatory motion of the jet, in turn, pumps energy into the duct modes. Thus, the duct mode oscillations and the instability wave form a feedback cycle, as illustrated in Fig. 6.5. It is also believed that the mechanism responsible for the AEDC test cell resonance is very similar. Accordingly, the theoretical work was divided into two parts mirroring the two links of the feedback loop. They are:

a. Computation of the ejector duct modes.

b. Computation of the instability waves of the jet.

6.2.1 Ejector Duct Mode Calculations

The results of the theoretical investigation have been documented by Ahuja, et al. in Ref. 6.4. It was found that the presence of a jet in the center of an ejector did not significantly affect the frequencies of the lower-order duct modes. For first-order calculation, therefore, following Eq. (4.1), the simplified duct mode frequency formula

$$f_{nm} = \sigma_{nm} \, a_0/(\pi D) \qquad n = 0, 1, 2,... \;; \quad m = 1, 2, 3,... \qquad (6.1)$$

may be used for an infinitely long circular cylinder. In Eq. (6.1) f_{nm} is the frequency of the n_{th} azimuthal and m^{th} radial, mode. a_0 is the speed of sound. D is the diameter of the duct, and σ_{nm} is the mth root of $J_n{}'$ (the derivative of the n_{th} order Bessel function), e.g., $\sigma_{11} = 1.841$, $\sigma_{12} = 5.331$, $\sigma_{13} = 8.536$, etc. (Here terminology 1 described earlier in Section 4.4.2 is used.)

6.2.2 Jet Instability Wave Calculations

Initially, instability wave calculations were confined to cold jets alone. The most amplified jet instability wave Strouhal number (f D_j/u_j) over the Mach number (M_j) range of 1.0 to 2.0 was determined where f is the wave frequency, D_j is the effective jet diameter, and u_j is the fully expanded jet velocity. The results are shown in Fig. 6.6. It turns out that at low supersonic Mach numbers, the axisymmetric mode (n = 0) is the most amplified. At higher Mach number, say above 1.3, the helical mode (n = 1) is the most amplified. This finding provides a natural explanation of why supersonic jets undergo axisymmetric screech oscillations at low supersonic Mach number and helical oscillation's mode at higher Mach number. (For further details, see Ref. 6.4.)

An examination of the results of the instability wave calculation and the ejector duct mode calculation indicated that cold supersonic jet could not produce super-resonance at 140-Hz (full scale) frequency. The cold-jet resonance frequency is much higher. This is consistent with experimental measurements reported in our earlier investigation (Ref. 6.4).

One critical difference between the theoretical and experimental model used in Ref. 6.4 and the actual test condition at AEDC is the jet temperature. In a real engine the jet is hot, typically at a total temperature between 1,500° and 2,000°R. We have shown that, as the jet temperature increases, the frequency of the most amplified jet instability waves decreases. Thus, higher temperature would tend to move the super-resonance frequency in the right direction. Extensive instability wave characteristics at higher jet-to-ambient temperature ratios were, therefore, calculated as a part of the present investigation and are described below. A close agreement between the circumferential ejector duct mode and first the heated jet instability for the AEDC facility is found, strongly supporting the contention that super-resonance is the mechanism responsible for test cell resonance at AEDC.

6.3 TEST CELL SUPER-RESONANCE

In Ref. 6.1, Jones and Lazalier described certain violent acoustic resonances encountered in the AEDC high-altitude turbine engine test facility. Figure 6.1 is a schematic diagram of the baseline configuration of the test cell. They reported that when an axisymmetric jet from a convergent nozzle of 2-ft diameter at a total temperature of approximately 1,800°R and a Mach number of 1.3 was being tested, the jet underwent violent oscillation, and a discrete tone at 140 Hz was emitted. The cause of the resonance was unknown. However, they were able to suppress the resonance by conventional engineering methods.

The test cell resonance is evidently related to the ducted jet feedback resonance illustrated schematically in Fig. 6.5. The normal modes, in this case, are the acoustic modes of the cylindrical/conical duct piece of the facility as shown in Fig. 6.7. The geometry of the cylindrical/conical duct piece is very similar to that of a circular duct of diameter D and length L with one open and one closed end. The normal mode frequencies, flmn, of such a finite length duct are given by Eq. (4.1) and repeated below for convenience.

$$f_{lmn} = \sqrt{\sigma_{nm}^2 + l^2 \left(\frac{\pi D}{2L}\right)^2} \frac{a_0}{\pi D}$$

$$l, n = 0, 1, 2, \ldots$$
$$m = 1, 2, 3, \ldots$$

(6.2)

where l, n, m are the longitudinal, azimuthal, and radial mode numbers, respectively. a_0 is the sound speed inside the duct. s_{nm} is the m_{th} root of J_n' (prime denotes derivative); i.e., J_n' (σ_{nm}) = 0. J_n' is the Bessel function of order n. The presence of a jet inside a finite length duct invariably modifies the acoustic normal mode frequencies. An analysis of the presence of a vortex sheet jet inside a duct has been carried out. Numerical results, however, reveal that the jet alters the low-order duct mode frequencies by only a negligible amount. Therefore, as a first estimate, Eq. (6.2) is used. The diameter of the cylindrical/conical duct piece is not exactly

constant. It varies from 10.75 ft at the open end to 8.5 ft at the closed end. The average is 9.63 ft, which is used in the computation below. The length of the duct piece is 8.08 ft. Jones and Lazalier estimated that the ambient gas surrounding the jet has a temperature of about 250°F or 710°R so that the sound speed a_0 is 1,300 ft/sec. On noting that $\sigma_{11} = 1.841$ ($n = m = 1$), it is easy to find from Eq. (6.2) that the normal mode frequency of the (1, 1, 1) mode; i.e., f_{111} is equal to 144 Hz. This is very close to the observed tone frequency of 140 Hz. The good agreement suggests that the test cell resonance is primarily related to the $n = \pm 1$ azimuthal (helical or flapping) jet instability wave mode.

Since the observed test cell resonance is associated with extremely high tone intensity and large amplitude jet oscillations, it is probably not just a case of simple resonance. From an energy standpoint, the strong oscillation has to be driven by a large-amplitude instability wave of the jet (the only large source of energy available). As a working hypothesis of the mechanism responsible for the test cell screech phenomenon, it is proposed that the oscillation was driven by a feedback loop consisting of the (1, 1, 1) mode of the inlet cylindrical/conical duct and the instability wave of the jet. Since the oscillation was reported to be very violent, the instability wave involved must be the most amplified wave, a situation hereby referred to as super-resonance. To demonstrate that the test cell tone and pressure fluctuations are indeed generated by super-resonance, we must first determine the frequency of the most amplified instability wave of the jet at the test condition.

Figures 6.8a-c show the calculated total growth of the instability waves of a Mach 1.3 jet at three different temperature ratios as a function of the Strouhal number for the three lowest azimuthal modes ($n = 0$, 1, and 2). It is evident from these figures that the helical mode ($n = 1$) is the dominant instability wave mode. As temperature increases from $T_j/T_a = 1.0$ to 2.0, (T_j is the fully expanded jet temperature and T_a is the ambient temperature) the Strouhal number of the most amplified instability wave decreases from 0.25 to 0.13. Now the AEDC test cell resonance was observed at a jet Mach number, M_j, equal to 1.3, total temperature around $1,800^\circ$R, ambient gas temperature about 250°F (710°R) and a jet nozzle exit diameter, D, of 2 ft. By using the above parameters as input, the frequency of the most amplified jet instability wave can be calculated as follows.

$$T_j = \frac{T_r}{1 + (\Upsilon - 1)\frac{M_j^2}{2}} = \frac{1800}{1 + 0.175 \times 1.3^2} = 1389^\circ R \ (\Upsilon = 1.35) \tag{6.3}$$

Hence $T_j/T_a = 1.96$, say 2.0. The effective diameter of the jet, D_j, is related to the nozzle exit diameter D by the formula

$$\frac{D_j}{D} = \left(\frac{1 + \frac{\Upsilon - 1}{2}M_j^2}{1 + \frac{\Upsilon - 1}{2}M_d^2} \right)^{\frac{1 + 1}{4(\Upsilon - 1)}} \sqrt{\frac{M_d}{M_j}} = 1.033 \tag{6.4}$$

where M_d is the nozzle design Mach number; $M_d = 1.0$ for a convergent nozzle. Also the jet velocity, U_j, is equal to $M_j a_j$ (a_j = sound speed inside the jet). At a temperature of $1,389°R$ it is easy to find that $a_j = 1,798$ ft/sec.

From Fig. 6.8c at $T_j/T_a = 2.0$ the Strouhal number, fD_j/u_j, of the most amplified instability wave is equal to 0.13. Thus,

$$f = \frac{0.13 U_j}{D_j} = \frac{0.13 \times 1798 \times 1.3}{2 \times 1.033} = 147 Hz \qquad (6.5)$$

Therefore, the frequency of the most amplified jet instability wave is, indeed, nearly equal to the observed resonance frequency and the frequency of the second radial duct mode of the test cell inlet cylindrical/conical duct piece.

In the original GTRI experiments with unheated jets presented in Ref. 6.4 and those presented here, resonance at 140 Hz (full scale) frequency was/is not observed. However, unlike in the AEDC facility only cold jets were used. Thus, even if super-resonance did occur, it would occur at a higher frequency and would not be noticed. Now following the above computation procedure, it is possible to determine the condition under which super-resonance occurs. If super-resonance did occur, it can be confirmed by re-examining the experimental data.

It appears that for the ejector with both ends open, as in our experimental study (without orifice baffle inserts) the second radial duct mode provides super-resonance.

By means of Eq. (6.1), the frequency of the second radial duct mode of the ejector used in the GTRI experiment is 8.54 kHz. In Fig. 6.9, the curve in the Strouhal number versus Mach number plot (cold jets) corresponding to this frequency is shown in broken line segments. Also shown in this figure is the curve of the most amplified instability waves of cold supersonic jets given earlier in Fig. 6.6. The intersection of these curves provides the Mach number at which the frequency matching condition of super-resonance is satisfied, i.e., the frequency of the duct mode matches the frequency of the most amplified jet instability wave. As can be seen from this figure, the intersection point lies between Mach number 1.5 and 1.6. Therefore, if super-resonance occurs in the unheated test in the GTRI sub-scale experiments, it would occur when the operating Mach number of the jet is between 1.5 and 1.6.

Figures 6.10a-d are the in-duct microphone sound pressure level spectra measured at jet Mach numbers 1.4, 1.5, 1.6, and 1.7, respectively. From these data, it can be seen that there are dominant tones in the spectra. The highest sound pressure level occurs at $M_j = 1.6$ at 8.0 kHz. The highest sound pressure level at Mach number 1.4 and 1.5 are about the same and occur at 9.8 kHz and 8.8 kHz, respectively.

This sound pressure level is considerably higher than the tone sound pressure level at $M_j = 1.7$. Thus, it is conceivable that a strong resonance could have occurred at a Mach number between 1.5 and 1.6 at a frequency of 8.54 kHz for the unheated conditions, just as the theory predicts.

109

Similarly, when the orifice baffle inserts shown in Fig 4.31 are used, one should use Eq (6.2) to approximate a close-open end ejector duct. This provides a frequency of 11.967 kHz for the 1st circumferential mode corresponding to $\sigma_{11} = 1.84$.

Note that this configuration is a better representation of the AEDC configuration for which super-resonance has been demonstrated to occur for $\sigma_{11} = 1.84$. A re-examination of the spectra with the orifice baffle insert indeed shows high peaks in the vicinity of 12 kHz, as seen in Figs 4.39 and 4.40.

The data with the inserts were obtained near the contractual termination date and were outside the original scope of the contract. Further data need to be acquired and need to be analyzed in the light of the new insights gained on the topic of super-resonance.

6.4 CONCLUDING REMARKS

The mechanism responsible for the AEDC test cell resonance has been investigated. It is believed that the oscillations are generated by a feedback loop involving the second radial acoustic mode of the inlet cylindrical/conical duct piece of the test facility and the most amplified instability wave of the jet. To see how the feedback loop maintains itself, one may begin by noting that associated with a duct mode oscillation there are pressure and velocity fluctuations. These fluctuations can easily excite the instability wave of the jet near the nozzle exit where the mixing layer is thin. Once excited, the instability wave grows rapidly as it propagates downstream by extracting energy from the mean flow of the jet. When the instability wave attains a large enough amplitude, it forces the jet to oscillate, thus pumping energy back into the duct mode. In this way, the oscillations of the jet are coupled to the acoustic oscillations of the duct mode, forming feedback resonance. The oscillations would be most violent when the most amplified instability wave of the jet is involved --- the case of super-resonance. It is determined that at the AEDC test conditions, the frequency of the most amplified instability wave is around 147 Hz. This is very close to the observed resonance frequency of 140 Hz and also the frequency of the second radial duct mode of the inlet piece of the facility. The good match of these frequencies provides strong support for the hypothesis that super-resonance is the cause of the test cell resonance.

The budget and time constraints did not allow us to completely understand the effect of temperature on the coupling between the jet instability and the duct resonance. It appears that we are on the correct path of understanding as our measurements of the screech frequencies of heated jets follow the theoretically predicted trend. That is, the screech frequencies increase with increasing jet temperature ratio. Our measurements indicated the presence of the same screech frequencies for the ducted configuration in which the amplitudes at these frequencies were much higher.

We were also able to identify a number of discrete tones for the ducted configuration at frequencies corresponding to various duct mode resonances. The amplitudes of all duct mode-related tones increased with increasing Mach numbers and with increasing temperature.

Since our work has demonstrated that the peak frequency of the jet instability wave changes with temperature and that high-amplitude duct resonance tones are generated at a range of

frequencies, it will not be surprising to find that at certain Mach numbers, super-resonance does not occur at unheated conditions, but does occur at heated conditions, and vice versa.

6.5 RECOMMENDATIONS FOR FUTURE WORK

The present project ended before we could acquire more detailed data to properly close the gap in our understanding of the phenomenon underlying the coupling between jet instabilities and duct resonances.

It is recommended that the future studies include the following as a minimum:

1. Acquire data similar to those obtained to date at finer intervals of jet temperature and pressure ratios and validate the concept of super-resonance for a range of suitably selected diffuser diameters and operating conditions.

2. In all future studies, make detailed flow and acoustics measurements inside the diffuser.

3. Conduct a similar study, both experimental and analytical/computational, for rectangular jets.

4. Develop appropriate scaling methodology and design charts for estimating the occurrence of strong resonances in test facilities to support the analysis of future exhaust systems.

5. Develop methods of controlling the acoustic interactions between altitude test facilities and jet engine plumes.

TEST CELL CONFIGURATION
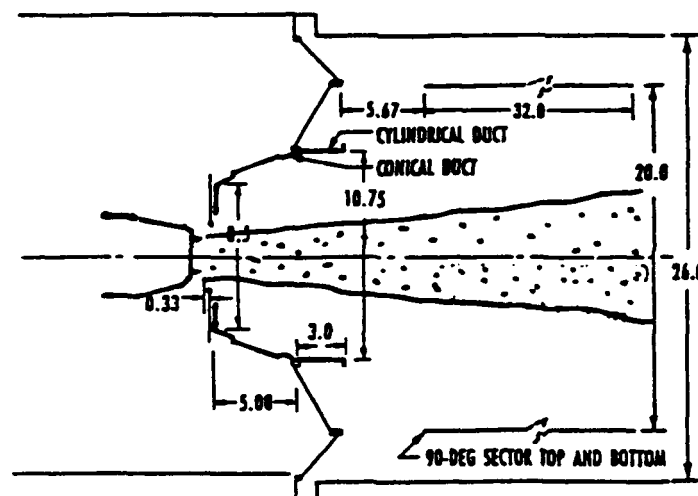
Figure 6.1 Baseline configuration at AEDC.
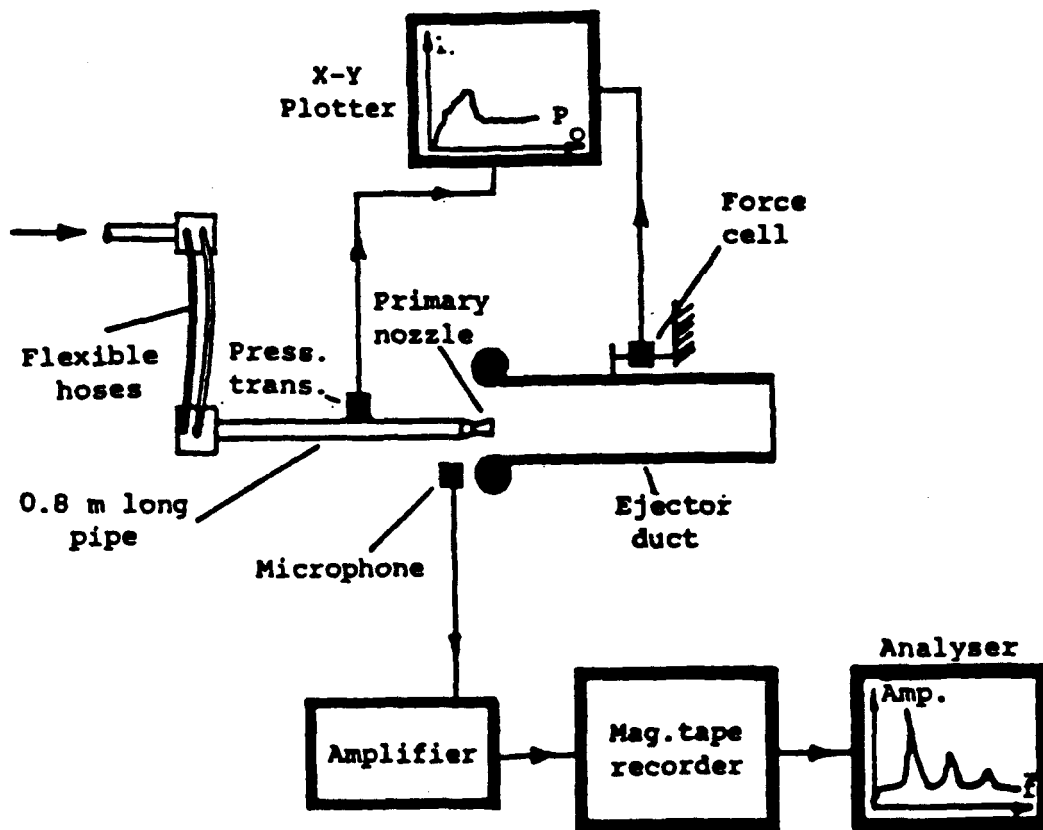
Figure 6.2 Schematic diagram of the experimental apparatus used by Abdel-Fattah and Favaloro (Ref. 6.3, Figure 1).
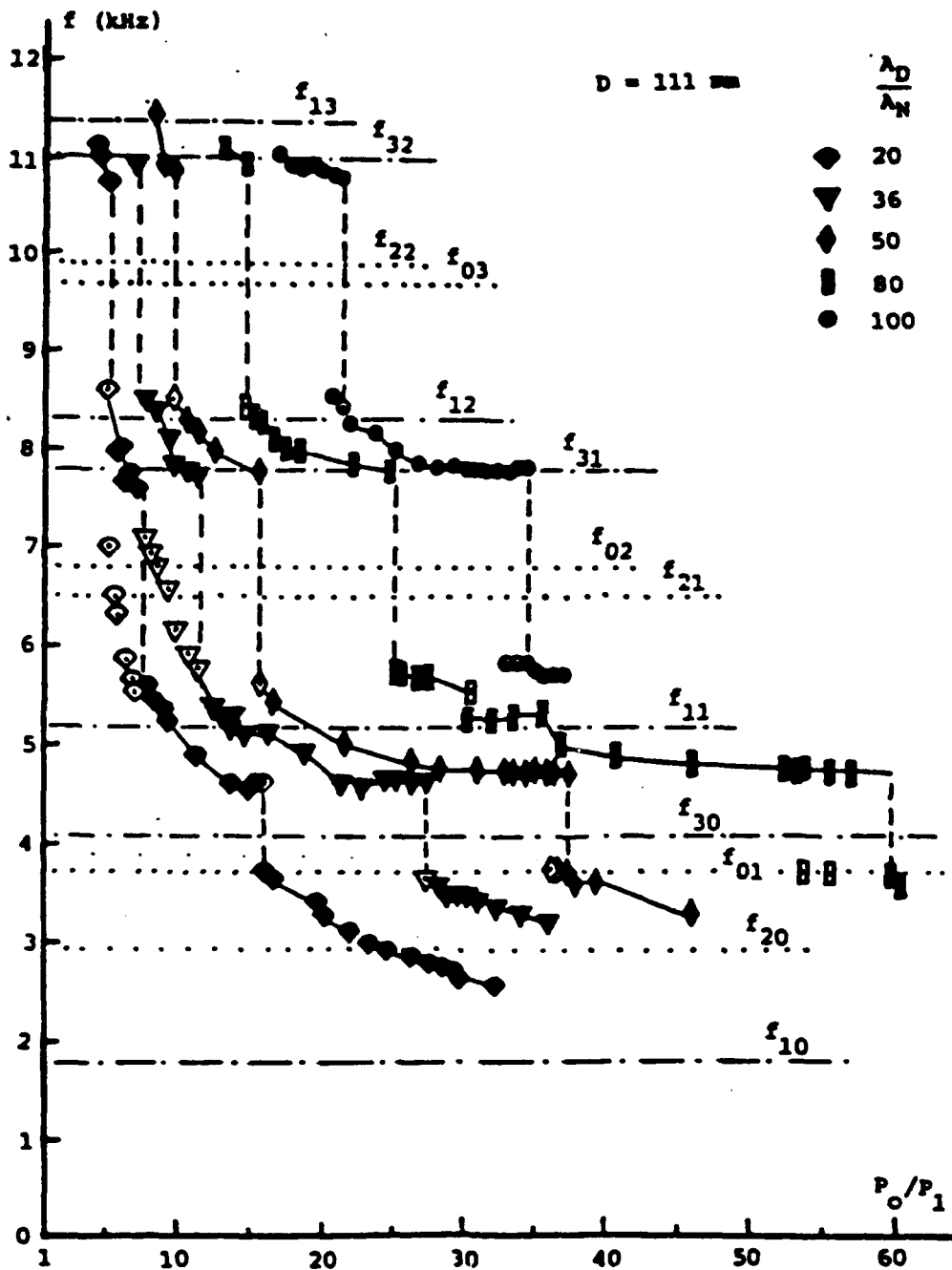
Figure 6.3. Discrete tone fundamental frequency measured by Abdel-Fattah and Favaloro in their ejector thrust enhancement experiment (Ref. 6.3, Figure 7).
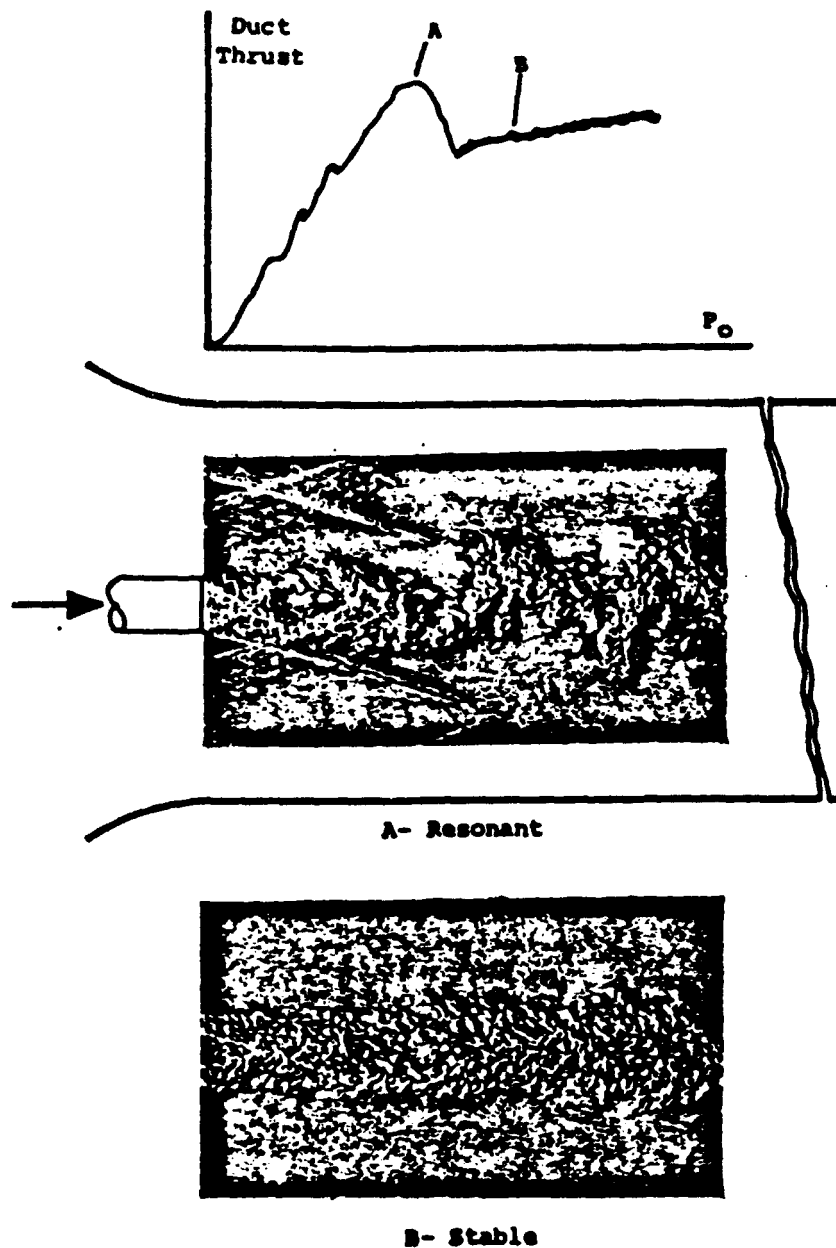
Figure 6.4. Schlieren photographs of the axisymmetric jet in the square duct dur-
ing resonant and relatively stable flow conditions corresponding to
points A and B on the thrust characteristics respectively (Ref. 6.3, Fig.
12.

114
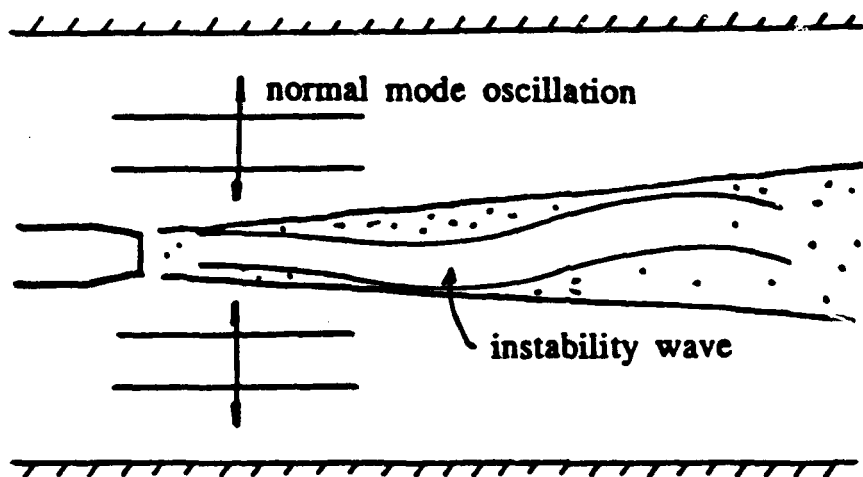
Figure 6.5. Super-resonance — feedback cycle formed by a normal mode of the
duct and the most amplified instability wave of the jet.
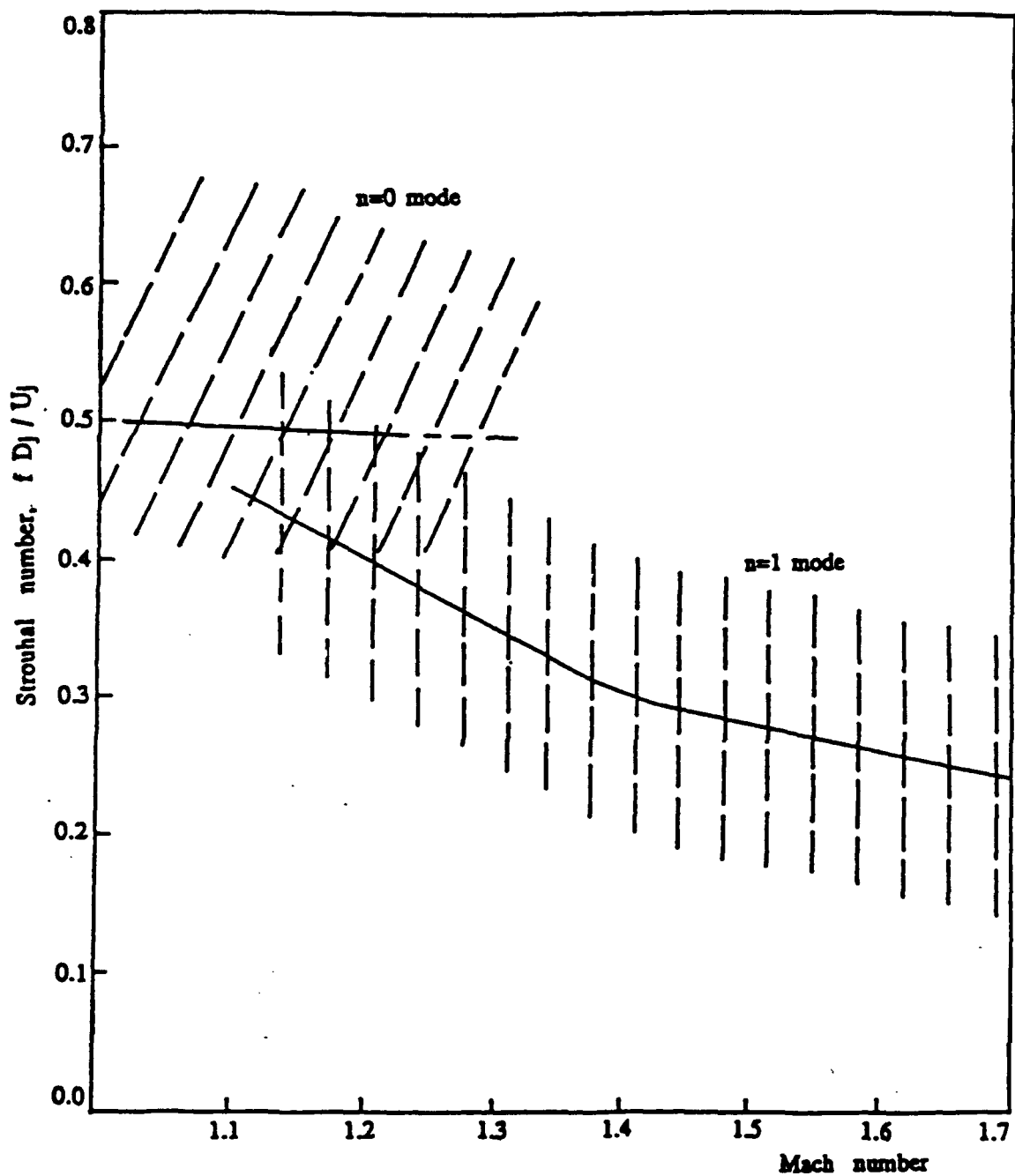
Figure 6.6. Range of the most amplified axisymmetric and helical instability wave
modes of cold supersonic jets.
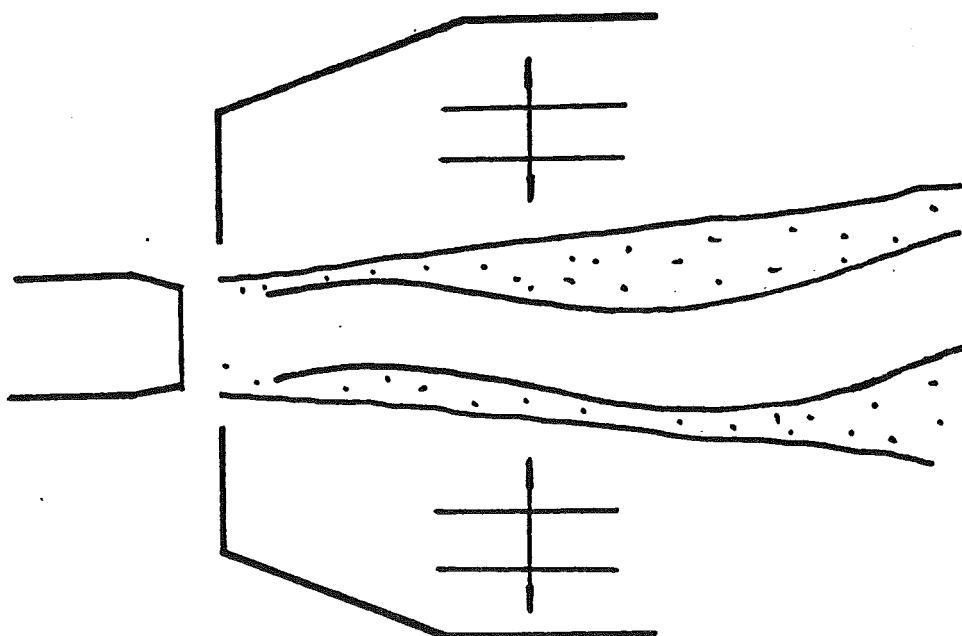
Figure 6.7. Super-resonance formed by the feedback oscillations of the second radial duct mode of the inlet cylindrical/conical piece and the most amplified instability wave of the jet.
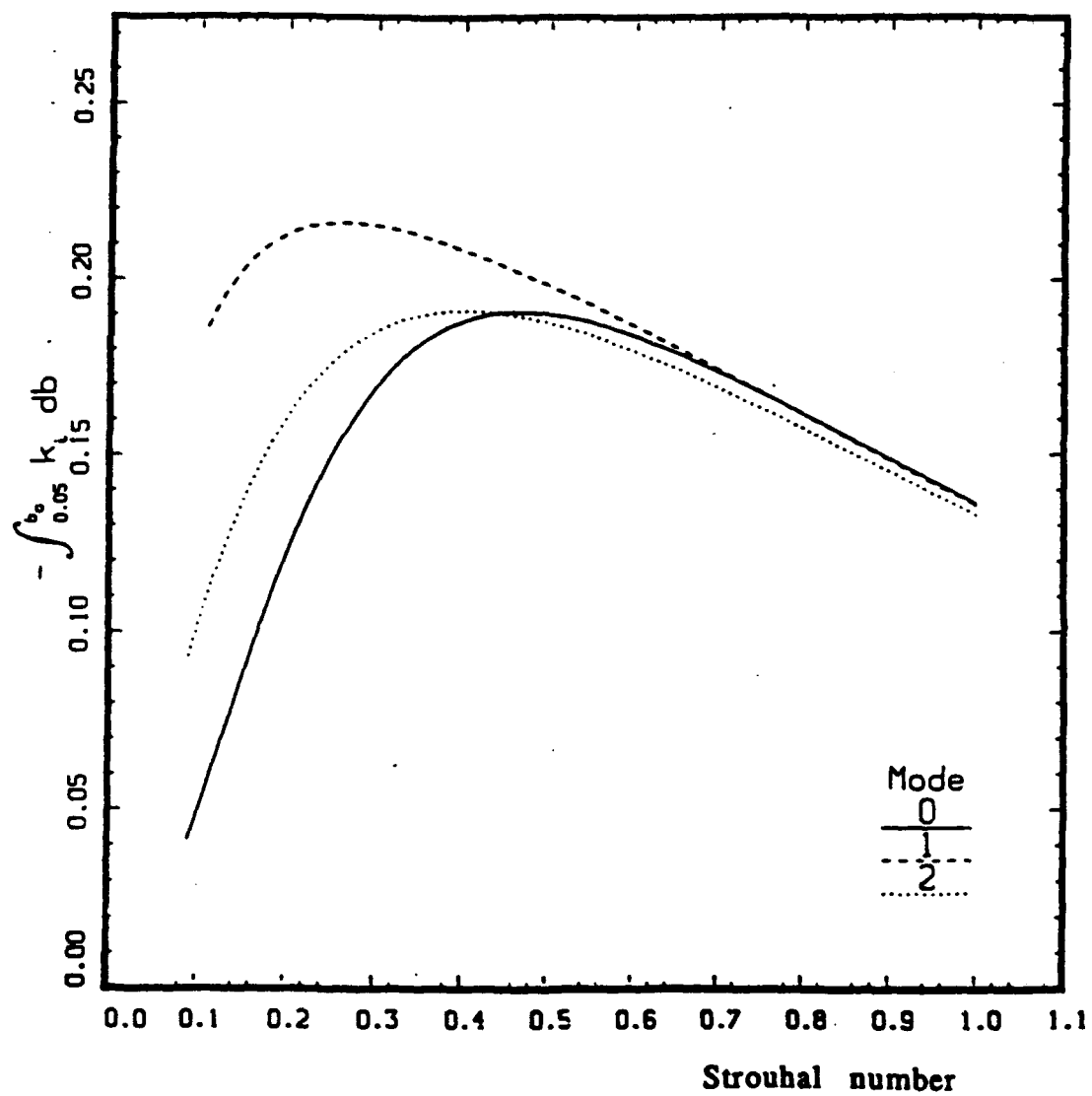
Figure 6.8a. Total growth versus the Strouhal number of a Mach 1.3 jet at $T_j/T_a = 1.0$.
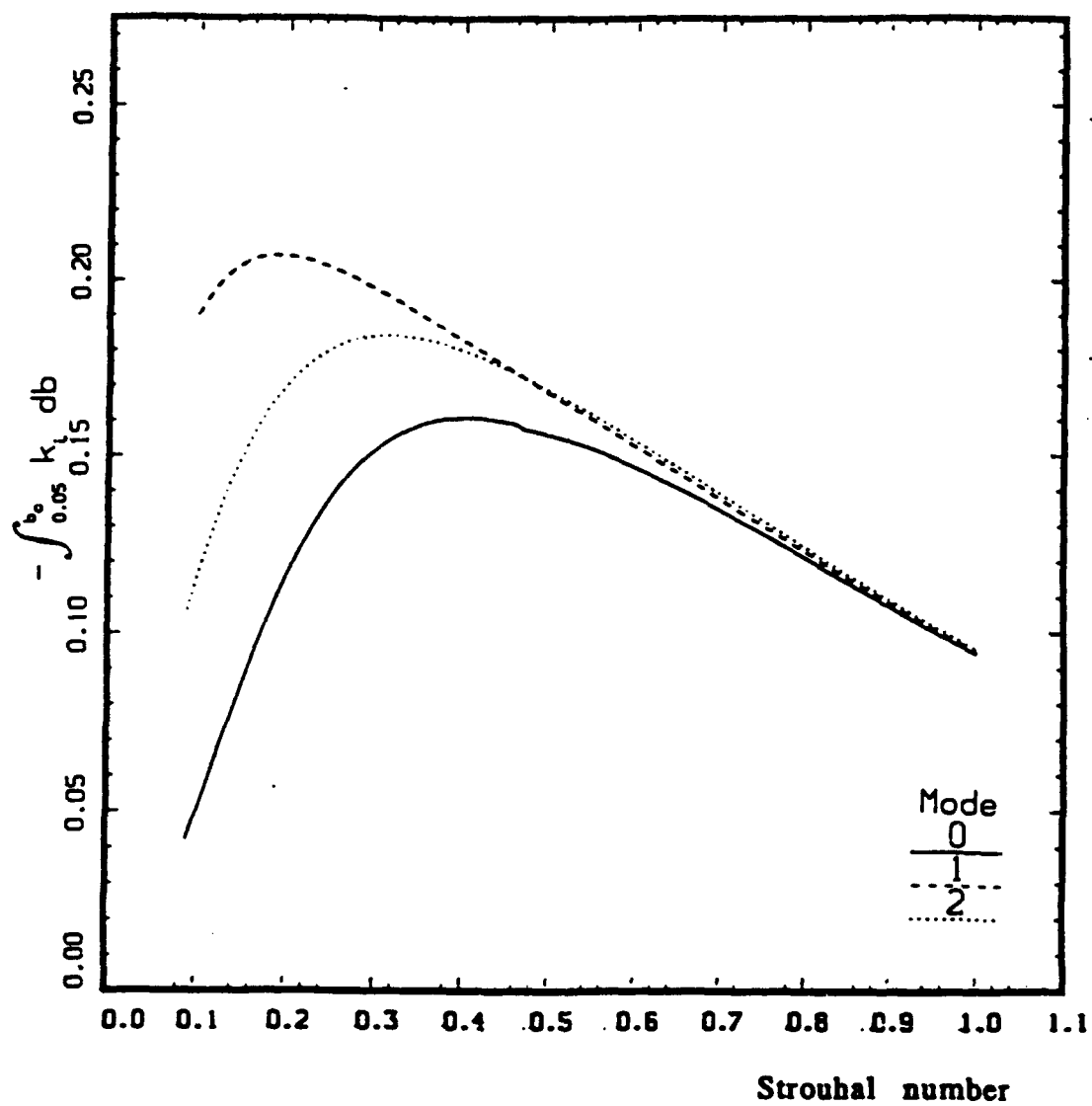
Figure 6.8b. Total growth versus the Strouhal number of a Mach 1.3 jet at $T_j/T_a = 1.4$.

119
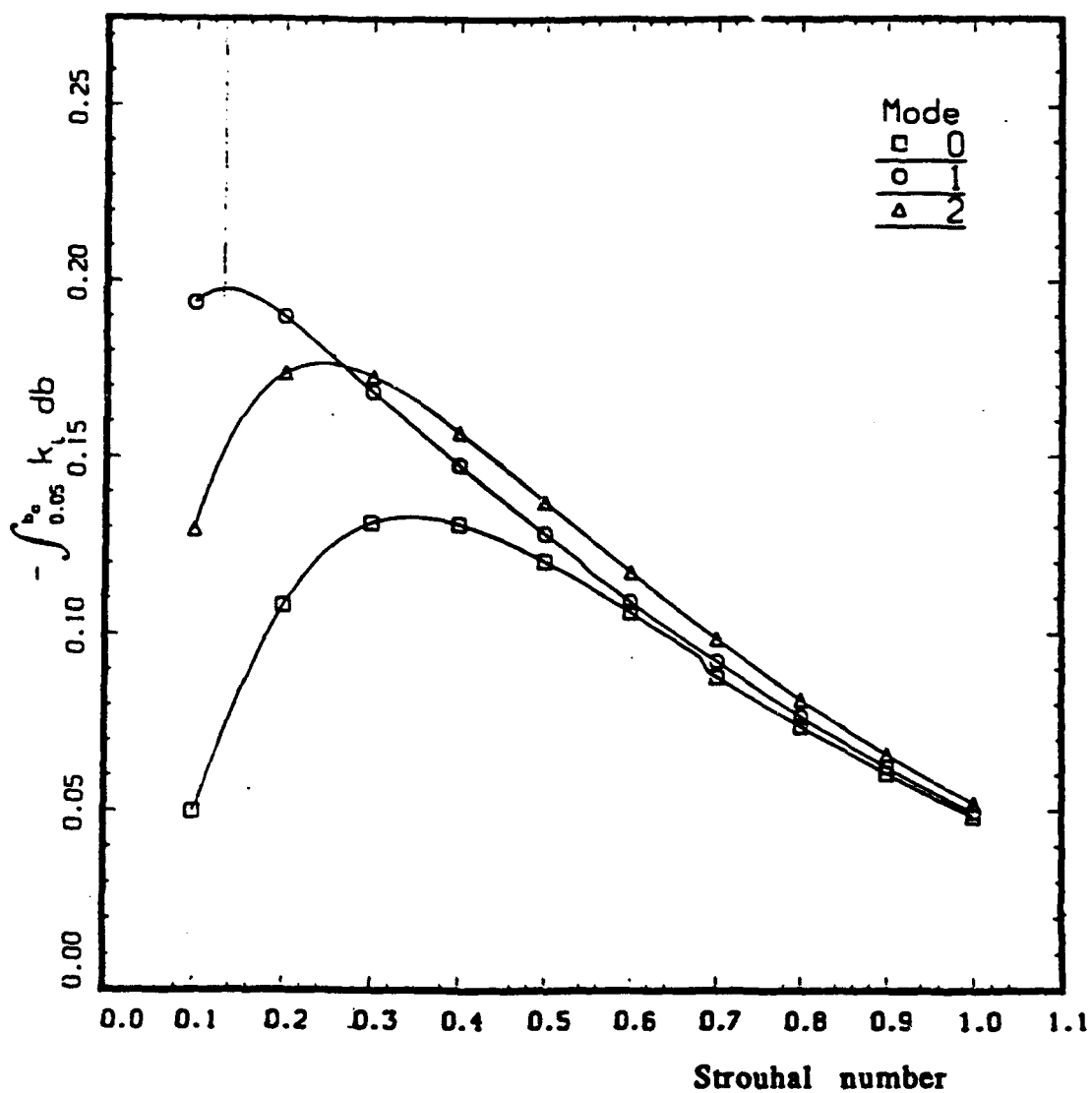
Figure 6.8c. Total growth versus the Strouhal number of a Mach 1.3 jet at $T_j/T_a = 2.0$.
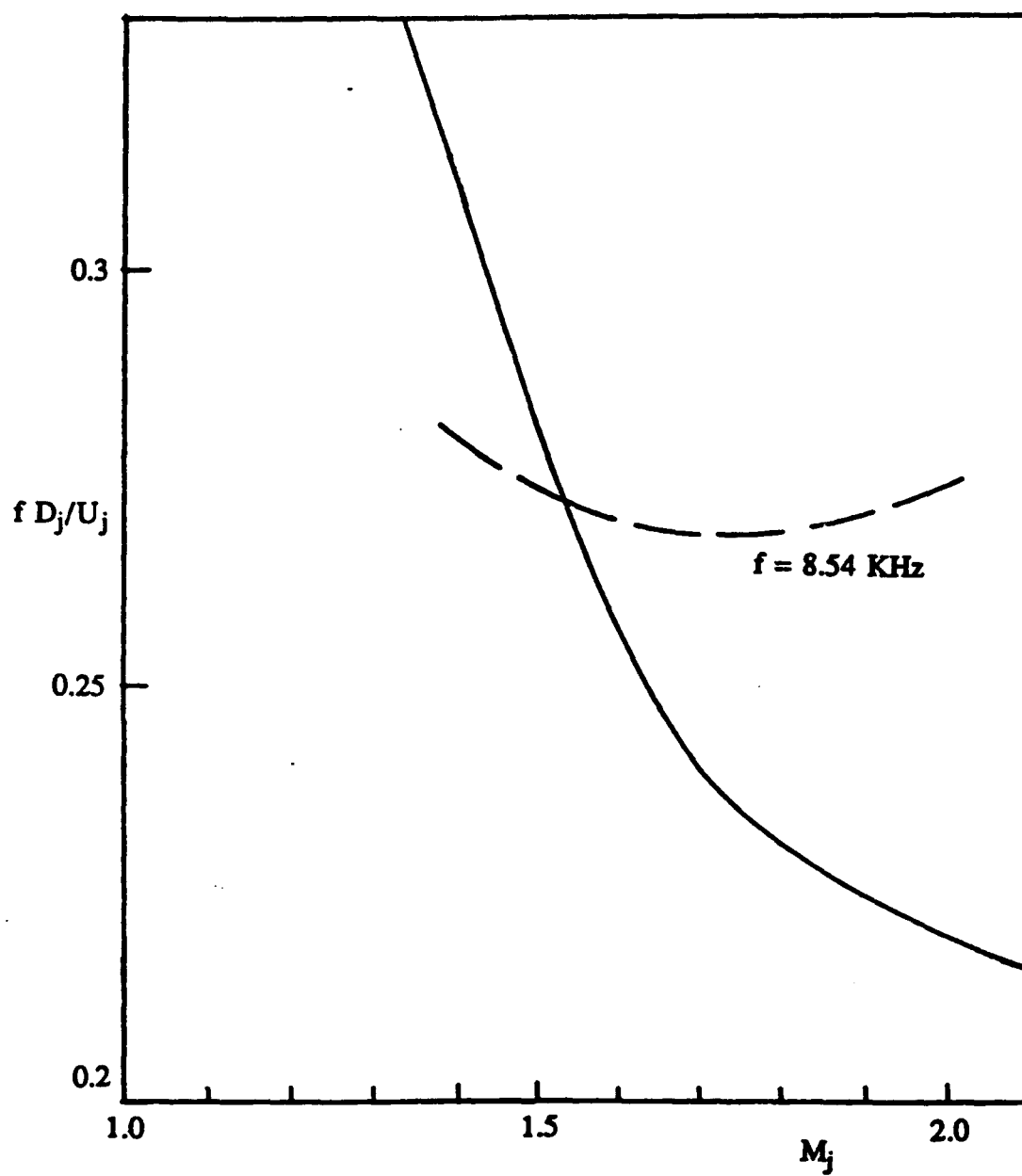
Figure 6.9. Locating the super-resonance condition for the GTRI experiments (cold jets).
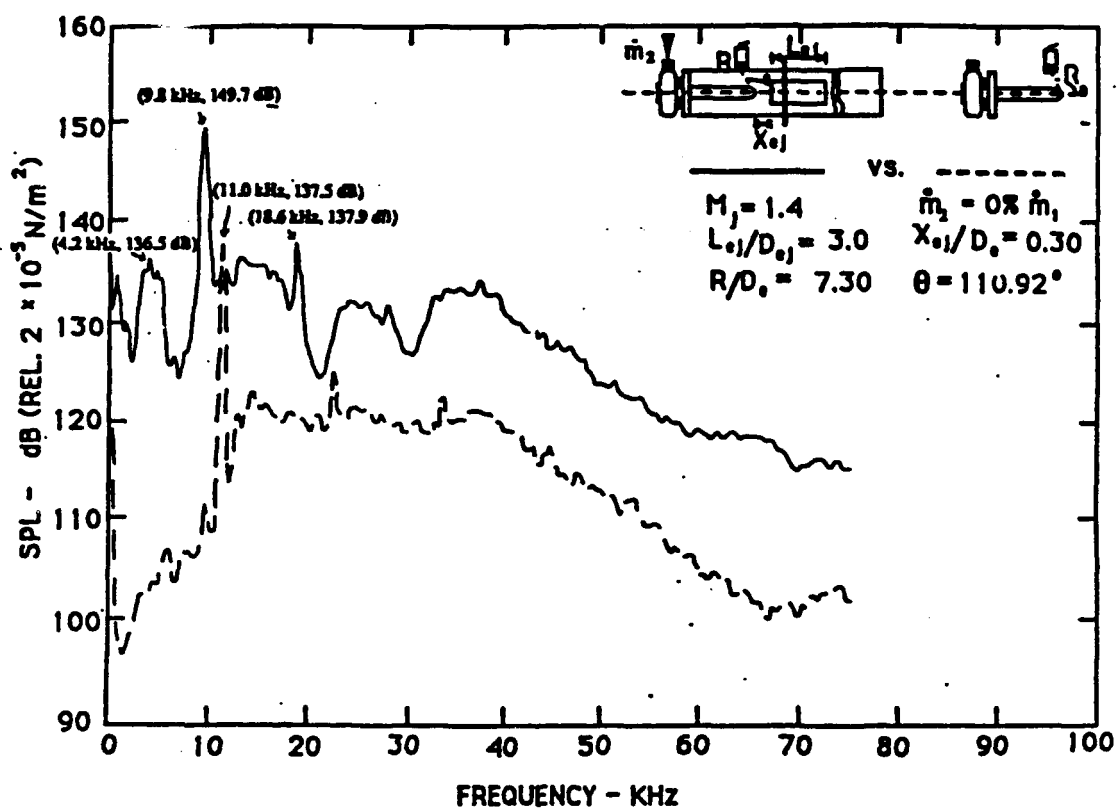
Figure 6.10a. Sound pressure level spectrum at M_j = 1.4.
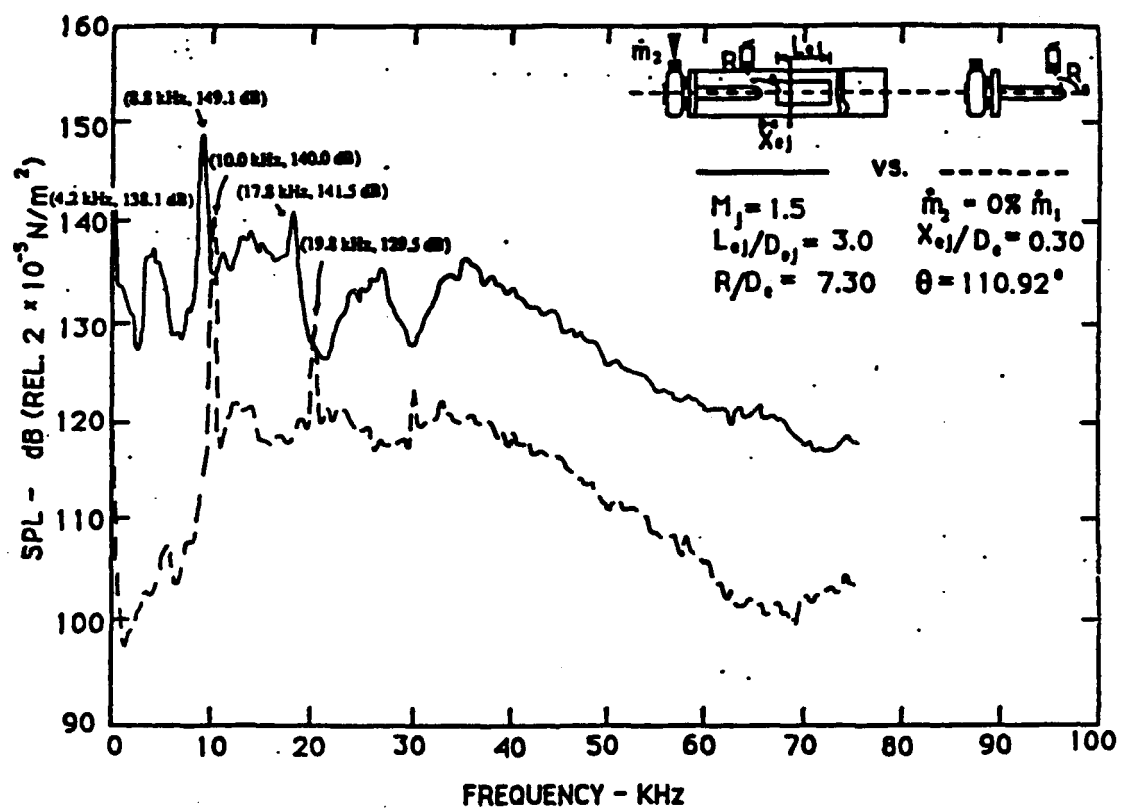
Figure 6.10b. Sound pressure level spectrum at M_j = 1.5.
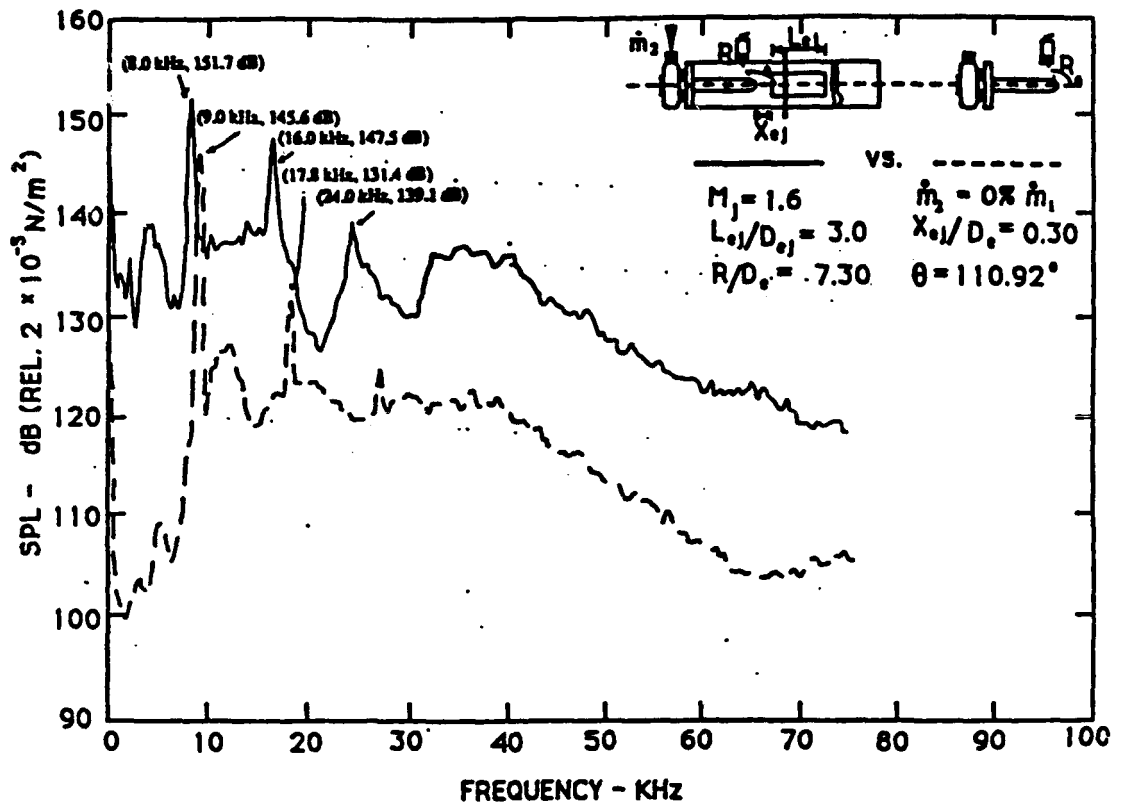
Figure 6.10c. Sound pressure level spectrum at M_j = 1.6.
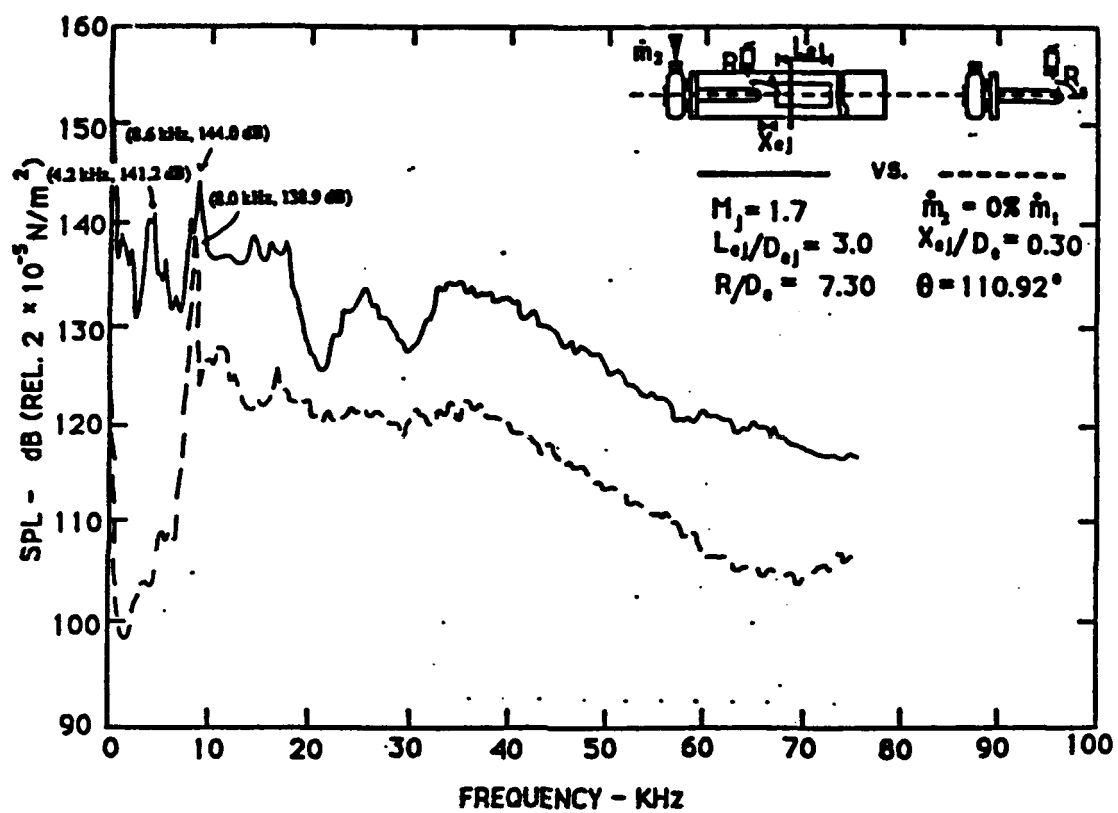
Figure 6.10d. Sound pressure level spectrum at M_j = 1.7.
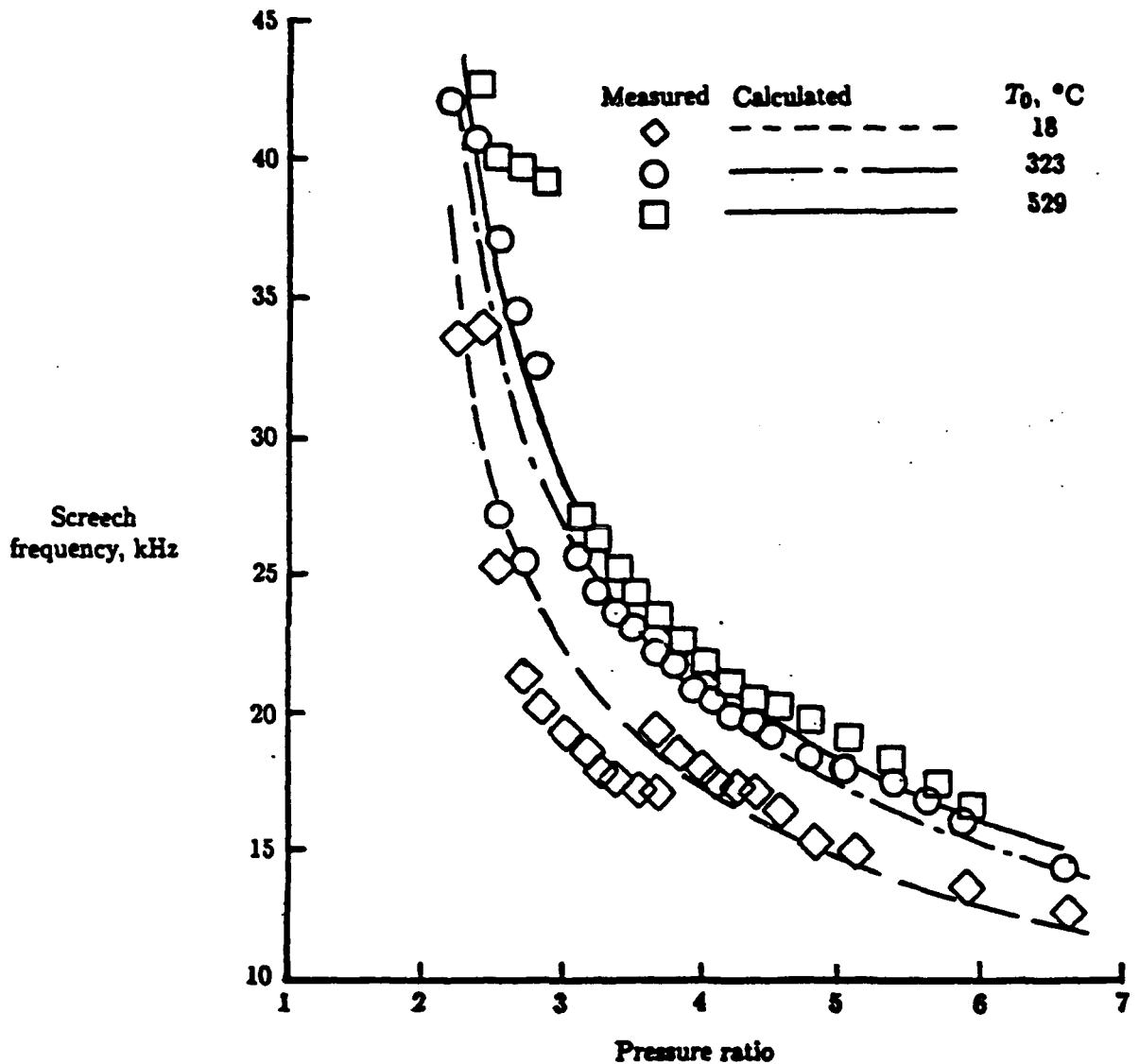
Figure 6.11. Dependence of screech frequency on jet pressure ratio at different total temperatures measured by Rosfjord and Toms.

126
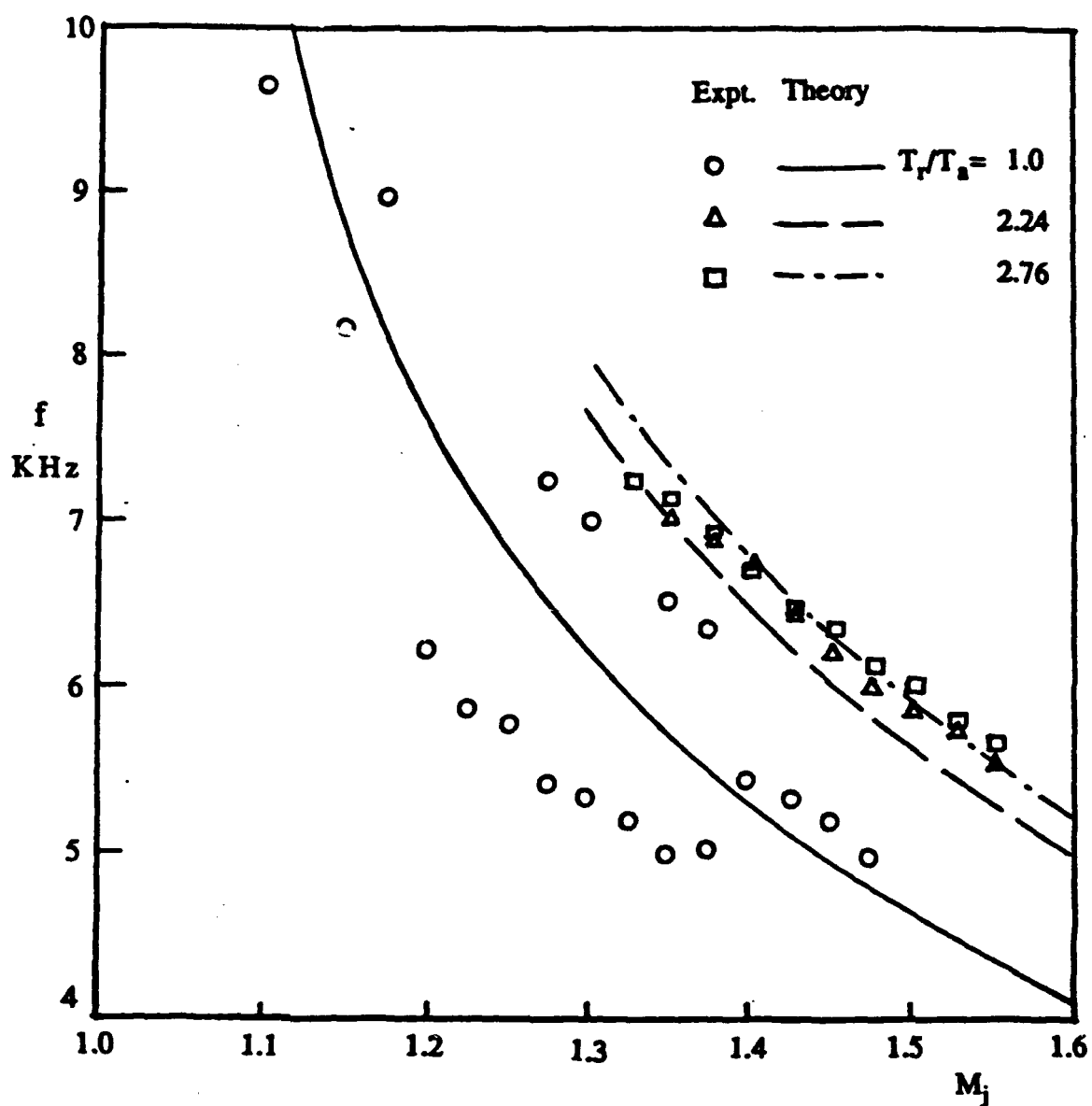
Figure 6.12. Comparisons between calculated and measured screech tone frequencies at different temperature ratios.

REFERENCES

1.1. Jones, R. R. III and Lazalier, G. R. "The Acoustic Response of Altitude Test Facility Exhaust Systems to Axisymmetric and Two-Dimensional Turbine Engine Exhaust Plumes." AIAA Paper 92-02-131, 1992.

1.2. Tam, C. K. W. "Jet Noise Generated by Large-Scale Coherent Motion." Chapter 6 in Aeroacoustics of Flight Vehicles: Theory and Practice, NASA RP-1258, 1991.

1.3. Ahuja, K. K., Tam, C. W., Massey, K. C., Fleming, A. J.,and Jones, R. R. III. "Acoustic Interactions Between an Altitude Test Facility and Jet Engine Plumes." AEDC- TR- 91-20, January 1992.

1.4. Jones, R. R. III, Ahuja, K. K., Tam, C. W.,and Abdelwahab, M. "Measured Acoustic Characteristics of Ducted Supersonic Jets at Different Model Scales." AIAA Paper 93-0731, 1993.

1.5. Lepicovsky, J., Ahuja, K. K., Brown, W. H., Salikuddin, M., and Morris, P. J. "Acoustically Excited Heated Jets - II, In Search of a Better Understanding." NASA Report 4129, 1988.

1.6. Tam, C. K. W., Ahuja, K. K., and Jones, R. R. III. "Screech Tones From Free and Ducted Supersonic Jets." AIAA Paper 93-0732, Reno 1993; also AIAA Journal, Vol. 32, No. 5, May 1994.

2.1. Lepicovsky, J., Ahuja, K. K., Brown, W. H., Salikuddin, M., and Morris, P. J. *Excited Heated Jets, Part I: Internal Excitation*. Journal of Sound and Vibration, Vol. 102(1), pp. 71-91, 1985.

2.2. Lepicovsky, J., Ahuja, K. K., and Burrin, R. H. *Tone Excited Jets-Part III: Flow Measurements*. NASA CR-4129, 1988.

3.1. Tam, C. K. W. "Jet Noise Generated by Large-Scale Coherent Motion." Chapter 6 in Aeroacoustics of Flight Vehicles: Theory and Practice, NASA RP-1258, 1991.

3.2. Massey, K. C., Ahuja, K. K., Jones, R. R. III and Tam, C. K. W. "Screech Tones in Supersonic Heated Free Jets." AIAA Paper 94-1041, Reno, NV, 1994.

3.3. Lepicovsky, J., Ahuja, K. K., Brown, W. H., Salikuddin, M., and Morris, P. J. "Acoustically Excited Heated Jets - II, In Search of a Better Understanding." NASA Report 4129, 1988.

3.4. Tam, C. K. W., Seiner, J. M., Yu, J. C. "Proposed Relationship Between Broadband Shock Associated Noise and Screech Tones." Journal of Sound and Vibration, Vol. 110, pp. 309-321, 1986.

3.5. Tam, C. K. W. and Tanna, H. K. "Shock Associated Noise of Supersonic Jets from

Convergent-Divergent Nozzles." Journal of Sound and Vibration, Vol. 81, pp. 337-358, 1982.

3.6. Tam, C. K. W. "Jet Noise Generated by Large-Scale Coherent Motion." Chapter 6 in Aeroacoustics of Flight Vehicles: Theory and Practice, NASA RP-1258, 1991.

3.7. Tam, C. K. W., Ahuja, K. K., and Jones, R. R. III. "Screech Tones From Free and Ducted Supersonic Jets." AIAA Paper 93-0732, Reno, NV, 1993; also AIAA Journal, Vol. 32, No. 5, May 1994.

4.1. Ahuja, K. K., Tam, C. W., Massey, K. C., Fleming, A. J., Jones, R. R. III. "Acoustic Interactions Between an Altitude Test Facility and Jet Engine Plumes." AEDC-TR-91-20, January 1992.

4.2. Jones, R. R. III, Ahuja, K. K., Tam, C. W. ,and Abdelwahab, M. "Measured Acoustic Characteristics of Ducted Supersonic Jets at Different Model Scales." AIAA Paper 93-0731, 1993.

4.3. Tam, C. K. W., Ahuja, K. K., and Jones, R. R. III. "Screech Tones From Free and Ducted Supersonic Jets." AIAA Paper 93-0732, Reno, NV, 1993; also AIAA Journal, Vol. 32, No. 5, May 1994.

6.1. Jones, R. R. III and Lazalier, G. R. "The Acoustic Response of Altitute Test Facility Exhaust Systems to Axisymmetric and Two-Dimensional Turbine Engine Exhaust Plumes." AIAA Paper 92-02-131, 1992.

6.2. Caruthers, John E., Vakili, Ahmad D., Raviprakash, G. K., and Jones, R. R. III. "Aeroacoustic Interaction of Jets/Test Cells." AIAA Paper 92-02-132, 1992.

6.3. Adell-Fattah, A.M., and Favalaro, S. C. "Duct Resonance and Its Effect on the Performance of High-Pressure Ratio Axisymetric Ejectors." AIAA Journal, Vol. 26, No. 7, July 1988.

6.4. Ahuja, K. K., Tam, C. W., Massey, K. C., Fleming, A. J.,and Jones, R. R. III, "Acoustic Interactions Between an Altitude Test Facility and Jet Engine Plumes." AEDC-TR-91-20, January 1992.

D.1. Streeter, Victor. Handbook of Fluid Dynamics,. McGraw-Hill, 1961.

APPENDIX A

Free-Jet Data for 1-in. Nozzle
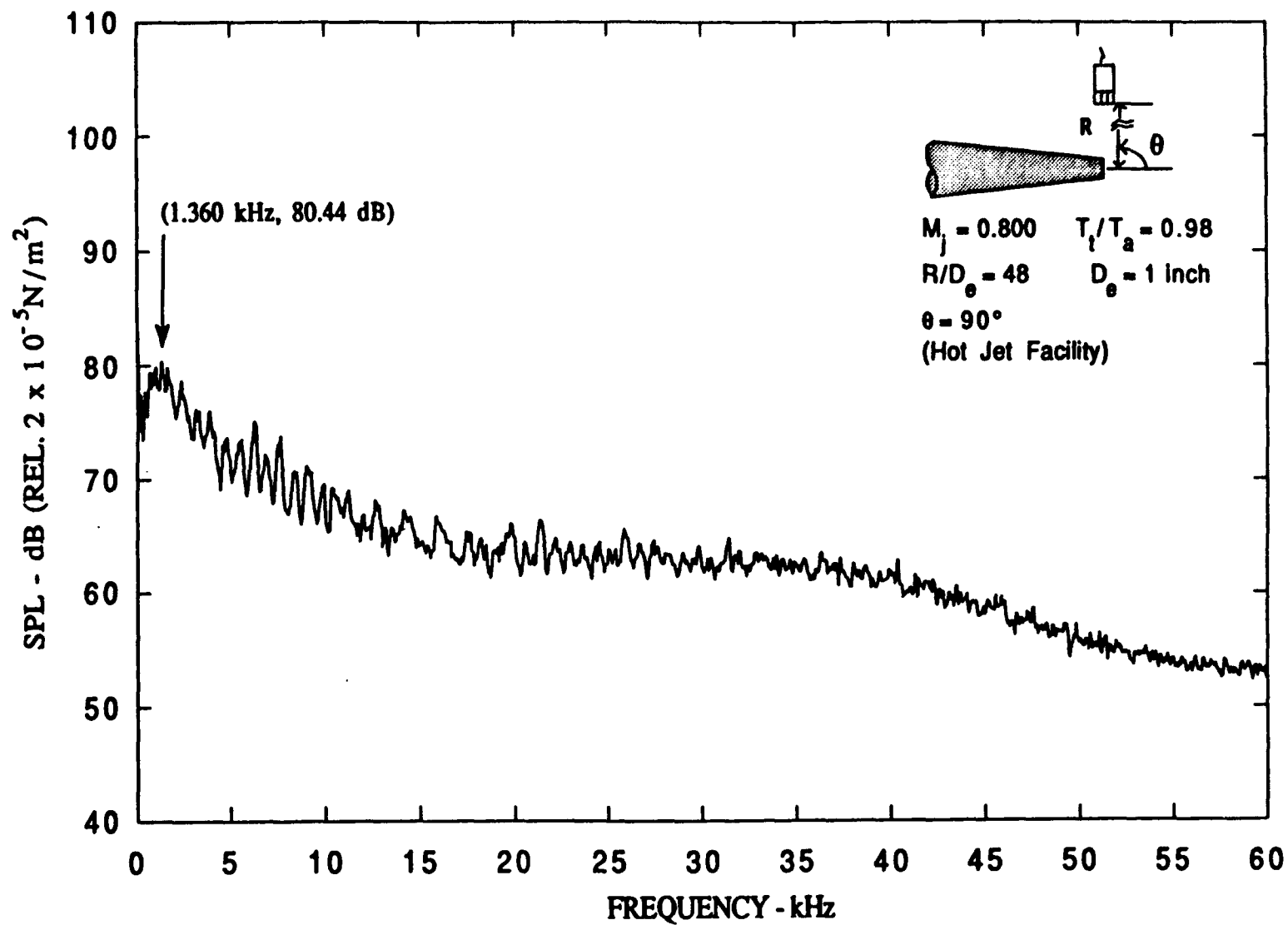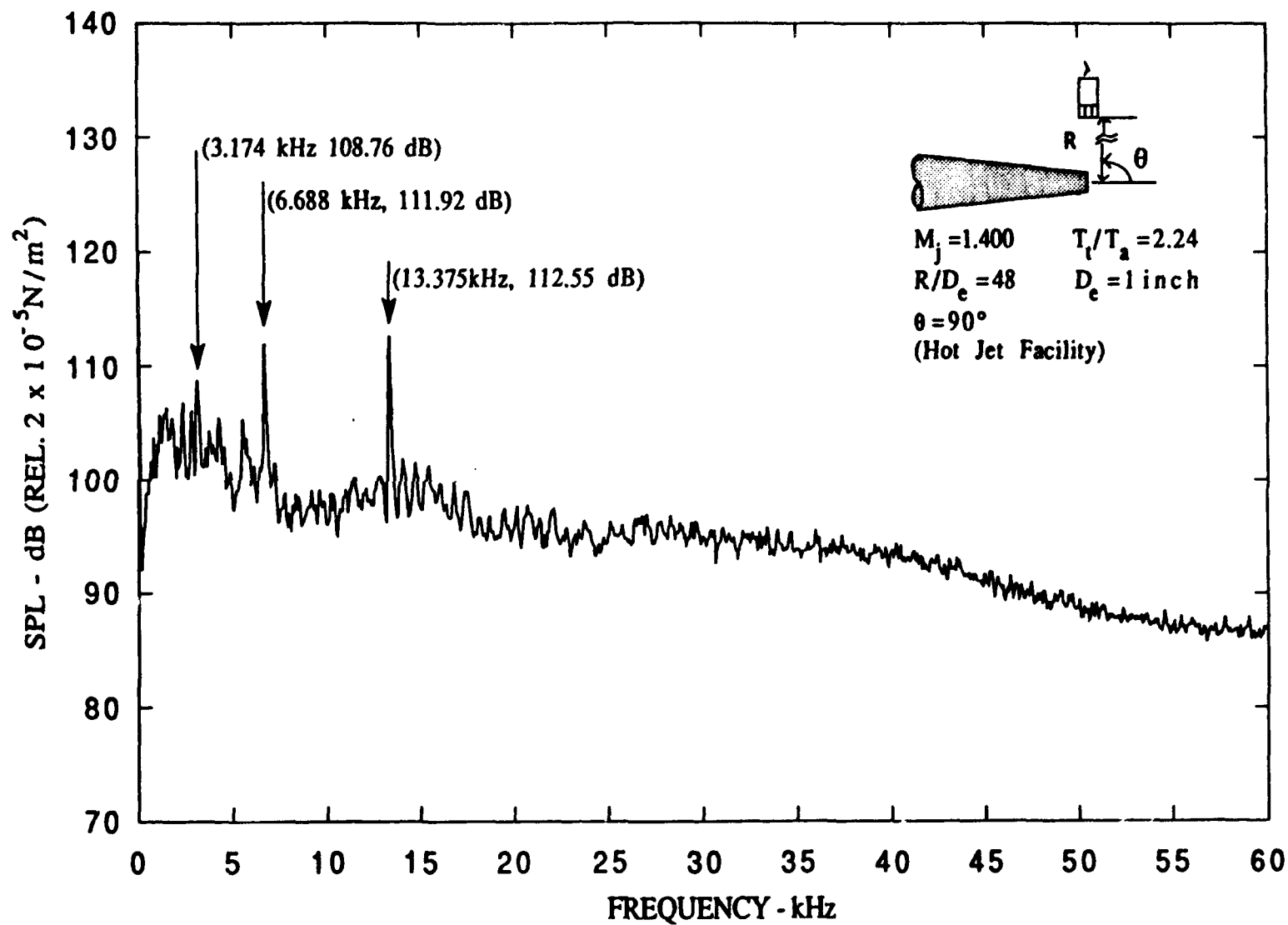
Figure A-1. Narrow band spectra ($\Delta f = 62.5$ Hz), $M_j = 0.800$, $T_t/T_a = 0.98$.
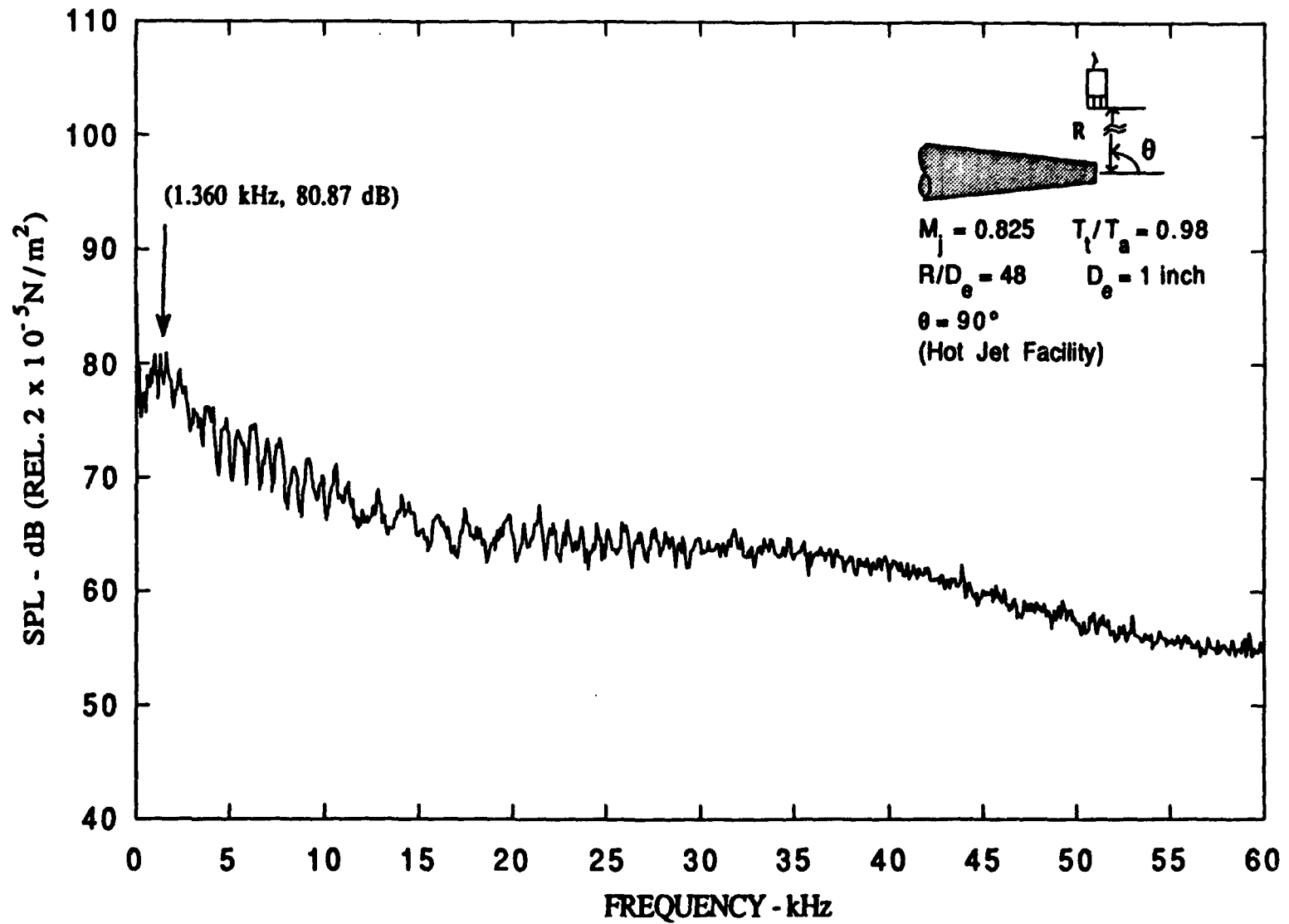
Figure A-2. Narrow band spectra (Δf = 62.5 Hz), M_j = 0.825, T_t/T_a = 0.98.
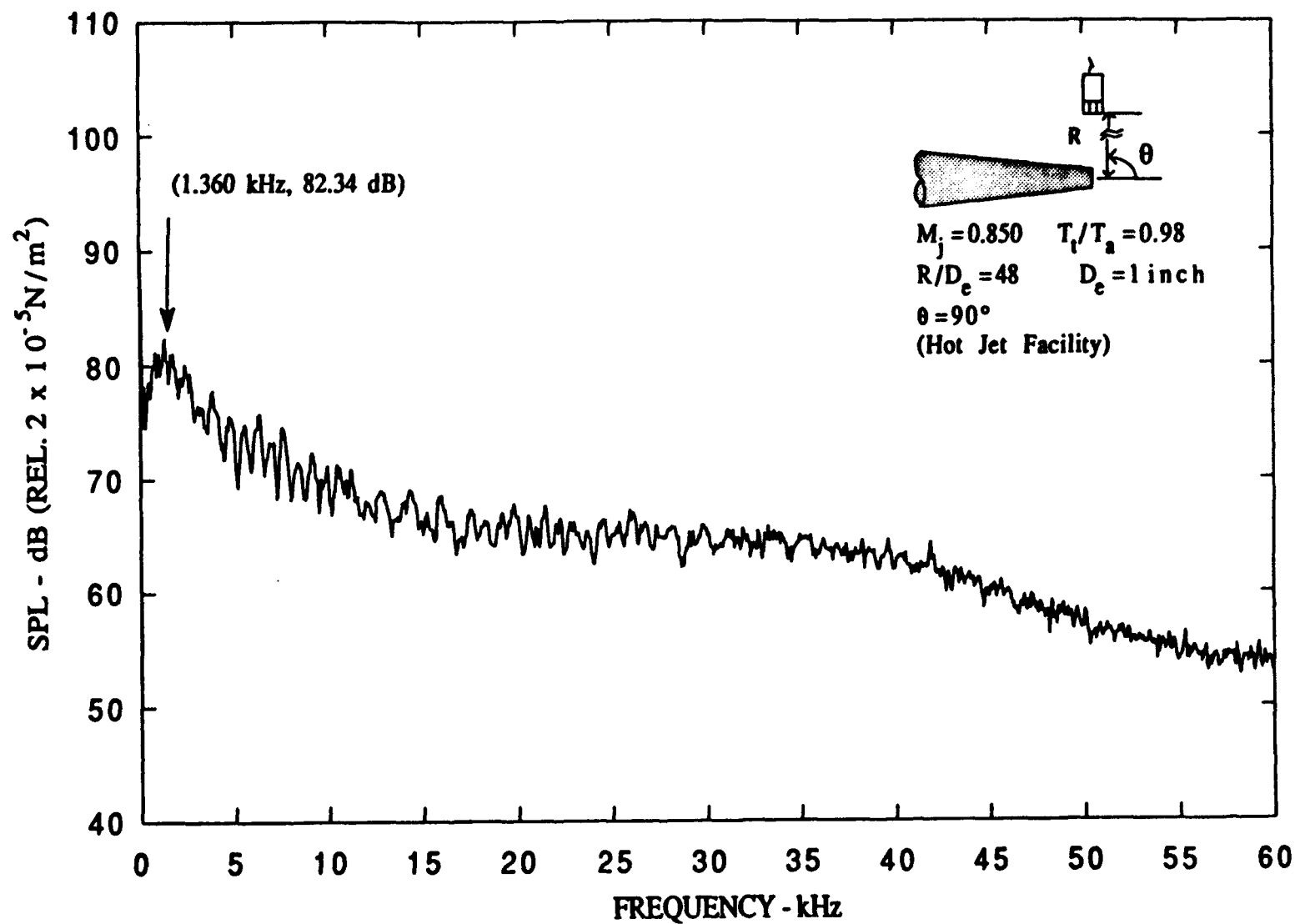
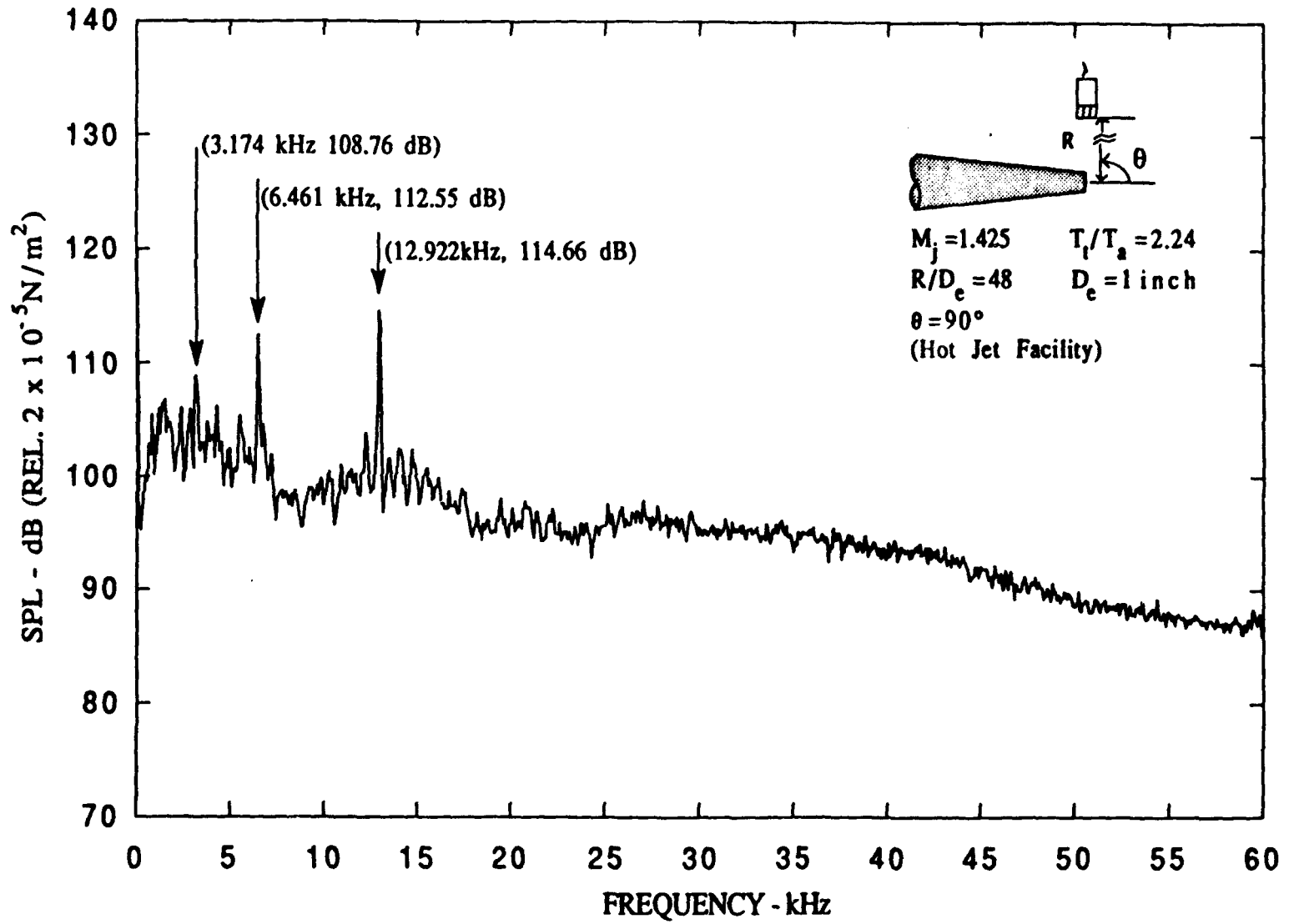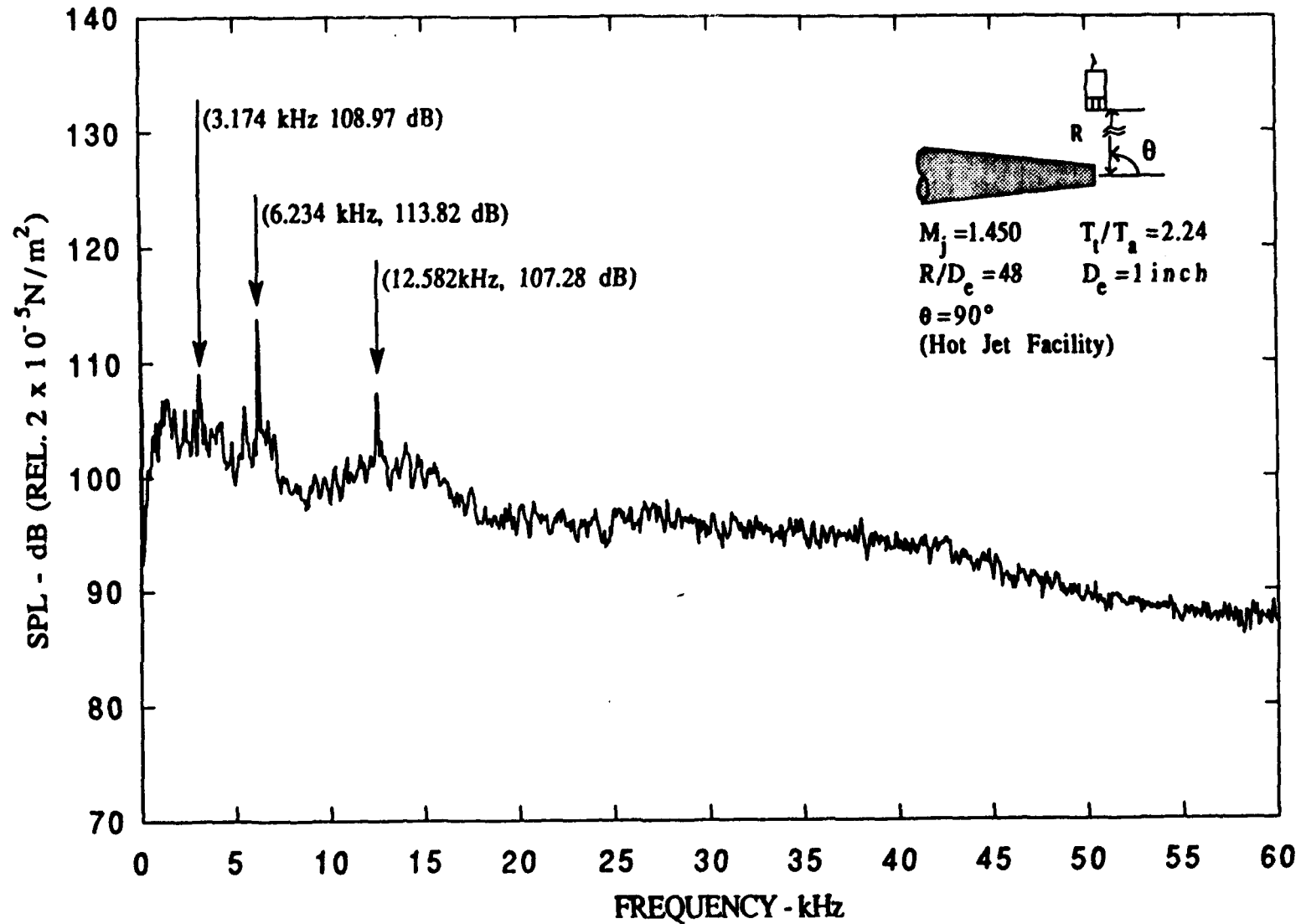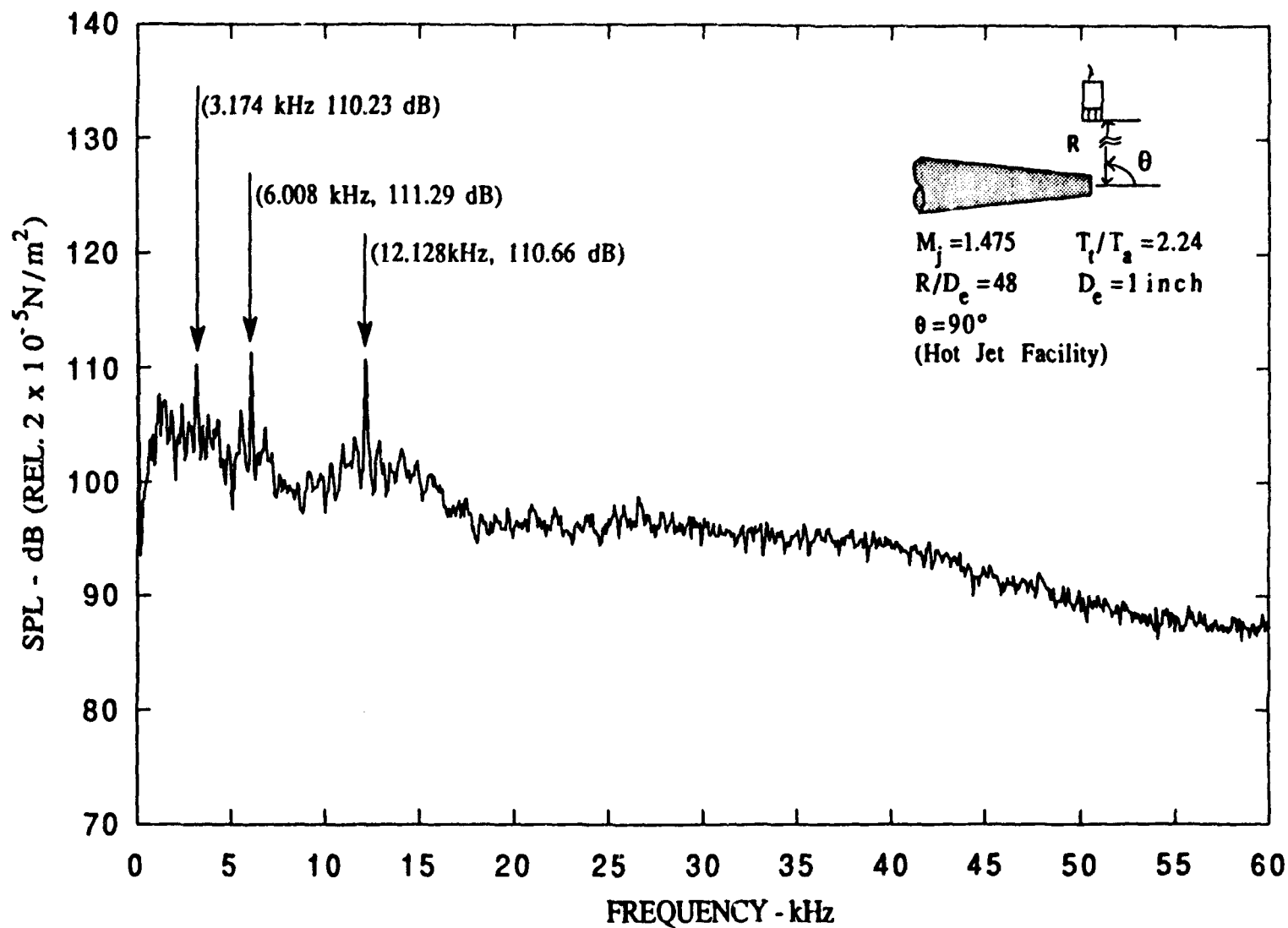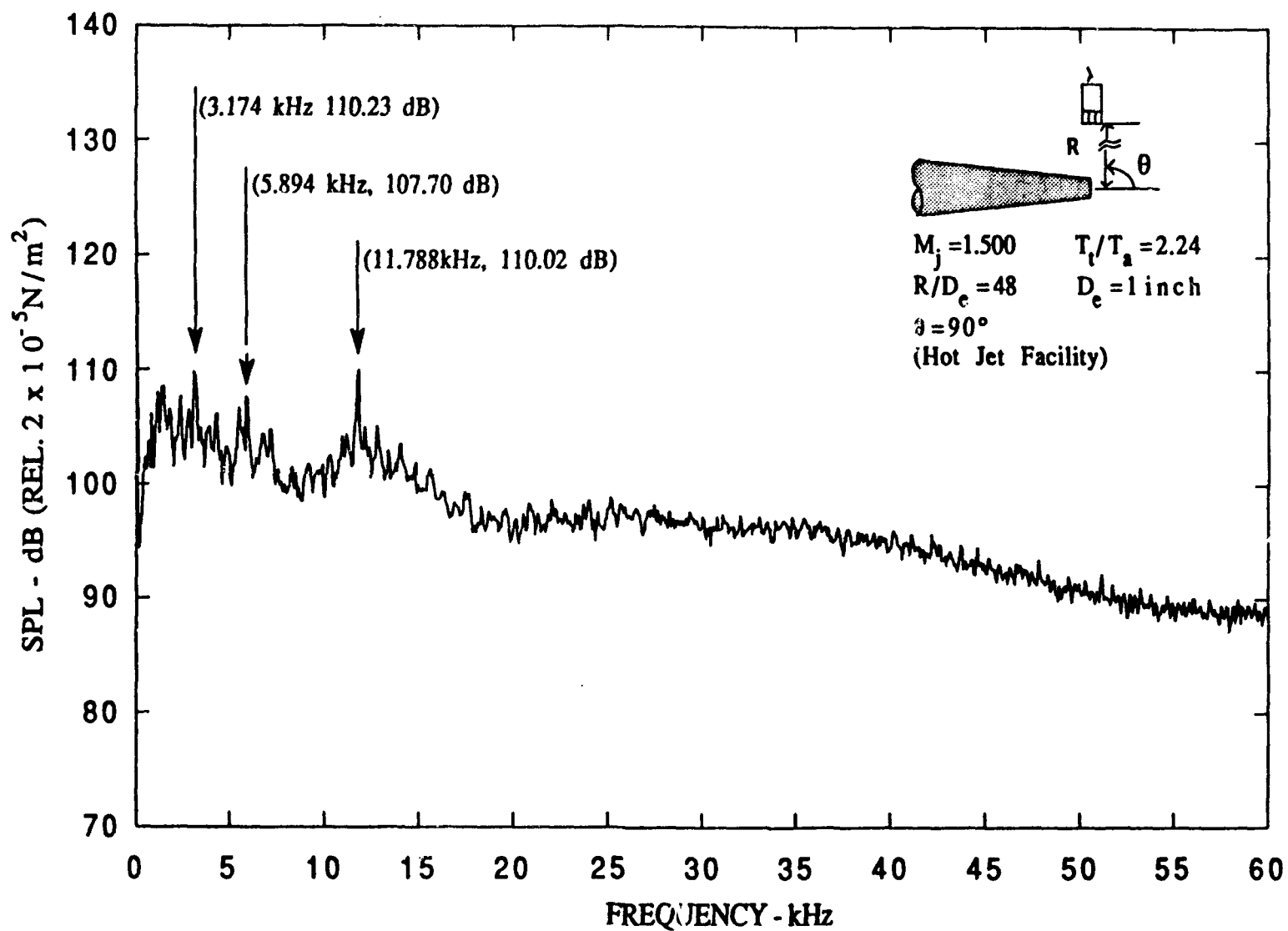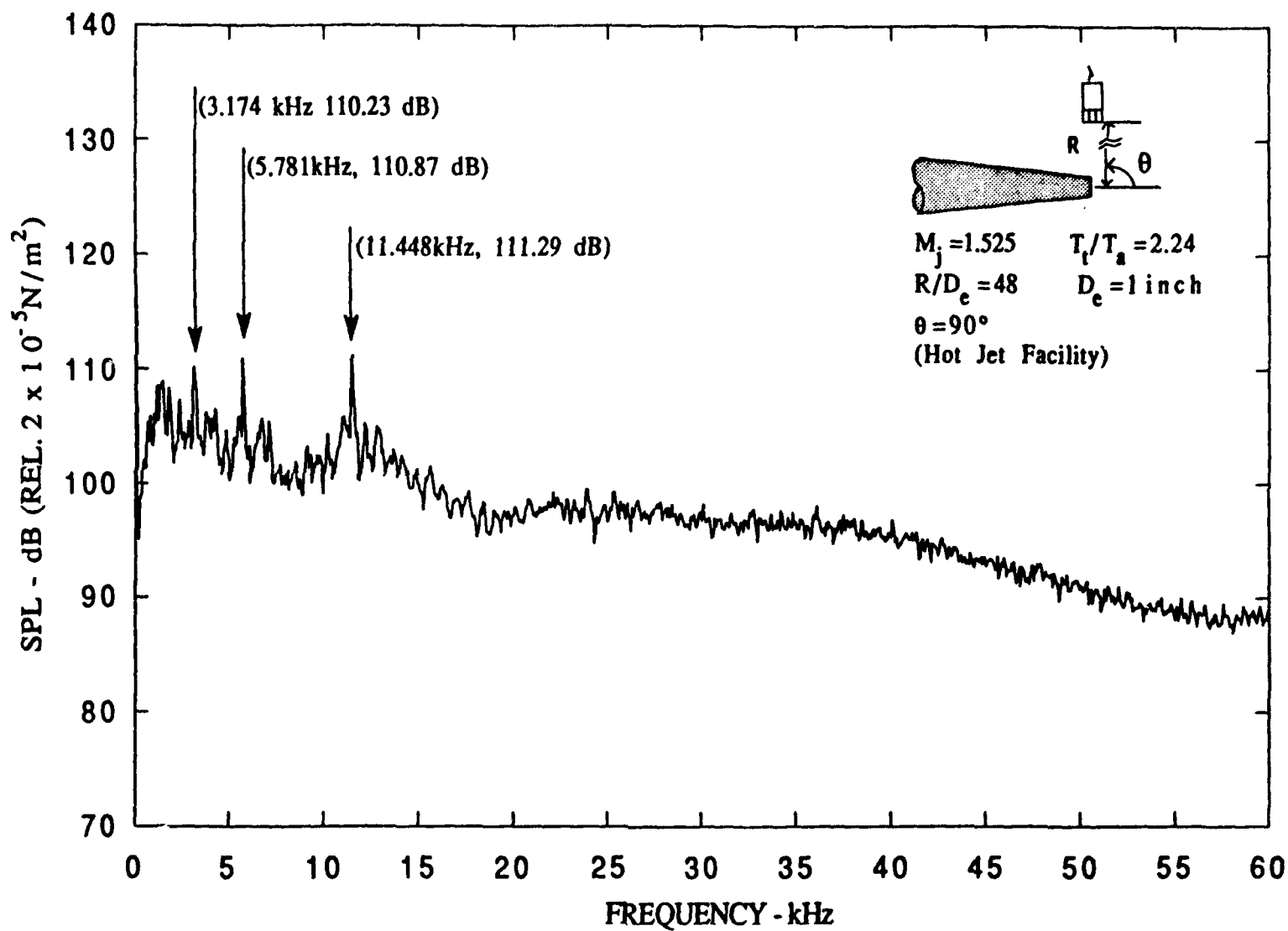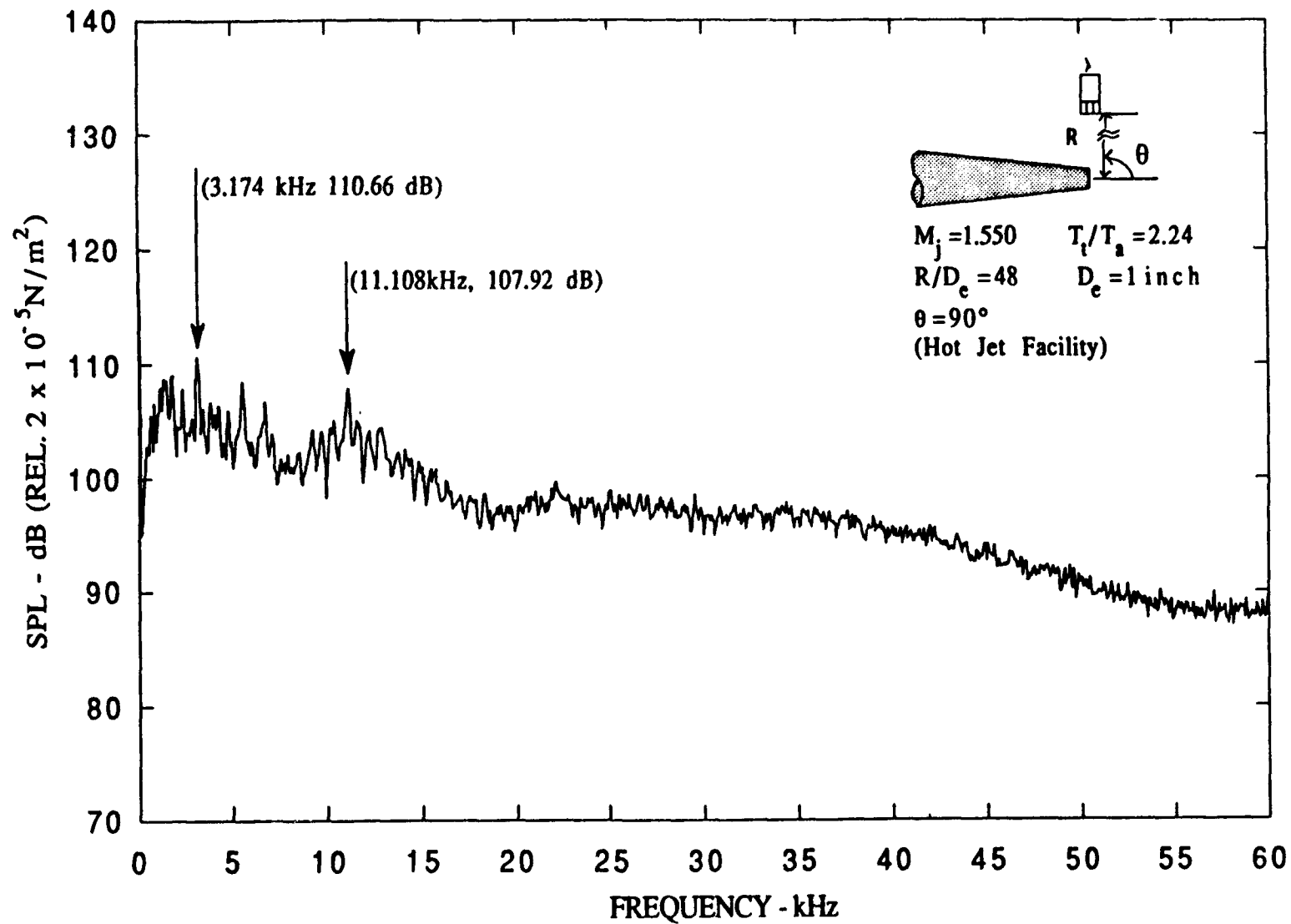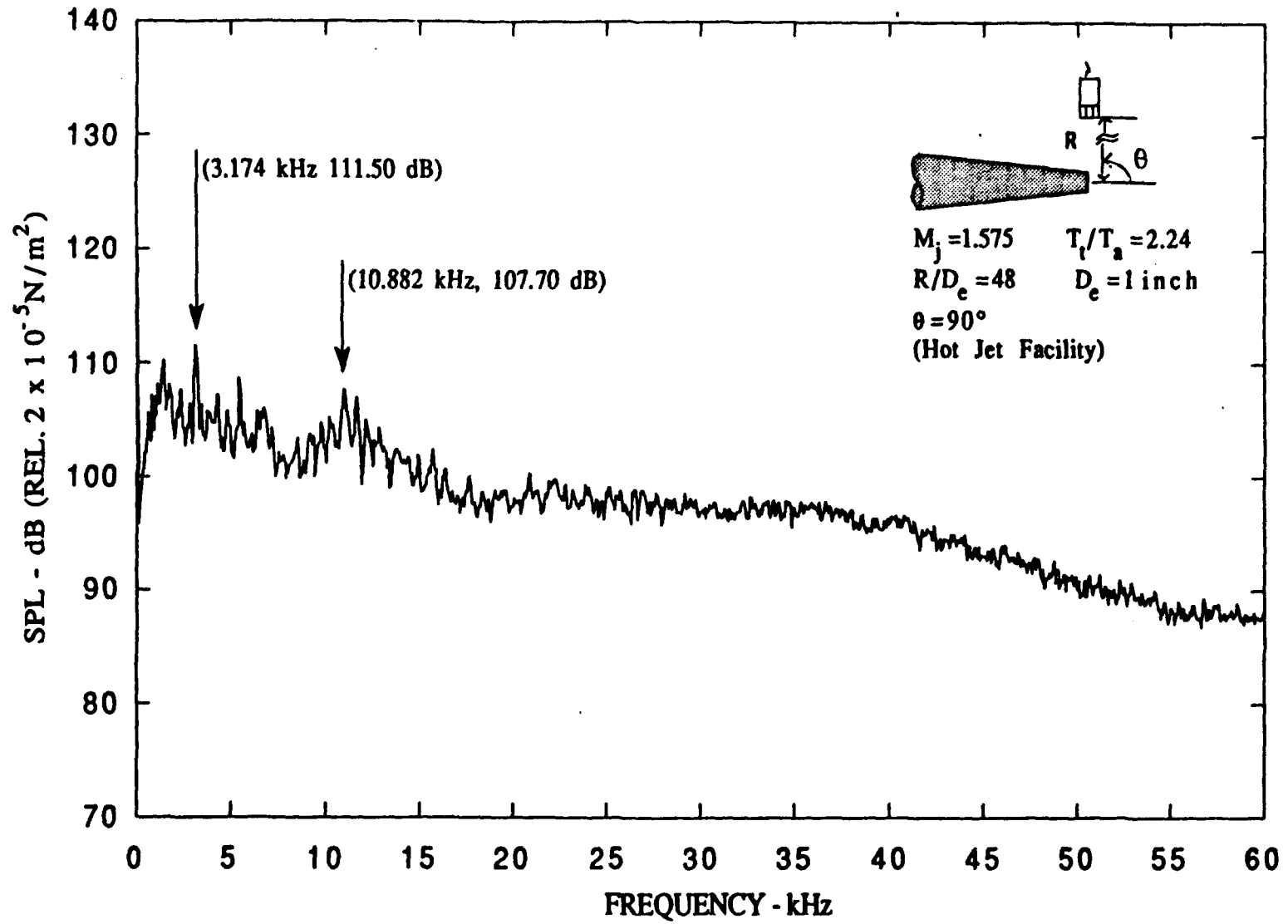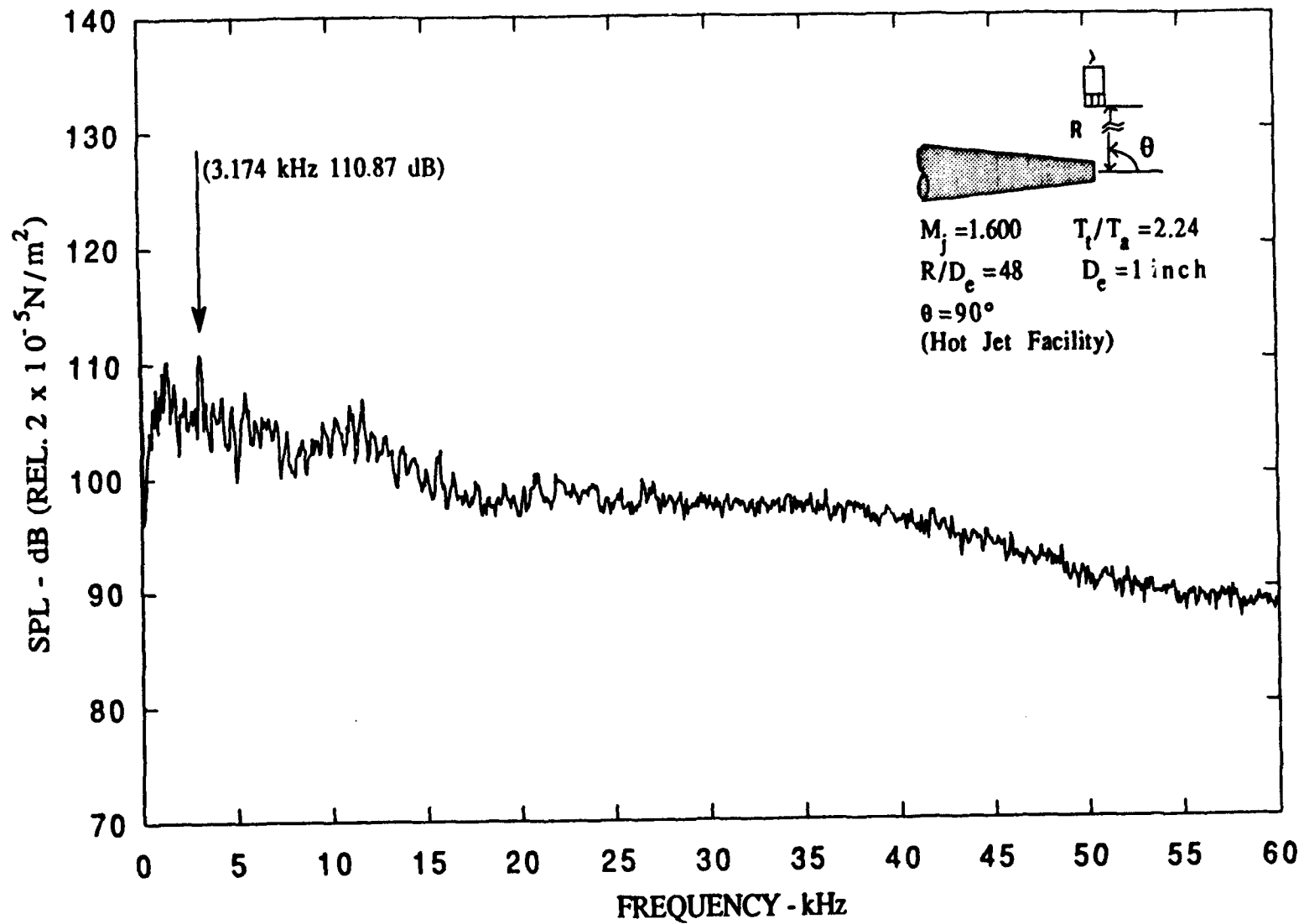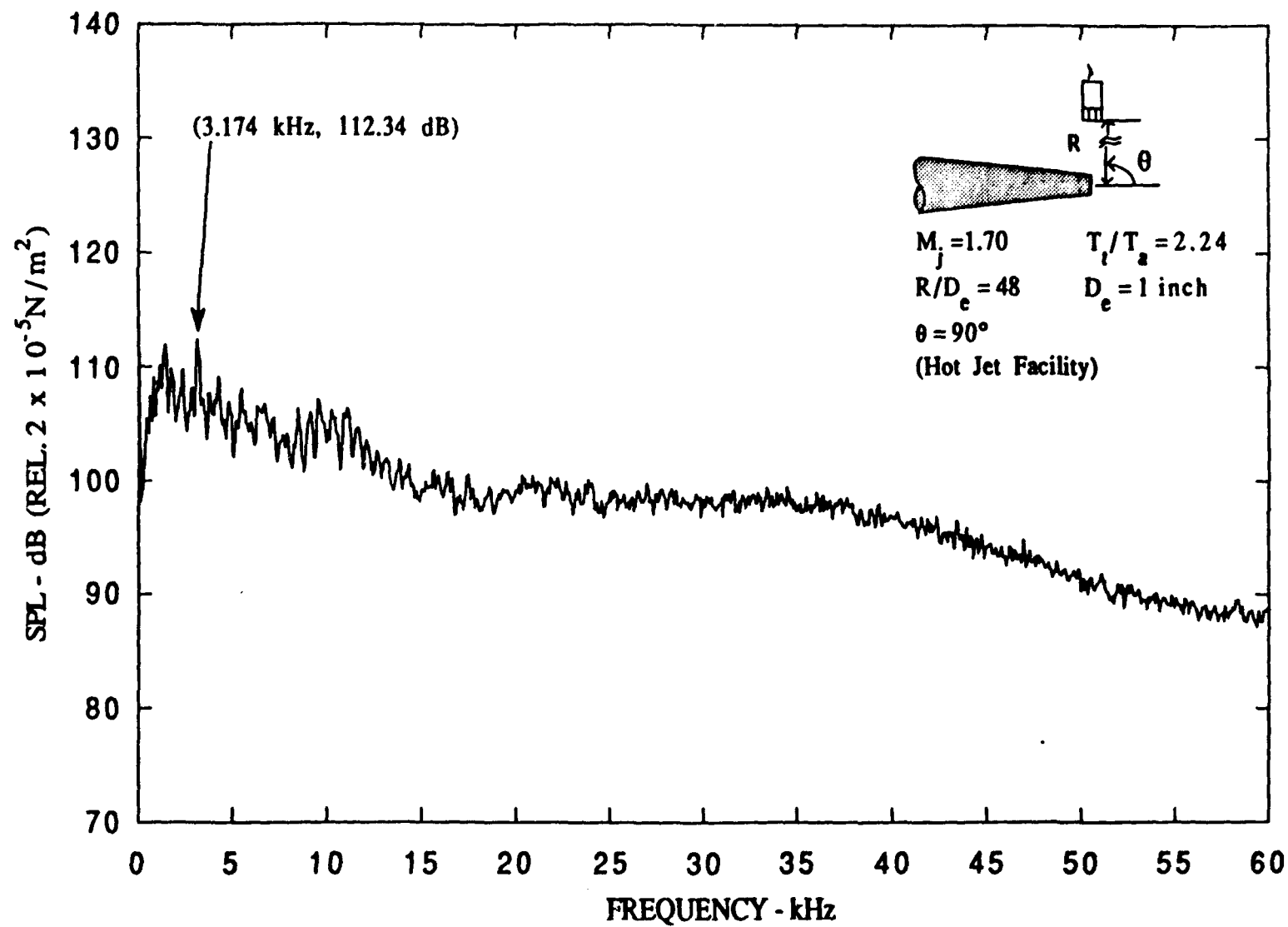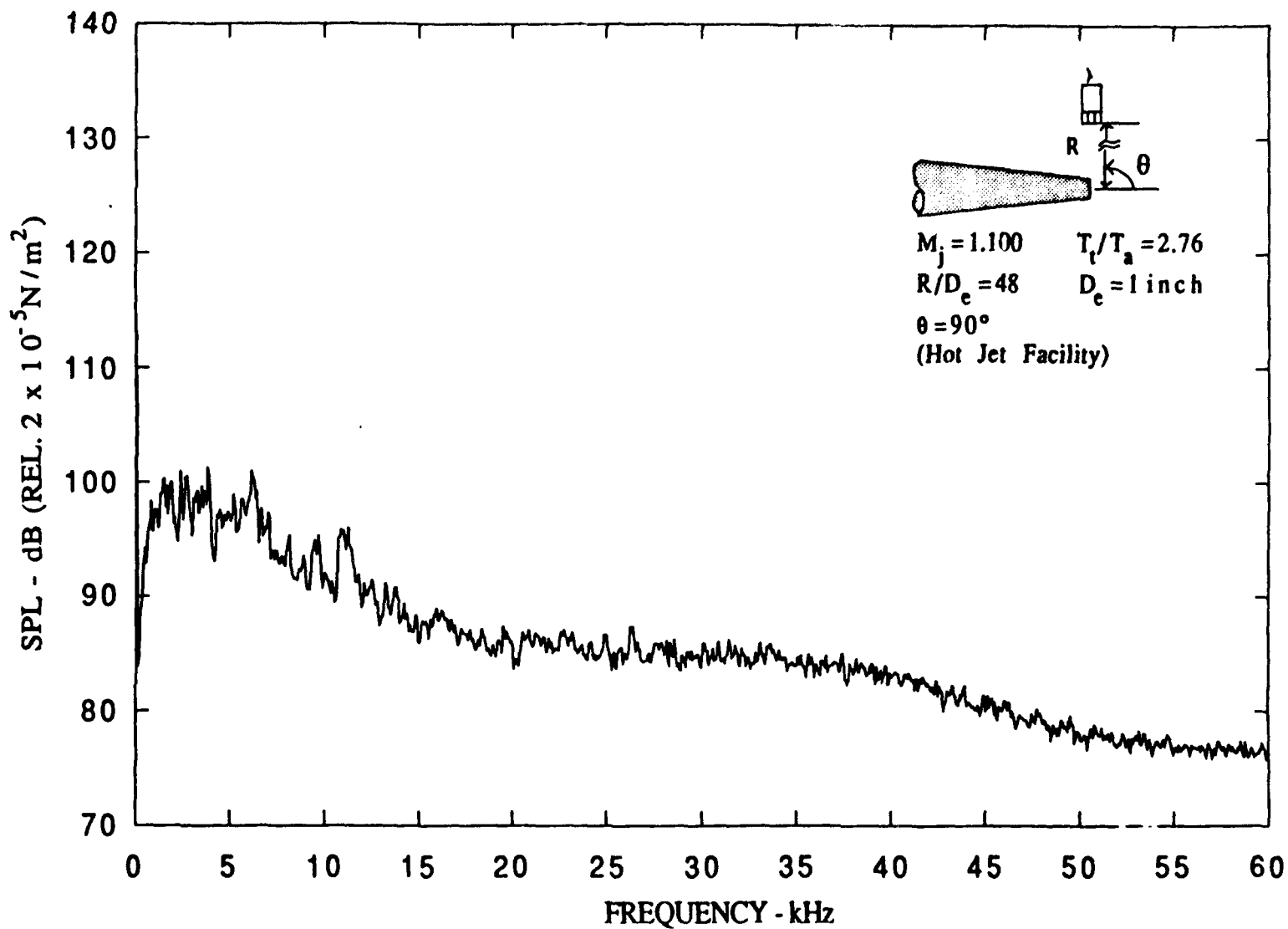Figure A-3. Narrow band spectra (Δf = 62.5 Hz), M_j = 0.850, T_t/T_a = 0.98.
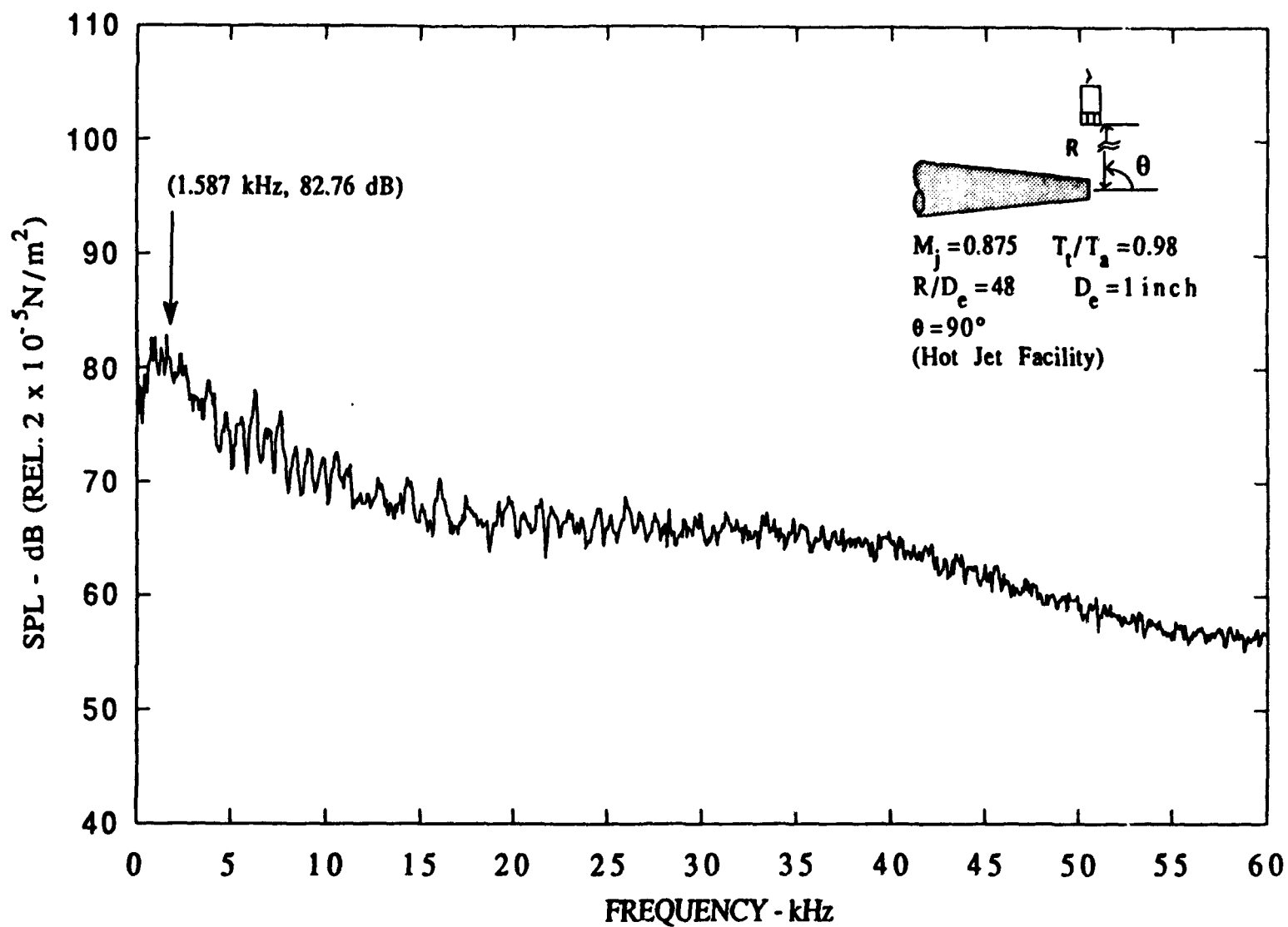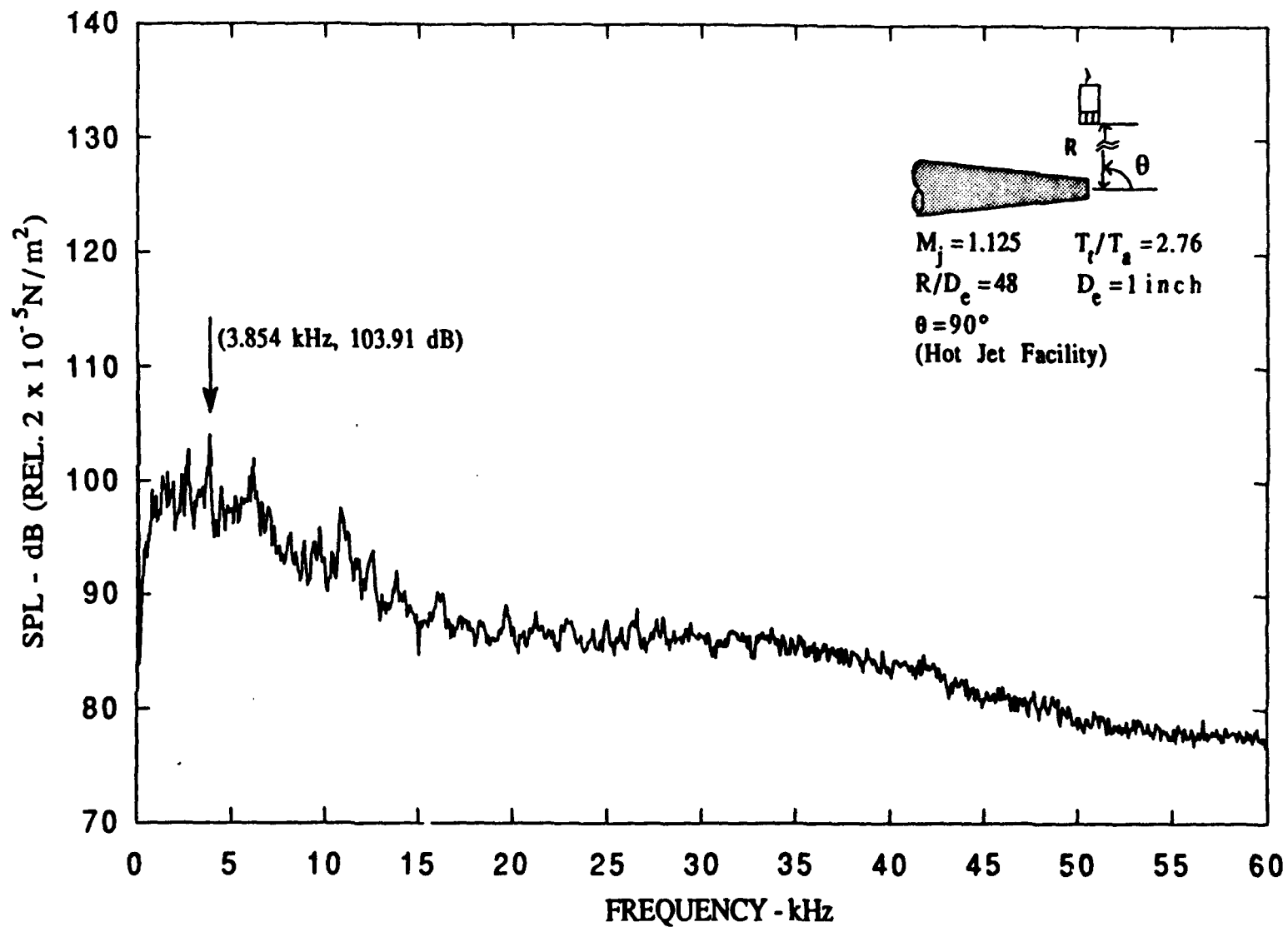
Figure A-4. Narrow band spectra ($\Delta f = 62.5$ Hz), $M_j = 0.875$, $T_t/T_a = 0.98$.
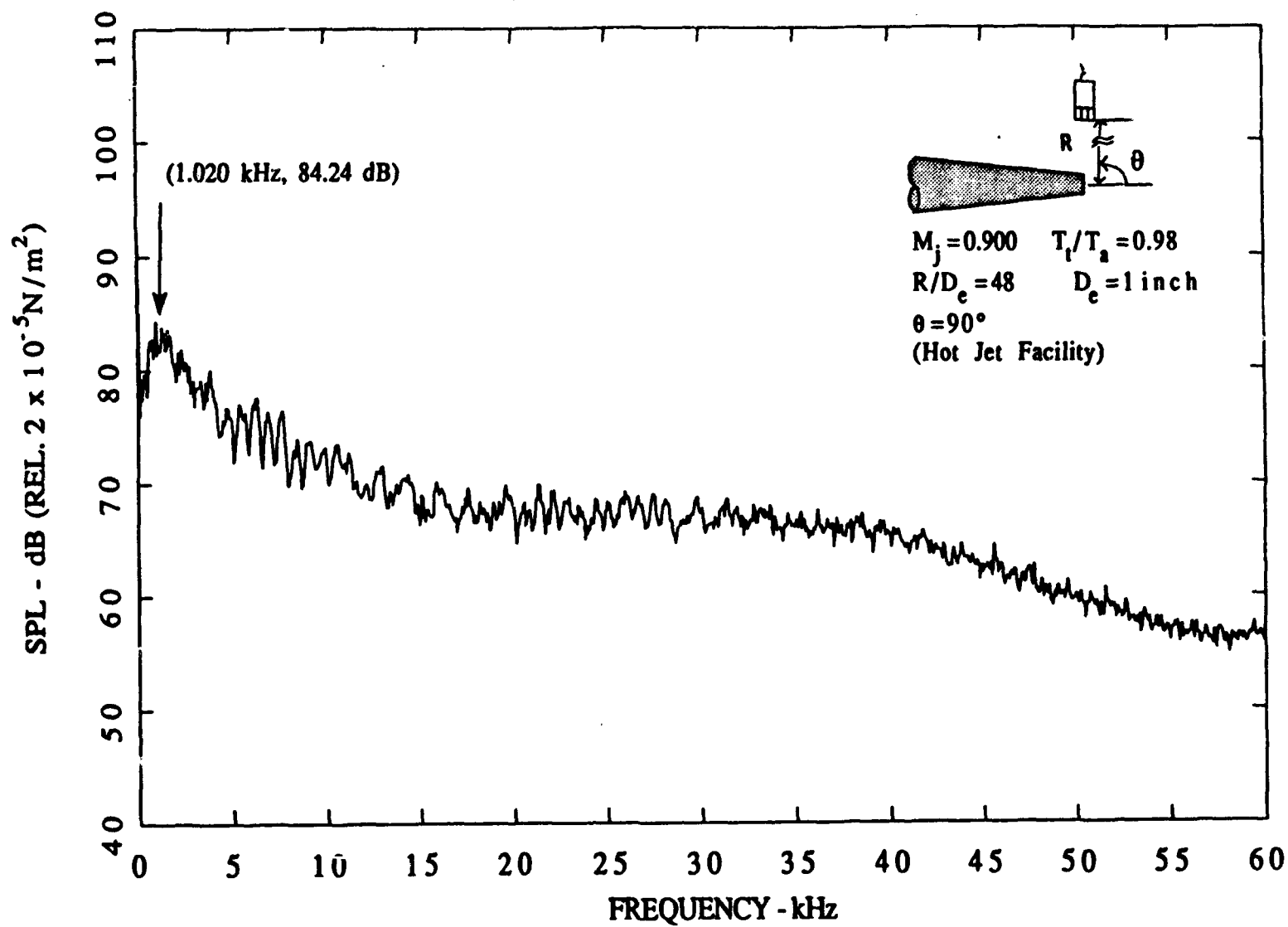
Figure A-5. Narrow band spectra (Δf = 62.5 Hz), M_j = 0.900, T_t/T_a = 0.98.
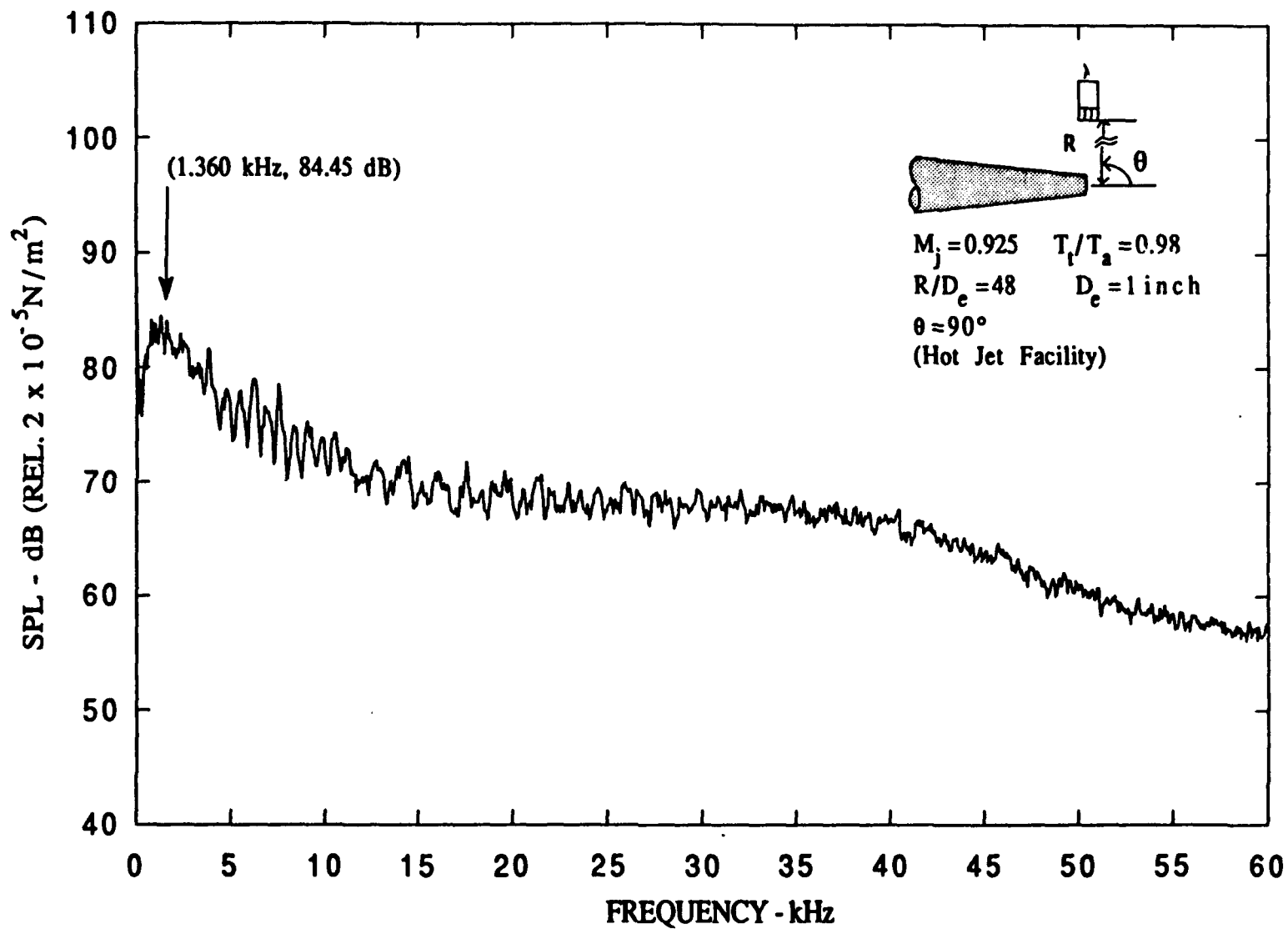
Figure A-6. Narrow band spectra ($\Delta f = 62.5$ Hz), $M_j = 0.925$, $T_t/T_a = 0.98$.
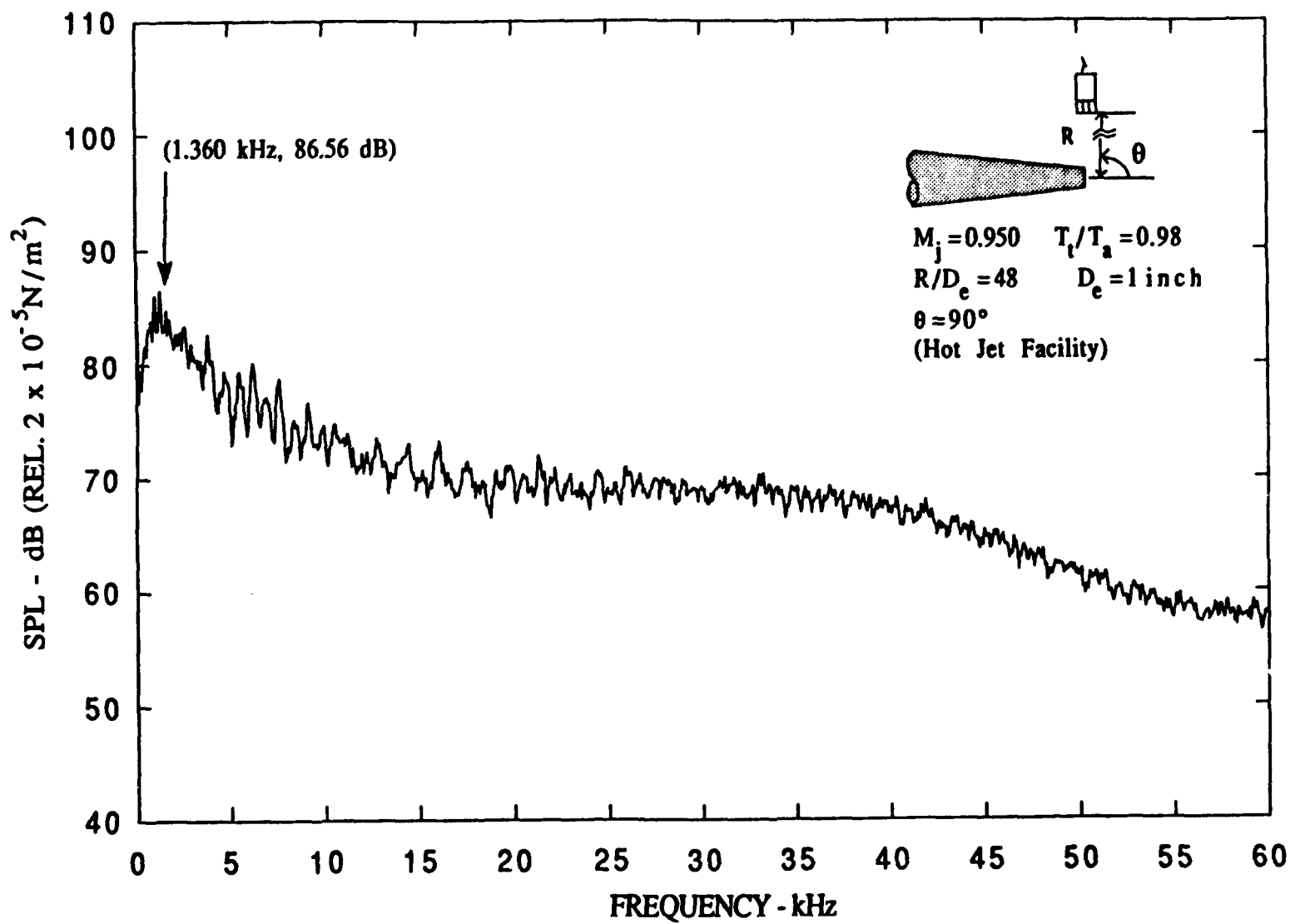
Figure A-7. Narrow band spectra (Δf = 62.5 Hz), M_j = 0.950, T_t/T_a = 0.98.
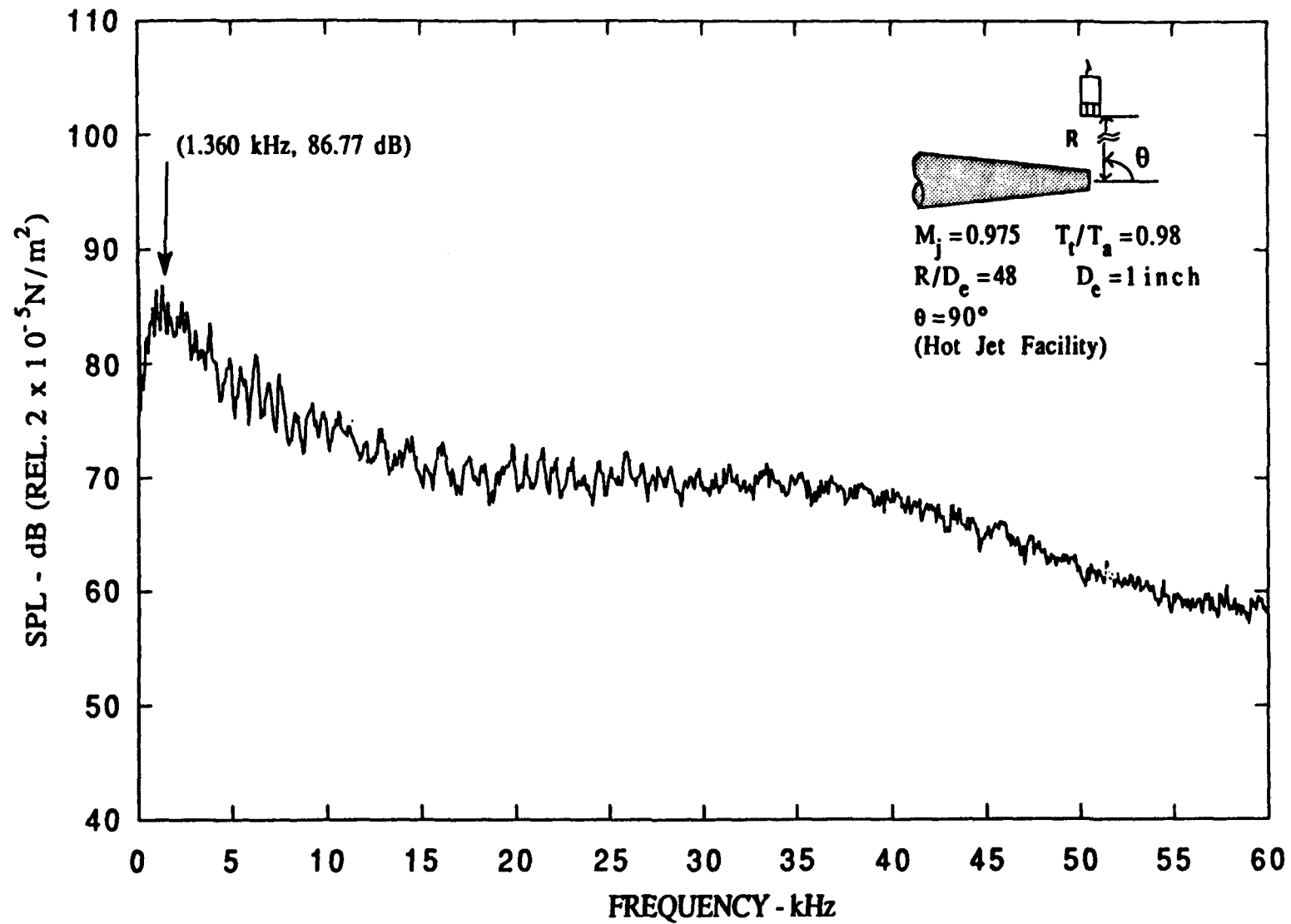
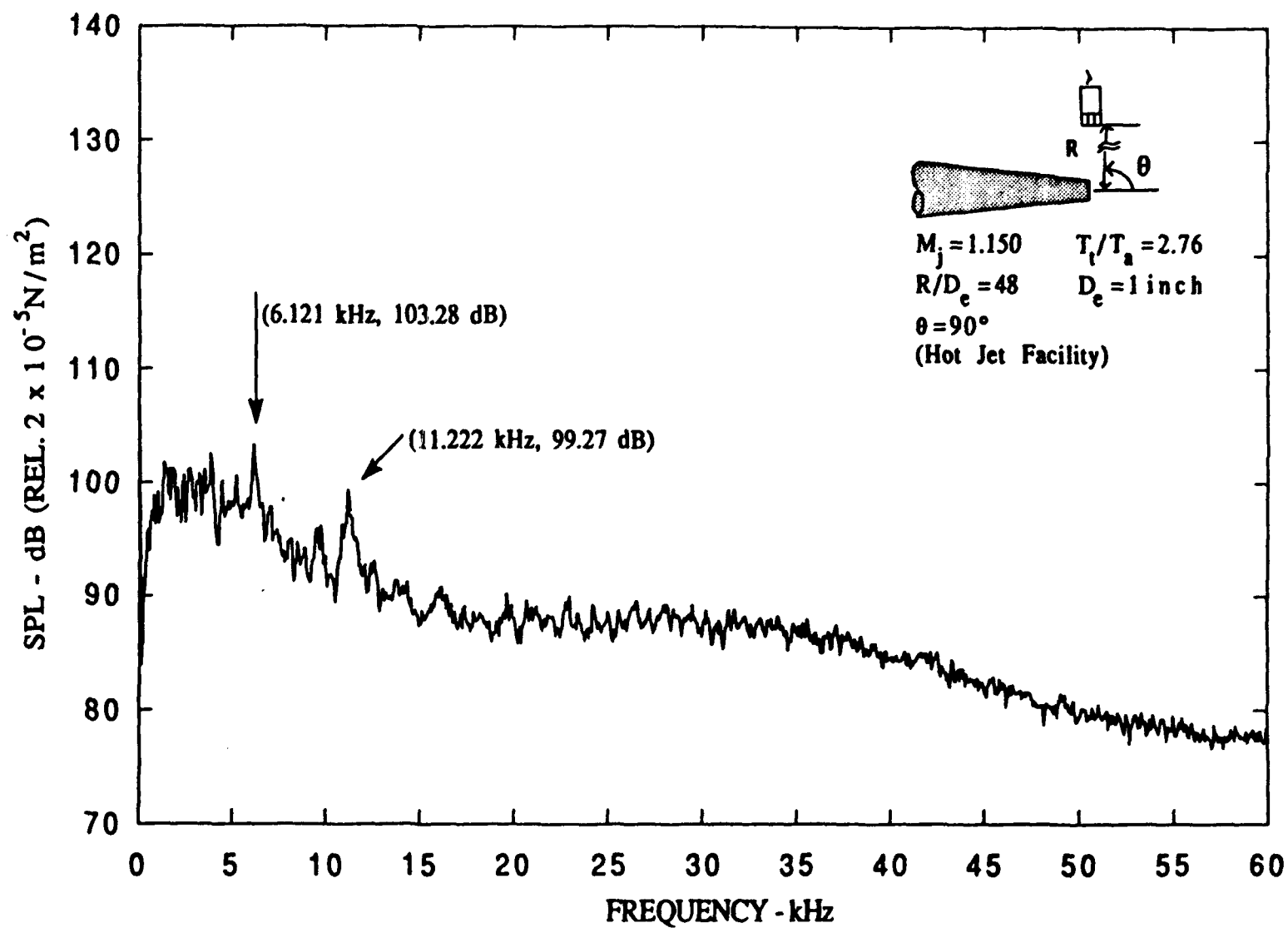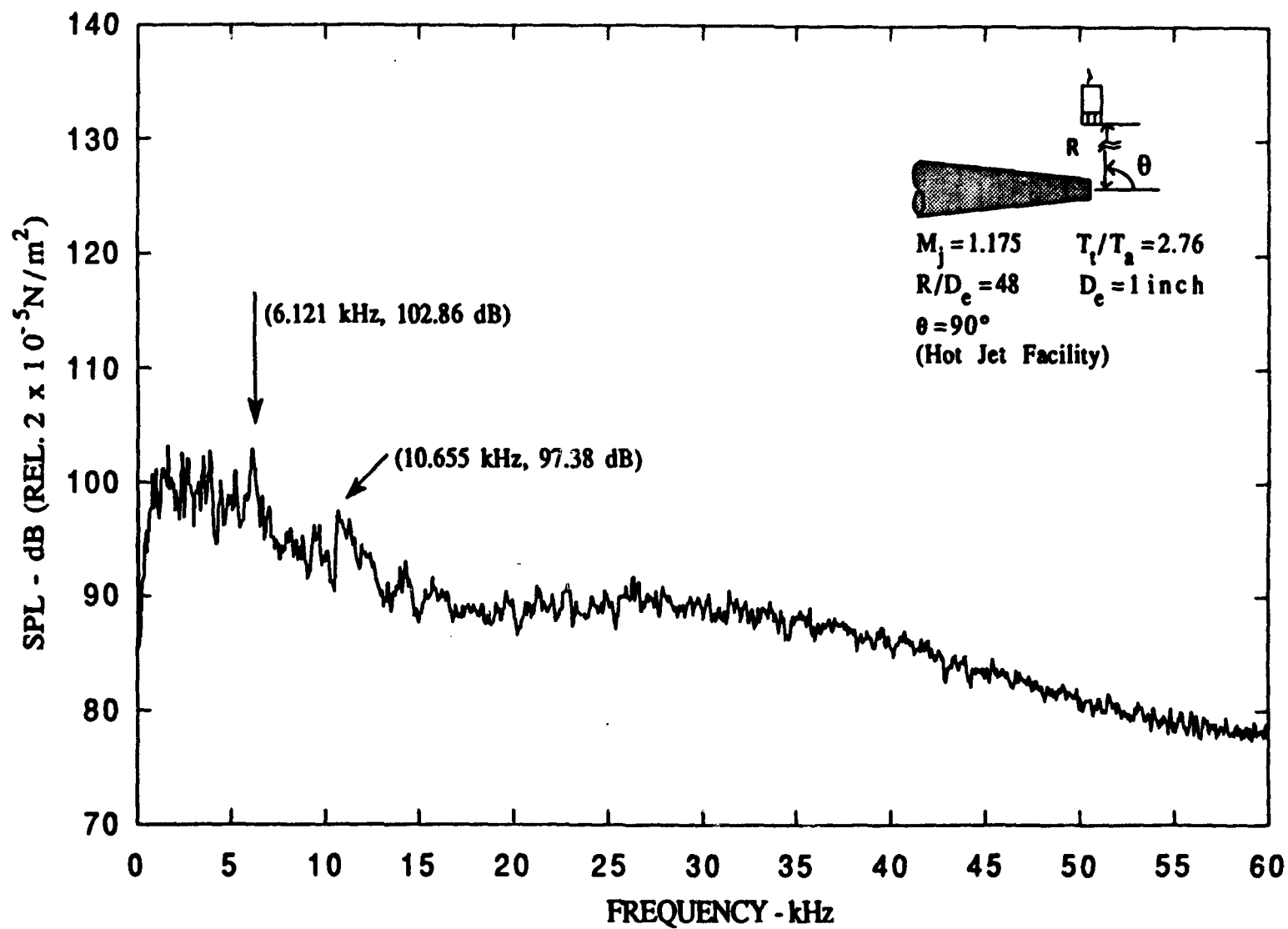Figure A-8. Narrow band spectra ($\Delta f = 62.5$ Hz), $M_j = 0.975$, $T_t/T_a = 0.98$.
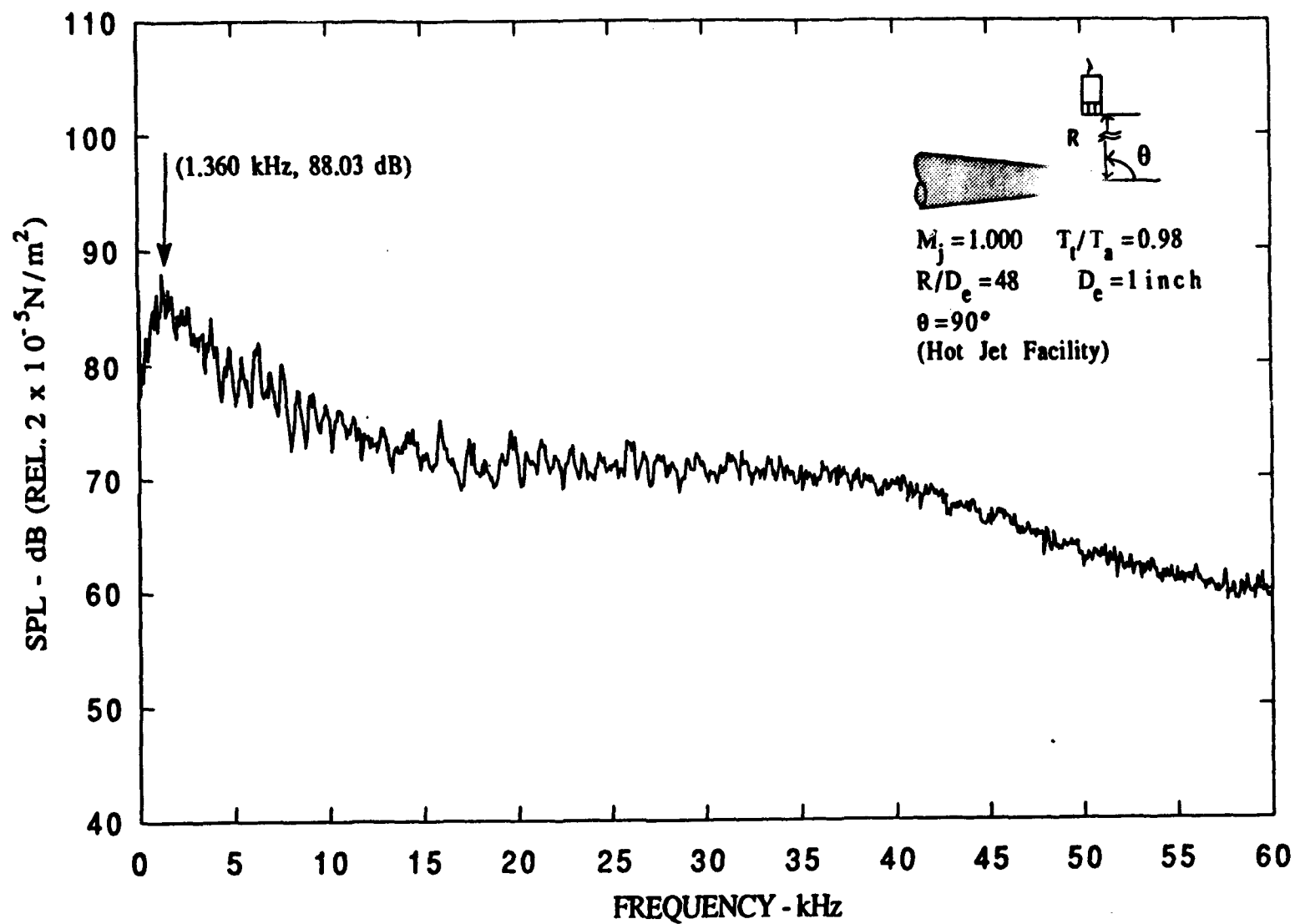
Figure A-9. Narrow band spectra ($\Delta f = 62.5$ Hz), $M_j = 1.000$, $T_t/T_a = 0.98$.
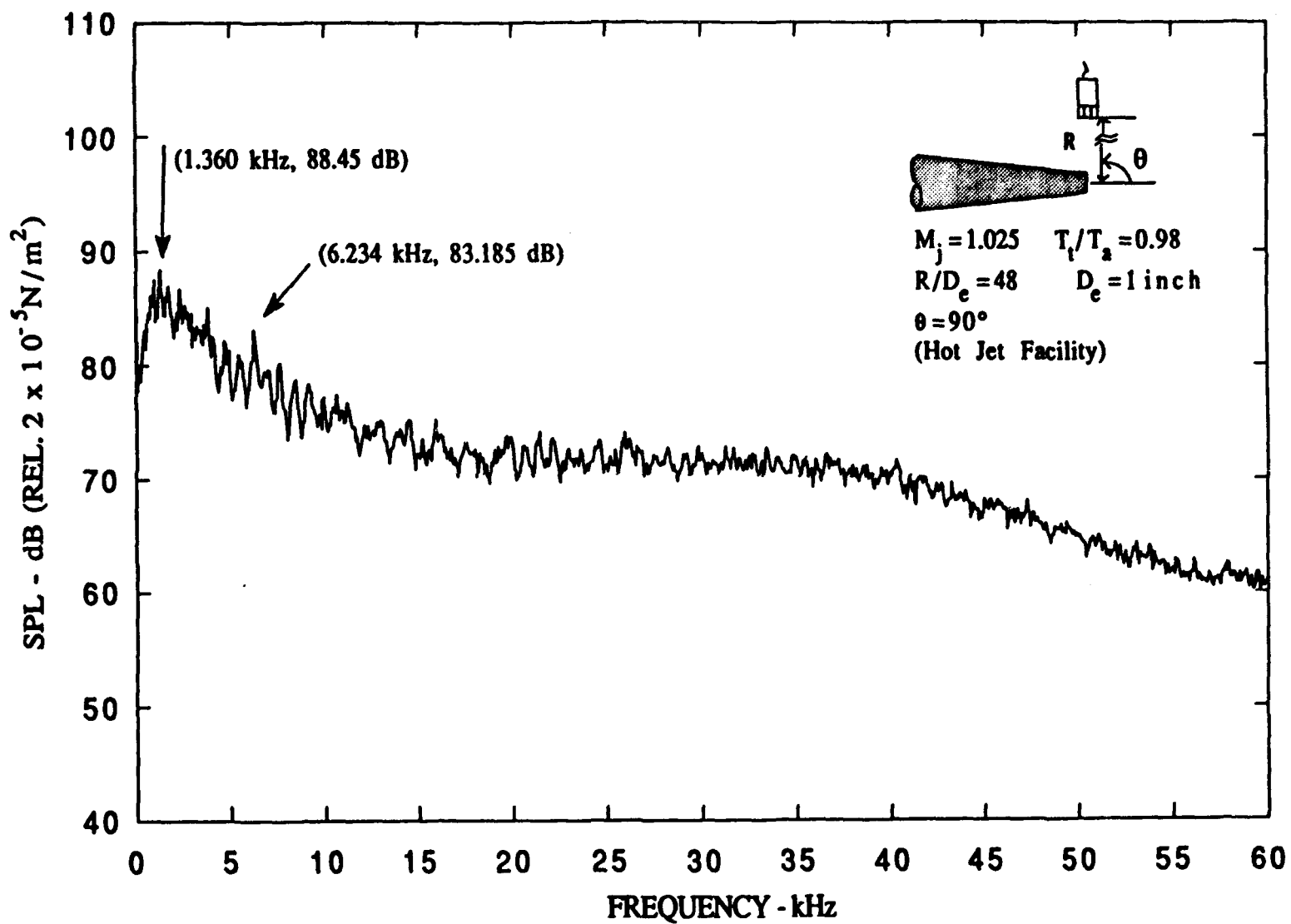
Figure A-10. Narrow band spectra ($\Delta f = 62.5$ Hz), $M_j = 1.025$, $T_t/T_a = 0.98$.
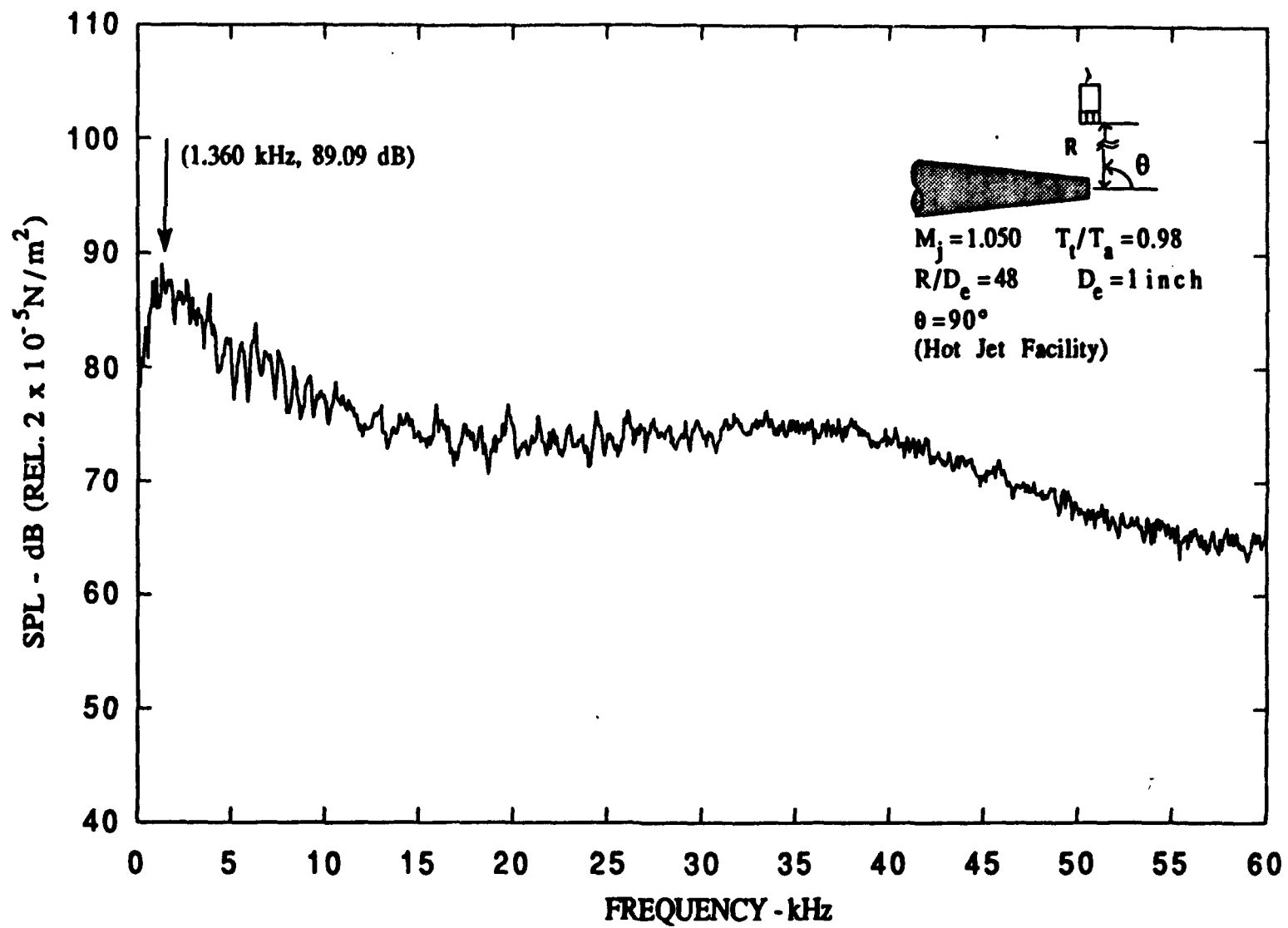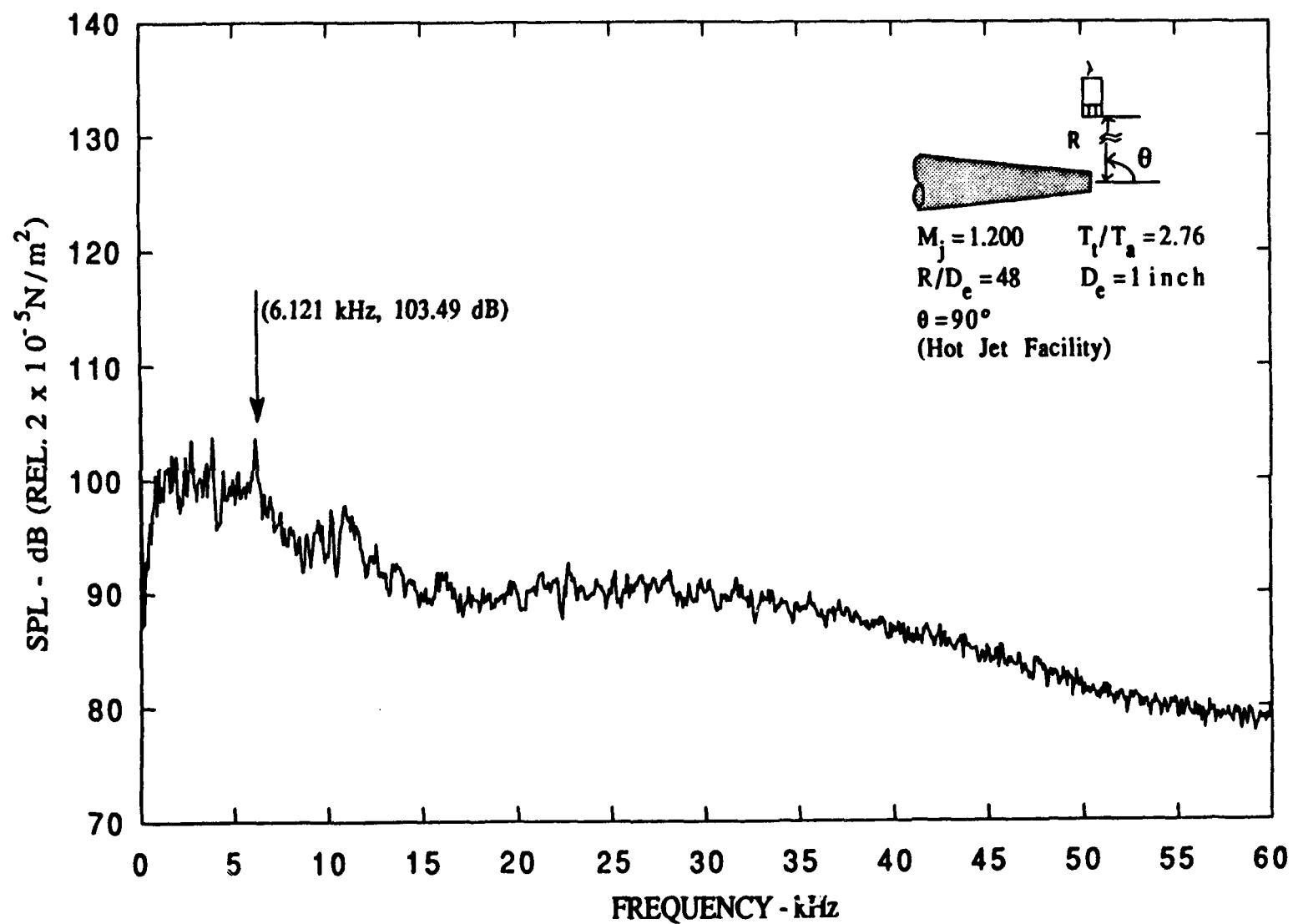
Figure A-11. Narrow band spectra ($\Delta f = 62.5$ Hz), $M_j = 1.050$, $T_t/T_a = 0.98$.
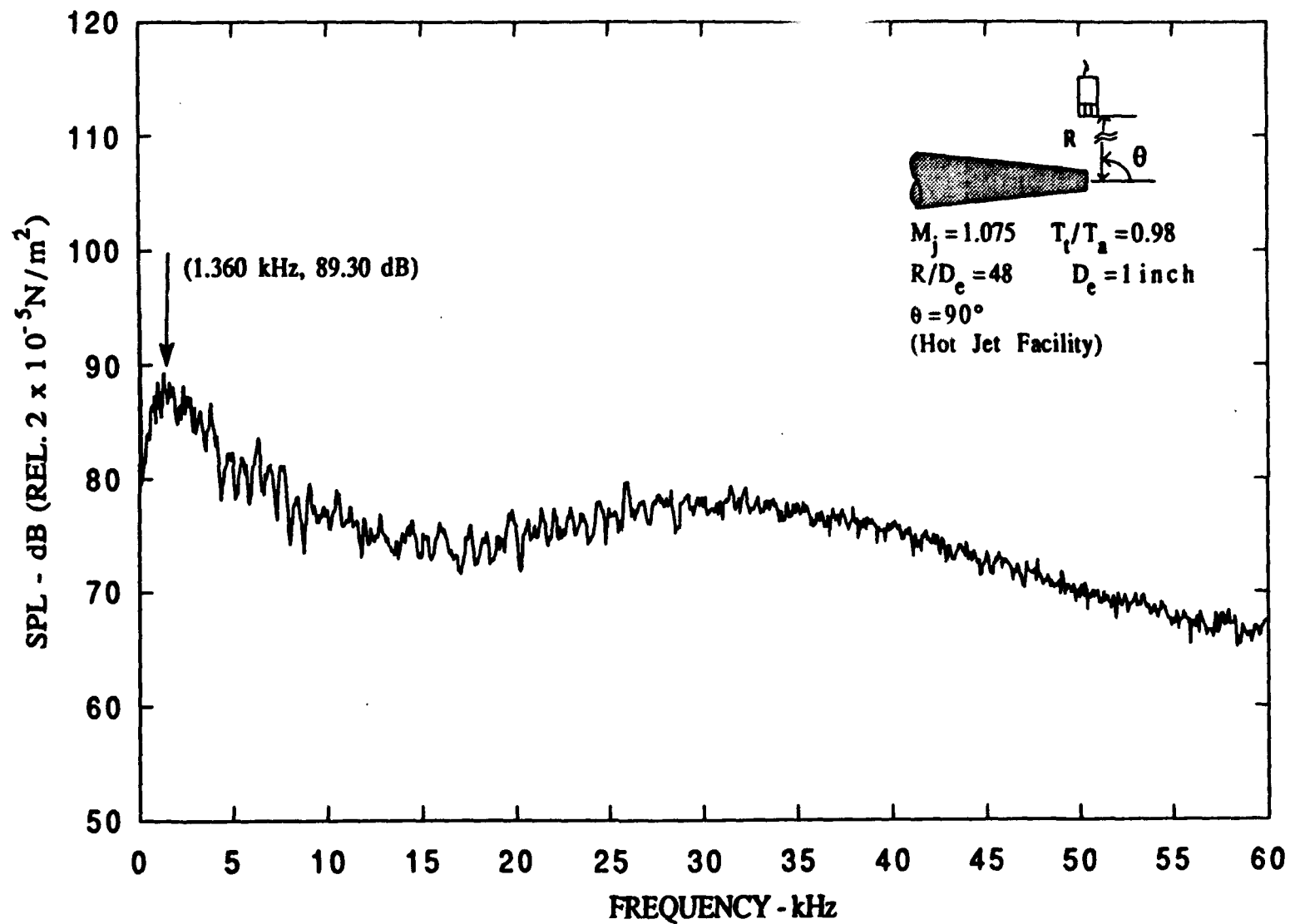
Figure A-12. Narrow band spectra ($\Delta f = 62.5$ Hz), $M_j = 1.075$, $T_t/T_a = 0.98$.
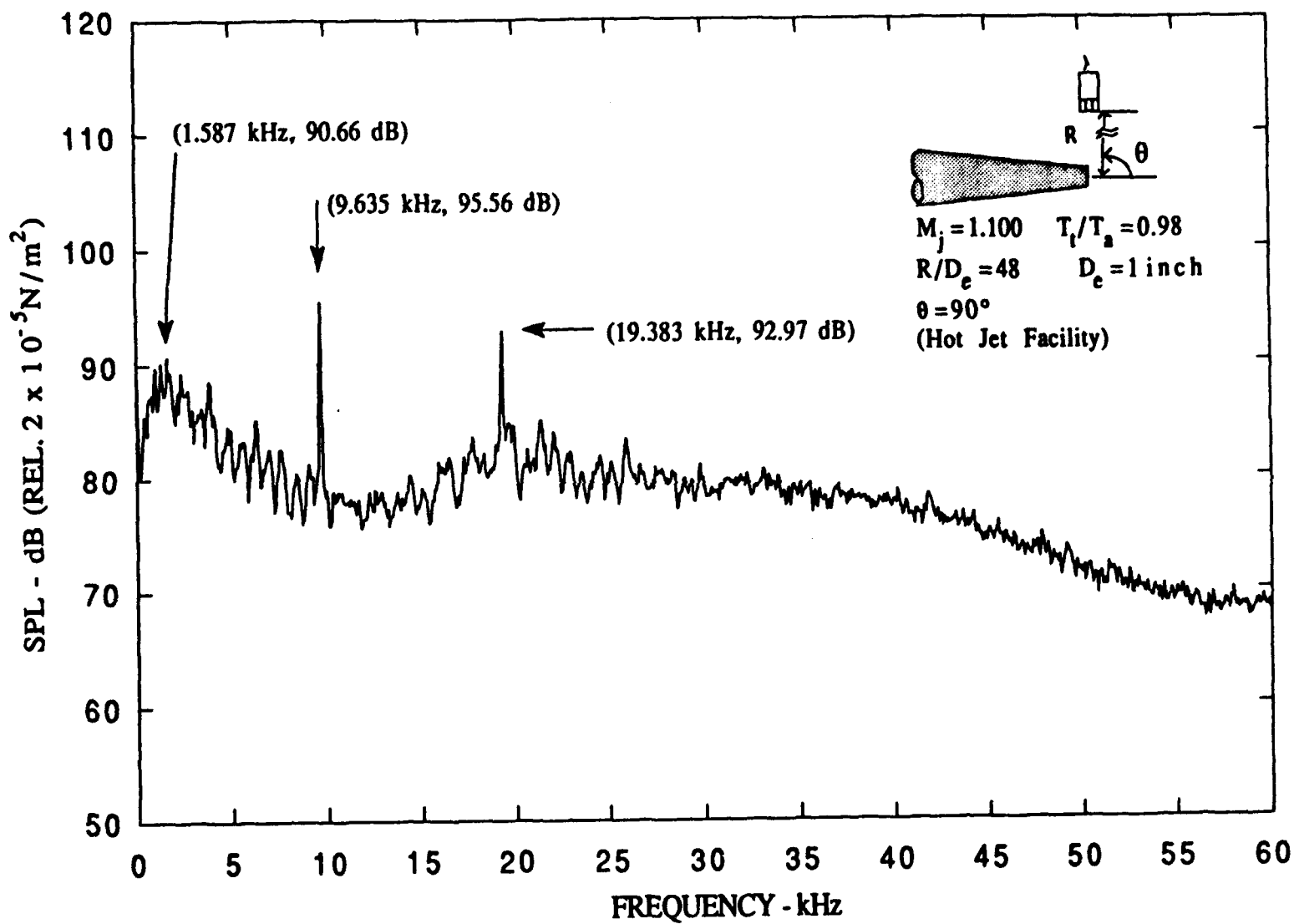
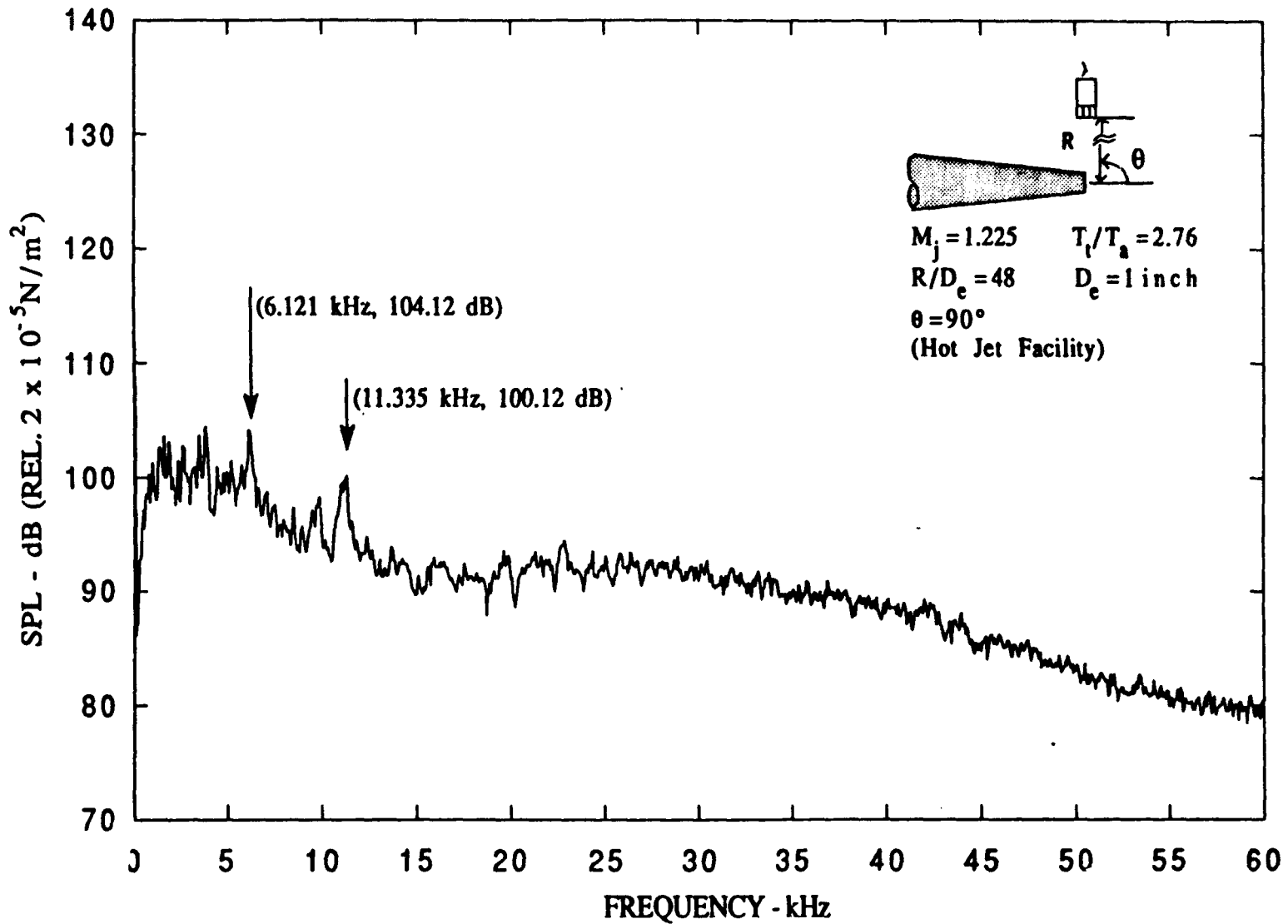Figure A-13. Narrow band spectra ($\Delta f = 62.5$ Hz), $M_j = 1.100$, $T_t/T_a = 0.98$.
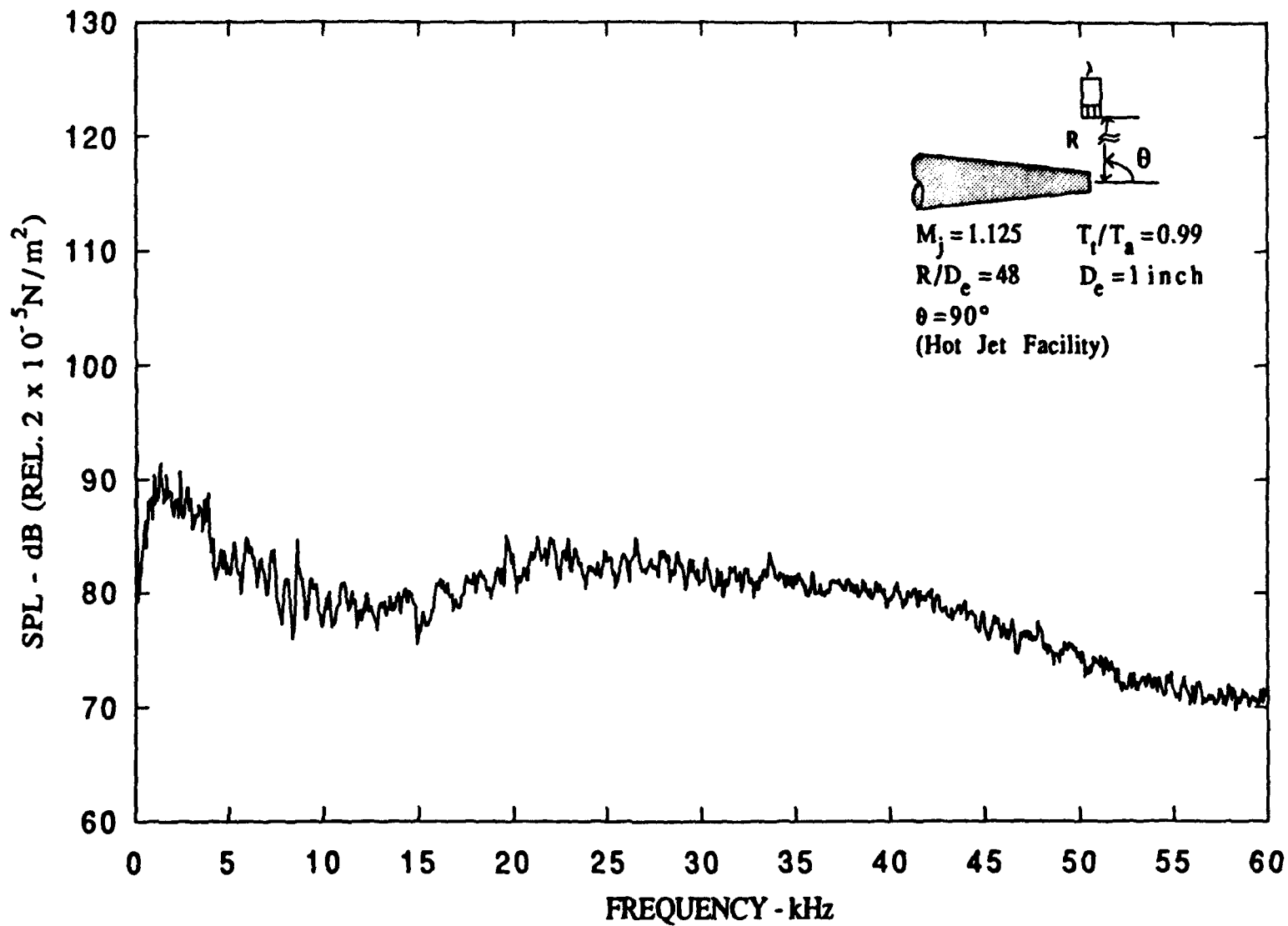
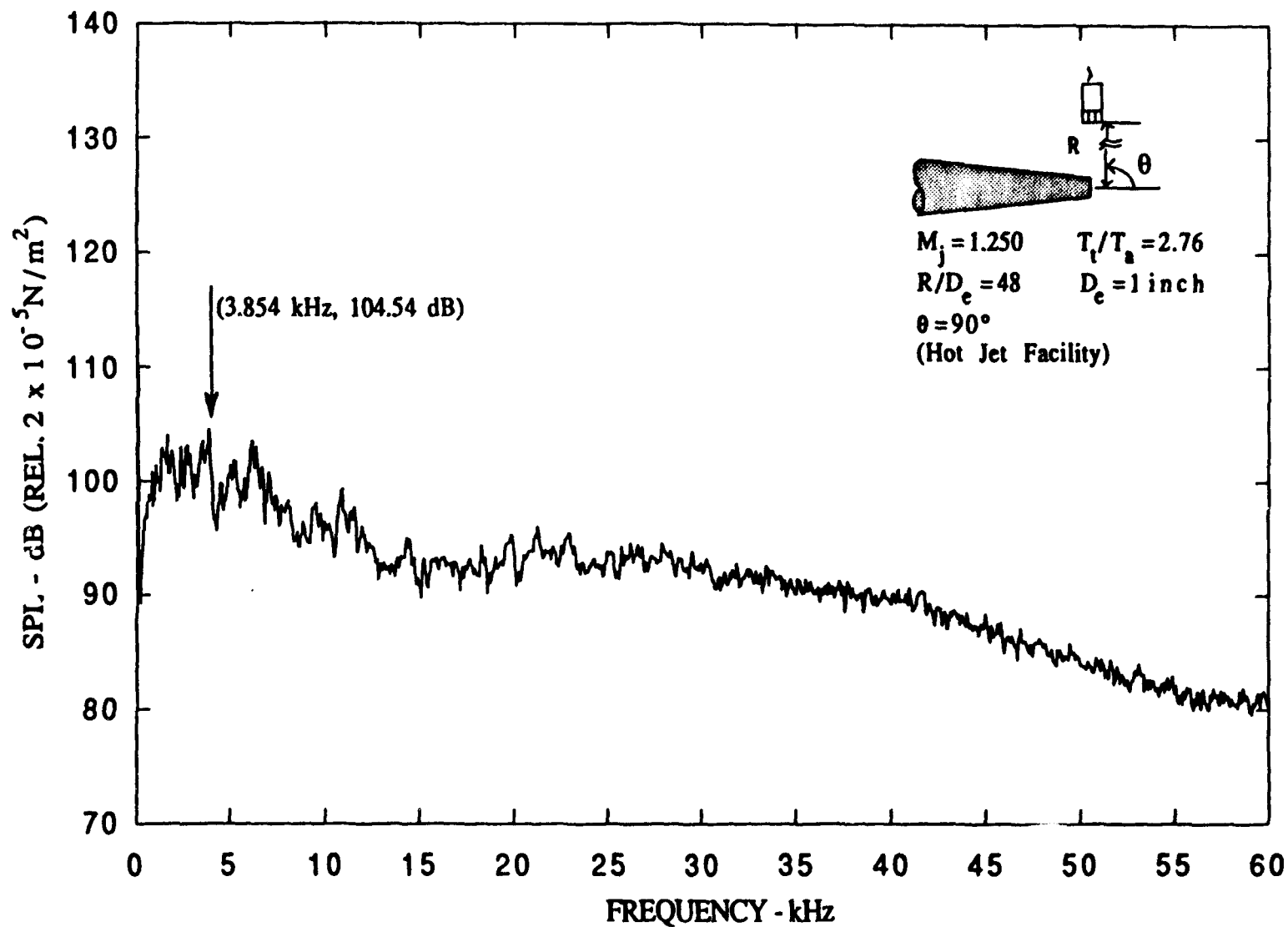Figure A-14. Narrow band spectra ($\Delta f = 62.5$ Hz), $M_j = 1.125$, $T_t/T_a = 0.99$.
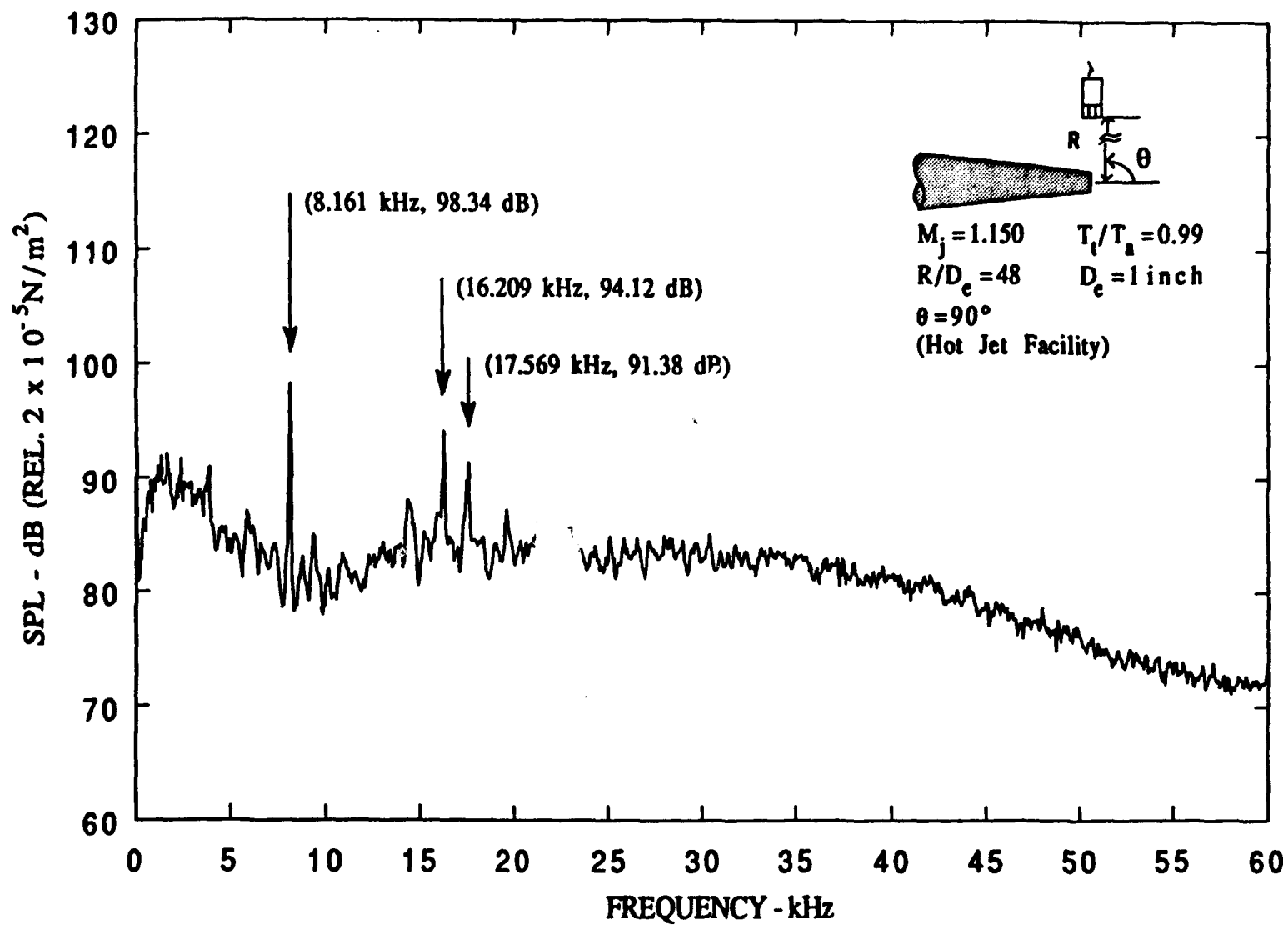
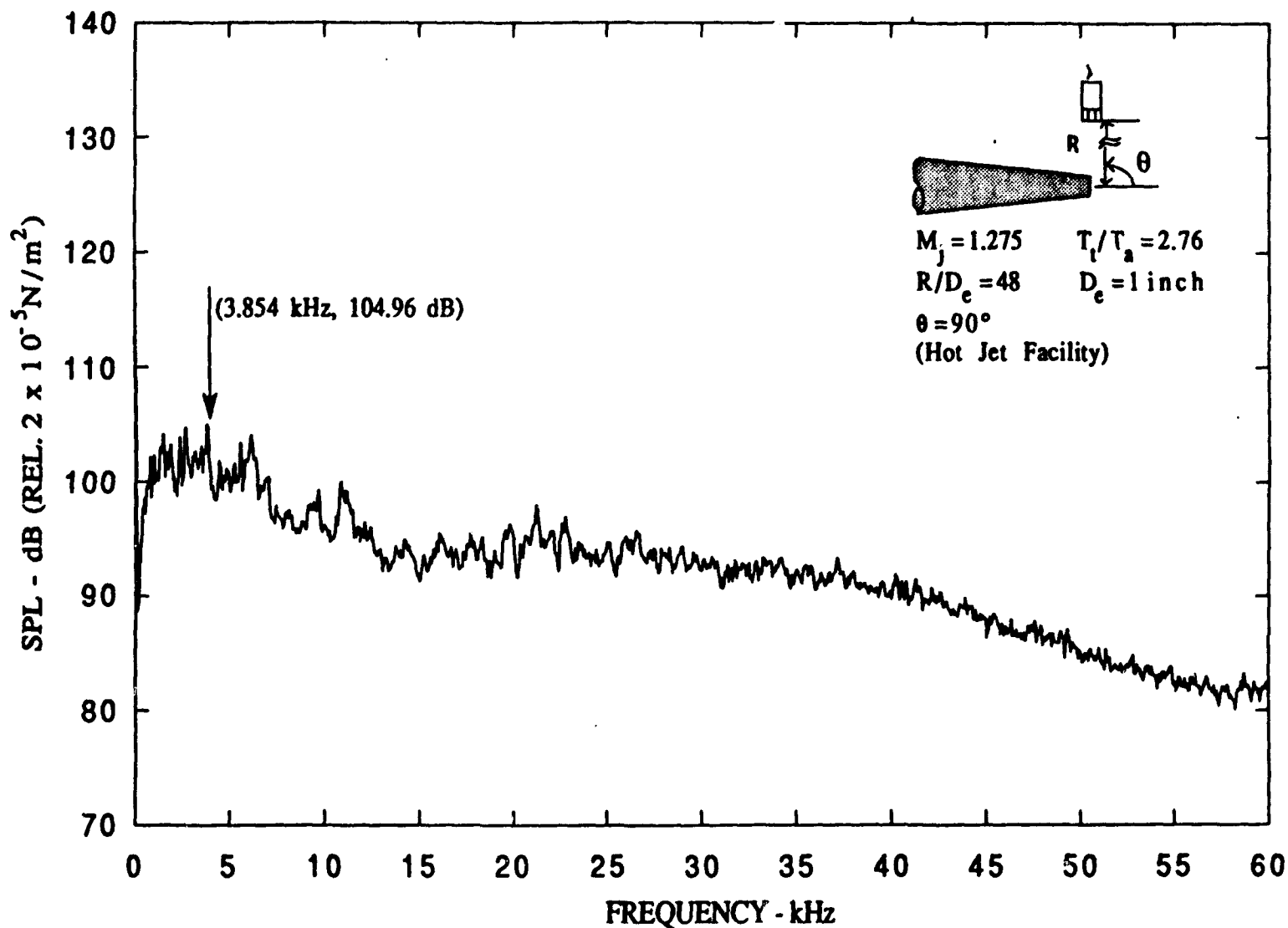Figure A-15. Narrow band spectra ($\Delta f = 62.5$ Hz), $M_j = 1.150$, $T_t/T_a = 0.99$.
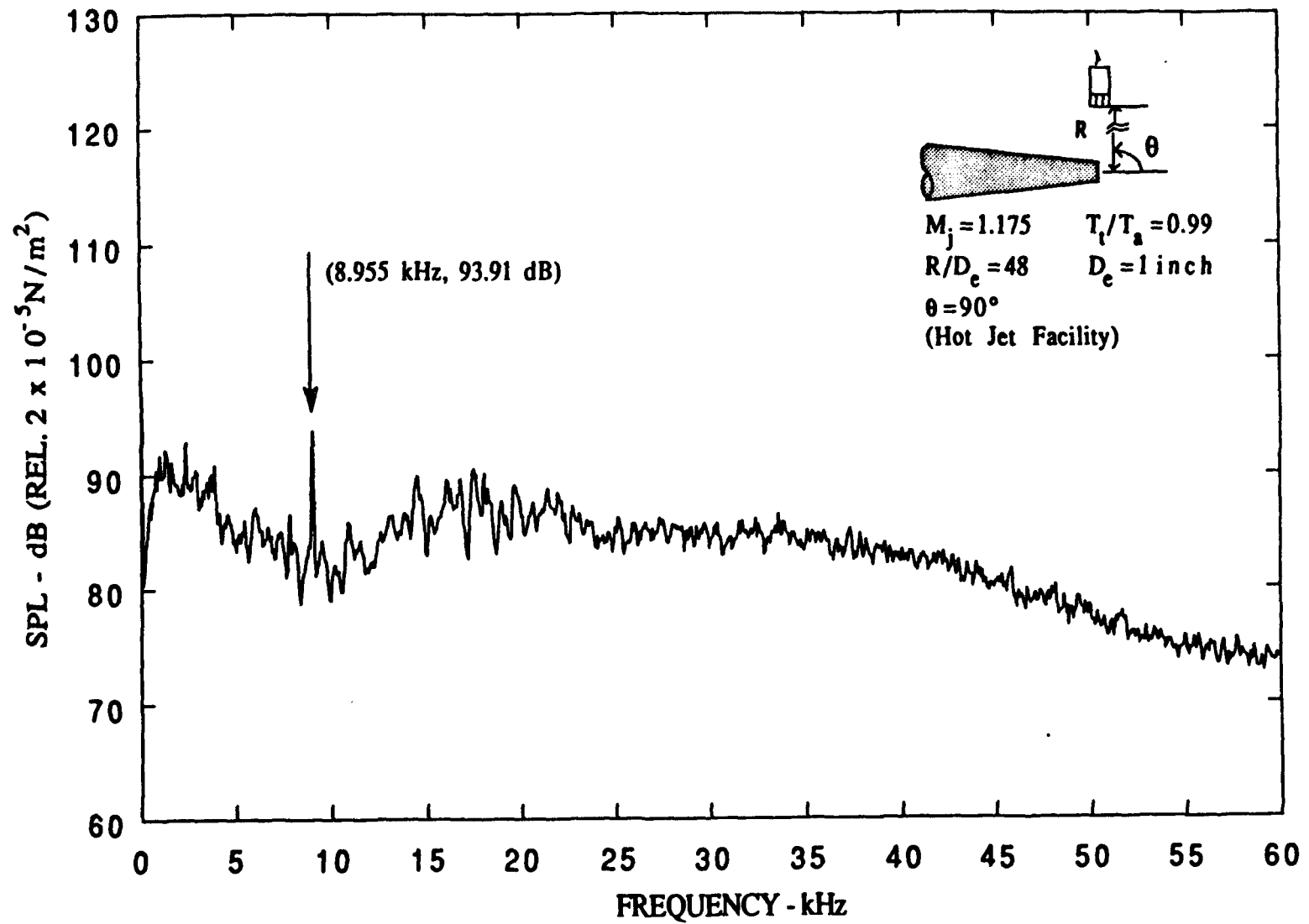
Figure A-16. Narrow band spectra ($\Delta f = 62.5$ Hz), $M_j = 1.175$, $T_t/T_a = 0.99$.
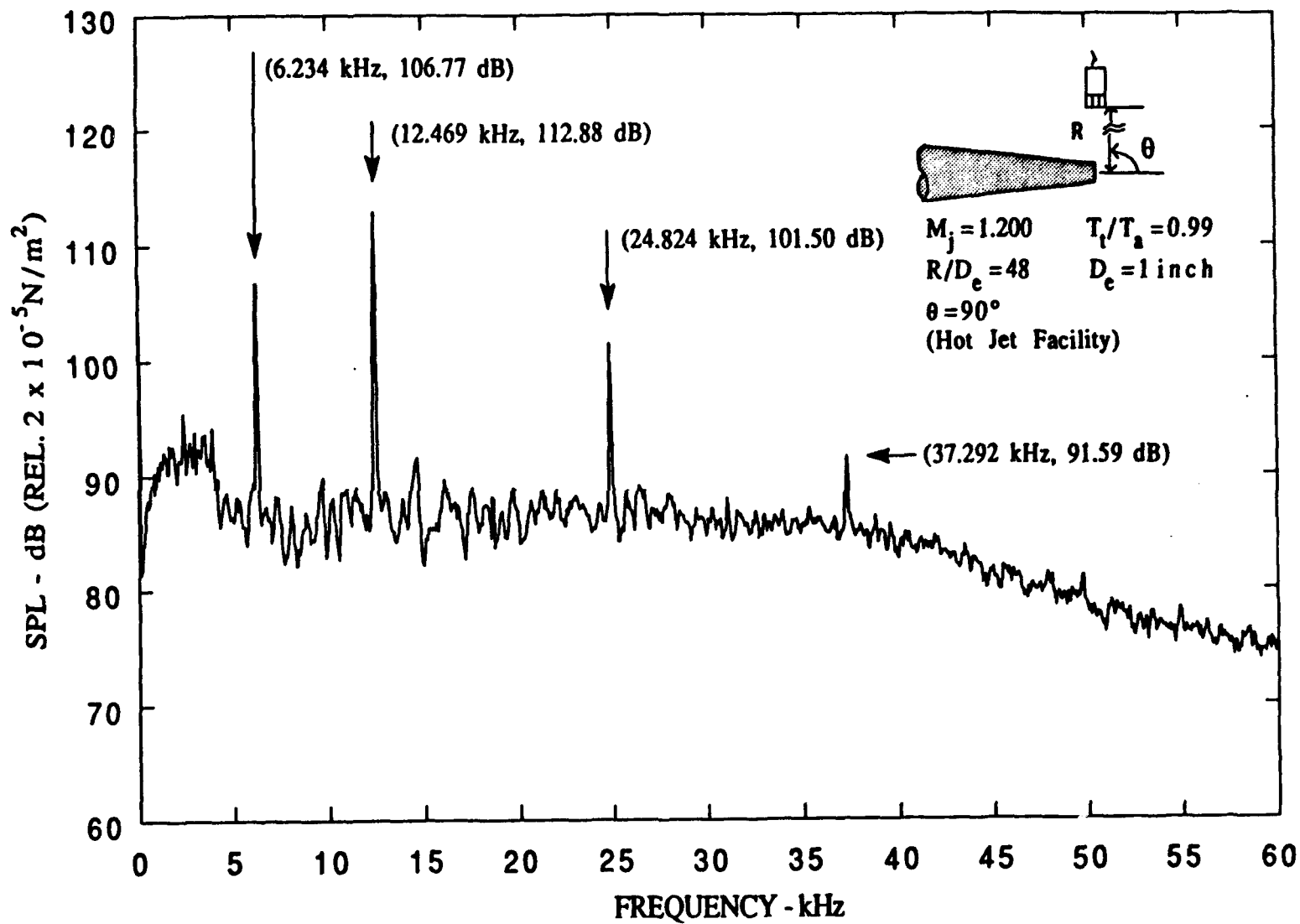
Figure A-17. Narrow band spectra ($\Delta f = 62.5$ Hz), $M_j = 1.200$, $T_t/T_a = 0.99$.
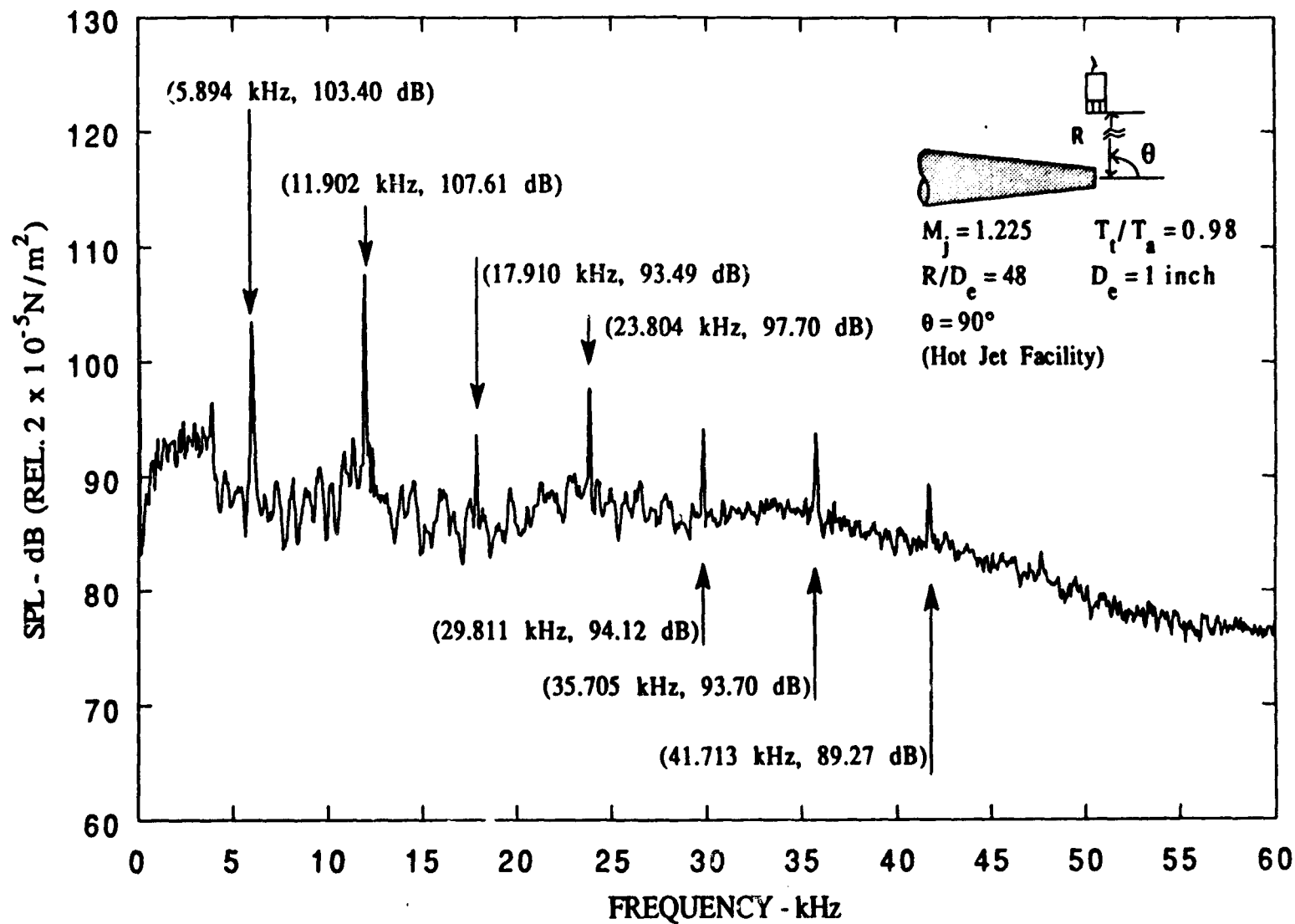
Figure A-18. Narrow band spectra ($\Delta f = 62.5$ Hz), $M_j = 1.225$, $T_t/T_a = 0.98$.
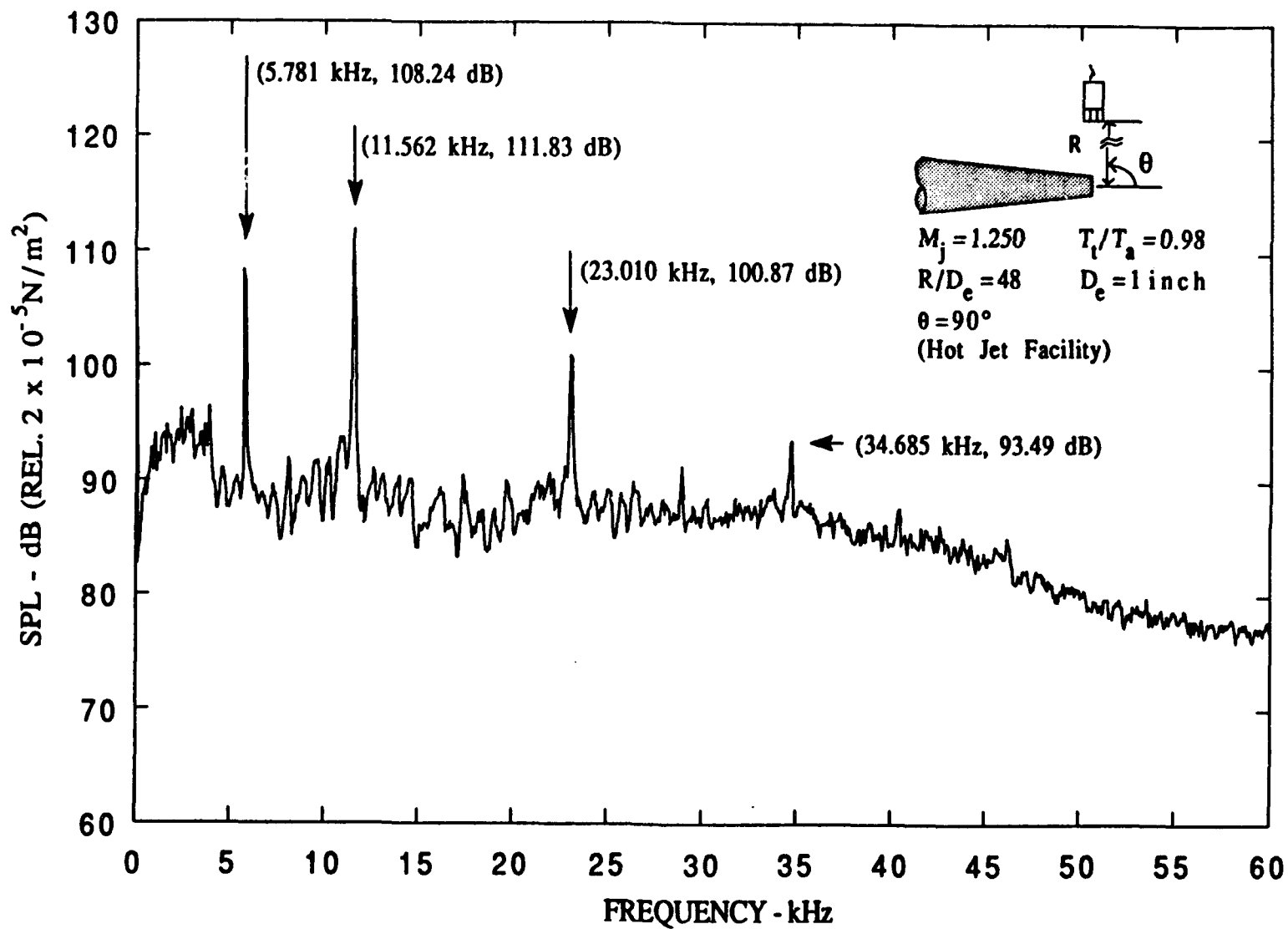
Figure A-19. Narrow band spectra ($\Delta f = 62.5$ Hz), $M_j = 1.250$, $T_t/T_a = 0.98$.
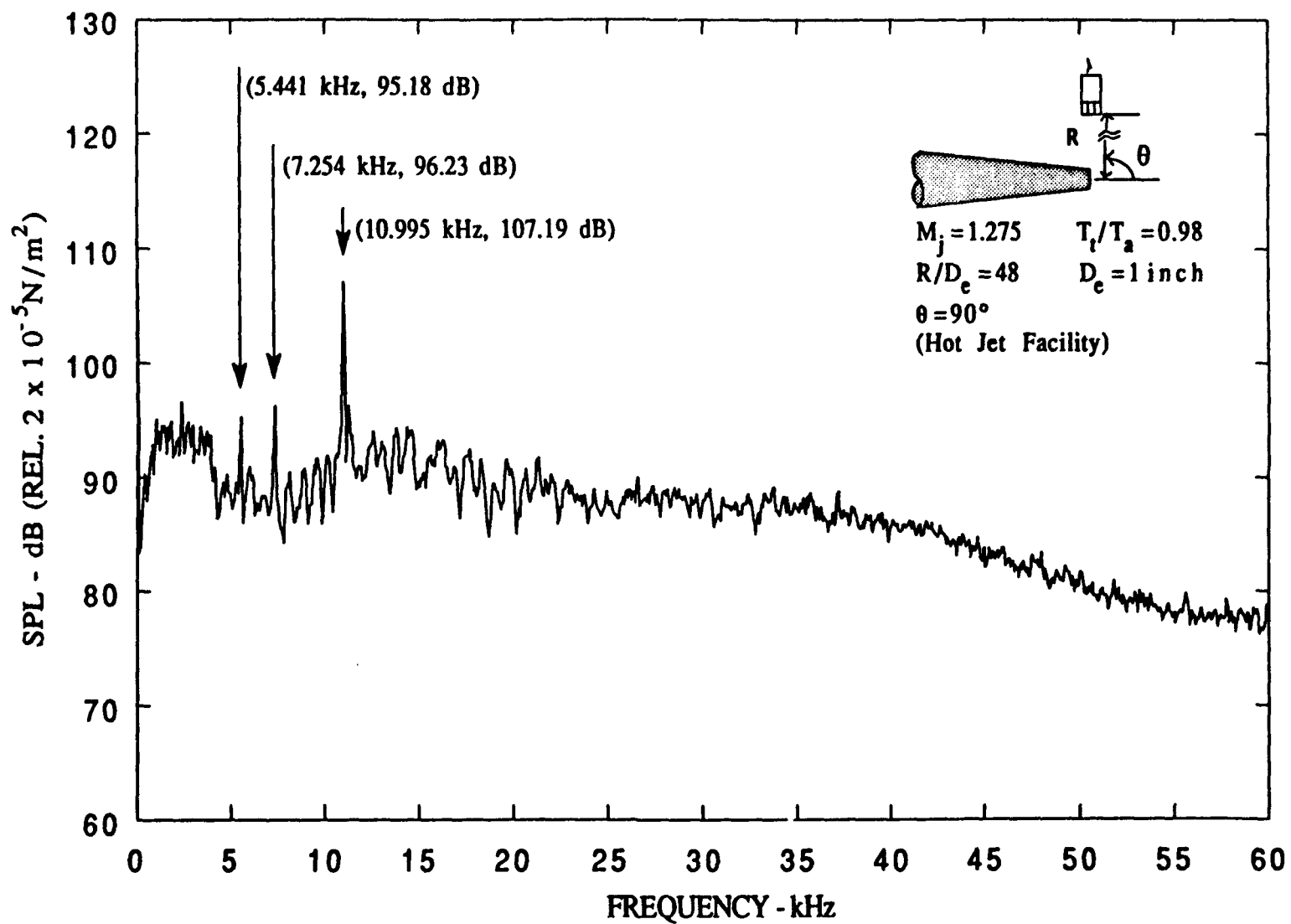
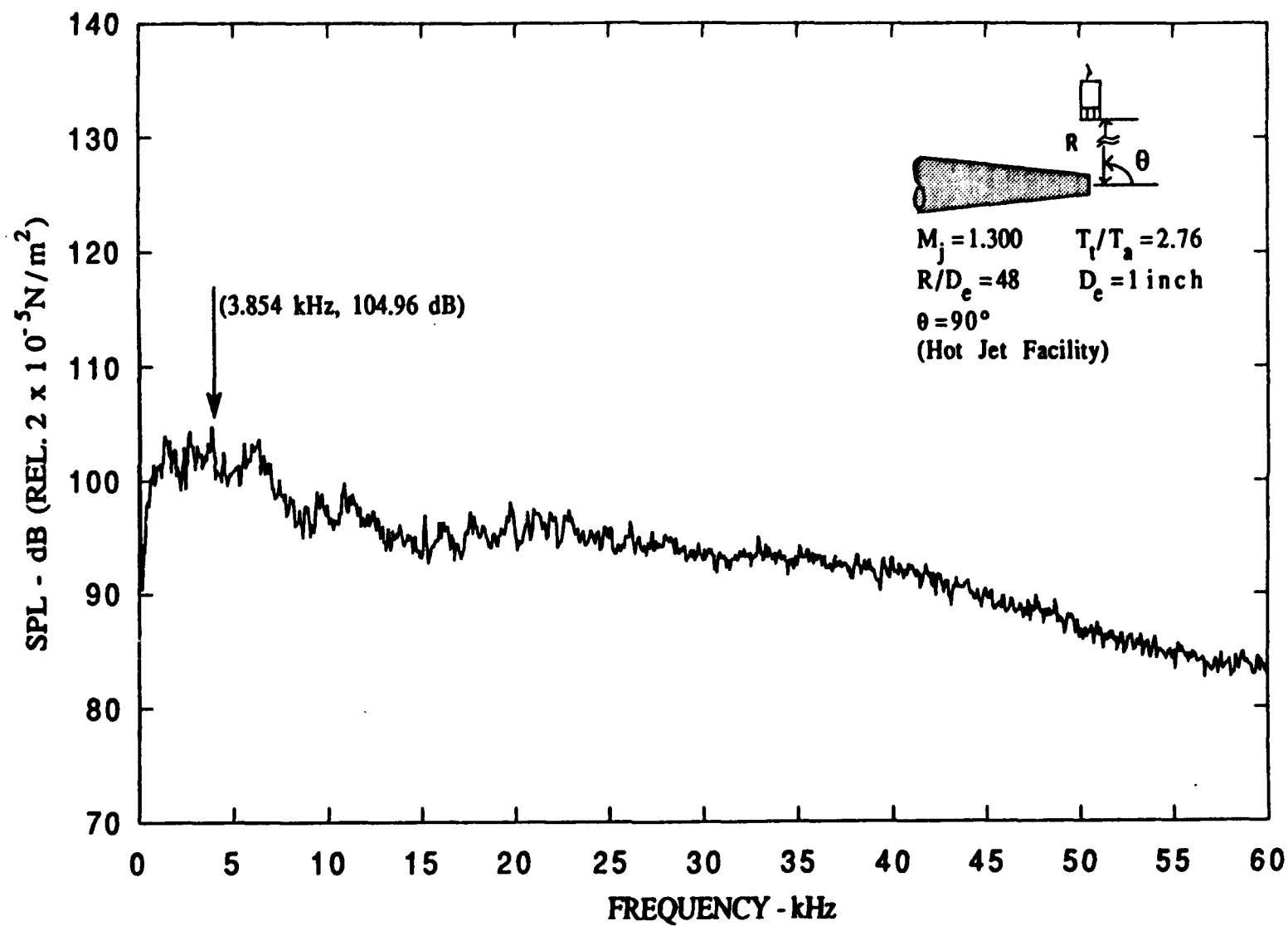Figure A-20. Narrow band spectra ($\Delta f = 62.5$ Hz), $M_j = 1.275$, $T_t/T_a = 0.98$.
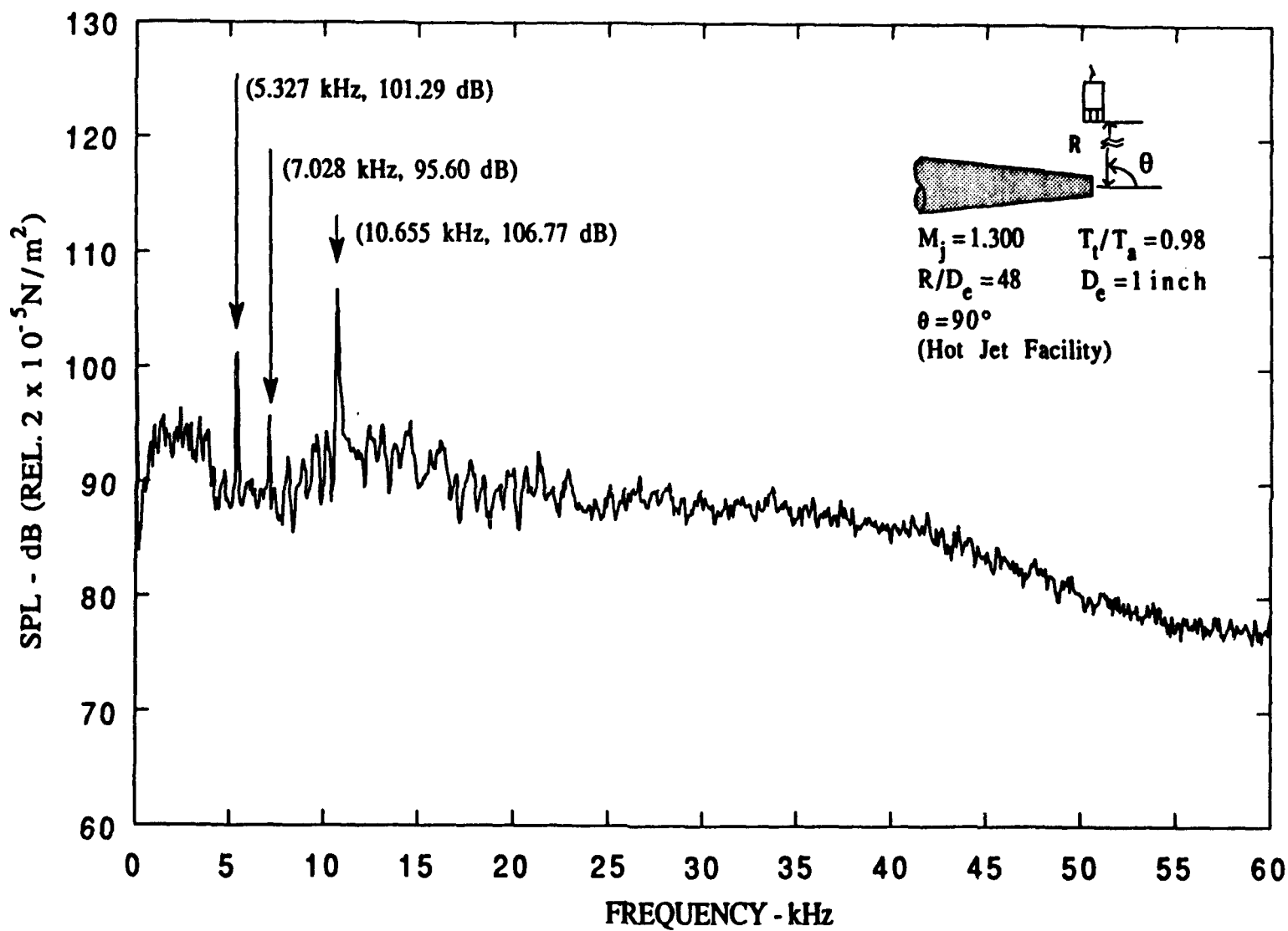
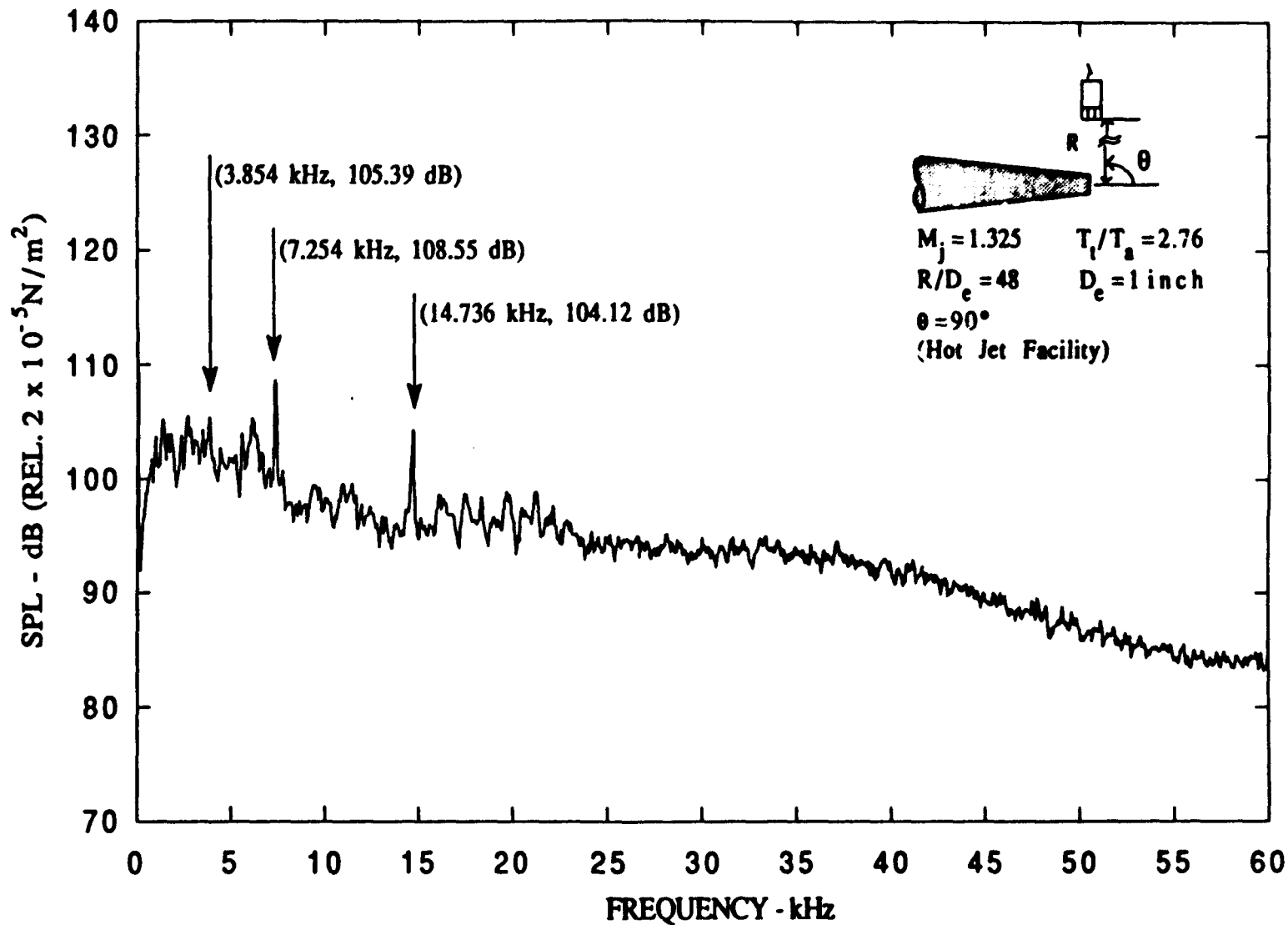Figure A-21. Narrow band spectra ($\Delta f = 62.5$ Hz), $M_j = 1.300$, $T_t/T_a = 0.98$.
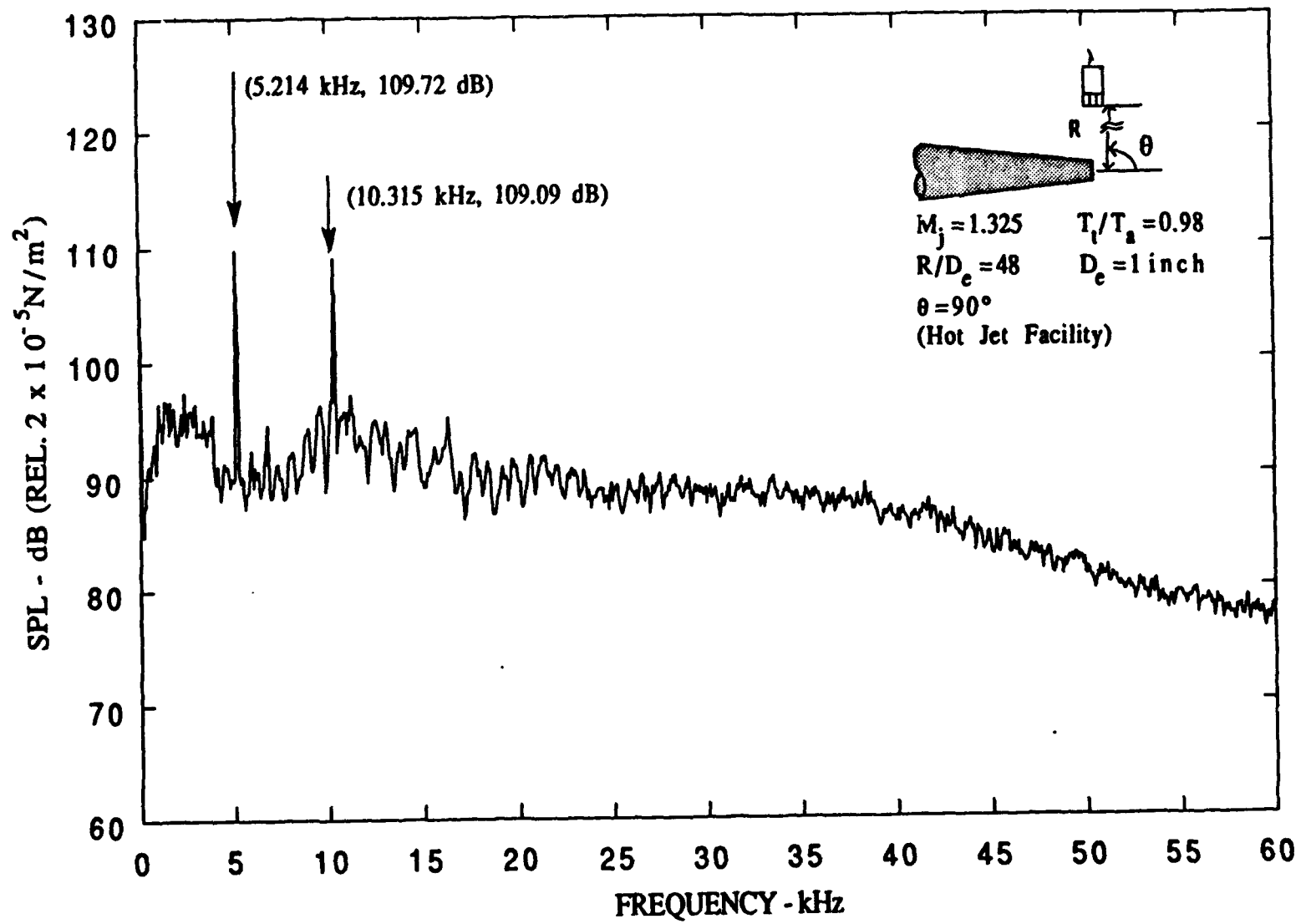
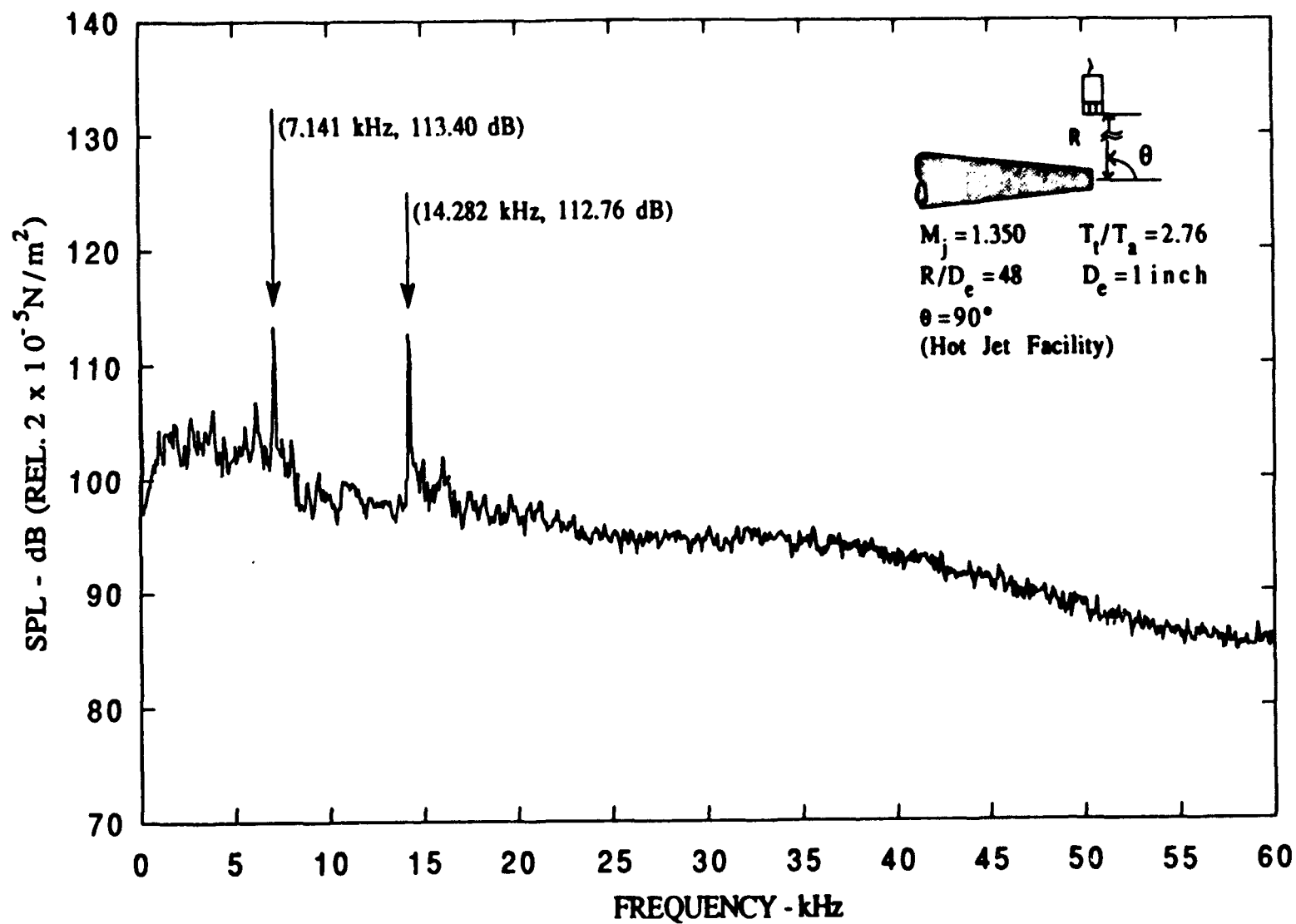Figure A-22. Narrow band spectra ($\Delta f = 62.5$ Hz), $M_j = 1.325$, $T_t/T_a = 0.98$.
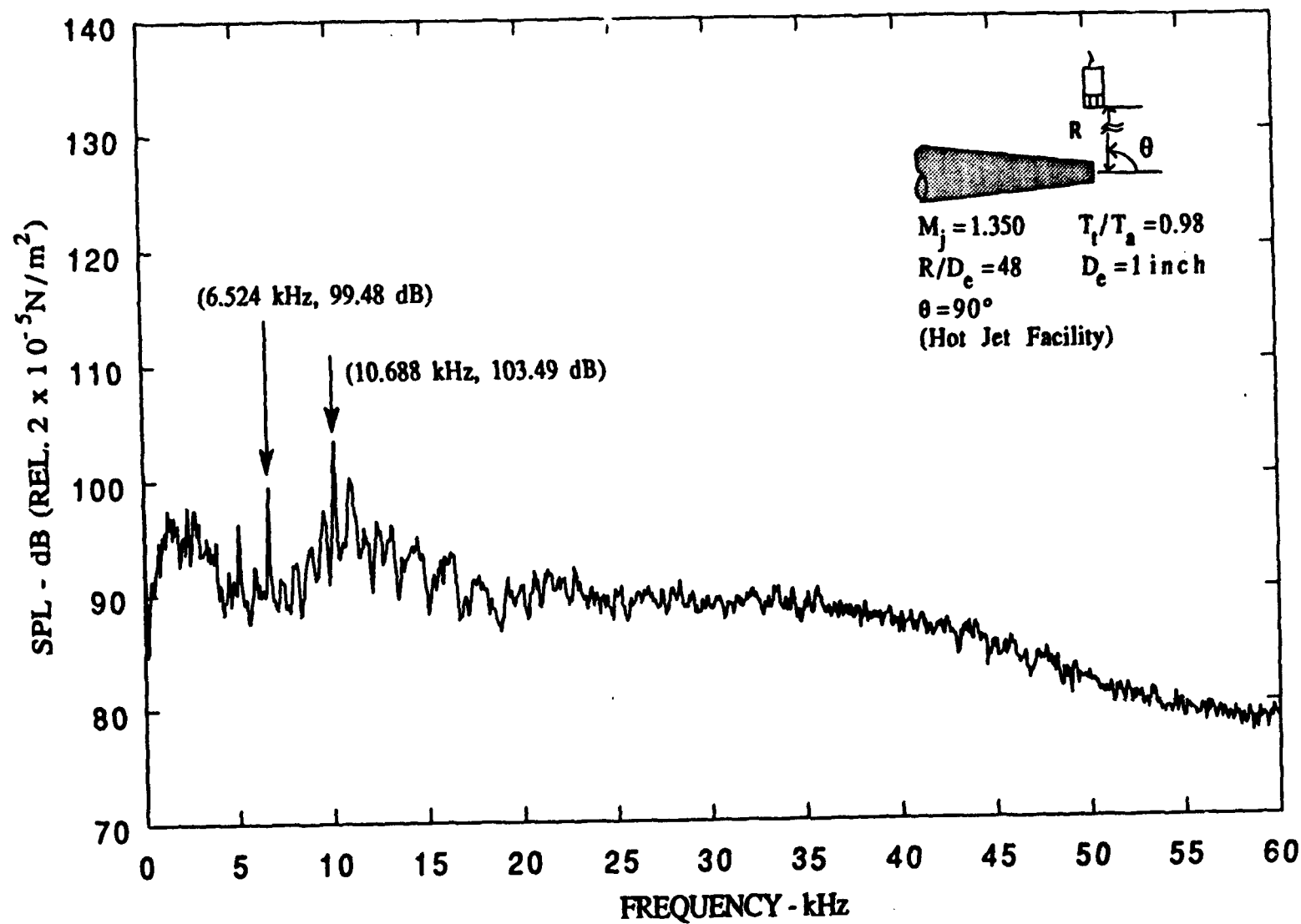
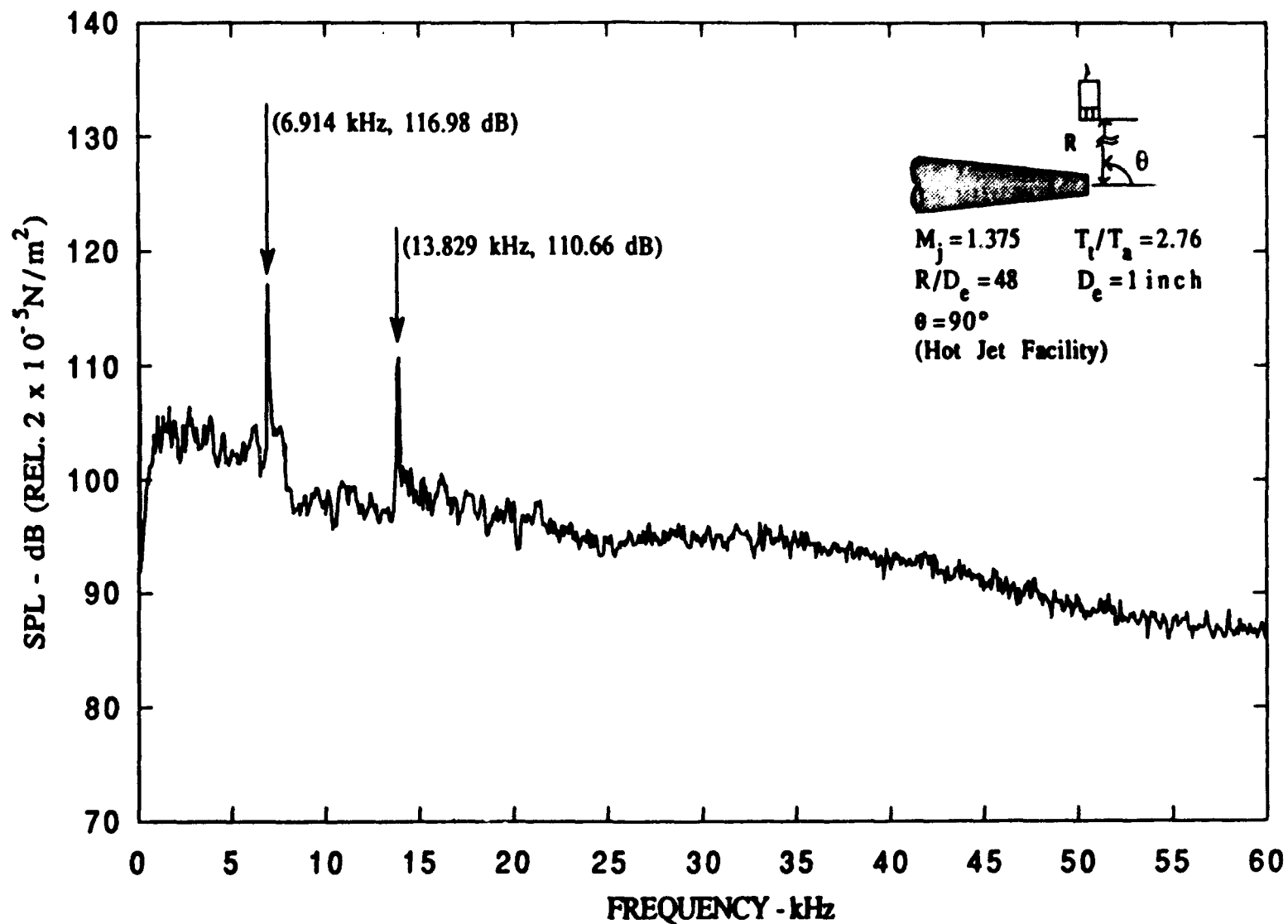Figure A-23. Narrow band spectra ($\Delta f = 62.5$ Hz), $M_j = 1.350$, $T_t/T_a = 0.98$.
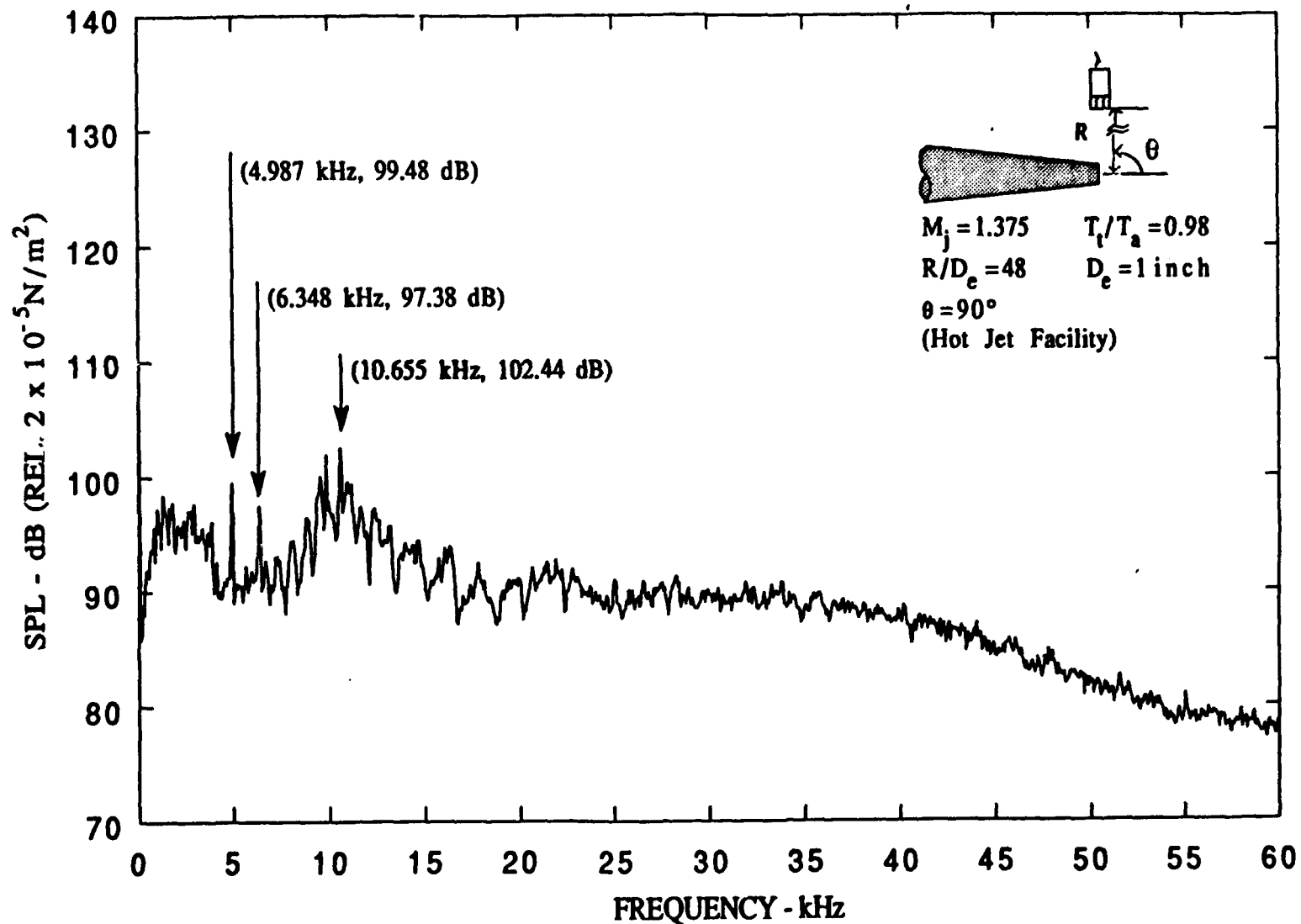
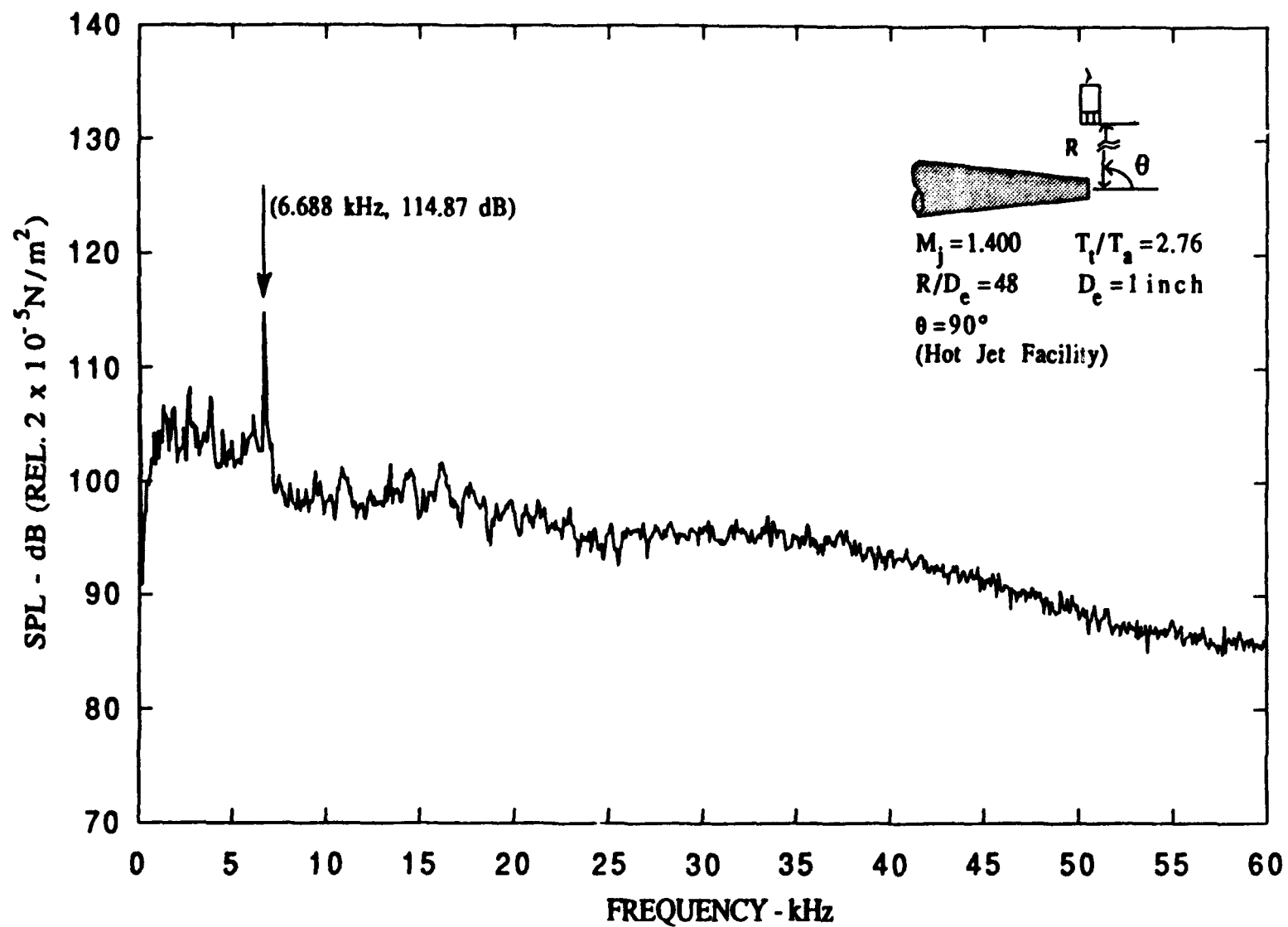Figure A-24. Narrow band spectra ($\Delta f = 62.5$ Hz), $M_j = 1.375$, $T_t/T_a = 0.98$.
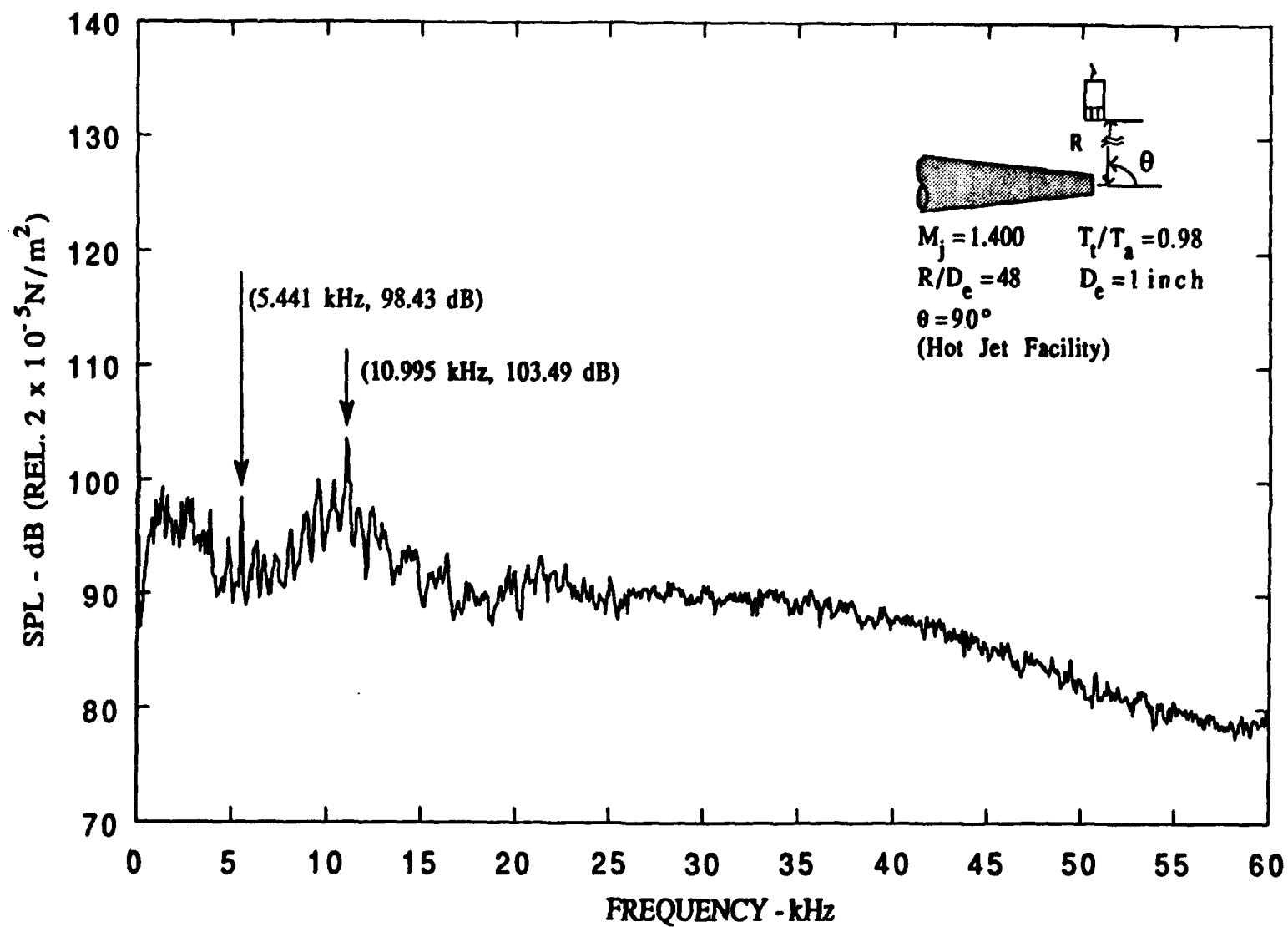
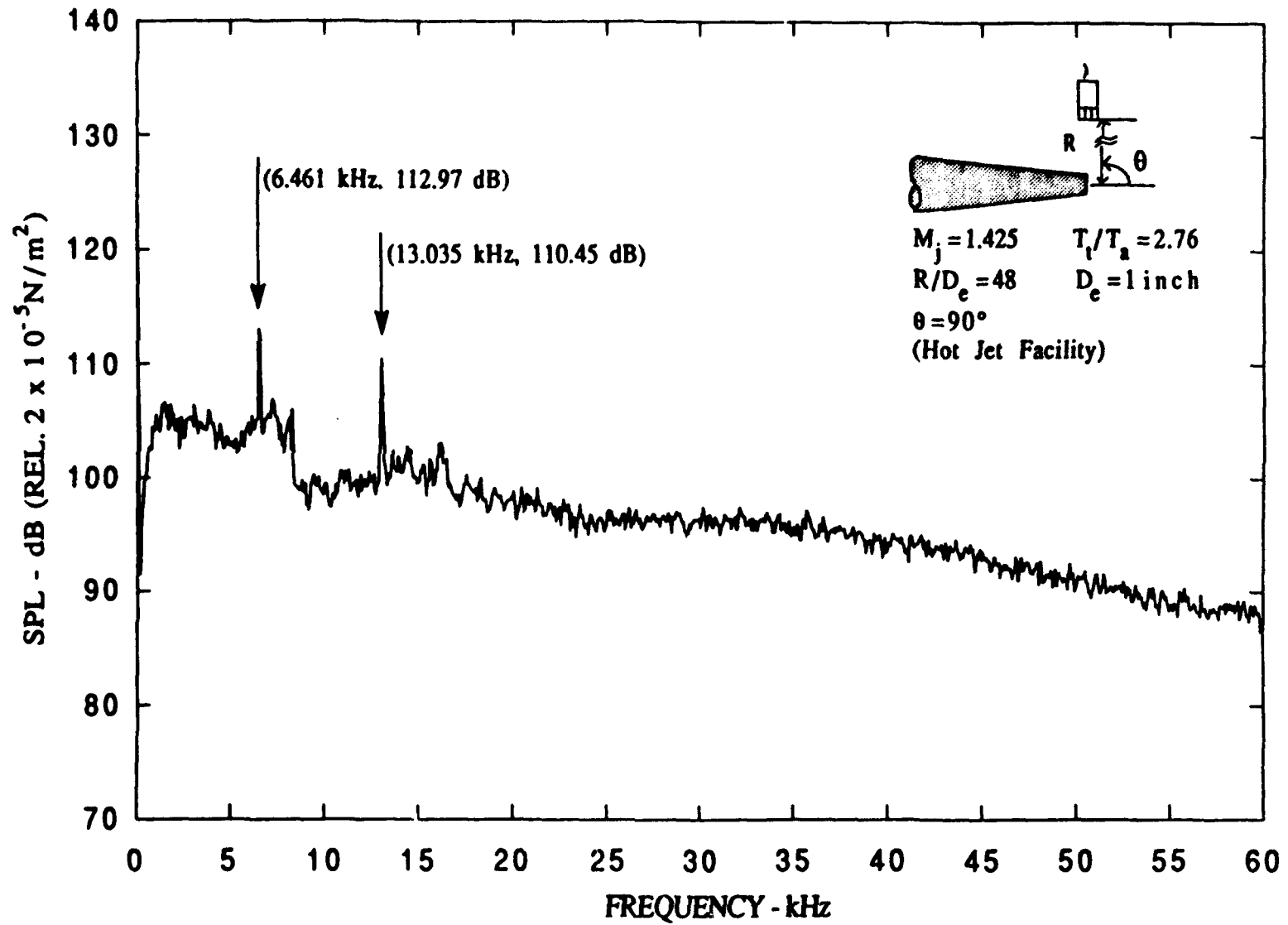Figure A-25. Narrow band spectra ($\Delta f = 62.5$ Hz), $M_j = 1.400$, $T_t/T_a = 0.98$.
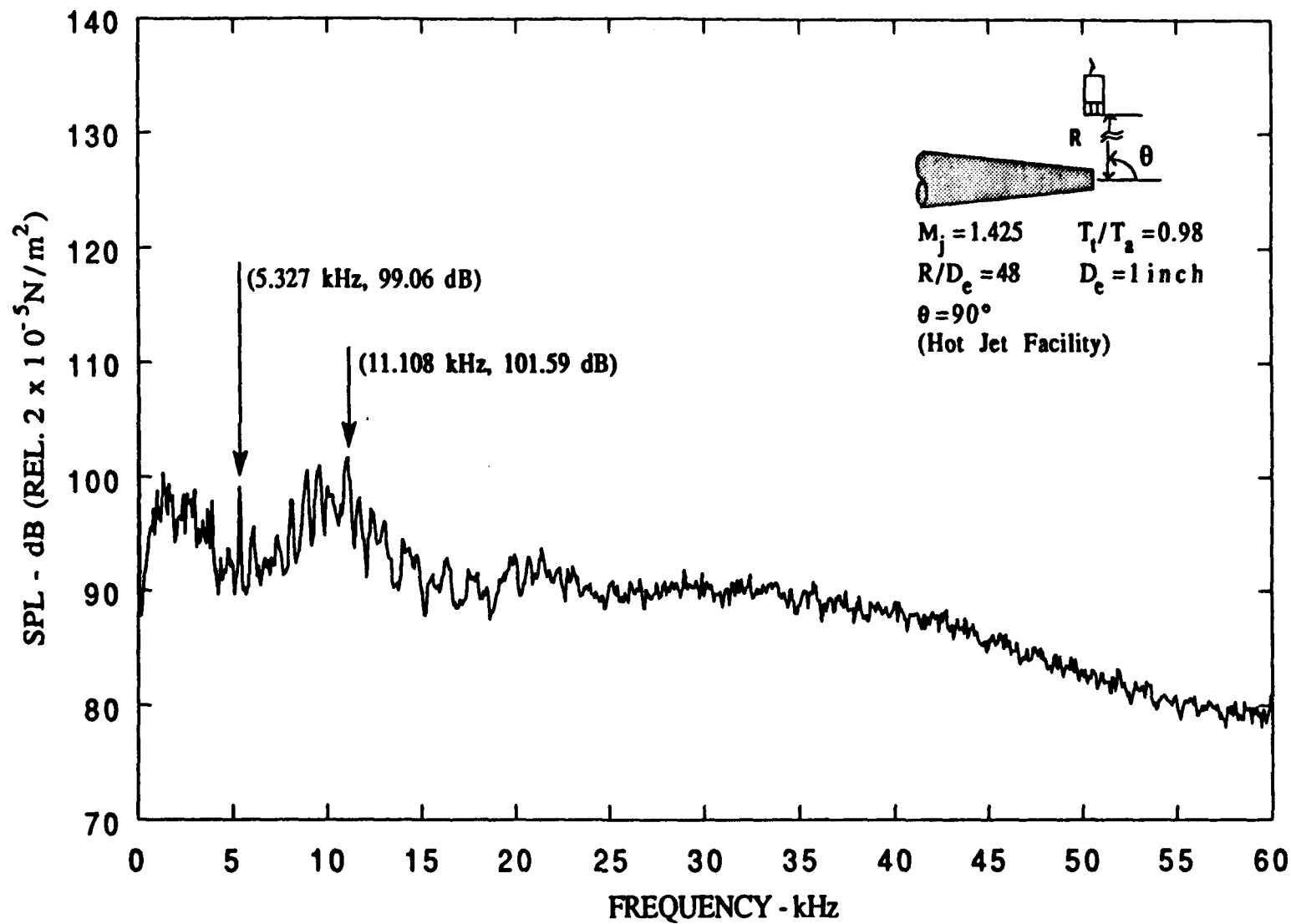
Figure A-26. Narrow band spectra ($\Delta f = 62.5$ Hz), $M_j = 1.425$, $T_t/T_a = 0.98$.
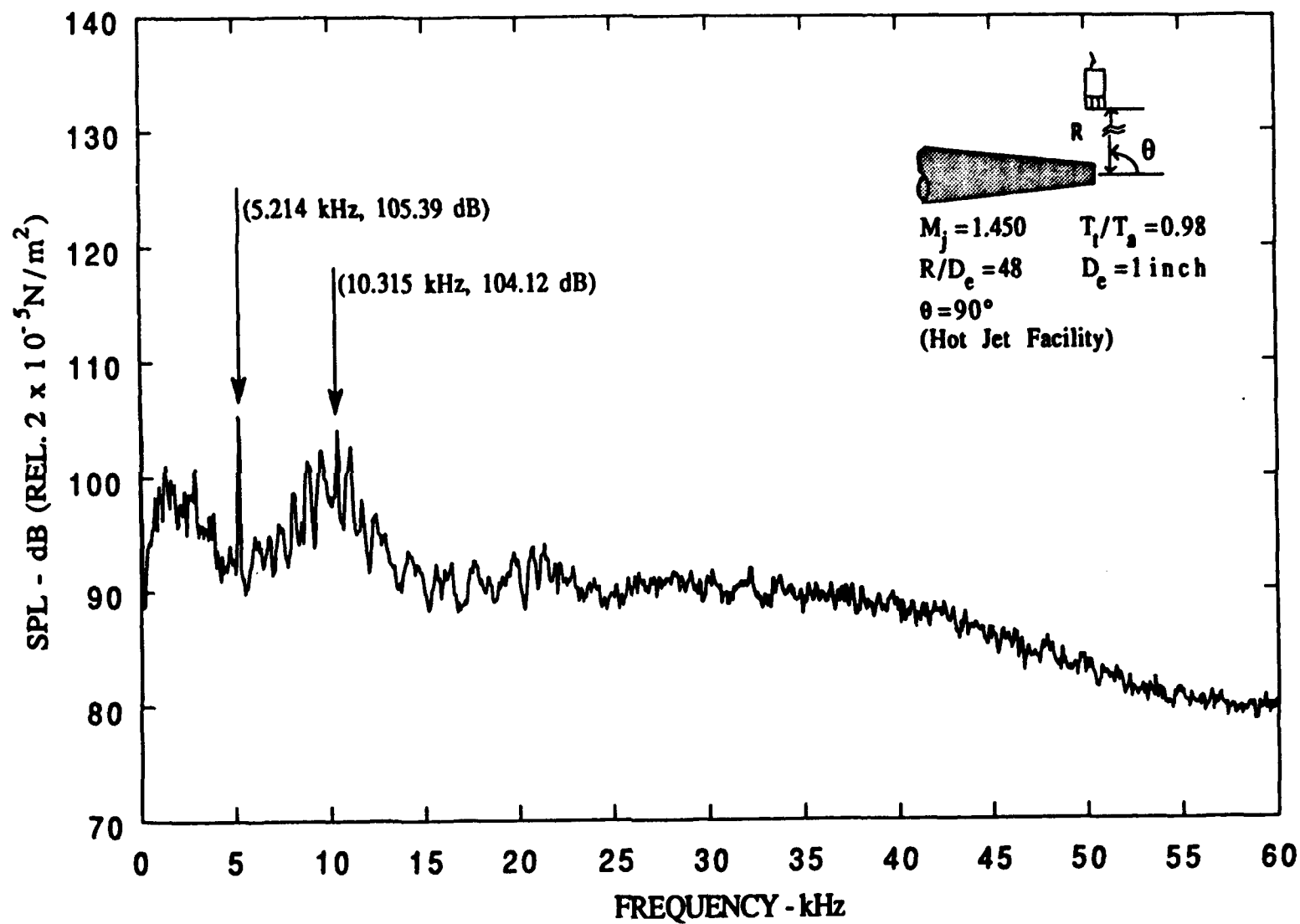
Figure A-27. Narrow band spectra ($\Delta f = 62.5$ Hz), $M_j = 1.450$, $T_t/T_a = 0.98$.
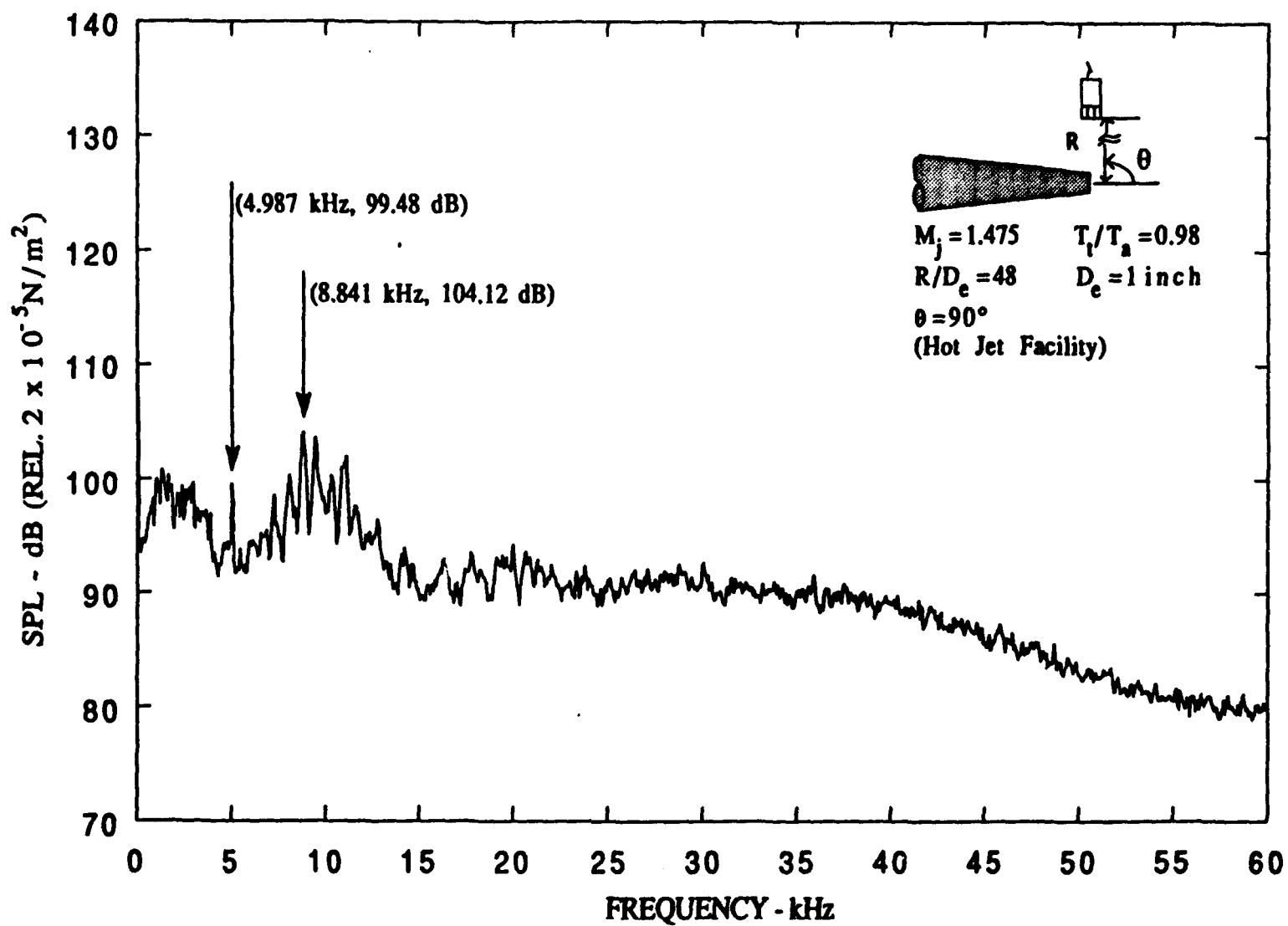
Figure A-28. Narrow band spectra (Δf = 62.5 Hz), M_j = 1.475, T_t/T_a = 0.98.
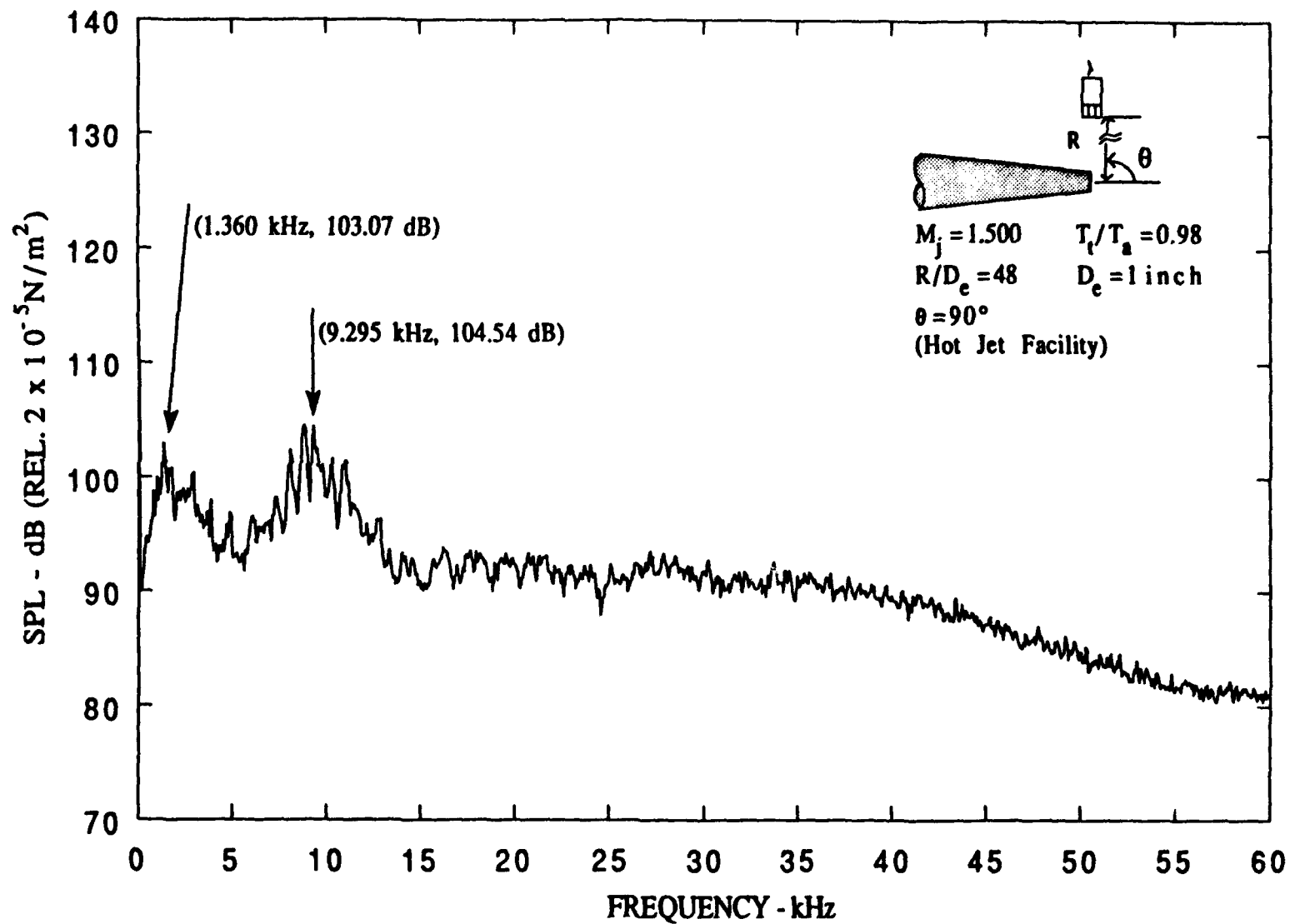
Figure A-29. Narrow band spectra ($\Delta f = 62.5$ Hz), $M_j = 1.500$, $T_t/T_a = 0.98$.
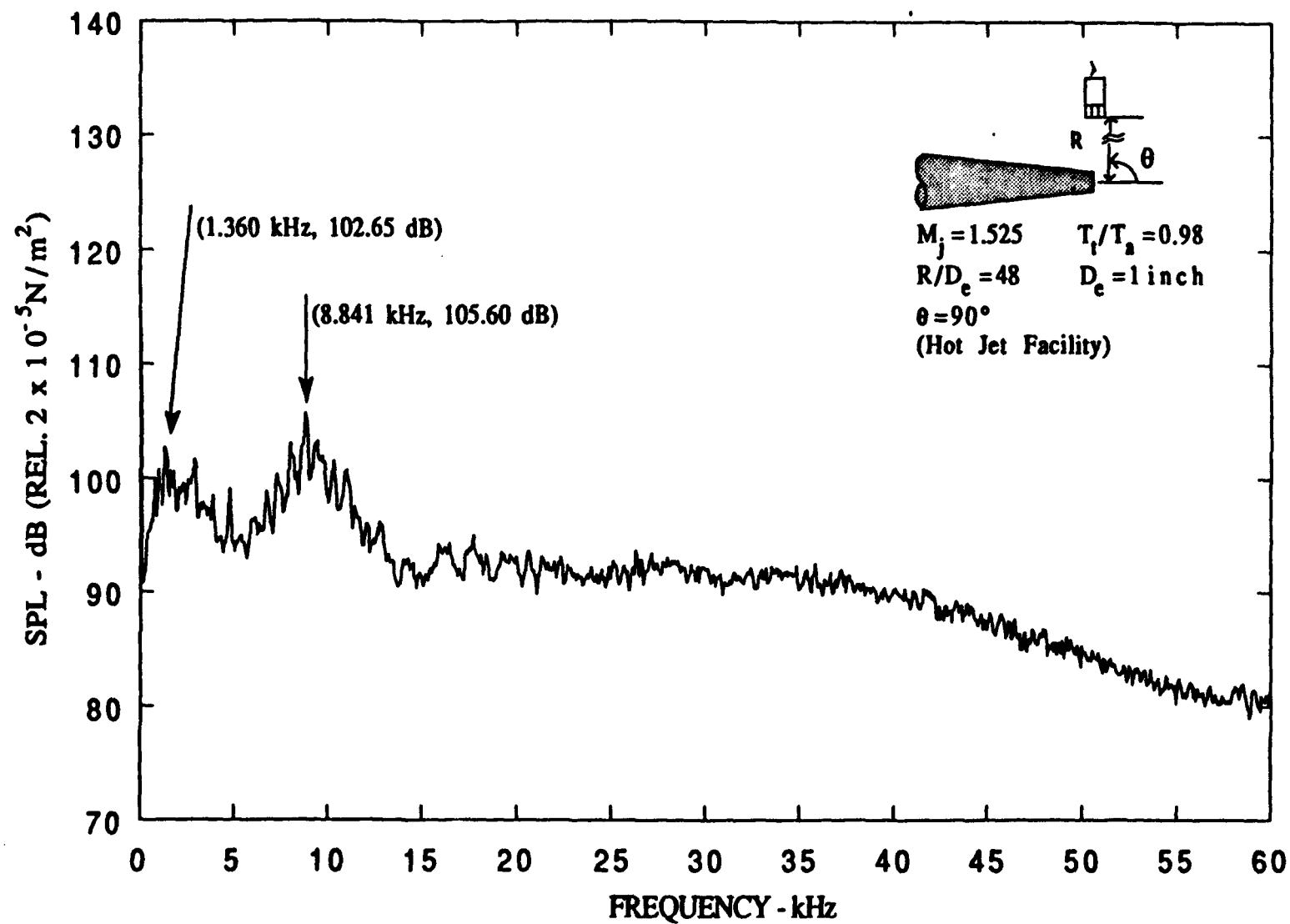
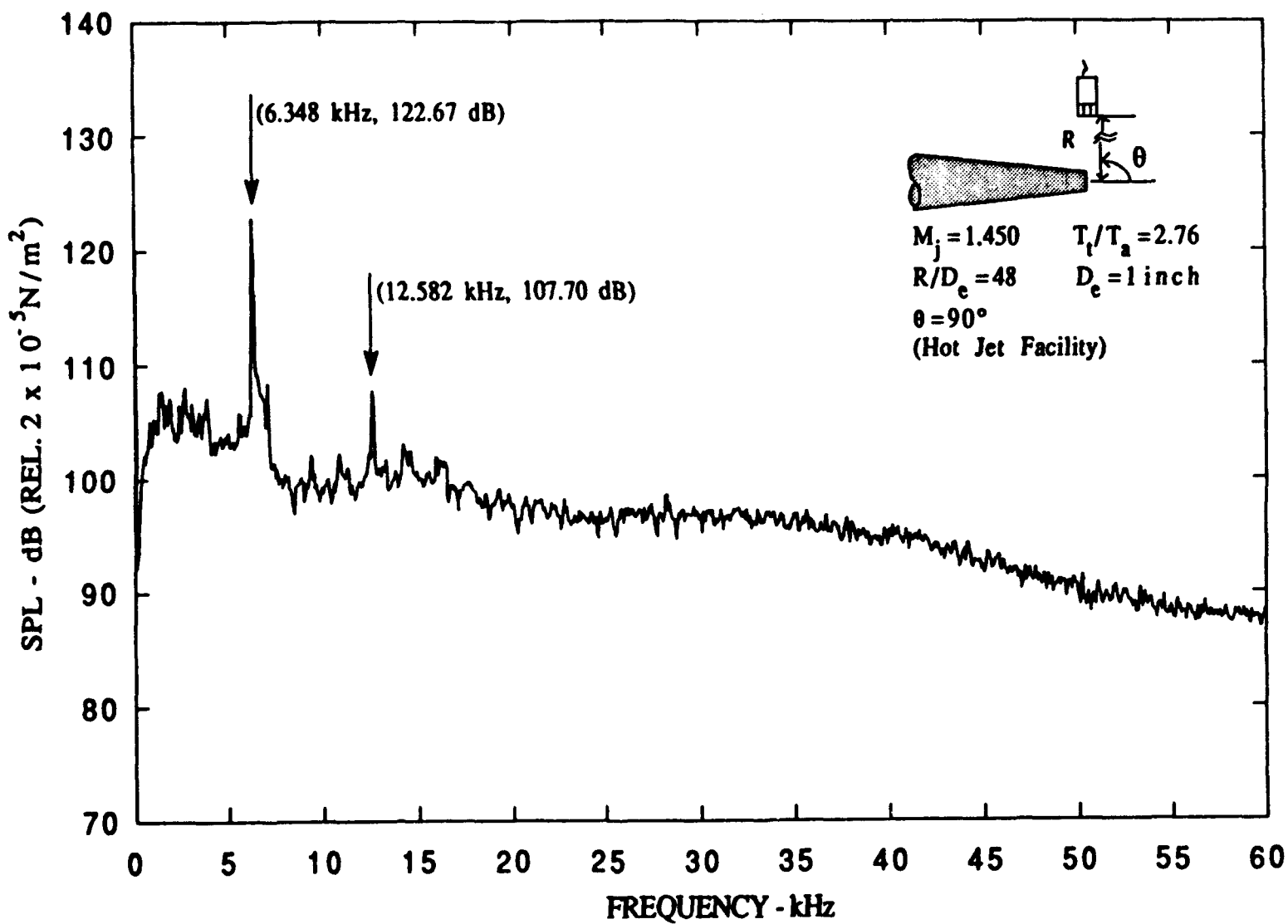Figure A-30. Narrow band spectra ($\Delta f = 62.5$ Hz), $M_j = 1.525$, $T_t/T_a = 0.98$.
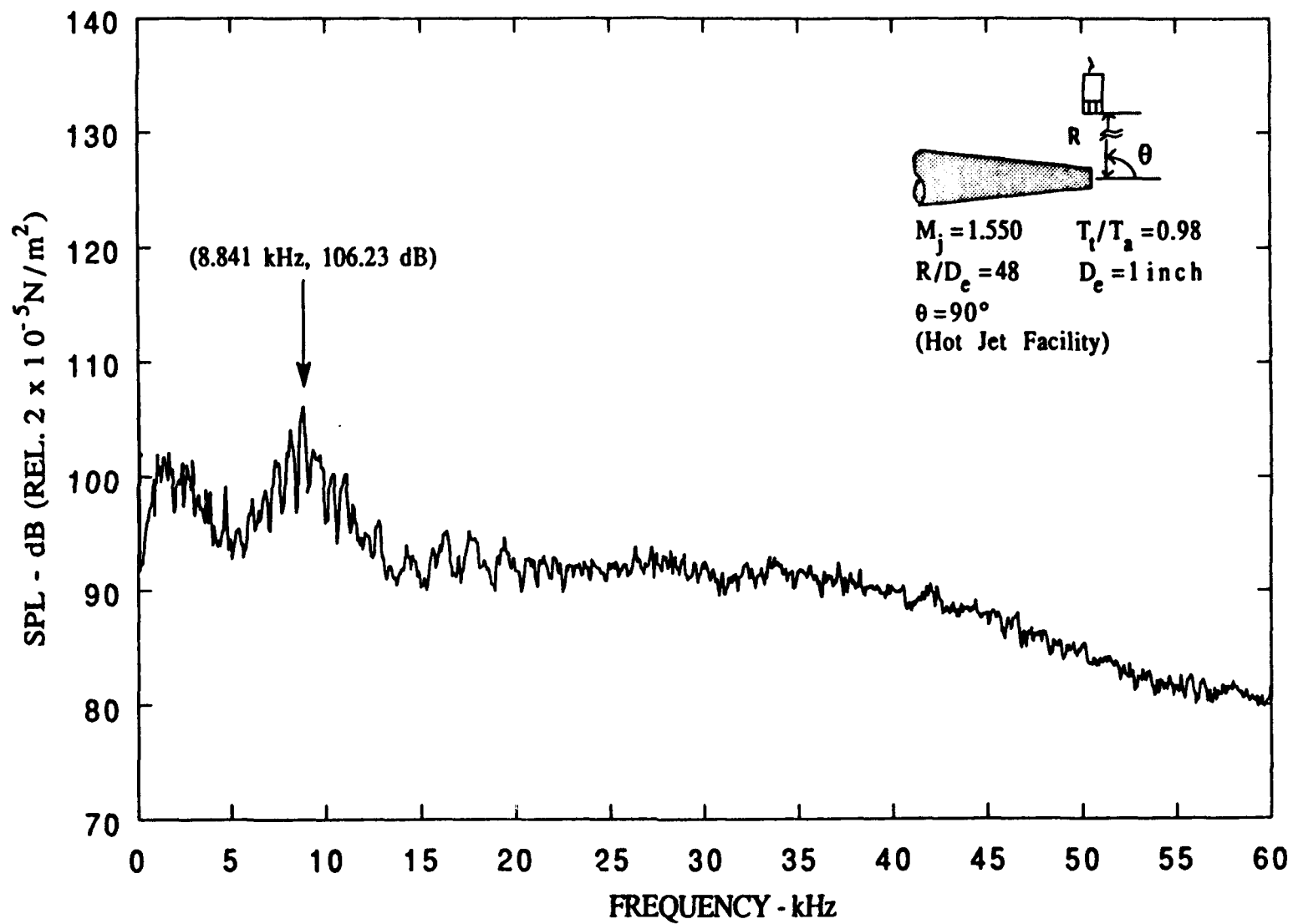
Figure A-31. Narrow band spectra ($\Delta f = 6.5$ Hz), $M_j = 1.550$, $T_t/T_a = 0.98$.
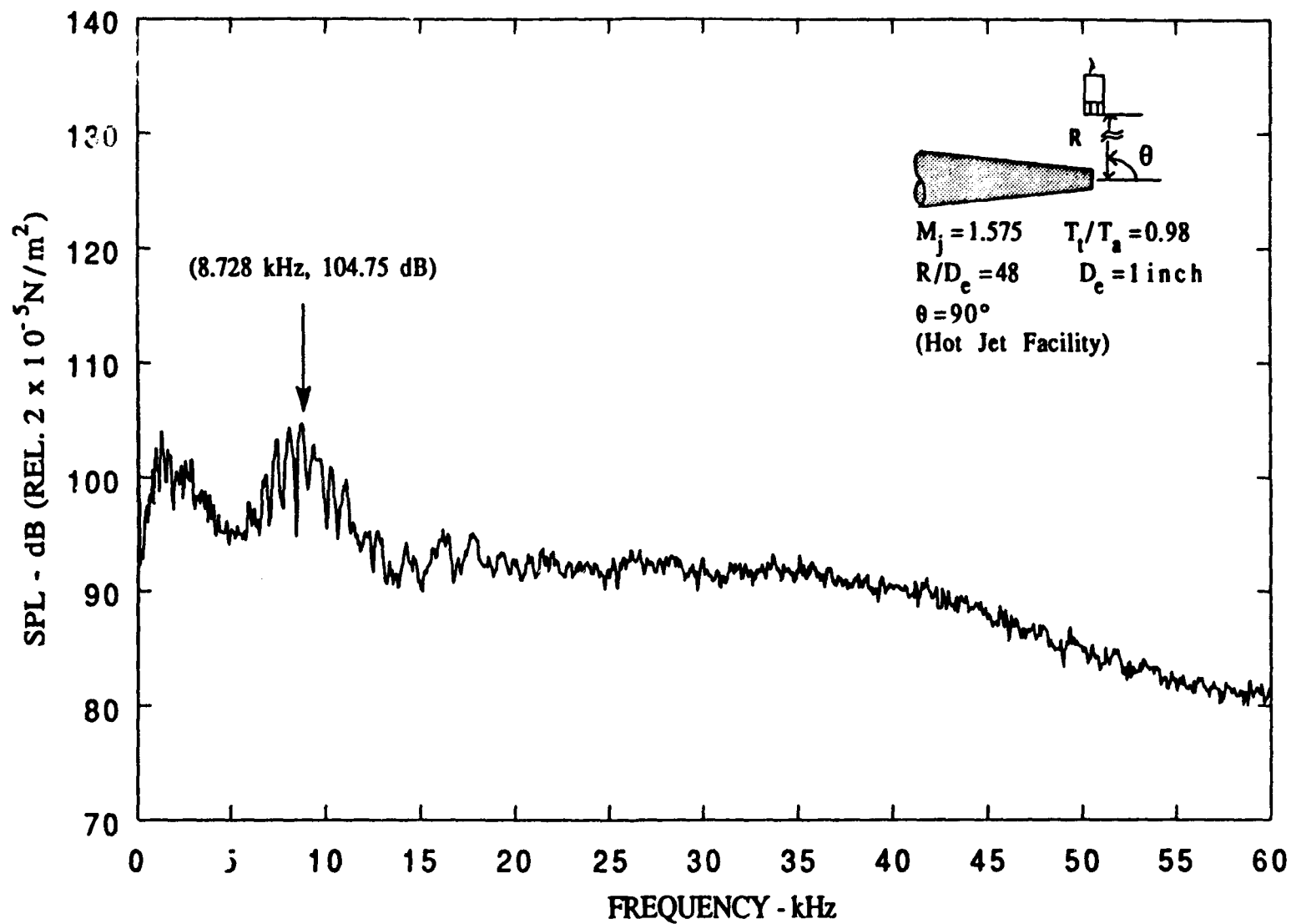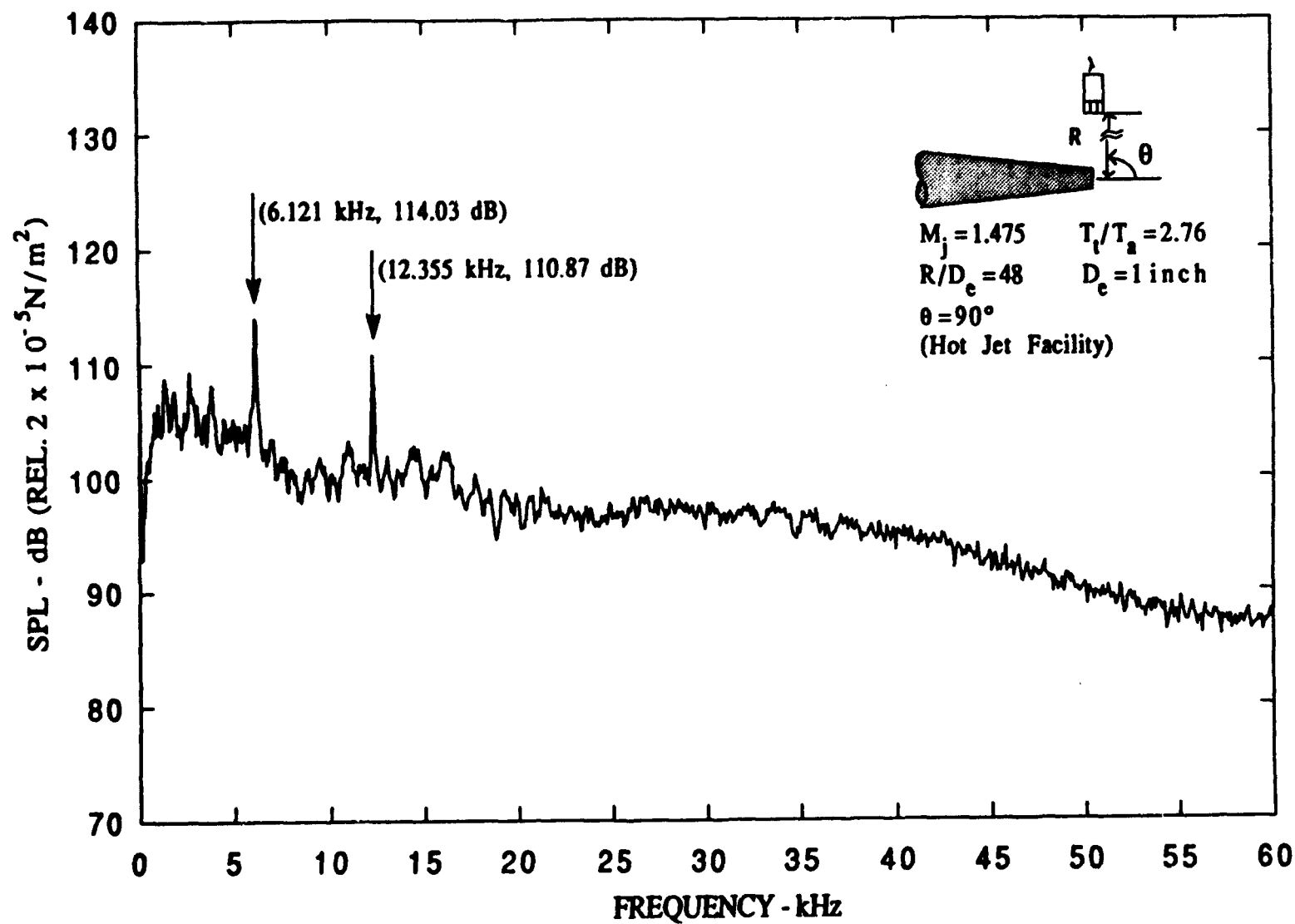
Figure A-32. Narrow band spectra (Δf = 62.5 Hz), M_j = 1.575, T_t/T_a = 0.98.
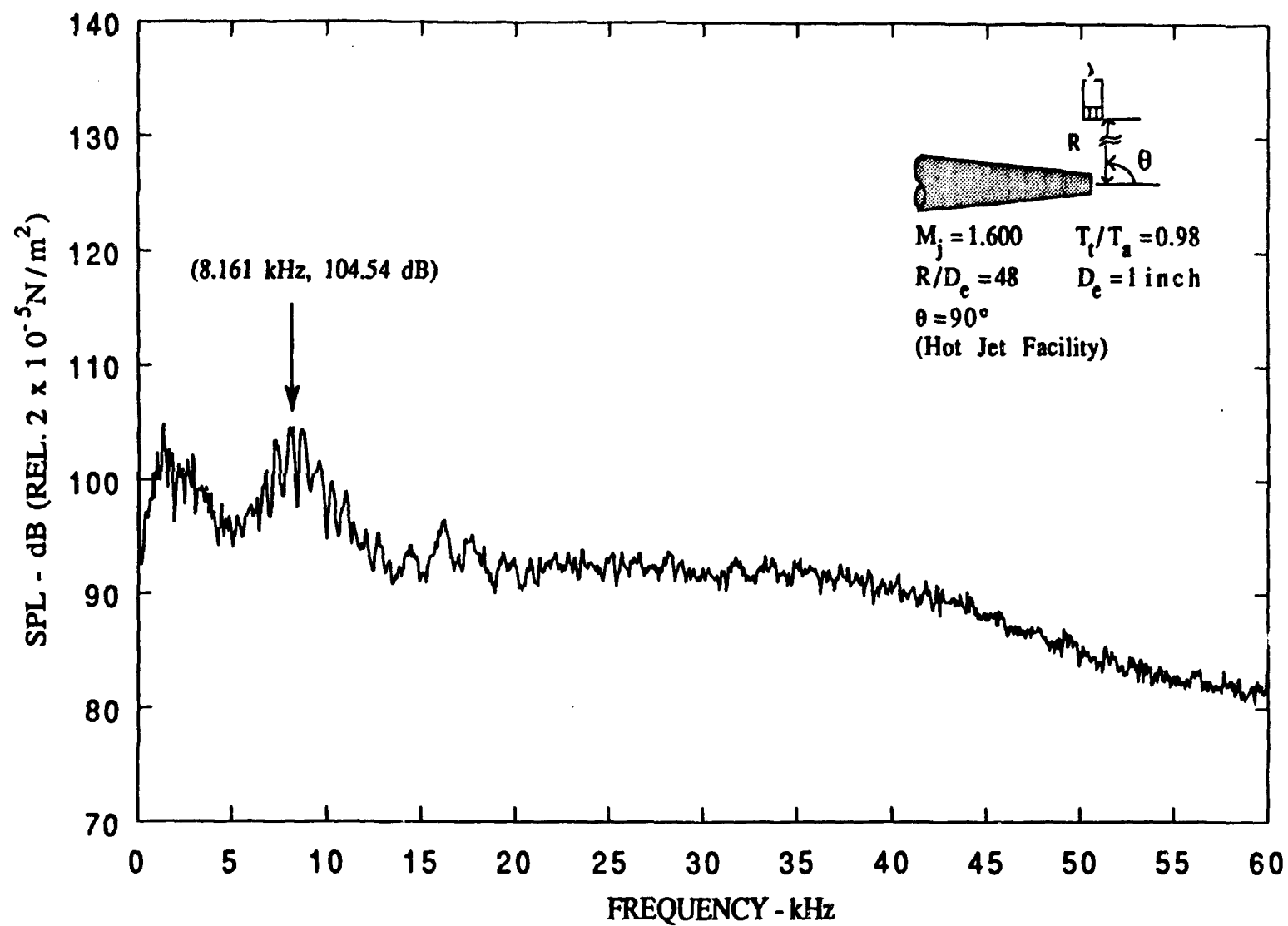
Figure A-33. Narrow band spectra (Δf = 62.5 Hz), M_j = 1.600, T_t/T_a = 0.98.
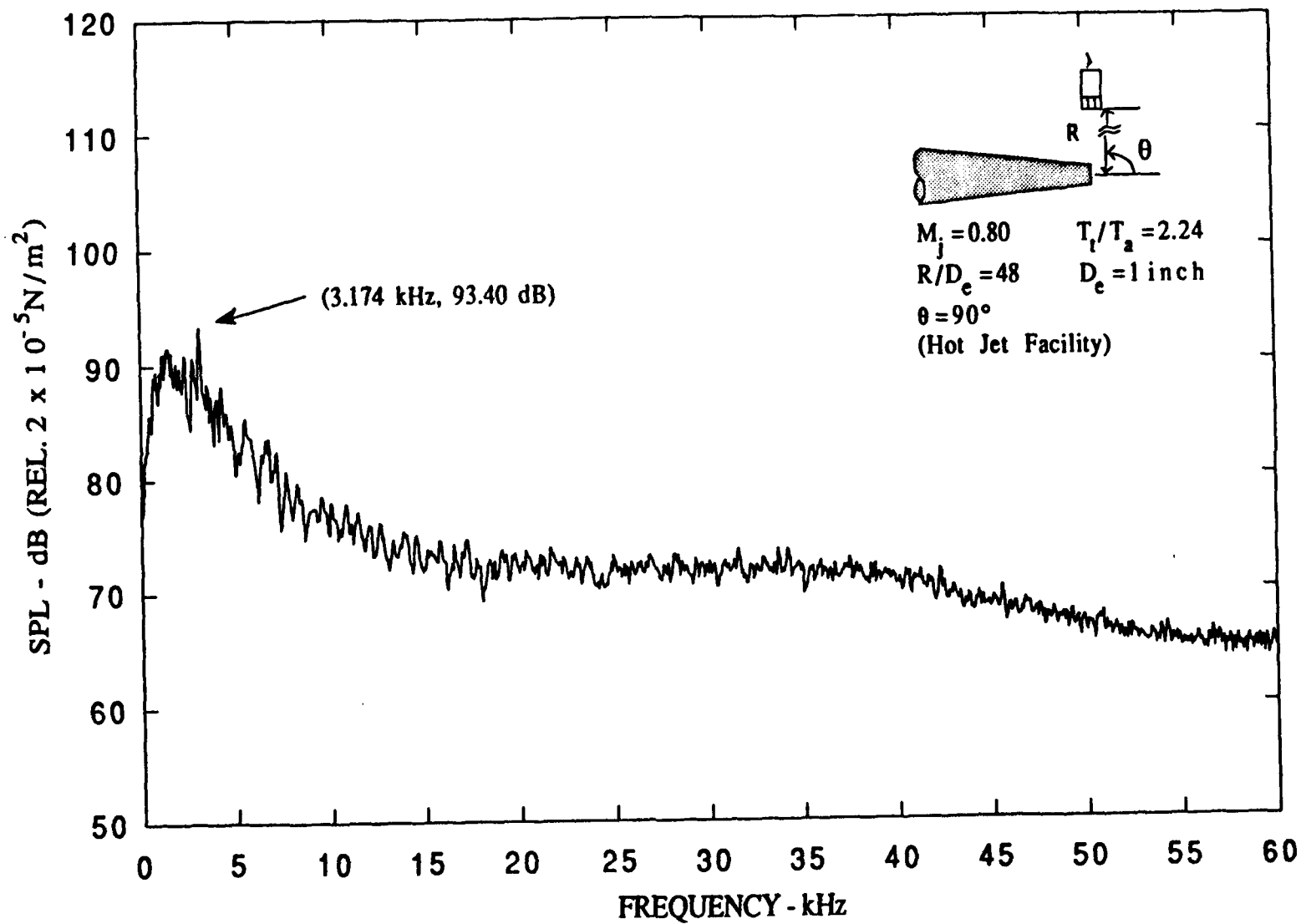
Figure A-34. Narrow band spectra (Δf = 62.5 Hz), M_j = 0.80, T_t/T_a = 2.24.
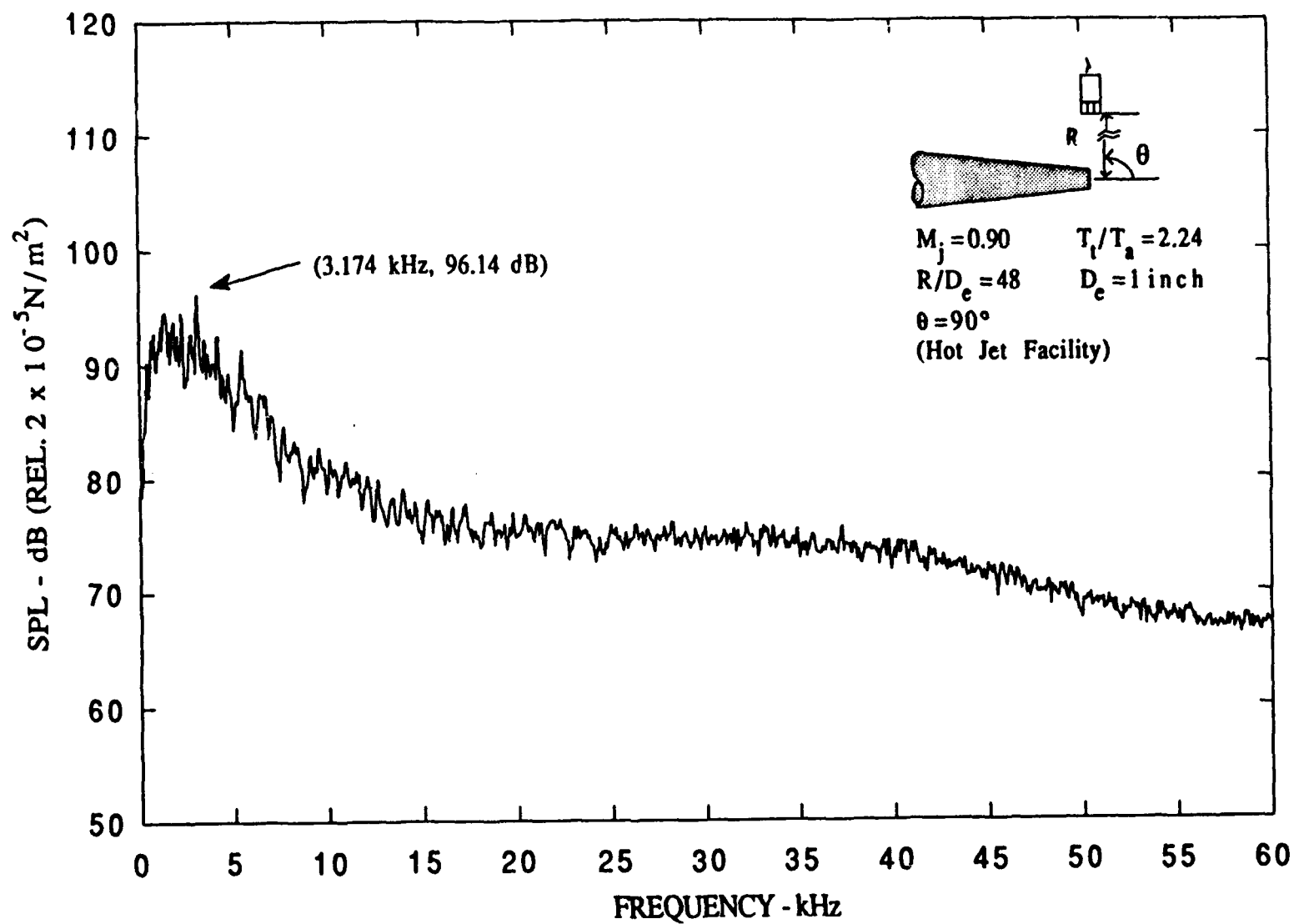
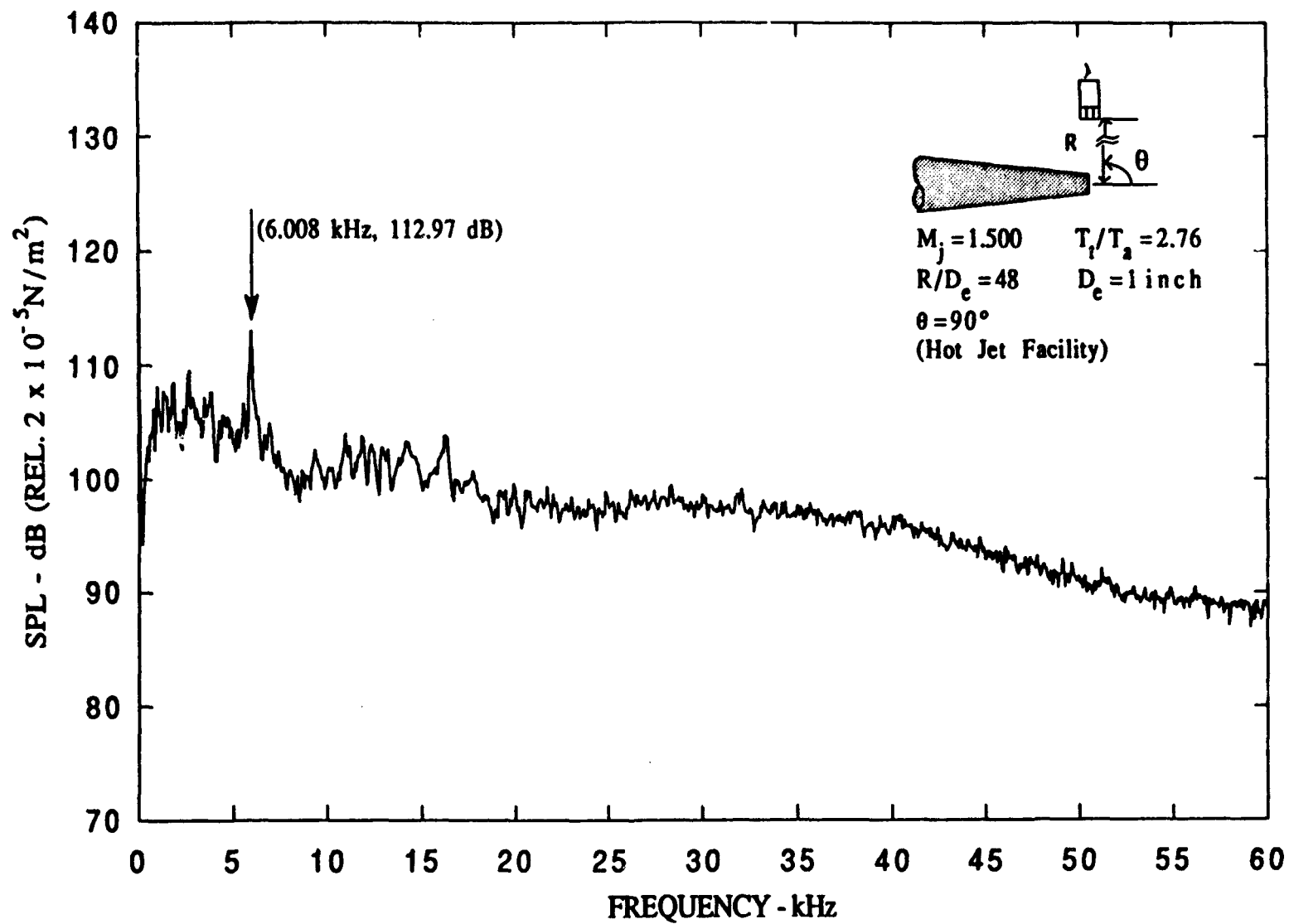Figure A-35. Narrow band spectra (Δf = 62.5 Hz), M_j = 0.90, T_t/T_a = 2.24.
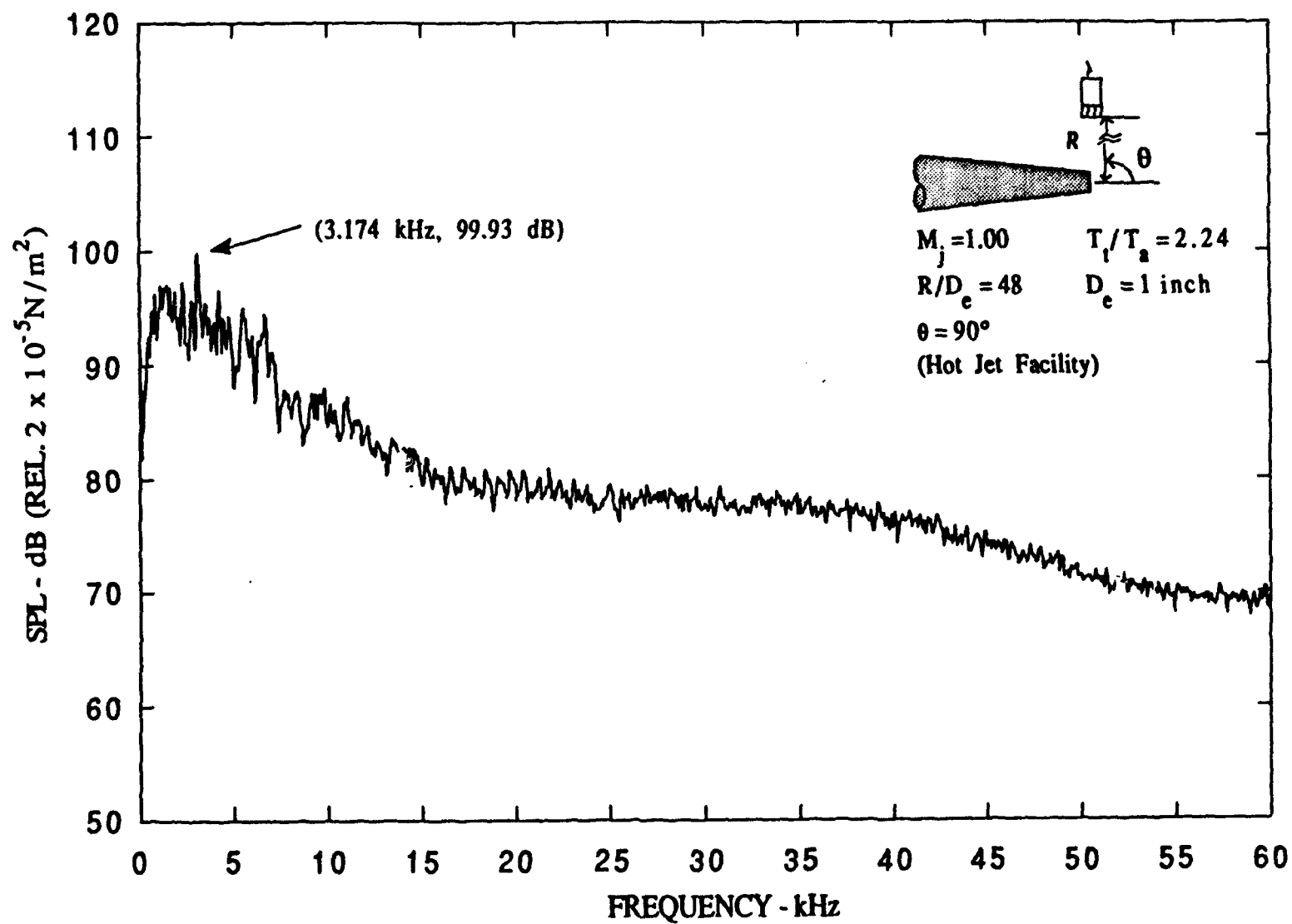
Figure A-36. Narrow band spectra ($\Delta f = 62.5$ Hz), $M_j = 1.00$, $T_t/T_a = 2.24$.
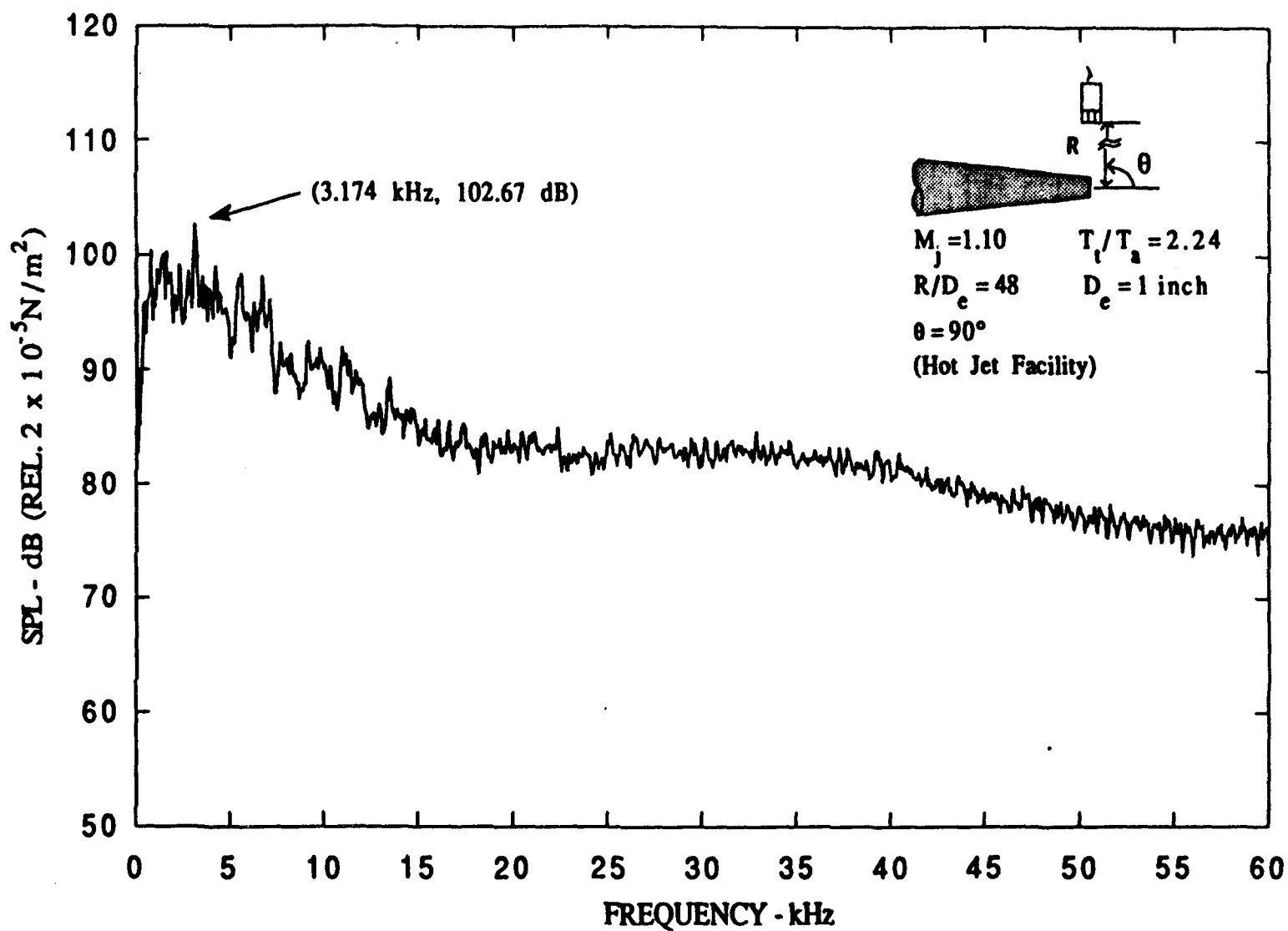
Figure A-37. Narrow band spectra ($\Delta f = 62.5$ Hz), $M_j = 1.10$, $T_t/T_a = 2.24$.
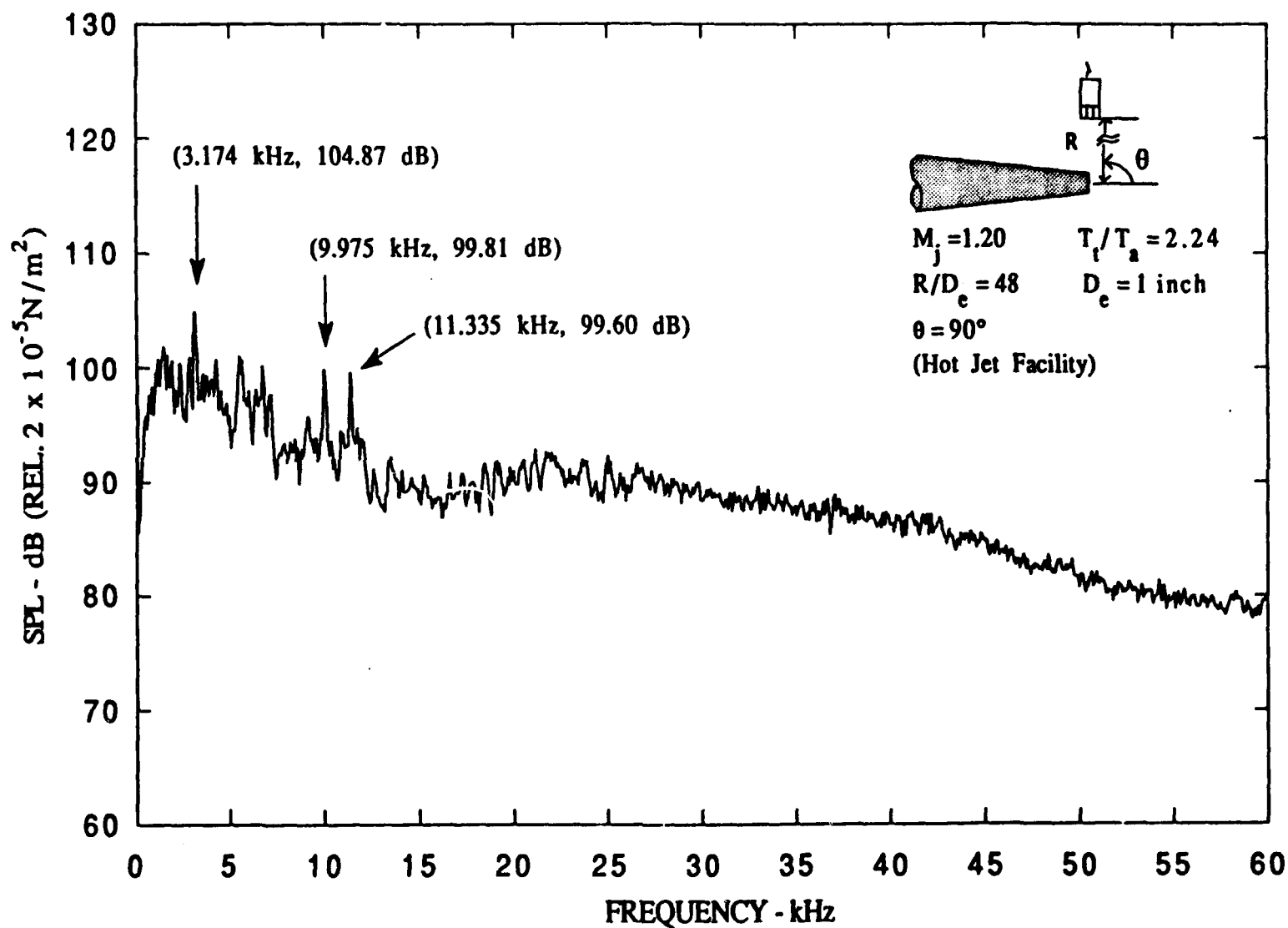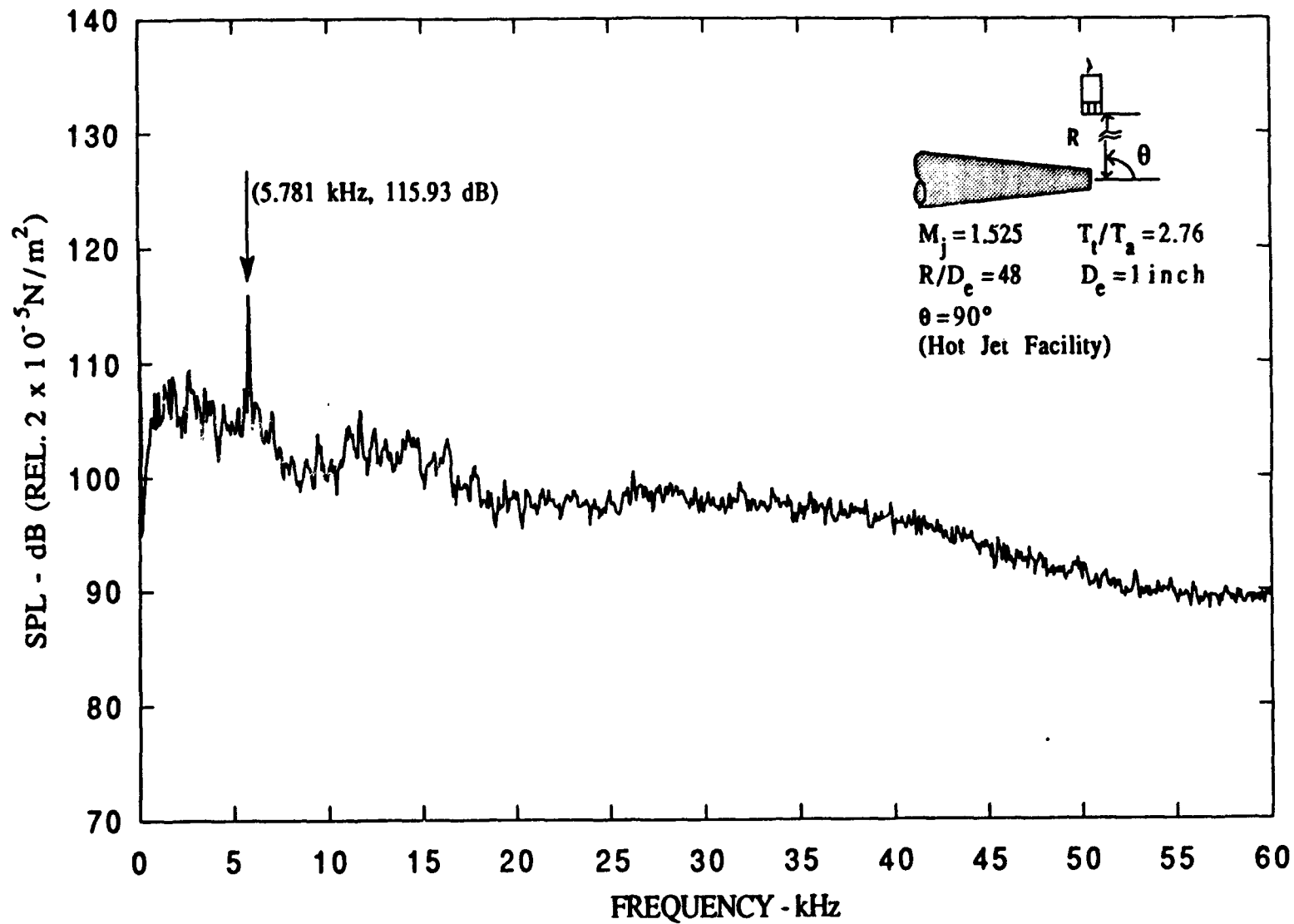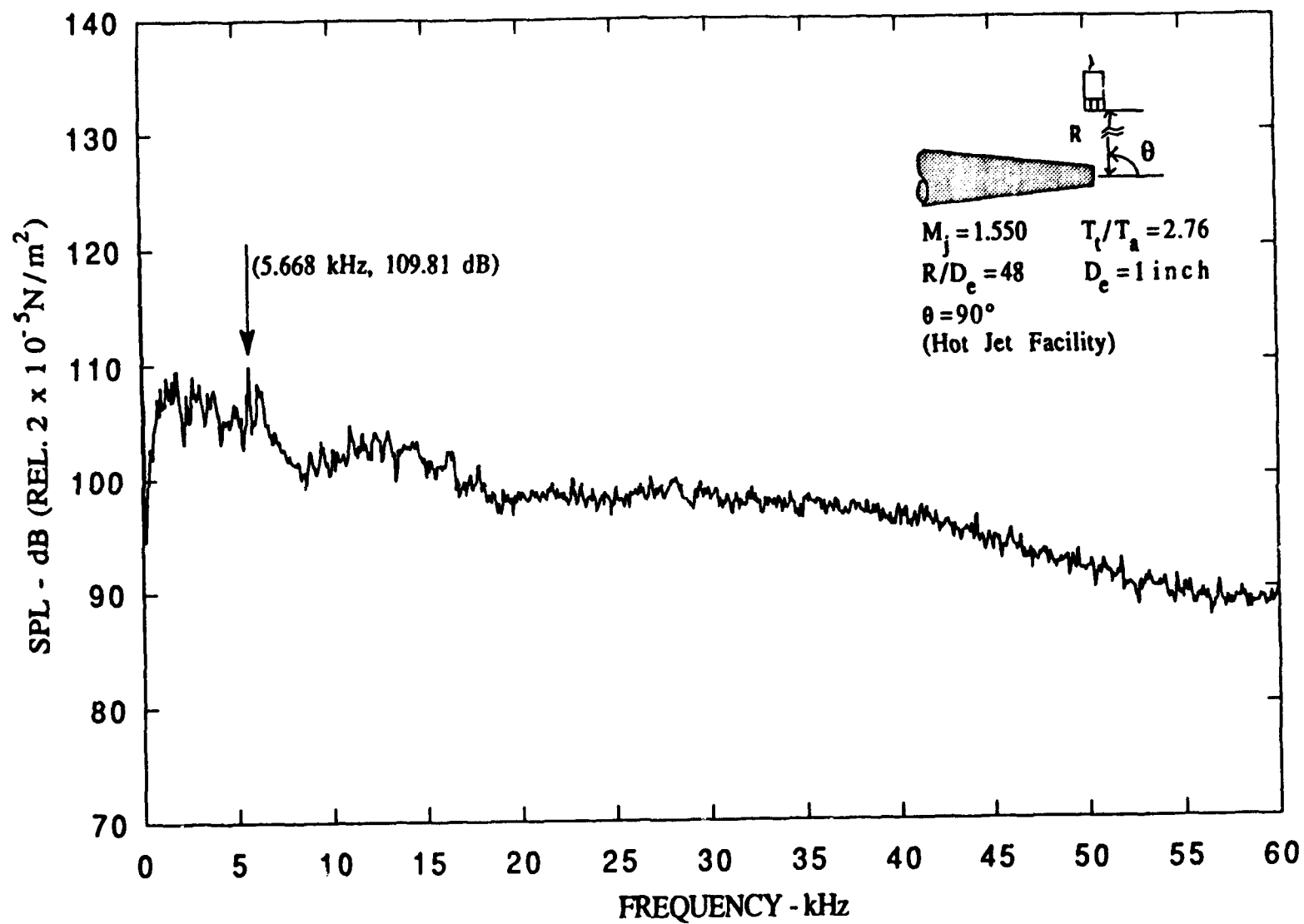
Figure A-38. Narrow band spectra ($\Delta f = 62.5$ Hz), $M_j = 1.20$, $T_t/T_a = 2.24$.
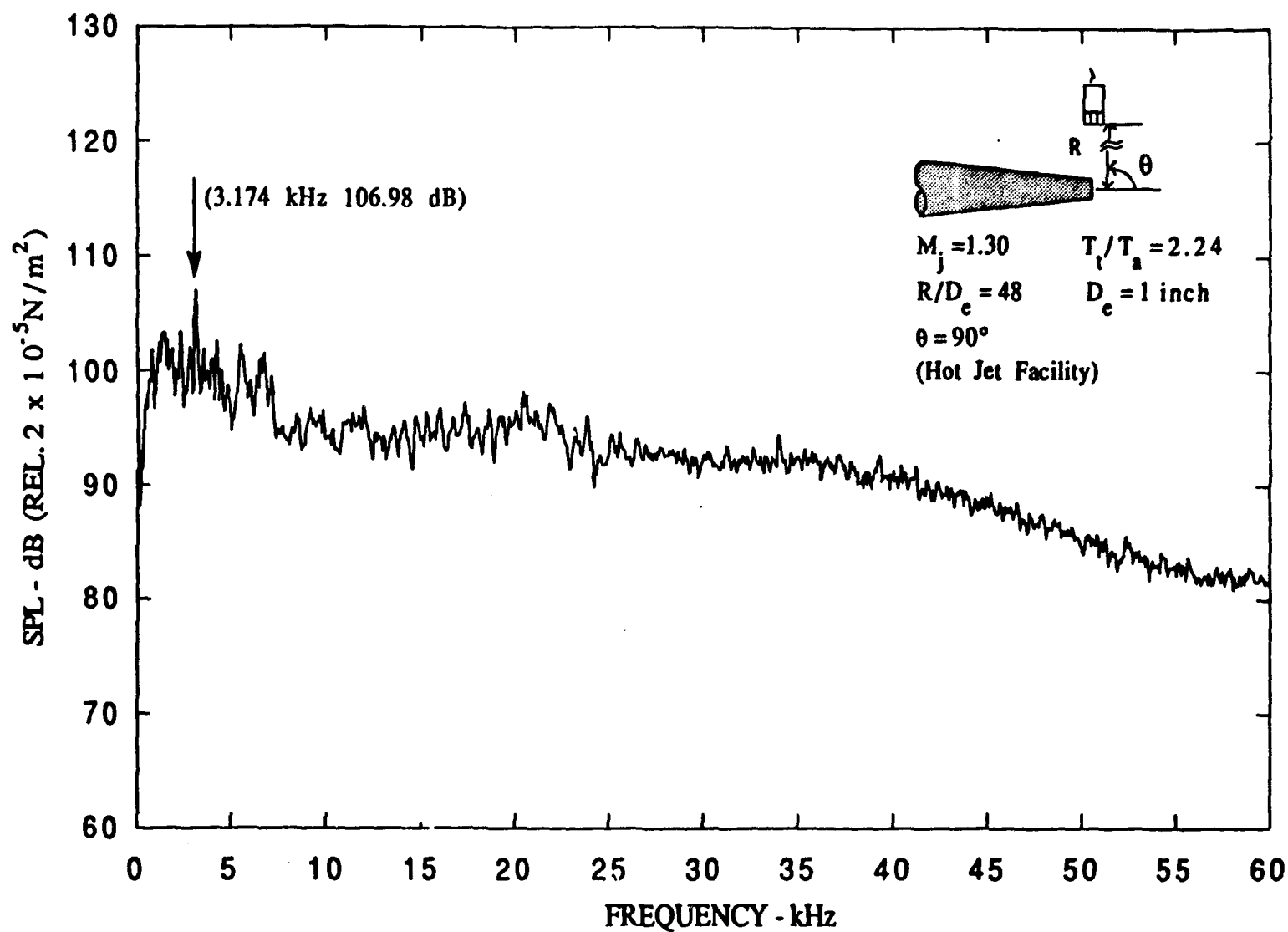
Figure A-39. Narrow band spectra (Δf = 62.5 Hz), M_j = 1.30, T_t/T_a = 2.24.
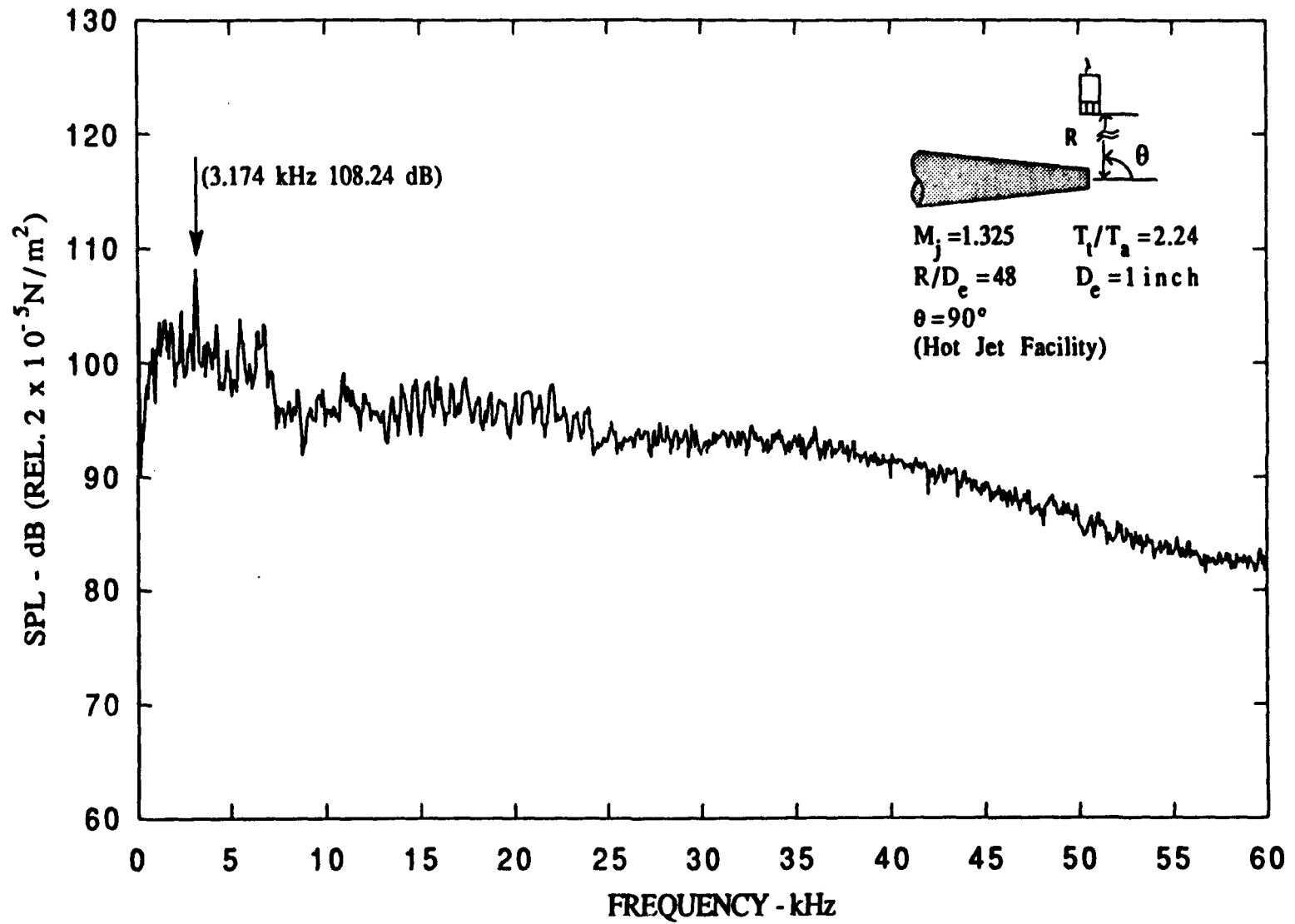
Figure A-40. Narrow band spectra ($\Delta f = 62.5$ Hz), $M_j = 1.325$, $T_t/T_a = 2.24$.
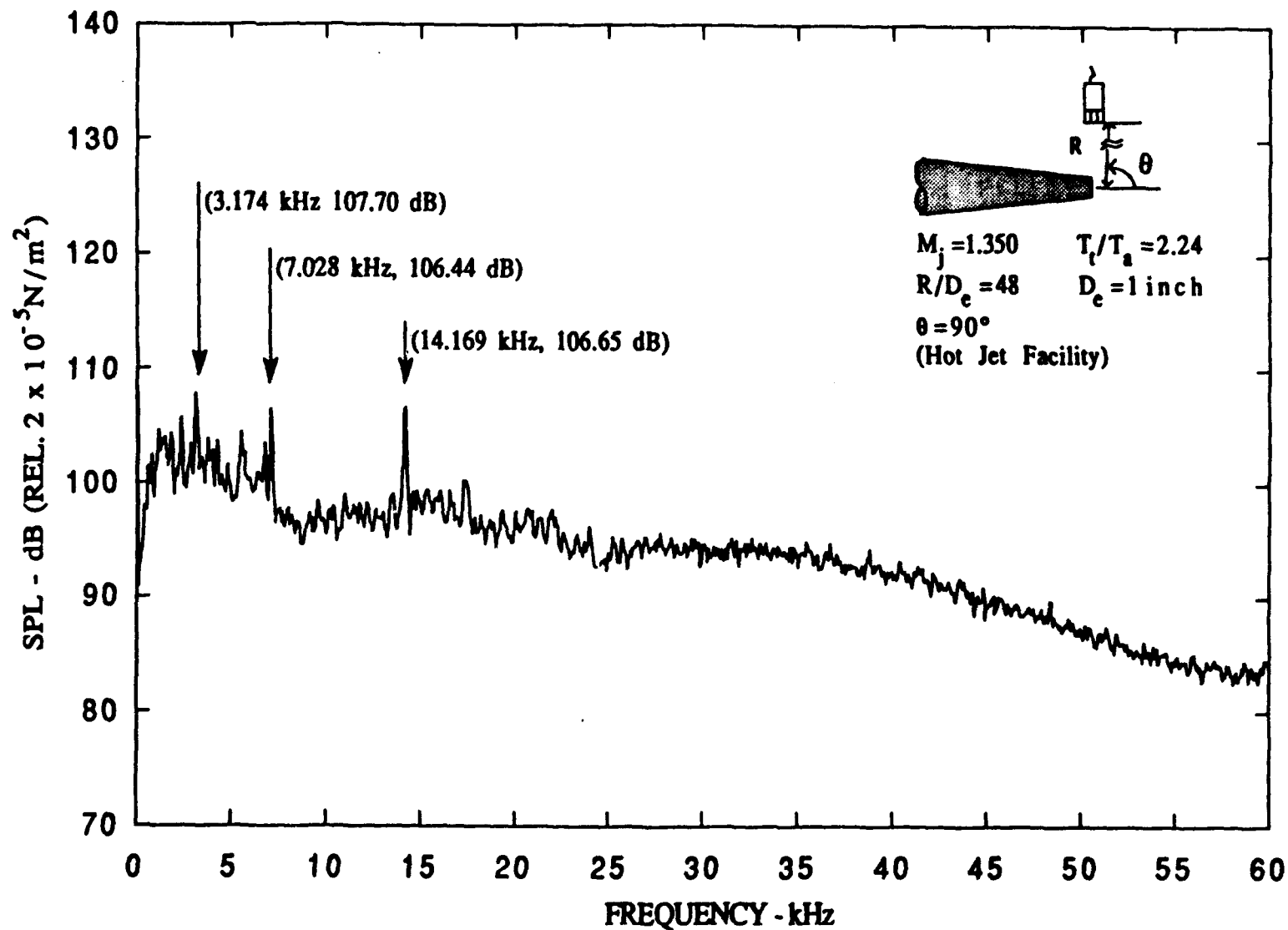
Figure A-41. Narrow band spectra (Δf = 62.5 Hz), M_j = 1.350, T_t/T_a = 2.24.
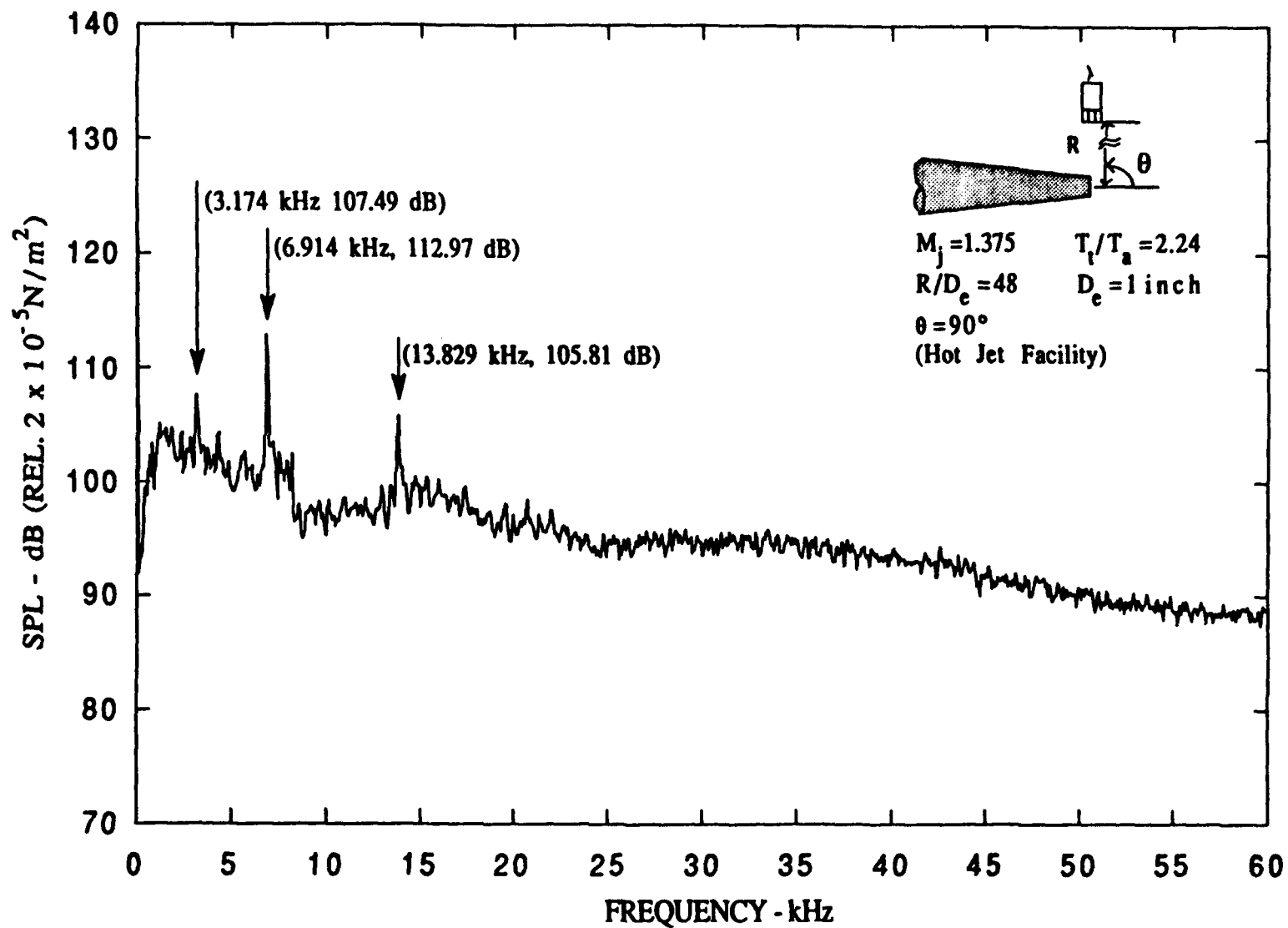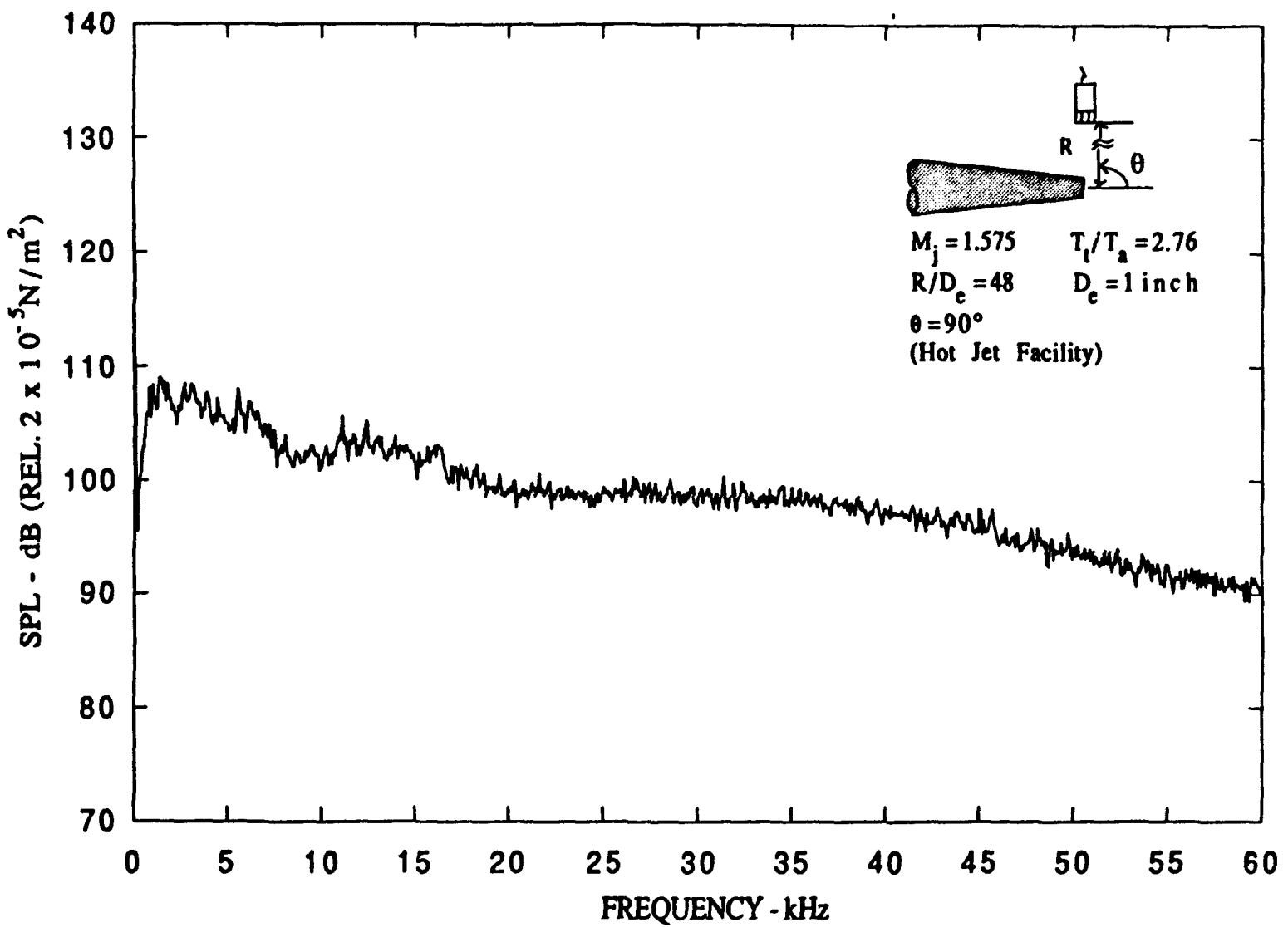
Figure A-42. Narrow band spectra ($\Delta f = 62.5$ Hz), $M_j = 1.375$, $T_t/T_a = 2.24$.

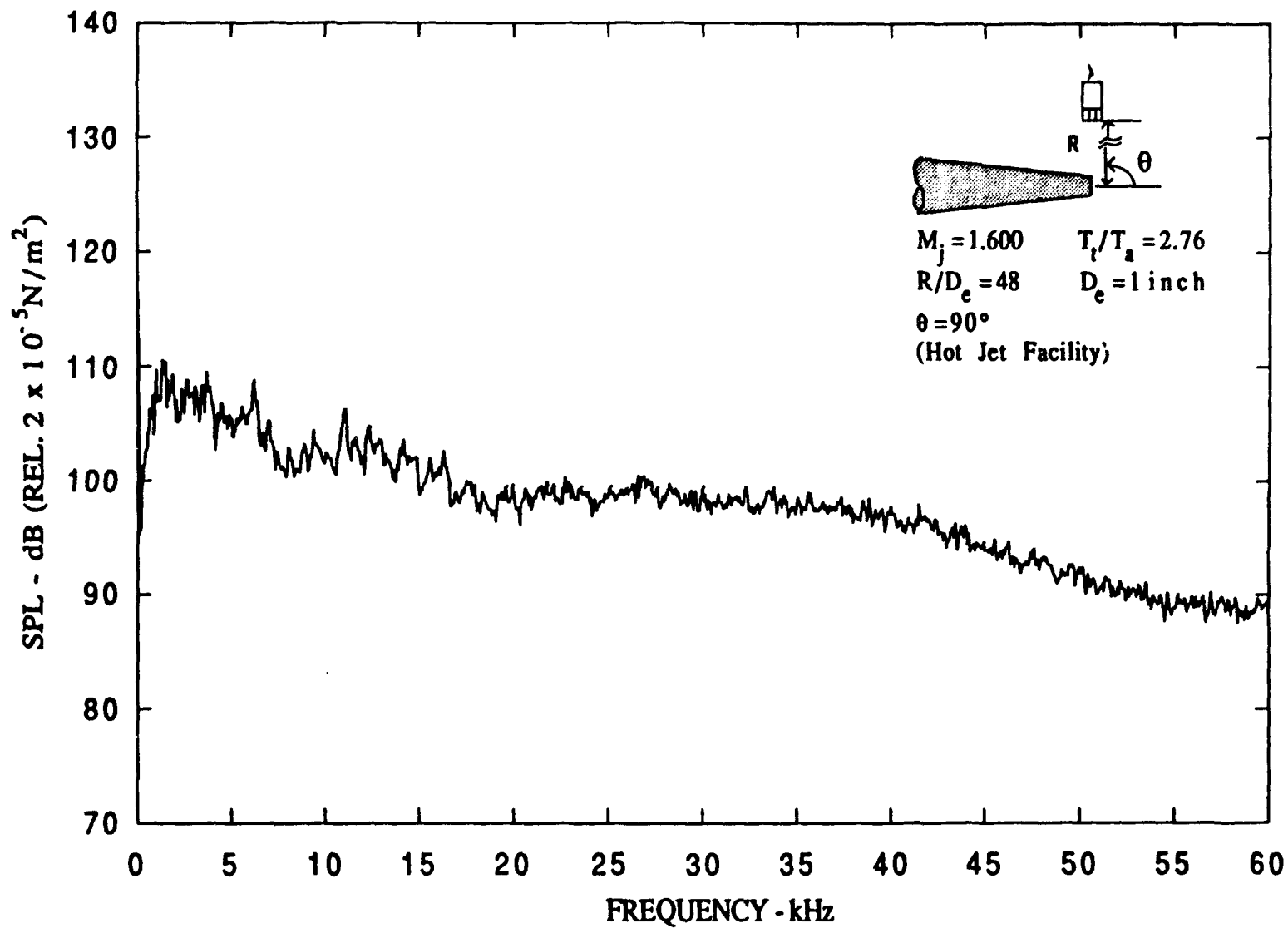Figure A-43. Narrow band spectra (Δf = 62.5 Hz), M_j = 1.400, T_t/T_a = 2.24.

Figure A-44. Narrow band spectra (Δf = 62.5 Hz), M_j = 1.425, T_t/T_a = 2.24.

Figure A-45. Narrow band spectra (Δf = 62.5 Hz), M_j = 1.450, T_t/T_a = 2.24.

Figure A-46. Narrow band spectra ($\Delta f = 62.5$ Hz), $M_j = 1.475$, $T_t/T_a = 2.24$.

Figure A-47. Narrow band spectra ($\Delta f = 62.5$ Hz), $M_j = 1.500$, $T_t/T_a = 2.24$.

Figure A-48. Narrow band spectra ($\Delta f = 62.5$ Hz), $M_j = 1.525$, $T_t/T_a = 2.24$.

Figure A-49. Narrow band spectra (Δf = 62.5 Hz), M_j = 1.550, T_t/T_a = 2.24.

Figure A-50. Narrow band spectra (Δf = 62.5 Hz), M_j = 1.575, T_t/T_a = 2.24.

Figure A-51. Narrow band spectra (Δf = 62.5 Hz), M_j = 1.600, T_t/T_a = 2.24.

(3.174 kHz, 112.34 dB)

$M_j = 1.70$ $T_t/T_a = 2.24$
$R/D_e = 48$ $D_e = 1$ inch
$\theta = 90°$
(Hot Jet Facility)

Figure A-52. Narrow band spectra ($\Delta f = 62.5$ Hz), $M_j = 1.70$, $T_t/T_a = 2.24$.

Figure A-53. Narrow band spectra (Δf = 62.5 Hz), M_j = 1.100, T_t/T_a = 2.76.

Figure A-54. Narrow band spectra ($\Delta f = 62.5$ Hz), $M_j = 1.125$, $T_t/T_a = 2.76$.

Figure A-55. Narrow band spectra (Δf = 62.5 Hz), M_j = 1.150, T_t/T_a = 2.76.

Figure A-56. Narrow band spectra (Δf = 62.5 Hz), M_j = 1.175, T_t/T_a = 2.76.

Figure A-57. Narrow band spectra ($\Delta f = 62.5$ Hz), $M_j = 1.200$, $T_t/T_a = 2.76$.

Figure A-58. Narrow band spectra ($\Delta f = 62.5$ Hz), $M_j = 1.225$, $T_t/T_a = 2.76$.

Figure A-59. Narrow band spectra (Δf = 62.5 Hz), M_j = 1.250, T_t/T_a = 2.76.

Figure A-60. Narrow band spectra ($\Delta f = 62.5$ Hz), $M_j = 1.275$, $T_t/T_a = 2.76$.

Figure A-61. Narrow band spectra ($\Delta f = 62.5$ Hz), $M_j = 1.300$, $T_t/T_a = 2.76$.

Figure A-62. Narrow band spectra (Δf = 62.5 Hz), M_j = 1.325, T_t/T_a = 2.76.

Figure A-63. Narrow band spectra ($\Delta f = 62.5$ Hz), $M_j = 1.350$. $T_t/T_a = 2.76$.

Figure A-64. Narrow band spectra ($\Delta f = 62.5$ Hz), $M_j = 1.375$, $T_t/T_a = 2.76$.

Figure A-65. Narrow band spectra ($\Delta f = 62.5$ Hz), $M_j = 1.400$, $T_t/T_a = 2.76$.

Figure A-66. Narrow band spectra (Δf = 62.5 Hz), M_j = 1.425, T_t/T_a = 2.76.

Figure A-67. Narrow band spectra (Δf = 62.5 Hz), M_j = 1.450, T_t/T_a = 2.76.

Figure A-68. Narrow band spectra ($\Delta f = 62.5$ Hz), $M_j = 1.475$, $T_t/T_a = 2.76$.

Figure A-69. Narrow band spectra (Δf = 62.5 Hz), M_j = 1.500, T_t/T_a = 2.76.

Figure A-70. Narrow band spectra (Δf = 62.5 Hz), M_j = 1.525, T_t/T_a = 2.76.

Figure A-71. Narrow band spectra (Δf = 62.5 Hz), M_j = 1.550, T_t/T_a = 2.76.

Figure A-72. Narrow band spectra (Δf = 62.5 Hz), M_j = 1.575, T_t/T_a = 2.76.

Figure A-73. Narrow band spectra ($\Delta f = 62.5$ Hz), $M_j = 1.600$, $T_t/T_a = 2.76$.

APPENDIX B
Free-Jet Data for 0.48-in. Nozzle
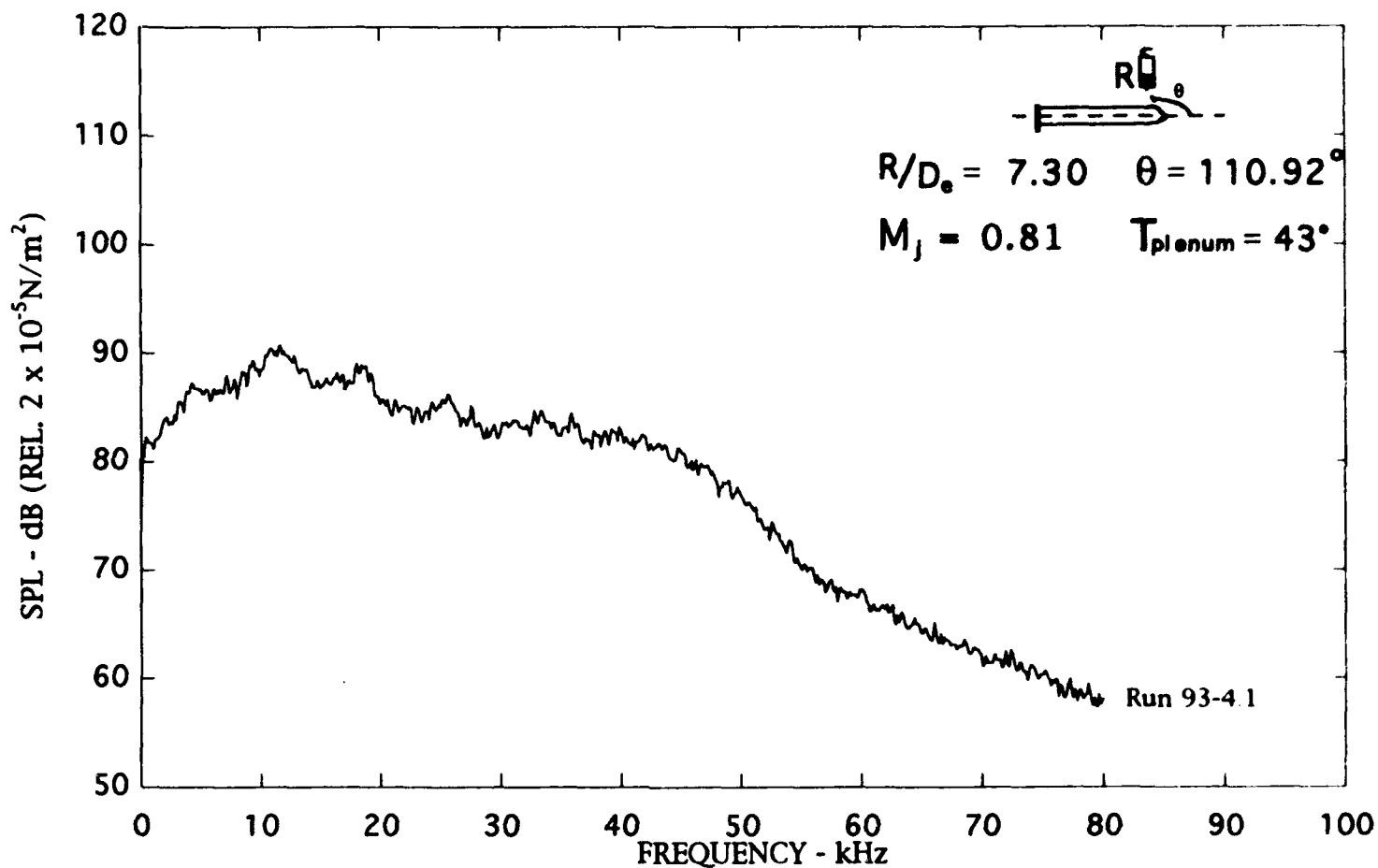
Figure B-1. Narrow band ($\Delta f = 128$ Hz) noise spectra of round nozzle (cold flow), $M_j = 0.81$.
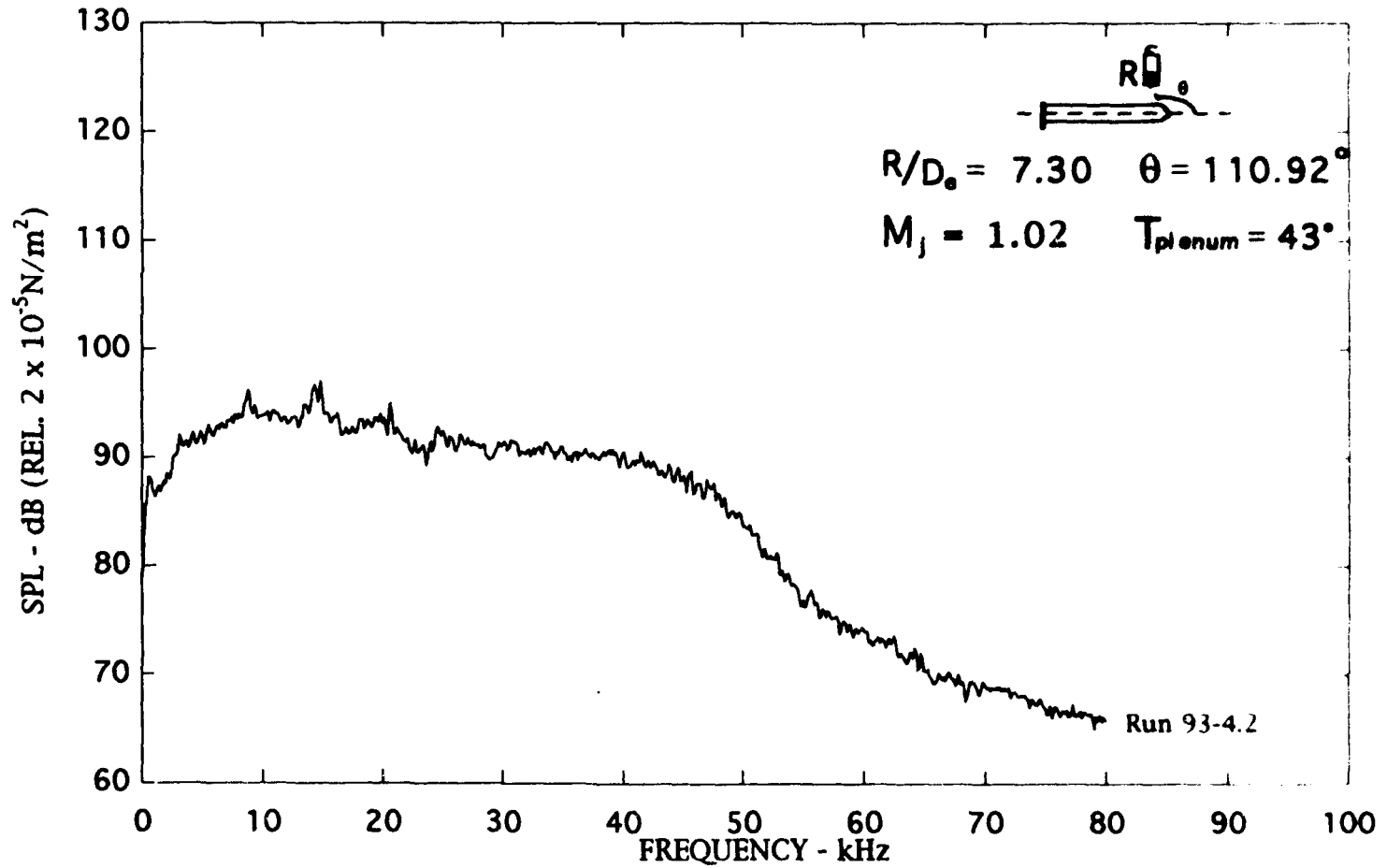
Figure B-2. Narrow band (Δf = 128 Hz) noise spectra of round nozzle (cold flow), M_j = 1.02.
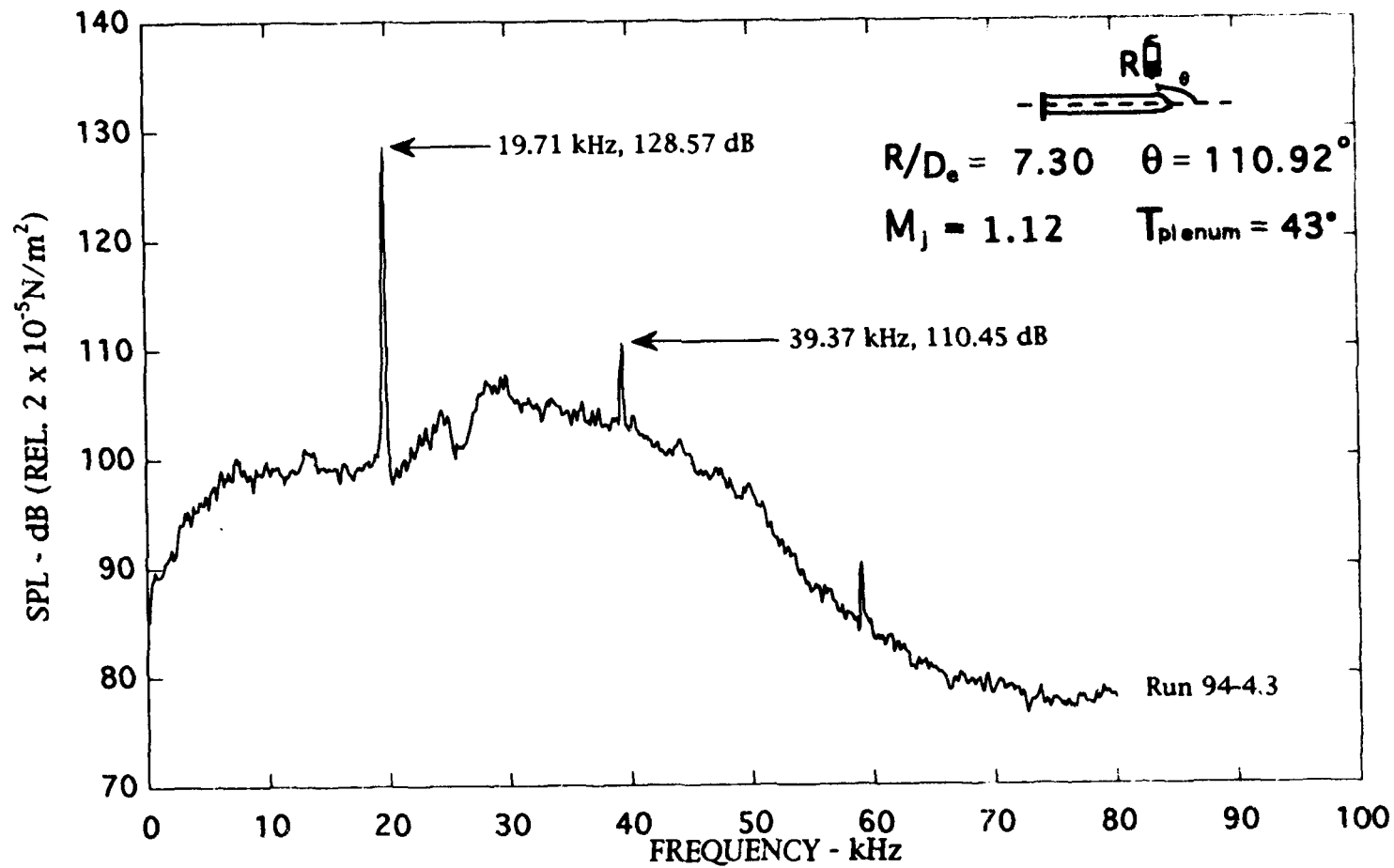
Figure B-3. Narrow band ($\Delta f = 128$ Hz) noise spectra of round nozzle (cold flow), $M_j = 1.12$.
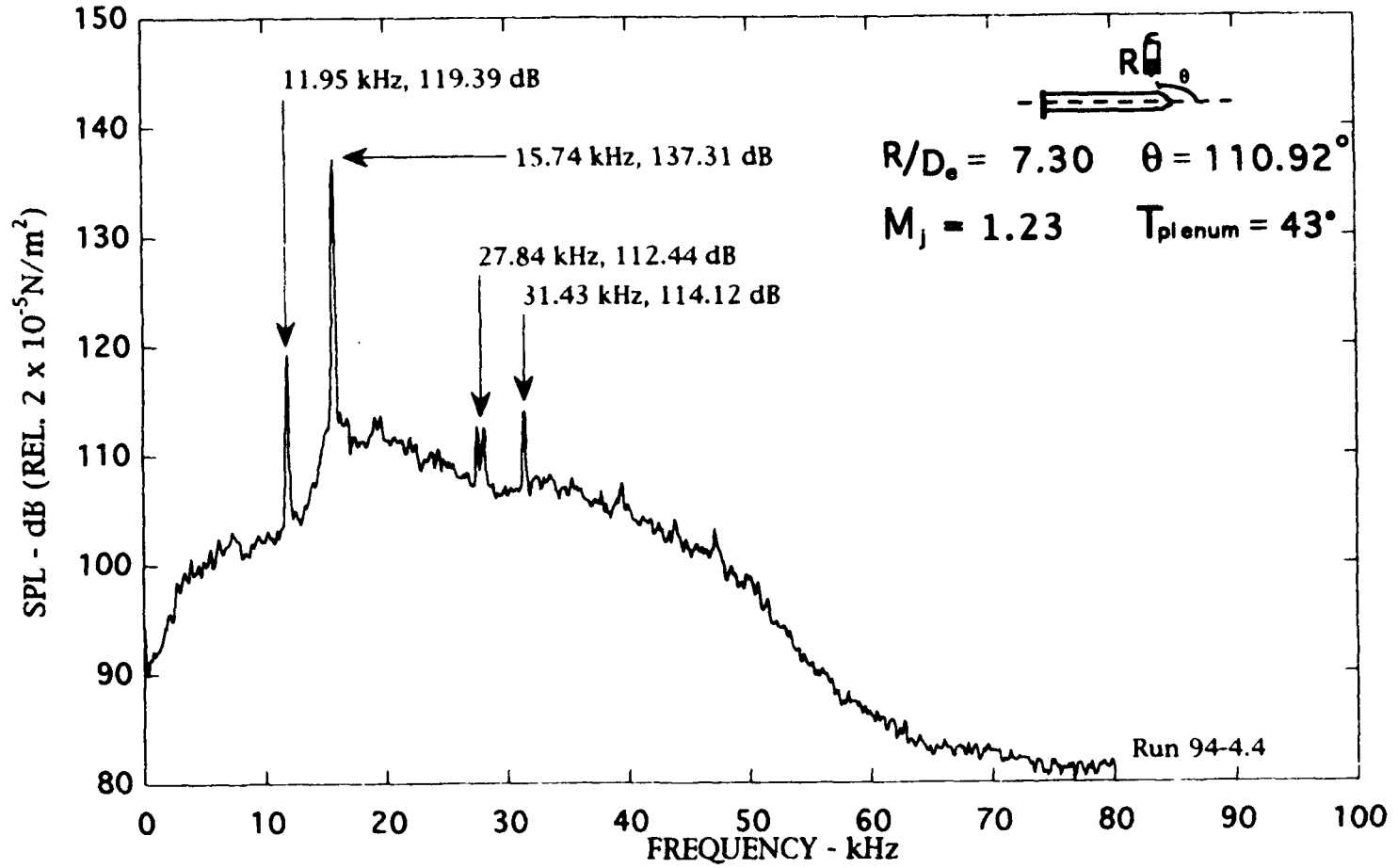
Figure B-4. Narrow band ($\Delta f = 128$ Hz) noise spectra of round nozzle (cold flow), $M_j = 1.23$.
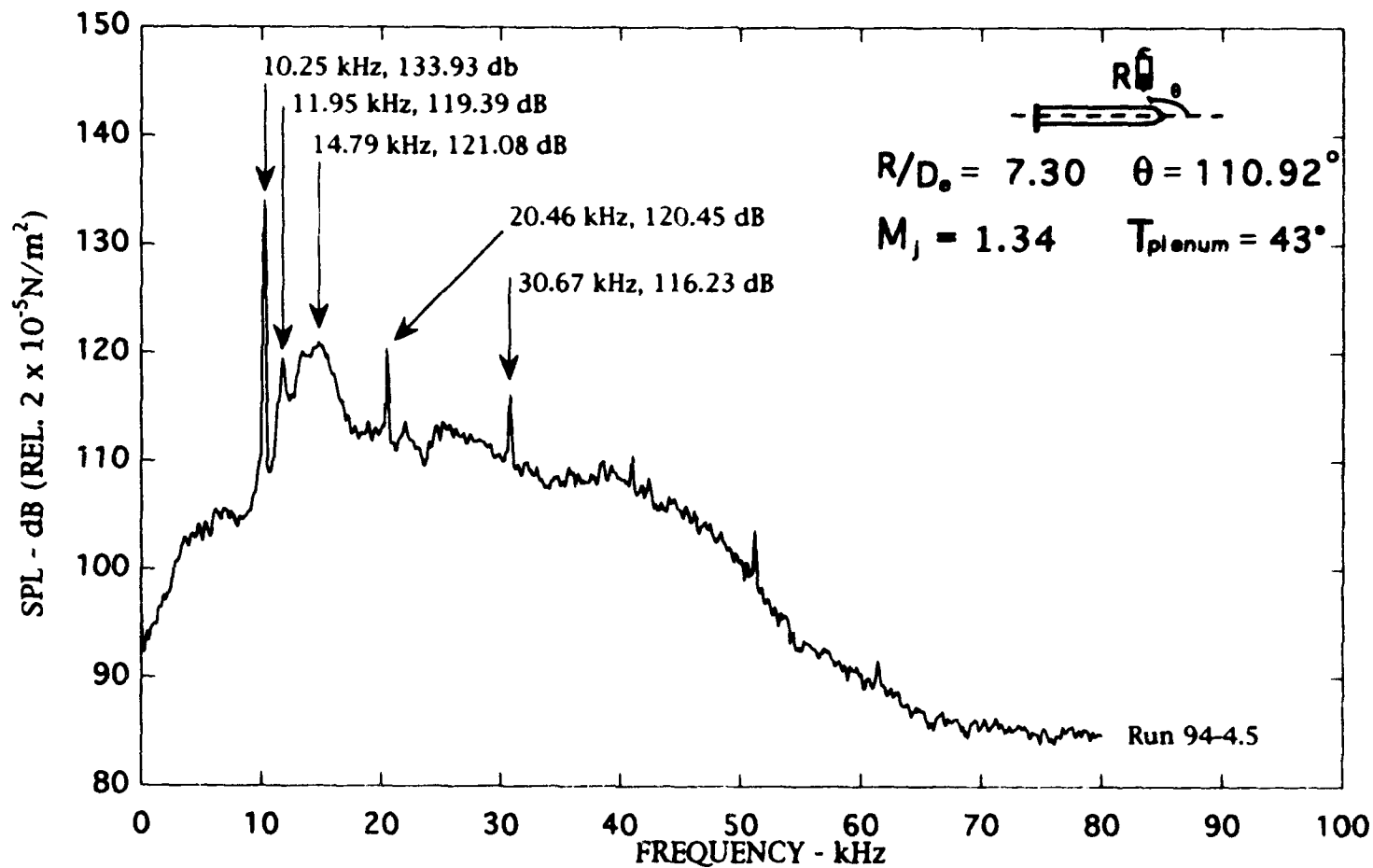
Figure B-5. Narrow band ($\Delta f = 128$ Hz) noise spectra of round nozzle (cold flow), $M_j = 1.34$.
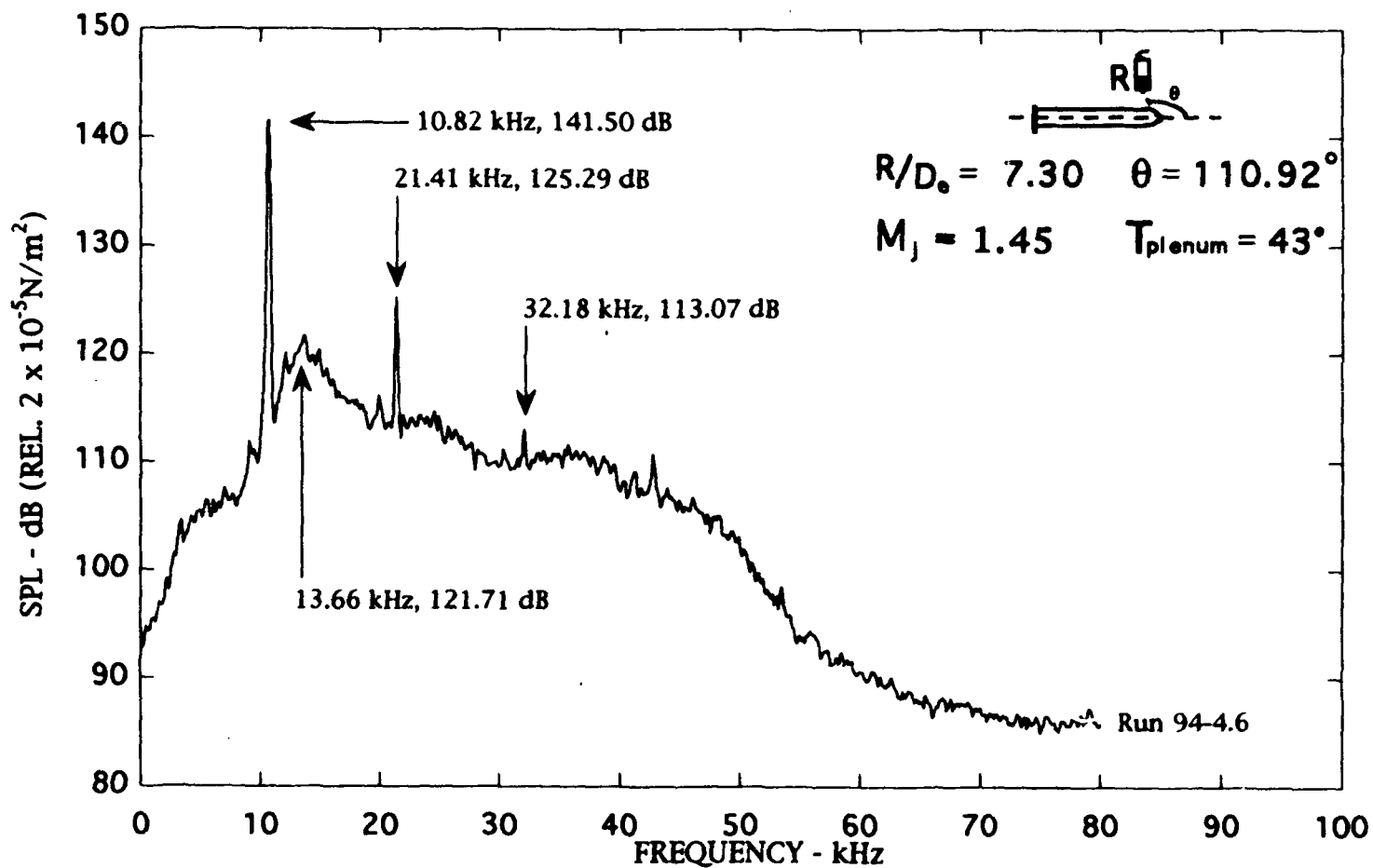
Figure B-6. Narrow band ($\Delta f = 128$ Hz) noise spectra of round nozzle (cold flow), $M_j = 1.45$.
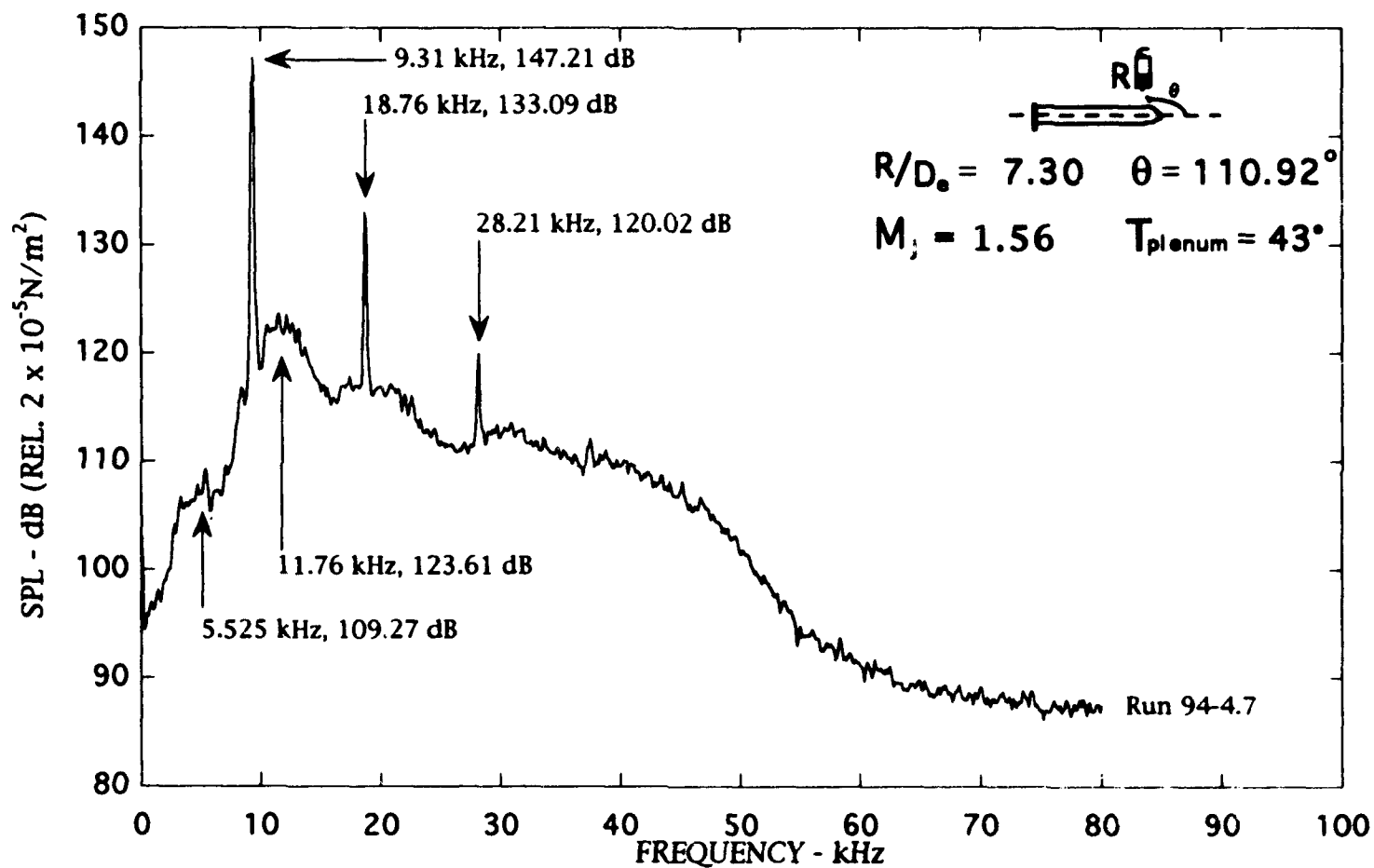
Figure B-7. Narrow band ($\Delta f = 128$ Hz) noise spectra of round nozzle (cold flow), $M_j = 1.56$.
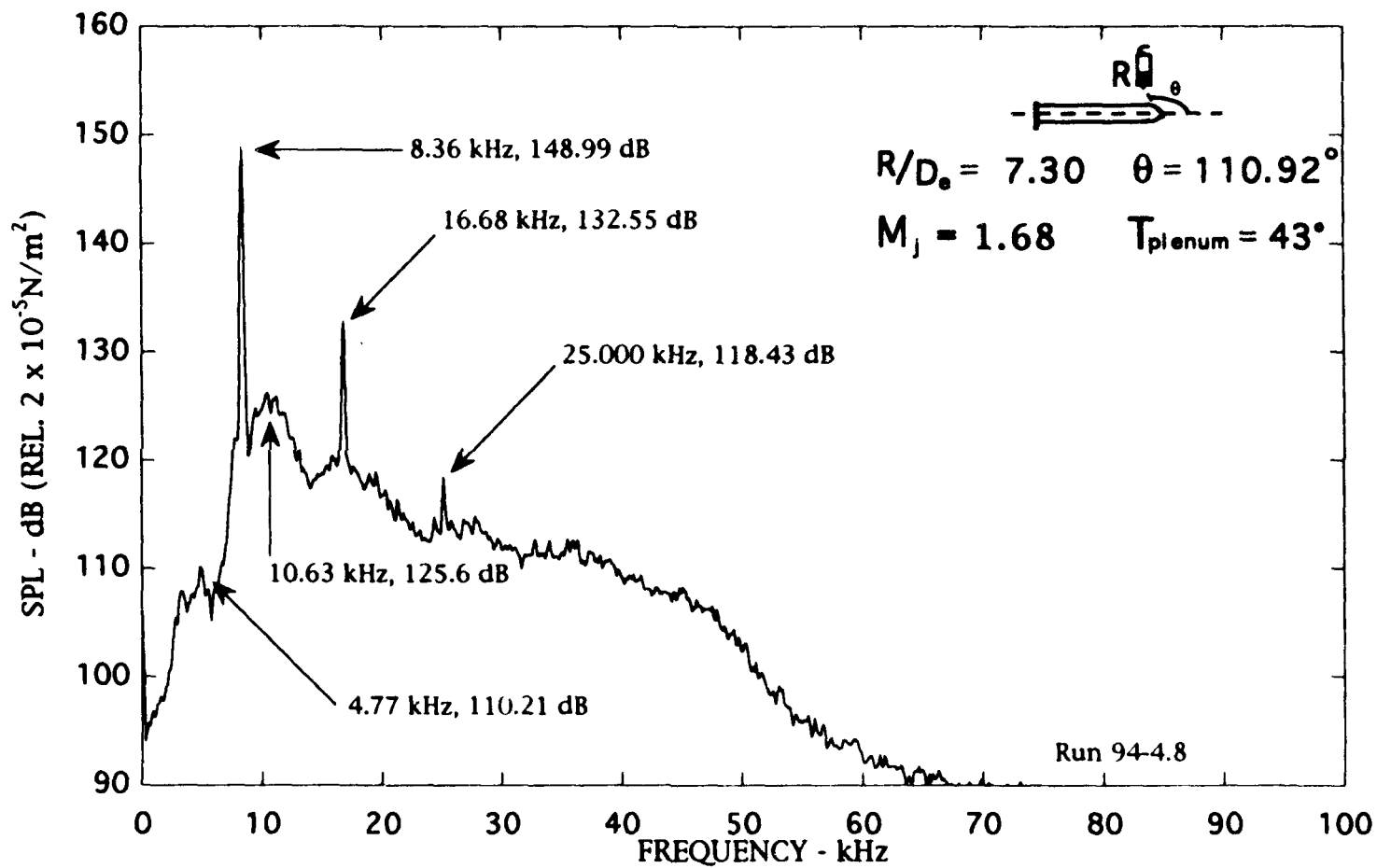
Figure B-8. Narrow band (Δf = 128 Hz) noise spectra of round nozzle (cold flow), M_j = 1.68.
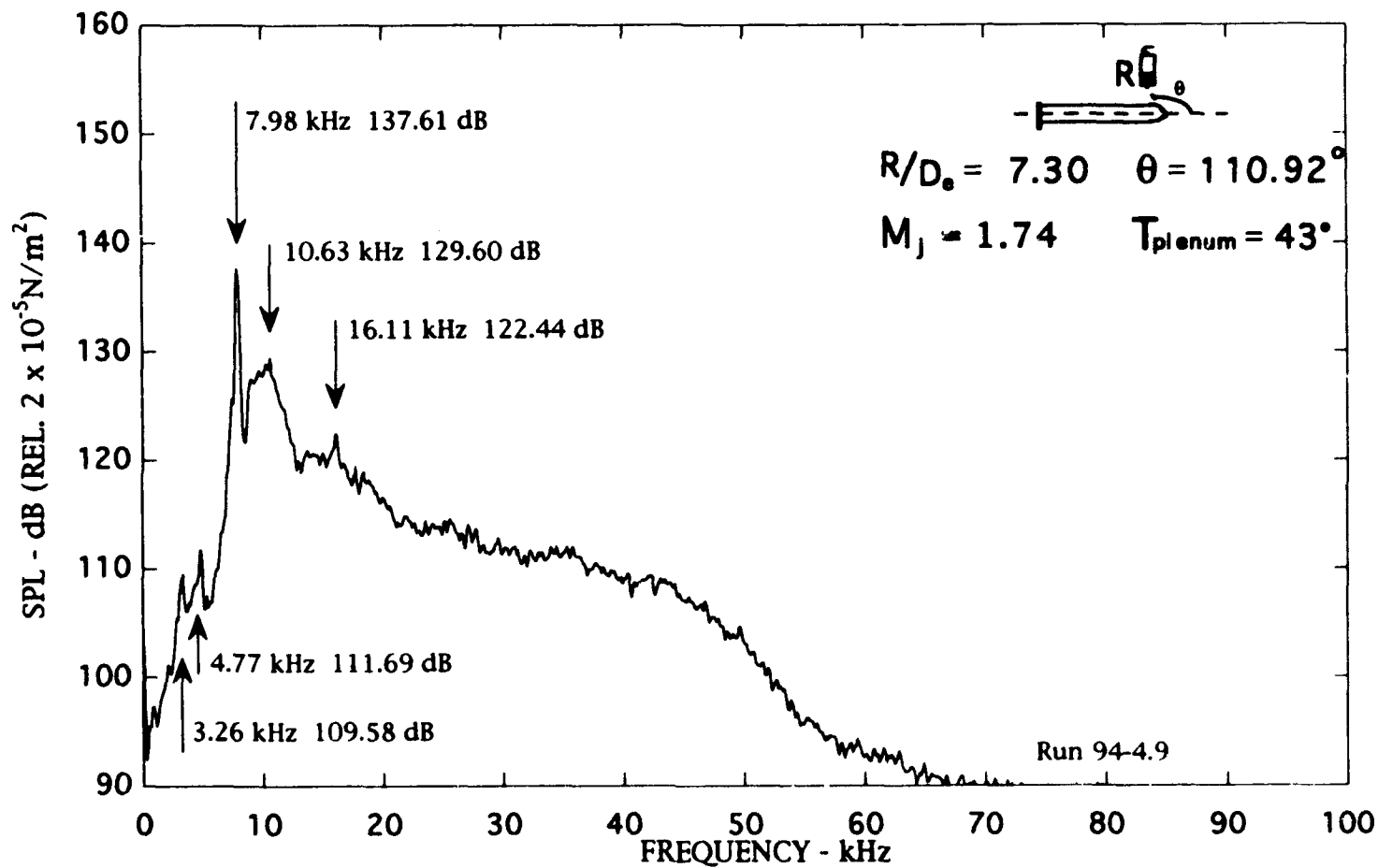
Figure B-9. Narrow band (Δf = 128 Hz) noise spectra of round nozzle (cold flow), M_j = 1.74.
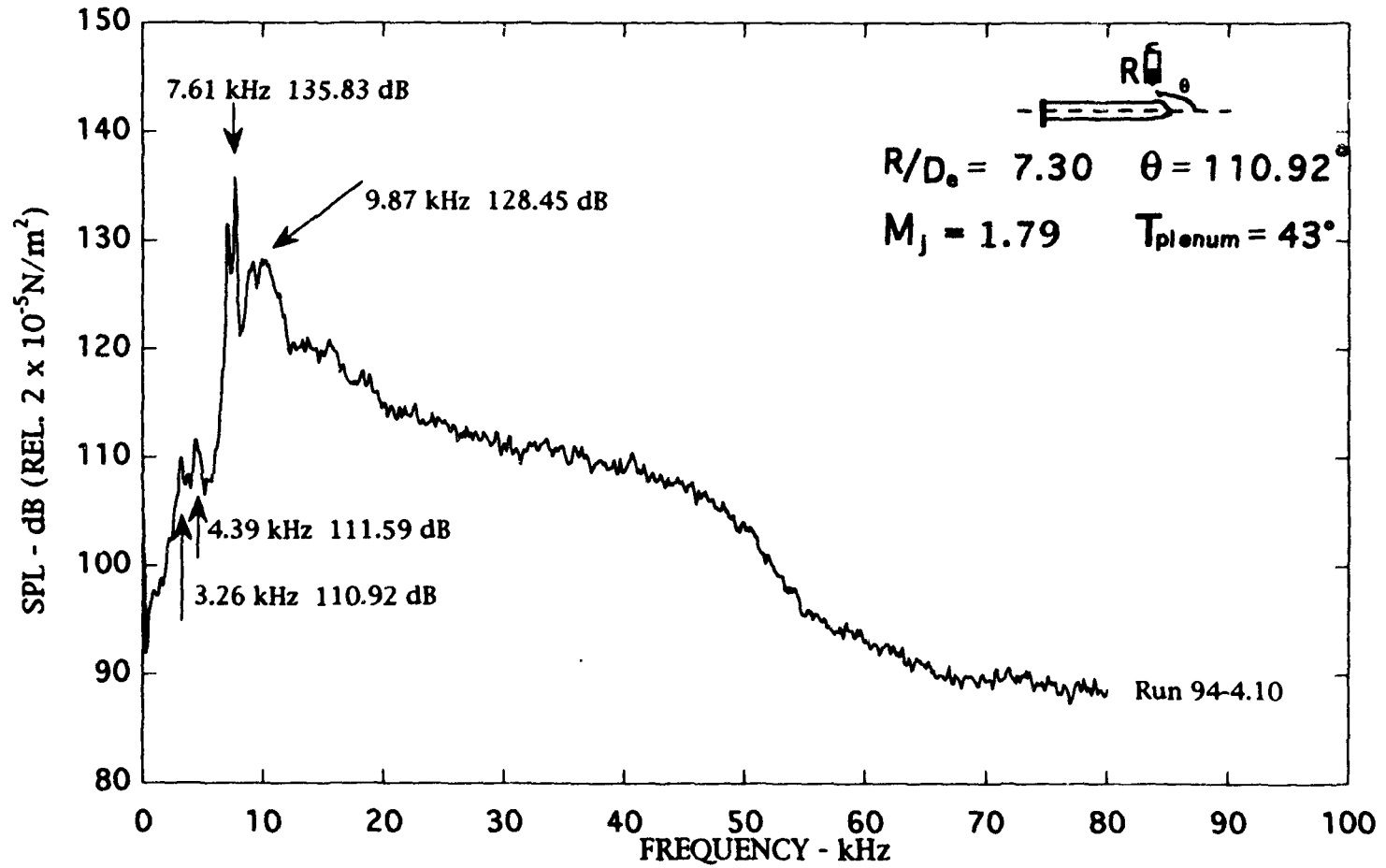
Figure B-10. Narrow band (Δf = 128 Hz) noise spectra of round nozzle (cold flow),
M_j = 1.79.
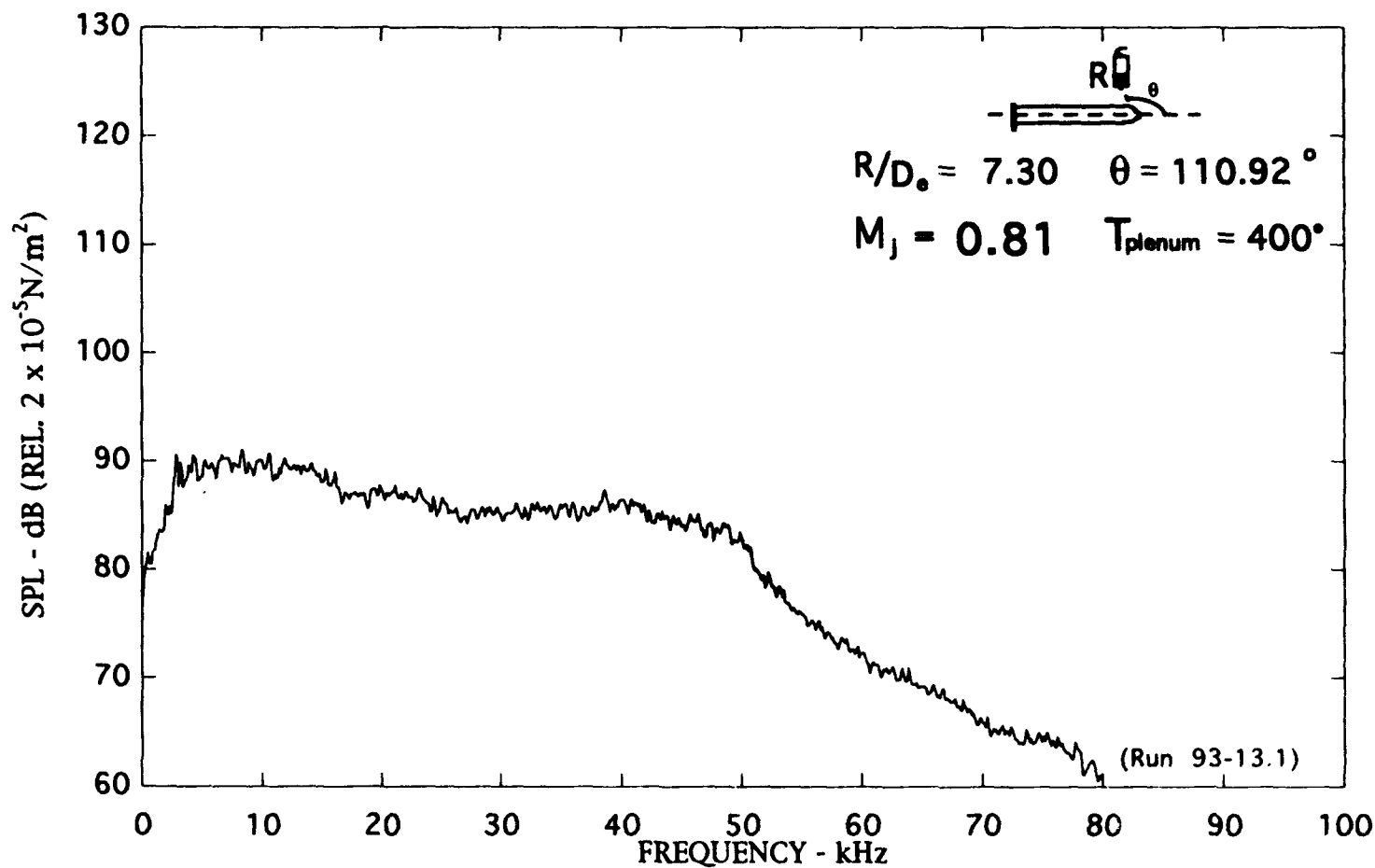
Figure B-11. Narrow band (Δf = 128 Hz) noise spectra of the free jet, M_j = 0.81.
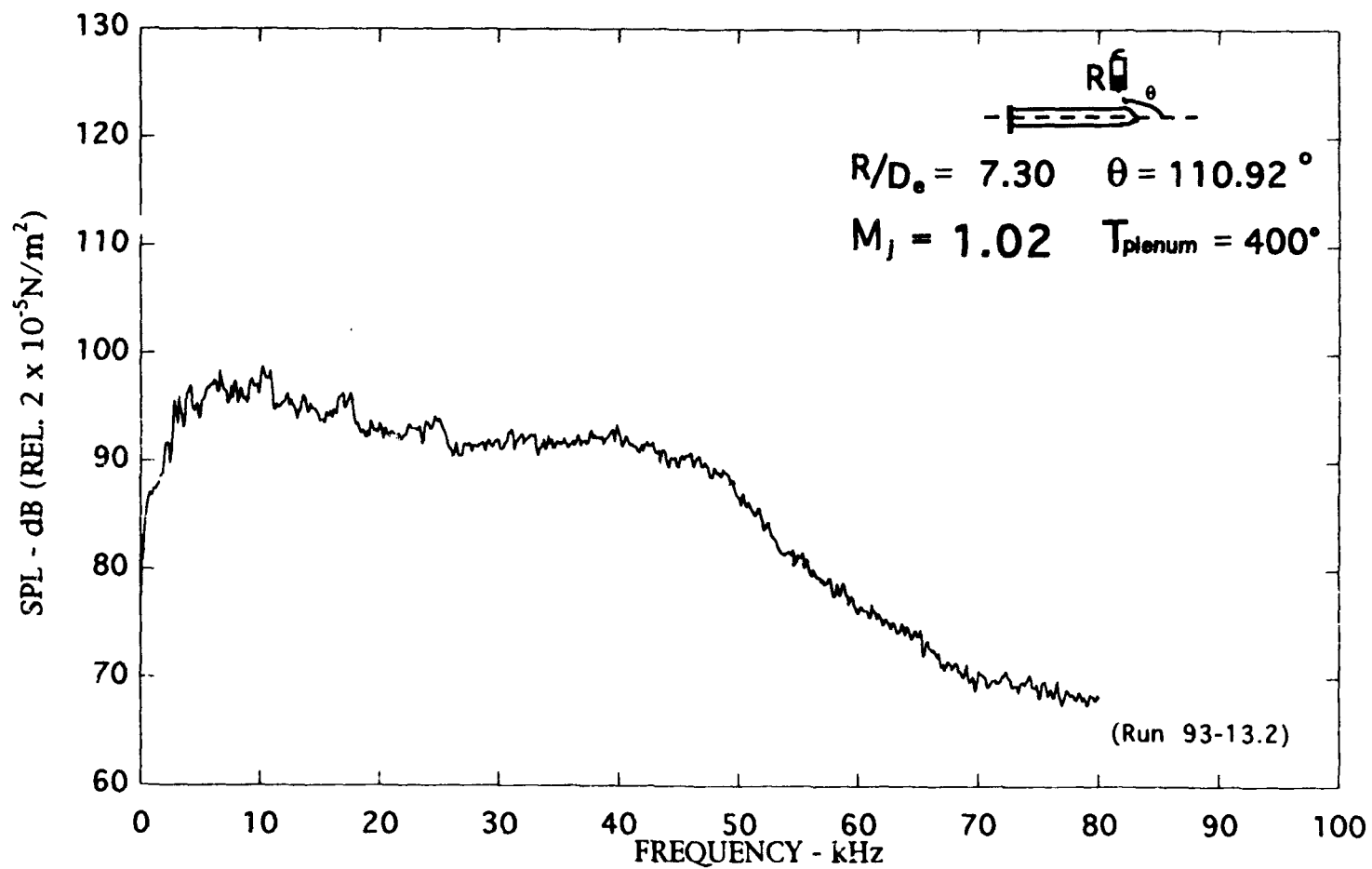
Figure B-12. Narrow band ($\Delta f = 128$ Hz) noise spectra of the free jet, $M_j = 1.02$.
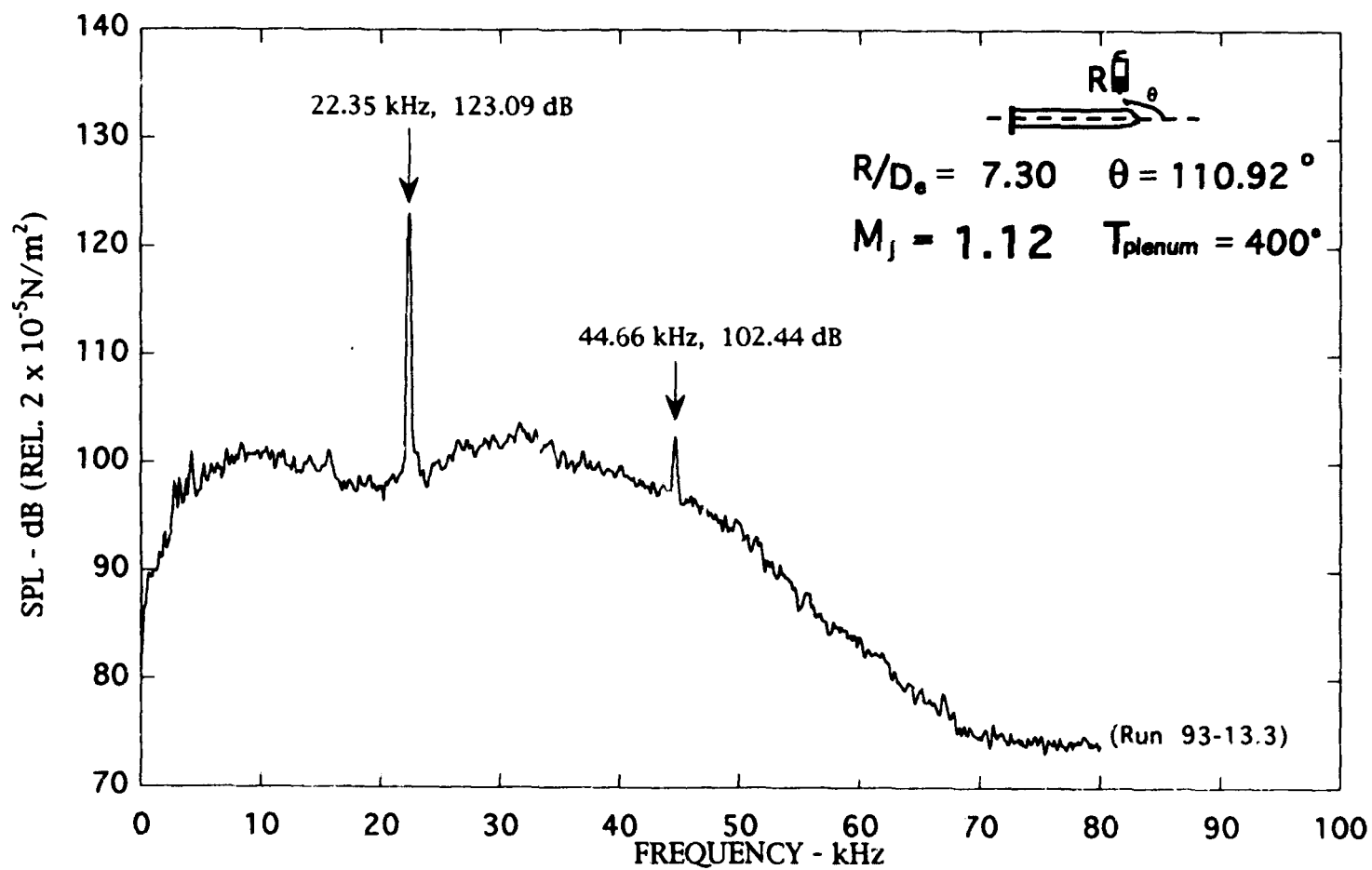
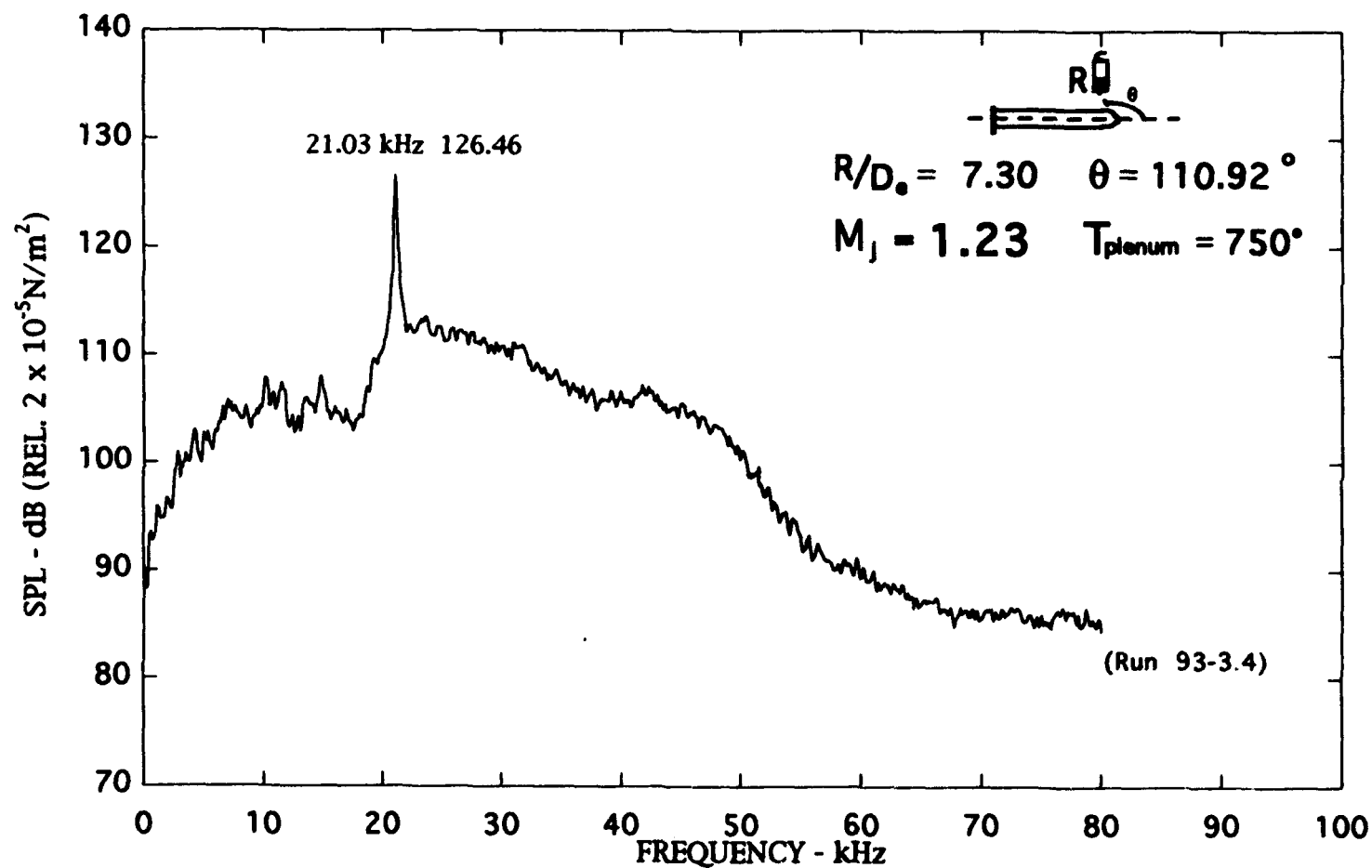Figure B-13. Narrow band ($\Delta f = 128$ Hz) noise spectra of the free jet, $M_j = 1.12$.

The figure shows a plot of SPL - dB (REL. 2 x 10^{-5} N/m^2) versus FREQUENCY - kHz. Annotations on the plot read:

22.35 kHz, 123.09 dB

44.66 kHz, 102.44 dB

$R/D_e = 7.30 \quad \theta = 110.92\,^\circ$

$M_j = 1.12 \quad T_{plenum} = 400\,^\circ$

(Run 93-13.3)
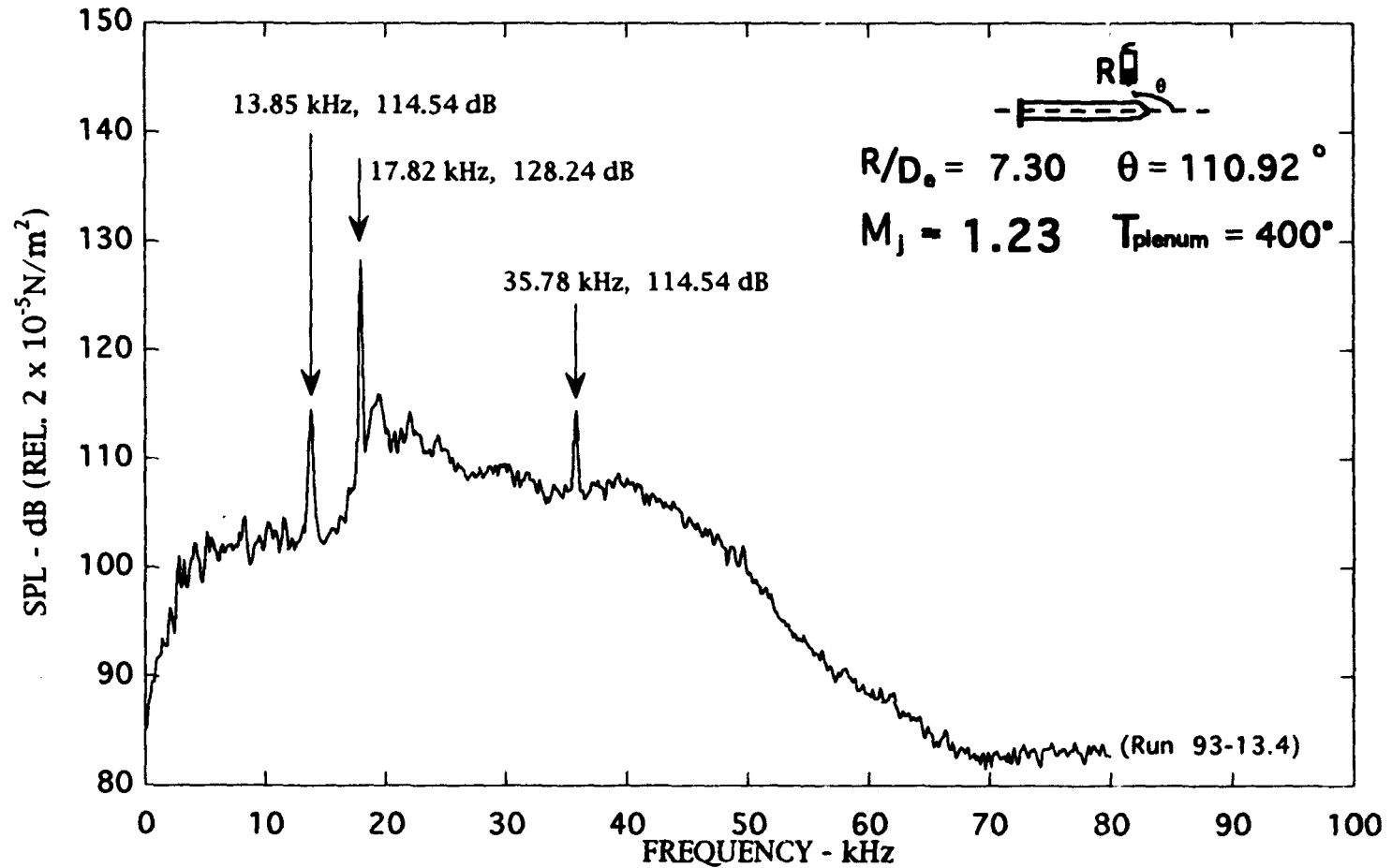
Figure B-14. Narrow band ($\Delta f = 128$ Hz) noise spectra of the free jet, $M_j = 1.23$.
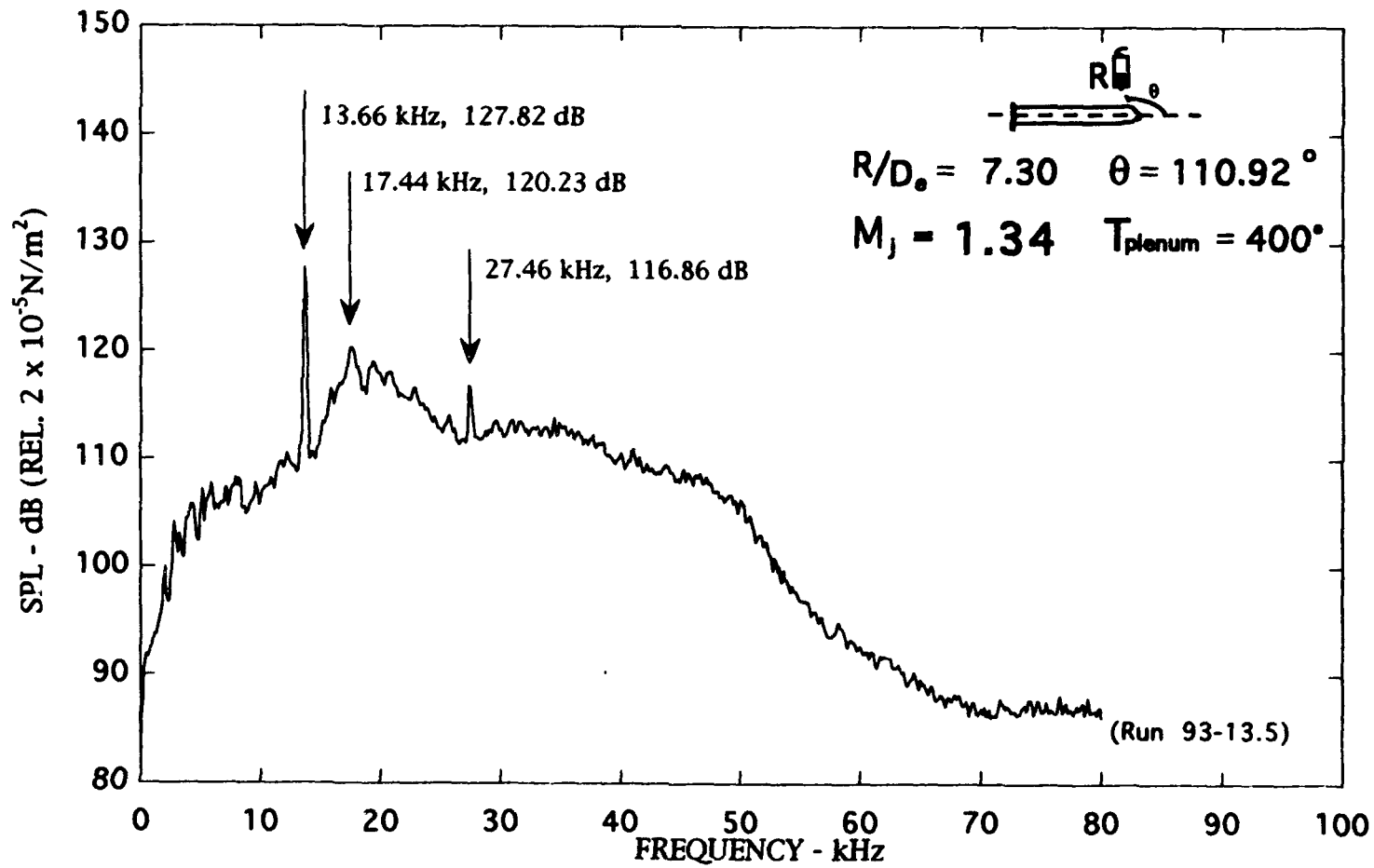
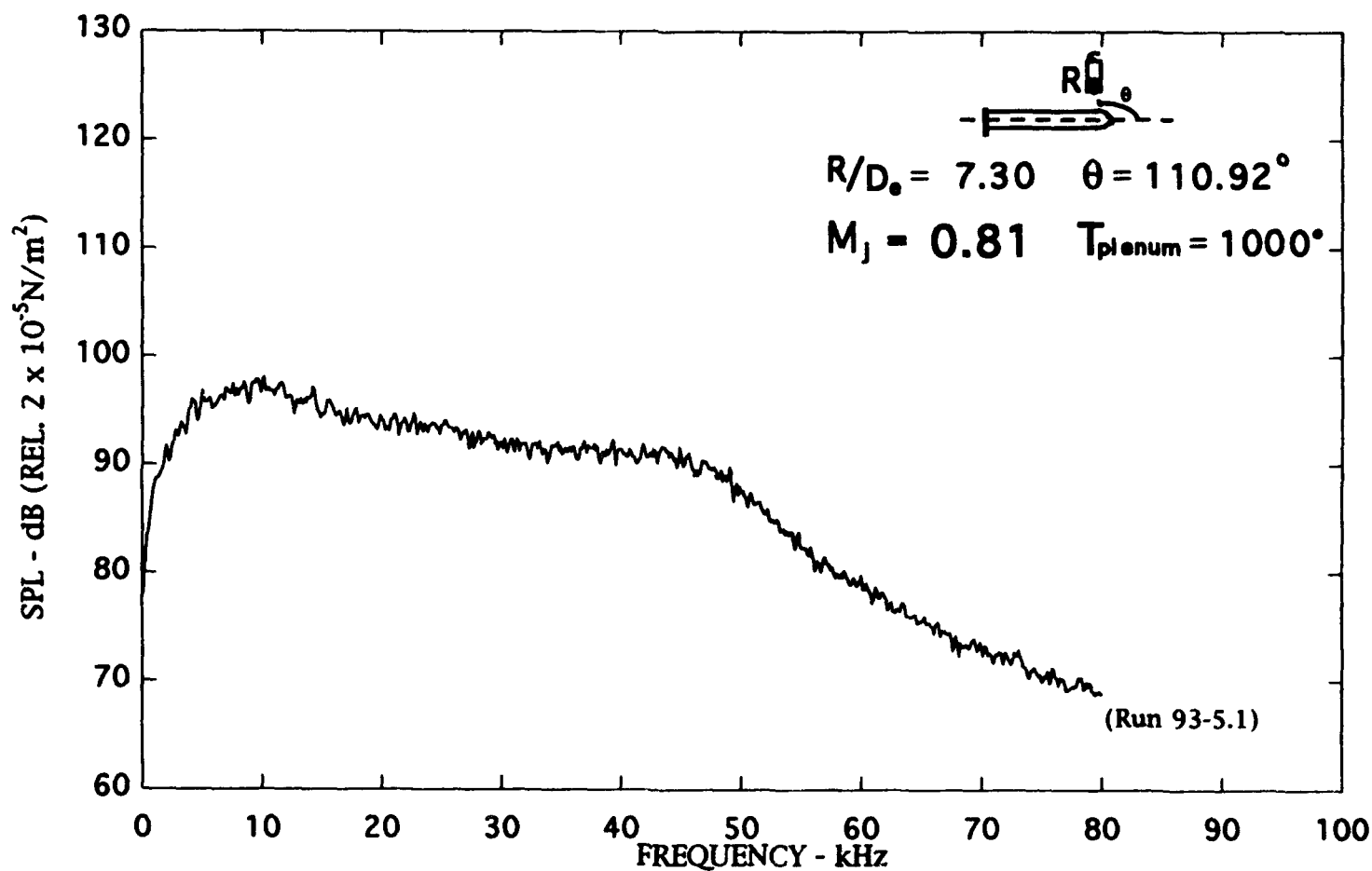Figure B-15. Narrow band (Δf = 128 Hz) noise spectra of the free jet), M_j = 1.34.
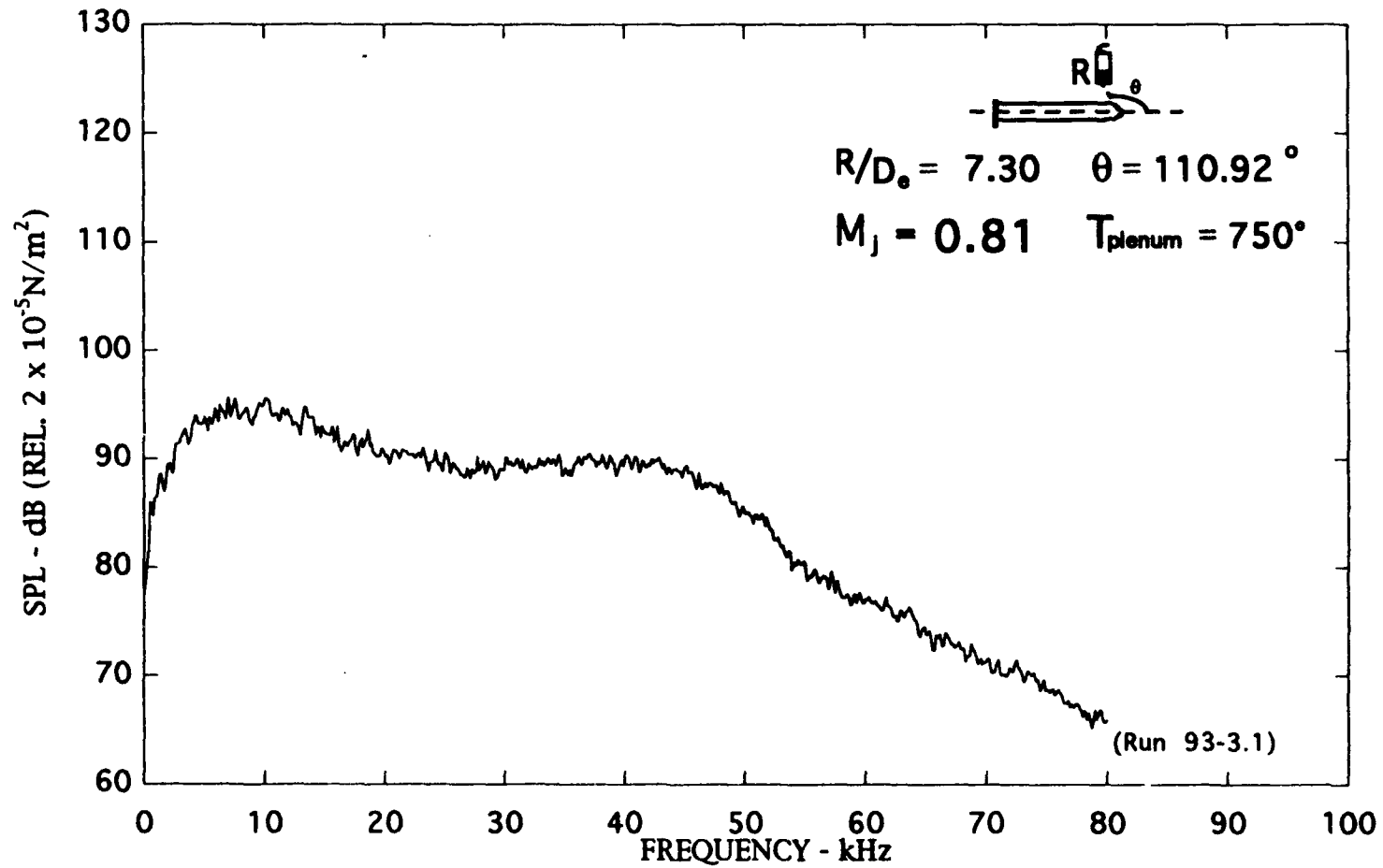
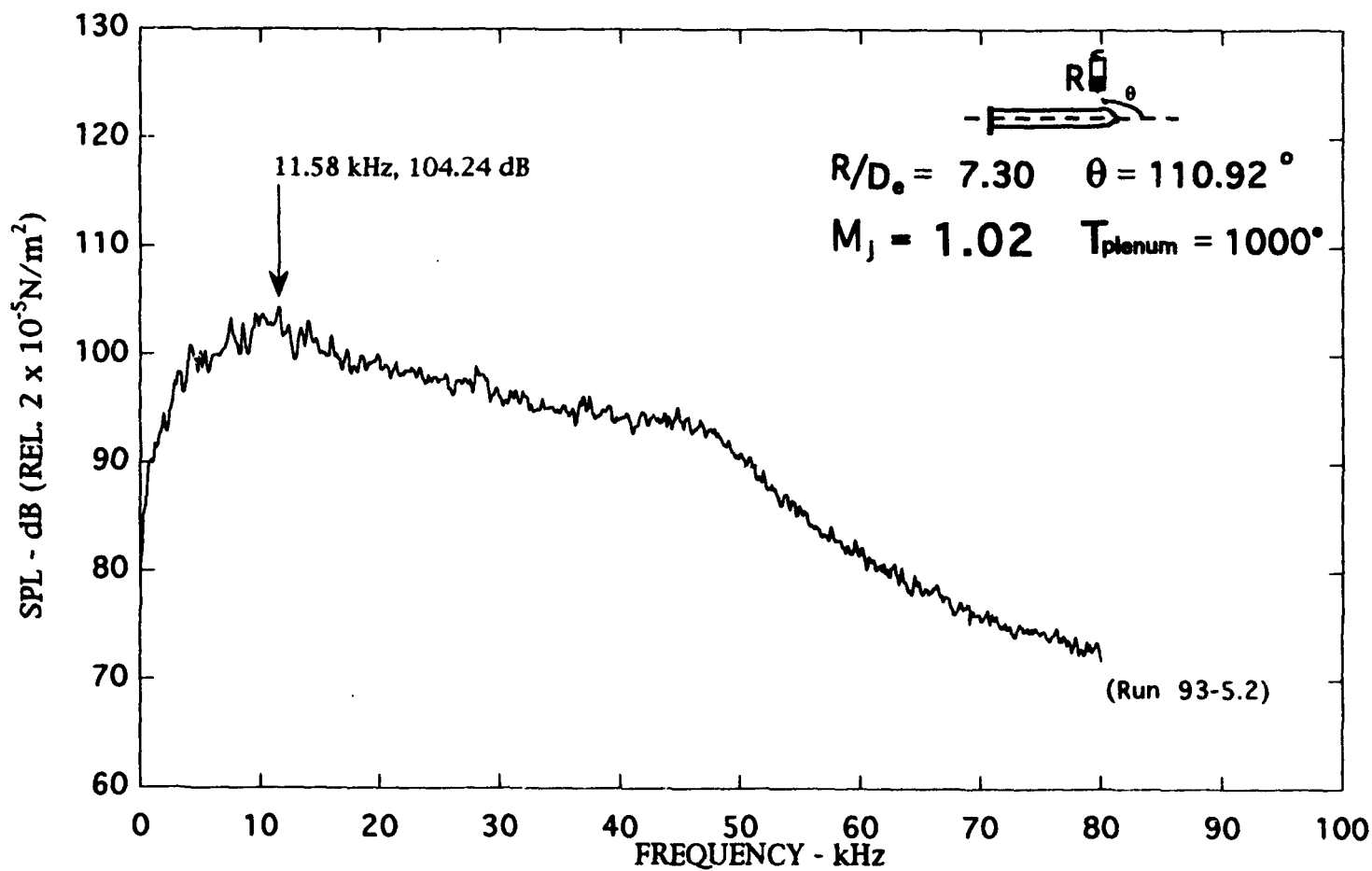Figure B-16. Narrow band (Δf = 128 Hz) noise spectra of the free jet), M_j = 0.81.
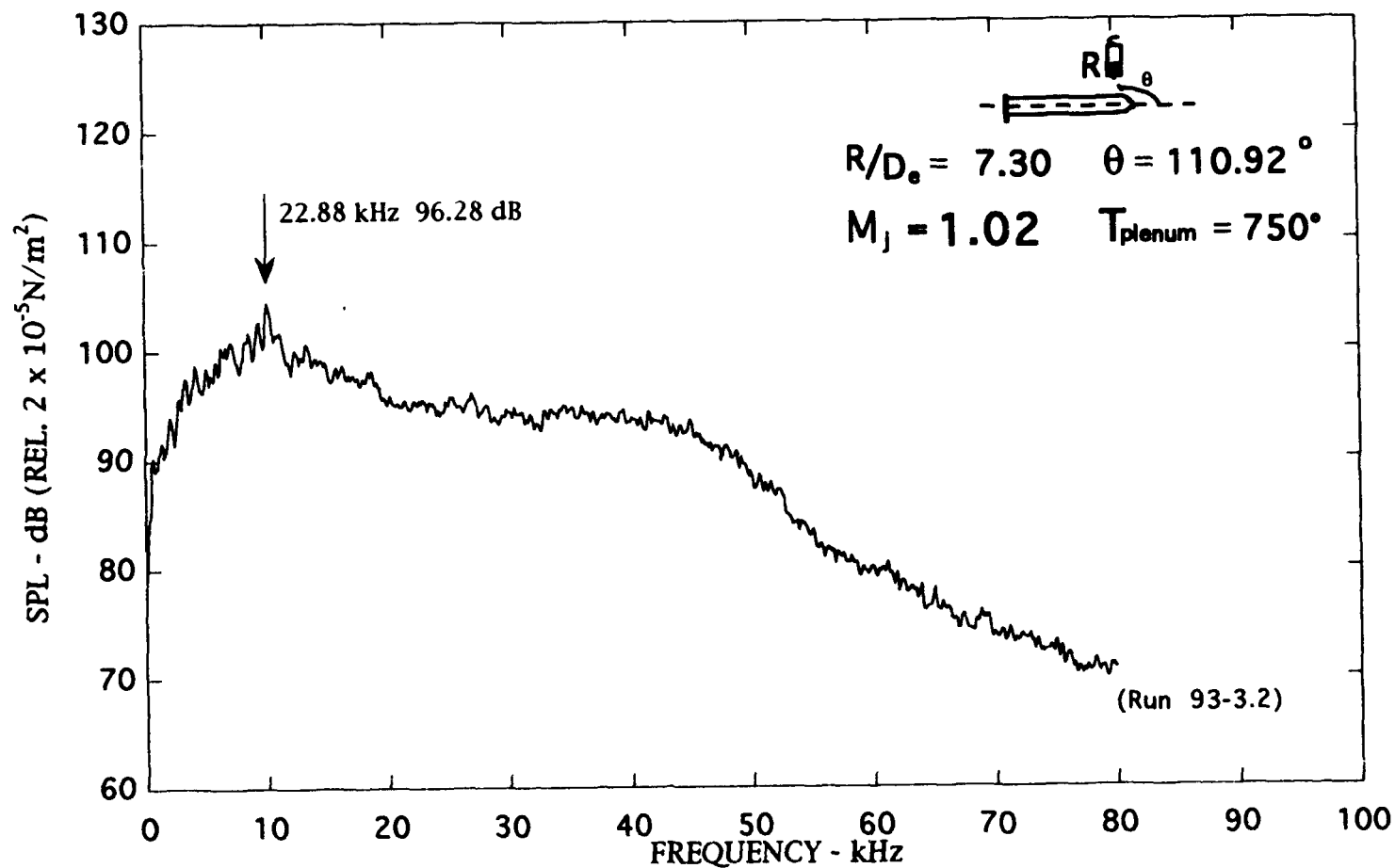
Figure B-17. Narrow band ($\Delta f = 128$ Hz) noise spectra of the free jet), $M_j = 1.02$.
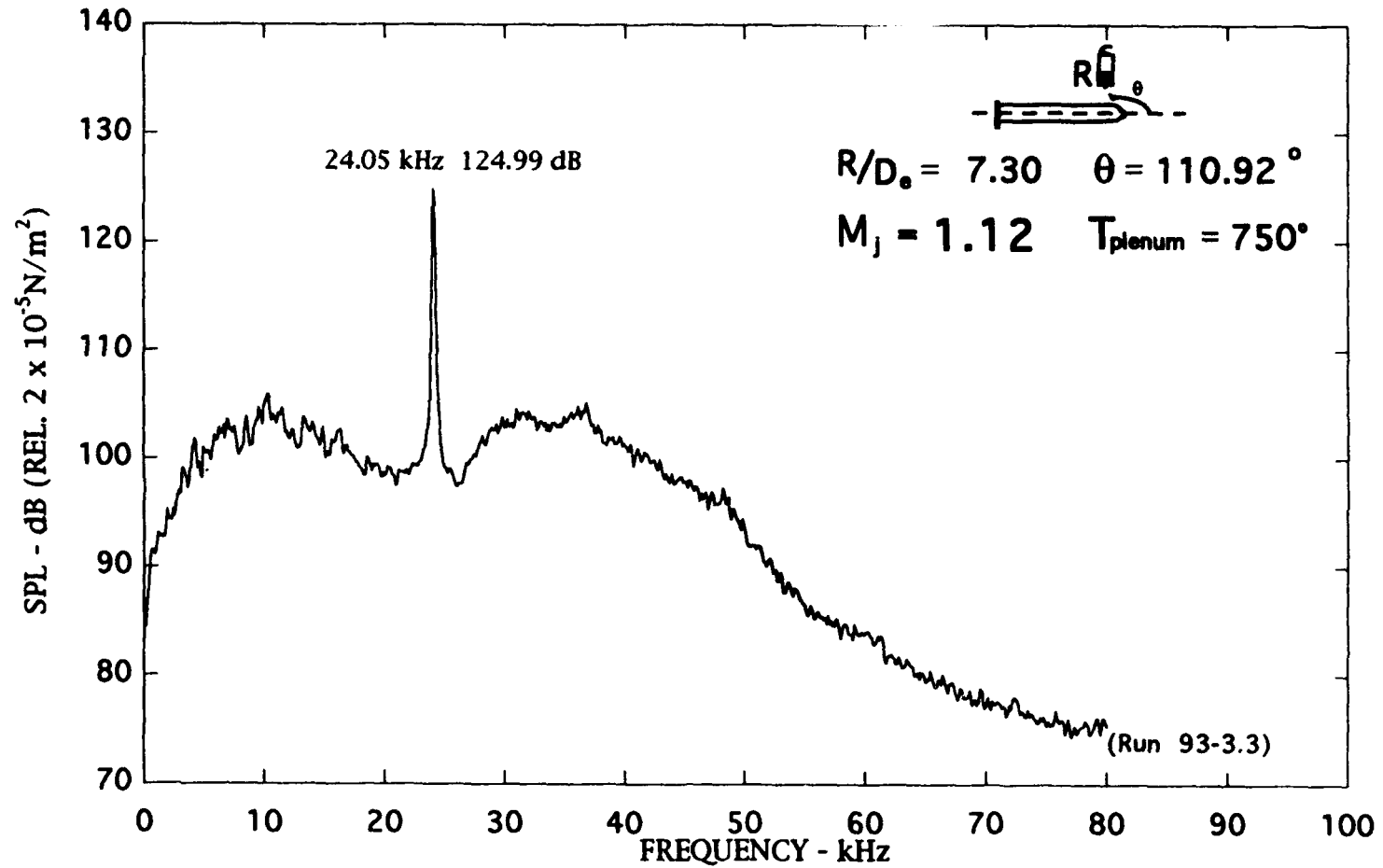
Figure B-18. Narrow band (Δf = 128 Hz) noise spectra of the free jet), M$_j$ = 1.12.
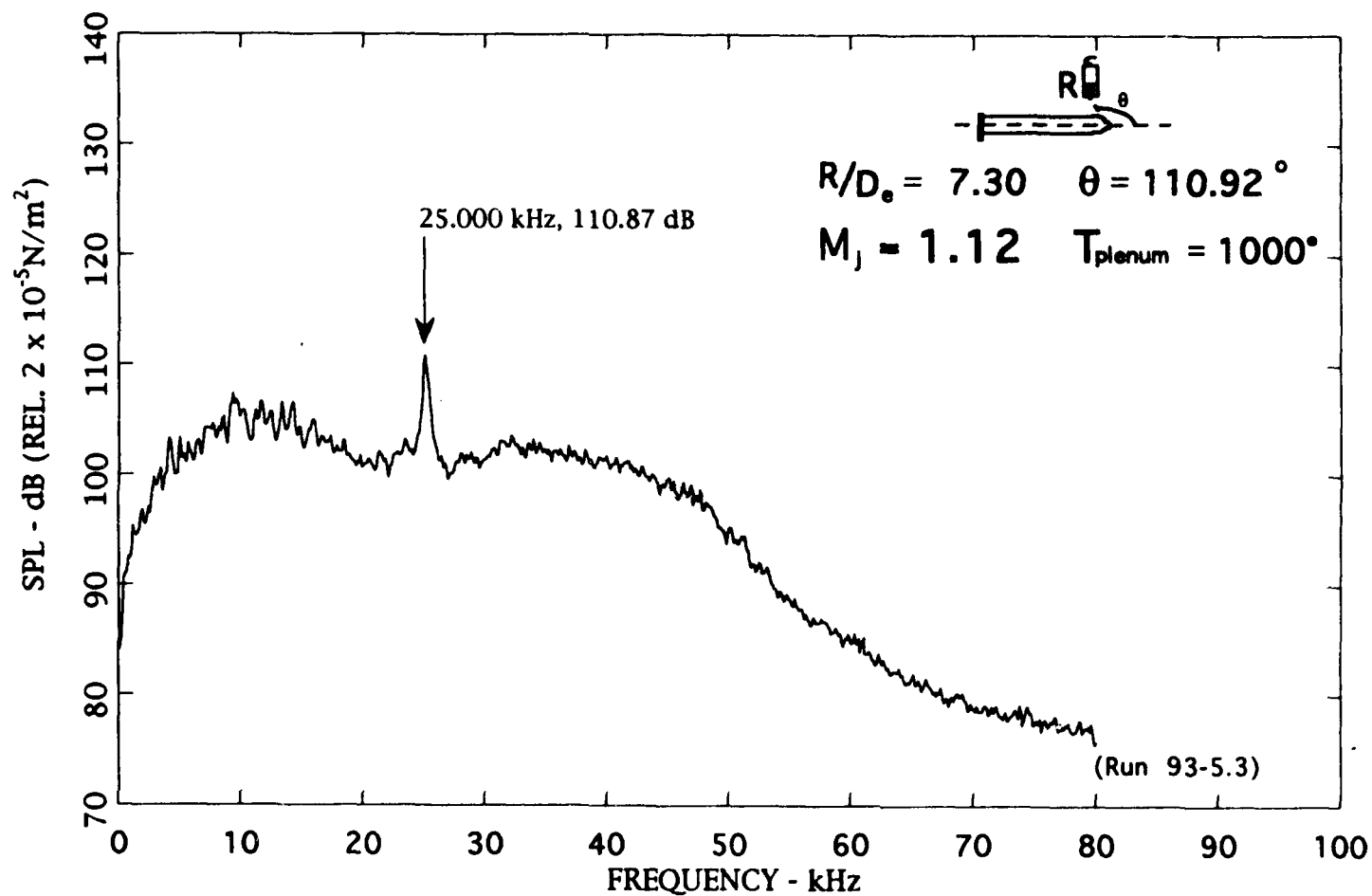
Figure B-19. Narrow band ($\Delta f = 128$ Hz) noise spectra of the free jet), $M_j = 1.23$.
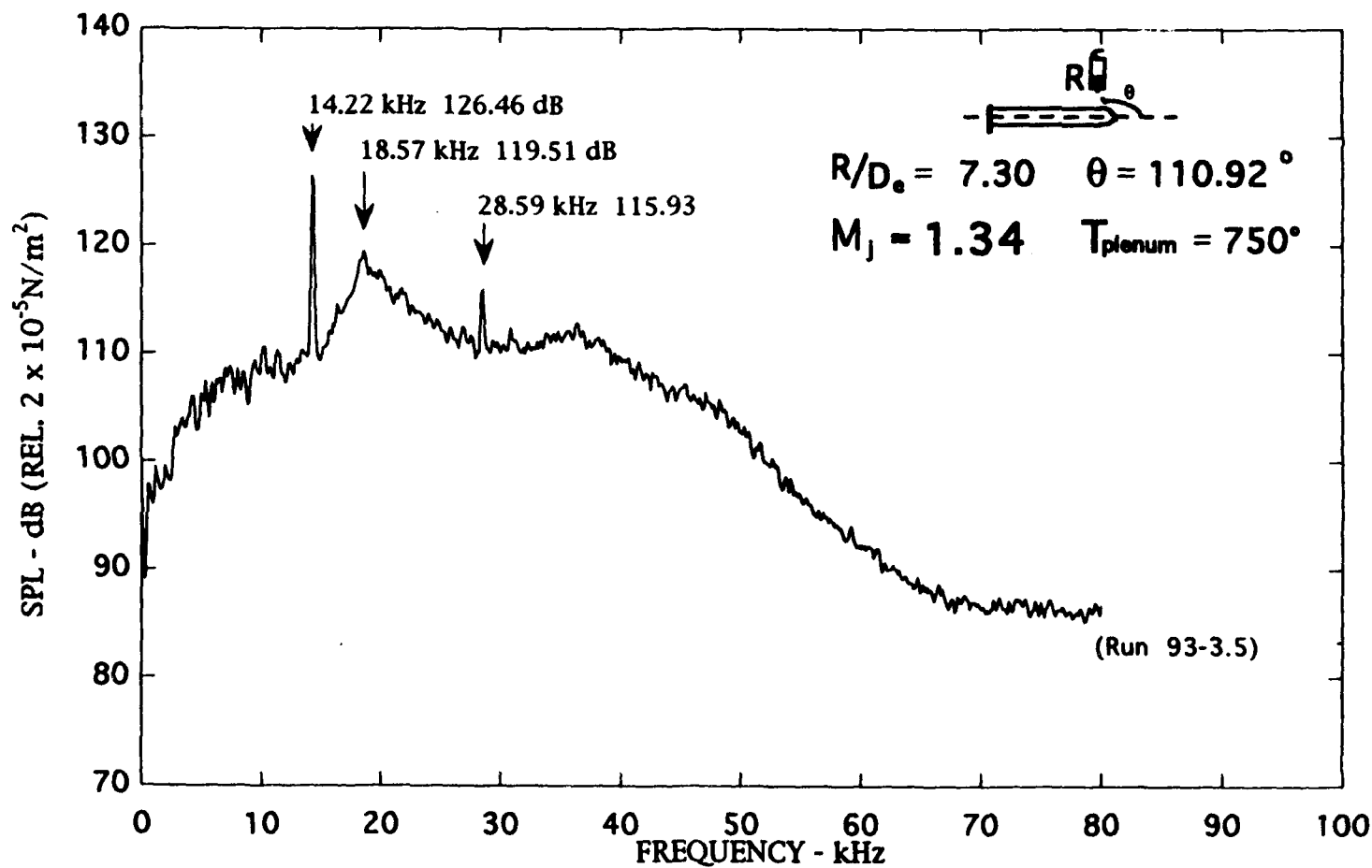
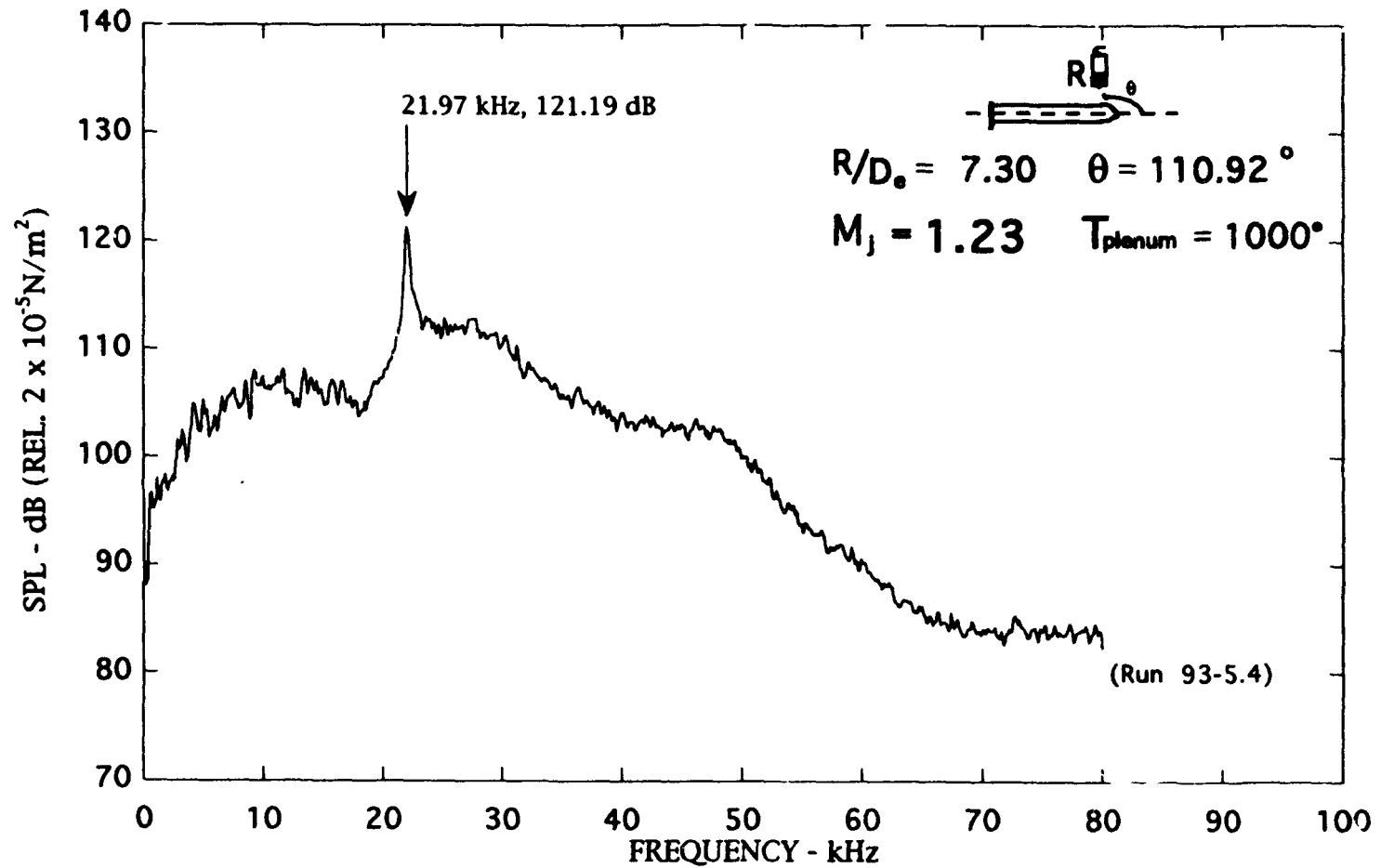Figure B-20. Narrow band ($\Delta f = 128$ Hz) noise spectra of the free jet), $M_j = 1.34$.
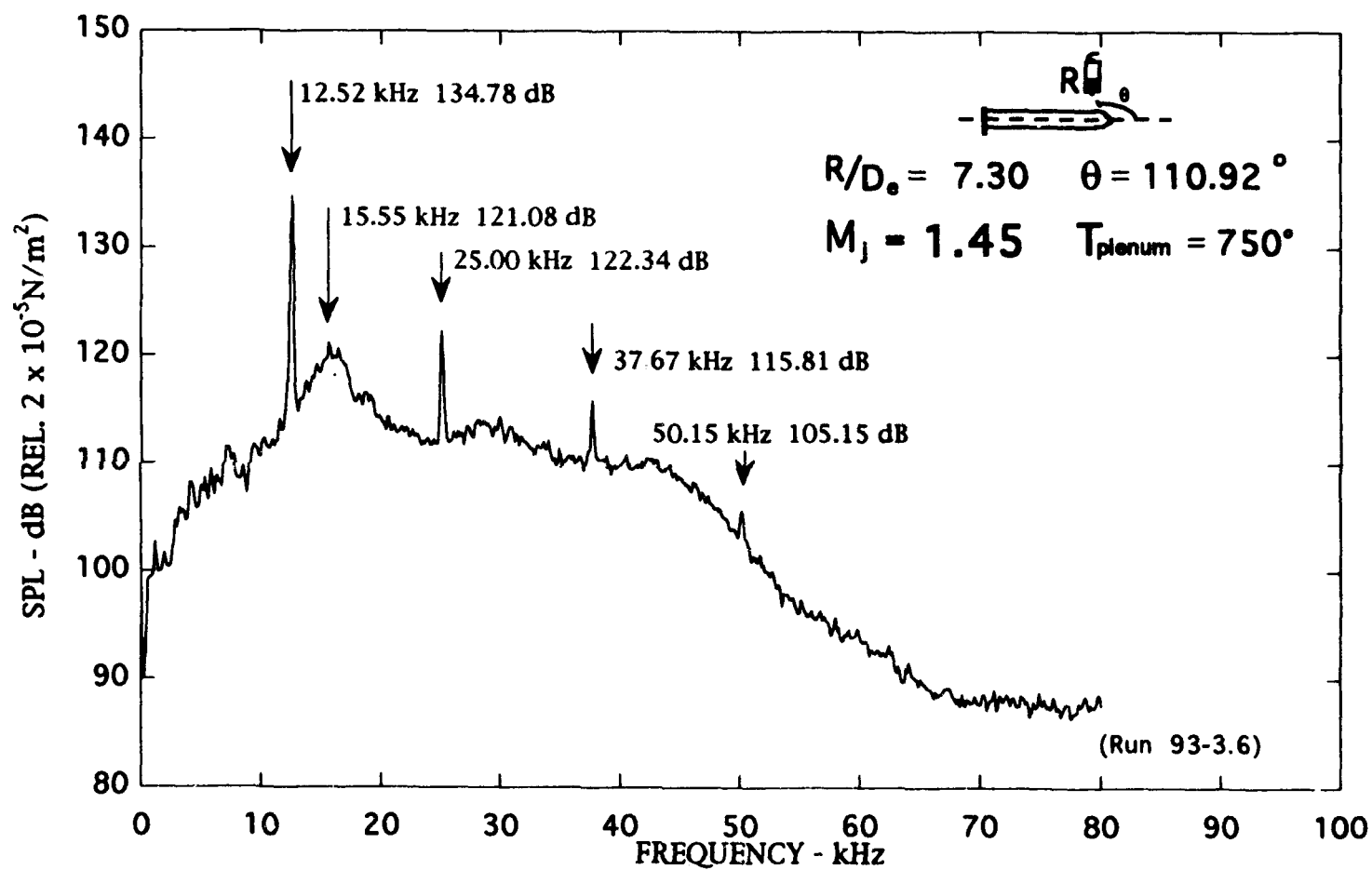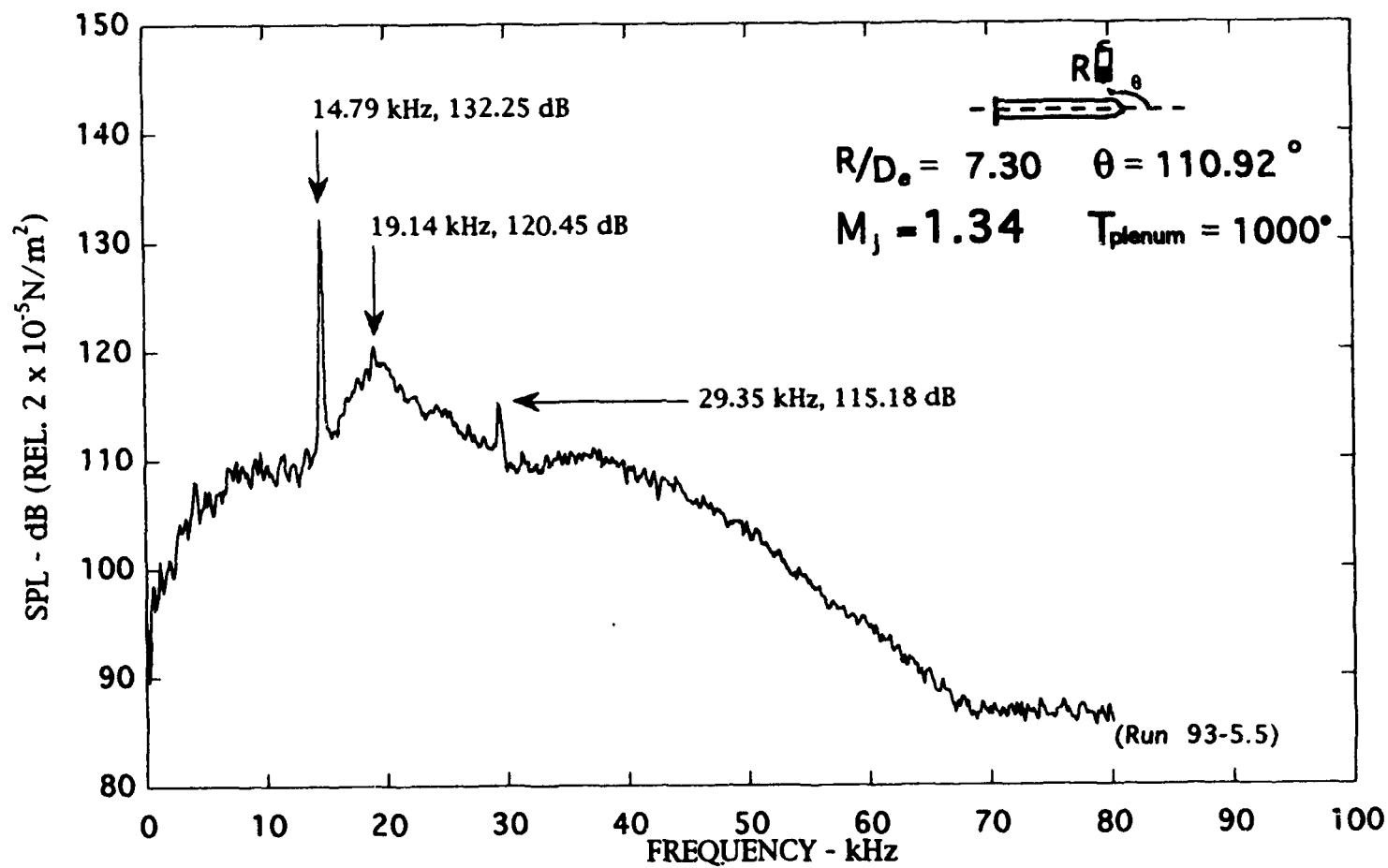
Figure B-21. Narrow band (Δf = 128 Hz) noise spectra of the free jet), M_j = 1.45.
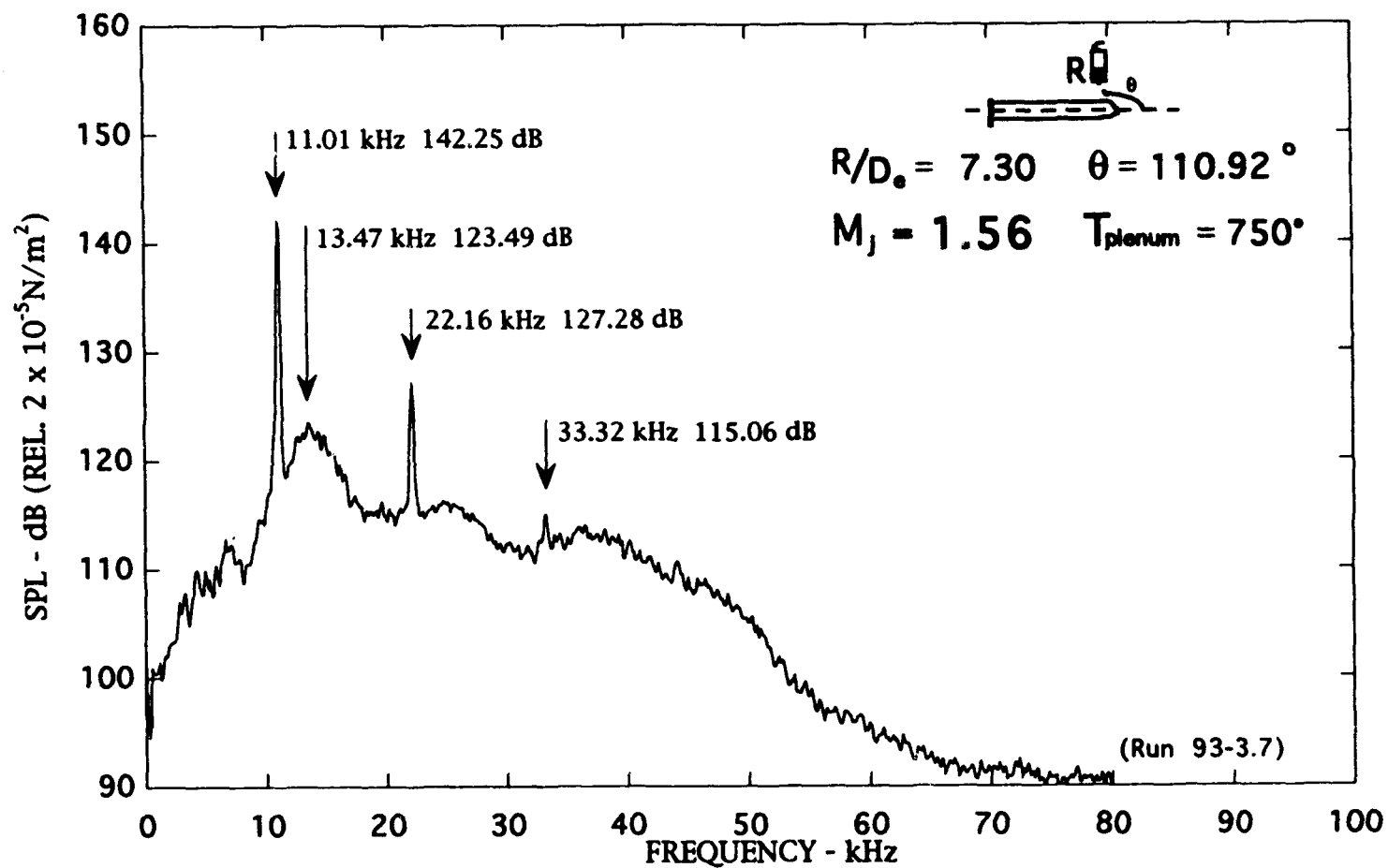
Figure B-22. Narrow band (Δf = 128 Hz) noise spectra of the free jet), M$_j$ = 1.56.

Figure B-23. Narrow band (Δf = 128 Hz) noise spectra of the free jet), M_j = 0.81.

R/D_e = 7.30   θ = 110.92°

M_j = 0.81   T_plenum = 1000°

(Run 93-5.1)

Figure B-24. Narrow band (Δf = 128 Hz) noise spectra of the free jet), M_j = 1.02.

Figure B-25. Narrow band ($\Delta f = 128$ Hz) noise spectra of the free jet), $M_j = 1.12$.

Figure B-26. Narrow band ($\Delta f = 128$ Hz) noise spectra of the free jet), $M_j = 1.23$.

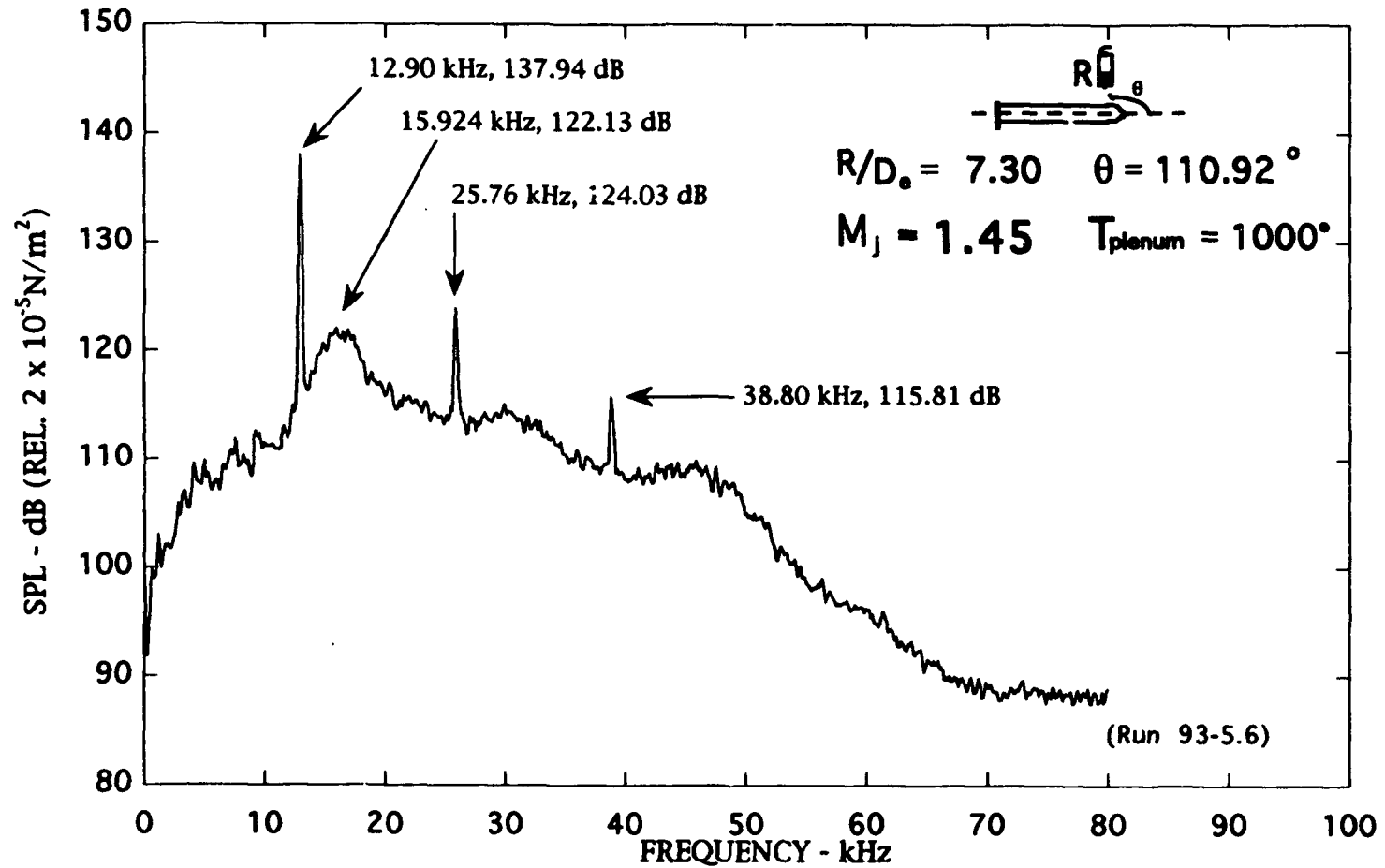Figure B-27. Narrow band (Δf = 128 Hz) noise spectra of the free jet), M_j = 1.34.

Figure B-28. Narrow band (Δf = 128 Hz) noise spectra of the free jet), M_j = 1.45.

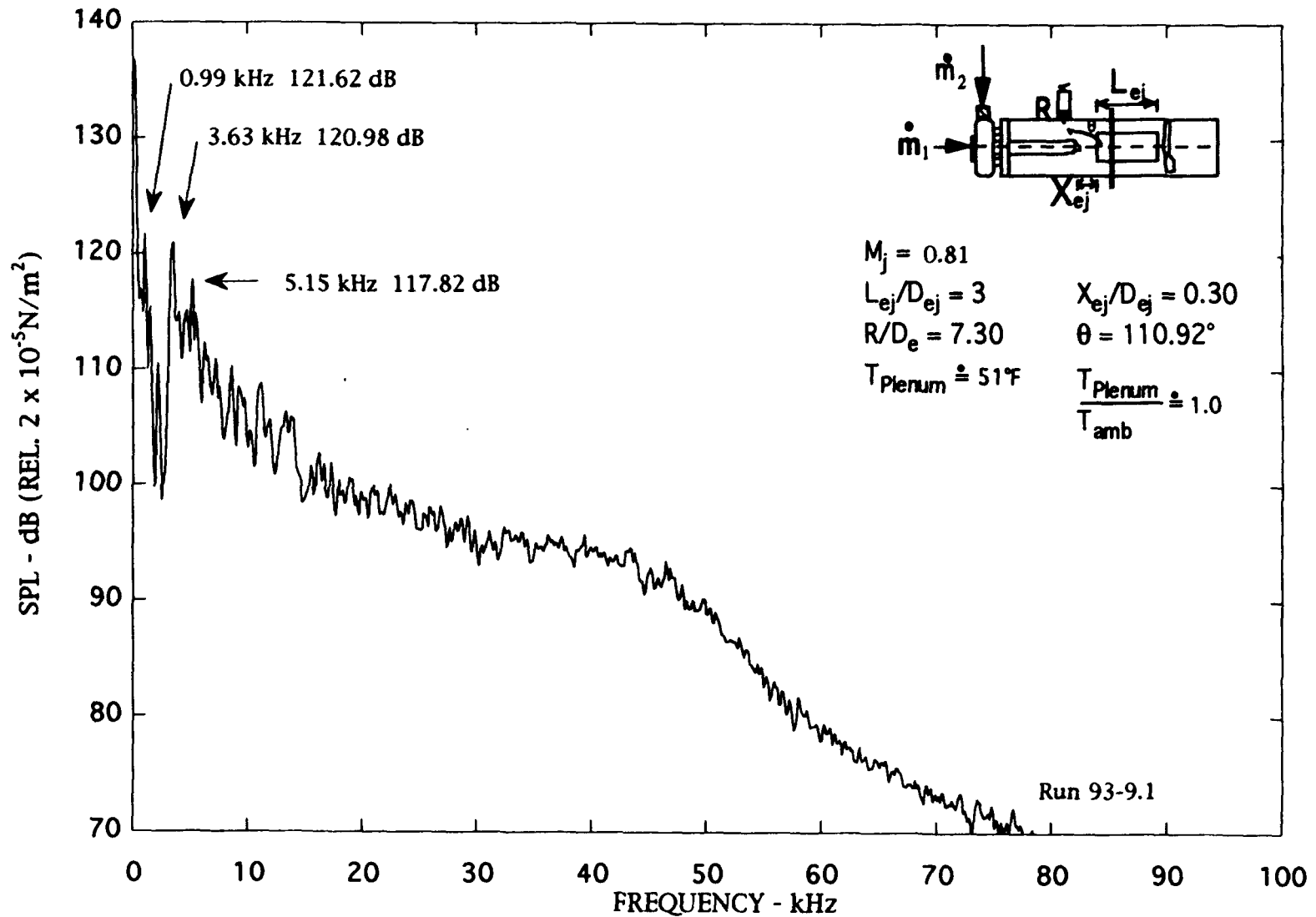# APPENDIX C

Individual Spectra with the Venturi in Place

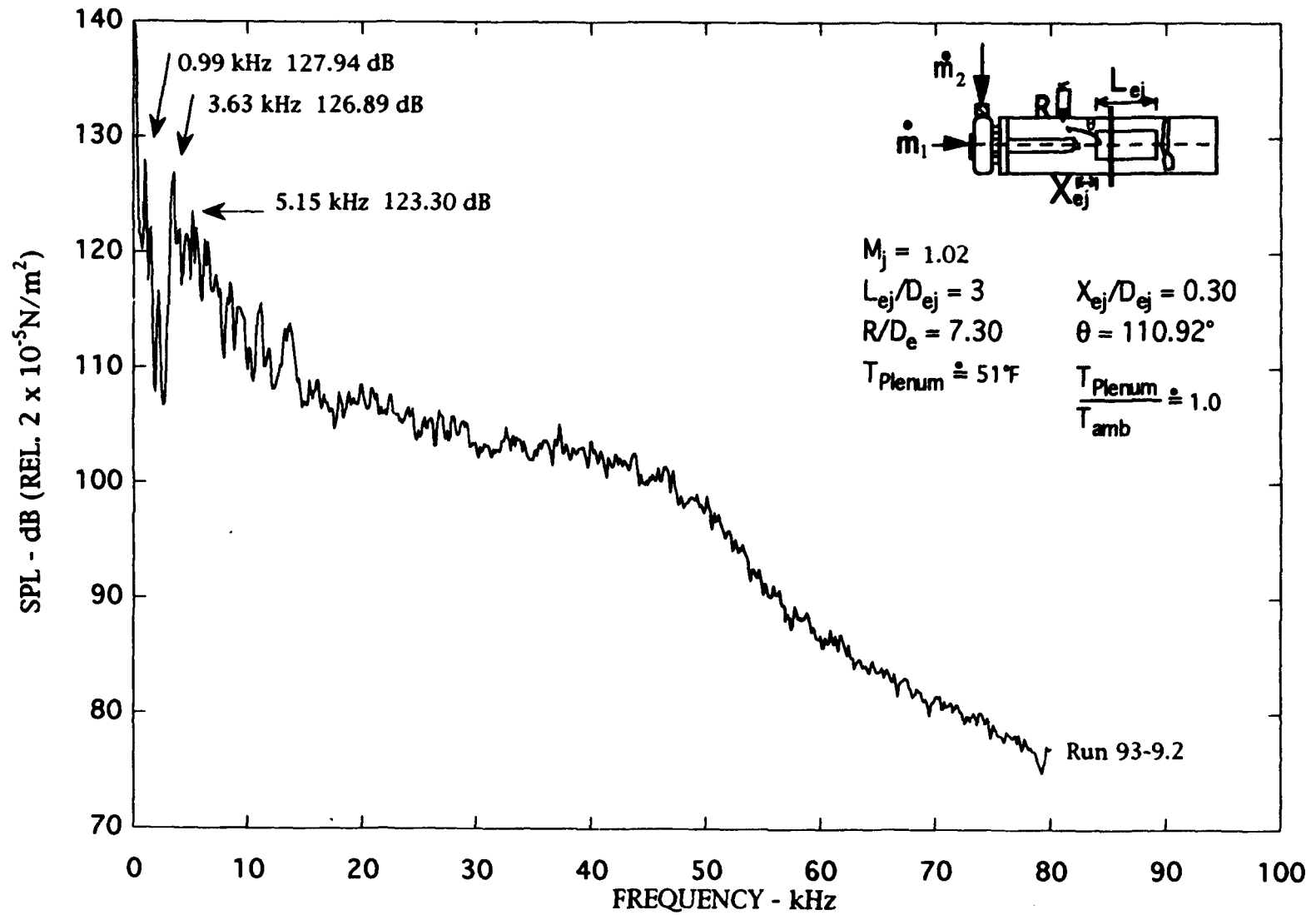Figure C-1. Narrow band ($\Delta f = 128$ Hz) noise spectra of ducted jet), $M_j = 0.81$.

Figure C-2. Narrow band ($\Delta f = 128$ Hz) noise spectra of ducted jet), $M_j = 1.02$.
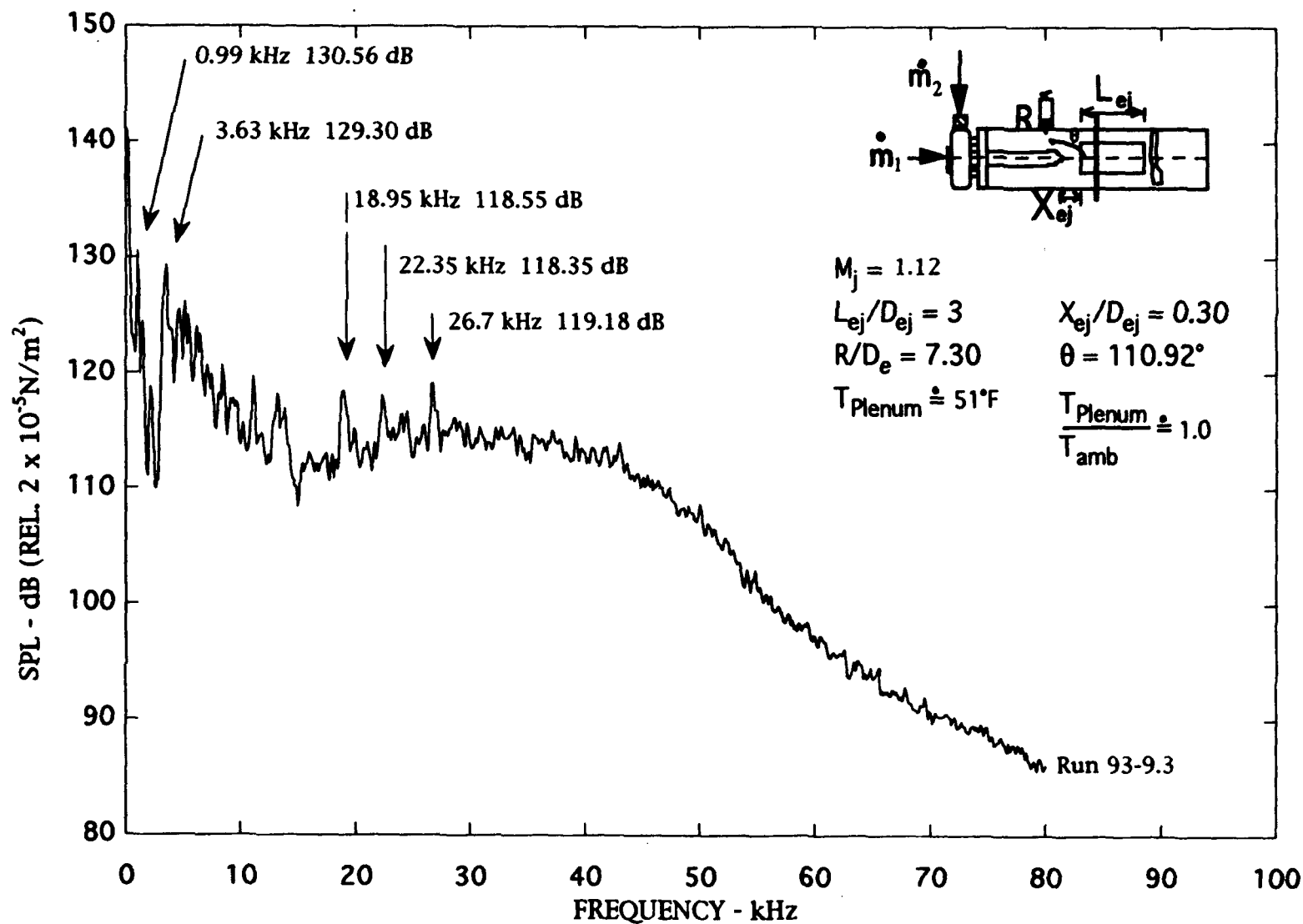
Figure C-3. Narrow band ($\Delta f = 128$ Hz) noise spectra of ducted jet), $M_j = 1.12$.
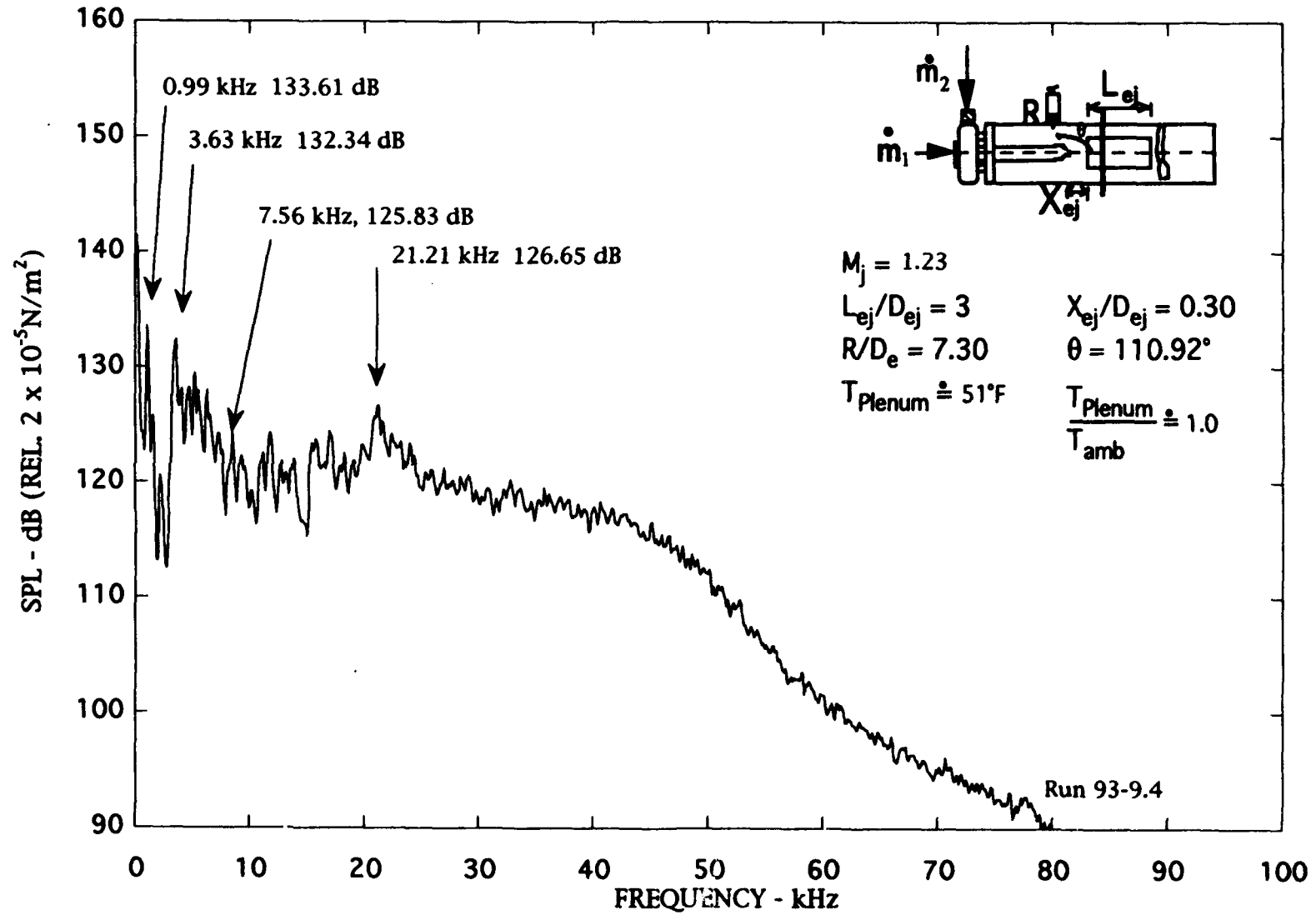
Figure C-4. Narrow band ($\Delta f = 128$ Hz) noise spectra of ducted jet), $M_j = 1.23$.

Figure C-5. Narrow band ($\Delta f = 128$ Hz) noise spectra of ducted jet), $M_j = 1.34$.

Figure C-6. Narrow band ($\Delta f = 128$ Hz) noise spectra of ducted jet), $M_j = 1.45$.

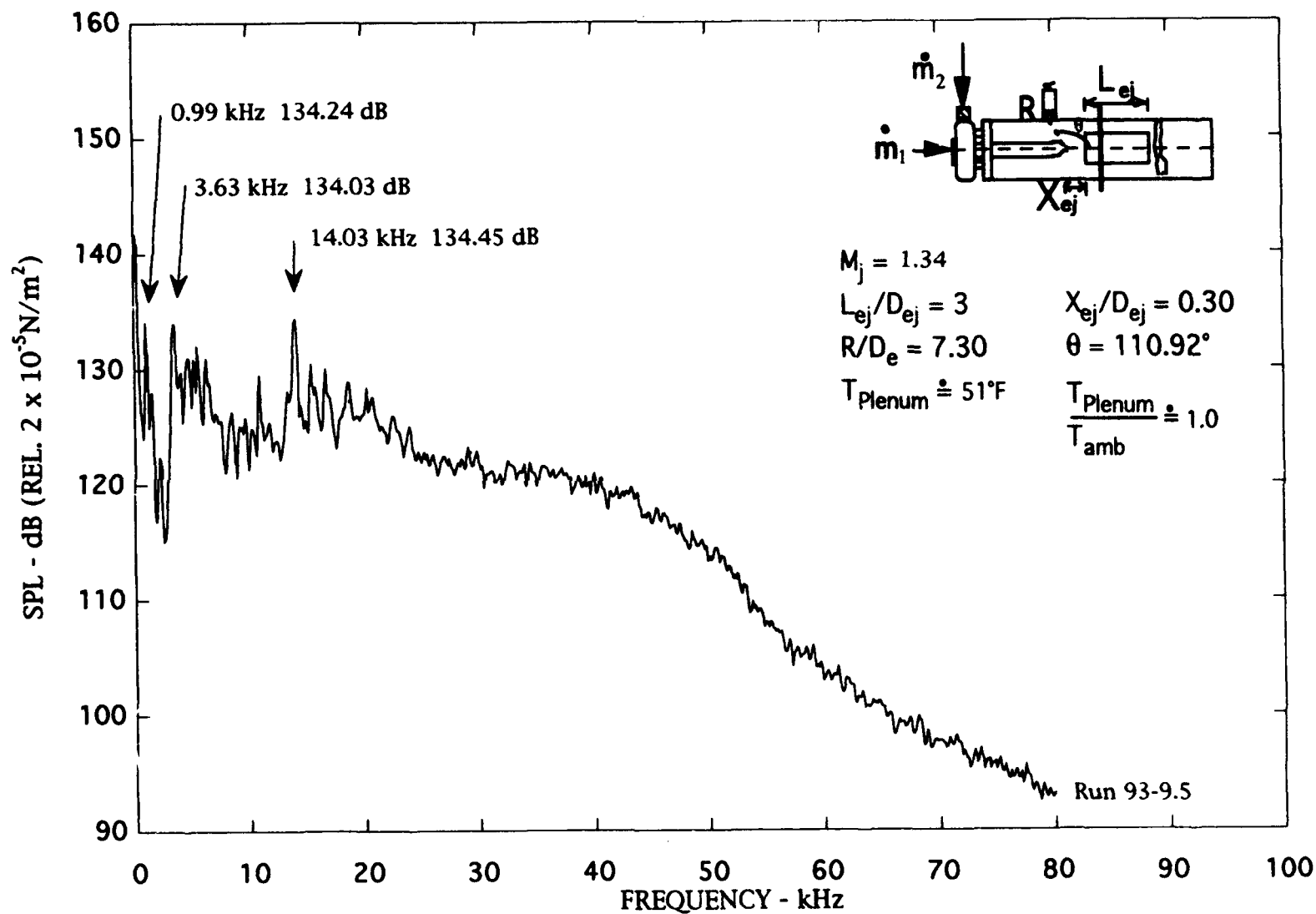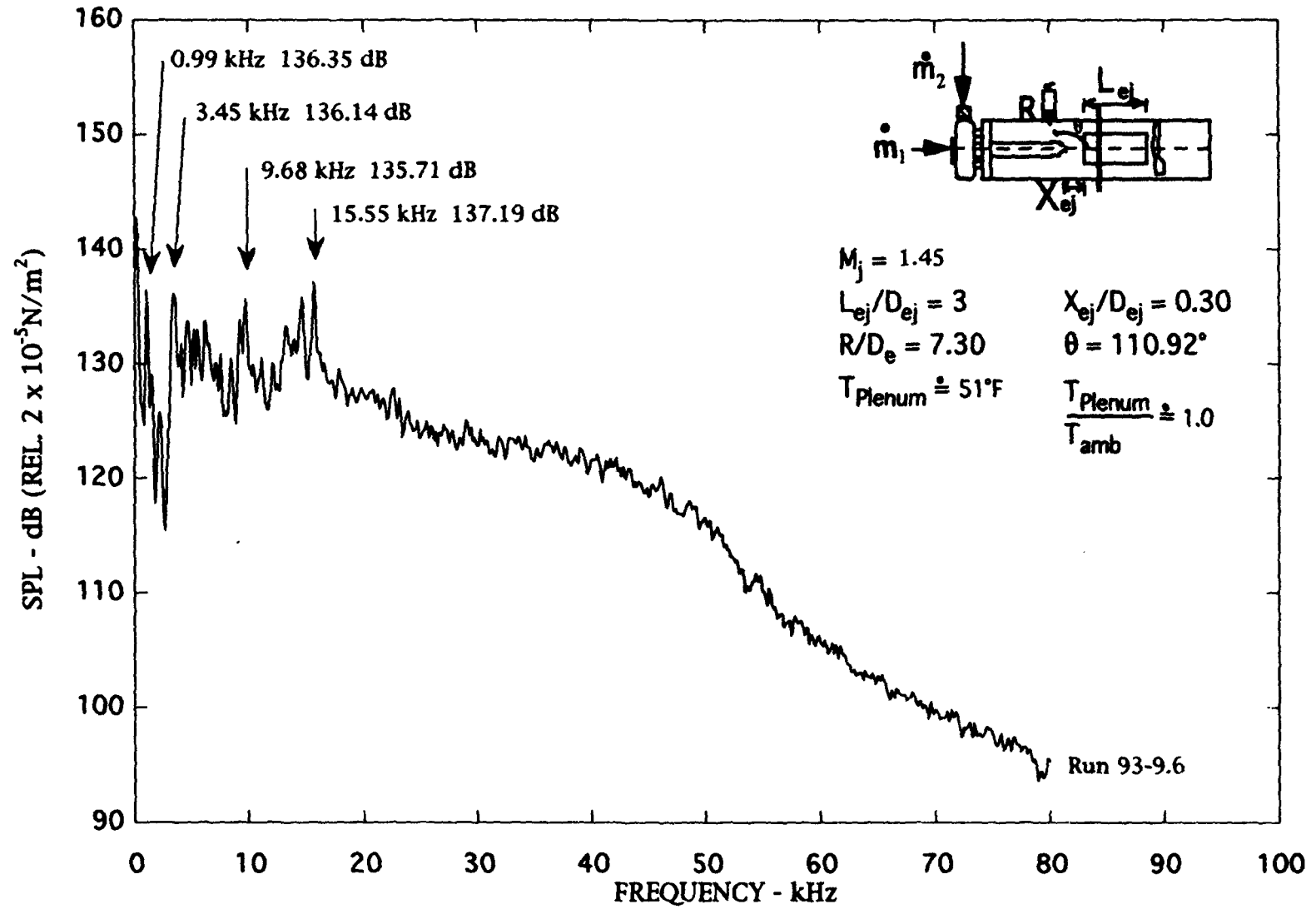Figure C-7. Narrow band ($\Delta f = 128$ Hz) noise spectra of ducted jet), $M_j = 1.56$.

Figure C-8. Narrow band (Δf = 128 Hz) noise spectra of ducted jet), $M_j \approx 1.68$.
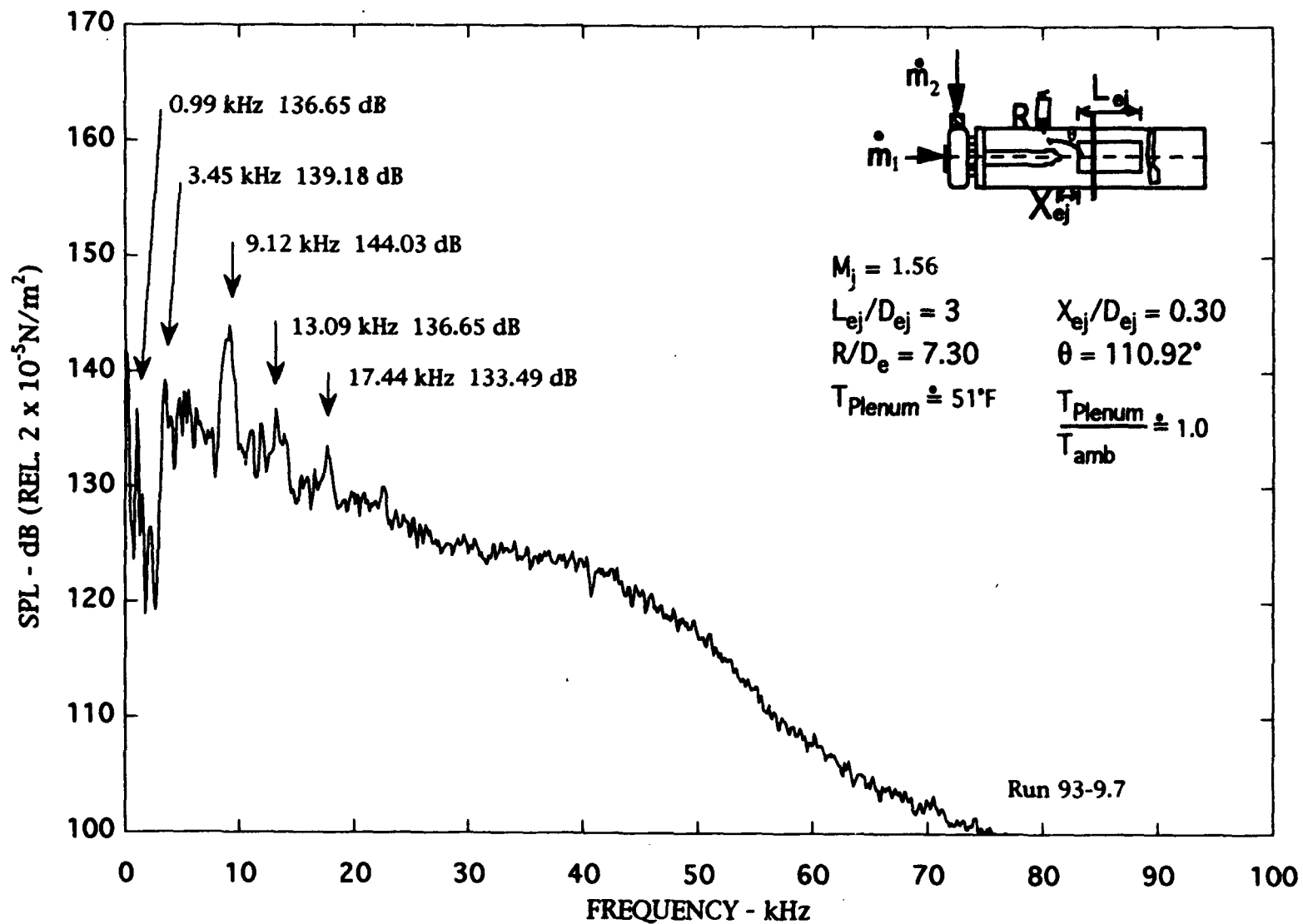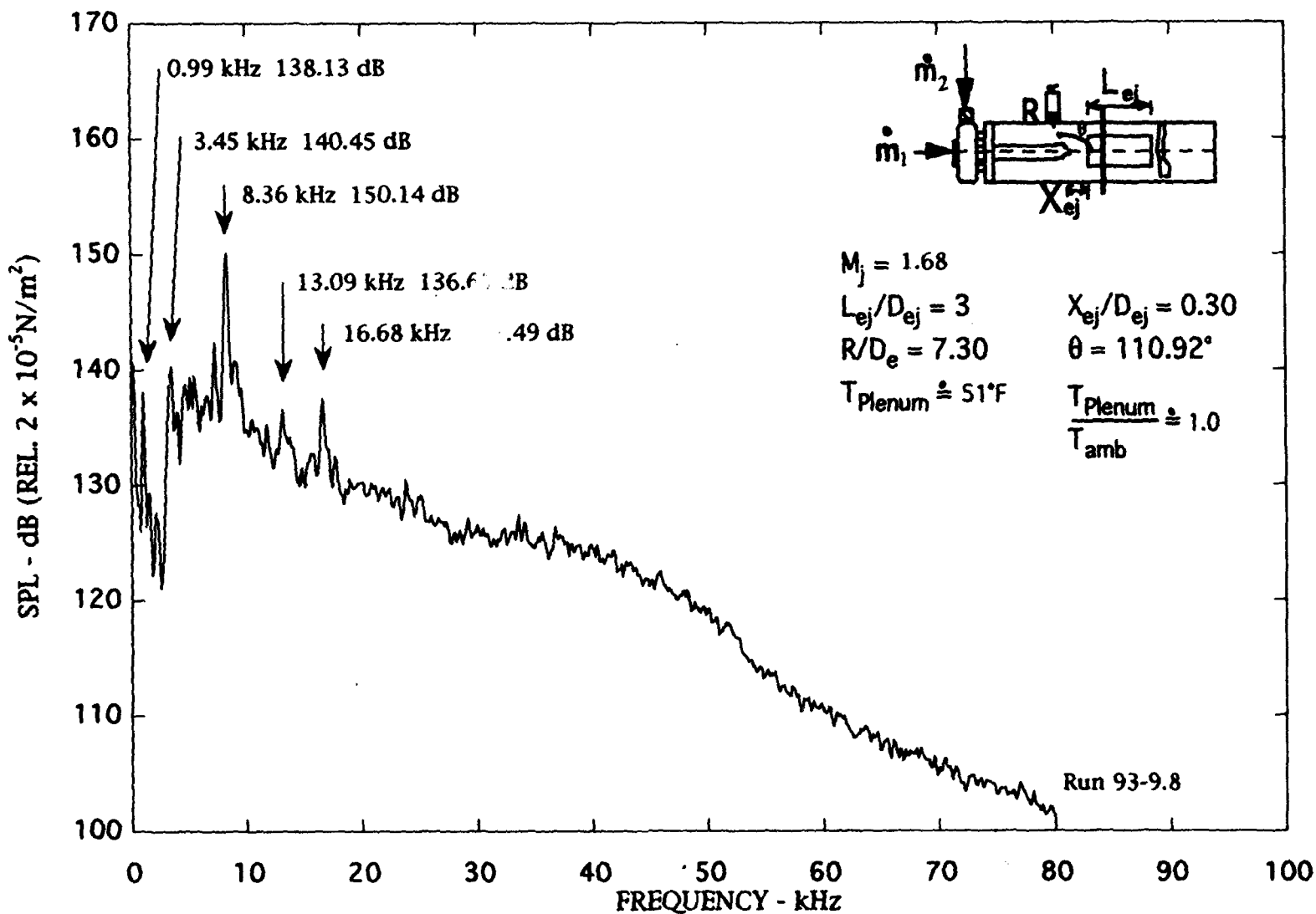
Figure C-9. Narrow band ($\Delta f = 128$ Hz) noise spectra of ducted jet), $M_j = 1.74$.

Figure C-10. Narrow band ($\Delta f = 123$ Hz) noise spectra of ducted jet), $M_j = 1.79$.

Figure C-11. Narrow band ($\Delta f = 128$ Hz) noise spectra of ducted jet), $M_j = 0.81$.

Figure C-12. Narrow band (Δf = 128 Hz) noise spectra of ducted jet), M$_j$ = 1.02.

Figure C-13. Narrow band ($\Delta f = 128$ Hz) noise spectra of ducted jet), $M_j = 1.12$.

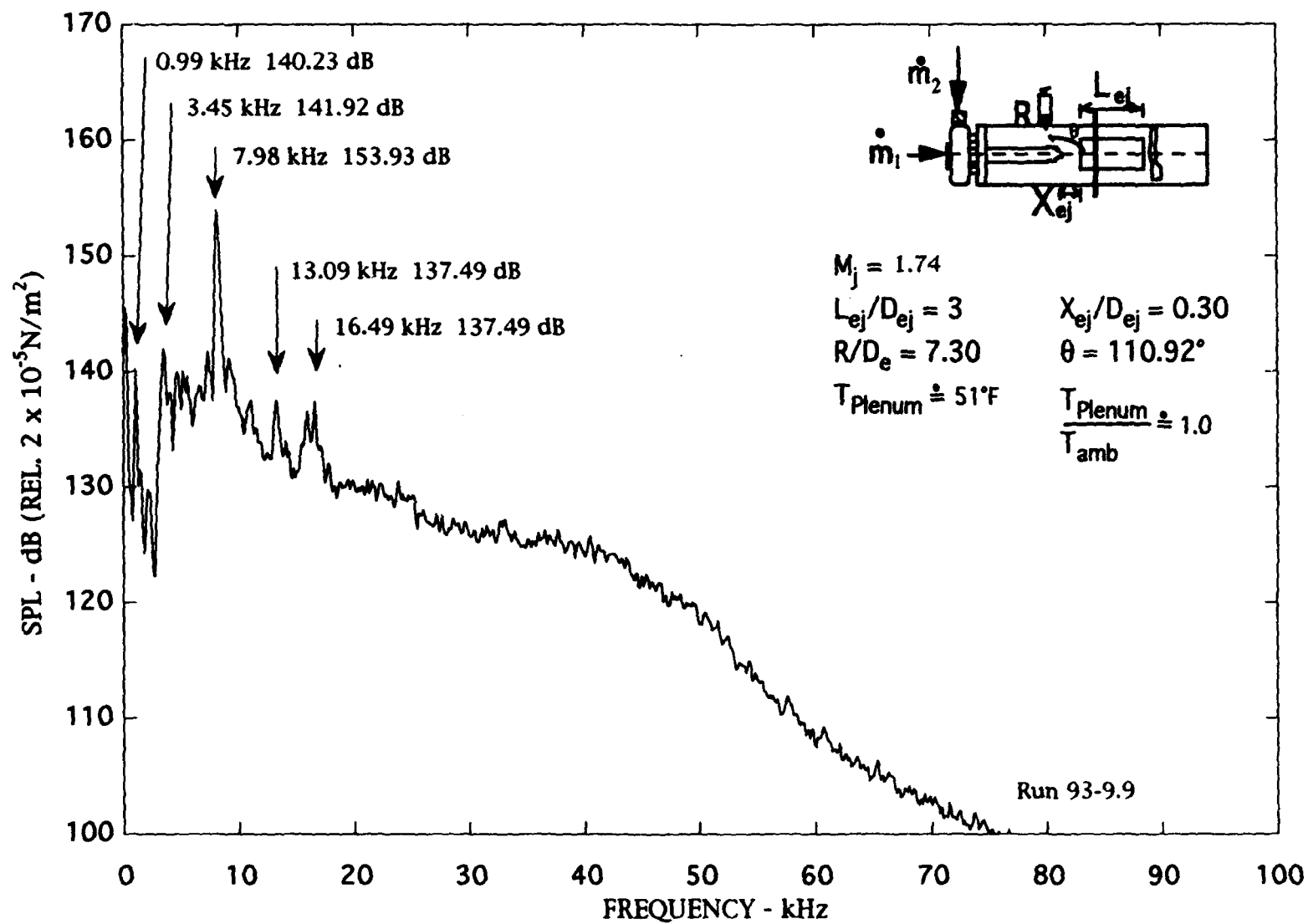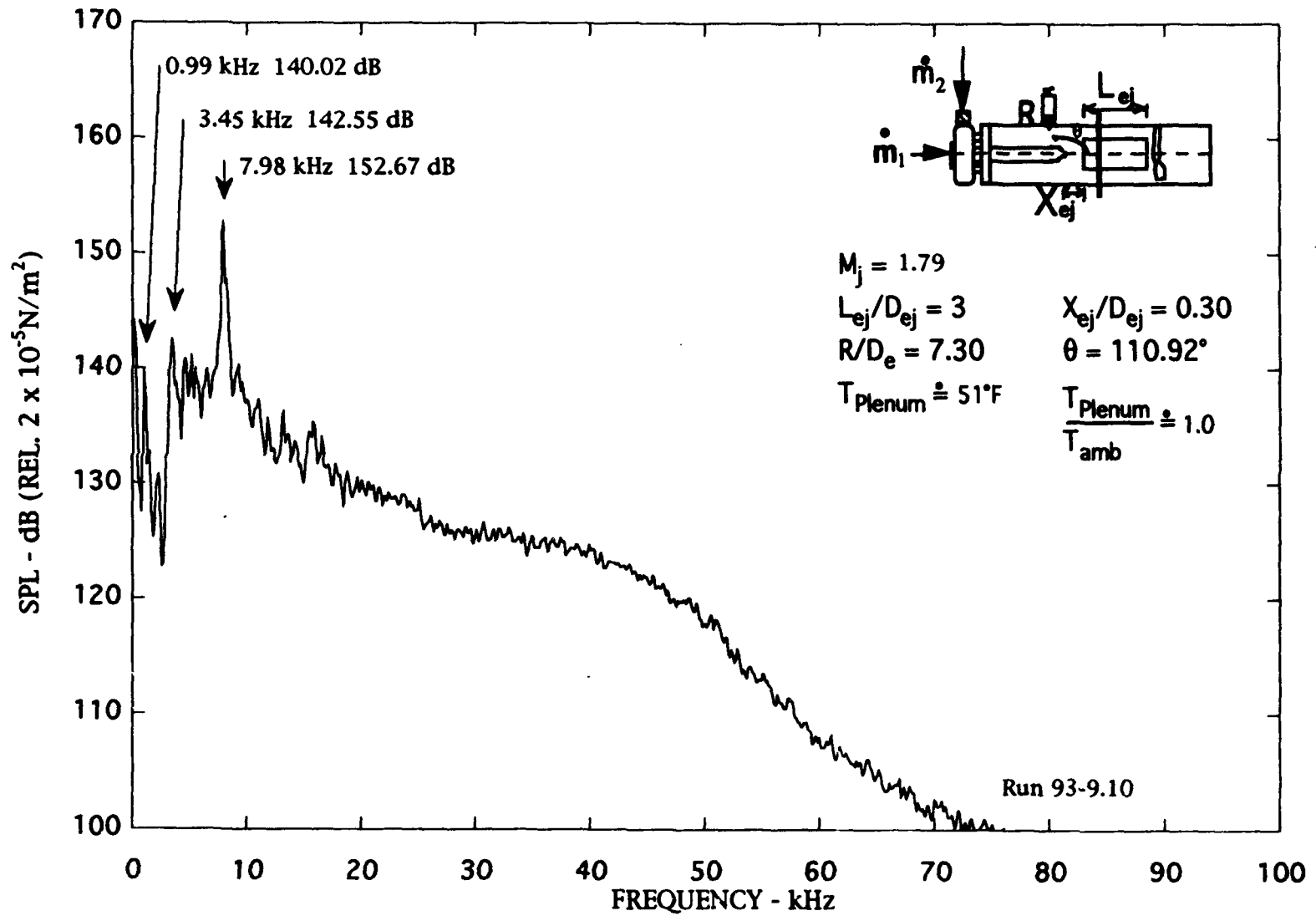Figure C-14. Narrow band ($\Delta f = 128$ Hz) noise spectra of ducted jet), $M_j = 1.23$.

Figure C-15. Narrow band ($\Delta f = 128$ Hz) noise spectra of ducted jet), $M_j = 1.34$.

The figure shows:
- 1.37 kHz 134.24
- 6.09 kHz 131.29 dB
- 7.94 kHz, 129.41 dB
- 19.71 kHz 130.02 dB
- 26.32 kHz 129.81 dB

$M_j = 1.34$

$L_{ej}/D_{ej} = 3$ $X_{ej}/D_{ej} = 0.30$

$R/D_e = 7.30$ $\theta = 110.92°$

$T_{Plenum} \doteq 750°F$ $\dfrac{T_{Plenum}}{T_{amb}} \doteq 2.37$

Run 93-7.5

X-axis: FREQUENCY - kHz

Y-axis: SPL - dB (REL. $2 \times 10^{-5} N/m^2$)

Figure C-16. Narrow band (Δf = 128 Hz) noise spectra of ducted jet), M_j = 1.45.

Figure C-17. Narrow band ($\Delta f = 128$ Hz) noise spectra of ducted jet), $M_j = 1.56$.

Figure C-18. Narrow band ($\Delta f = 128$ Hz) noise spectra of ducted jet), $M_j = 1.68$.

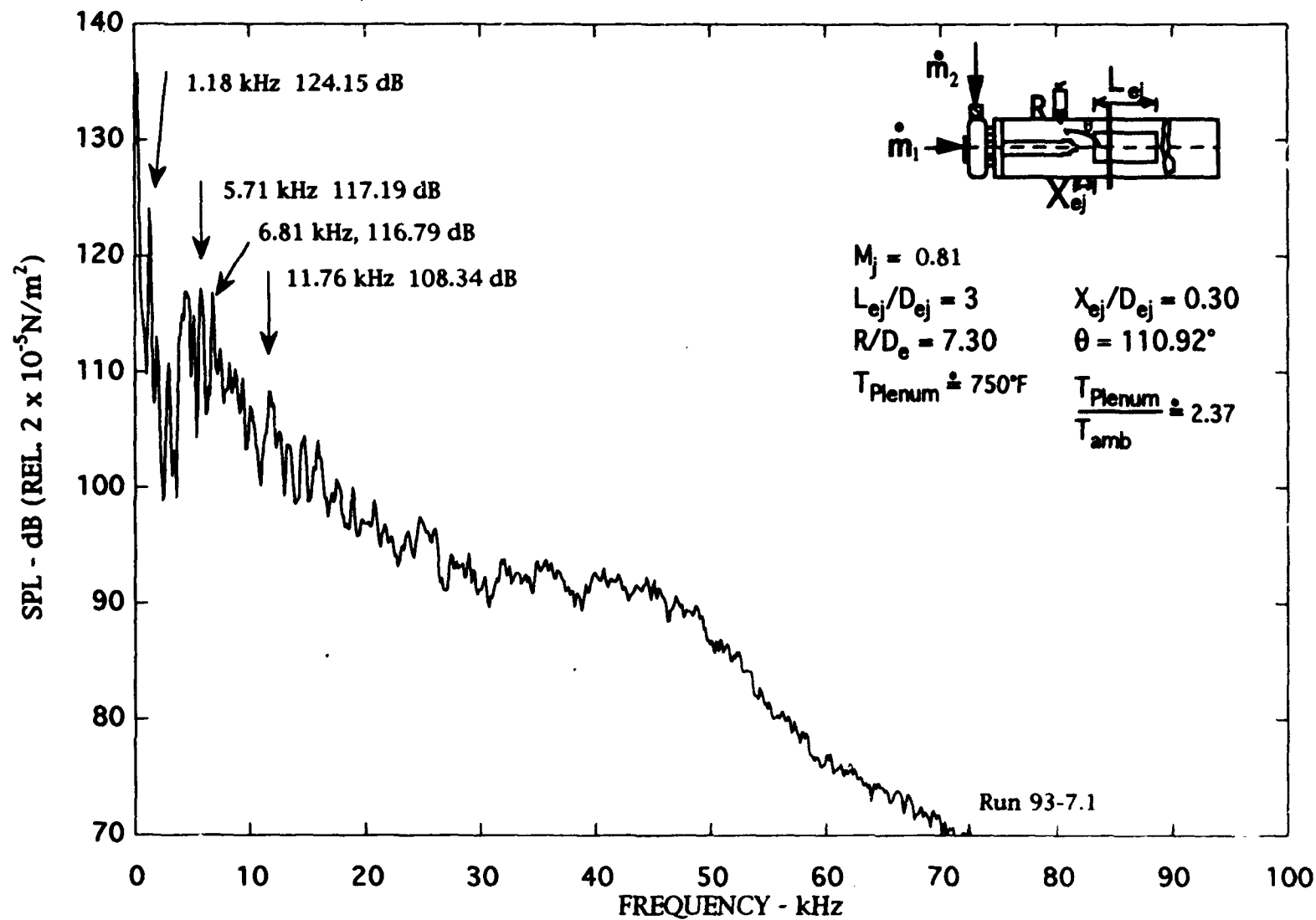Figure C-19. Narrow band ($\Delta f = 128$ Hz) noise spectra of ducted jet), $M_j = 0.81$.

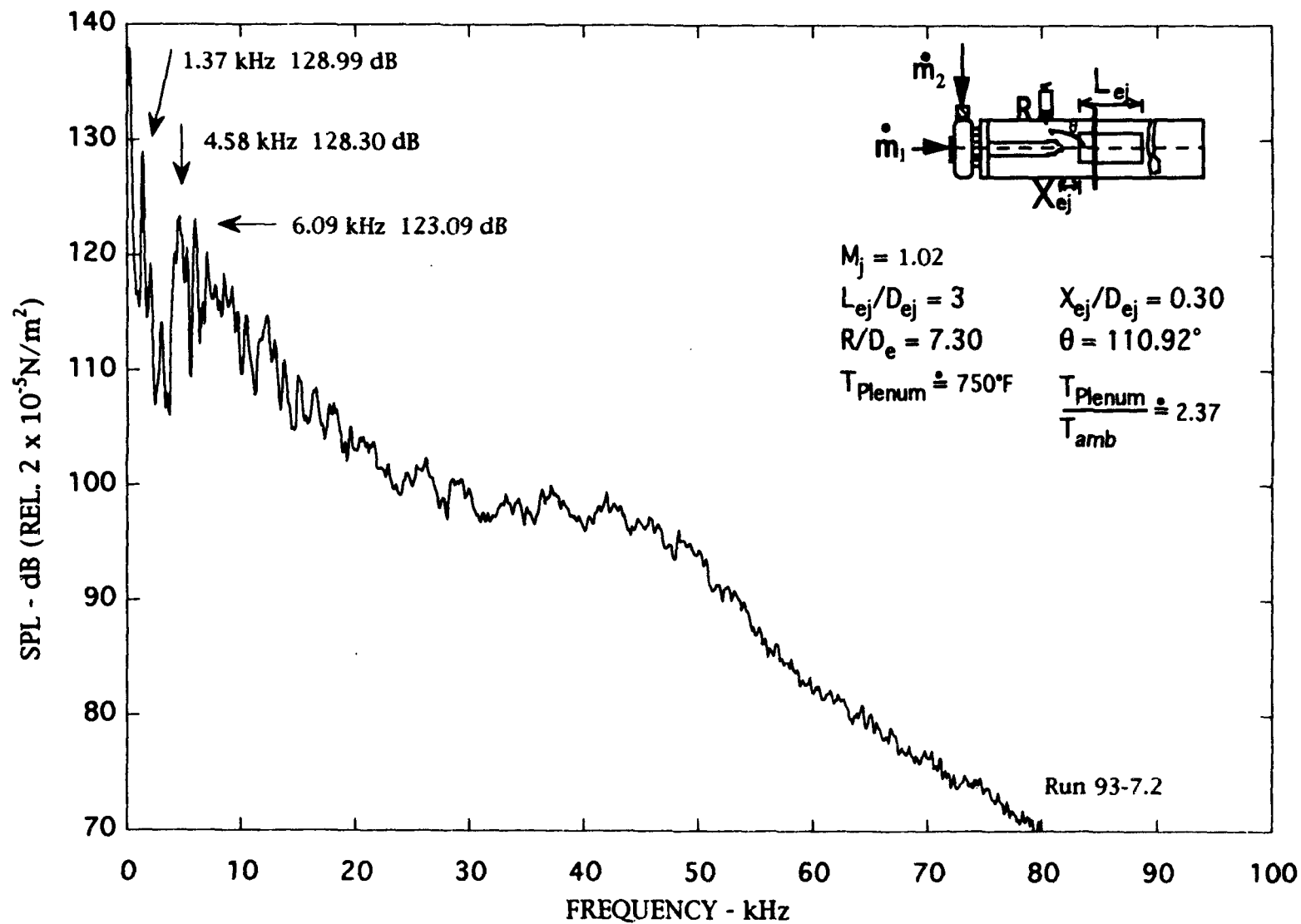Figure C-20. Narrow band ($\Delta f = 128$ Hz) noise spectra of ducted jet), $M_j = 1.02$.

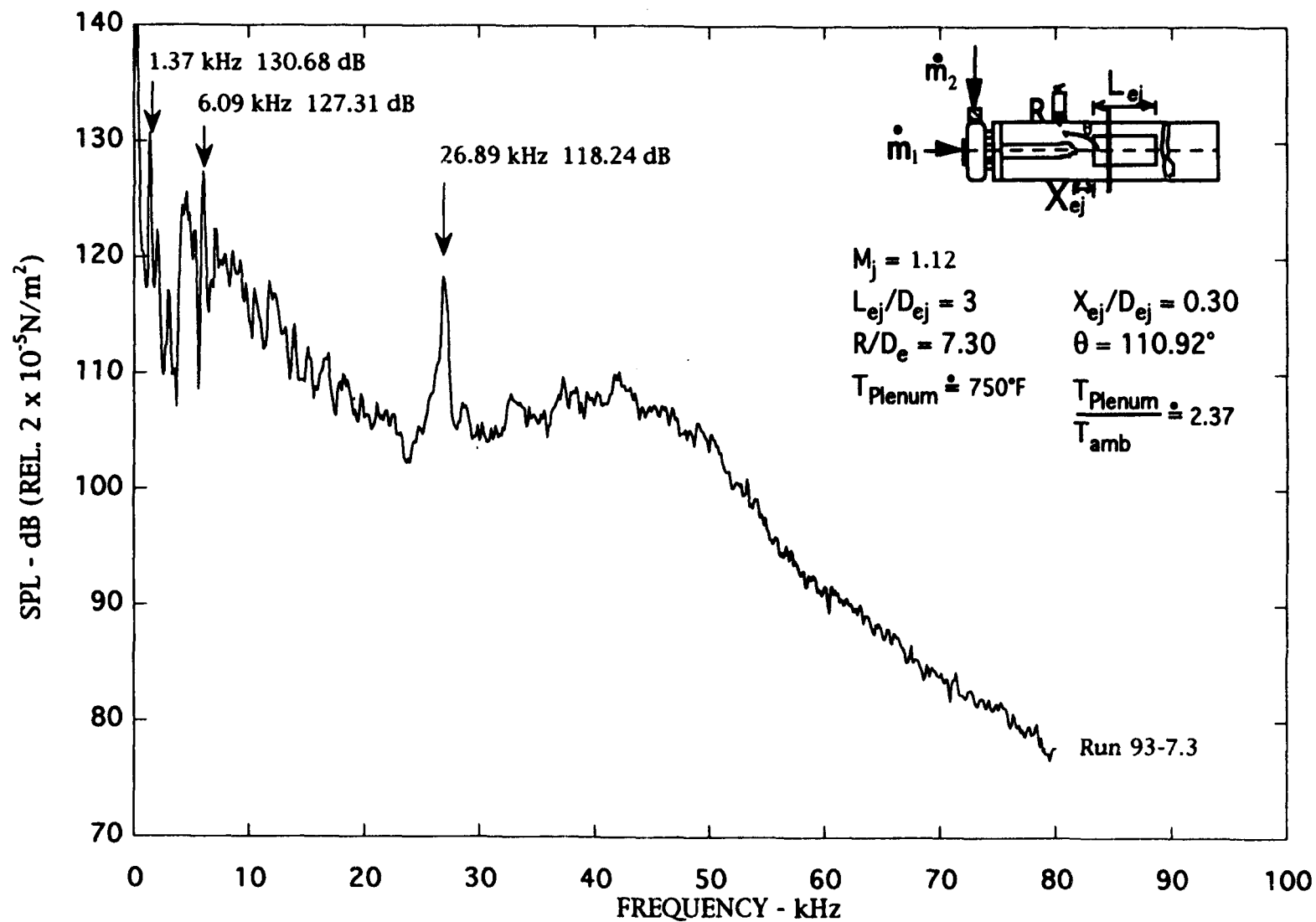Figure C-21. Narrow band ($\Delta f = 128$ Hz) noise spectra of ducted jet), $M_j = 1.12$.

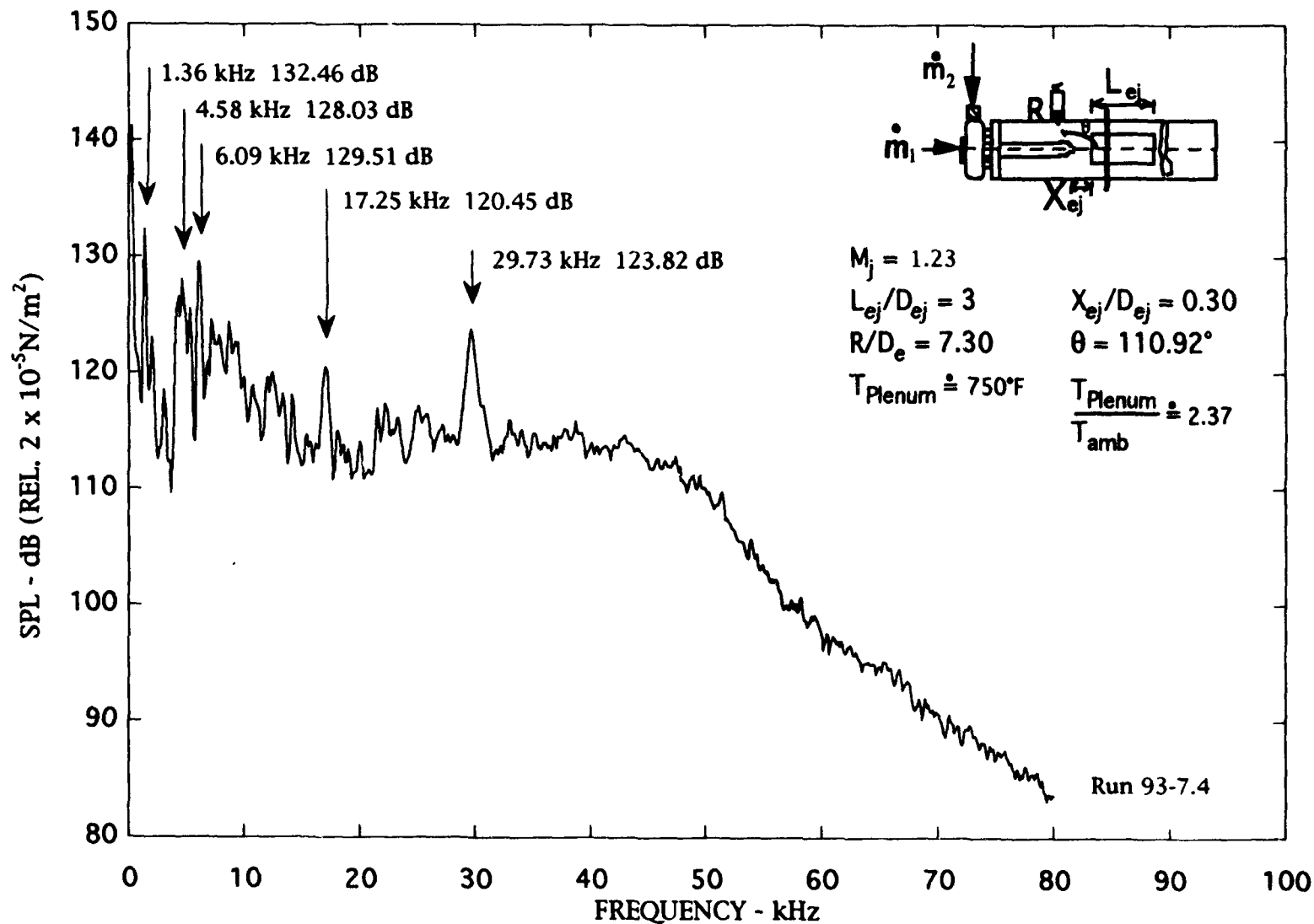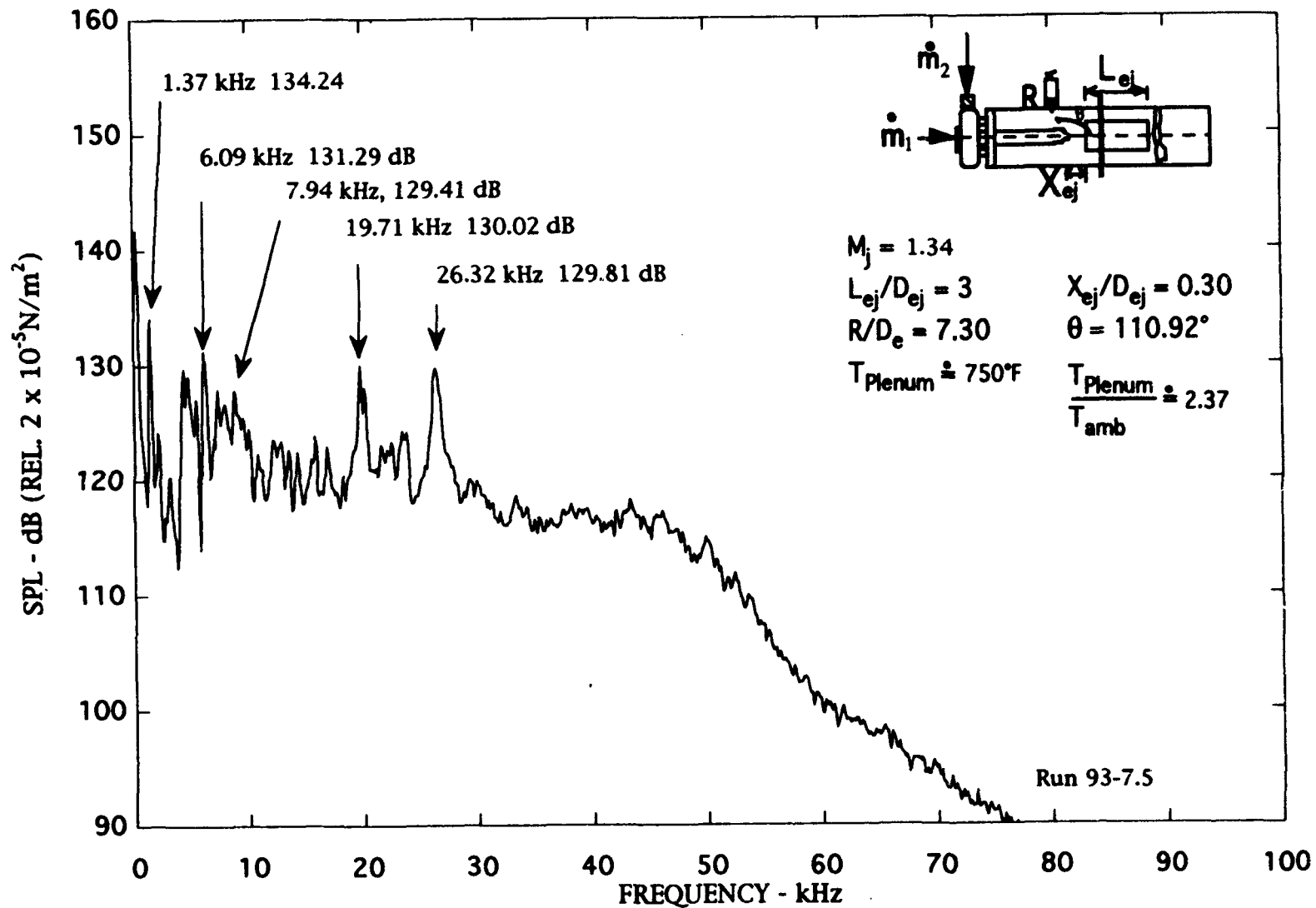Figure C-22. Narrow band ($\Delta f = 128$ Hz) noise spectra of ducted jet), $M_j = 1.23$.

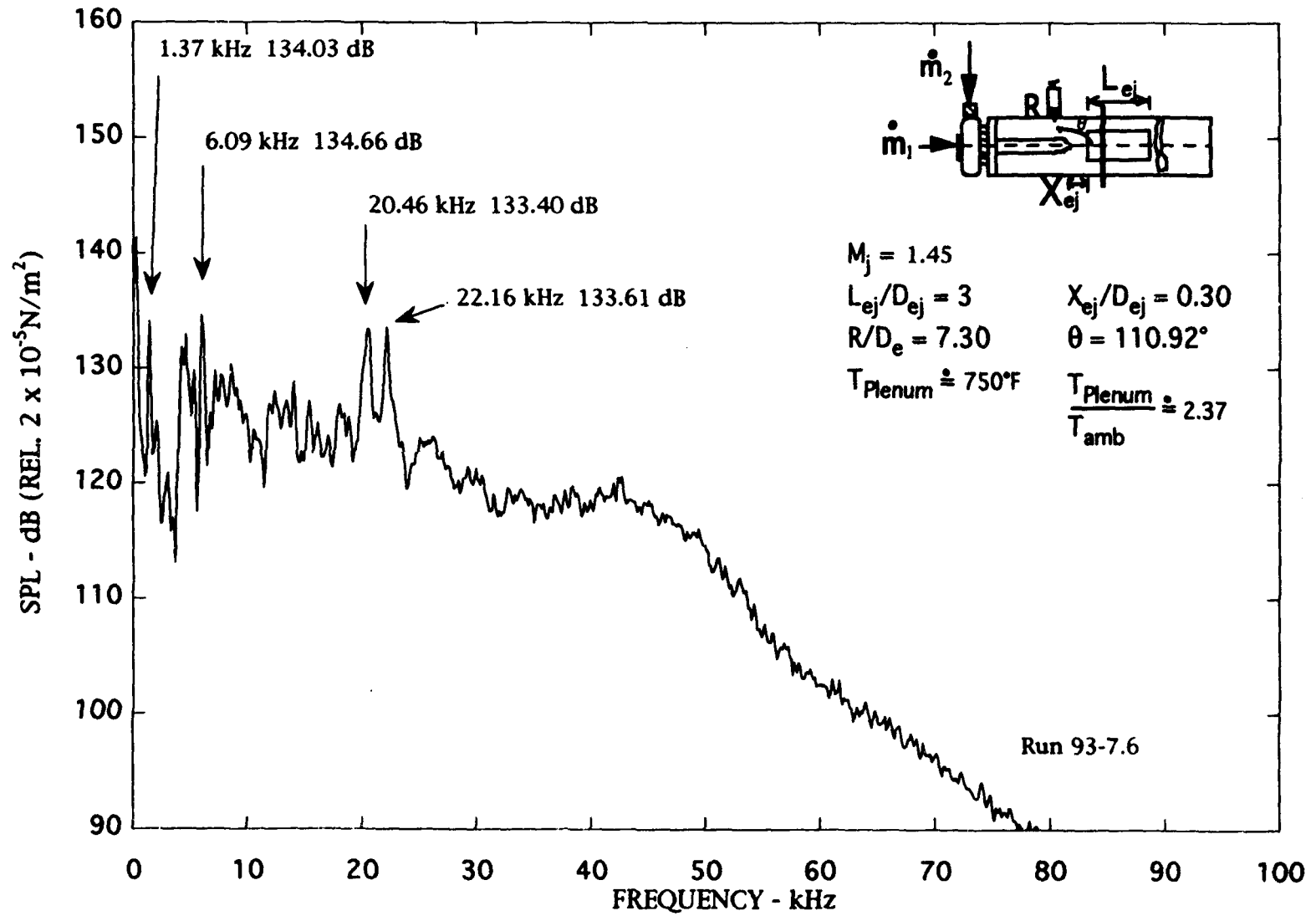Figure C-23. Narrow band ($\Delta f = 128$ Hz) noise spectra of ducted jet), $M_j = 1.34$.

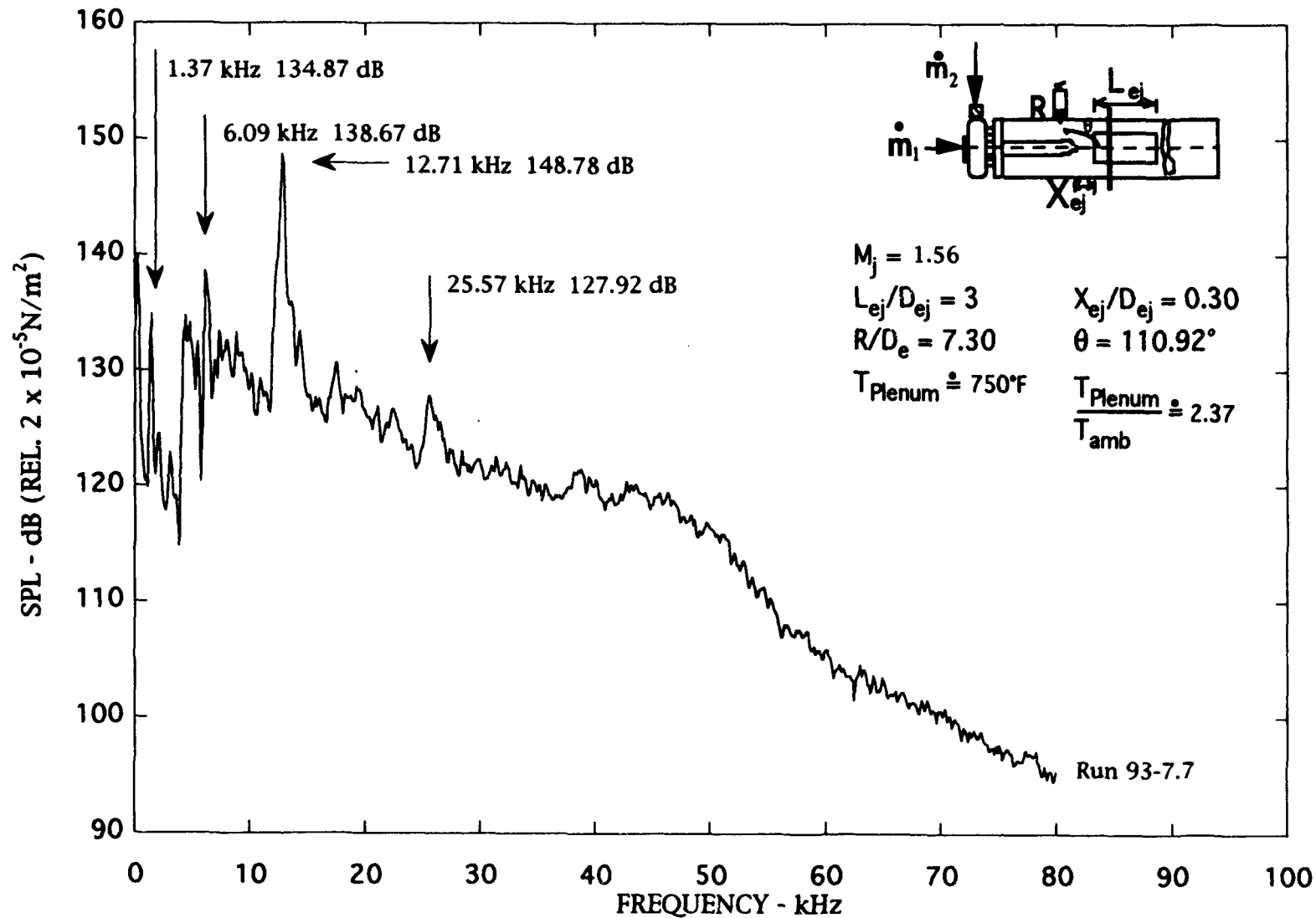Figure C-24. Narrow band (Δf = 128 Hz) noise spectra of ducted jet), M_j = 1.45.

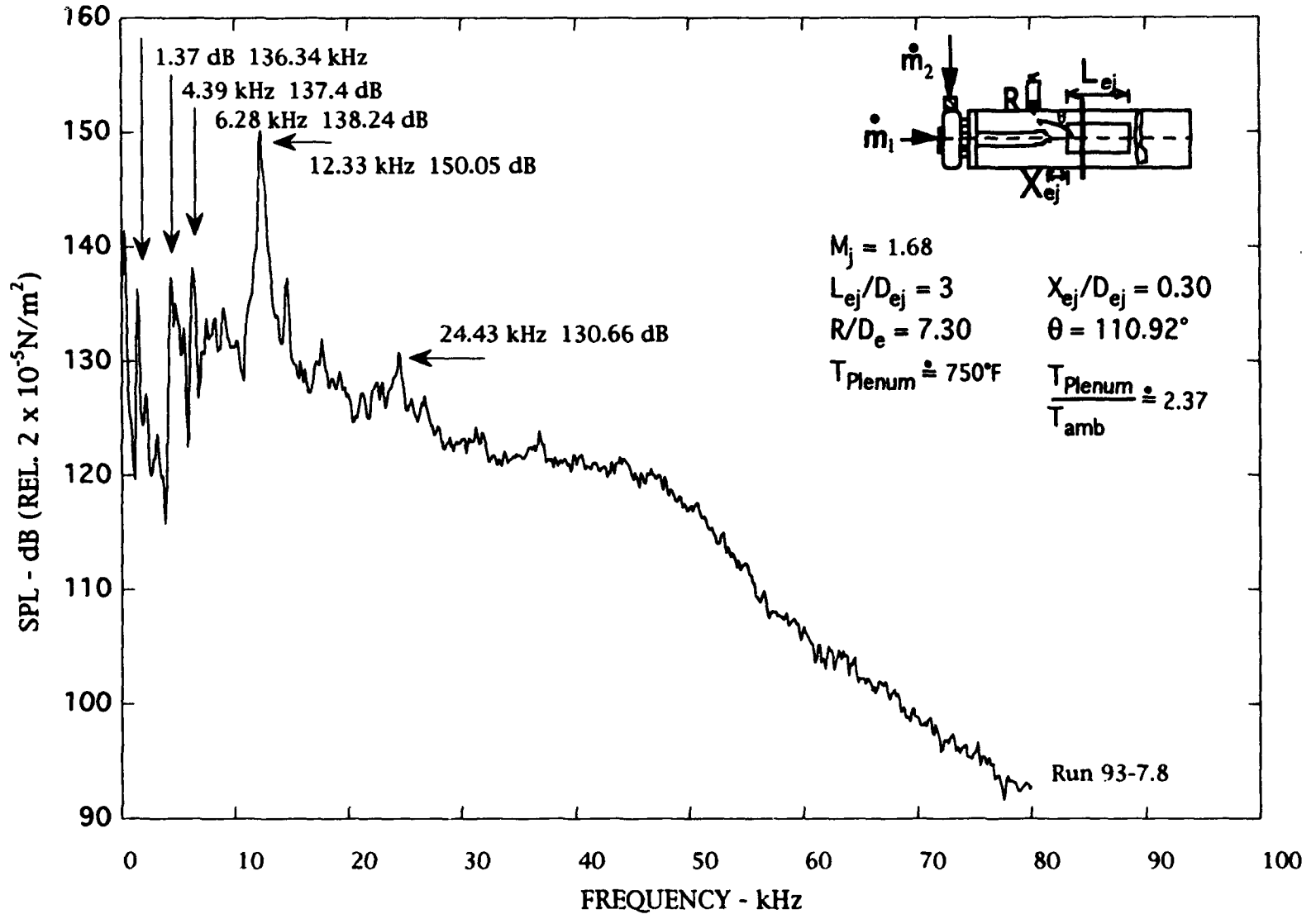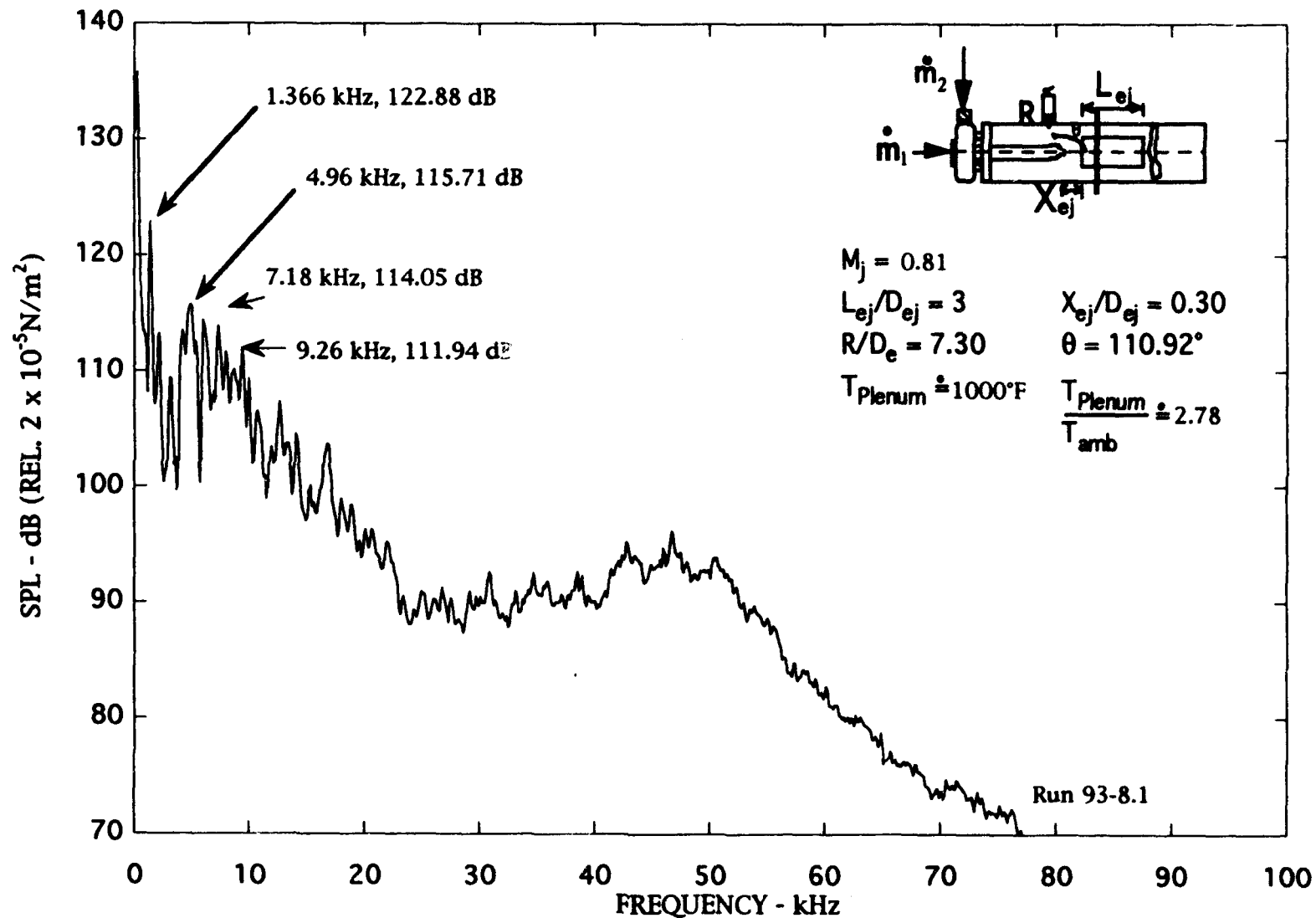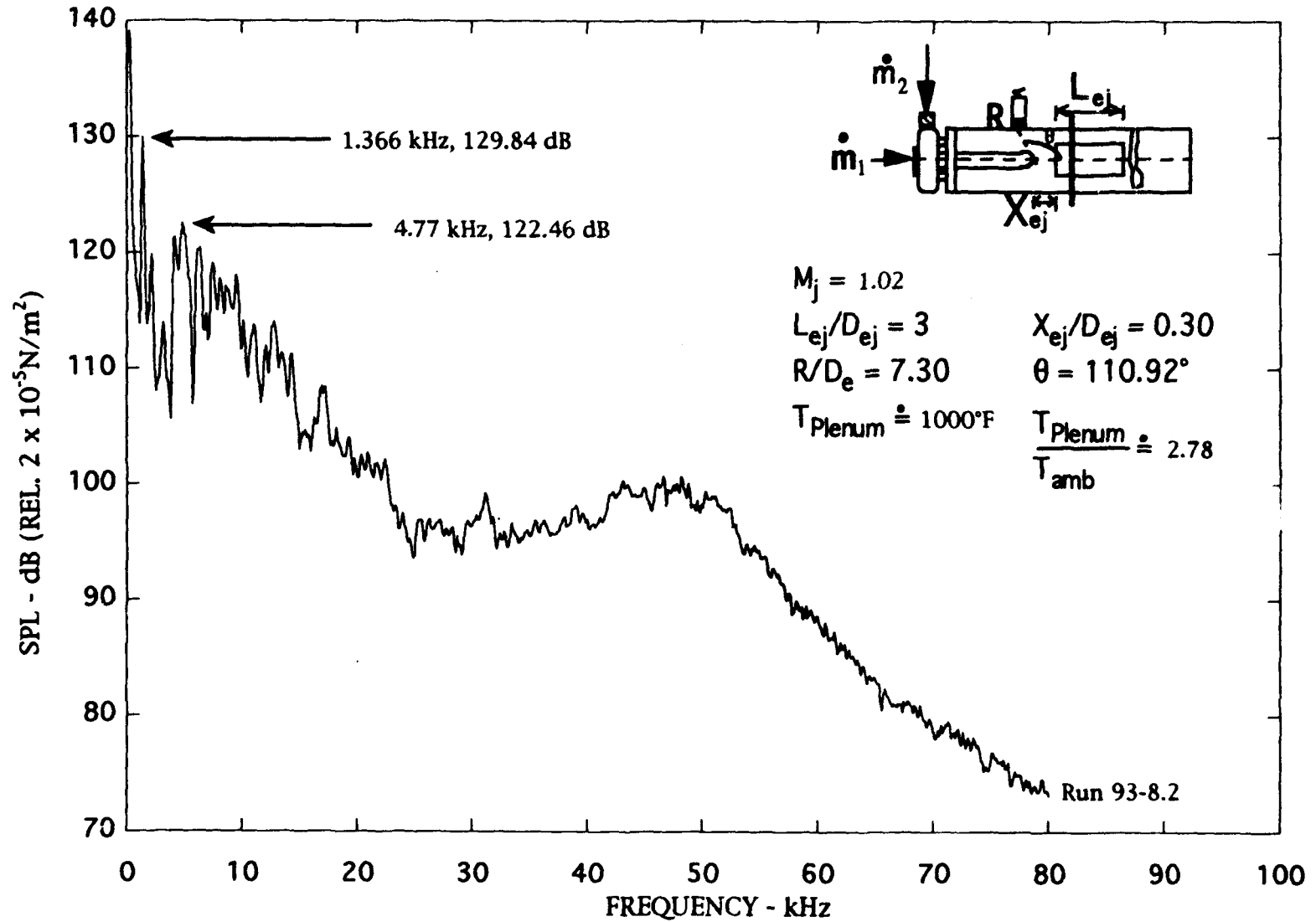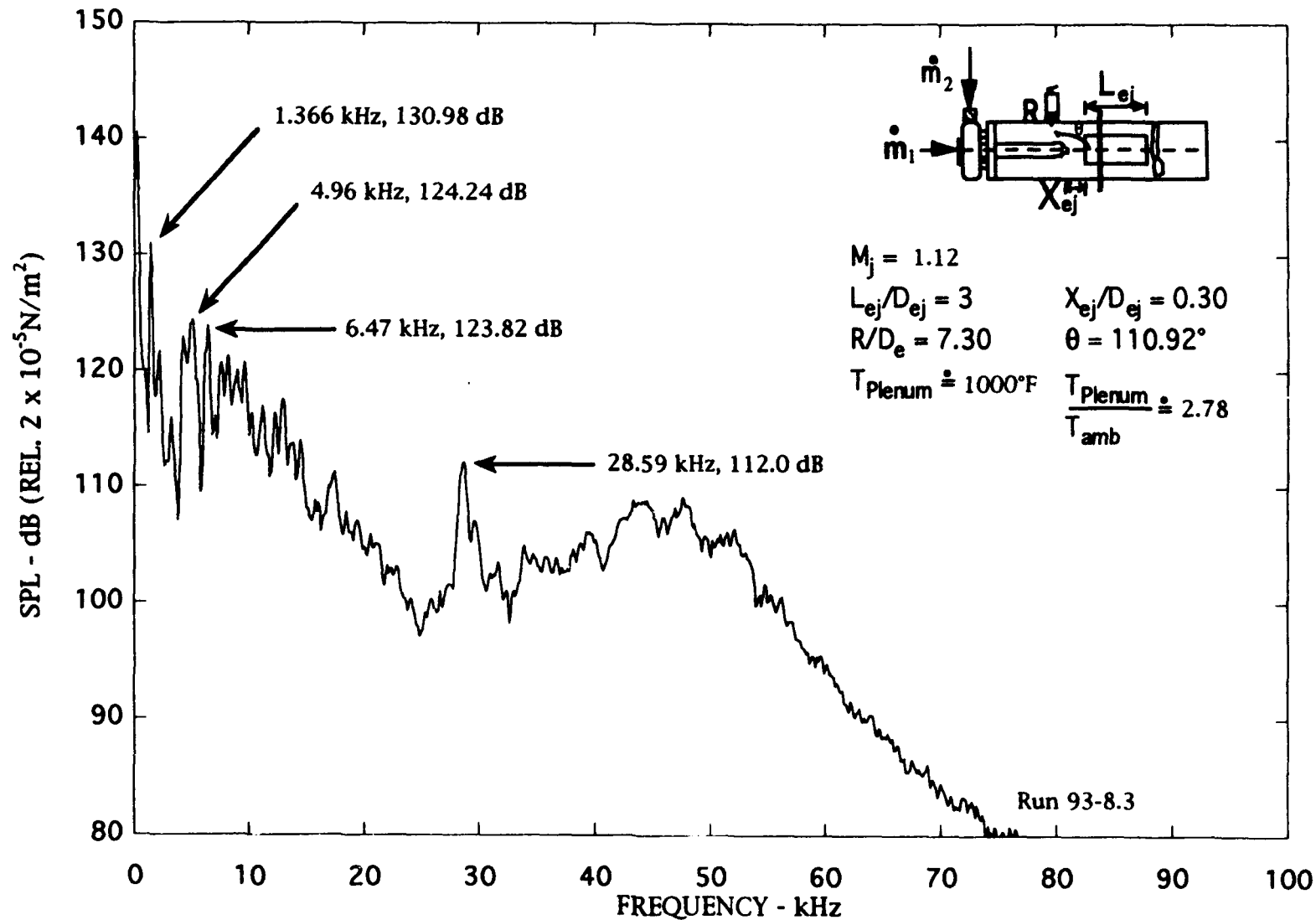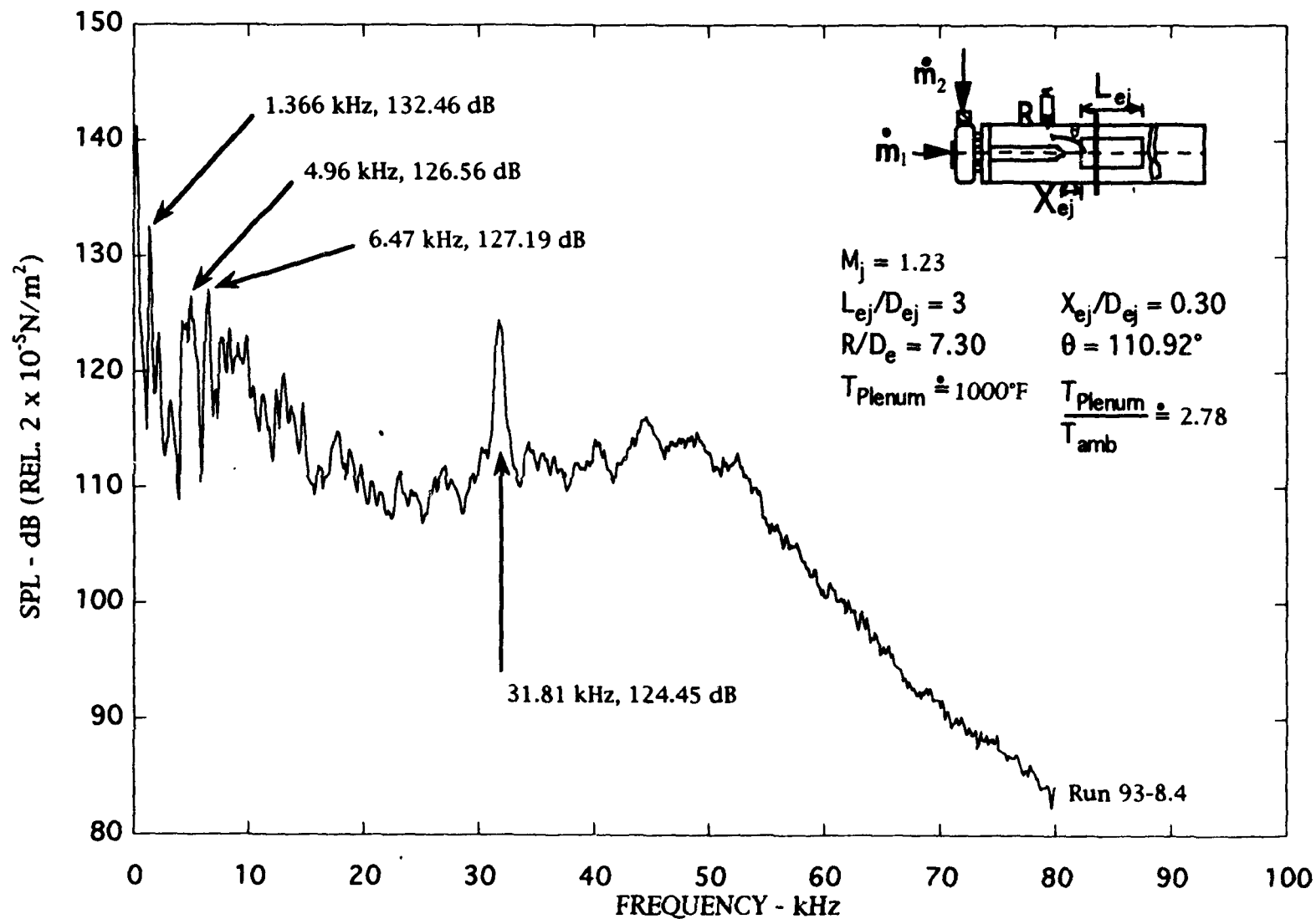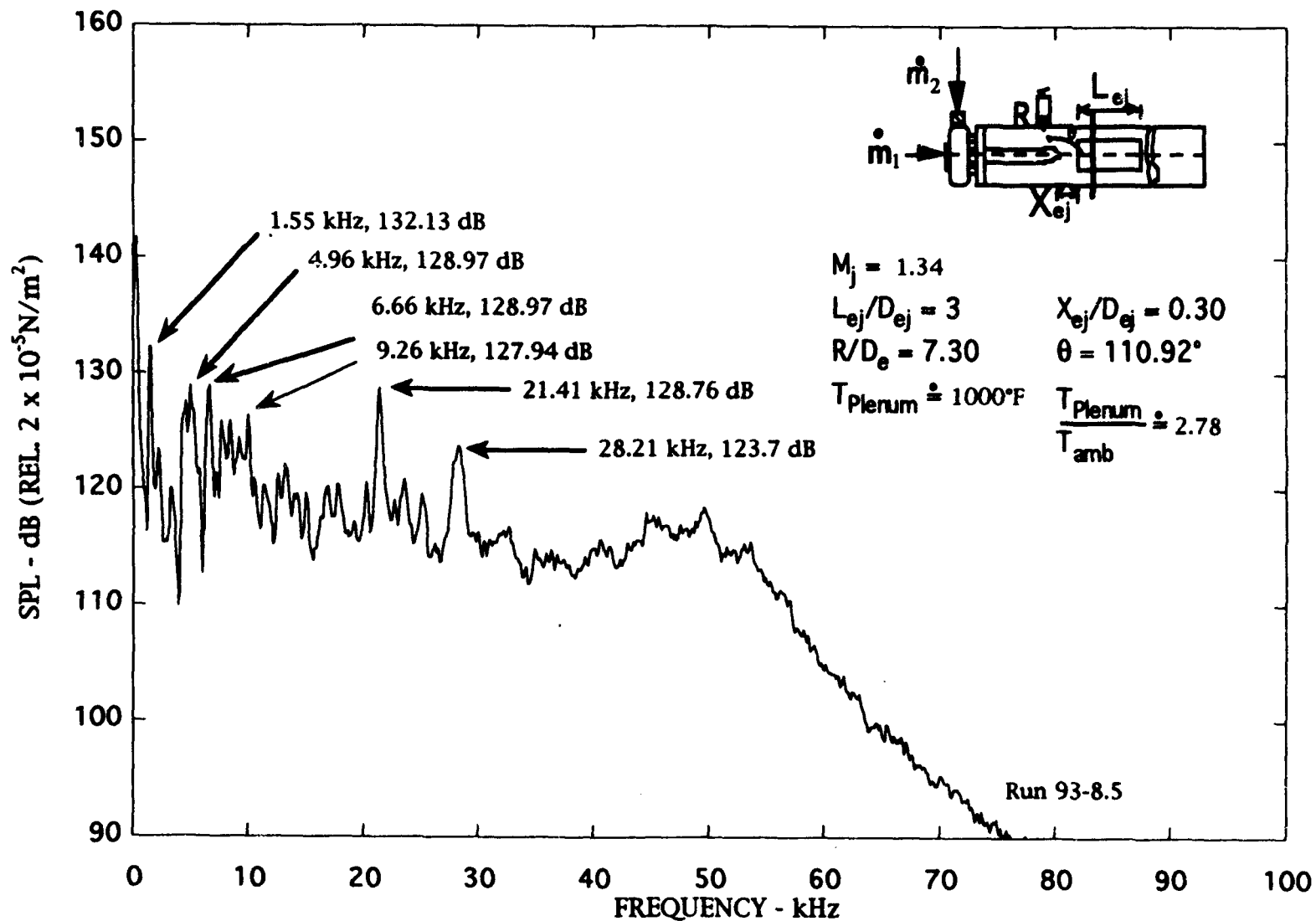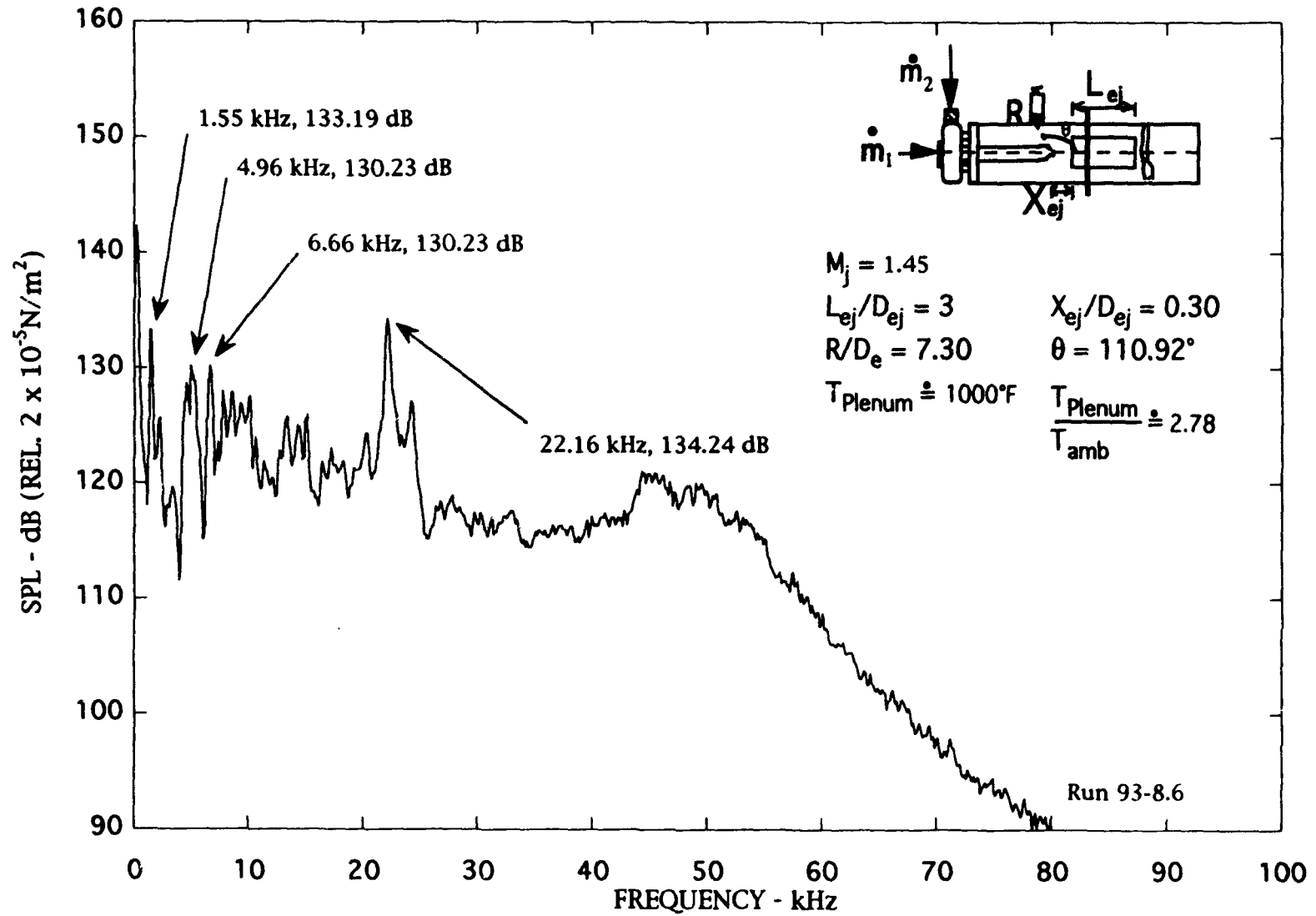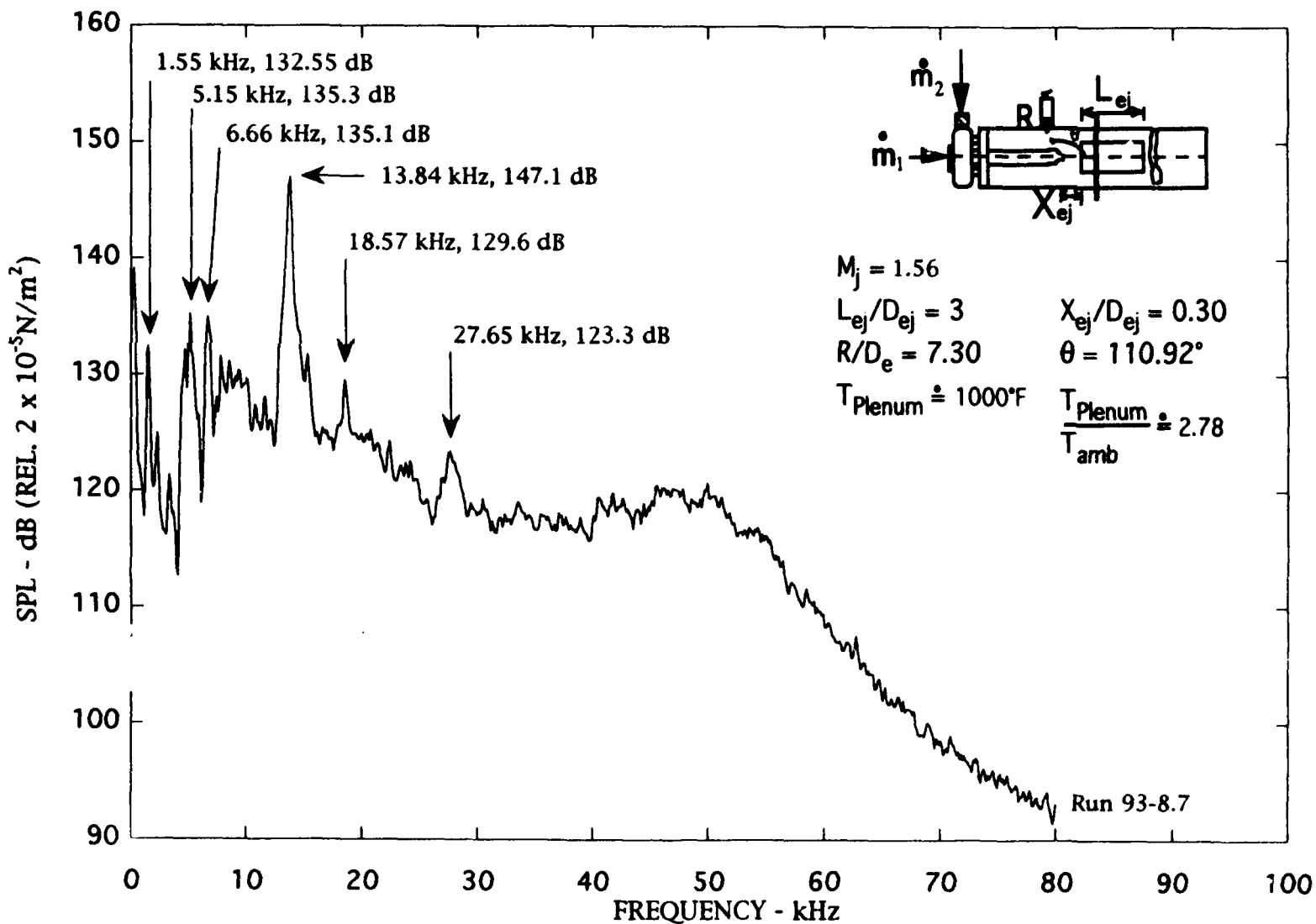Figure C-25. Narrow band (Δf = 128 Hz) noise spectra of ducted jet), M_j = 1.56.
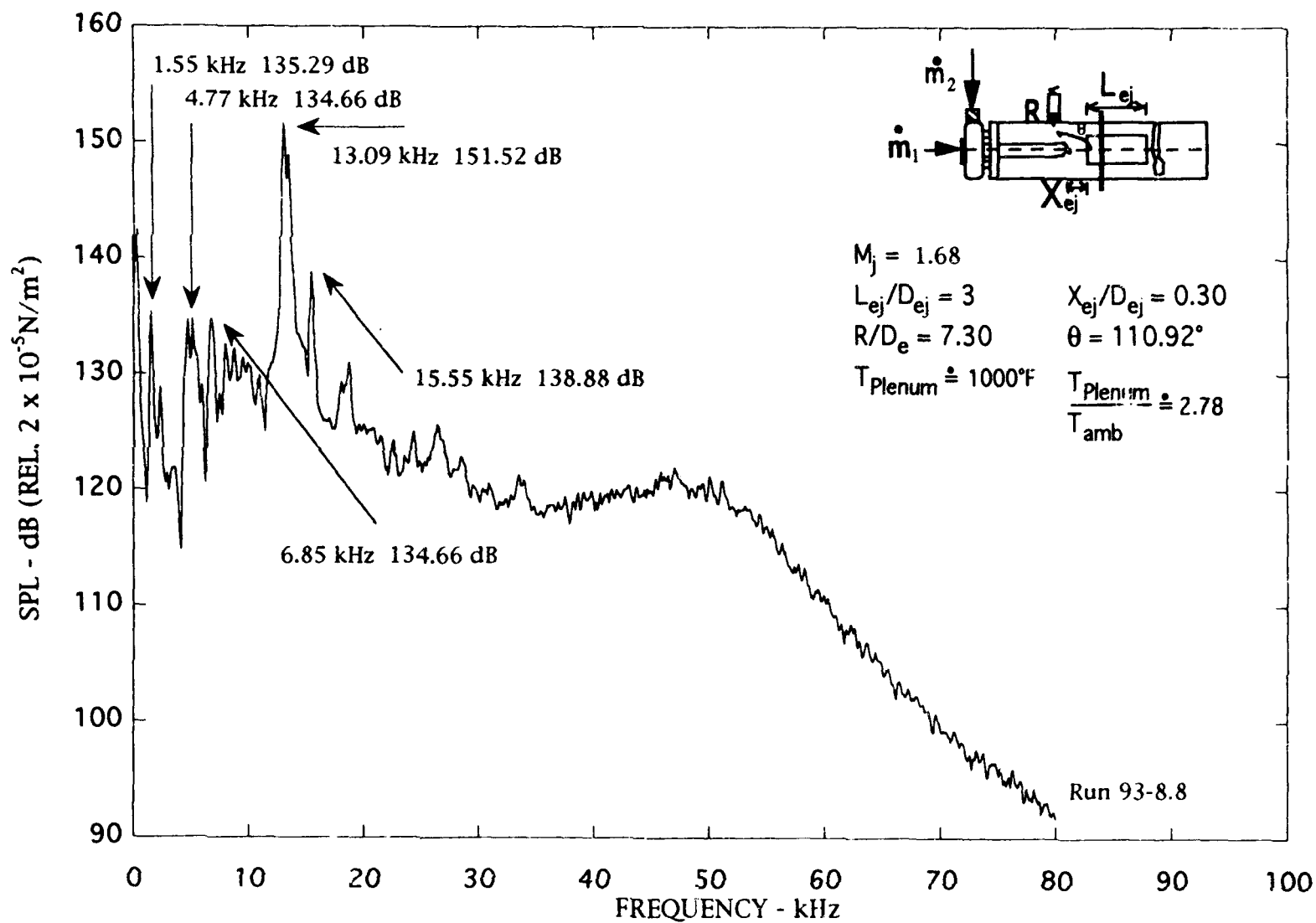
Figure C-26. Narrow band (Δf = 128 Hz) noise spectra of ducted jet), M_j = 1.68.
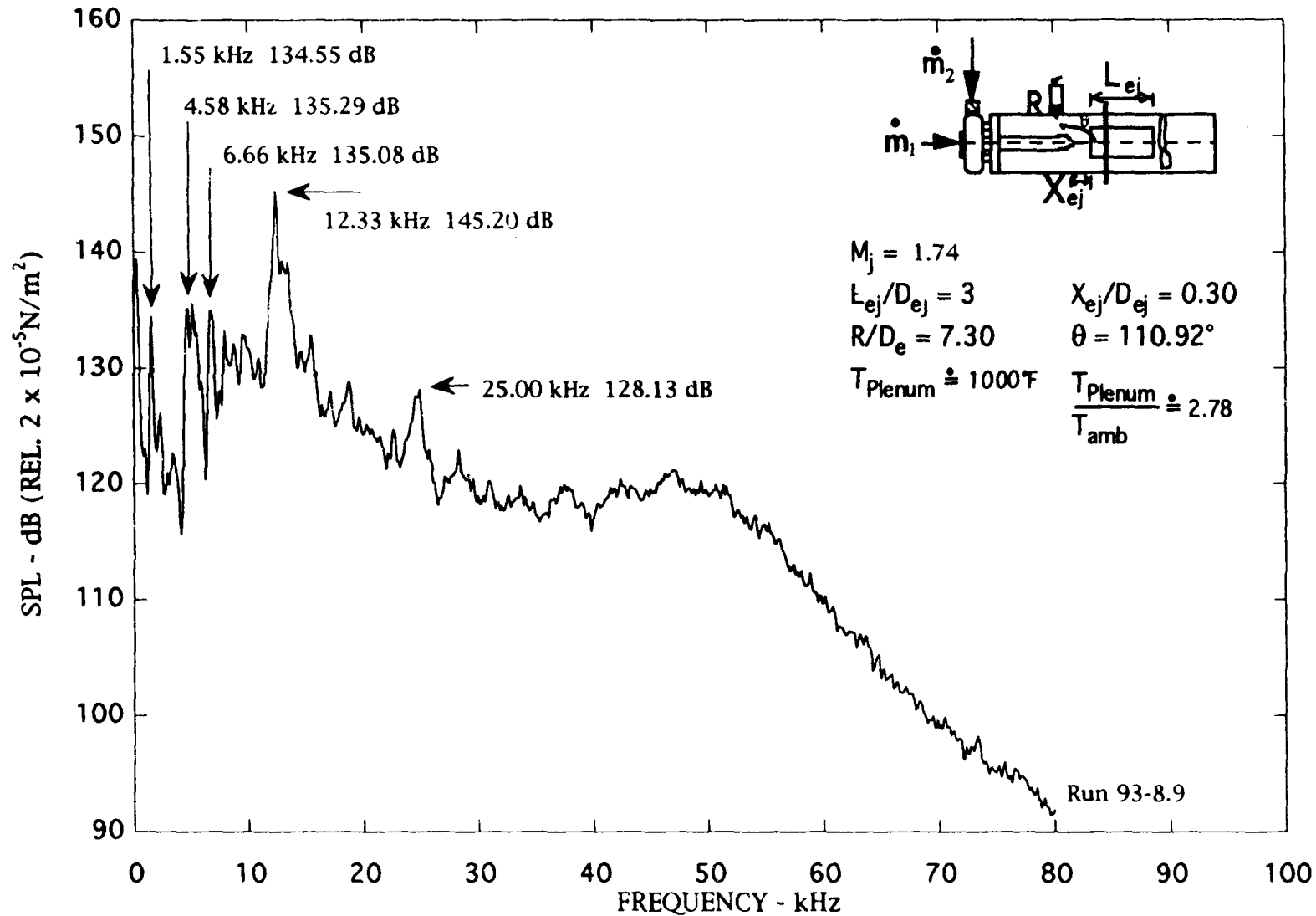
Figure C-27. Narrow band (Δf = 128 Hz) noise spectra of ducted jet), M_j = 1.74.

APPENDIX D

Mass Flow Calculations

D.1 Calculation of the Primary Jet Mass Flow Rate $\dot{m}_1$

For this calculation the following isentropic mass flow relation was used;

$$\dot{m}_1 = A \frac{P_o \sqrt{\gamma}}{\sqrt{RT_o}} \left(\frac{1}{1 + \frac{\gamma-1}{2} M^2} \right)^{\frac{\gamma+1}{2(\gamma-1)}}$$

where $A = \pi \left(\dfrac{0.484/2}{12} \right)^2 = 0.001278 \text{ ft}^2$. P_o and T_o are the plenum pressure and temperature, respectively, and where the Mach number, M, is equal to 1 if the jet is supersonic.

D.2 Calculation of the Secondary Mass Flow Rate $\dot{m}_2$

D.2.1 The Secondary Manifold Equipped with Venturi

The pressure difference across the venturi was measured and recorded for each pressure ratio tested.

The calculations for the mass flow through the venturi were based on the methods given in the Handbook of Fluid Dynamics by Streeter (Ref. D.1) for compressible flow through a venturi. The equation for calculating weight flow was given as

$$W = K A_2 \gamma Y \sqrt{\frac{2g(p_1 - p_2)}{\gamma}} \quad \text{lb}/\text{s}$$

where K is a flow coefficient based on Reynolds number that was taken to be equal to 1, A_2 is the area at the throat of the venturi, γ here represents the specific weight (32.2 * density), Y is the 'expansion factor' for the venturi, g represents the acceleration due to

267

gravity, and p_1 and p_2 represent the pressure at the venturi intake and throat respectively. The above formula was used to find the mass flow rate by dividing by 32.2 ft/s^2

For the venturi used, the diameter of the intake was 0.61 inches and the diameter at the throat was 0.08 inches. This yielded the following values

$$\frac{D_2}{D_1} = 0.1311$$

$$A_2 = 3.4907 * E - 5 \text{ ft}^2$$

The density was taken to be the density at ambient conditions as given above since the venturi entrained the ambient air.

The expansion factor was determined from the graph below.

Expansion Factors vs. Pressure Ratio
for γ = 1.4
Adapted from Handbook of Fluid Dynamics
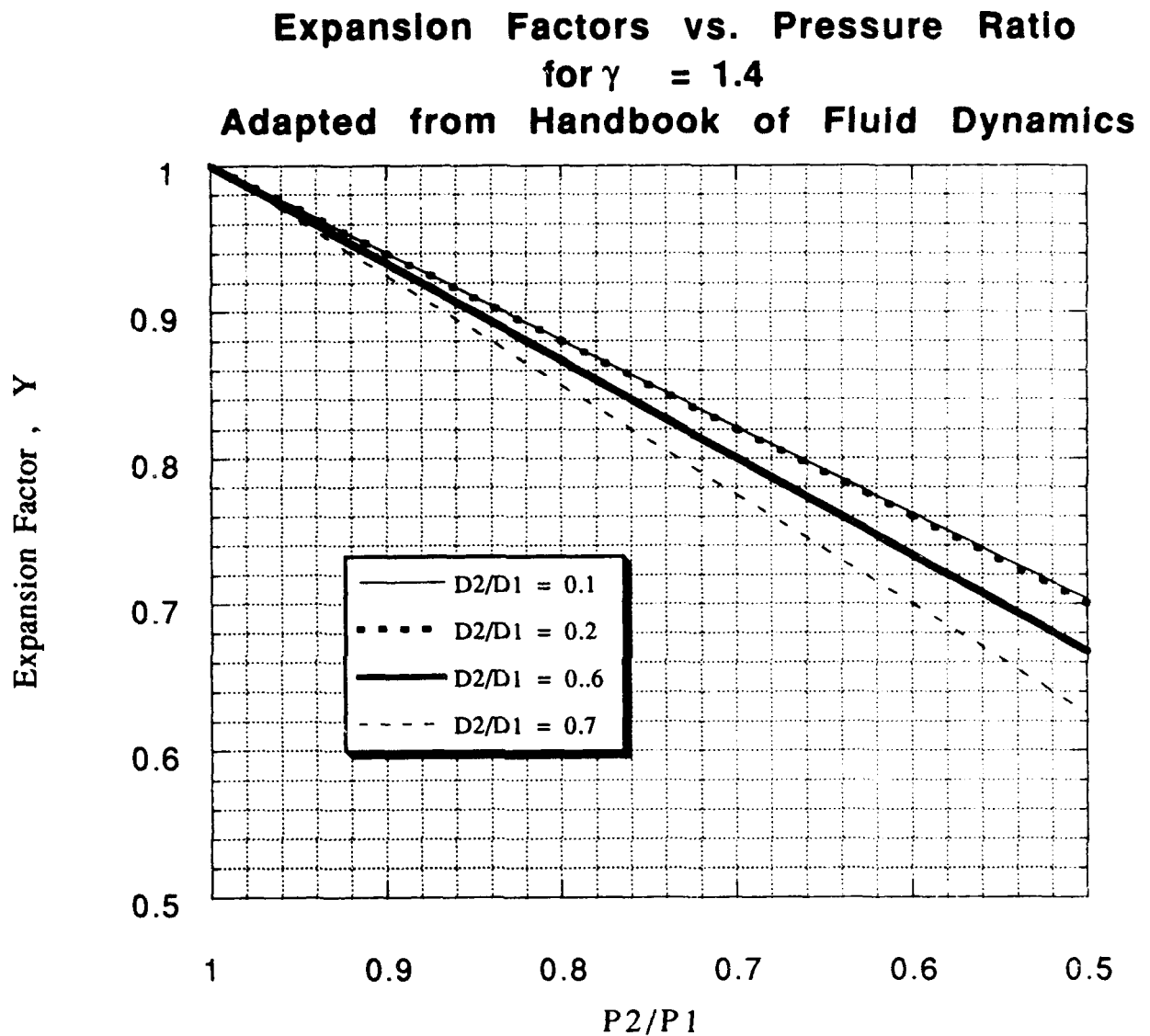
This graph is based on the values given in Ref. D.1, and the line for D_2/D_1 was extrapolated from the given values. This essentially resulted in using the expansion factors given for D_2/D_1 = 0.2 which is close to the actual value of 0.13.

D.2.2 The Manifold Without the Venturi

Here the mass flow rate is given by

$$\dot{m}_2 = \rho \, A \, V$$

where the density is taken as the standard density as above and the area is given by the manifold area, which in some cases is halved since half of the manifold was closed off, and the velocity was determined as follows.

The velocity was measured by a pitot static probe. An effort was made to ensure that the velocity was uniform over the entire area of the manifold intake. The velocity did indeed appear to be uniform as the measured pressure difference was only slightly lower at the walls and uniform elsewhere in a line across the intake. From this pressure difference the velocity was calculated as follows;

$$V = \sqrt{\frac{2(p_0 - p_s)}{\rho}}$$

APPENDIX E

Calibration of Kistler® Transducers

One of the initial goals of the experiments was to acquire the tone amplitude and phase measurements inside the diffuser to determine the mode of the jet inside of the diffuser. To acquire these data a special diffuser was constructed which contained many ports for water-cooled Kistler pressure transducers. To accurately measure the phase, it is necessary to know the relative amplitude and phase of each transducer with respect to a reference transducer. Thus it was necessary to measure the relative amplitudes and phases of each of these transducers in a controlled experiment where they each receive the same input. This experiment and some preliminary results are presented below. The results are described as preliminary since a decision was made not to make the phase measurements part way through the program and thus this part the experiment was not carried to its completion.

E.1 Experimental Setup

Several different setups were used to try to provide the same acoustic signal to multiple transducers at the same time. A sound distribution device, shown in part in Figure E.1 was used for this purpose. This device consisted of a port in which the sound was introduced that impinged on a sharp cone. Radially distributed around this cone were 12 circular ports to which the transducers were mounted. At first, an attempt was made to use a speaker to output white noise into the sound distributor, but it was found that the amplitude was to low for the transducers. This setup is shown in Figure E.2. Figure E.3 shows the transducers protruding from the sound distributor in the foreground. Letting a subsonic jet impinge on the opening of the sound distributor was found to create the acoustic amplitude necessary. This setup is shown in Figure E.4 and schematically in E.5.
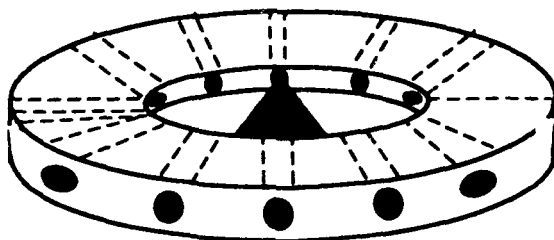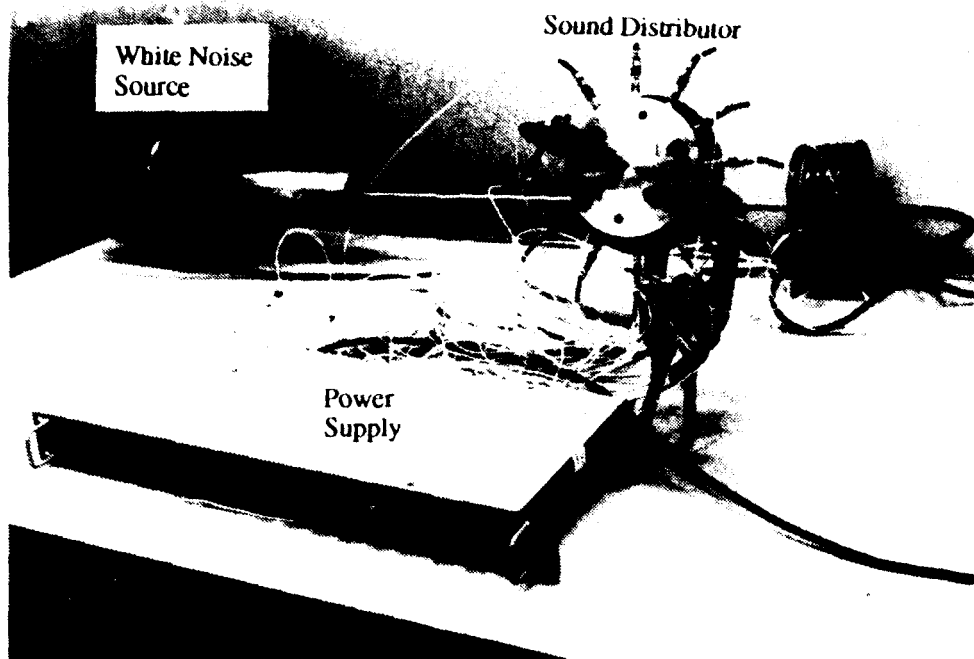

Figure E-1. Sound distribution device.

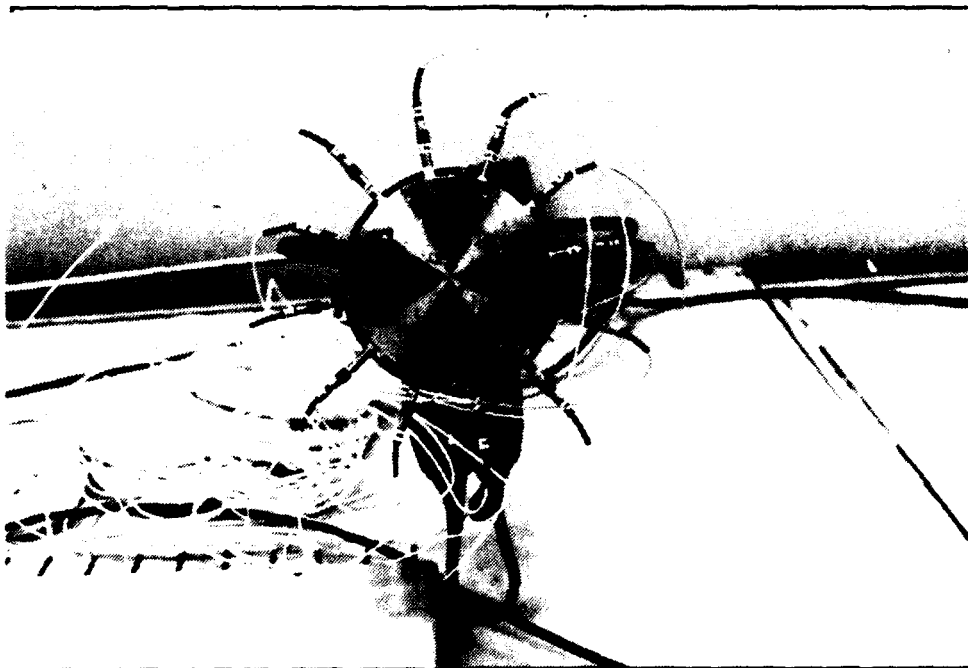**Figure E-2. Speaker setup for Kistler calibration.**

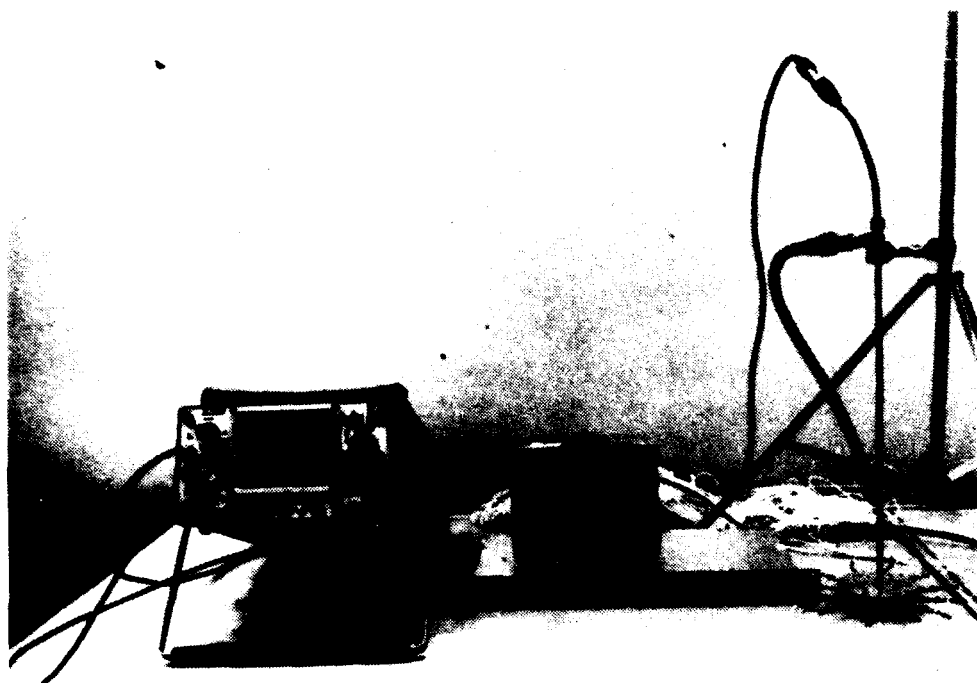**Figure E-3. Close up of sound distributor and transducers.**

Figure E-4. Impinging jet schematic for Kistler calibration.
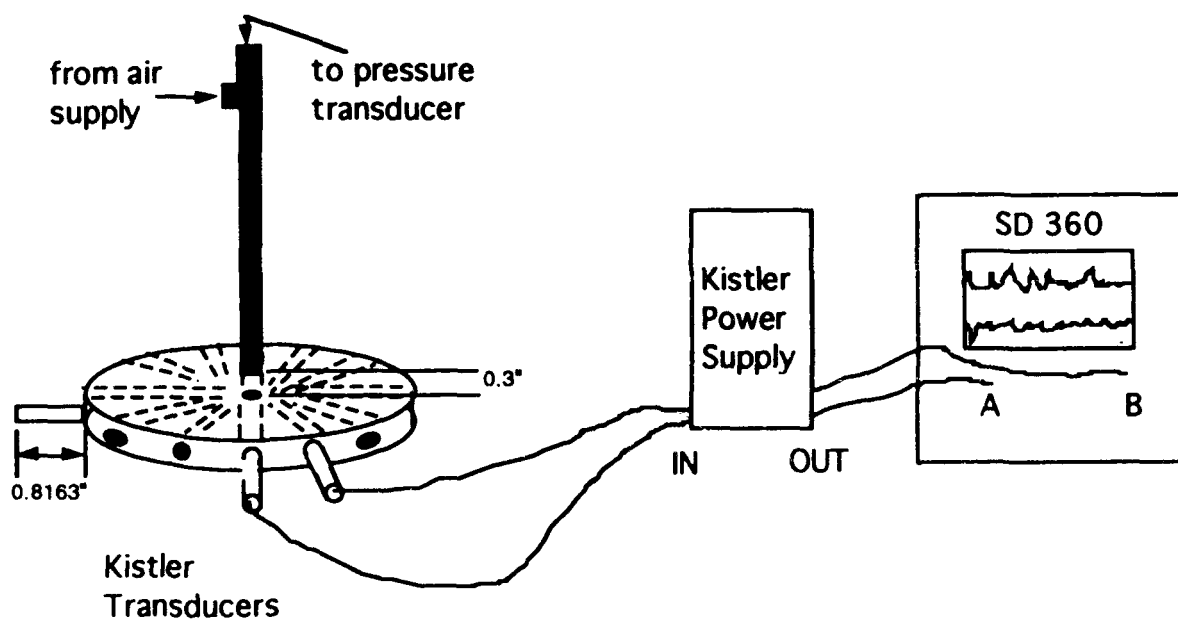

Figure E-5. Impinging jet schematic for Kistler calibration.

273

It was found that by running the jet with a line pressure of approximately 11 psi with the jet 0.3 inches above the entrance to the sound distributor yielded a highly reproducible acoustic signal. At a frequency of 26.6 kHz this signal was found to be 26.2 dB above the ambient/electronic noise.

(Note: A 120 Hz tone, that is electronic in origin, was found to be present in all measured spectra.)

The repeatability of the data as well as the level relative to the ambient noise is shown in Figure E.6.

E.2 Test of Sound Distributor Device

An attempt was made to confirm that the sound that enters through the small orifice in the sound distributor propagates evenly to each port.

Method
1) Cover all ports except port #1.
2) Record noise at port #1 with transducer #1 on Channel #1.
3) Cover all ports except port #2.
4) Record noise at port #2 with transducer #1 on Channel #1.
5) Repeat the above procedure for other ports.

The transducer depth into each port was determined by using precision dial calipers, and the transducer had 2.163 inches of its length protruding into the port for any given measurement. The line pressure was maintained at 10.6 psi for all data taken.

The effectiveness of the sound distribution device is shown in Figure E.7.

E.3 Transducer Relative Amplitude Measurements

Method
1) All 12 transducers were mounted as in the previous test.
2) The jet was positioned as in the previous test and was run at a line pressure of 10.6 psi.

3) The signal from each transducer was measured and the levels relative to transducer #1 were monitored at a frequency of 29.0 or 28.8 kHz.

4) An effort was made to adjust the output levels of each transducer by means of the "current adjust" switch on the power supply so that all transducers gave the same level at this frequency.

5) The transfer function spectra between a given transducer and transducer #1 was obtained using a real time frequency analyzer.

A representative transfer function between transducer 1 and 2 is shown as the lower curve in Figure E.8. This plot is typical of the preliminary results for the remaining transducers. (The upper curve is the phase spectra as described below.)

E.4 Transducer Relative Phase Measurement

Method

1) The setup of the transducers was the same as in the previous experiment.

2) The relative phase between transducer #1 and #2 was measured.

3) The relative phase between transducer #1 and #3 was measured.

4) This process was repeated for all 11 transducers.

A representative phase measurement is presented in Figure E.8 as the upper curve.
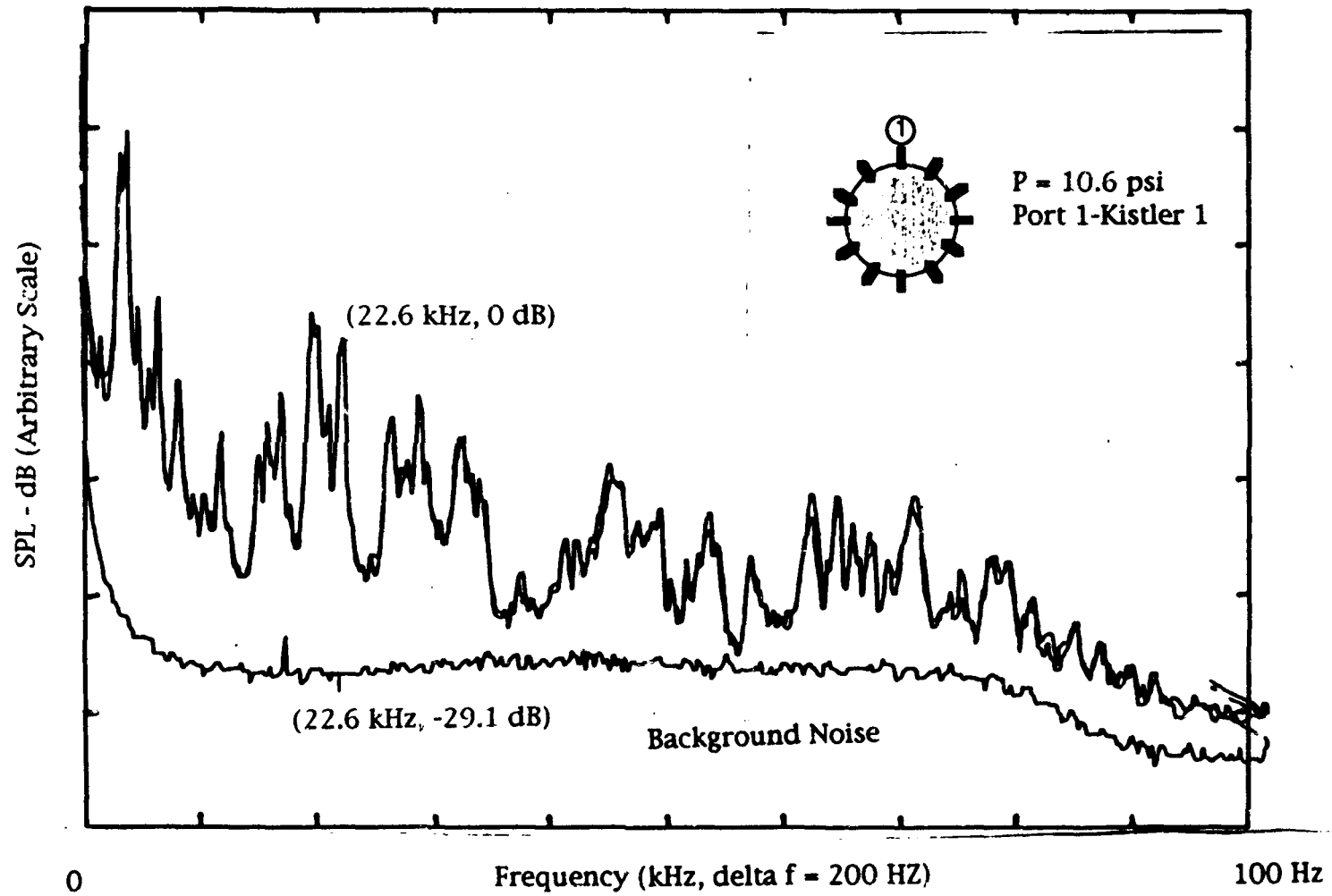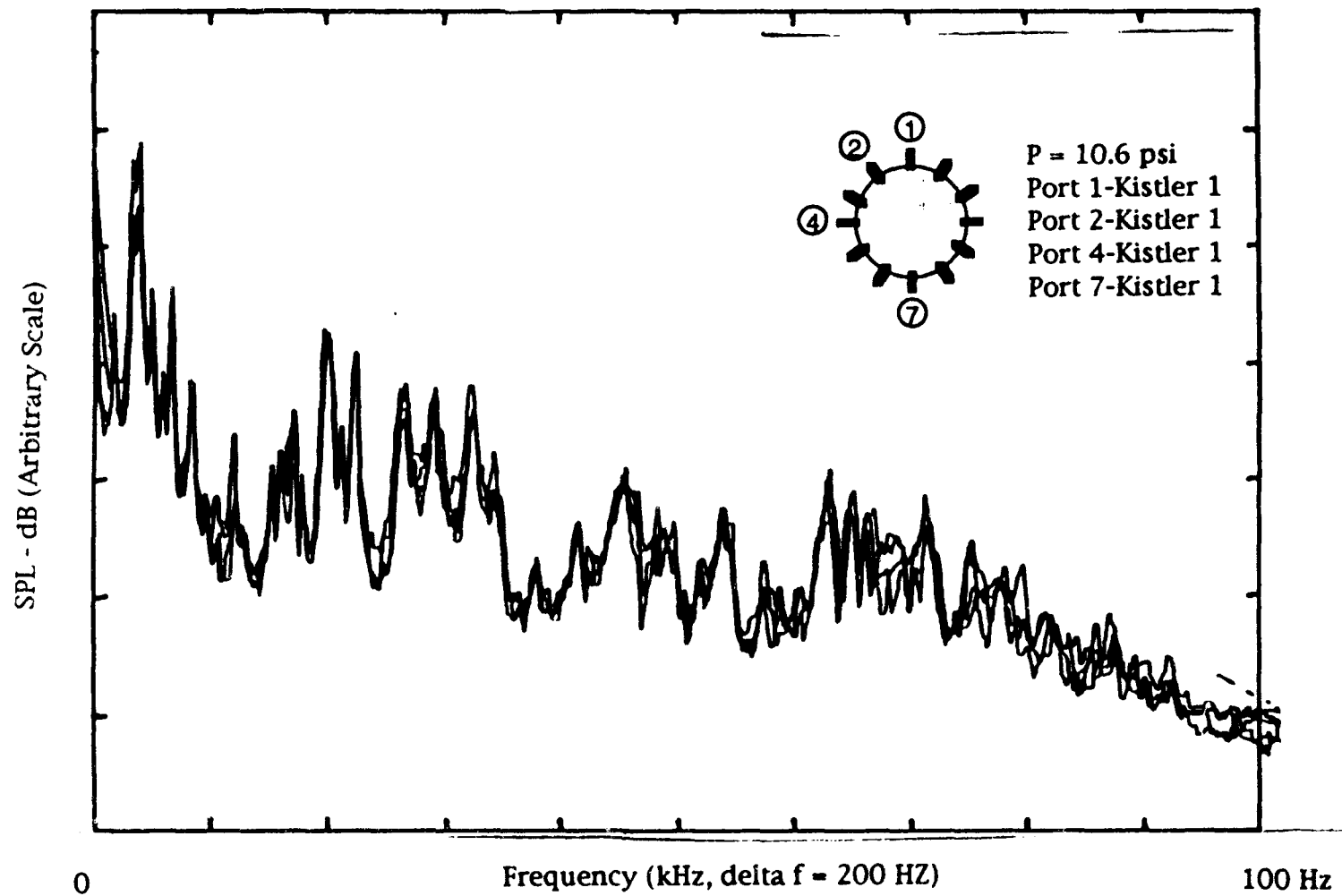
Figure E-6. Repeatability of data.

P = 10.6 psi
Port 1-Kistler 1
Port 2-Kistler 1
Port 4-Kistler 1
Port 7-Kistler 1

SPL - dB (Arbitrary Scale)

0   Frequency (kHz, delta f = 200 HZ)   100 Hz

Figure E-7. Sound propagation test.

P = 10.62 psi
Port 1-Kistler 1
Port 2-Kistler 2

(20.8, 147°)

Degrees (Arbitrary Scale)

at 0 Hz
Phase = 90.2°

SPL - dB (Arbitrary Scale)
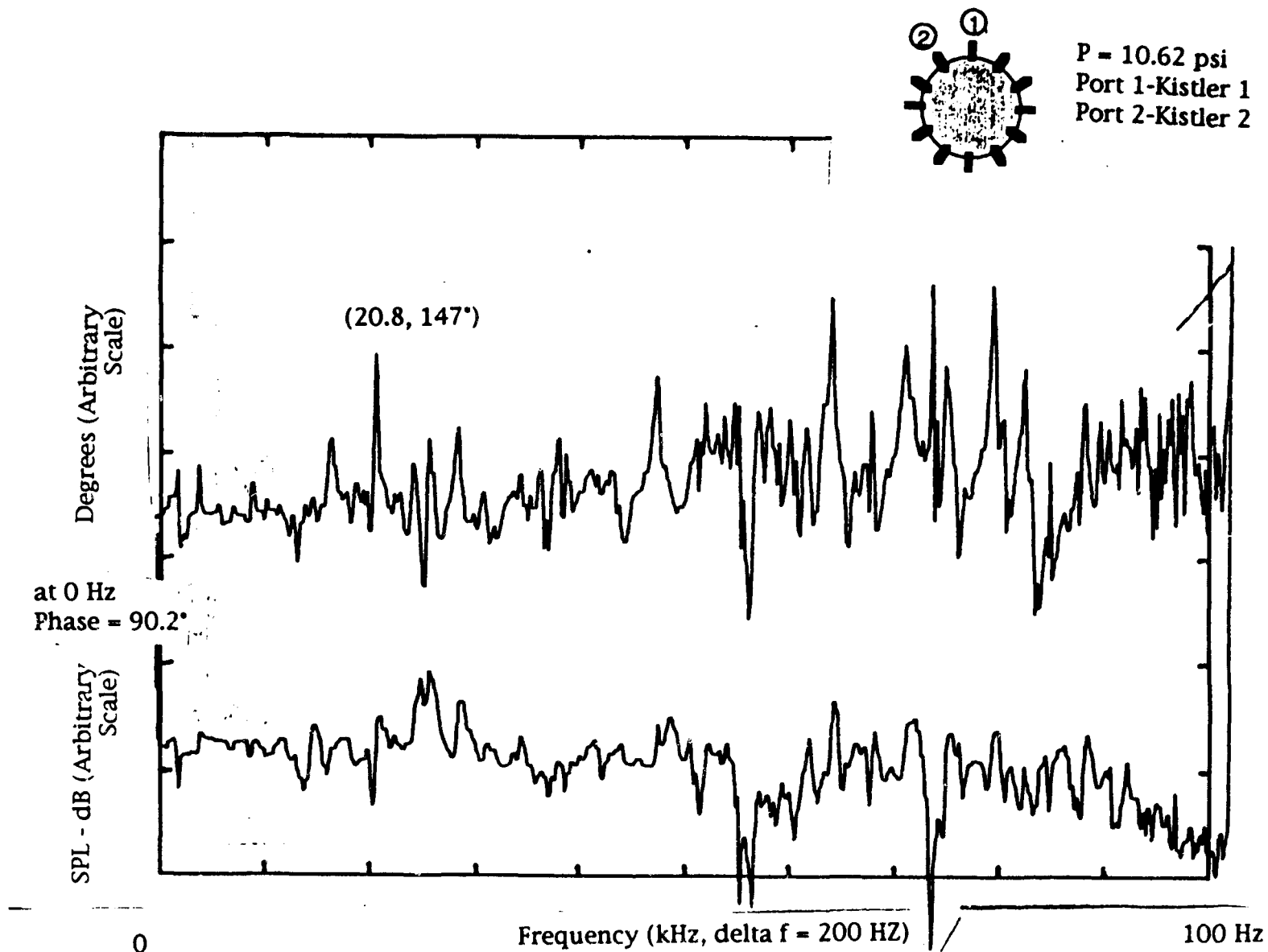
0

Frequency (kHz, delta f = 200 HZ)

100 Hz

Figure E-8. Phase of Kistler 2 versus Kistler 1.

E.5 Transducers in Water Jackets

Since it was planned to use these transducers in a high temperature environment, it was planned to mount them inside of water jackets while obtaining the acoustic measurements. A set of experiments was thus conducted to determine the effect of these waterjackets on the acoustic response of the transducers, if any.

To accomplish this task, it was decided to use an unheated free jet operated at a pressure ratio such that a high amplitude screech tone was present as a noise source. This was necessary to acheive the high amplitude necessary for the transducers. First a 'free standing'(i.e., without a water jacket) Kistler transducer was placed at a distance of 2.125 inches from the jet center, at the same radial distance as a B&K microphone, which was previously calibrated, in the exit plane of the jet. The Kistler transducer was then calibrated with respect to the B&K microphone. The Mach number was increased and the two time averaged signal were compared. As can be seen in Figure E.9, the two signals compare quite favorably until about 35 kHz after which the Kistler transducer's amlitude is considerably higher. This is due to the fact that the Kistler transducers are only sensitive to high amplitude pressure fluctautions. One can clearly see that these transducers only meaure levels in excess of the 115 dB range. This is the primary reason for using the screech tone of the jet to calibrate these transducers. In Figure E.10 one again sees relatively good agreement between the two.

The same transducer was now mounted inside a water jacket and placed at the same physical location. In Figure E.11, one can see that with the addition of the water jacket the two signals are quite different. There is a 20 dB increase from 1-10 kHz, a 10 dB increase from 10-20 kHz, and additional tones appear to be added. The transducer did however measure the screech frequency accurately although at a level 4.3 dB lower than that measured by the B&K. For the higher Mach number similar but worse results were obtained.

Due to changes in the scope of the program this phenomenon was not resolved, and at this point only speculation can be made into the cause of this phenomena. These results are included here primarily to provide the benefit of our experience on the problems associated with acoustic measurements at elevated temperatures.
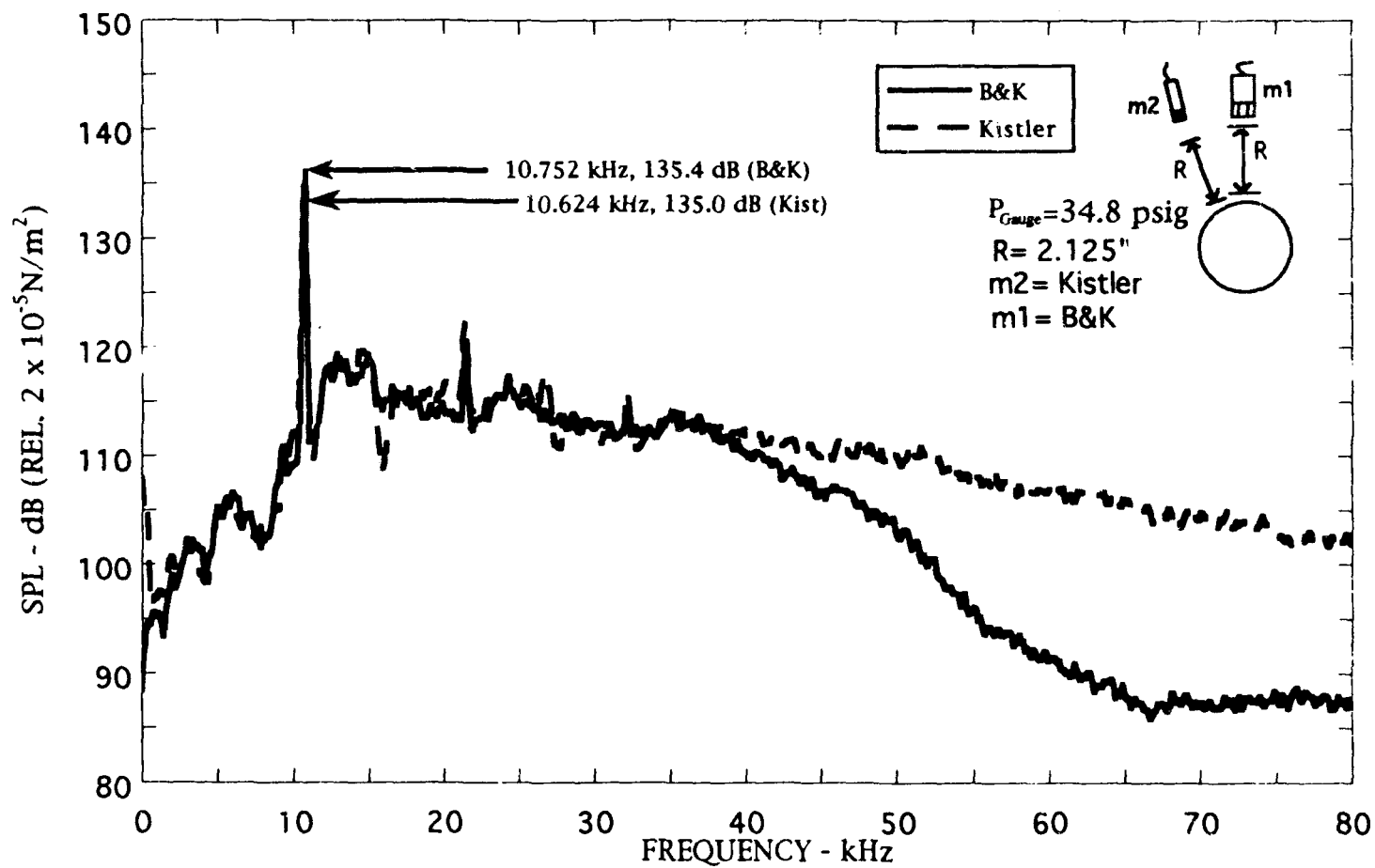
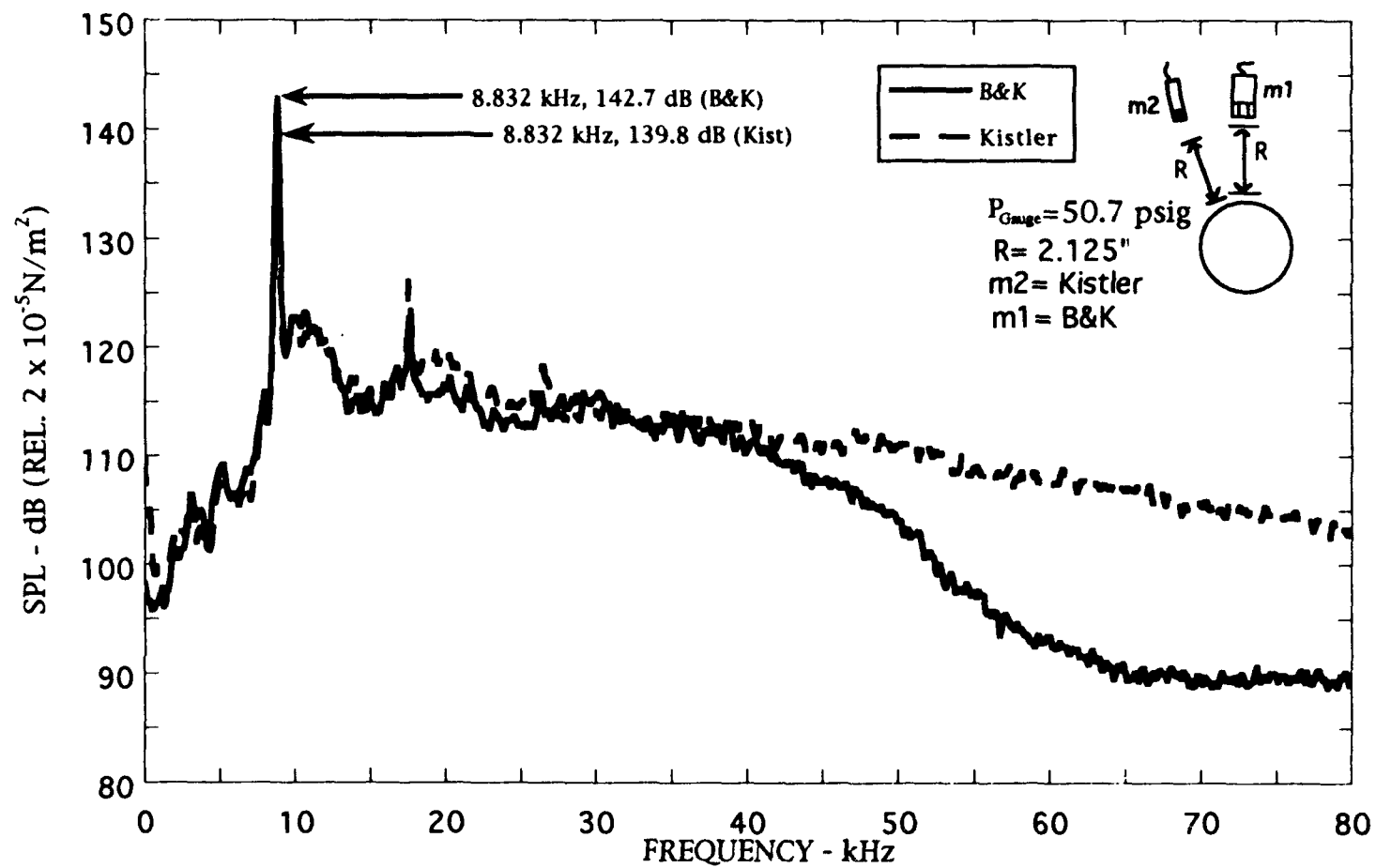**Figure E-9. B&K microphone versus Kistler transducer for Mach 1.35 jet.**

Figure E-10. B&K microphone versus Kistler transducer for Mach 1.65 jet.
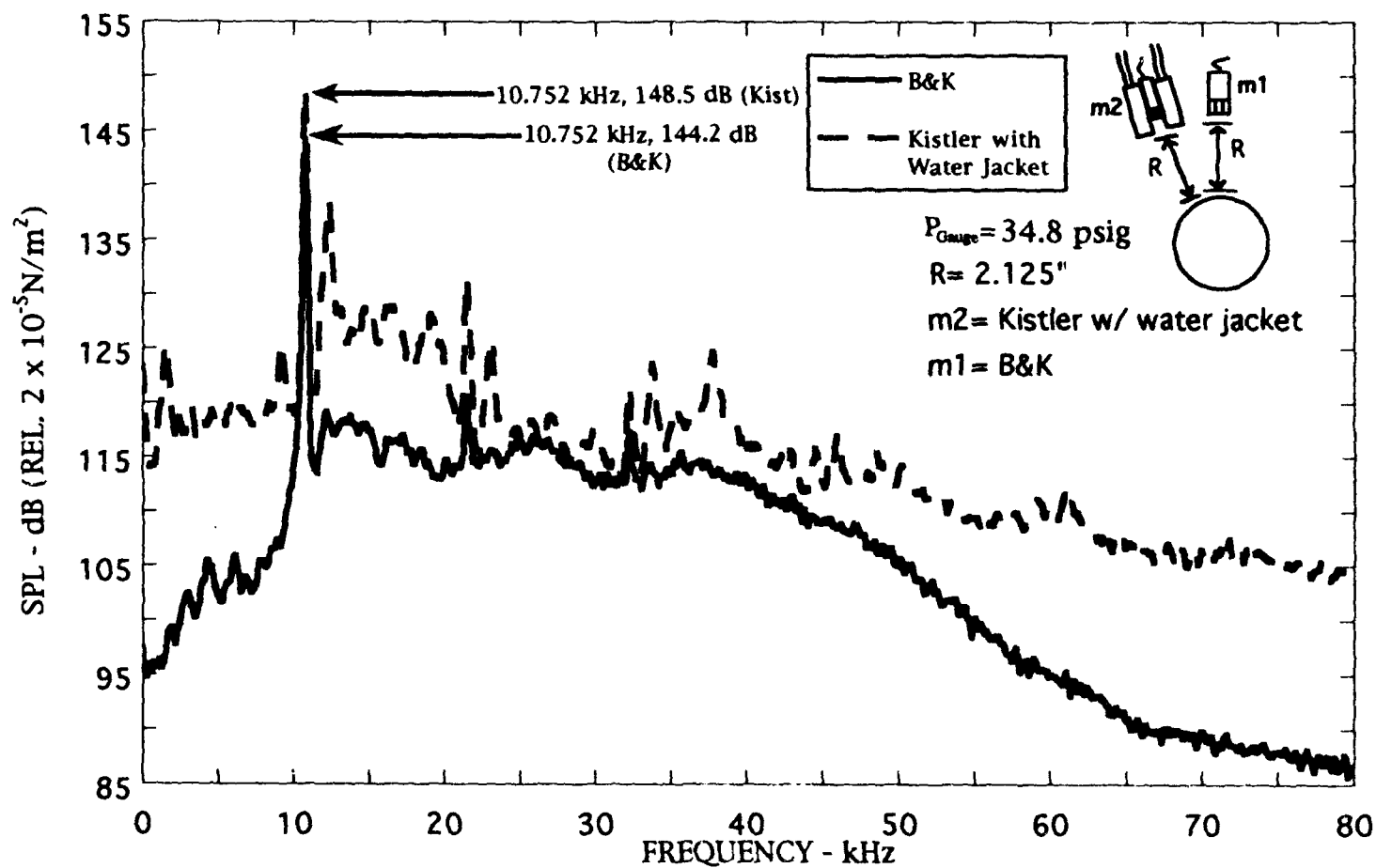
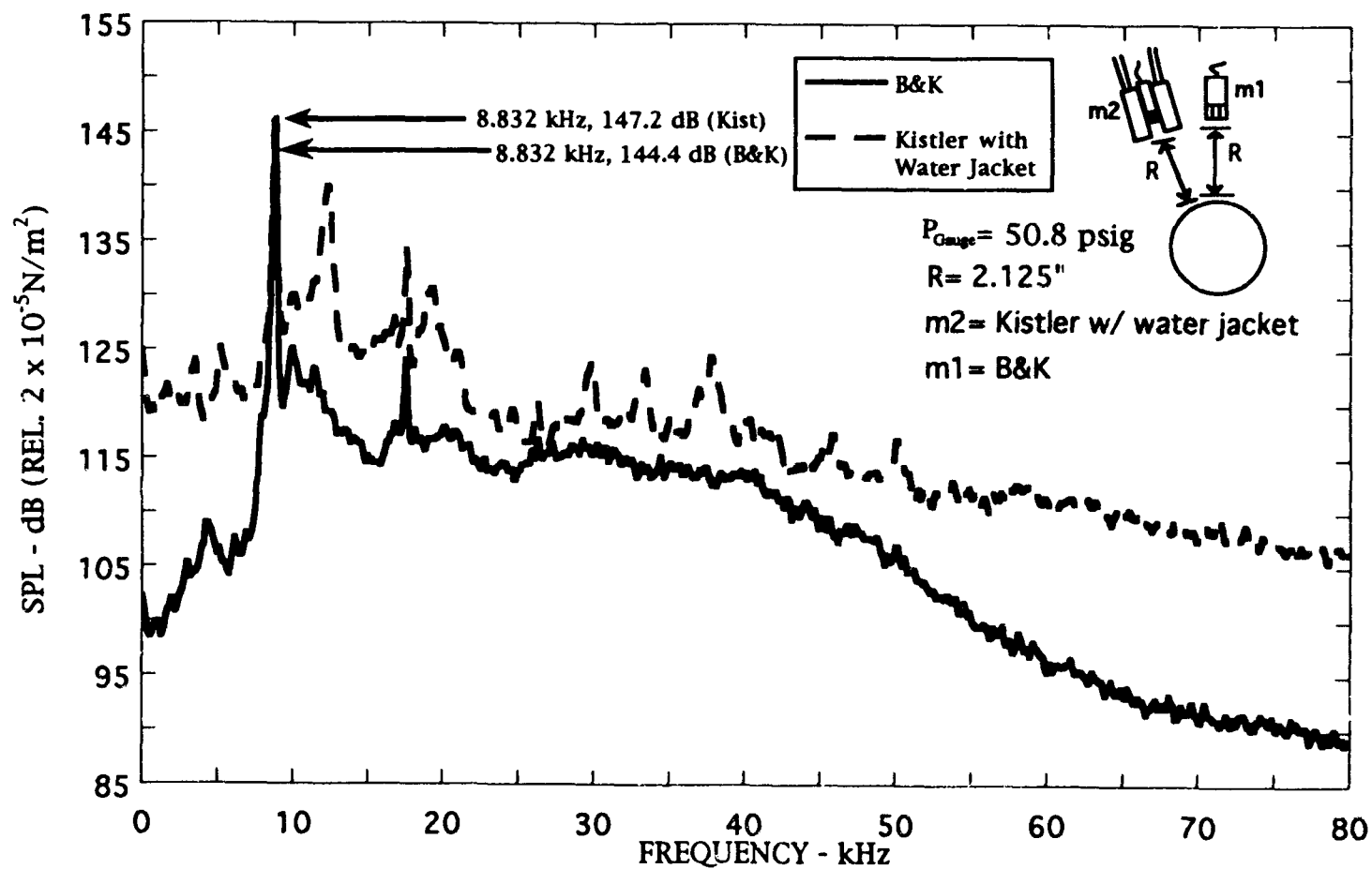Figure E-11. B&K microphone versus Kistler transducer inside waterjacket for Mach 1.35 jet.

Figure E-12. B&K microphone versus Kistler transducer inside waterjacket for Mach 1.65 jet.

APPENDIX F

Diffuser with Water Jackets

A diffuser was constructed with an array of fourteen water jackets to accommodate pressure transducers for the purpose of mode detection inside the diffuser. As the experiments progressed, it was jointly decided by the experimenters and AEDC personnel to pursue the mode detection at a later time and concentrate on acquiring the acoustic data, consequently this diffuser was not used in these experiments as other facets of the program became more important. For the sake of completeness, however, the diffuser is described here, since it presents a unique capability that could be exploited at a later time.

The diffuser is shown in Figures F.1 and F.2 below. This diffuser has a L/D of 3.0 and has 14 water jackets downstream of the test cell bulkhead. These water jackets are mounted so that 8 are radially distributed just downstream of the test cell bulkhead and there are 6 more mounted along axial lines on opposite sides of the diffuser. This configuration allows for unsteady pressure data to be acquired by 8 transducers simultaneously at a given radial location, and for data to be acquired along the diffuser axis by 8 transducers with four on each side (two transducers have multiple roles). Furthermore the diffuser design allowed the radial ring of water jackets to be moved axially on the diffuser, thus allowing easier model detection at different axial locations.
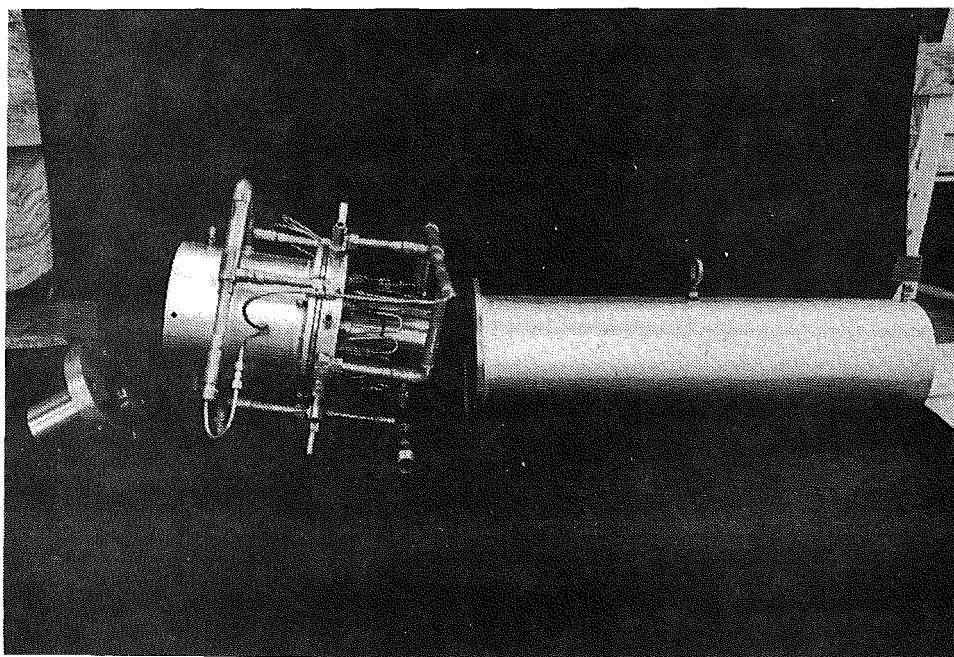

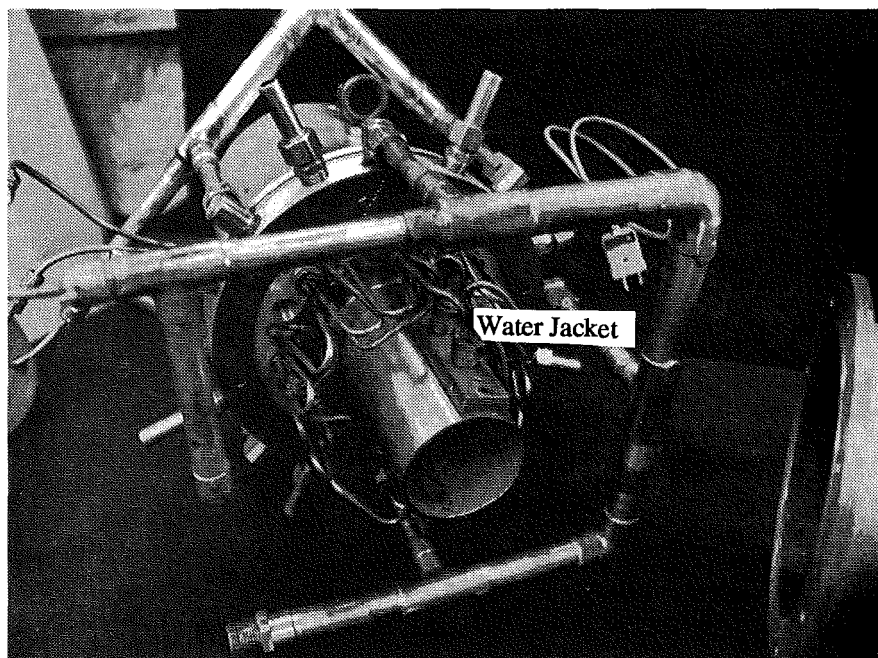Figure F-1. Ducted jet components with diffuser with water jackets.

285

Figure F-2. Close up of diffuser with water jackets.

APPENDIX G

Effect of L/D

A test was conducted for unheated flow into the effect of changing the length to diameter ratio of the diffuser. The L/D of this diffuser was 1.64 which is the ratio for the actual AEDC facility. Data for this diffuser were compared with data from a L/D = 3.0 diffuser. For all practical purposes, the spectra of these two test were identical, although the shorter ejector tended to increase the tones described in previous sections by approximately 2-3 dB. A comparison between the two diffusers is presented in Figures G.1 - G.9.
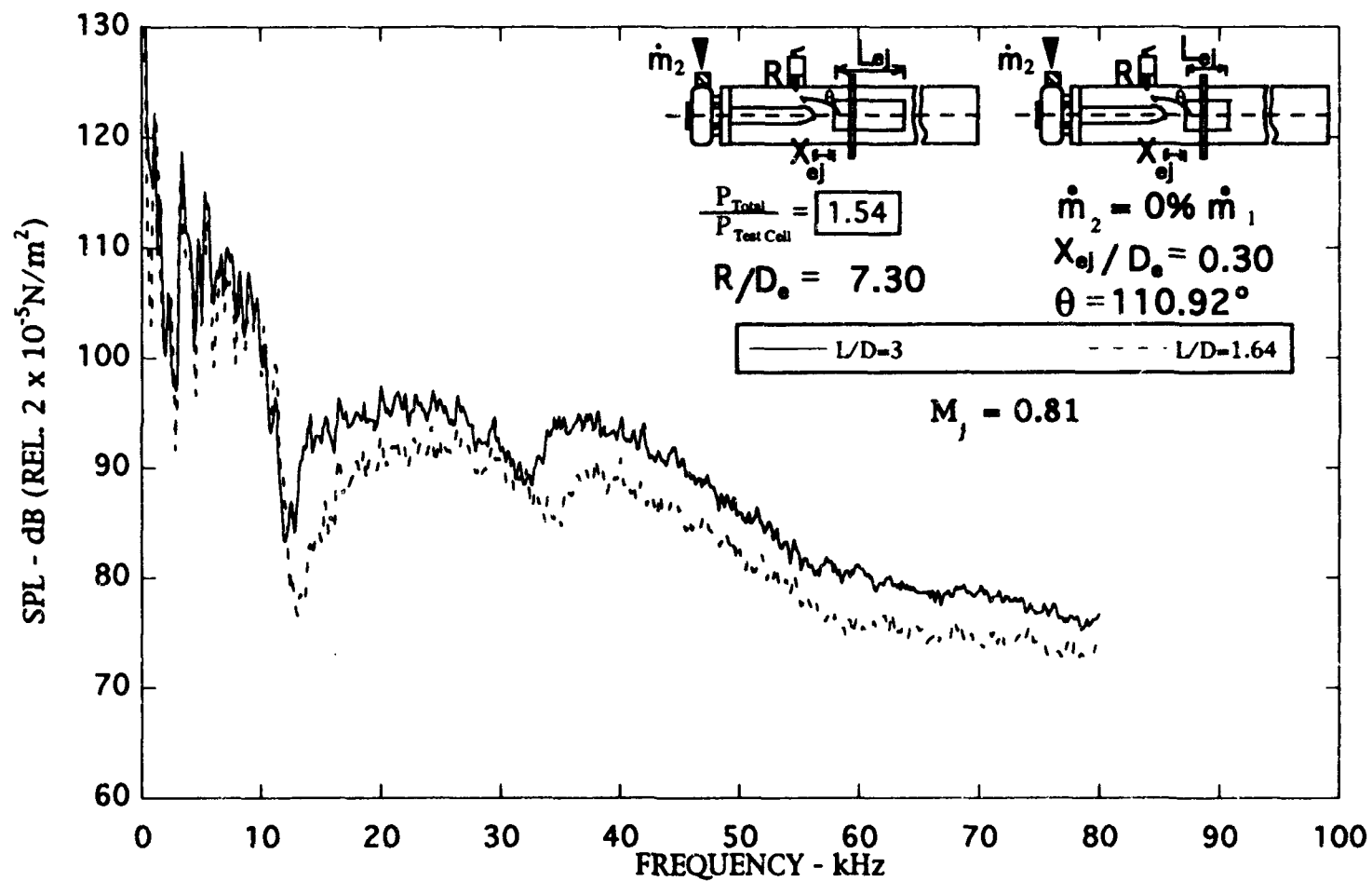
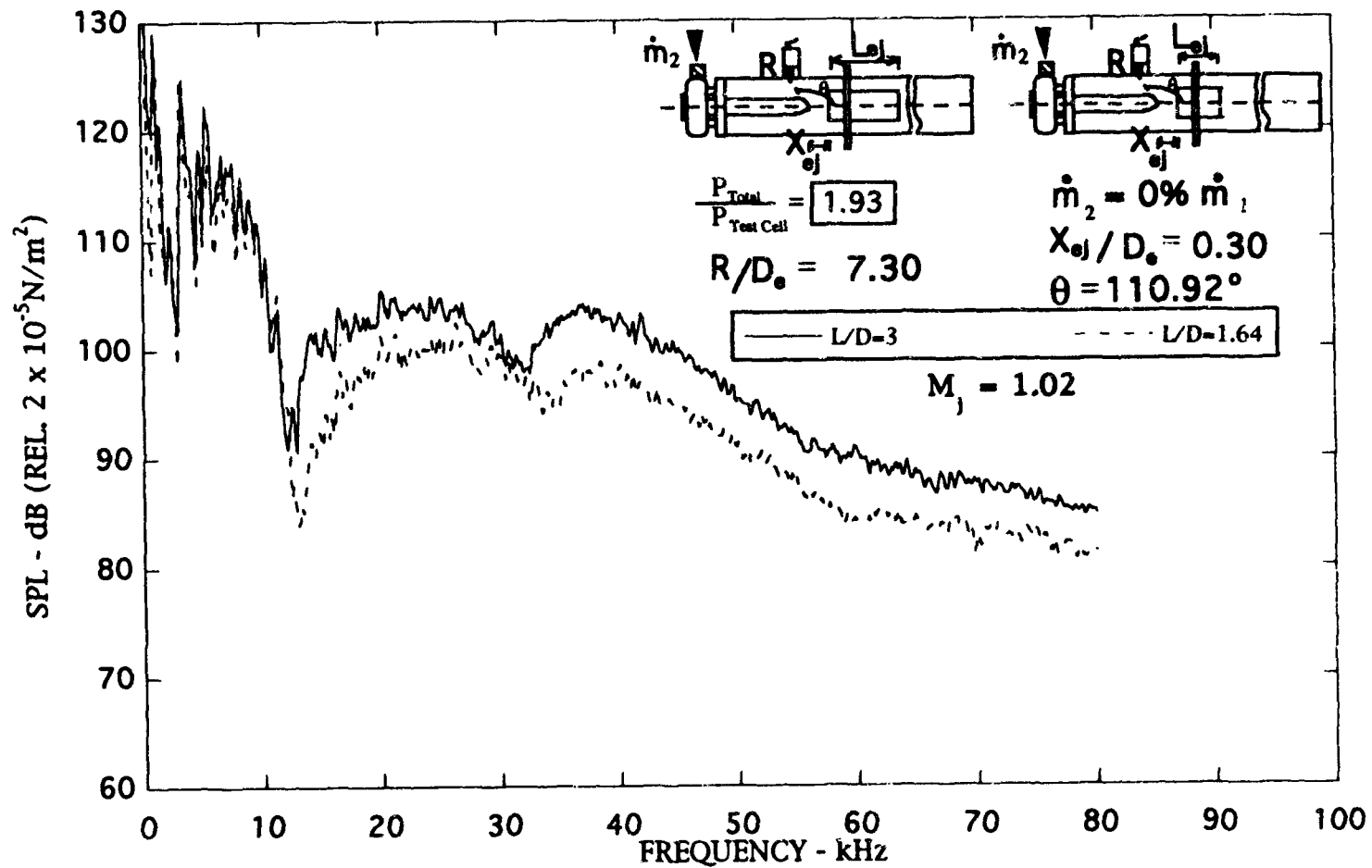Figure G-1. Cold flow ejector length comparison L/D = 3 versus L/D = 1.64.

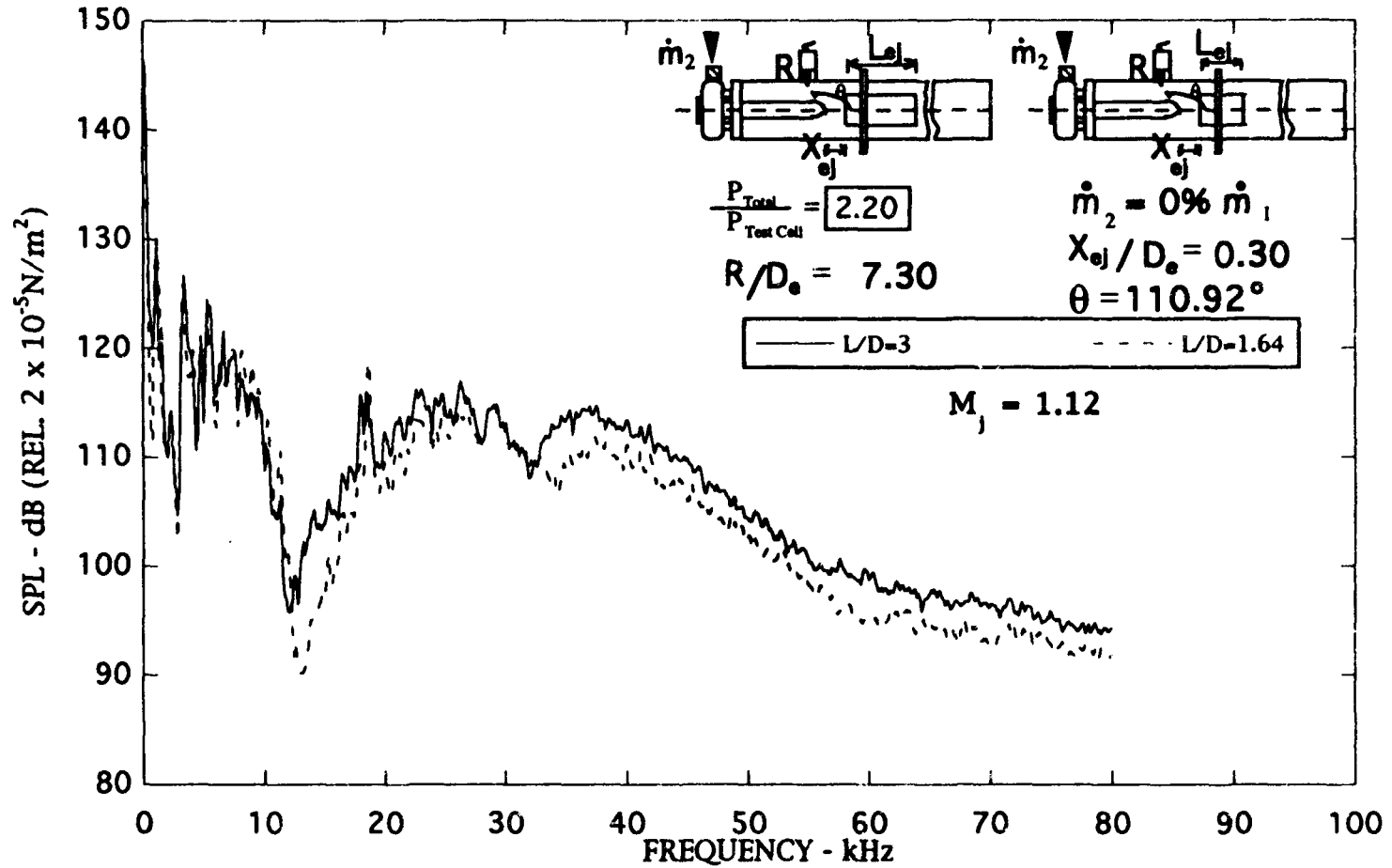Figure G-2. Cold flow ejector length comparison L/D = 3 versus L/D = 1.64.

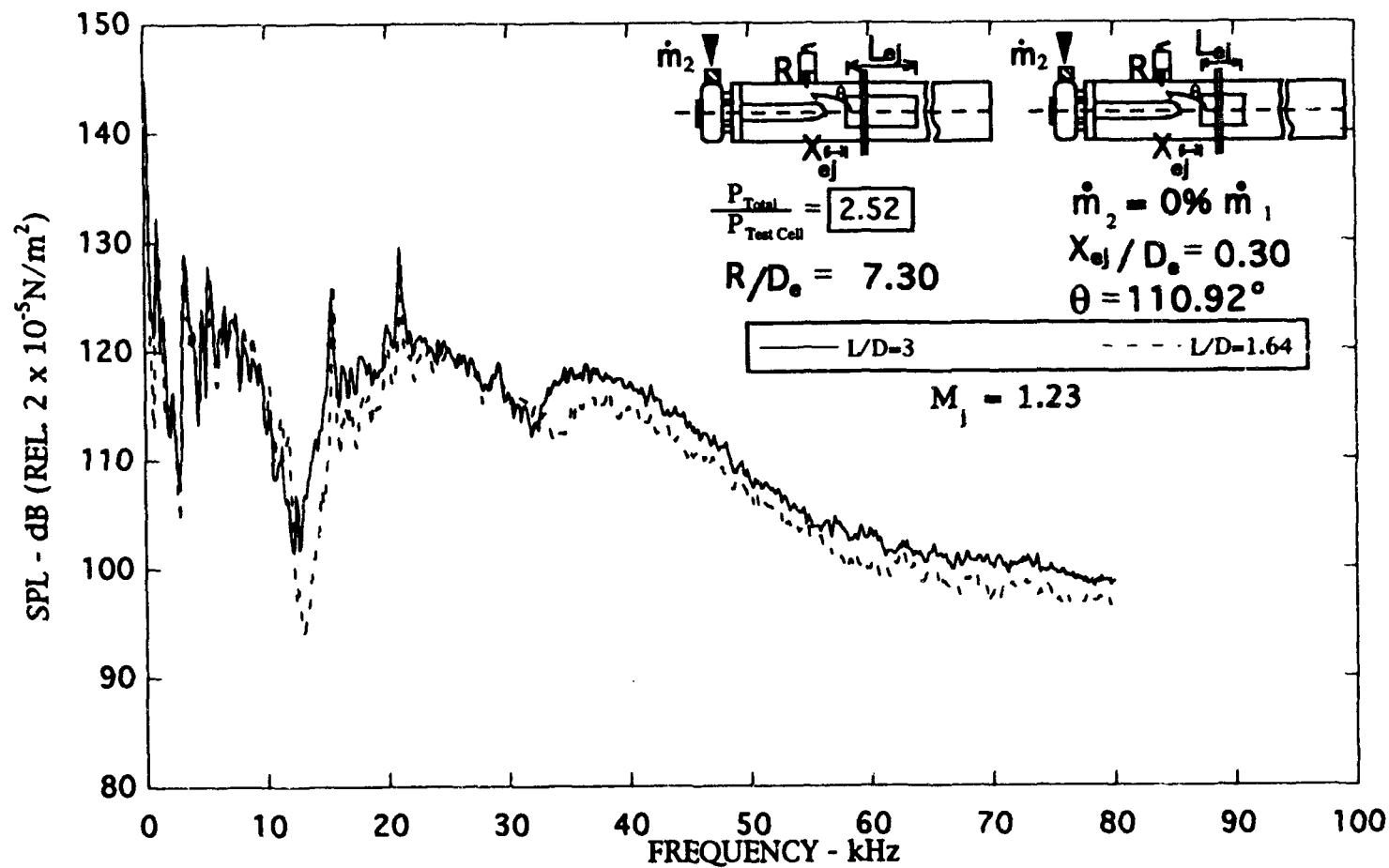Figure G-3. Cold flow ejector length comparison L/D = 3 versus L/D = 1.64.

Figure G-4. Cold flow ejector length comparison L/D = 3 versus L/D = 1.64.
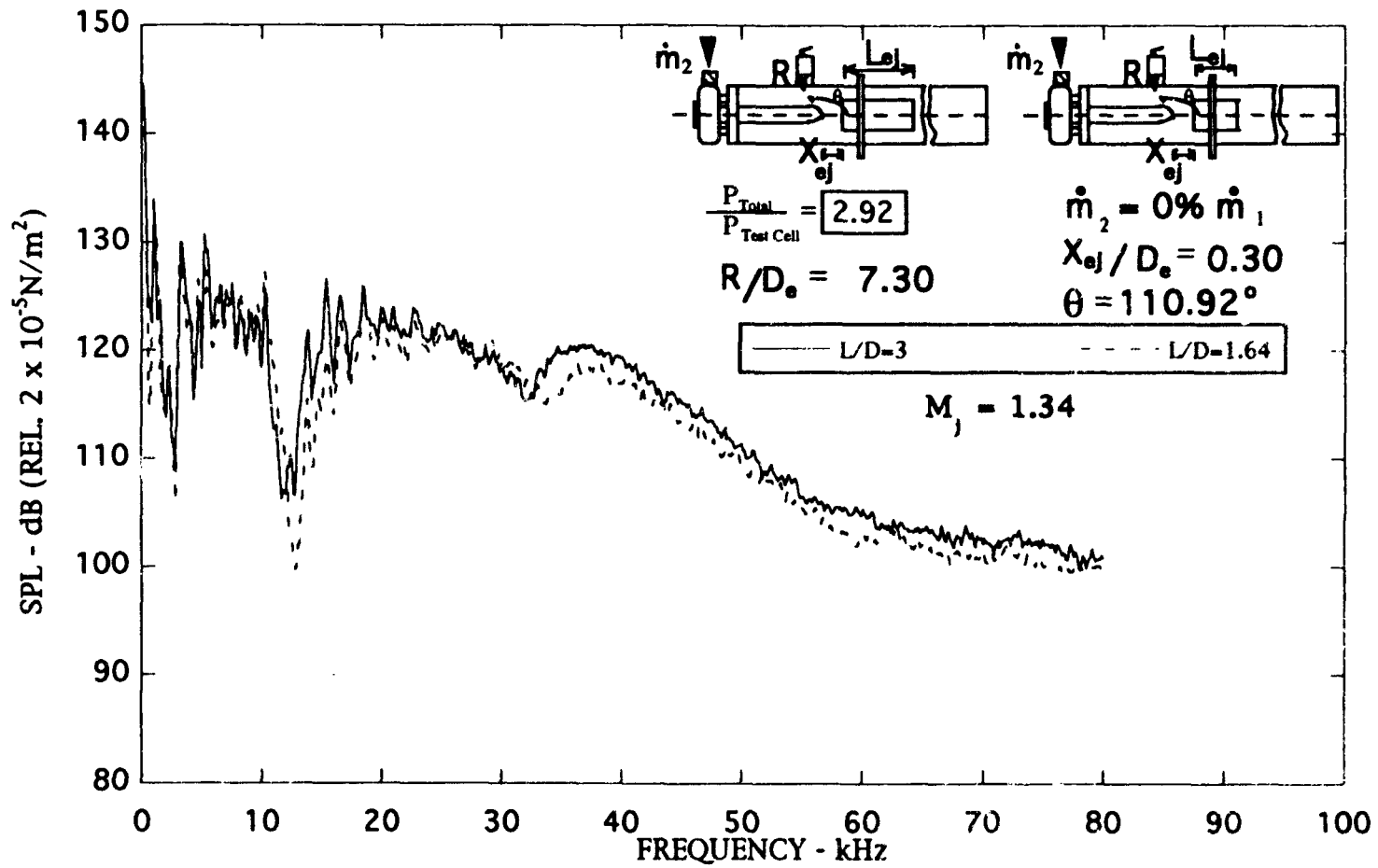
Figure G-5. Cold flow ejector length comparison L/D = 3 versus L/D = 1.64.

Figure G-6. Cold flow ejector length comparison L/D = 3 versus L/D = 1.64.

Figure G-7. Cold flow ejector length comparison L/D = 3 versus L/D = 1.64.
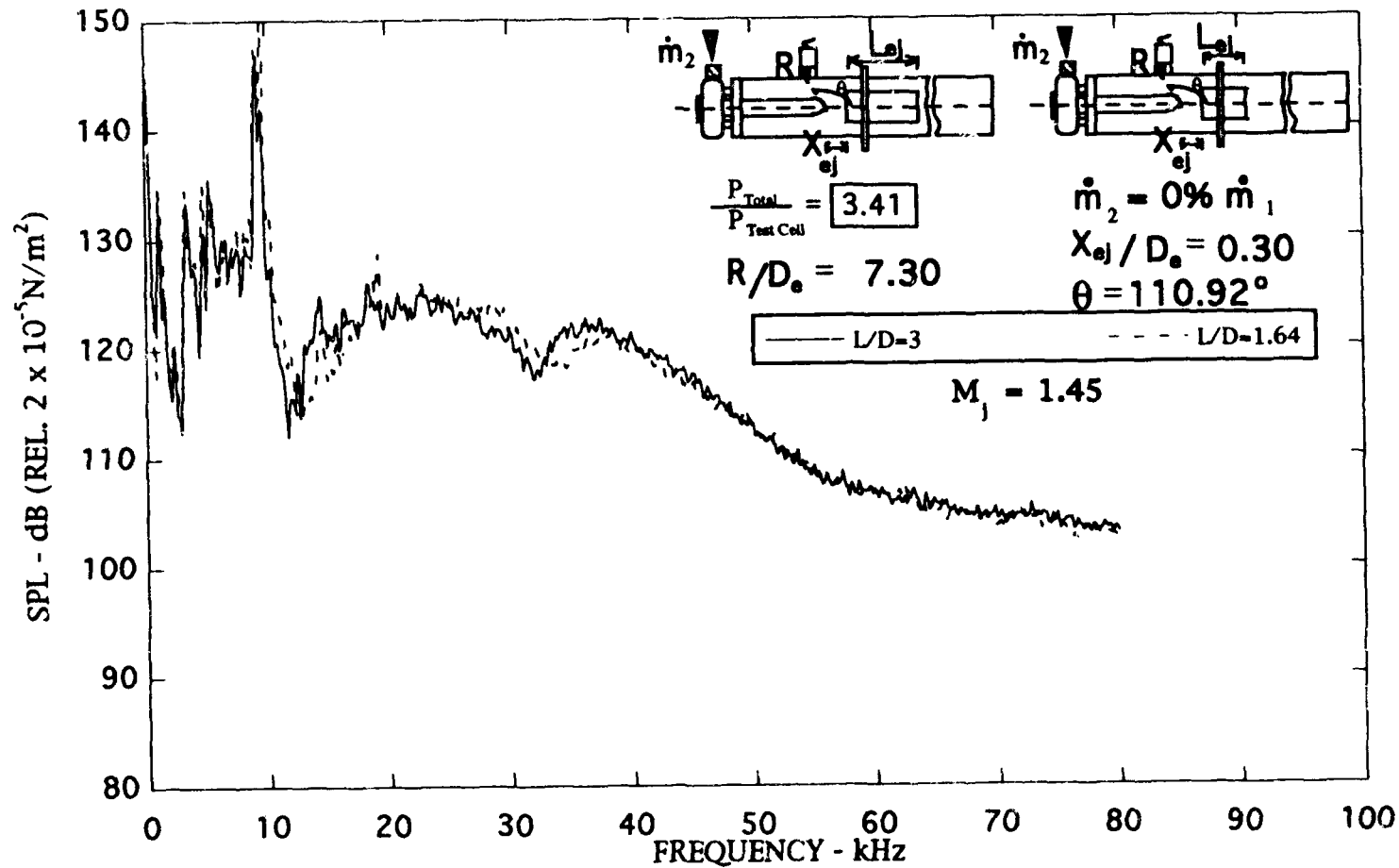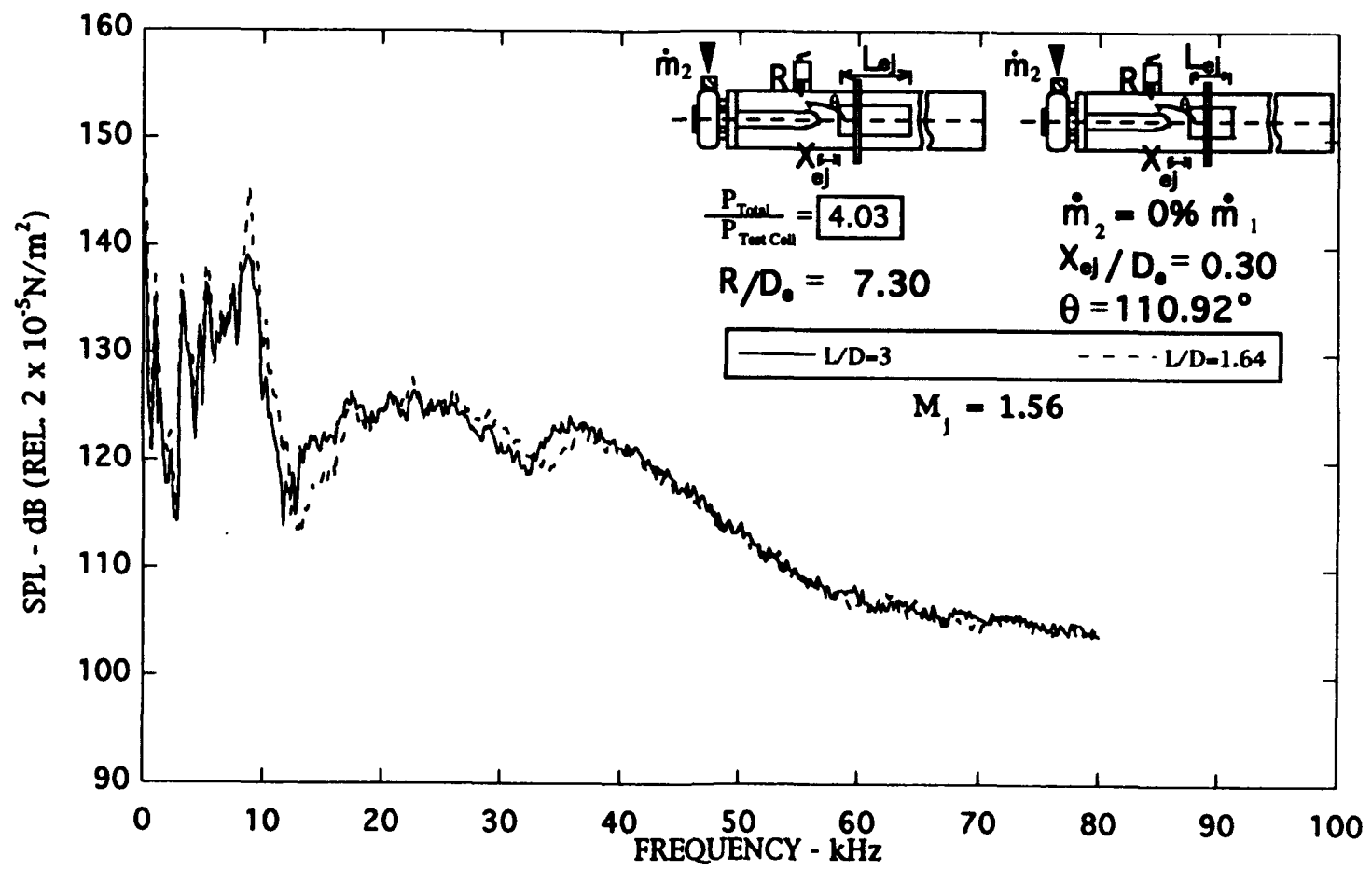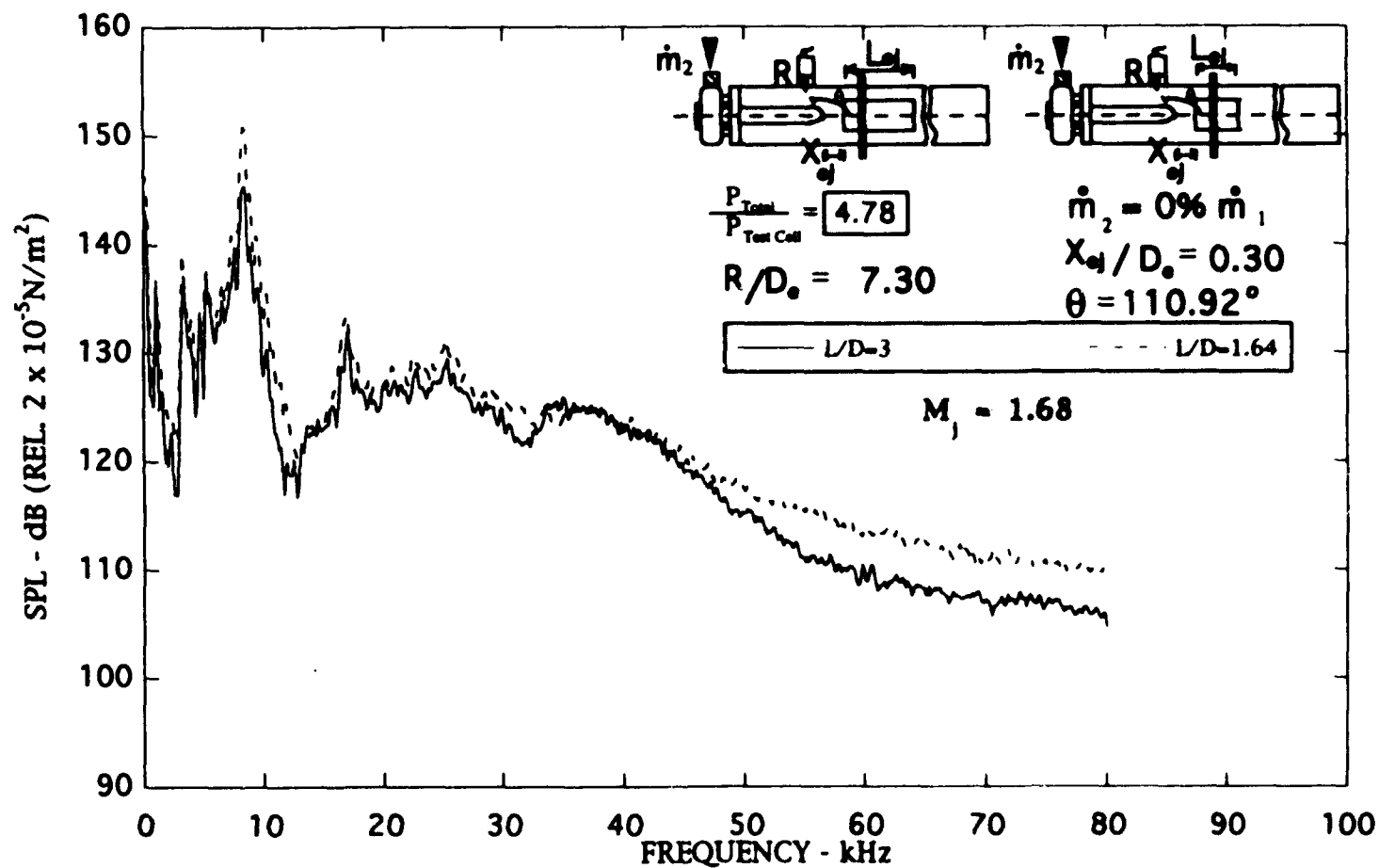
Figure G-8. Cold flow ejector length comparison L/D = 3 versus L/D = 1.64.

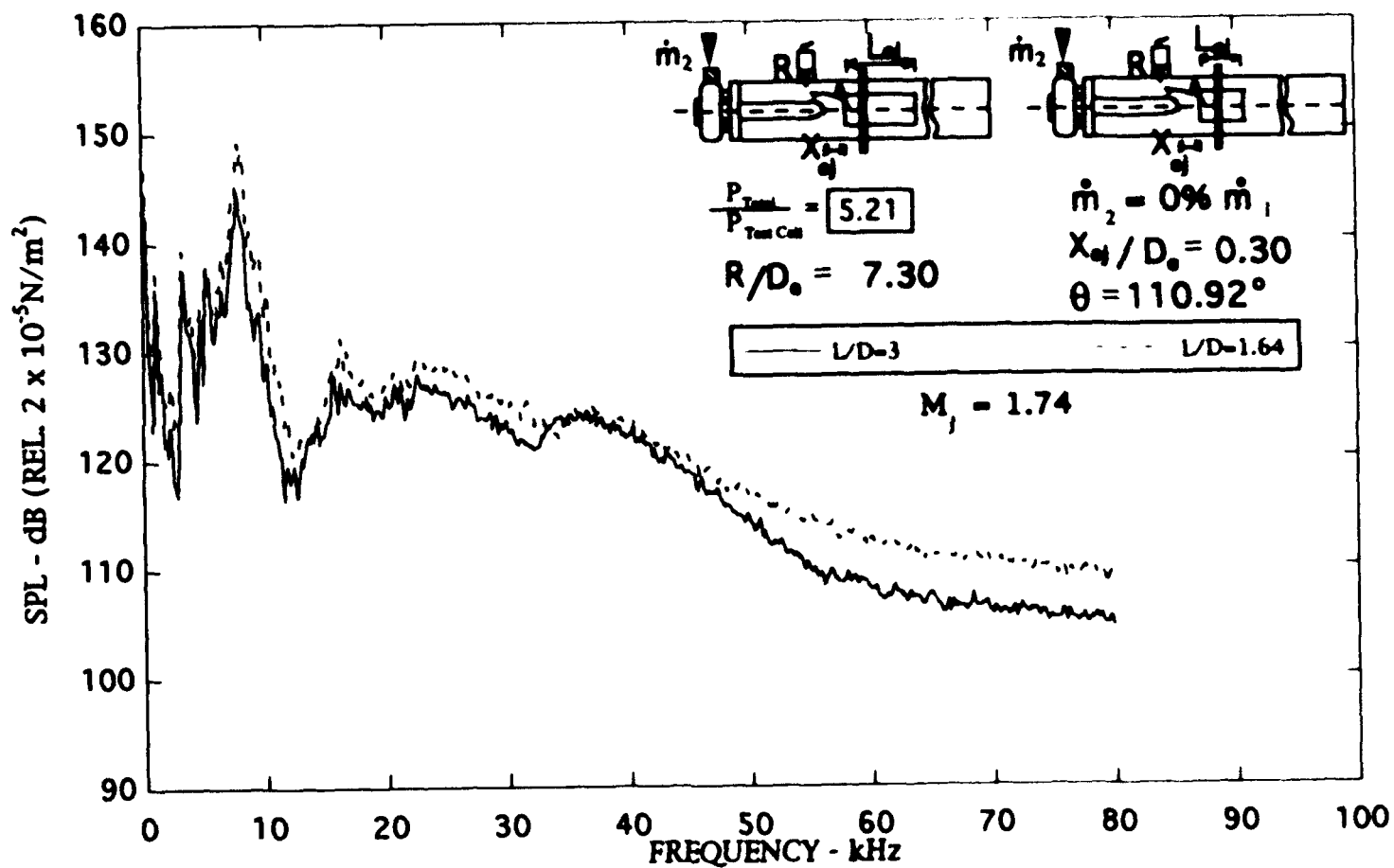Figure G-9. Cold flow ejector length comparison L/D = 3 versus L/D = 1.64.

NOMENCLATURE

D_e	- exit diame~~ter of t~~he nozzle
D_j	- exit diameter of the nozzle, alternatively the fully expanded jet diameter from Ref. 3.5
Δf	- bandwidth of the data
L/D or L_{ej}/D_{ej}	- length of diffuser over the diameter of the ejector
M_j	- tunderexpanded jet Mach number
M_d	- design Mach number of the jet
$\dot{m}_1$	- primary (jet) mass flow rate
$\dot{m}_2$	- secondary (manifold) mass flow rate
$\dot{m}_2/\dot{m}_1$	- nondimensional secondary mass flow rate
R/D_e	- nondimensional radial distance to the microphone
SPL	- Sound Pressure Level, typically measured in decibels
T_a	- temperature into which the jet expands
T_j	- jet total temperature
T_p or T_r	- temperature in the plenum reservoir
T_{tc}	- temperature in the test cell
T_r/T_a	- temperature ratio of the jet
θ	- polar angle relative to the jet centerline of the microphone location
U_j	- underexpanded jet velocity
X_{ej}/D_e	- nondimensional distance from the ejector to the nozzle exit